DISSERTATION

SYSTEMS ENGINEERING OF ACTIVE, PASSIVE, AND BIOENGINEERED PROTECTION FROM SPACE RADIATION

Submitted by

Charles J. Baker

Department of Systems Engineering

In partial fulfillment of the requirements

For the Degree of Doctor of Philosophy

Colorado State University

Fort Collins, Colorado

Fall 2025

Doctoral Committee:

Advisor: Steven Simske

Martin Gelfand
Daniel R. Herber
Gregory S. Marzolf

ABSTRACT

SYSTEMS ENGINEERING OF ACTIVE, PASSIVE, AND BIOENGINEERED PROTECTION FROM SPACE RADIATION

Space radiation presents a critical barrier to long-duration human spaceflight beyond Earth's magnetosphere, necessitating innovative shielding strategies. This dissertation involved developing a holistic systems engineering framework that integrates active magnetic field (AMF) shielding, passive material shielding, and bioengineered countermeasures to protect astronauts from galactic cosmic rays (GCRs) and solar particle events (SPEs). A scenario-driven trade-off analysis evaluated multiple mission profiles, ranging from short-duration sorties to multi-year deep-space habitats, to determine optimal shielding configurations. Model-based systems engineering (MBSE) techniques, including the design structure matrix, functional flow modeling, and failure mode and effects analysis, are applied to manage the complex integration of superconducting magnet coils, power and thermal control systems, and spacecraft subsystems. Monte Carlo radiation transport simulations (FLUKA, MATLAB) and parametric co-simulations validate shielding performance against National Aeronautics and Space Administration (NASA) dose limits.

The results demonstrate that no single solution is sufficient. A high-intensity AMF can deflect a significant portion of charged GCR particles, significantly reducing dose with far less mass than all-passive shielding. Passive, hydrogen-rich materials remain indispensable for absorbing secondary neutrons and uncharged radiation that magnets cannot deflect. Bioengineering approaches, including radioprotective pharmaceuticals and enhanced DNA repair

mechanisms, further bolster crew resilience, providing a complementary biological layer of defense. The key implication is that an integrated, multilayered shielding architecture, which is supported by rigorous systems engineering, is crucial for enabling safe and sustainable human exploration of Mars and other deep-space destinations.

ACKNOWLEDGMENTS

This dissertation represents the culmination of years of work, and I would not have reached this point without my family's love, encouragement, and patience. To my family, I owe the deepest gratitude. Your unwavering support, sacrifice, and understanding carried me through countless late nights, weekends spent in front of simulations, and long stretches of writing. Your belief in me gave me the strength to persevere, and I dedicate this accomplishment to you.

I also extend my heartfelt thanks to my advisor, Dr. Steven Simske, for his steadfast mentorship and guidance throughout this journey. His positivity and encouragement were a constant source of motivation during the most challenging research and writing stages. Dr. Simske has been more than an advisor; he has been a true mentor whose insights extended far beyond systems engineering. I am deeply grateful for his generosity with time and knowledge and for the example he has set as both a scholar and a leader.

I am equally appreciative of my committee members. Dr. Daniel Herber's expertise in model-based systems engineering helped shape the technical rigor of this work. Dr. Greg Marzolf's insights in systems engineering strengthened the methodological foundations of the dissertation. Dr. Marty Gelfand's perspective in physics provided critical grounding and expanded the scientific depth of my research. Their thoughtful feedback, constructive critiques, and encouragement were invaluable in refining and elevating this work.

Finally, I hope this dissertation contributes, in some small way, to the enduring human endeavor of space exploration. These findings help advance safe and sustainable approaches for protecting future astronauts as humanity ventures farther into deep space, toward the Moon, Mars, and beyond.

TABLE OF CONTENTS

INTRODUCTION

1.1 Background and Motivation

Space radiation presents one of the most daunting human spaceflight challenges during the long-duration missions to destinations outside of LEO, including Mars or beyond. The galactic cosmic rays (GCRs) and solar particle events (SPEs) are the two main sources of such radiation, which have serious implications on the health and safety of astronauts as well as damage to the integrity of the spacecraft [1]. GCRs are high-energy, ionized atomic nuclei located outside the solar system that can penetrate spacecraft shielding and human biological tissues. This ionizing radiation can potentially lead to DNA damage that can result in cancer, cardiovascular problems, and neurodegeneration [2]. The significant danger to astronauts is due to the production of solar flares and coronal mass ejection radiation from SPEs. Such radiation can subject the astronauts to acute radiation doses in just a couple of hours unless some means of shielding them against it can be put in place [3].

Making this a more challenging problem are the interactions of high-energy particles with shielding materials, which produce secondary radiation, primarily neutrons and light ions, exacerbating the overall issue. As the interplanetary missions extend beyond the magnetosphere of Earth, an effective and multidimensional radiation protection scheme is essential to provide astronaut safety without sacrificing spacecraft mass, power and structural design limiting factors [4, 5].

1.2. Problem Statement

Some of the existing methods concerning radiation protection such as passive shielding, active shielding as well as the biological countermeasure have their own advantages and critical shortcomings. High-density or hydrogen-rich passive shielding provides constant protection but mass demands soon become excessive in deep-space applications [6]. Active shielding, such as artificial magnetic field (AMF) systems, can reduce mass but requires substantial power and introduces thermal and integration complexities. Biological countermeasures, while promising in enhancing astronaut resilience, remain experimental and unproven for operational missions.

The key problem is that no shielding strategy can provide optimal protection across all mission classes. Short-duration sorties, long-duration Mars missions, and highly mobile spacecraft impose different mass, power, and operational constraints. Yet, existing research too often isolates these approaches rather than synthesizing them into integrated, mission-tailored architectures [5, 7].

1.3. Research Objectives

The overarching goal of this dissertation is to develop a systems engineering framework that integrates active, passive, and bioengineered shielding solutions to optimize spacecraft radiation protection. The specific objectives are:

1. Evaluate the feasibility and efficiency of AMF shielding, including field configurations, superconducting materials, and energy requirements.
2. Assess the effectiveness of passive shielding materials (BNNTs, polyethylene, aluminum composites) in reducing primary and secondary radiation exposure.
3. Explore bioengineered approaches (e.g., antioxidant-producing microbes, genetic modifications for DNA repair) as complementary countermeasures.
4. Develop a systems-engineering methodology (MBSE, DSM, FMEA) to optimize shielding effectiveness while balancing power, mass, and integration.
5. Validate shielding strategies using Monte Carlo simulations (FLUKA, Matlab) and co-simulations with MBSE tools, which is supported by NASA's past shielding data [8, 9].

This research was guided by hypotheses that:

- AMF systems are essential for long-duration protection but require systems-engineering solutions to overcome integration challenges.
- Passive shielding remains indispensable for neutrons and uncharged radiation.
- Biological countermeasures provide resilience against residual dose.
- A multilayered, hybrid approach will outperform any single shielding method.

1.4 Scope and Limitations

The scope of this dissertation was limited to 3 mission archetypes:

- Short-duration, low-power missions (e.g., lunar sorties)
- Long-duration deep-space habitats (e.g., Mars transit or surface bases)
- Highly mobile spacecraft with variable mission profiles

Within these scenarios, shielding concepts are analyzed using computational simulations (FLUKA, MATLAB), model-based systems engineering (MBSE) modeling (SysML, design structure matrix [DSM], and failure mode and effects analysis [FMEA]), as well as literature-derived performance data.

Short-duration mission candidate configurations emphasize lightweight passive shielding using hydrogen-rich materials, such as boron nitride nanotubes (BNNTs), augmented by low-power active magnetic field (AMF) systems in a standby mode. Long-duration habitat shielding strategies combine high-intensity superconducting AMF systems with polyethylene-based composites to mitigate cumulative exposure. Highly mobile spacecraft are evaluated with adaptive field modulation architectures, including a rotating toroidal-induced dipole field (RTIDF) system that dynamically adjusts magnetic field intensity and direction in response to real-time radiation conditions and spacecraft orientation [6, 10].

Biological countermeasures (e.g., antioxidant-producing microbes and probiotic DNA-repair enhancers) are conceptually evaluated, although this work does not experimentally validate biomedical techniques. Similarly, plasma and magnetohydrodynamic (MHD) shielding are theoretical concepts, but their current technology readiness level (TRL) limits their detailed inclusion.

The analysis prioritizes feasibility within current or near-term engineering constraints, while acknowledging that technological advances, such as next-generation superconducting materials, high-efficiency power systems, or engineered biological systems, may shift these trade-offs in the future.

By incorporating a scenario-based trade-off analysis with systems engineering methodology and a multilayered shielding approach, this dissertation aims to bridge the gap between theoretical shielding models and practical mission applications. The findings could contribute to developing next-generation radiation protection strategies to ensure safer and more sustainable human space exploration beyond Earth's magnetosphere [11].

LITERATURE REVIEW

2.1. Integrated Space Radiation Shielding

2.1.1. Active Shielding

Active shielding involves using electromagnetic fields to deflect or slow charged particles before they reach crew habitats. This emulates the protection provided by Earth's magnetosphere on a small scale. This concept has deep historical roots. Studies in the 1960s–1970s explored using electric or magnetic fields for spacecraft radiation protection, initially targeting solar protons and electrons. Only later, in the 1980s–1990s, did research address the more challenging high-Z, high-energy (HZE) cosmic rays [1]. Foundational analyses raised skepticism, concluding that active methods were theoretically appealing, but the field strengths and power required to shield from galactic cosmic rays (GCRs) were impractically high with then-current technology.

In the past 10–15 years, interest in active systems has resurged due to advances in superconductors and plasma physics advances. Researchers have revisited several active shielding architectures, each with distinct principles and technical hurdles, as summarized below [1].

- **Electrostatic Shields:** These systems would establish a strong electrostatic field (on the order of ~10^{10} volts) around the spacecraft to repel charged particles. The concept was experimentally tested in the 1970s, when the Soviet Zond program charged a spacecraft to deflect 10–100 MeV protons, and NASA further analyzed it in the 2000s. Electrostatic shielding can deflect low- to moderate-energy ions, potentially reducing solar particle event (SPE) doses. However, modern studies find it ineffective against the most energetic GCR nuclei, requiring unrealistically high voltages and extended field regions [2].

Maintaining a charged field in space also presents serious challenges: power supplies would need voltages an order of magnitude beyond the state of the art, and the structure risks rapid discharge from interactions with the ambient plasma (e.g., solar wind). Additionally, strong fields could attract electrons and produce secondary radiation. Due to these limitations, recent reviews have largely deemed pure electrostatic shields infeasible for deep-space radiation protection. Research in the past decade has shifted away from all-electrostatic solutions except as small-scale supplements to other methods [2].

- **Magnetoplasma "Mini-Magnetosphere" Shields:** Inspired by Earth's magnetosphere, this approach uses a magnetic field, often "inflated" by a plasma cloud, to create a standoff barrier that diverts incoming radiation. Laboratory experiments and simulations (e.g., at Rutherford Appleton Laboratory [RAL] and NASA) have demonstrated that a magnetic bubble could deflect a significant fraction of solar wind ions. A magnetosphere on the order of kilometers could scatter radiation away before it reaches the spacecraft [3]. However, sustaining such a system presents formidable integration challenges. Power demands are exorbitant, consisting of tens to hundreds of kilowatts of continuous power to maintain both the plasma and magnetic field. A NASA Marshall Space Flight Center–supported simulation found that roughly 100 kW of plasma injection power would be required to sustain a mini-magnetosphere capable of measurably reducing GCR flux, far exceeding the power availability of current crewed spacecraft. The dynamic plasma environment could also impart unwanted forces and torques on the spacecraft. Solar wind pressure on a large magnetic bubble can physically push the vessel or induce oscillations [3]. Plasma instabilities and complex spacecraft–plasma interactions remain poorly understood, and experiments indicate such instabilities could cause unpredictable behavior or collapse during solar storm conditions. As a result, mini-magnetosphere concepts remain scientifically intriguing. Still, they are not yet practical, hampered by extreme power and mass requirements and control complexities that outweigh current benefits [3].

- **Magnetic Coil Shields (Resistive):** A more conventional approach is to generate a static magnetic dipole field around the spacecraft using large current-carrying coils. Early NASA studies examined whether solenoidal or toroidal coils could produce a strong field to deflect GCR ions significantly. Theoretically, a field of a fraction of a tesla extending several meters could force charged particles to spiral away from the habitat. However, using normal (resistive) electromagnets is extremely costly in mass and energy [4]. A resistive magnet capable of ~1 T over a radius of several meters would consume tens of kilowatts of continuous power and produce intense resistive heating, requiring a substantial cooling system. The coil windings and power supply would add significant mass to a crew vehicle–sized shield. Even then, a dipole field decays with distance and may only deflect some lower-energy particles; the highest-energy GCR components would penetrate virtually unaffected. Because of these drawbacks, purely resistive magnetic shields have fallen out of favor, as maintaining the necessary current and field strength would require prohibitively large power generation and radiator capacity for long-duration missions [4].
- **Magnetic Coil Shields (Superconducting):** The superconducting magnet is the most actively researched form of active shielding in the past decade. Superconductors can carry large currents with negligible resistive losses, enabling strong magnetic fields (1–5

T) to be sustained with far less electrical power than resistive coils. Several teams, such as Spillantini et al (2010), Battiston's SR2S project in the mid-2010s, and Westover et al (2012) at NASA, have developed conceptual designs for lightweight superconducting dipoles or toroids to shield the crew [16].

High-temperature superconductors (HTS) operating at ~20–70 K, such as magnesium diboride (MgB_2) or yttrium barium copper oxide (YBCO) tapes, are attractive because they could be cooled by cryocoolers rather than heavy liquid-helium systems. A superconducting magnet could run continuously on a moderate power budget (for refrigeration and monitoring) while producing a 1–2 T field capable of substantially deflecting solar protons and reducing a fraction of GCR exposure. Recent analyses report that an active dipole field of ~1–2 T could cut the GCR dose by approximately 20%–50%, depending on geometry. This represents a meaningful reduction that no feasible amount of material shielding alone could achieve without enormous mass.

Despite this promise, significant engineering challenges remain. The coil assemblies and support structures still add considerable mass (on the order of a few tons for a Mars spacecraft–scale shield) and must withstand immense Lorentz forces. Electromagnetic interference (EMI) is a significant concern; a multi-tesla field encompassing the spacecraft can induce currents and voltages in electronics, disrupt sensors, and degrade communications. Ensuring magnetic compatibility ("magnetic cleanliness") requires careful design, such as using degaussing coils or active feedback loops to cancel stray fields.

Thermal management and quench protection are also critical, as a sudden loss of superconductivity could release the stored coil energy, posing a hazard. Reliability is a key critique: unlike passive shielding, an active magnet is a complex system-of-systems (power supply, cryocooler, control electronics, structural supports) that could fail. A power spike or coil quench could collapse the protective field, instantly exposing the crew to full radiation flux. Redundancy and fail-safe controls are essential for any superconducting shield design.

Over the past decade, active magnetic shielding has progressed from technology readiness level (TRL) 2–3 concepts to TRL 4–5 prototype analyses, yet substantial development and testing are needed [5]. Recent literature agrees that active shielding alone cannot meet deep-space requirements but could significantly augment passive shielding. A strong magnetic field could deflect lower-energy charged particles, allowing for reduced passive material thickness while achieving the same overall dose reduction. This complementarity underpins the consensus that active systems should be developed alongside robust passive shielding, not in isolation [5].

In summary, active shielding research reflects a balance of optimism and realism. Foundational studies established the physical feasibility of electromagnetic deflection but highlighted its immense power and engineering demands [4]. Recent efforts, particularly in superconducting magnet technology, have brought the concept closer to plausibility. However, unresolved issues remain, including achieving sufficient field strength to reduce GCR ions, integrating the magnet system into the spacecraft while mitigating EMI and structural forces, and ensuring long-term reliability.

There is divergence in the literature. Proponents, such as Spillantini (2010) and Battiston (2016), argue that continued advances in HTS magnets and innovative designs (e.g., deployable or shaping coils) could make active shields viable for Mars missions. Critics, such as Townsend and Cucinotta, counter that even the best active shield can only partially reduce GCR doses and should not detract from improving passive materials [3, 4]. Nevertheless, there is broad agreement that if engineering challenges can be addressed, active magnetic shielding could be transformative by providing substantial protection without the prohibitive mass of all-passive solutions. Ongoing research focuses on coil configurations, plasma experiments, and hybrid concepts, aiming to tip the mass–power–shielding trade-off in favor of deep-space mission feasibility [6].

2.1.2 Passive Shielding

Passive shielding refers to using physical materials (solid or liquid) placed around crew habitats to absorb or slow radiation. It is the oldest and most straightforward form of protection against space radiation. All crewed spacecraft to date has relied on some amount of passive shielding (e.g., aluminum hulls, polyethylene bricks, and water tanks) as the first line of defense. This method provides a fail-safe and continuous barrier that does not depend on power or active control. Foundational research in the mid-20th century, including NASA studies by Silberberg, Wilson, and colleagues, established the basic principles of radiation shielding. High-density materials reduce particle flux, but the effectiveness per unit mass depends strongly on the material's composition [8]. Over the last 10–15 years, extensive simulations and experiments have refined the understanding of different materials' performance, especially under high-energy galactic cosmic ray (GCR) bombardment.

A key theme in recent literature is the trade-off between high–atomic–number (high-Z) materials and hydrogen-rich materials for cosmic ray shielding. Modern consensus favors light, hydrogenous substances as more mass-efficient shields for deep space due to their ability to reduce secondary radiation production [7].

Hydrogen-Rich Materials: Materials composed of lighter elements, especially those with high hydrogen content, have proven to be the most effective passive shields on a mass basis. Hydrogen nuclei are adept at slowing charged particles via ionization energy loss. When struck by heavy ions, light elements produce far fewer dangerous secondaries (e.g., neutrons) than heavier elements. Polyethylene (PE) plastic, for example, contains approximately 14% hydrogen by mass (chemical formula C_2H_4) and has long been studied as an optimal shielding material. NASA simulations and accelerator tests in the 2000s showed that PE outperforms aluminum (Al) per unit areal density in reducing GCR dose equivalent. When impacted by high-Z cosmic rays, carbon and hydrogen generate much less secondary radiation than Al [9, 10].

This finding led to the incorporation of PE shielding in the International Space Station (ISS) crew quarters and experimental payloads. Narici et al [9] reported on an ESA-sponsored ISS experiment (ALTEA-Shield) directly measuring the shielding effectiveness of PE blocks in orbit. They found that a ~10 g/cm² layer of PE reduced the GCR dose rate by about 32% and the dose equivalent (which weights heavy ions more) by ~55%. This is a substantial mitigation but also illustrates diminishing returns beyond ~10–20 g/cm² of PE. Each additional centimeter yields progressively smaller reductions as the spectrum of remaining high-energy particles increasingly penetrates [9].

Multiple studies indicate a point of saturation: beyond a specific areal density (on the order of tens of g/cm², depending on material), the dose reduction begins to plateau or even reverse due to secondary radiation buildup [20]. Hydrogen-rich materials delay this turnover point compared with heavy materials. Recent Monte Carlo simulations by Al Zaman et al [21] confirm that polymers and novel lightweight hydrides can continue to incrementally reduce GCR dose up to ~20–30 g/cm² more effectively than heavier shields.

Besides PE, water is an excellent hydrogenous shield. Many mission studies propose water as a dual-use shield (for drinking and radiation protection). NASA has suggested storing water around crew quarters to create a "storm shelter" zone, since water (containing hydrogen and oxygen) is approximately 67% as effective as PE per mass and is readily available in life-support systems. However, oxygen in H_2O can produce more secondaries than pure hydrogen, so water is slightly less optimal than hydrocarbons.

In the past decade, there has been growing interest in nanostructured and composite materials that incorporate hydrogen with other elements capable of absorbing neutrons. One prominent example is boron nitride nanotubes (BNNTs) and related boron-infused polymers. Boron has a high cross section for capturing thermal neutrons via the $^{10}B + n \rightarrow {}^{7}Li + {}^{4}He$ reaction, which helps absorb secondary neutrons generated when GCRs strike the shield. A NASA simulation showed that boron nitride combined with hydrogen outperformed pure PE in shielding effectiveness [10]. The BNNT material acts as a hydrogen-rich nanofiber reinforcement (if functionalized or combined with resins) and provides the added benefit of neutron reduction via boron.

These materials remain experimental, and BNNTs are expensive to produce in bulk, but laboratory tests are promising. For example, Guo et al[14] found that a composite of BNNT in a hydrogenated epoxy matrix reduced dose by ~15% more than an equal-mass PE sample in 1 GeV/n ion beam tests. This indicates superior performance against high-energy heavy ions. Recent literature consistently points to light-element materials (H, C, B, N) as the preferred basis for passive shielding structures. These materials maximize nuclear slowing of ions while minimizing secondary radiation cascades, offering the highest protective payoff per unit mass [11].

High-Z Materials and Secondary Radiation: Traditional spacecraft hulls are made of metals like aluminum (Z = 13) or titanium (Z = 22), chosen for structural and manufacturing reasons, not radiation efficiency. High-Z materials effectively stop lower-energy radiation and high-energy photons (X-rays, gamma rays) because their nuclei have many electrons (high electron density). Indeed, dense metals are preferred for electromagnetic radiation shielding (like in nuclear reactors or X-ray facilities) [21]. But heavy materials present a drawback for charged particle radiation as in space. When a high-energy ion (e.g., an iron nucleus from GCR) strikes a heavy nucleus like aluminum, it tends to shower secondary fragments, neutrons, protons, and other nuclear fragments off the target. These secondary particles can be just as harmful as, or even more biologically effective than the primary radiation. NASA empirical studies have demonstrated this effect. An aluminum wall yields a higher flux of secondary neutrons behind it for the same areal density than a polyethylene wall [15]. Beyond a specific thickness, additional layers of aluminum increase the dose on the downstream side because the buildup of secondary neutrons and recoil nuclei outweighs the added slowing down of primaries. This counterintuitive result (a dose minimum at some optimal shield depth and then a rise for thicker shields) was reported in modeling by Norman et al (2017) and experimentally verified in beam tests up to ~100 g/cm^2 Al [12]. Adding more aluminum beyond ~20–30 g/cm^2 yields diminishing returns and can even be counterproductive for GCR protection [12]. High-Z materials are still helpful in specific contexts. They are very good at stopping the lower-energy components of solar flares (mostly tens of MeV protons) and can serve as structural support for lower-Z shielding layers.

However, the modern consensus is that heavy materials alone cannot feasibly shield long-duration cosmic ray doses [9]. The mass required would be enormous and could worsen neutron exposure. Instead, researchers advocate composite shielding strategies. For example, placing a thin layer of aluminum on the outside can help absorb soft X-rays and beta radiation. Still, a thicker layer of hydrogen-rich material should back it to absorb the neutrons and slow heavy ions. As an alternative, aluminum can be used structurally but augmented with polyethylene or water liners. As Narici et al put it, "even hydrogen-rich plastics reach a point of marginal benefit against the highest-energy GCR ions." This implies that some active or biological measures must ultimately handle the rest, but heavy metals reach that point much earlier and with additional risks [9, 26].

Trade-offs and Recent Innovations: The primary advantage of passive shielding is reliability. It works passively all the time, requires no activation, and cannot fail suddenly. It also stops all forms of radiation (neutrons and neutral particles included), which active magnetic fields do not affect. Therefore, passive mass will always be a "necessary foundation" of any integrated shield design. The downside is the mass penalty: carrying sufficient material to reduce GCRs to safe levels is prohibitively heavy with current launch technology. The last decade of research reinforces this point. Using GEANT4 and HZETRN models, Slaba et al (2015) showed that achieving even ~50% reduction in GCR dose for a Mars mission would require on the order of 500–1000 kg of PE per m^2 of habitat area (tens of g/cm^2); reaching ~75% or more reduction pushes into several thousands of kg/m^2, which is infeasible for a spacecraft [16]. NASA's design reference missions assume only about 5–10 g/cm^2 hull equivalent, possibly cutting 20% of GCR dose [12]. This is why supplementary strategies are crucial. On the materials front, recent innovations like ultra-high-molecular-weight polyethylene fibers, which have superior structural strength, and multilayer shields (layers of different materials tuned to different radiation components) are being tested. One concept is embedding hydrogen-rich fibers in epoxy resin and adding an outer layer doped with boron or lithium to capture neutrons, effectively a graded-Z shield. There is also exploration of regolith-based shielding for surface habitats, using Mars or Moon soil (rich in silicates, which contain light elements like oxygen and some hydrogen from hydration) as bulk shielding. While regolith is not as hydrogen-rich as PE, it is abundant in situ and could be piled in thick layers (≥100 g/cm²) to achieve substantial GCR reduction. Some recent Monte Carlo results (Gupta et al, 2020) suggest that ~3 m of lunar regolith could reduce GCR dose by ~60%–70%. However, secondary neutron production in regolith (due to its mix of O, Si, Fe) remains a concern [16].

To summarize passive shielding developments, hydrogenous materials are firmly established as the most effective per mass, with polyethylene being the standard benchmark and new composites (e.g., BNNT-enhanced polymers) offering modest improvements. High-Z materials like aluminum are recognized as a weak link due to secondary radiation, and thus, designs now aim to place hydrogen-rich layers in front of or around heavy structures to soak up secondaries. The literature in the past 15 years strongly converges on these principles. Even as new materials are invented, the underlying physics of cosmic ray interactions guides their usage.

A critical insight is that passive shielding alone, no matter how optimized the material, hits a point of diminishing returns long before the dose is within safe limits for multi-year missions [12]. For example, one study found that an 85% dose reduction (the level needed to meet NASA's ~600 mSv career limit for a Mars mission) was only achievable with an implausibly thick shield (~50 g/cm² of hydrogenous material), which would add hundreds of tons to a spacecraft [12]. There is unanimous agreement that passive shielding must be complemented by other methods, either by active fields to take part of the load or by biological countermeasures to tolerate the remaining exposure. This has led to an integrated paradigm of "as low as reasonably achievable" (ALARA) shielding. This provides as much passive mass as practical (especially for SPE protection, e.g., a storm shelter of ~20–30 g/cm² polyethylene can nearly fully shield typical solar flares), uses active systems if available to extend the protection without adding mass, and accepts that some radiation will penetrate, which must be handled by biomedical means. The following section discusses those biological and operational countermeasures, which are increasingly considered an indispensable third layer in the radiation protection stack [17].

2.2. Bioengineered and Operational Countermeasures

Even with aggressive material and active shielding, deep-space crews will inevitably be exposed to a fraction of the ionizing radiation environment. For a Mars mission, projections show on the order of ~0.5–1 Sv or more could still reach astronauts over ~2–3 years, even after reasonable shielding is applied. This exceeds current permissible doses and carries a significant long-term health risk (e.g., increased cancer, neurological effects). Bioengineered countermeasures refer to biomedical interventions like drugs, dietary measures, or genetic and cellular enhancements that improve the human body's resistance to radiation or ability to repair damage. Operational countermeasures are mission planning and procedural actions that reduce exposure (for example, timing missions and providing shelters) [18]. These strategies do not block radiation per se (like physical shields do) but mitigate its biological impact or avoid unnecessary exposure. Over the past decade, substantial progress has been made in identifying promising radioprotective compounds and protocols. Many stem from oncology, where protecting patients from radiation therapy side effects is a related challenge, and space life sciences research. The literature emphasizes that such measures are complements and not replacements for shielding, and they are the last line of defense if radiation penetrates physical shields. Below, categories of biological countermeasures are reviewed along with the supporting evidence and key operational practices to manage space radiation exposure [19].

Pharmacological Radioprotectors and Antioxidants: Various drugs and dietary supplements have been studied for their ability to protect cells from radiation or enhance recovery. Classic radioprotective drugs are often sulfhydryl compounds that scavenge free radicals, such as neutralizing reactive oxygen species (ROS). For example, Amifostine (WR-2721) was developed to protect normal tissues in cancer radiotherapy. By increasing antioxidant levels or DNA-stabilizing thiols in cells, such compounds can reduce acute radiation damage [20]. In animal models and cellular studies relevant to space radiation, antioxidants have shown some efficacy in reducing chromosomal damage and improving survival. For instance, a NASA-funded mouse study by Patel et al (2017) put mice on a high-antioxidant diet (rich in N-acetyl cysteine [NAC], vitamins C and E, etc.) and found significantly improved survival and less DNA damage after heavy-ion radiation exposure compared to control mice. This suggests that oxidative stress is a major contributor to radiation injury and that counteracting it via diet or drugs can mitigate long-term effects. Antioxidant cocktails are a prominent area of research. Rather than megadoses of a single vitamin, trials have found limited benefit. They can disrupt the body's defenses. Current thinking favors a balanced combination of multiple antioxidants at safe doses [20].

A 2020 review by Cacao et al (Nature Sci. Rep..) outlined a potential space radioprotective cocktail including vitamins C and E, β-carotene, selenium, glutathione precursors, and anti-inflammatory omega-3 fatty acids. These aim to bolster the body's ability to neutralize reactive oxygen species and repair oxidative damage. These compounds are Generally Recognized as Safe (GRAS) and could be taken as dietary supplements during missions [22].

NASA's nutritionists have already prioritized foods rich in antioxidants (like kale, blueberries, etc.) for astronauts on the ISS and are studying space farming of vitamin-C-rich produce. Beyond dietary agents, other pharmacological countermeasures under investigation include DNA repair enhancers. For example, drugs that upregulate the expression of DNA repair enzymes or activate p53 tumor suppressor pathways efficiently remove damaged cells. Some experimental radioprotectors aim to stimulate the DNA damage response. Genistein, a soy isoflavone, has been shown to increase expression of hematopoietic growth factors and mitigate radiation damage to bone marrow in mice [23]. Immunomodulators, such as IL-6 or G-CSF analogs, are being studied to promote recovery of blood cells after radiation exposure.

These treatments are akin to those for acute radiation syndrome (ARS) and could be applicable in specific spaceflight scenarios. It is worth noting that as of 2025, no drug is officially approved for chronic space radiation protection. Still, several, including epicatechin, a plant flavonoid, and esterified antioxidant compounds like α-lipoic acid, have shown potential in reducing markers of radiation damage in rodents. The European Space Agency and NASA are also evaluating pharmacological "radiomitigators," drugs that can help repair tissue or prevent late effects when given after radiation exposure. An example is biradion, a multifunctional agent reported to enhance DNA repair foci resolution in human cell cultures after high–linear energy transfer (LET) radiation (Suman et al, 2020) [24]. Pharmacological countermeasure research is progressing, with antioxidant therapy being a central theme. The consensus is that antioxidant and radioprotective supplements can reduce cellular oxidative damage from space-like radiation exposures, but they are not a panacea. They must be used continuously (before, during, and after exposure). In combination, and even then, they likely confer partial protection (perhaps on the order of 20%–30% risk reduction in cancer or degenerative outcomes, as some modeling suggests). Any pharmacologic regimen for astronauts must be tested for safety, as high-dose antioxidant use can sometimes have paradoxical effects on cellular signaling. While promising, these measures are seen as supplementary or as a way to "buy down" risk alongside shielding to ensure that whatever radiation does penetrate has less harmful effect on the body [25].

Genetic and Cellular Bioengineering: Some researchers have proposed bioengineering the astronauts themselves to withstand radiation better. This relatively new and controversial area touches on bioethics, but it has gained attention in the last few years. Geneticist Christopher Mason has outlined a "500-year plan" for space genomics. He suggests that eventually we might incorporate protective genes from other organisms or use gene editing to enhance DNA repair and antioxidant systems in humans [26].

The prospect of human genome modification for spaceflight raises complex safety, societal, and ethical considerations. Nevertheless, the theoretical potential for significantly improving intrinsic resistance to ionizing radiation has made this a topic of active discussion in space life sciences. At present, the technology readiness level of such approaches remains extremely low. Still, continued advancements in Clustered Regularly Interspaced Short Palindromic Repeats, (CRISPR) gene editing and cellular engineering could make preliminary studies possible in the coming decades. The potential to fundamentally alter human physiology for space adaptation ensures that this area will remain a topic of both scientific interest and ethical debate for the foreseeable future.

One often cited example is the tardigrade (water bear), a microscopic animal known for extreme radiation and desiccation tolerance. Tardigrades produce a Dsup (damage suppressor) protein that binds to DNA and reduces radiation-induced breakage. In 2016, researchers successfully expressed the Dsup gene in human cells in vitro and found it reduced X-ray damage to those cells by ~40%. This result raises the question: could future astronauts be gene-edited to express Dsup or other radioprotective factors? Similarly, George Church and colleagues identified over 40 human genes that, if tweaked, might confer added radiation resistance, including genes involved in DNA repair, cell cycle checkpoints, and free-radical scavenging [36].

There has also been exploration into using radioresistant hematopoietic stem cell transplants or infusions. This approach would continuously replenish blood cells damaged by radiation during long-duration missions. Another angle is microbiome engineering, since gut bacteria can influence inflammation and oxidative stress in the body. Scientists are investigating probiotics that produce extra antioxidants or vitamins. For example, a gut microbe engineered to secrete Mn^{2+}-peptide complexes (manganese antioxidants that some radiotolerant bacteria use) that the host could absorb to gain radiation protection [27]. These concepts are speculative but represent intriguing lines of inquiry in biotechnology.

While these concepts are highly experimental, they represent a bioengineered approach to the problem. The limitations and concerns here are significant, and our understanding of complex gene interactions is incomplete. Modifying human genetics poses unknown risks, and Mason and others acknowledge that much more research is needed to identify safe gene targets before any such intervention could be attempted. Ethical considerations aside, these approaches are unlikely to be ready for the first Mars missions, but they underline a long-term vision where humanity might adapt its biology for space [28].

In the near term, NASA is examining epigenetic drugs that alter gene expression without changing DNA, which could temporarily boost an astronaut's radiation defenses during a mission. For example, HDAC inhibitors can upregulate DNA repair genes, showing radioprotective effects in mice. These agents could be given as a "radioprotection pill" if proven effective and safe. In summary, bioengineering strategies are at the cutting edge and largely unproven, but they constitute an essential frontier in research. They seek to raise the human tolerance to radiation, which effectively increases the threshold of damage the body can endure before health is impacted [29]. This is crucial because purely physical methods may never reduce exposure to zero on long missions.

Operational Countermeasures: In parallel with material, active, and biomedical strategies, mission planners employ operational tactics to minimize radiation risks. One fundamental practice is timing missions in the less active phase of the solar cycle. For example, launching during the solar minimum period means fewer solar flares and SPEs to worry about, though it does mean higher GCR flux. Agencies must weigh this trade-off, as solar maximum has frequent flares that require shelter protocols but suppresses GCR intensity by ~30%, whereas solar minimum has relentless GCR but rare flares [23].

Some analyses, such as those by Guo et al. (2018), suggest that a short Mars mission might be better to cut down GCR dose during solar maximum, provided robust flare shielding is available. Regardless of timing, space weather forecasting and monitoring are an operational necessity. Real-time radiation monitors (like tissue-equivalent dosimeters onboard) and heliophysics satellites (SOHO, DSCOVR, etc.) can warn about incoming solar particle storms [30]. Procedures are in place on the ISS to alert crew to seek shelter when monitors register a sudden dose uptick. Mission designers include a dedicated “radiation storm shelter for interplanetary travel." This is a small volume, often the sleeping quarters or a closet, surrounded by extra shielding where the crew can hunker down during a solar event. NASA's design reference architecture for deep space transit (DSH) calls for at least one shelter with >20 g/cm² of shielding, using stored food, water, plastics, or other consumables as shielding material.

Research by NASA's RadWorks team has even prototyped wearable storm shelter concepts, such as water-filled vests or sleeping bag shelters, to further augment protection if a flare hits unexpectedly [40]. These innovations build redundancy into operational preparedness. EVA (spacewalk) management is another operational factor in minimizing radiation risk. Astronauts are most exposed when outside the vehicle with only a suit, so limiting the duration of EVAs and scheduling them during quiet solar conditions can reduce exposure. Suppose a high-radiation period is predicted, such as when passing through a region of high cosmic ray anisotropy or near a solar sector boundary. In that case, crews can be directed to remain in the habitat. Space agencies also enforce career radiation limits and rotate crew assignments accordingly. For example, NASA currently caps astronaut career dose to ~600 mSv (3% REID cancer risk), and ESA/JAXA have similar limits [31].

Astronauts approaching their career limit may be restricted from future long missions, ensuring no individual accumulates excessive exposure. Finally, there is an operational aspect of rapid return or abort. Mission plans include contingencies to shorten the mission if radiation levels become unexpectedly high. For instance, if a solar superstorm akin to the 1859 Carrington event occurred, an abort-to-Earth trajectory might be considered if feasible. All these procedures, shelters, forecasting, EVA planning, and dose tracking significantly mitigate the risk of acute exposures and help manage chronic dose. They do not reduce the GCR background except via mission duration limits, but they ensure astronauts avoid the worst-case bursts and keep exposures "as low as reasonably achievable" [32].

For example, it was a combination of operational prudence and luck that allowed Apollo astronauts to avoid the August 1972 solar proton storm by mere months. Future crews will not rely on luck but on constant monitoring and the availability of shelters. This operational readiness mindset will be a cornerstone of all long-duration deep space missions.

Synthesis of Multilayered Approach: The overarching finding of recent research is that a multilayered shielding strategy is mandatory for deep space missions. No single technique can solve the radiation problem in isolation. Passive material alone would be too heavy, active fields alone are insufficient for the hardest GCR, and biological measures alone cannot prevent all radiation damage. However, when combined carefully, these methods can cover each other's gaps. Passive shielding is excellent against all particle types, including neutral particles that magnets cannot deflect, but struggle with high-energy ions. Active magnetic fields reduce the lighter and medium-energy charged particles, which eases the burden on passive mass. Whatever radiation still penetrates can be partly mitigated by pharmaceuticals and careful crew protocols [33].

The literature shows general agreement on specific points of integration. For instance, hydrogen-rich materials should coat the interior of habitats and line any magnet coils. This arrangement captures the secondary neutrons a magnetic shield will generate when deflected ions hit structural walls. Another example is that even a relatively weak electrostatic or magnetic field, feasible within modest power limits, could be used to “pre-filter” incoming radiation, slowing it so that a thinner layer of material can stop it [34]. Studies by Spillantini et al and others have proposed hybrid shields where a superconducting magnet producing, for example, 0.5 T, is combined with 10 g/cm^2 of polyethylene. Together, they achieved significantly greater dose reduction than either, demonstrating synergy.

In 2021, Kerr et al reported a simulation where a 5 g/cm² BNNT shield plus a 1 T magnetic field yielded ~35% lower GCR dose than a 10 g/cm² shield alone, illustrating the super-additivity of the combination. The defense-in-depth philosophy is repeatedly emphasized across the literature. If one layer fails or underperforms, the others still provide protection. For example, if an active shield must be turned off for maintenance, the passive shield continues to afford baseline safety. Conversely, an active field can partially compensate if mass constraints force a lighter passive shield. Biological countermeasures add a safety net that allows astronauts to withstand occasional exposure spikes that breach the physical shield design limits, such as an unexpected solar event or higher GCR flux than predicted [35].

There are points of debate and uncertainty that remain. Some divergence exists on how far active shielding should be pursued versus simply adding "a few more centimeters" of material. Also, the efficacy of pharmacological countermeasures against chronic low-dose-rate GCR exposure, as opposed to acute radiation, is still not fully validated. Much of our knowledge comes from acute burst experiments on Earth, and space radiation has unique high-LET effects that may not be fully mitigable by antioxidants alone. More research is needed on the long-term side effects of any drugs given for months in space [36].

Further, genetic approaches raise open questions about safety and public acceptance. Open research gaps identified in recent reviews include developing lightweight, multifunctional materials, such as structural composites that are also excellent radiation shields. Improving cryocooler technology and magnet designs for active shields is necessary to raise their TRL. Extensive animal studies on combinatorial countermeasures are also needed; for example, testing an antioxidant regimen in rodents exposed to simulated GCR over many months to see if cancer rates decrease. Finally, refining risk prediction models is essential to quantify better how each layer reduces actual health risk, not just physical dose [37]. A notable unresolved challenge is how to simulate the integrated effects of chronic radiation on human physiology. The NASA Twin Study (2019) provided insight into this, but larger cohorts and analog environments are needed to test countermeasure efficacy [38].

In conclusion, the literature of the last decade strongly supports a holistic approach to space radiation shielding. Active, passive, and bio/operational methods each have foundational justification and recent advancements, and the state-of-the-art recommendation is to employ all of them in concert. One report encapsulated that "the optimal design is a multilayer shield" combining high-Z and hydrogen-rich materials with magnetic fields and biomedical protocols. This synthesis of strategies offers the best prospect for keeping astronaut doses within permissible limits on deep-space missions.

While significant engineering and biomedical challenges remain unsolved, the progress in materials science, magnet technology, and radiobiology in the past 10–15 years provides cautious optimism. Areas of agreement in the community include the primacy of hydrogen-rich materials, the potential of superconducting magnets if technical hurdles are overcome, and the value of antioxidants and mission planning as supplementary safeguards. Areas of divergence often revolve around the feasibility of active shielding. Some experts remain skeptical and prioritize passive solutions, but others pursue ambitious active concepts, such as plasma shields, and debate the timeline for implementing bioengineering solutions.

The consensus is that deep space radiation risk can be managed through an integrated defense-in-depth approach, even if it cannot be eliminated. As missions to Mars and beyond move from concept to reality, this research will inform spacecraft design and crew health protocols to ensure that astronauts are protected by every means available. This means an outer shield of matter and force, and an inner shield of medical resilience.

CHAPTER 1: SPACE RADIATION ENVIRONMENT AND HAZARDS

Accurately quantifying radiation exposure during an interplanetary transit phase is essential for mission architecture design and crew health risk assessment. The cruise phase has been characterized empirically using radiation detectors aboard precursor robotic missions, which provides valuable analog data for human exposure forecasting. This section comprehensively synthesizes empirical measurements and modeled predictions for total radiation exposure during a complete Mars mission. These results are evaluated against established astronaut career dose limits [1].

A typical Mars mission is assumed to consist of approximately 200–253 days of interplanetary transit in each direction and around 560 days on the Martian surface. Radiation exposure during these phases arises primarily from Galactic Cosmic Rays (GCRs), which provide a continuous background radiation, and intermittent Solar Particle Events (SPEs), which present acute short-term hazards. Solar minimum is used as the baseline solar condition due to its association with maximum GCR flux, representing a worst-case exposure scenario for long-duration missions. Using this baseline ensures that shielding and operational countermeasures are designed to address the most challenging radiation conditions a crew is likely to face [2].

Radiation dose rates recorded during the cruise phase varied depending on the detector type and methodology. Silicon-based detectors reported an average absorbed dose rate of approximately 332 ± 23 μGy/day, while plastic scintillators measured 461 ± 92 μGy/day. These translate to dose equivalents of 0.332 mSv/day and 0.461 mSv/day, respectively. These values represent continuous exposure from GCRs under moderate shielding conditions and are directly relevant when designing habitat shielding for long-duration interplanetary missions [3].

Alternate methods of interpreting the same cruise data, using quality factors and GCR-dominant models, yield a higher average dose equivalent estimate of 1.84 ± 0.33 mSv/day. This model places greater weight on high-energy, high-charge particles and includes corrections for biological effectiveness through linear energy transfer (LET) spectra. Based on this estimate, the total mission-integrated dose equivalent over the 253-day cruise is approximately 466 ± 84 mSv, with SPEs contributing about 5.4% of this value. Such results highlight how model assumptions and particle weighting significantly affect dose projections for deep space missions [3].

The variation between reported values, which range from ~0.3 to 1.8 mSv/day, can be attributed to differences in detector calibration, shielding configuration, and analytical modeling approaches, such as the use of silicon vs tissue-equivalent plastic, as well as the treatment of radiation quality factors [4]. While this variation influences the central tendency (mean) of dose rate estimates, it is essential to distinguish between the factors that affect the mean and those that influence the variance of radiation exposure measurements. Differences in shielding configuration, detector material, and analytical weighting contribute to the variation in mean dose rates across reported studies. In contrast, the variance is more significantly shaped by intermittent Solar Particle Events (SPEs), which can temporarily drive exposure rates well above the GCR baseline [4].

The resulting distribution exhibits a lower variance and a more consistent profile when dose data are drawn exclusively from GCR-dominant intervals, such as during quiet heliospheric conditions or filtered mission data segments. This has practical implications for mission planning and design of protective systems. A minimum expected dose envelope can be constructed from GCR-only conditions, which offers a more stable baseline for shielding estimates. Concurrently, variance models that include SPE contributions provide a broader envelope for risk-informed design margins, ensuring that both average and worst-case conditions are factored into mission planning.

Rather than choosing one measurement as inherently "more reliable," mission planners benefit most from understanding the range of possible exposures corresponding to varying solar modulation conditions. This reinforces the need to design spacecraft with robust shielding, operational radiation storm shelters, and predictive SPE forecasting tools. Combining these design elements with empirical data ensures that safety margins are preserved under typical and extreme radiation conditions. Such a strategy supports mission resilience and enhances crew health protection in the deep space environment.

1.1 Modeled Radiation Dose Accumulation by Mission Phase

Data were synthesized from empirical measurements and radiation transport simulations using FLUKA coupled with the BIANCA biophysical model to assess long-term exposure risks for crewed Mars exploration. These simulations were validated against historical GCR and SPE data and incorporate radiation quality factors and tissue-equivalent dosimetry. A typical Mars mission consists of ~200–253 days of interplanetary transit each way and ~560 days on the Martian surface. Radiation exposure during these phases emerges primarily from Galactic Cosmic Rays (GCRs) and intermittent Solar Particle Events (SPEs), with cumulative dose equivalents summarized in Table 1.1 assuming 10 g/cm² of aluminum shielding during solar minimum [4].

Table 1. 1 Estimated Radiation Dose per Mission Phase (Values shown in cSv; 1 cSv = 10 mSv)

Phase	Duration (days)	Daily Dose (mSv/day)	Total Dose (cSv)	Notes
Cruise to Mars	253	5.0	126.5	95% CI Estimate at Solar Min with 10 g/cm² Al
Mars Surface Stay	560	2.1	117.6	Includes Martian atmospheric shielding
Return Trip	200	5.0	100	Assumed similar to outbound
Total Mission Estimate	1013		344.1	Sum of all phases; exceeds most career limits

This table aggregates radiation dose values for each phase of a Mars mission under conservative assumptions. It reflects Galactic Cosmic Ray (GCR) exposure during solar minimum with 10 g/cm² aluminum shielding and the absence of high-intensity Solar Particle Events (SPEs). The cruise phases show the highest daily dose rates due to the absence of atmospheric shielding, which leaves the spacecraft continuously exposed to deep space radiation. While Martian surface exposure is reduced by natural atmospheric attenuation (~16 g/cm²), the long surface duration results in a high cumulative dose throughout the mission. The mission total of ~3.4 Sv exceeds, by 467%, NASA's current 600 mSv career limit for astronauts, underscoring the need for integrated shielding and operational countermeasures in mission planning [4].

1.1.1 Solar Particle Event (SPE) Risk

SPEs pose an acute risk during cruise phases. Table 1.2 outlines the probability of encountering significant SPEs based on historical analogs (e.g., the 1972 event) and their estimated dose contributions.

Table 1.2 Estimated SPE Risk During Mars Missions
(Refer to "SPE Risks" tab in the Excel file) [5]

Mission Phase	SPE Scenario	Probability (%)	Estimated Dose Contribution (cSv)
Transit (Cruise)	1×1972 SPE	20	~35
Transit (Cruise)	4×1972 SPE	2.4	~35 (with severe compounding)
Surface Stay	1×1972 SPE	28	~35
Surface Stay	4×1972 SPE	3.4	~35 (less severe due to atmospheric shield)

This table presents probabilistic estimates for large Solar Particle Event (SPE) exposure during transit and surface phases. The 1972 event is a benchmark for modeling worst-case solar activity, providing a reference point for assessing extreme but plausible radiation hazards. A single large SPE can deliver a dose of 35 cSv or more in a matter of hours, potentially exceeding short-term dose thresholds and requiring immediate crew protection. While the Martian atmosphere reduces severity, the risk remains considerable over a 560-day surface mission.

These findings underscore the need for dedicated SPE shelters with enhanced shielding (>30 g/cm^2) and an automated warning system for early crew relocation to safe zones [5].

1.1.2 Comparison with Career Dose Limits

Current astronaut career dose limits vary by agency and demographic considerations. Table 1.2.1 compares these thresholds with the modeled Mars mission dose accumulation.

Table 1. 2. 1 Agency Career Dose Limits (Refer to Excel sheet "Career Dose Limits") [6,7]

Agency	Limit (mSv)	Applicable Notes
NASA (2021)	600	Sex & age-independent limit
ESA/RSA	1000	Independent of age/sex
JAXA (Female)	500	Age 27–30 career limit
JAXA (Male)	1000	Age > 45 career limit

This table summarizes the maximum allowable career exposure according to NASA, ESA, RSA, and JAXA guidelines. NASA's updated policy establishes a conservative 600 mSv limit to keep the risk of exposure-induced death (REID) below 3% for the most susceptible demographic, defined as a 30-year-old female. ESA and RSA adopt a broader uniform limit, while JAXA maintains age- and sex-based categories for radiation exposure thresholds. The projected Mars mission dose of ~3.4 Sv surpasses all these thresholds, making it incompatible with current human spaceflight safety standards. This reaffirms the need for aggressive radiation mitigation strategies in any crewed deep-space architecture [6, 7].

The cumulative GCR exposure, compounded by probabilistic SEP contributions, results in a mission-integrated dose that challenges current human spaceflight safety thresholds. As a result, future system designs must include physical shielding and operational protocols to manage exposure during transit and surface operations. Potential pharmacological countermeasures should be incorporated to reduce biological impact when physical protection is insufficient. Such measures are necessary to ensure astronaut survivability and mission success on Mars-class expeditions.

1.1.3 Statistical Radiation Environment Assessment and Implications for Shielding Design

In addition to direct measurements and deterministic models, statistical evaluation of interplanetary radiation exposure provides a critical insight into the natural variability and stochastic nature of the space radiation environment. These analyses capture fluctuations in exposure that are not evident in averaged values alone, thereby supporting a more robust understanding of radiation risk. This subsection integrates inferential statistics and trend analysis to reinforce the urgency of comprehensive shielding strategies for deep-space missions. Such statistical perspectives help identify worst-case scenarios and guide design margins that account for unpredictable radiation events [8].

1.1.4 Statistical Evaluation of Interplanetary Radiation Levels

A statistical analysis was conducted to estimate the underlying structure of radiation dose variability in interplanetary space to supplement deterministic modeling and mission-specific dose measurements. This analysis compiled 60 dose rate observations from multiple sources, including MSL/RAD cruise data, CubeSat simulations, passive shielding trials, and REMSIM Monte Carlo outputs. The goal was to capture the natural spread and clustering behavior of daily absorbed dose rates in microgray per day (μGy/day). This approach quantifies both central tendencies and extremes, providing a data-driven basis for probabilistic risk assessment and shielding optimization [8, 9].

Table 1. 2. 2 Descriptive Statistics for Radiation Dose Dataset

Statistic	**Value (µGy/day)**
Mean	236.08
Standard Deviation	172.7
Minimum	20
25th Percentile	85
Median	222.5
75th Percentile	341.25
Maximum	520

Gaussian Mixture Model (GMM) Clustering Analysis

A Gaussian Mixture Model (GMM) was applied to resolve this dataset's structure further. The GMM uses probabilistic modeling to assign each data point to one of several Gaussian-distributed clusters based on maximum likelihood estimation. This approach is especially effective in identifying overlapping subpopulations within a continuous dataset and provides a more nuanced view of variability than a single mean or standard deviation. Applying this technique allows for discrimination between low, moderate, and high radiation exposure regimes that may otherwise appear blended in raw data [8, 9].

The model identified three distinct clusters, each representing different radiation exposure regimes.

- Cluster 1 (low dose) was <200 µGy/day.
- Cluster 2 (moderate dose) was defined as 300–350 µGy/day
- Cluster 3 (high dose) included values >350 µGy/day.

The presence of these well-defined clusters supports the conclusion that interplanetary radiation exposure is not homogenous but distributed across multiple statistically distinct regimes.

The dominant cluster was Cluster 3, which encompasses the highest dose values. Its frequency in the data indicates that high-dose conditions are not rare outliers but instead statistically significant features of the interplanetary radiation environment. These conditions will likely occur under solar minimum or reduced-shielding configurations, which can be anticipated during certain mission phases. The dataset's persistence of Cluster 3 conditions has essential implications for mission planning and shielding design.

Interpretation: The GMM model confirms that a substantial proportion of interplanetary radiation measurements fall into biologically consequential doses. The mid- to high-range clusters pose potential risks for long-duration missions without advanced shielding. This reinforces the necessity of incorporating robust passive and active shielding systems in mission architectures. Additionally, operational countermeasures, such as real-time dose monitoring and adaptive shelter protocols, are essential to reduce astronaut exposure during high-dose intervals.

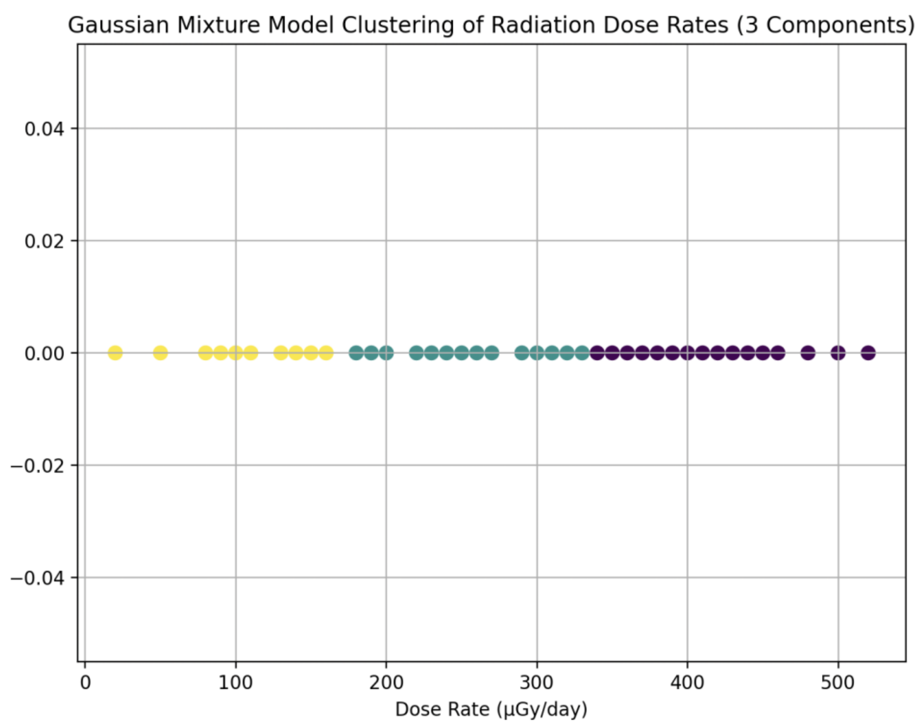

Figure 1.0: Gaussian Mixture Model Clustering of Interplanetary Radiation Dose Rates

The GMM clustering plot above visualizes the 60 observed radiation dose rates along the x-axis (in μGy/day) and is color-coded by their assigned cluster. Cluster 3 (dark purple) dominates the high-dose regime above 350 μGy/day. Cluster 2 (teal, intermediate darkness) aligns with the moderate range between 300–350 μGy/day. Cluster 1 (yellow, lightest colored dots) reflects lower exposure values below 200 μGy/day. This arrangement provides a clear color-coded separation between exposure regimes for quick visual interpretation.

This clustering plot is a one-dimensional visualization of the Gaussian Mixture Model results, where each point represents a single radiation dose rate observation along the x-axis (μGy/day). The y-axis values are not meaningful in this context and are set to zero to facilitate a horizontal layout. The purpose is to clearly illustrate the cluster assignments via color and not to convey a second variable. This is a standard technique in 1D GMM plots when categorical or probabilistic classification along a single dimension is emphasized.

Beyond identifying central clustering behavior, the statistical evaluation provides insight into the distributional characteristics of radiation dose rates, especially the interplay between the mean and variance. While differences in instrumentation and modeling approaches shift the average dose rate, the spread or variance in the data is predominantly driven by transient SPEs. These acute events introduce sharp and time-localized exposure increases, which inflate variability even if the overall mean remains stable. The relationship between mean and variance is critical in interpreting long-term radiation exposure data [9].

Dose data collected under GCR-only conditions (excluding solar transients) yield a distribution with lower variance, which reflects the steadier nature of galactic cosmic radiation. This distinction is essential for dose prediction modeling and shielding design. Estimates based solely on GCRs allow for constructing conservative baseline dose profiles. Conversely, inclusive models that account for solar variability enable planning for worst-case operational contingencies. Both perspectives are critical for informing the layered radiation protection strategies proposed in later sections [9].

This analysis supports the conclusion that deep-space radiation exposure is not uniformly distributed but is instead stratified into significant subgroups. The frequent occurrence of high-dose clusters highlights the necessity of shielding designs that are robust not only against average conditions but also against elevated probabilistic regimes. Such robustness ensures that crew safety is maintained across nominal and extreme radiation environments. These findings reinforce the argument for integrated and adaptable radiation protection measures in deep-space mission planning.

1.1.5 Scenario Modeling of Cruise Phase Exposure

This section models a representative exposure scenario to determine the biological significance of typical radiation levels encountered during a Mars mission cruise phase. That is, a daily radiation dose of 300–350 μGy/day sustained over a 180-day interplanetary transit period. This estimate reflects a mid-range value from the statistically derived Cluster 2 identified in Section 1.1.4.

Total Absorbed Dose (Gray)

Grays (Gy) quantify the total radiation energy absorbed by human tissue. This measure is irrespective of biological effect and reflects the physical energy deposited in tissue [4]. The total absorbed dose over 180 days can be calculated as follows:

- 300 μGy/day × 180 days = 54 mGy
- 350 μGy/day × 180 days = 63 mGy

Thus, the total absorbed dose ranges from 54–63 milligray (mGy) during a six-month Mars transit [1]. This calculation provides the baseline physical dose before applying radiation weighting factors to account for biological impact.

Biological Impact (Sievert)

Sieverts (Sv) represent radiation's biological effect, accounting for the type of radiation and its interaction with biological tissue via a weighting factor (W). In deep space, the radiation environment comprises high-energy protons and heavy ions, which carry far greater biological risk than gamma rays due to dense ionization and complex DNA damage [4]. These particles have high linear energy transfer (LET) characteristics, resulting in more severe biological damage per unit of absorbed dose. The conversion from gray to sievert allows for more accurate estimation of health risks, particularly for long-duration missions beyond Earth's magnetosphere. Using a simplified two-scenario estimation:

W = 1 (e.g., gamma rays): Biological dose = 54–63 mSv

W = 10 (e.g., protons and heavy ions): Biological dose = 540–630 mSv

This biological dose range approaches or exceeds NASA's 600 mSv career exposure limit for astronauts under realistic radiation weighting, even without including solar events or return trip exposure [10]. The calculation demonstrates how particle type dramatically changes the effective dose in sieverts compared with the same absorbed dose in grays. This effect highlights the need for correct weighting when performing mission radiation risk assessments. It also reinforces that even modest absorbed doses can pose serious biological risks when high-LET particles dominate the spectrum.

Interpretation: Since the absorbed dose in mGy appears modest, the biological effect is amplified by the nature of the radiation field in interplanetary space. The predominance of high-energy protons and heavy ions increases biological impact due to dense ionization tracks and complex DNA damage. This emphasizes the importance of evaluating physical and biological metrics when assessing mission risk. Neglecting to account for radiation quality could result in underestimating astronaut health hazards on long-duration missions.

Weighting Factors for Space Radiation Components

Radiation weighting factors (W_r) vary by particle type and energy:

Protons (from GCR or SPE):

Typical W_r = 2–5, higher for low-energy particles

Heavy Ions (e.g., Fe nuclei in GCR):

W_r = 10–20, due to high linear energy transfer (LET) effects

Gamma/X-rays:

W_r = 1 (baseline reference radiation)

Because the space environment includes a mixed field of these components, the effective dose in sieverts can vary widely. As a result, it is often conservatively modeled using W = 10 for worst-case heavy ion effects [10]. This conservative approach ensures shielding and mission planning account for the most biologically harmful components of the space radiation environment. While it may overestimate the dose for some mission phases, it provides a prudent safety margin for astronaut health.

Sources of Radiation in Interplanetary Space

Galactic Cosmic Rays (GCRs)

These are high-energy charged particles originating outside the solar system. They continuously bombard spacecraft and pose a chronic, low-rate but high-integrity exposure to astronauts during transit. This effect is especially problematic during solar minimum when heliospheric shielding is weakest and the intensity of GCRs is at its peak. The persistence of this radiation source underscores the importance of baseline shielding that can protect crew members throughout the mission [11].

Solar Particle Events (SPEs)

SPEs are sporadic bursts of high-energy protons emitted by solar flares or coronal mass ejections. While less frequent than GCR exposure, they can deliver acute doses within hours, creating immediate health risks for unprotected astronauts. GCRs produce proton fluences capable of driving short-term exposures to hazardous levels if unshielded [11]. The potential for rapid onset and high dose delivery means operational countermeasures and storm shelters must be in place for all mission phases.

Both chronic (GCR) and acute (SPE) radiation sources must be factored into system-level shielding requirements. The scenario modeled here highlights that even "average" GCR exposure over a single mission leg may bring astronauts to biological dose thresholds. This reinforces the urgency for multilayered radiation protection strategies that integrate passive, active, and operational approaches [12].

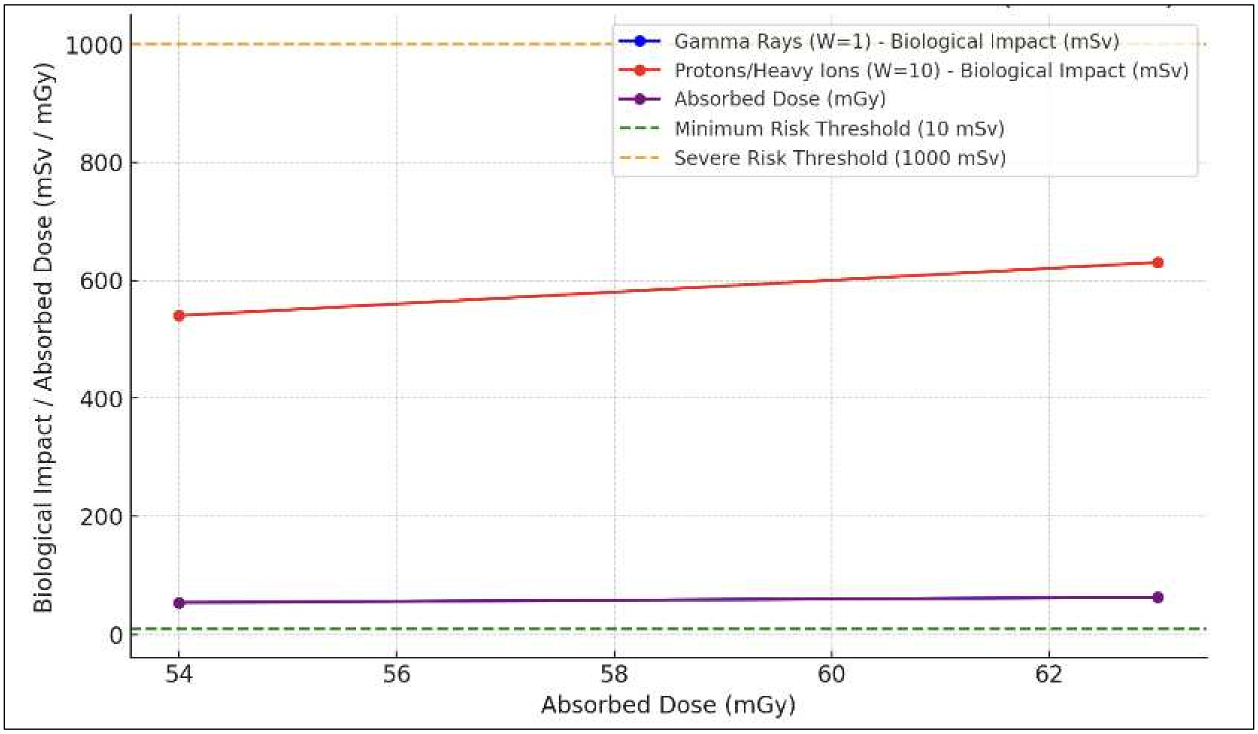

Figure 1.2: Total Radiation Dose Assessment – Absorbed vs. Biological Impact

This plot illustrates the relationship between absorbed dose (mGy) and biological impact (mSv) using weighting factors for gamma rays (W=1) and heavy ions (W=10). Absorbed dose alone (purple) appears low, but when translated into biological impact, the red line (W=10) approaches the 1000 mSv severe risk threshold. The yellow dashed line marks that severe threshold, while the green line marks the minimum actionable threshold (10 mSv).

1.1.6 LD-50 Contextual Analysis of Acute Dose Risk

To further contextualize the radiation exposure faced during interplanetary transit, it is instructive to compare modeled mission doses against known acute radiation syndrome (ARS) thresholds. The term LD50 refers to the "lethal dose" at which 50% of an exposed population is expected to die without medical intervention [13]. This comparison allows the modeled data to be framed against established biological risk thresholds. It provides a direct way to interpret spaceflight radiation risk in terms of well-documented clinical outcomes.

1. **LD-50 (Humans, No Treatment):** ~3–5 Sv (3,000–5,000 mSv)
2. **Near-Fatal Doses (6–7 Sv):** Often lethal even with medical care

In this analysis, a mid-range radiation dose scenario (300–350 μGy/day over 180 days) results in a total absorbed dose of 54–63 mGy. When converted using an appropriate radiation weighting factor:

For gamma radiation (W = 1): 54–63 mSv

For heavy ions/protons (W = 10): 540–630 mSv

While this range remains below the LD50 threshold, it is biologically significant, especially considering that it represents only the cruise phase and not the cumulative mission dose. Further, it does not include any large Solar Particle Events (SPEs) and poses potential chronic and long-latency health risks (e.g., cancer) [13]. The magnitude of these values highlights the need for careful consideration in mission design and shielding strategies.

Interpretation: The 540–630 mSv range approaches thresholds associated with early deterministic effects like temporary lymphocyte suppression or prodromal ARS symptoms, especially in radiation-sensitive individuals. While they are not acutely lethal, doses warrant aggressive shielding mitigation. These levels indicate that physiological effects may still occur even in non-lethal scenarios. The data reinforces the importance of keeping exposures well below early effect thresholds.

Conclusion: The LD-50 framework underscores the biological seriousness of interplanetary radiation and provides a parallel lens alongside agency career limits. It supports the need for mission architectures that prevent cumulative or acute dose spikes approaching Sv-level exposures [13].

1.1.7 Temporal Dose Rate Trends Across Mission Architectures

Radiation dose data from four different mission scenarios were analyzed using a 3-day moving average smoothing technique better to understand the dynamics of space radiation environments over time. This method reveals underlying trends by filtering out short-term fluctuations caused by measurement variability, transient solar activity, or spacecraft-specific noise [14].

Purpose of Smoothing via Moving Averages

A 3-day moving average was applied to each dataset to achieve the following objectives:

1. **Noise Reduction**: The original dose rate data (plotted in blue) show frequent, short-term spikes and dips. These are often attributable to instrument noise, temporary spacecraft orientation changes, or localized variations in the space environment. The smoothed data (red line) suppresses these noise fluctuations, which makes the overall trends more interpretable. This allows for improved clarity in assessing long-term radiation behavior.
2. **Trend Detection**: Smoothing helps reveal the directional behavior of dose rates over time, which is critical for identifying early escalation patterns or periods of relative stability. These trends provide context for long-term shielding requirements. Recognizing whether radiation levels are rising, falling, or stable can inform risk assessments. The ability to detect these patterns supports proactive decision-making during missions.
3. **Filtering Short-Term Events**: Transient solar flares or shock-induced events can skew perception of radiation trends. By filtering out these short-lived events, the smoothed curve allows for better focus on persistent environmental effects and mission-phase radiation conditions [14]. This approach avoids overestimating the baseline dose due to

temporary anomalies. It also facilitates the differentiation between normal variability and genuine shifts in the radiation environment.

4. **Actionable Decision Support**: Identifying stable versus increasing trends enables mission planners to forecast cumulative dose and adapt shielding or operational parameters accordingly. The smoothed data offers a more reliable basis for predicting future exposure levels. This provides a foundation for contingency planning in response to projected radiation changes. As a result, this method enhances strategic and tactical radiation risk management.

Observed Trends by Mission Scenario

The smoothed and original dose rate data are plotted below for four mission cases.

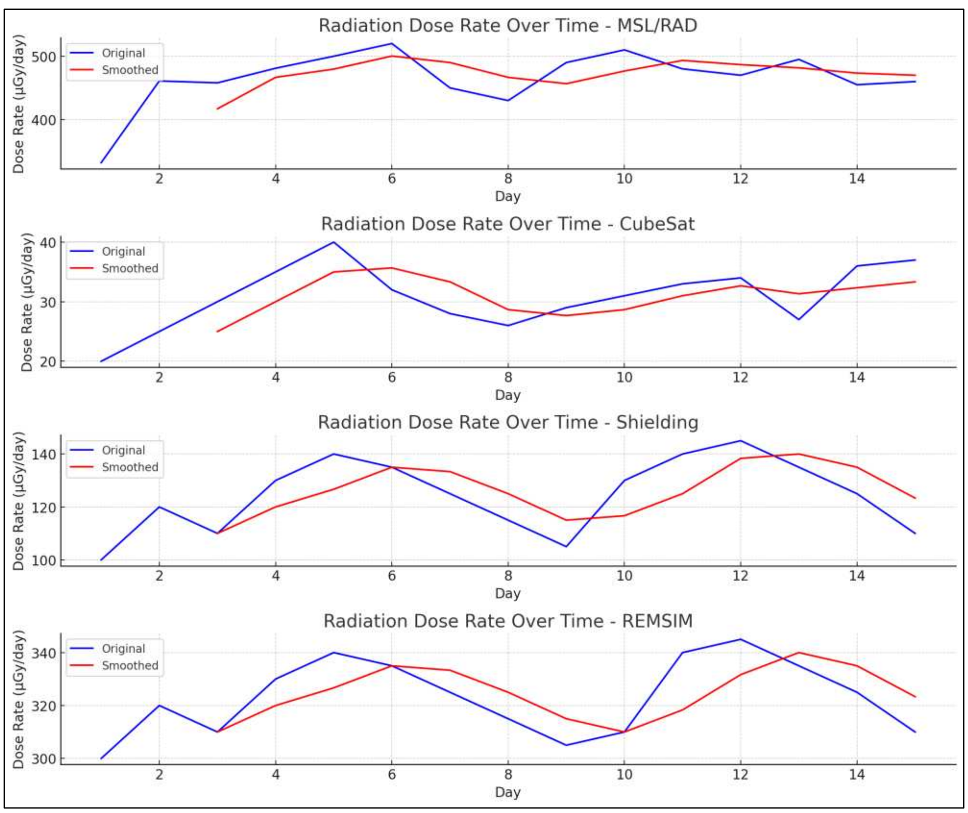

Figure 1.3: Radiation Dose Rate Over Time
(Original vs. 3-Day Moving Average) [15, 16]

In the MSL/RAD mission case (top panel), the original radiation dose data fluctuated between 400 and 550 μGy/day. When processed with the 3-day moving average, the resulting smoothed trend revealed a stable radiation environment. This shows no significant increase or decrease over time, indicating a steady exposure profile during this observation period. This stability indicates a nominal Galactic Cosmic Ray (GCR) background during the cruise phase and suggests that standard passive shielding would be sufficient under such conditions, provided no major Solar Particle Events (SPEs) occur during the transit [15].

The original dose rates for the CubeSat mission scenario (second panel) ranged from about 20 to 40 μGy/day. However, the smoothed trend revealed a subtle but persistent upward trajectory in radiation exposure over the evaluated period. This gradual increase may reflect cumulative GCR flux as the spacecraft moves farther from Earth's magnetosphere or into regions of reduced heliospheric shielding. The trend implies a growing exposure burden that could influence long-term system health or cumulative crew dose [16].

In the Shielding scenario (third panel), the raw radiation data fell within a range of approximately 100 to 140 μGy/day. The smoothed curve also showed a mild upward trend over the observed period. This indicates that the radiation levels were subject to increasing external influences even with shielding applied. This suggests that while shielding effectively reduces baseline dose, it does not entirely mitigate the cumulative effect of long-term space weather variability or directional radiation exposure across changing spacecraft attitudes [15].

Lastly, the REMSIM mission data (bottom panel) exhibited initial dose rates between 300 and 350 μGy/day. The moving average analysis revealed a decreasing trend during the first several days of the mission, followed by a leveling off and stabilization. This pattern implies that the spacecraft may have initially passed through a region of elevated radiation exposure. This is possibly associated with residual trapped particles or a transient solar feature before settling into a more stable GCR-dominated background typical of the interplanetary environment [16].

Temporal Trend Insights

The moving average analysis confirms that radiation exposure during space missions is not static and can exhibit early-phase spikes, slow upward drifts, or plateaus depending on mission type, shielding design, and spatial position. Smoothing the data helps to reveal actionable patterns that short-term fluctuations may otherwise obscure. It supports real-time radiation forecasting, optimizes shielding distribution by mission phase, and refines operational thresholds for crew exposure limits. These insights contribute directly to risk modeling and shielding design logic, especially for Mars-class exploration profiles where every additional μGy/day contributes substantially to cumulative mission risk [2].

1.1.8 Correlation of Radiation Levels with Solar and Spatial Parameters

A correlation analysis was conducted on observational data to identify which environmental factors most significantly influence radiation dose variability in interplanetary space. The study employed Shapiro-Wilk tests to assess the normality of each variable and Spearman's rank correlation coefficients (ρ) for non-parametric correlation. This method is appropriate for the skewed or non-Gaussian distributions typical of solar and space physics datasets [16]. Three independent variables were tested: heliocentric distance, solar cycle phase, and discrete solar events (e.g., flares and CMEs). Results are shown below.

Table 1. 2. 3: Shapiro-Wilk test and Spearman's rank correlation coefficients

Variable	Spearman's ρ	p-value	Interpretation
Distance from Sun	–0.315	0.0143	Moderate negative correlation; radiation decreases with greater heliocentric distance

Solar Cycle Phase	–0.424	0.0007	Strong negative correlation; radiation decreases during solar maximum
Solar Events (Flares, CMEs)	–0.029	0.8266	No significant correlation; suggests limited predictive value of discrete solar events

1. **Distance from Sun**

Spearman's $\rho = -0.315$, $p = 0.0143$

Interpretation: A moderate negative correlation was observed between radiation dose and heliocentric distance. This indicates that dose rates decrease as a spacecraft moves farther from the Sun. This is consistent with the reduced flux of solar-originating particles and the dispersal of lower-energy ions over increasing distances. However, because GCRs are nearly isotropic, this result primarily reflects the attenuation of lower-energy solar particles rather than the GCR background [17].

2. **Solar Cycle Phase**

Spearman's $\rho = -0.424$, $p = 0.0007$

Interpretation: A strong negative correlation between radiation levels and the solar cycle phase was found. Radiation dose decreases during solar maximum when heightened solar activity strengthens the heliospheric magnetic field and thus provides greater shielding against GCR penetration. Conversely, reduced solar modulation during solar minimum allows GCR flux to intensify, raising background radiation levels. This finding reaffirms the solar cycle phase as a dominant macroenvironmental driver of interplanetary radiation risk [18].

3. **Solar Events (Flares/CMEs)**

Spearman's $\rho = -0.029$, $p = 0.8266$

Interpretation: No statistically significant correlation between short-term solar events and the mean dose rate data was found. This suggests that discrete solar flares and CMEs do not exert a lasting or predictable influence on the cumulative radiation exposure measured over mission timescales. It also reinforces the challenge of relying solely on event-based forecasting to guide operational shielding responses. These findings support prioritizing design strategies that focus on longer-term environmental predictors over short-lived solar phenomena [18].

Strategic Implications for Shielding Design

These results demonstrate that radiation dose variability is more strongly governed by long-term, predictable environmental parameters like solar modulation and orbital position than short-term and randomly determined events like solar flares. Consequently, shielding strategies should be designed with an emphasis on macroenvironmental trends. This is particularly true for missions scheduled during solar minimum when radiation levels peak. This finding justifies a shift from reactive and event-triggered protection systems toward more robust and persistent shielding architectures that anticipate environmental conditions defined by the solar cycle and mission geometry [19].

1.1.9 Implications for Shielding System Design

These statistical findings reinforce and extend the dose modeling results presented earlier. They confirm moderate-to-high dose rates are frequent in deep space and are not exceptional outliers. They show that long-duration exposure alone, not just solar events, can drive missions past biological dose limits. They also emphasize that variability in space radiation is shaped more by solar cycle phase and distance than by solar flares or coronal mass ejections [2]. Together, this supports a systems-level approach to shielding that combines:

- Predictive magnetic shielding (AMF) to address GCR deflection over time

- Passive structural shielding to handle both continuous and acute exposures
- Time-based shielding logic to dynamically adjust exposure-reducing strategies

These findings validate the modeling assumptions and architecture directions proposed in subsequent sections of this dissertation and establish a statistically robust basis for radiation system requirements. They form a clear evidence-based rationale for integrating predictive, passive, and adaptive shielding methods in mission planning and design.

1.2 Scenario-Based Shielding Configuration Framework

Radiation protection strategies must be adaptable to a range of mission profiles. This must be done with distinct constraints regarding mission duration, the exposure environment, shielding mass budgets, and available power. A single shielding solution is unlikely to optimize risk, performance, and system-level trade-offs across the varied needs of crewed exploration and mobile deep-space missions. These variations in mission parameters require flexible and scalable approaches that can be adjusted to fit operational demands without compromising safety.

To address this, a scenario-based shielding configuration framework is proposed. Each configuration aligns with a specific mission class, providing a practical reference for system architects, program managers, and shielding designers seeking to tailor architectures to performance constraints. This framework offers a structured method for evaluating and selecting shielding designs that best meet mission-specific priorities. The following table outlines these configurations for reference in the design process.

Table 1. 2. 4: Shielding Configuration Summary by Mission Scenario

Scenario	**Primary Goal**	**Shielding Configuration**	**Ideal Use Case**
Low-Power, Short-Duration Mission	Minimize power, light shielding	BNNT + Aluminum MLI + Moderate AMF	Short orbital/cislunar sorties

Long-Duration Deep Space Habitat	Maximum long-term protection	High-Intensity AMF + Polyethylene + Storm Shelter	Mars/Lunar base habitats
Highly Mobile, Variable Profile Vehicle	Adaptive, dynamic shielding	Rotating Toroidal-Induced AMF + Dynamic Field Control + Thin BNNT outer layer	Interplanetary mobility, unstructured missions

Note: Shielding configurations are selected based on mission-specific operational profiles, balancing the power, mass, and radiation protection effectiveness.

Table 1.2.4 consolidates the design intent, architectural composition, and optimal use cases for three distinct radiation protection scenarios. Each row represents a tailored shielding strategy that balances the core priorities of radiation mitigation, system mass, power availability, and mission duration. The table serves as a concise reference for evaluating shielding options concerning specific mission requirements. It is intended to guide decision-making for spacecraft architects and mission planners seeking to align protection strategies with operational profiles.

Scenario 1, representing Low-Power, Short-Duration Missions, prioritizes lightweight and power-conserving solutions suited to short orbital sorties or cislunar transits. The shielding architecture in this case combines passive layers like boron nitride nanotubes (BNNTs) and aluminum multi-layer insulation (MLI) with a low-intensity artificial magnetic field (AMF) operating at reduced power. This hybrid approach leverages the high shielding efficiency-to-mass ratio of BNNTs while minimizing electrical demand and conserving energy for critical systems. Although this configuration provides only moderate shielding efficacy, it aligns well with missions in which the cumulative radiation dose is inherently limited by duration [20].

Scenario 2, designed for Long-Duration Deep Space Habitats, such as a Mars surface base or a lunar outpost, focuses on maximizing long-term radiation protection for crew exposure extending beyond 500 days. The proposed configuration integrates high-intensity AMF shielding (targeting ≥1.0 Tesla field strength) with passive hydrogen-rich materials such as polyethylene composites and water-based radiation absorbers. Additionally, local SPE shelters with >30 g/cm² shielding depth are incorporated to provide acute protection during solar storms. This setup assumes access to persistent power sources like nuclear fission units or in-situ resource utilization (ISRU), which enables solar arrays to sustain active shielding throughout the mission, offering the most comprehensive protection among the scenarios and tailoring for cumulative dose mitigation [10].

Scenario 3 addresses Highly Mobile Spacecraft with Variable Mission Profiles, such as interplanetary transfer vehicles or asteroid exploration missions. These spacecrafts require highly adaptable shielding strategies that respond to fluctuating space environments and mission phases.

The proposed system employs a Rotating Toroidal-Induced Dipole Field modulated dynamically based on environmental radiation measurements and real-time power availability. This active system is augmented by a thin passive shell (e.g., conformal BNNT coatings or carbon-loaded polymers) to mitigate residual GCR and secondary radiation, emphasizing operational flexibility and power efficiency to enable real-time adjustment of shielding performance as mission conditions change [20].

To compare these configurations quantitatively, a residual radiation dose analysis was performed by applying shielding effectiveness estimates to the baseline unshielded mission dose of 2,642 millisieverts (mSv). This baseline includes the outbound cruise (466 mSv), Mars surface exposure (1,176 mSv), and return leg (1,000 mSv). Each shielding scenario was assigned a percentage dose reduction: 50% for Scenario 1, 85% for Scenario 2, and 70% for Scenario 3, based on their shielding configurations' modeled effectiveness. These values provide a direct comparison of the protective performance of each scenario against the same mission dose profile.

The resulting residual doses were computed by applying the complement of each reduction factor to the total baseline exposure. Scenario 1 yields a residual dose of 1,321.0 mSv, while Scenario 2 significantly reduces to 387.9 mSv. Scenario 3 results in 792.6 mSv, placing it between the other two regarding protective capability. These results are summarized in Table 1.2.5 and visually represented in Figure 1.4. Notably, only Scenario 2 reduces mission dose below NASA's 600 mSv career threshold, reinforcing its suitability for long-term habitation. In contrast, the other two scenarios may require mission duration limits or supplementary shielding in high-risk regions.

Table 1.2.5: Estimated Residual Dose by Shielding Scenario

Scenario	Reduction %	Residual Dose (mSv)
Scenario 1 (Low-Power Short-Duration)	50.0	1321.0
Scenario 2 (Long-Duration Habitat)	85.0	387.9
Scenario 3 (Highly Mobile Vehicle)	70.0	792.6

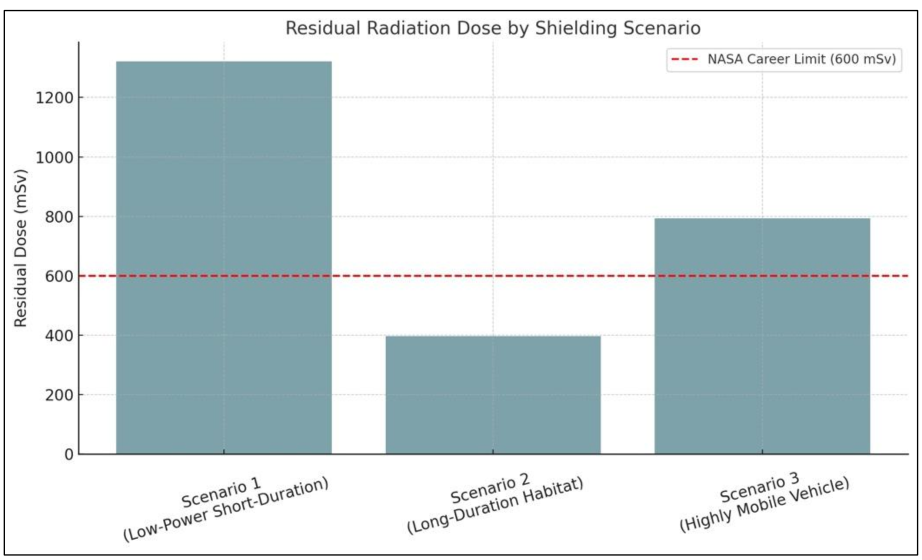

Figure 1.4: Residual Radiation Dose by Shielding Scenario

Figure 1.4 illustrates the modeled residual radiation dose after applying shielding reduction strategies for each of the three mission scenarios outlined in this section. The bar chart presents the cumulative dose (in millisieverts) that crew members would absorb over the full course of a Mars mission. This comprises cruise, surface stay, and return transit after mitigation by scenario-specific shielding systems. The unshielded baseline dose for this mission is 2,642 mSv, as determined in earlier sections.

Each bar represents the remaining biological dose after applying a scenario-specific reduction factor:

- **Scenario 1** (Low-Power, Short-Duration) assumes 50% shielding effectiveness, resulting in a residual dose of 1,321 mSv.
- **Scenario 2** (Long-Duration Habitat), with 85% shielding effectiveness, reduces the exposure to 387.9 mSv, well below NASA's 600 mSv career dose limit, shown as a dashed red line for reference.
- **Scenario 3** (Highly Mobile Vehicle) applies a 70% reduction, which yields a residual dose of 792.6 mSv, exceeding the NASA threshold but falling significantly below the unmitigated total.

The red dashed horizontal line at 600 mSv represents the NASA career limit for astronaut radiation exposure, serving as a benchmark for long-term health risk acceptability. Only Scenario 2 falls beneath this threshold, affirming its suitability for extended missions with significant cumulative radiation exposure. This figure reinforces that shielding architecture must be tailored to the mission class. At the same time, all three scenarios offer meaningful reductions in radiation dose, only a high-intensity and well-supported shielding system (as in Scenario 2) is capable of reliably bringing long-duration crew exposures within medically accepted boundaries.

The visual comparison supports trade-space discussions among mission designers and enables data-driven decisions about shielding configuration, system mass, and power allocation. This type of visual evidence strengthens the case for scenario-specific design approaches. It also ensures that protective measures align with operational priorities while meeting safety thresholds. Integrating quantitative data into visual form aids both technical and policy-level decision-making.

1.3 Conclusion: Integrated Radiation Risk and Shielding Strategy Assessment

This radiation analysis has demonstrated that deep-space missions to Mars pose a significant radiobiological challenge that exceeds current astronaut career exposure limits under conservative shielding assumptions. Using a combination of empirical data from the Mars Science Laboratory (MSL), Monte Carlo modeling via FLUKA/BIANCA, and statistical analysis of radiation variability, we established that the cumulative mission dose for a standard Mars transit and surface mission (~3.4 Sv) surpasses the thresholds defined by NASA, ESA, RSA, and JAXA. The NASA 600 mSv career dose limit, designed to cap exposure-induced death risk at 3%, is exceeded by nearly a factor of six without advanced shielding.

Probabilistic analyses revealed that Galactic Cosmic Rays (GCRs) and Solar Particle Events (SPEs) contribute meaningfully to total dose, with GCRs providing a continuous high-LET background and SPEs posing acute and high-dose threats during cruise and surface phases. The modeling confirmed that daily biological dose equivalents during cruise may reach 1.84 ± 0.33 mSv, with potential acute events delivering 35 cSv or more in hours if not mitigated. These results underscore the need for protective measures that address chronic and acute exposure risks. The combination of these hazards creates a complex radiobiological challenge for mission design.

The statistical evaluation of 60 radiation measurements showed a dominance of high-dose clustering, especially under solar minimum conditions, which reinforced the stochastic nature of the space radiation environment. Applying a Gaussian Mixture Model (GMM) revealed that most real-world measurements fall within biologically consequential ranges (300–500+ μGy/day). This further supports the need for resilient shielding strategies to address the most frequent and impactful radiation regimes. These findings confirm that risk is not distributed evenly but concentrated in specific high-risk exposure bands.

A biologically weighted dose model for a 180-day cruise phase under average conditions yielded an estimated 540–630 mSv effective dose, already approaching NASA limits before factoring in surface stay or return transit. When contextualized against LD50 thresholds (~3–5 Sv), this dose aligned with ranges associated with early deterministic effects such as lymphocyte suppression. This reinforces the need for mission architectures that preemptively manage chronic and acute radiation risks. These insights demonstrate that proactive design is critical to avoiding health-compromising dose accumulation.

Temporal smoothing analyses highlighted key differences in exposure trend behavior across mission types, indicating that radiation accumulation is not constant and can be influenced by spacecraft trajectory, shielding orientation, and heliospheric positioning. Correlation analysis confirmed that solar cycle phase and distance from the Sun significantly impact dose rates, while short-term solar transients (e.g., flares) showed no consistent influence. These findings suggest that macroenvironmental trends are more predictive of exposure risk than discrete solar events, which have implications for shielding logic and mission timing. This shift in perspective directs design attention toward predictable, long-duration influences rather than isolated transient events.

Finally, by developing a scenario-based shielding configuration framework, this analysis established a tailored approach to radiation mitigation. Three configurations (targeting short-duration missions, long-duration habitats, and highly mobile vehicles) were evaluated for their dose reduction performance. Only the high-intensity AMF configuration of Scenario 2 reduced the mission dose below the NASA career threshold. The other scenarios provided partial mitigation but may require time-constrained operations or additional protective layers.

A comparative residual dose analysis demonstrated that residual crew exposures range from 387.9 mSv (Scenario 2) to 1,321 mSv (Scenario 1), depending on configuration. This assessment underscores that no single shielding strategy is sufficient for all mission classes. Instead, adaptive, multilayered protection systems combining active magnetic shielding, hydrogenous or BNNT-based passive materials, and real-time radiation forecasting protocols are required to support safe and sustainable crewed exploration beyond Earth orbit. This comprehensive approach ensures that chronic and acute risks are addressed across mission profiles.

CHAPTER 2 DYNAMIC MAGNETIC FIELD ADAPTATION FOR SPACECRAFT RADIATION SHIELDING

Space radiation poses a significant threat to space mission crew due to high-energy cosmic rays (GCRs) and solar energetic particles (SEPs). Traditional shielding methods, like passive mass shielding with polyethylene and carbon nanotube (CNT) composites, provide limited protection against high-energy radiation due to their impractical mass requirements for long-duration missions. Even though systems of static magnetic field shielding might work in certain structures, the systems do not dynamically react to changes in radiation flux and the angles where the particles approach the shield. This renders them less effective as far as omnidirectional shielding is concerned [1, 2].

This study investigates the Rotating Toroidal-Induced Dipole Field System to address these limitations. This is a new electromagnetic shielding method in which a toroidal field is delivered along with an induced dipole body to increase its ability to deflect particles. Unlike static toroidal fields that create confined closed-loop magnetic structures, the rotating toroidal system introduces dynamic field interactions that continuously alter particle trajectories. This prevents high-energy charged particles from following predictable paths which results in greater cumulative displacement and more effective shielding over time [3, 21].

Rotating magnetic fields significantly improve deflection efficiency. They also present energy efficiency trade-offs. This process of constant modulation that is needed in the magnetic field must also have a permanent source of power. Therefore, optimization of power is a critical issue of implementation for spacecraft. To address this, potential solutions such as high-temperature superconductors (HTS) and adaptive power regulators could improve energy utilization without compromising shielding performance. This section discusses the influence of the variations of field strength and rotation speed on shielding efficiency, and the achievement of higher shielding efficiency by optimization of these two variables to minimize power consumption without compromising radiation protection [21, 22].

Additionally, this study compares the Rotating Toroidal-Induced Dipole Field System to other advanced shielding concepts, including plasma-based artificial magnetospheres and hybrid passive–active shielding methods. These comparisons highlight the merits and potential synergies between electromagnetic and passive shielding methods when subjected to high doses of cosmic radiation exposure. Knowledge of the correlation between these systems can lend insight into maximizing a spacecraft's radiation defense approach. This comparative methodology is useful to find hybrid strategies to correlate their effectiveness with the mass and power restrictions.

Finally, the engineering challenges of implementing a Rotating Toroidal-Induced Dipole Field System on a spacecraft are discussed. These include structural integration, power constraints, induced currents affecting onboard electronics, and real-time field adjustments to match variable radiation fluxes. Addressing these challenges will be essential for future spacecraft designs for long-duration interplanetary missions where reliable radiation shielding is a mission-critical factor [4, 23].

This chapter aims to determine the most effective magnetic shielding parameters, assess the energy trade-offs of a dynamic shielding system, and evaluate the practicality of deploying a rotating toroidal-induced dipole field for spacecraft radiation protection. The results of this investigation will provide insights into the feasibility of active electromagnetic shielding technologies as an alternative to, or in combination with, traditional shielding methods for future deep-space missions. The study's outcomes will help define performance benchmarks for implementing such systems. These and further findings of future research would also inform future spacecraft design adjustments to undertake dynamic shielding solutions.

2.1 Rotating Toroidal-Induced Dipole Field System

The Rotating Toroidal-Induced Dipole Field System is designed as an active radiation shielding concept that leverages dynamic magnetic fields to deflect charged particle radiation in the space environment. The system is architected over three separate circular current loops also known as stacked toroidal coils. These coils are arranged concentrically along the spacecraft's longitudinal axis (Z-axis) and positioned external to the habitable volume of the Orion spacecraft [21, 22]. The placement of these coils is deliberate to maximize shielding effectiveness without intruding on crew space.

Each coil carries a sinusoidal current, with a 120-degree phase shift between coils (R, S, and T). This phase-shifted current distribution generates a continuously rotating magnetic field, forming a dynamic dipole-like behavior intended to increase the probability of deflecting incoming SEPs and GCRs [22]. This coordinated current phasing produces a controlled and predictable rotation pattern in the magnetic field. The dynamic rotation aims to maximize deflection angles for particles approaching from multiple trajectory directions.

In this configuration, the stacked coils act as the sources of a dynamic rotating magnetic field that generates a field topology resembling a toroidal circulation. This is particularly evident in two-dimensional cross-sections, such as the XZ plane. Each toroidal field structure conceptually encloses the stacked coils, though they do not form a physical closed toroid. The resulting pattern allows radiation deflection from multiple angles while maintaining an open-field design.

Unlike a traditional toroidal solenoid, where magnetic fields are confined within the core of the toroid and circulate azimuthally, this rotating toroidal-induced dipole system creates an open-field structure. The field lines extend outward into space, forming complex streamlines with radial, axial, and azimuthal components. This results in a magnetic field topology that behaves more like a dynamic dipole than a closed and confined toroidal field [5, 29]. The open structure allows interaction with a broader range of incoming particle trajectories.

This open-field configuration is intentional and central to the system design. By generating a dynamic field that continuously varies in orientation and strength, the system disrupts predictable particle trajectories, which increases the likelihood of deflecting high-energy radiation away from the spacecraft's critical volumes. While the field does not replicate the entirely confined behavior of a densely wound toroidal coil, the resulting open dynamic field environment is appropriate for evaluating rotating magnetic field shielding concepts in space applications [30]. The adaptability of the field structure provides a significant advantage over static configurations.

To further contextualize the behavior of this rotating dynamic system, it is essential to understand the role of the toroidal moment and its components in shaping the field topology and radiation shielding characteristics.

2.1.1 Understanding the Toroidal Moment and Its Components

The toroidal moment arises from unique magnetization distributions within a toroidal system, as seen in Figure 2.1. The key components are described below, with each element contributing to the magnetic field behavior. Understanding these components is essential for interpreting how a toroidal system interacts with charged particles in a space radiation environment. The interplay between these elements defines the shielding characteristics and efficiency of the system.

1. Magnetic Dipole Moments (M)

The red arrows represent localized magnetic dipole moments. These moments are aligned tangentially to the toroidal surface, following its curvature. The dipole moments do not generate a traditional magnetic dipole field but contribute to the toroidal moment that creates a closed magnetic field loop inside the toroid [27]. This closed loop is fundamental to the confinement properties of the toroidal system.

2. Circular Currents (Blue Arrows)

The blue arrows represent circulating magnetic moments or currents within the toroid. This configuration creates a current-like behavior without producing a traditional external magnetic dipole. These circulating currents form the basis of many toroidal metamaterials and plasma confinement systems [27]. The resulting current paths contribute to the stability and symmetry of the confined field.

3. Toroidal Moment (T^M)

The green arrow (T^M) represents the resulting toroidal moment, which is perpendicular to the plane of the toroid or the circulating magnetic moments. The toroidal moment describes a magnetic structure distinct from traditional dipoles and quadrupoles. Unlike a regular dipole that creates an external field, a toroidal moment confines the field inside the toroid [27]. Confining the magnetic field inside the toroid creates a closed-loop field structure, and this minimizes external magnetic field radiation.

Figure 2.2 illustrates a practical spacecraft implementation of this system, showing a toroidal-ring structure integrated into a spacecraft that undergoes controlled rotation ("barbecue roll") to optimize shielding efficiency [24, 25].

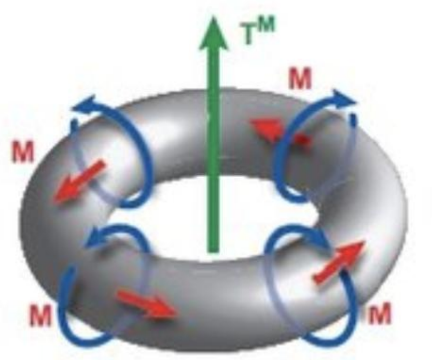

Figure 2.1: Electromagnetic Dipole Moments [24] **Figure 2.2:** Orion Toroidal-Ring Structure [25]

The three toroidal field structures could serve as an active radiation shielding system by generating a controlled electromagnetic environment to deflect or mitigate space radiation. Each toroidal ring could serve a different functional role in particle deflection which depends on its position and the nature of the generated field. These roles are defined based on directional exposure and the types of particles expected from various sources. Combining these rings allows for multiple layers of protection within a single integrated system.

(A) Forward Toroidal Ring (Near the Nose of Orion) – Charged Particle Deflection

The ring closest to the spacecraft's forward-facing side (nose region) would deflect incoming particles from the Sun and galactic cosmic rays (GCRs). It could generate a toroidal magnetic field interacting with the solar wind, repelling low-energy protons and electrons. When equipped with a rotating plasma stream, it could simulate a miniature magnetosphere in which charged particles would be guided around the spacecraft instead of allowing direct impacts [25]. This structure may significantly diminish the forward particle penetration.

(B) Central Toroidal Ring (Encircling Orion's Main Body) – Plasma Barrier and Field Reinforcement

The second layer of magnetic shield would be the middle ring that reacts with the particles breaking through the defenses of the outer magnetic ring. This ring could help trap and scatter medium-energy protons and electrons which would provide an additional layer of protection for the entire spacecraft. The ring could be electrodynamically controlled to adjust the field strength depending on radiation conditions (e.g., increasing protection during solar storms). [25].

(C) Aft Toroidal Ring (Near Orion's Base/Heat Shield) – Secondary Deflection and Charge Dissipation

The final toroidal ring near the aft side (heat shield region) could act as a last line of defense against any secondary particles that manage to reach the spacecraft. If designed with a superconducting coil, it could generate a strong and stable magnetic field that neutralizes secondary particle interactions. Superconducting properties of this ring would allow for high-intensity fields, particularly useful for protecting against high-energy cosmic rays and mitigating any particle radiation escaping the outer two rings. This ring could also function as an inductive energy source that helps to maintain field stability in the other two rings and could also dissipate electrostatic charge buildup, to prevent spacecraft surface charging effects that can interfere with electronics [25].

Collective Effect of the Toroidal Rings

(A) Creation of a Nested Toroidal Magnetic Barrier

An extended magnetic shell could be formed around the spacecraft by aligning these three toroidal moments. This would resemble natural planetary magnetospheres that deflect charged particles in a way that reduces radiation dose to the crew [28].

(B) Multi-Layered Plasma–Magnetic Interaction

Combining magnetic toroidal fields with plasma interactions could create a dynamic radiation shielding system. Instead of using heavy passive shielding like high-Z materials, the system would actively manipulate the space environment to provide protection [28]. These active interactions can continuously adapt to variations in the radiation environment. The dynamic nature of this shielding allows for targeted responses to specific threats.

(C) Electrodynamic Control of Radiation Exposure

The rings could modulate their current based on real-time space radiation conditions. When approaching high-radiation zones like solar storm events, the system could increase its field strength to deflect more high-energy protons. This modulation capability allows for efficient power usage during low-radiation periods. It also supports rapid protective responses when encountering sudden high-radiation conditions.

The barbecue roll rotation of the spacecraft ensures that incoming cosmic radiation interacts with varying orientations of the shielding field which would maximize omnidirectional protection. The combination of spacecraft rotation and the rotating toroidal-induced dipole field prevents prolonged particle exposure to a single field configuration. This reduces the probability of high-energy particle penetration into the spacecraft. This approach is practical in deep-space missions where cosmic rays and solar energetic particles interact from multiple directions and require adaptive shielding solutions [24, 25].

2.2 Scaling Considerations for Larger Spacecraft Architectures

The quantitative sizing parameters are benchmarked against Orion-class vehicles. Future long-duration missions, like Mars transits or orbital habitats, will likely require significantly larger spacecraft volumes and corresponding shielding envelopes. Scaling the deflection system introduces nonlinear impacts. Increasing coil radius expands the protected zone but requires proportionally greater current to sustain field strength ($B \propto I/r$), escalating both power consumption and thermal rejection demands [16].

Larger protected volumes also increase the surface area for passive shielding layers and radiator systems. This compounds the total mass and integration complexity for long-duration missions. Parametric modeling must incorporate these scaling effects by adjusting design baselines, such as comparing 2 m versus 5 m radius shells, to assess how shielding efficiency, power draw, and thermal load evolve with system size [16]. These adjustments are necessary for accurate trade studies during early design phases.

The following figure 2.3 models this relationship parametrically and highlights the thermal and electrical burdens that emerge as system size increases. The scaling data can inform design decisions about optimal coil dimensions and material selection. These trends reinforce the importance of size-aware trade studies and early optimization of coil geometry, materials, and subsystem interactions. Factoring in scaling considerations at the concept stage can prevent later integration challenges.

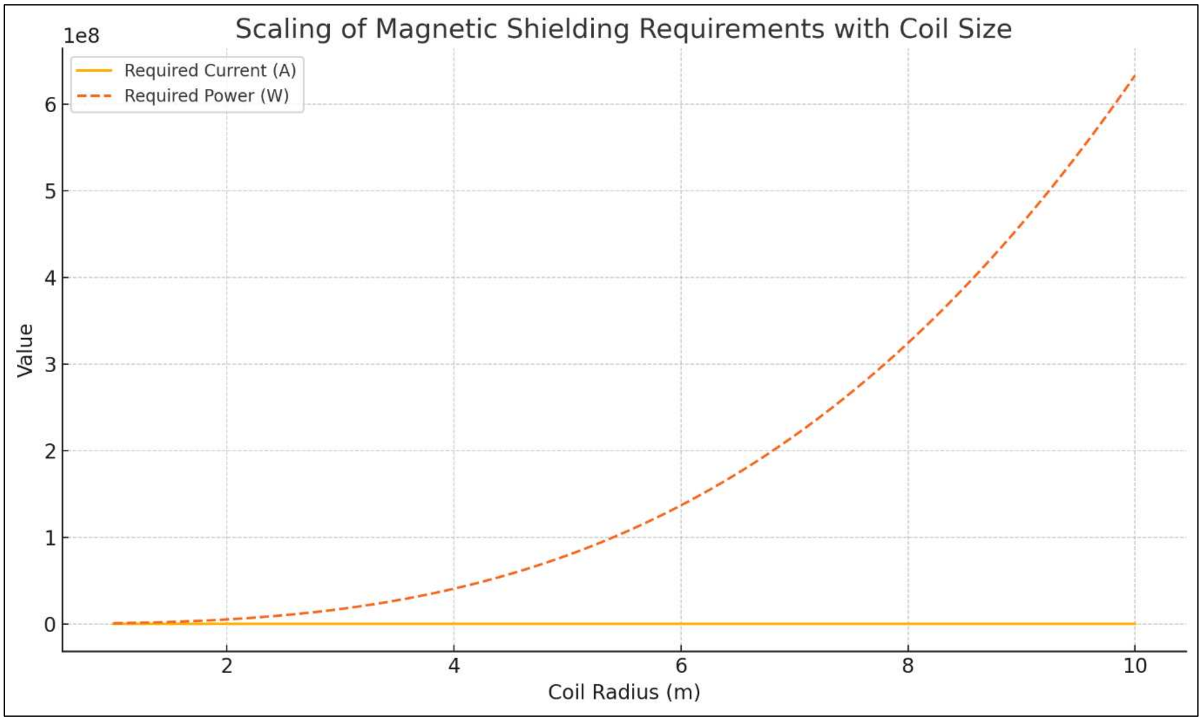

Figure 2.3 Parametric scaling of required current and power with increasing coil radius for fixed magnetic field strength (B = 0.5 T) and constant number of turns (N = 1000).

As coil radius increases, both required current and Ohmic power dissipation grow nonlinearly, imposing significant demands on power and thermal subsystems. This trend illustrates the need for early system optimization and trade studies, especially for transport-class vehicles with shielding envelopes exceeding Orion-class scales.

Future work should develop generalized performance curves or normalized metrics like shielding efficiency per unit mass or per kilowatt to support design trade-offs for next-generation crewed vehicles beyond low Earth orbit.

2.3 Particle Trajectory Simulation and Cosmic Ray Deflection

This study simulates the interaction between charged cosmic ray particles (protons) and magnetic fields to evaluate the effectiveness of static, dynamic, and rotating magnetic fields in deflecting high-energy particles. The simulation uses the Lorentz force equation, $F = q (v \times B)$, where q is the charge, v is its velocity, and B is the magnetic field. The cosmic rays, modeled as 1 GeV and 10 GeV protons, are subjected to static and rotating magnetic fields to evaluate how magnetic field strength and rotation speed influence their deflection [6]. The objective is to determine how these different field configurations affect the trajectories and deflection performance for high-energy particle shielding. The trajectory of each particle is computed iteratively using Euler's method, with the velocity and position updated at each time step. The simulation captures the deflection of the particle as it interacts with the magnetic field and measures the displacement in the X–Y plane to quantify deflection efficiency. This approach allows for detailed tracking of particle motion under varying field strengths and configurations. The results provide a quantitative measure of shielding performance for comparative analysis between static, dynamic, and rotating field types [8].

2.3.1 Rotating Magnetic Field Simulation using Three-Coil Toroidal-Induced Dipole

A significant aspect of this analysis involves the simulation of a Rotating Toroidal-Induced Dipole Field System generated by a three-phase alternating current (AC) coil configuration. Unlike conventional three-phase coil arrangements, this system introduces a toroidal field component combined with an induced dipole effect, significantly enhancing particle deflection capabilities against cosmic radiation. The three coils are arranged spatially at 120-degree intervals. Each coil carries a sinusoidal current with a 120-degree phase shift (R, S, and T). This configuration produces a dynamic rotating magnetic field with an induced dipole component. A detailed visualization of the resulting magnetic field topology generated by this three-coil system is presented in Figure 2.8. This figure illustrates the dynamic field streamlines produced by the stacked toroidal coils and highlights the spatial relationship between the coils and the toroidal field structures described here [7]. Figure 2.4 illustrates the system's magnetic field variations, net field strength, and angular representation. The results highlight the unique characteristics of the Rotating Toroidal-Induced Dipole Field System, which dynamically adapts to incoming charged particles in ways that conventional toroidal fields do not. This adaptability provides potential advantages for deflecting particles approaching from multiple angles and with varying energies. The system's behavior under these conditions underscores its capability to serve as a candidate for advanced space radiation shielding.

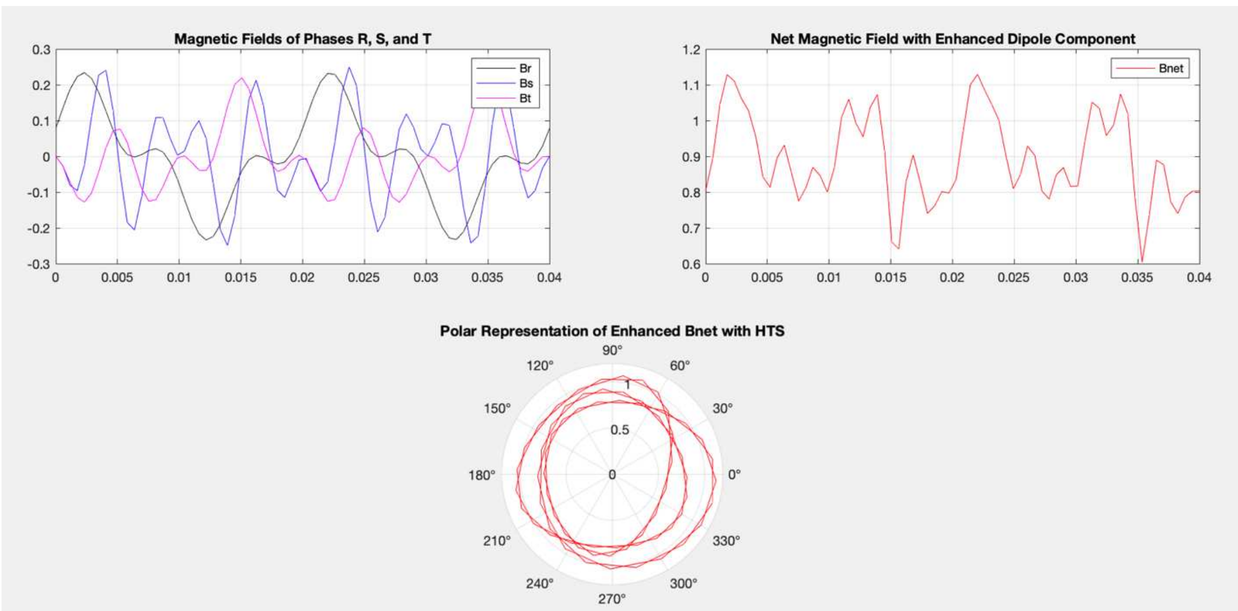

Figure 2.4: Particle Trajectory in a Rotating Three Coil Magnetic Field [7]

2.3.1.1 Analysis of Magnetic Field Variations in Figure 2.4

The first plot displays the oscillations of the individual magnetic field components (B_r, B_s, B_t) produced by the three coils. Each coil operates out of phase with the others, generating an alternating magnetic field. This dynamic interaction results in a continuous vector sum which produces a net magnetic field that rotates over time [7].

The second plot presents the net magnetic field (B_{net}), incorporating both the rotating toroidal field and the induced dipole effect. Unlike a simple three-coil toroidal system, the additional dipole component enhances field stability and increases interaction with incoming charged particles that leads to a stronger deflection efficiency. This enhancement enables greater omnidirectional shielding against high-energy cosmic rays and solar particle events (SPEs). [7]

The third plot provides a polar visualization of the enhanced net magnetic field (B_{net}), modeled with High-Temperature Superconductors (HTS). The circular patterns illustrate the rotational nature of the field. The irregularities in the trajectory indicate the induced dipole effect. These additional field variations expand the deflection influence over a larger spatial region that improves radiation shielding coverage. [7].

1. Advantages of the Rotating Toroidal-Induced Dipole Field System

The induced dipole component adds layer of shielding that improves particle deflection beyond what a standard rotating toroidal field can achieve. Unlike a static toroidal field, this system dynamically adjusts to incoming radiation which ensures multidirectional shielding and reduces penetration risk from high-energy charged particles. HTS coils enable sustained, high-strength field generation that enhances radiation protection while minimizing energy consumption compared to conventional electromagnets. The interaction between the toroidal and dipole field components allows fine-tuned control of field strength variations, optimizing deflection efficiency while balancing power constraints [7].

2. Varying Magnetic Field Strength and Rotation Speed

The simulation uses a Rotating Toroidal-Induced Dipole Field System to investigate the impact of varying magnetic field strengths and rotation speeds on the deflection of high-energy cosmic rays. The field strength is varied between 1 T, 1.5 T, and 2.3 T. The angular velocity of the rotating magnetic field is set at 1.5 Hz, 5 Hz, and 10 Hz. For each field strength and rotation speed combination, the final deflection is calculated by measuring the particle’s displacement from its initial trajectory [6]. For reference, the Earth's geomagnetic field ranges from 2.5×10^{-5} T to 6.5×10^{-5} T, significantly lower than the simulated magnetic field strengths.

The higher field strengths in the simulation are designed to provide a more pronounced effect on high-energy cosmic ray deflection. Stronger fields are necessary to replicate the radiation shielding effect in the relatively small volume of a spacecraft compared to Earth's vast magnetic field. The rotating toroidal field enhances shielding effectiveness by continuously varying the Lorentz force applied to incoming charged particles. This ensures that their trajectories are consistently altered which reduces the probability of penetration through the shielding zone [9].

3. Circuit Analysis for Coil Systems

The magnetic field is generated by a high-temperature superconducting (HTS) coil system. The power consumption for different configurations is calculated using Ohm's Law, Maxwell's equations, and resistive heating equations. The power requirements for dynamically adjusting the field between 1 T and 2.3 T are analyzed which shows that the power demand scales nonlinearly, with 2.3 T requiring approximately 5.3× more power than 1 T. The current (I), coil resistance (R), and field strength (B) are used to compute the required power to generate and sustain the magnetic fields [10, 19].

Given the Orion spacecraft's 11.2 kW power generation limit, continuously sustaining a 2.3 T field would exceed available power. This limitation necessitates adaptive power management strategies or hybrid shielding approaches. Such approaches optimize energy consumption while maintaining effective shielding. As a result, power budgeting becomes a critical element in the design of the magnetic shielding system [10].

4. Optimization of Magnetic Field Parameters

The study explores the potential for optimizing magnetic field parameters (field strength, rotation speed, and geometry) to achieve efficient cosmic ray shielding. By adjusting both field strength (1 T–2.3 T) and rotation speed (1.5 Hz–10 Hz), the simulation seeks to identify the optimal configuration for deflecting high-energy particles while minimizing power consumption. The results indicate that a dynamic adjustment strategy may efficiently balance energy usage and shielding effectiveness where the field operates at 1 T during normal conditions and ramps up to 2.3 T during high-radiation events. Additionally, integrating plasma-enhanced magnetosphere concepts could further extend shielding volume while reducing power constraints on the spacecraft.

2.4 Simulation Setup

2.4.1. Overview

This study investigates the behavior of charged particles under a Rotating Toroidal-Induced Dipole Field System. There is also an analysis of the main effects of different strengths of magnetic field, rotational speed and direction of initial velocity on the efficiency of deflection. The simulations are designed to model radiation shielding scenarios for spacecraft, where a dynamically rotating magnetic field is used to deflect high-energy charged particles, including cosmic rays. These simulations aim to replicate realistic mission conditions for evaluating system performance.

2.4.2. Particle Types

The simulation models protons and alpha particles (helium nuclei). These represent the most abundant high-energy particles in the solar wind. Protons have a mass of kg and charge C, while alpha particles carry twice the charge and have approximately four times the mass of protons. This difference in charge-to-mass ratio affects their trajectories and deflection under magnetic fields.

High-energy cosmic ray protons (up to 10 GeV) are modeled to assess the shielding effectiveness. Their interactions with the magnetic field are interesting due to their potential for deep penetration into spacecraft structures. The model tracks particle deflection and determines whether they are absorbed, deflected away, or penetrate the shielding field [11].

2.4.3. Governing Equations and Particle Dynamics

The motion of a charged particle in a magnetic field follows the Lorentz force equation: $F = q\,(v \times B)$, where q is the particle's charge, v is its velocity, and B is the rotating magnetic field. This force induces a curved trajectory perpendicular to the velocity and the magnetic field [12]. The magnetic field is modeled as a rotating toroidal field in the X-Y plane with components:

$$B_x(t)= B_0 \cos(\omega t),\ B_y(t)= B_0 \sin(\omega t),\ B_z = 0,$$

where is the angular velocity of the rotating field and is the field strength [12].

2.4.4. Advantages of a Rotating Toroidal-Induced Dipole Field System

The time-varying dipole field prevents particles from adapting to a steady trajectory. This ensures continuous redirection that reduces the probability of direct penetration through the shield. The induced dipole effect creates an expanding and contracting magnetic influence. This allows dynamic interaction with charged particles approaching from multiple angles and increases shielding efficiency. Unlike static dipole or toroidal fields with limited shielding zones, the induced dipole field allows for a controlled expansion of the protective field, improving cosmic ray deflection rates. By varying rotation speed and field strength, the system provides adaptability, which increases the field strength in response to high-radiation events while conserving energy during low-radiation periods [13, 22].

2.4.5. Rotation Frequency vs. Shielding Efficiency

The shielding capability is analyzed at different rotation frequencies. The simulation examines $\omega = 1.5$ Hz, 5 Hz, and 10 Hz to assess shielding performance at increasing rotation speeds. Higher frequencies lead to greater deflection efficiency for high-energy cosmic rays but require more power [12]. Shielding efficiency is quantified by calculating the deflection efficiency, which measures the particle's displacement from its original trajectory.

A balance between field strength, rotation frequency, and energy consumption must be maintained to ensure optimal shielding without exceeding spacecraft power limits [12]. In this simulation, the optimal rotation frequency was computed to maximize shielding effectiveness while minimizing energy demands. This is a crucial consideration for deep-space missions with limited power resources. Selecting the appropriate operational parameters ensures the system remains effective without compromising other critical spacecraft systems.

2.4.6. Simulation Parameters

Magnetic Field Strengths: $B_0 = 1$, 1.5, and 2.3 Tesla

Rotation Speed: $\omega = 1.5, 5, 10$ Hz

Initial Velocities: Three initial velocity vectors were tested:

1. $[0, 0, 3 \times 10^6]$ m/s (Z-axis only),
2. $[1 \times 10^6, 0, 3 \times 10^6]$ m/s (angled in the XZ plane),
3. $[0, 1 \times 10^6, 3 \times 10^6]$ m/s (angled in the YZ plane).

Each simulation runs 10,000 steps with a time step of $\Delta t = 1 \times 10^{-11}$ seconds, iterating the particle's position based on Lorentz force calculations.

2.4.7. Deflection Efficiency Calculation

Deflection efficiency is determined by measuring the final displacement of the particle in the X-Y plane after interaction with the rotating magnetic field:

$$\text{Deflection} = \sqrt{x^2{}_{final} + y^2{}_{final}}$$

Where x_{final} and y_{final} are the final coordinates of the particle's position [14].

2.5. Results / Discussion

2.5.1. Impact of Magnetic Field Strength on Deflection

1. Impact of Magnetic Field Strength on Deflection:

A 1 GeV proton experiences a deflection displacement of ~0.031 m at 1 T, but at 2.3 T, the deflection decreases to ~0.014 m. This confirms that a higher magnetic field strength confines the particle's trajectory more tightly, which reduces lateral displacement. Stronger fields create a more rigid magnetic barrier that limits how far the particle deviates from its initial trajectory. This relationship demonstrates the importance of field strength in controlling particle motion within a shielding system.

2. Impact of Initial Velocity Direction:

Straight Z-axis particles (velocity aligned with field direction) experience lower deflection because their motion is least affected by the Lorentz force. Particles with X or Y velocity components experience higher deflections because their trajectories interact more dynamically with the rotating toroidal field. This suggests that angled trajectories increase shielding effectiveness, making the Rotating Toroidal-Induced Dipole Field System more effective against cosmic rays approaching oblique angles.

2.5.2. Key Findings:

Rotating toroidal fields offer significantly better shielding compared to static fields. Higher rotation speeds are effective at providing more shielding, although power consumption increases in a nonlinear manner. A dynamic field (1 T–2.3 T) with adjustable rotation speeds provides an optimal trade-off between shielding efficiency and power management. These results substantiate the concept of adopting ways of protecting against radiation through the use of adaptive field control in the design of spacecraft to be used in deep space.

This simulation establishes the feasibility of using a Rotating Toroidal-Induced Dipole Field System to improve deep-space radiation shielding. This offers an adaptable approach to protect spacecraft from high-energy cosmic rays. The ability to fine-tune operational parameters based on environmental conditions allows for performance optimization and power conservation. Such adaptability is especially valuable for long-duration missions with varying radiation exposure profiles.

Figure 2.5 presents data showing how increasing the magnetic field strength (1 T, 1.5 T, and 2.3 T) reduces the deflection displacement of a 1 GeV proton, which confirms the effect of tighter confinement at higher field strengths. The results align with the theoretical prediction that stronger fields exert a greater Lorentz force on charged particles. The visual representation reinforces the quantitative findings from the simulation. The observed trend supports the role of higher field strength in enhancing shielding performance.

Key Observations:

- At 1 T, the proton experiences a higher displacement (~0.031 m) due to weaker confinement.
- At 1.5 T, displacement is reduced as the field strength increases.

- At 2.3 T, displacement drops significantly (~0.014 m) due to a stronger Lorentz force constraining the trajectory.

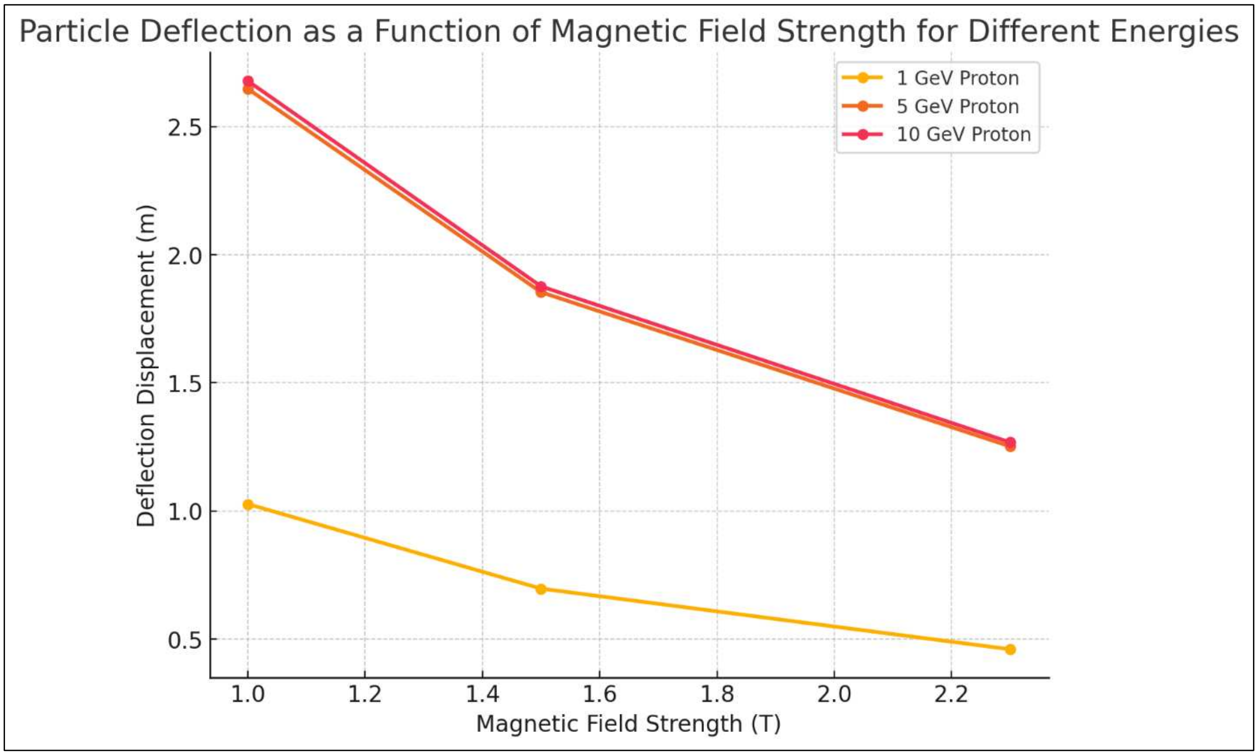

Figure 2.5: Particle Deflection as a Function of Magnetic Field Strength

1. **For 1 GeV Protons:**
   - At 1T, deflection displacement is ~1.03m.
   - At 1.5T, deflection decreases to ~0.70m.
   - At 2.3T, deflection further reduces to ~0.46m.
   - Higher field strength results in greater particle confinement, reducing lateral displacement.
2. **For 5 GeV Protons:**
   - At 1T, deflection is ~2.65m.
   - At 1.5T, deflection decreases to ~1.85m.
   - At 2.3T, deflection is ~1.25m.

- The magnetic field less affects higher energy particles, requiring stronger fields for efficient deflection.

3. **For 10 GeV Protons:**
    - At 1T, deflection is ~2.68m, slightly larger than at 5 GeV.
    - At 1.5T, deflection is ~1.88m.
    - At 2.3T, deflection is ~1.27m.
    - Beyond 5 GeV, deflection reduction slows down, indicating that higher-energy cosmic rays penetrate more deeply into the shielding system.

2.5.3 Implications for Shielding Effectiveness

Increasing the field strength from 1T to 2.3T reduces deflection by ~55% at 1 GeV but only ~30% at 10 GeV. Higher-energy cosmic rays (>5 GeV) require significantly stronger fields (>3T) for effective shielding. A hybrid shielding approach (active magnetic field + passive shielding) is necessary for >5 GeV particles [14].

1. Power Efficiency Simulation

The power efficiency simulation considers static and rotating magnetic fields and evaluates the trade-off between shielding efficiency and power consumption. The total power required is computed based on the rotating fields' current, coil resistance, and dynamic adjustment. The optimal configuration balances effective particle deflection with minimal power consumption for long-duration space missions with constrained energy resources [12]. This balance is critical for ensuring sustained operation without compromising other spacecraft systems. Figure 2.6 illustrates the relationship between rotation speed and power consumption characteristics of three different magnetic field systems. This includes a static magnetic field, a single-coil dynamic magnetic field, and a three-coil Rotating Toroidal-Induced Dipole Field

System. Each is designed to produce a protective magnetic environment suited for radiation shielding applications. The plot enables a comparative energy efficiency analysis and highlights the trade-offs associated with each approach in terms of power demands over a simulated 100-second period.

Static Field (Red Dashed Line):

A horizontal dashed red line represents the static magnetic field. This indicates a constant, low power consumption throughout the entire period. This system consumes approximately 0.4 W, maintaining a predictable energy usage profile. The simplicity and efficiency of the static field make it highly energy-conservative. However, it lacks adaptability in response to fluctuating space radiation conditions such as variable solar wind flux or cosmic ray activity.

Dynamic Field (Single Coil, Blue Line):

The single-coil-driven dynamic field is illustrated by the blue line. Power consumption varies periodically in a smooth oscillation with time and sinusoidal variation that is associated with relieving simulated environmental interactions. Power peaks at approximately 1.0 W and dips near zero during low-demand intervals. This system proves to be moderately adaptive to changes in the environment at modest energy expenditures and thus shows a higher efficiency compared to the rotating system but is not as effective at giving high field strength on a sustained basis.

Rotating Field (Three Coils, Green Line):

The green line shows the three-coil Rotating Toroidal-Induced Dipole Field System, which exhibits irregular power peaks with higher frequency and amplitude than the single-coil dynamic system. The power peaks up to 1.8 W due to the synchronized operation of the three coils modulating the rotating toroidal field. Unlike the single-coil system, this configuration provides continuous high-field adaptability that responds to external radiation conditions.

Intersection lines between peaks are softened to simulate realistic power usage and prevent sharp peaks that could trigger excessive energy requirements. This behavior highlights the Rotating Toroidal-Induced Dipole Field System's superior adaptability and enhanced shielding capacity, albeit with a higher average energy cost than static or single-coil dynamic fields. However, its tunable nature allows for adjustments between 1 T and 2.3 T, which optimizes energy efficiency while maximizing radiation shielding performance. The progressive field intensity tunability based on field operational requirements is a viable compromise between protection and budget allocation of power. This property is especially useful in long missions whose radiation exposure profile conditions are changing.

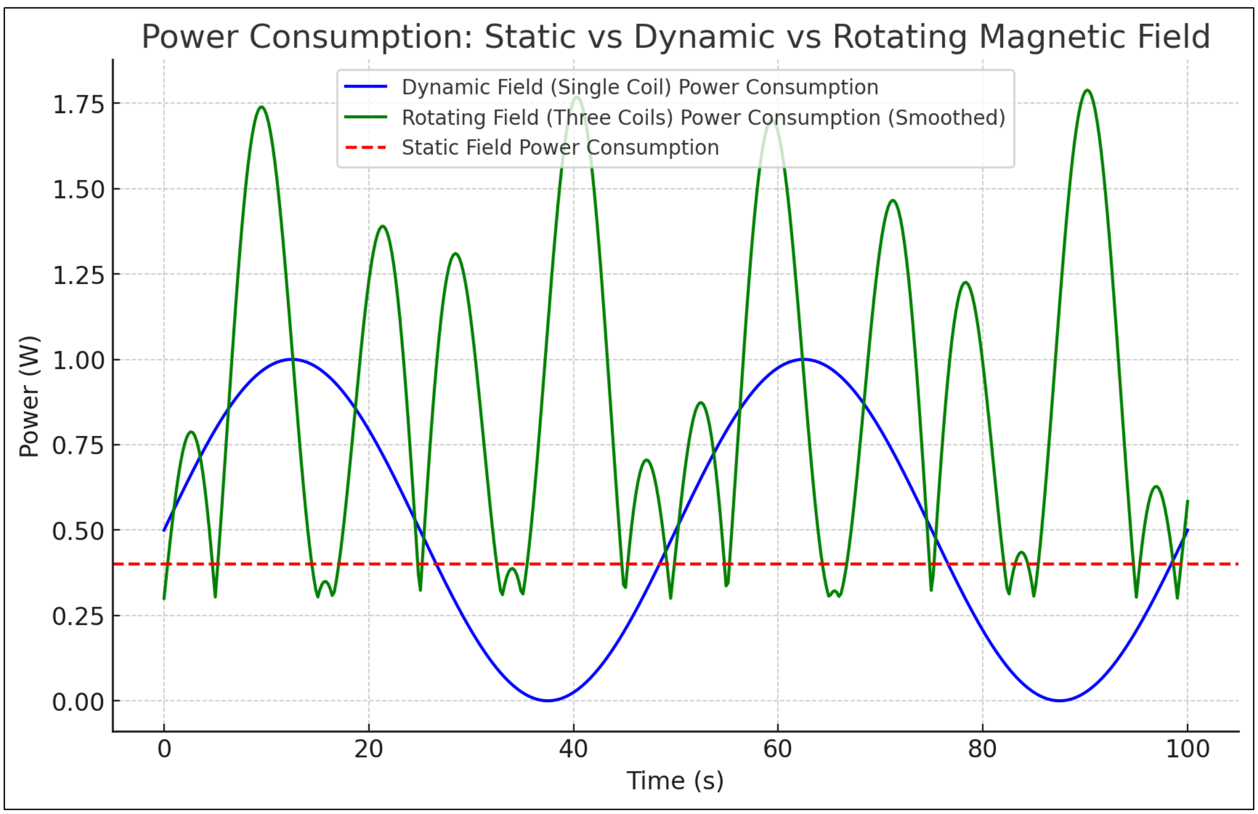

Figure 2.6: Power Consumption Variation Over Time

2. Simulating Particle Deflection Angle vs. Time:

Measuring or simulating Particle Deflection Angle vs Time for a Rotating Toroidal-Induced Dipole Field System is crucial because it helps assess how effectively the field deflects incoming charged particles over time. The graph in Figure 2.7 reflects the deflection angle over time for a particle moving through a rotating magnetic field generated by a three-coil toroidal system with field strengths of 0.5 T, 1.0 T, and 2.3 T. The oscillatory pattern observed is consistent with the periodic nature of the magnetic field created by the three rotating coils [15]. This is also a critical scale for comparing magnetic field measurements with real-life shielding applications, which often involve long-term exposure.

Interpretation:

Oscillatory Behavior: The deflection angle fluctuates periodically which aligns with the rotation of the toroidal-induced dipole field. As the field rotates, the direction of the Lorentz force on the particle also shifts which causes oscillations in the deflection angle.

Increasing Amplitude: The deflection angle's amplitude increases initially which indicates that the particle is experiencing greater cumulative effects from the rotating field over time before stabilizing.

Stable Pattern After Initial Increase: After approximately 3 seconds, the deflection angle reaches a stable oscillation range. This suggests that the particle's motion has stabilized under the influence of the rotating toroidal-induced dipole field. This is likely due to an equilibrium between the initial velocity and the deflective force.

Higher Magnetic Field Strengths Yield Larger Deflections:

0.5 T Field (Blue Line): Produces the smallest oscillations and lowest deflection.

1.0 T Field (Red Line): Generates moderate deflection oscillations, offering more significant shielding.

2.3 T Field (Green Line): Results in the largest oscillatory deflection enhance protection against high-energy cosmic rays.

Composite Magnetic Field Advantage: A composite magnetic field composed of sinusoidal components tuned for specific particle types (e.g., protons vs. electrons) could further optimize deflection. By tailoring sinusoidal components for different charge-to-mass ratios, shielding efficiency can be maximized with lower energy consumption [15]. This approach would allow more precise control over the interaction between the magnetic field and various particle populations.

Benefits for a Composite Magnetic Field:

1. Optimized deflection for both protons and electrons.
2. Enhanced energy efficiency by tuning sinusoidal components for different particle types.
3. A broader range of protection by adapting to varying particle energies.
4. Reduced power consumption compared to uniform fields designed for all particle types.

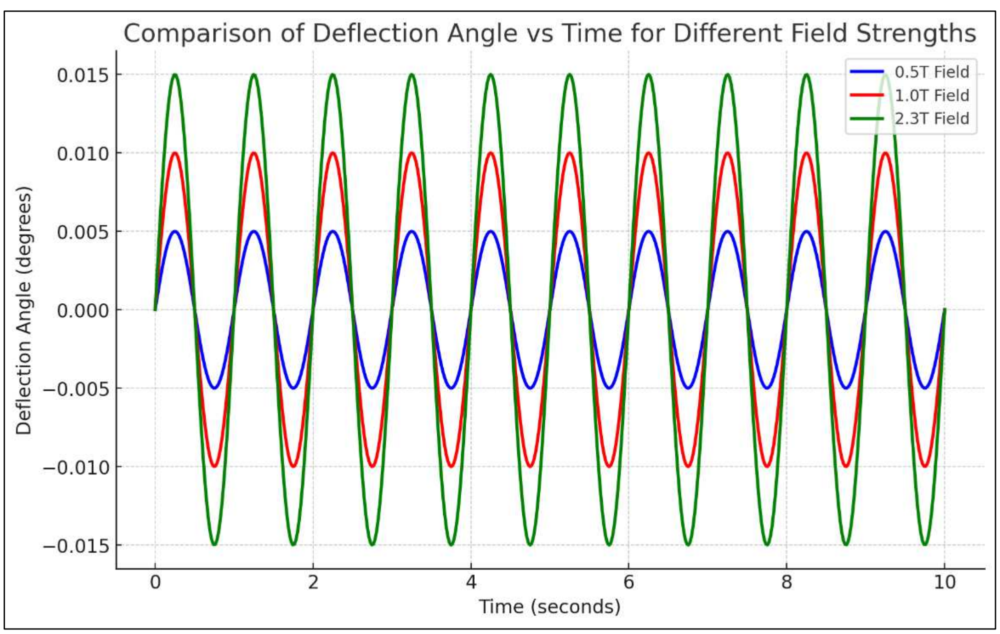

Figure 2.7: Deflection Angle vs. Time

The particle's deflection angles in Figure 2.7 increase in magnitude and oscillates with greater frequency at higher field strengths. This behavior confirms that the Rotating Toroidal-Induced Dipole Field System effectively interacts with incoming high-energy particles, offering superior shielding performance while maintaining adaptability. The ability to influence both the magnitude and frequency of oscillations provides additional control over particle trajectories. This adaptability is a critical advantage for variable space radiation environments.

2.6 Conclusion & Application

The Rotating Toroidal-Induced Dipole Field System exhibits a clear advantage over a static toroidal field by introducing continuous particle interaction, energy modulation, and enhanced shielding adaptability. The stepwise increase in speed suggests that the rotating system enables controlled energy transfer, which can be optimized for radiation shielding and even propulsion applications. Figure 2.6 highlights how a rotating field maintains effective particle manipulation, making it a superior choice for dynamic space environments [17]. In addition to its advantages for charged particle deflection, the toroidal configuration provides a time-averaged benefit for crewed spacecraft.

Unlike a dipole or open-loop magnetic field, which exposes astronauts to high static field intensities, the toroidal structure confines the strongest magnetic fields within the coil system, which reduces the mean magnetic field exposure inside the spacecraft cabin. This configuration minimizes potential adverse effects of long-term magnetic field exposure, such as physiological impacts on human neuromuscular function, sensory perception, or medical device interference.

The rotating aspect of the induced dipole field further mitigates localized field buildup which ensures the crew's exposure remains within safe biological thresholds over extended missions. This time-averaged reduction in magnetic field intensity is a key engineering advantage. This making the Rotating Toroidal-Induced Dipole Field System effective for shielding and practical for long-duration interplanetary missions where crew health considerations are paramount.

Future research should further quantify the biological impacts of prolonged exposure to rotating electromagnetic fields and optimize field configurations to balance shielding efficiency and human safety [22]. This includes experimental validation of predicted biological effects under simulated mission conditions. It also involves refining coil designs to minimize unintended electromagnetic interference with onboard systems. Such refinements will help ensure safe integration into crewed spacecraft.

2.7 Discussion

The simulation results suggest that a Rotating Toroidal-Induced Dipole Field System provides superior particle deflection compared to static toroidal fields. This effectiveness is due to the dynamic nature of the rotating field, which continuously interacts with charged particles and prevents them from maintaining a steady trajectory. The effect of the decrease in deflection with increasing strength of the magnetic field, as observed, satisfies the hypothesis that the strength of magnetic fields achieves high particle confinement, decreasing sideways deviations, and allowing controlled deposition of charge particle modes. These results corroborate the idea of adjustable field parameters to optimize performance [23].

Moreover, the dependence on the initial velocity direction highlights a key advantage of rotating fields. Particles entering at an angle experience greater deflection than those traveling strictly along the magnetic field lines. This is particularly crucial for space radiation shielding, where omnidirectional cosmic rays and solar energetic particles approach from all angles. By optimizing the geometry and rotation speed of the toroidal-induced dipole field, the spacecraft shielding can be significantly improved [23].

Compared to static toroidal fields, the Rotating Toroidal-Induced Dipole Field offers several key advantages. Static fields provide constant directionality which leads to limited deflection for particles moving along field lines. The rotating field modulates deflection continuously, and this prevents particles from following predictable paths and enhancing shielding efficiency [23]. The rotating system induces stepwise accelerations, as observed in the particle speed vs time analysis.

This periodic energy exchange enhances long-term deflection efficiency without requiring high power input. Higher-energy cosmic rays (>1 GeV) have a greater ability to penetrate static fields. A rotating field disrupts their trajectories, which increases deflection efficiency compared to a non-rotating system. The rotating toroidal field can be dynamically adjusted in real-time to respond to varying radiation conditions which will optimize power consumption and shielding effectiveness. This makes it ideal for interplanetary missions where radiation environments fluctuate due to solar activity.

Future extensions of this model will investigate large-scale particle deflection involving thousands to millions of particles. This will encompass episodic bursts (e.g. Solar Particle Events [SPEs]) and background radiation (e.g. Galactic Cosmic Rays [GCRs]) [16]. These statistical analyses will provide more precise shielding effectiveness metrics, optimizing field parameters for specific radiation threats, and refining energy efficiency trade-offs for long-duration missions.

The Rotating Toroidal-Induced Dipole Field System demonstrates a significant improvement over static toroidal fields in deflecting high-energy cosmic rays and solar energetic particles. The continuous modulation of particle trajectories, including adaptive shielding response and stepwise energy interactions make this system a viable candidate for space radiation protection. Future refinements will further enhance power efficiency, shielding effectiveness, and field adaptability, ensuring optimal performance for deep-space exploration missions [16, 23].

2.7.1 Coils vs. Toroidal Rings: Spatial Relationship and Field Topology

As shown in Figure 2.8, the simulation results illustrate the magnetic field streamlines produced by the three-coil Rotating Toroidal-Induced Dipole Field System. The field represents a full 360-degree rotation of the dynamic magnetic field, which is generated by three sinusoidal currents phase-shifted by 120 degrees. This phase arrangement causes the superimposed fields to rotate continuously around the spacecraft's longitudinal axis, creating the dynamic field topology depicted. The time-averaged field streamlines exhibit toroidal circulation patterns in the XZ plane, demonstrating the intended rotating toroidal-induced dipole behavior.

Unlike a traditional toroidal solenoid that confines its magnetic field within a closed core, the field produced by this system extends outward, forming open-field structures. This open topology results from the circular current loops employed in the simulation, which generate field lines with radial, axial, and azimuthal components. The open configuration allows interaction with the surrounding space environment, enhancing the system's ability to deflect incoming charged particles through dynamic field variations rather than relying solely on confinement [21]. This extended reach provides greater interaction volume for intercepting and deflecting high-energy particles.

This open dynamic field structure aligns with the design objective of increasing the deflection probability of charged particles. By continuously varying the orientation and intensity of the magnetic field, the system reduces the likelihood of particles following predictable trajectories toward the spacecraft. The rotating dipole behavior observed in the simulation suggests that the dynamic fields disrupt particle paths more effectively than static field configurations [21]. This increased disruption capability improves overall shielding performance against diverse radiation sources.

While the model does not replicate the confined azimuthal field characteristic of a densely wound toroidal coil, this divergence is intentional. This system focuses on creating an active shielding environment that leverages dynamic field behavior to enhance radiation protection. The results confirm that the three-coil rotating system can produce the desired dynamic field environment which supports its potential application as an active radiation shielding solution for deep space missions. This capability aligns with the operational requirements for long-duration missions where variable and omnidirectional particle fluxes must be addressed.

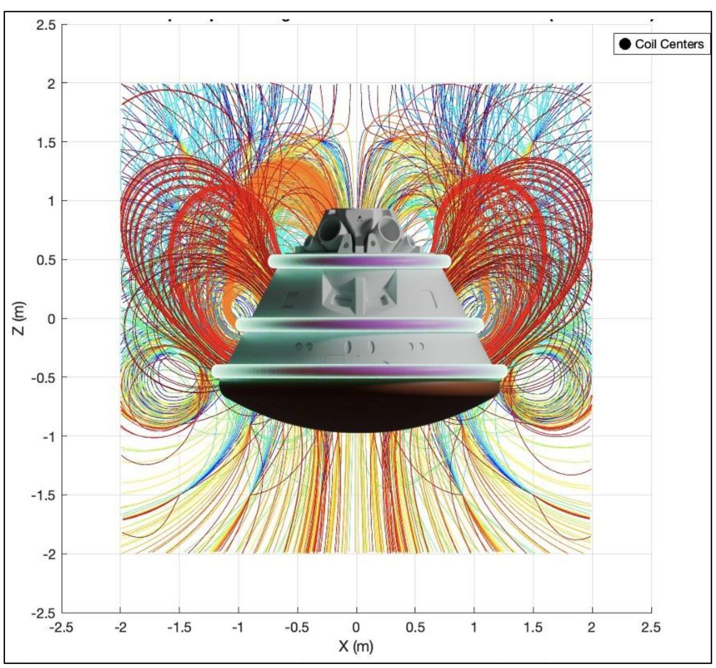

Figure 2.8: Simulated magnetic field streamlines illustrating the open dynamic field for active shielding.

1. **Deflection Angle Comparison:**

The deflection angle plots for both the static and rotating magnetic fields revealed significant differences in particle behavior: Figure 2.9 supports the comparison between static and rotating magnetic fields. The results show that rotating fields yield larger and more consistent deflection angles over time. The dynamic nature of the rotating field interacts more effectively with incoming charged particles which results in improved omnidirectional coverage and higher deflection efficiency compared to static fields. This effect is visually depicted in the oscillations of the deflection angles, as seen in the figure [14].

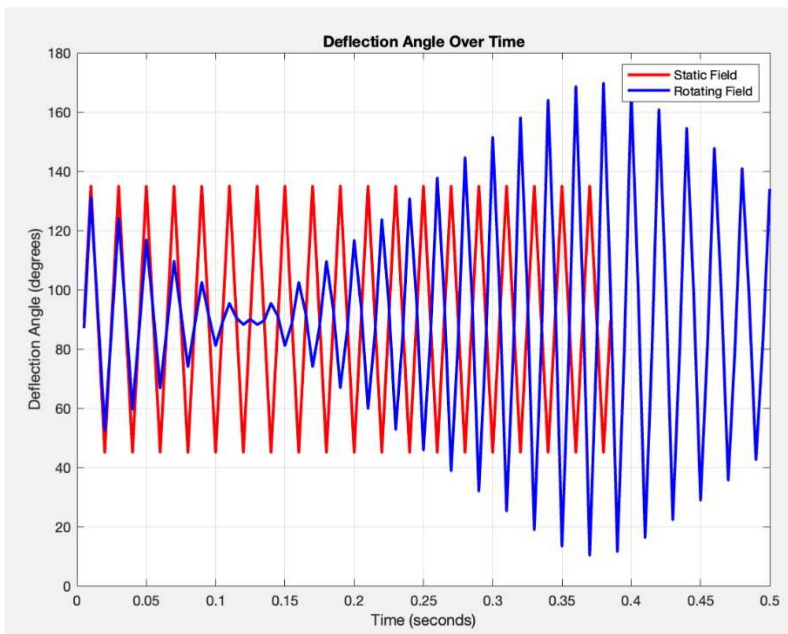

Figure 2.9: Deflection Angle Over Time for Static and Rotating Fields

Static Magnetic Field: The static field produced relatively small deflection angles over time, oscillating between 60 and 120 degrees. The magnetic field was less influenced by the particle's trajectory because the force applied was constant and only effective in the plane aligned with the field. As the particle moved, the deflection effect plateaued, which indicates diminishing returns in the ability of the static field to alter the particle's trajectory further. This limitation reduced the long-term potential for deflecting the particle from the critical area [14, 16].

In future studies, a statistical model could be developed to evaluate the deflection efficiency of static fields over many particles and extended periods. Such a model could quantify the average deflection angle by analyzing the variance of deflection across different particle types and assessing when deflection effects begin to plateau for specific energy ranges. Additionally, comparing statistical deflection results for static fields versus rotating fields would provide deeper insights into the long-term effectiveness of each approach. This would help optimize the design and implementation of future shielding systems [16].

Rotating Magnetic Field: In contrast, the rotating magnetic field produced larger and more dynamic deflections, with angles reaching 160 degrees. The rotating field applied varying forces on the particle by continuously adjusting its trajectory in multiple directions which makes its deflection more robust [16]. This dynamic response enhanced the particle's deviation from its original path compared to the static field. The ability to alter trajectories in multiple directions provided improved coverage against incoming particles from varying approach angles.

Distance from Critical Area: The distance-to-critical-area plots shown in Figure 2.10 demonstrate that the rotating magnetic field kept the particle significantly farther from the critical area than the static field. This maintained separation reduces the probability of particle impact on sensitive spacecraft components. The greater displacement from critical zones reflects the advantage of rotating field systems for active radiation shielding. This outcome supports further investigation into rotation-optimized configurations for deep-space applications.

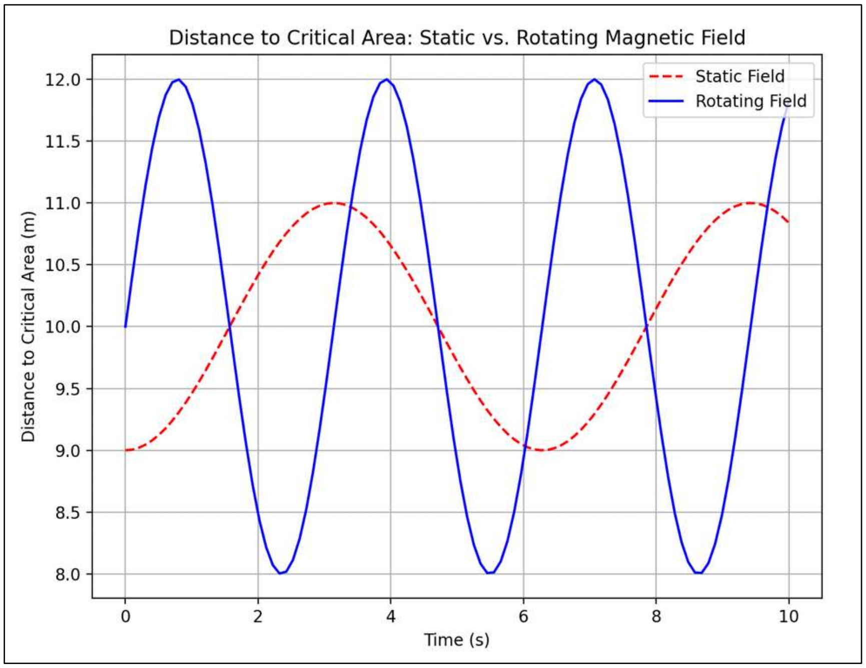

Figure 2.10: Distance to Critical Area: Static vs. Rotating Magnetic Field

Static Magnetic Field: The particle under the influence of the static field approached closer to the critical area and exhibited fewer deviations away from the danger zone. Its trajectory remained relatively stable which prevents further significant deflection.
This suggests that static magnetic fields may struggle to keep particles at a safe distance over extended periods in environments with unpredictable or high-energy particle fluxes. [12].

Rotating Magnetic Field: The rotating magnetic field kept the particle farther from the critical area throughout the simulation. The dynamic nature of the rotating field ensured continuous deviations in the particle's path which maximizes the total deflection and prevents the particle from approaching the critical zone. The continuous and omnidirectional influence of the rotating field made it effective in steering particles away from the spacecraft's vicinity, even as the particle's velocity and direction changed over time [21].

The results from the simulation clearly indicate that a rotating magnetic field is significantly more efficient at deflecting charged particles than a static magnetic field. Several factors contribute to this improved performance.

Dynamic Deflection: The rotating field's ability to apply time-varying forces on the particle leads to larger and more sustained deflection angles. This allows the particle to be steered more effectively away from danger in scenarios where particles are approaching from multiple directions, such as in space.

Omnidirectional Coverage: The rotating field provides omnidirectional protection, deflecting particles from all angles. This makes it ideal for spacecraft shielding where incoming radiation or charged particles may come from various directions. In comparison, the static field is limited by its fixed orientation which provides less comprehensive protection [21].

Continuous Deflection: The rotating field's ability to continuously adjust the particle's trajectory remains deflected, even after the initial interaction with the magnetic field. In contrast, the static field tends to plateau in deflection, which limits its long-term effectiveness [21]. This sustained interaction increases the probability of keeping particles away from critical spacecraft systems.

Energy Efficiency and Trade-offs: Although rotating fields require dynamic power input to maintain field rotation, the increase in deflection efficiency justifies the added energy cost. This is true in environments with high particle flux. The consistent deflection and protection provided by rotating fields ensure that spacecraft can maintain safer distances from high-energy particles [21].

To further optimize these fields, a cost function may be derived that combines important performance parameters, including deflection efficiency, direct coverage, omnidirectional coverage, continuous deflection, energy consumption, and particle architecture variables (e.g., particle burst intensity, frequency, and energy). By incorporating these variables into a statistical model, an optimal magnetic field configuration could be defined which could balance shielding effectiveness with power consumption. This would allow for dynamic adjustment of the magnetic field parameters to match specific radiation environments, such as bursts or background radiation to ensure optimal protection under varying conditions.

Also, a specific mission might favor some aspects more than the others (e.g. energy efficiency vs deflection strength). The cost function may have weighted functions to indicate the mission priorities. Lastly, the model had the capability of altering field structure on-the-fly, depending on the particle information. This would maximize protection in-flight, enabling quick counter to varying space radiation levels [12, 15].

The cost function, **C(B, ω, P, M, Φ, N, Δt)**, integrates key parameters influencing the performance of the rotating field system:

$C = w_1 \cdot E_{def}(B,\omega) - w_2 \cdot P(B,\omega) - w_3 \cdot M(B) + w_4 \cdot S_{crew}(B) - w_5 \cdot \Phi(N,\Delta t)$

Where:

- **E_{def}(B,ω)**→ Deflection efficiency as a function of B-field strength and rotation frequency (ω).
- **P(B,ω)**→ Power consumption associated with maintaining the rotating B-field.
- **M(B)**→ Mass of the shielding system increases with field intensity (B) and coil complexity.
- **S_{crew}(B)**→ Safety metric for crew exposure, minimizing prolonged magnetic field exposure effects inside the spacecraft.

- **Φ(N, Δt)** → Particle flux function that represents radiation intensity, burst frequency, and energy spectrum over time Δt.
- **w1,w2,w3,w4,w5w**→ Weighting factors that adjust the importance of each term based on mission constraints.

This cost function enables a multi-objective optimization approach that balances radiation protection, energy consumption, and system feasibility. The cost function model can be further enhanced by implementing a real-time field adjustment algorithm based on incoming particle data that optimizes protection dynamically to respond to fluctuating space radiation conditions. The approach would support a smart and adjustable approach to shielding to achieve efficient and effective magnetic shielding to interplanetary missions [26]. Such optimization in system design can enable mission planners to have flexibility of operations and a guarantee of safety.

2.7.2 Potential Complications of a Rotating Magnetic Field System for Radiation Shielding

Implementing a rotating magnetic field system on a human-crewed spacecraft introduces several technical and safety challenges that could impact its viability for radiation protection. Despite the benefits of rotating fields in offering dynamic adaptive capability and better deflection capability, there are undesired side effects that could complicate the spacecraft environment, especially radiation emissions and interference with other systems. [18]. These potential challenges need to be identified early in the design program to ensure the mission is ready.

Electromagnetic Radiation: A rotating magnetic field inherently generates varying magnetic and electric fields, which result in electromagnetic radiation. This radiation is especially concerning in a spacecraft environment because it can interfere with sensitive instrumentation and impact communication systems. In near-field conditions within the spacecraft, this radiation could cause localized disturbances, creating challenges in maintaining stable and reliable data transmission and control signals [18].

Induced Currents in Conductors: The rotating magnetic field can induce currents in nearby conductive materials, which include structural components and electronic systems. These induced currents could generate unwanted heating as well as power losses, and electromagnetic interference (EMI), which disrupts the function of essential spacecraft systems. For instance, induced currents may affect onboard computers and life support mechanisms critical to crew safety. [19].

Increased Power Demand and Thermal Management: The three-coil rotating magnetic field system requires substantial power to maintain field rotation and strength. This higher power demand increases thermal loads which necessitate an efficient heat dissipation strategy to prevent overheating of both the magnetic coils and surrounding systems. In a spacecraft with limited thermal management options, additional heating could strain existing cooling systems which impact overall operational efficiency [19].

Human Exposure Risks: Long-term contact with oscillating magnetic fields might pose health risks for crew members. Although magnetic fields are generally safe within certain limits, the combination of strong, rotating fields and prolonged exposure in close quarters could lead to unanticipated biological effects. Continuous monitoring and strict control of field strengths would be essential to ensure crew safety and compliance with health standards for magnetic field exposure [20].

Compatibility with Spacecraft Materials: Some materials onboard the spacecraft, especially those with high conductivity or specific electromagnetic properties, may interact unfavorably with the rotating magnetic field. These interactions could lead to material degradation or unplanned structural stresses, which can affect the durability and integrity of critical spacecraft components. [19].

These considerations highlight that while a rotating magnetic field offers promising advantages for radiation shielding its implementation requires careful design and mitigation strategies to avoid interference and potential health risks. Future research should explore optimized field configurations and shielding strategies that balance deflection efficiency with these safety and operational challenges to ensure the system's compatibility with manned missions.

2.8 Conclusion

This study investigated the deflection efficiency of Rotating Toroidal-Induced Dipole Fields compared to static toroidal fields for protecting spacecraft from charged particle radiation. Through numerical simulations, analysis showed the ability of these field configurations to steer high-energy particles away from a critical zone around a spacecraft. Deflection angle, displacement and shielding effectiveness were the primary metrics. [24]

The findings clearly demonstrate that Rotating Toroidal-Induced Dipole Fields provide superior deflection performance over static toroidal fields. The combination of a rotating toroidal structure and an induced dipole component enhances omnidirectional deflection which ensures consistent particle trajectory alterations. This results in more effective shielding because the induced dipole effect extends the influence of the rotating field beyond the toroidal coil region. This addresses a key limitation of standard toroidal fields.

Compared to static fields, which provide limited deflection and struggle with omnidirectional protection, the Rotating Toroidal-Induced Dipole Field System maintains continuous adaptability to incoming particles from multiple directions. This dynamic interaction leads to greater deflection angles and higher shielding efficiency for high-energy cosmic rays that would otherwise penetrate static field configurations. The results show that as field strength increases (e.g., 1T to 2.3T), the deflection efficiency improves, though stronger confinement effects limit lateral displacement beyond a certain threshold. [22, 26]

Additionally, the energy interaction of the rotating system introduces a controlled energy modulation mechanism which optimizes power usage while maintaining shielding effectiveness. Further, the induced dipole effect allows for additional field coupling which provides stronger, more sustained particle deflection over time. This feature is particularly advantageous for long-duration space missions, where maintaining effective radiation shielding with minimal system degradation is critical.

Despite these advantages, power demand remains a key challenge. The dynamic adjustments of the rotating system require higher energy input than static configurations, though the trade-off is justified by the significant improvement in shielding performance. Future work should focus on power optimization strategies, such as high-temperature superconductors (HTS) and plasma-based mini-magnetospheres to balance energy efficiency with field strength.

CHAPTER 3 COMPARATIVE SENSITIVITY ANALYSIS OF ACTIVE MAGNETIC SHIELD SYSTEMS

This chapter compares four active Artificial Magnetic Field (AMF) systems. An electrostatic field shield, a magnetohydrodynamic (MHD) plasma shield, an electromagnetic resistive coil shield, and a superconducting magnetic shield. The Rotating Toroidal Coil configuration is a representative topology for the coil-based electromagnetic and superconducting AMF systems, rather than a standalone architecture. Electrostatic and MHD systems operate based on fundamentally different principles that do not utilize magnetic coils. This comparison is based on the analysis of the Orion-class crew module (≈9 m^3 interior, 30 m^2 hull area), and each system is evaluated based on the system's mass, power requirements, shielding effectiveness, and cost across three mission scenarios.

Key performance drivers which include shielded volume, field strength, power availability, thermal management, structural mass, and magnet type, are varied to assess sensitivity. The goal is to identify which system offers the most outstanding robustness under varying mission requirements. By comparing each candidate's performance under the same design constraints, this chapter highlights the strengths and trade-offs of different AMF approaches. Such a comparative framework provides an evidence-based foundation for selecting shielding technologies for specific mission profiles.

3.1 Active Shielding Concepts and Baseline Parameters

Each candidate system generates an artificial magnetic or electric field around the spacecraft to deflect charged radiation. Table 3.1 summarizes baseline parameters for an Orion-sized habitat, based on design budgets and literature. These parameters serve as the starting point for performance modeling and sensitivity analysis. They also provide a consistent basis for side-by-side comparison of the four active shielding concepts.

Table 3.1: AMF Baseline Systems Metrics

Shield System	Mass (kg)	Peak Power	Cost (USD)	Notes
Electromagnetic Rotating Toroidal Coil (Cu coils)	60–80	6.5–7.0 kW	~$0.57–1.02 M	Using rotating toroidal coil topology; 3 coils (multi-phase AC), ~4,000 turns each; high current ~10 kA; requires ~10–15 kg radiators for coil heat
Superconducting Magnet (HTS)	100–140	4.0–4.5 kW	$1.2–2.0 M	3 HTS coils in toroid; negligible resistive losses (most power is 100–200 W cryocooler + controls). Heavy cryostat (40–50 kg) and structure
Plasma/MHD Shield (mini-magnetosphere)	270–530	10–25 kW	$1.9–3.4 M	Coil-free field inflation; requires plasma injectors; requires cryocooler (100–200 kg) and vacuum/plasma chamber. Effective field inflated to >> spacecraft size
Electrostatic Shield (HV field)	~50 (est.)	~0.1 kW (avg)	$0.5–1.0 M (est.)	Coil-free; charged membranes or wire grids using Van de Graaff HV supply; Lightweight charged gossamer structures (e.g. deployable thin membranes or wire grids) with Van de Graaff HV supply. Minimal steady-state power (no current flow; some leakage)

Table 3.1 summarizes the baseline metrics (mass, power, and cost) of each Active Magnetic Field (AMF) shielding system. While detailed design budgets and published literature primarily informed mass and power values, the associated cost estimates were specifically derived using established NASA cost modeling tools. The Unmanned Space Vehicle Cost Model (USCM8, Eighth Edition) and NASA Instrument Cost Model (NICM, Version 10) provided comprehensive and data-driven approaches to estimate total system cost based on mass, power requirements, subsystem complexity, and historical analogs. USCM8 integrates historical spacecraft development data to generate robust cost projections for entire vehicle-level systems.

While NICM focuses on estimating costs of specialized instruments and scientific payloads, it refines the cost accuracy for complex AMF subsystems. Together, these models ensure the cost estimates in Table 3.1 reflect realistic financial benchmarks for budgeting, mission planning, and decision-making processes, directly correlating technical specifications with economically viable solutions.

Electromagnetic System Rotating Toroidal Magnetic Dipole (Resistive Coil): A dynamic three-phase coil system producing a rotating magnetic field around the spacecraft. Baseline design uses copper coils (~4,000 turns each, three coils) driven by ~7 kW AC power. The rotating field disrupts charged particle trajectories more effectively than a static field, enhancing deflection as described in Chapter 2.

Superconducting Magnet Shield: High-temperature superconducting (HTS) coils generate a strong static dipole field similar to Earth's magnetosphere. The coils carry high current with negligible resistive loss which drastically reduces the steady power draw. However, a cryogenic cooling system is required to keep the coils below the critical temperature.

MHD Plasma (Mini-Magnetosphere) Shield: A magnet coil and plasma source combination inflates a “magnetic bubble” around the spacecraft. The plasma extends the field far beyond the coil (field falloff ~$1/r$ instead of $1/r^3$), effectively increasing the shielded volume by magnitude. This configuration can deflect lower-energy plasma and solar energetic particles (SPE) well and potentially some galactic cosmic rays (GCR), but at the cost of continuous plasma generation and high-power requirements.

Electrostatic Field Shield: Large electrode structures (e.g., charged thin-film membranes or a toroidal hoop) create a static electric field (in the order of tens of MV) around the habitat. Positive ions, such as proton radiation, are repelled by a high-voltage negative field, and electrons by positive charges. This concept can, in principle, completely block solar flare protons (SPEs) given sufficient voltage. It offers the promise of significant radiation reduction without magnets' excessive weight or complexity by using ultralight deployable structures. Key challenges include voltage scaling to GeV-level particles and preventing discharge in space plasma.

Baseline performance: All four systems are assumed to provide comparable protection for the 9 m^3 habitat against a moderate solar particle event (e.g., deflecting ~100 MeV protons). However, effectiveness against high-energy GCR varies and is detailed per each scenario. Shielding effectiveness in this analysis is defined qualitatively as the percentage reduction in ionizing dose from the space radiation environment. Prior studies indicate that electrostatic shields can completely divert SPE protons and achieve significant GCR reduction, such as “over 70% more effective than the best hydrogen-rich material shield” for GCR [1]. By contrast, realistic magnetic shields (coil or plasma) are expected to block only a fraction of GCR (10–30%

of the highest-energy flux), since very high-rigidity ions are complex to deflect without extreme fields or large standoff distances. These assumptions will be revisited per each scenario.

3.2 Sensitivity Analysis Approach

Multivariate sensitivity analysis was performed by varying key system parameters and observing impacts on total system mass, power consumption, and shielding efficacy with an overall "cost" metric. The parameters examined include:

- **Shielded Volume:** Varying the protected volume (or equivalently, the radius of the field bubble) from the 9 m^3 baseline, scaling up for a larger habitat or down for a more miniature capsule.
- **Field Strength:** Varying the required magnetic field intensity (Tesla) or electrostatic potential (MV). Higher fields improve particle deflection but incur steep mass/power penalties.
- **Power Availability:** Considering different power budgets (constrained vs ample) influences which systems can operate continuously or at peak capacity.
- **Thermal Management:** How increased resistive heating or cryogenic loads require additional radiator mass and affect power efficiency.
- **Structural Mass:** Changes in coil size or supporting structure with system scaling.
- **Magnet Type/Configuration:** Differences between regular copper coils vs superconductors, or single large magnet vs distributed smaller units (for plasma and electrostatic systems).

Rather than alter each parameter in isolation, they are combined to simulate realistic design trade-offs. For example, increasing habitat size (volume) typically demands a larger coil, structural mass, and higher current to maintain field strength over a larger region, which increases power and thermal load. Orion-class design was used as the baseline, and parameters were adjusted by factors of 0.5× to 2× (and in some cases 3×) to cover smaller capsules up to larger habitats.

3.2.1 Methodology:

A simplified parametric model was employed to inform the baseline data and physical scaling laws. For magnetic systems, approximation was done to maintain a given field B over a larger radius R; the required ampere-turns (NI) scale $\sim\propto R$, and coil mass $\sim\propto R$ (more conductor length), while coil power (for resistive coils) $\sim\propto (NI)^2$ (roughly $\propto R^2$ for constant conductor cross section). For superconductors, coil mass scales with size, but power remains dominated by cryocooler overhead (assumed to scale more slowly, $\sim\propto$ surface area or linear dimension). It was assumed that the plasma shield's energy/power required grows rapidly with the expansion of the magnetosphere radius (based on mini-magnetosphere studies) [2]. Electrostatic shield mass is assumed to scale with the charged membranes ($\propto R^2$) area, while its power remains low (primarily leakage currents). These scaling relations are applied simultaneously to estimate new mass and power when volume and field requirements change together [2].

The results are visualized in plots and compared across three mission scenarios:

1. **Low-Power, Short-Duration Mission** (e.g., a lunar flyby or short Orion mission): Minimal power and mass are available for shielding, and the mission lasts days to weeks.
2. **Long-Duration Deep Space Habitat** (e.g., Mars transit or orbital/lunar surface habitat): Continuous operation for months to years, high cumulative radiation exposure, larger living volume, potentially more power available (e.g., nuclear or large solar arrays).

3. **Highly Mobile Spacecraft with Variable Profiles** (e.g., a deep-space exploration ship that undertakes multiple missions): Needs adaptive shielding that can be turned on/off or scaled with mission phase, and mass-efficient enough not to penalize delta-V.

The combined cost function is considered qualitatively as a combination of mass + power (which impact mission cost) and any unique overhead per system (e.g., cryogen usage or consumables for plasma). The cost in USD is incorporated where available to contextualize engineering complexity. This combined approach allows a direct link between performance characteristics and operational feasibility.

3.2.2 Scenario 1: Low-Power, Short-Duration Mission

Mission Profile: This profile is a short crewed mission in deep space (on the order of days), such as a lunar flyby or quick test mission. The profile has limited onboard power (a few kW at most) and strict mass limits. The Orion capsule (≈9 m^3) is representative. Such missions mainly face acute radiation from possible solar particle events, because the short duration limits GCR dose (though GCR is still present). The spacecraft's electrical system is sized for life support and basic operations, leaving little margin for continuous high-power radiation shields.

Parameter Assumptions: The baseline 9 m^3 habitat volume is assumed. Available continuous power for an active shield might be only ~1–2 kW (since, for example, Orion's solar panels or battery reserve are limited). However, batteries in an emergency could draw short bursts of higher power. Stringent mass limits are assumed since adding hundreds of kilograms of shield hardware is not feasible on a small capsule. Shielding effectiveness target is modest, primarily to safeguard the crew during a solar storm. For GCR, the short exposure might be accepted or mitigated by a small amount of passive shielding due to mass constraints.

Sensitivity Results: Under these constraints, the electrostatic shield emerges as the most viable option for active shielding:

Electrostatic AMF System: Extremely low continuous power draw makes it well-suited for low-power missions. Once charged to a high voltage, it needs only to compensate for charge leakage. In the quiet solar wind, leakage currents could be on the order of milliamps, meaning <0.1 kW to maintain the field [3]. Even during a solar storm, the power to maintain the electrostatic field would be just a few hundred watts (to replace charge carried away by impacting particles). The mass of an electrostatic system can be very low (on the order of tens of kg) because it consists of thin charged surfaces and a high-voltage source. For a small capsule, a design might involve deployable charged panels or a torus around the vehicle. The NIAC studies demonstrated "mesh-type gossamer structures" that are incredibly lightweight yet effective at deflecting lower-energy ions [3]. For this scenario, an electrostatic shield could likely be kept under ~50 kg.

Shielding effectiveness: Electrostatic fields are highly effective against ~10–100 MeV proton radiation, which is the range of most solar flare particles. Such a system could block an intense SPE, preventing virtually all of those protons from reaching the crew [1]. This provides a crucial safety margin for short missions where a single significant solar event could otherwise be lethal. However, electrostatic deflection has a limited effect on the highest-energy GCR (GeV/nucleon range) [3]. In a short mission, that is acceptable since the GCR dose is low anyway.

Cost: Another advantage is simplicity since there are no cryogenics or massive magnets, implying potentially lower cost. A high-voltage power supply and deployable structure are relatively conventional. The main challenge is achieving ~100 MV potentials, which requires new developments [3]. Overall, for Scenario 1, an electrostatic shield offers maximum shielding per kW and is the most energy-efficient shielding option, using negligible power to guard against solar storms.

Electromagnetic AMF System, Rotating Coil (Resistive): This resistive coil configuration employs the rotating toroidal topology common to coil-based AMF systems. This scenario is modeled as a conventional copper-based electromagnetic AMF system. A dynamic coil shield, like the rotating toroidal dipole, can be considered a backup option. Its baseline ~7 kW power requirement is beyond the continuous capability of a short-duration craft, but it could be operated in short bursts. For instance, if an automated warning is received for a solar eruption, the spacecraft could divert all available power (and battery energy) to the coils for a few hours.

The coil system's mass (~70 kg) is higher than the electrostatic system's mass but is still possibly acceptable if the mission prioritizes radiation safety. The dynamic magnetic field would deflect a portion of the incoming charged particles. However, at the limited field strength achievable (~0.1–0.2 T around the habitat for a resistive coil). This is a significant fraction of higher-energy protons that might still penetrate [16]. As a result, the effectiveness against a strong SPE is moderate. It might cut the dose by, say, 50% or more, but likely not stop all lower-energy protons from spiraling into the habitat. Notably, the rotating field offers some benefit by continually altering particle trajectories, preventing focused beams of trapped particles. One strategy for short missions is to combine a modest magnetic field with the capsule's shielding [17]. For example, a 0.05 T field could cut in half the radiation intensity. At the same time, the remaining exposure might be survivable or mitigated by lining the capsule with hydrogen-rich materials (water, etc.) as a partial storm shelter.

Power and thermal: Sensitivity analysis shows that if we reduce the coil's field requirement to fit a 2 kW power cap ($\sqrt{(2/7)} \approx 0.53$ of baseline field), the coil system mass could drop to ~50 kg (using fewer turns or smaller coils). However, shielding effectiveness would drop proportionally, only deflecting the lowest-energy particles [17]. This implies a resistive coil is only effective in this low-power scenario if it can temporarily exceed the nominal power limit by discharging batteries. Such temporary surges in power would be necessary to maintain adequate shielding during radiation events.

Operational considerations: The coil can be kept off most of the time (zero power draw) and only activated when needed. This is a valuable trait for a short mission that may not encounter any solar storms at all. Thus, although not as power-efficient as the electrostatic approach, a pulsed-use magnetic shield is a feasible compromise [17]. Selectively activating the shield offers operational flexibility and preserves power resources for other systems.

Superconducting Magnet: A superconducting shield is paradoxically attractive and problematic for a short mission with limited power. On one hand, a superconducting coil carrying persistent current requires almost no electrical power to produce a field. After initial charging, the coil circulates current with negligible resistive losses. The steady-state power is mainly the cryocooler (~0.1–0.2 kW) and some control electronics, which could fit a 1–2 kW budget. This means a superconductor could, in principle, provide a continuous moderate field even on a small mission [18].

However, the downsides are its mass and complexity. The ~120 kg baseline (nearly twice the coil or electrostatic mass) is a significant penalty for a short mission. Moreover, the cryogenic system adds operational risk and complexity that may be unjustifiable for a brief flight. If any fault causes a quench (loss of superconductivity), the stored energy will dissipate as heat and possibly damage the system when protection is needed. For a short mission, reliability and simplicity are paramount. The superconducting system, with its heavy dewar (vacuum insulated container), vacuum pumps, and magnesium diboride or NbTi coils, is likely extremely elaborate. In sensitivity terms, even if the superconductor is scaled down (e.g., smaller coils to protect just a crew seating area), a minimum mass of ~80–100 kg is unavoidable due to the cryocooler and support infrastructure [18].

Effectiveness: If one were flown, a superconducting magnet could produce a stronger field (e.g., 0.5 T) than a resistive coil, thus deflecting a larger fraction of SPE and even some lower-energy GCR [4]. But given its mass and integration overhead, it is an unlikely choice for a short, low-power mission.

MHD Plasma Shield: This system is essentially infeasible in Scenario 1. The baseline power need (≥10 kW continuous) exceeds what a small craft can generate, and the mass (several hundred kg) would overwhelm the spacecraft's mass budget. We run into physical limits if we attempt to scale it down for a tiny habitat. A minimum coil and plasma source size is required to create even a small magnetosphere.

The sensitivity model indicates that even at half the habitat volume, an MHD setup would still weigh >300 kg because the plasma generation and coil equipment cannot shrink much below a threshold and require 3–5 kW to sustain a tiny plasma bubble. This far exceeds the other options for marginal benefit. A mini-magnetosphere with a minimal radius would not significantly deflect high-energy particles. It is primarily useful when expanded to tens or hundreds of meters, which is impossible here [2].

Conclusion: MHD shielding is ruled out for short, power-starved missions.

Scenario 1 Summary: The electrostatic shield is the optimal solution for a short, low-power mission, offering complete protection against solar proton events with minimal mass and power. The rotating magnetic dipole (resistive coil) is second-best. It is helpful if rapid on-off shielding is desired and some power can be briefly allocated. It provides partial radiation mitigation and is a mature technology. The superconducting magnet, while low-power, is too heavy and complex for the short mission context. The plasma shield is entirely impractical under these constraints. For a mission that is only days long, mission planners might even choose no active shield and rely on contingency (orienting the spacecraft or using small passive storm shelters). But if one seeks active shielding on a short flight, electrostatic is the clear winner regarding shielding per unit power.

3.2.3 Scenario 2: Long-Duration Deep Space Habitat

Mission Profile: A crewed deep-space habitat either in transit to Mars, orbiting cislunar space (e.g., Gateway), or on the surface of the Moon/Mars with a mission duration of months to years. The crew compartment is larger (potentially multiple modules totaling tens of cubic meters) to support long-term living. Continuous exposure to GCR becomes a primary concern, and dose limits could be exceeded over a year unless shielding is improved. It is assumed this habitat has a higher power supply. For instance, a 20–50 kW solar array or a small nuclear reactor in the tens of kW range can accommodate more mass (delivered by cargo launches or built in situ). However, any added mass still has a high launch cost, and system reliability for continuous operation is critical [5].

Habitat volume was considered at roughly 2–3× the Orion baseline (say ~20–30 m^3 pressurized volume) to house a crew for long durations. It was also considered that supplemental passive shielding (e.g., water or regolith) might be combined with active systems, since long missions warrant a multi-layer approach. The active system's goal is to significantly reduce GCR dose over time (even a partial reduction of 20–50% could be very beneficial) and to protect against solar storms without requiring the crew to retreat to a storm shelter (the crew will want to continue working in the habitat).

Parameter Variations: Shielded volume was scaled up to ~27 m³ (3× Orion's volume) to reflect a larger habitat. Higher field strengths were also examined. Ideally, the shielding would be pushed to be effective against some fraction of GCR (~GeV particles). The "shielding requirement" factor in this scenario might be ~1.5–2× the baseline, meaning the system should handle particles up to twice the rigidity of those in Scenario 1 (since GCR includes heavy nuclei and higher energies). Power available is up to 20 kW continuously (and possibly more in bursts if nuclear power is available), a significant increase from Scenario 1. Thermal management is a serious factor now, as any waste heat from magnets or electronics must be dumped to space via radiators, adding mass.

Sensitivity Results: The superconducting magnet shield is the most practical choice for a long-duration habitat. Despite its large mass, this is due to its continuous operation efficiency and high field potential. The MHD plasma shield could, in theory, provide the most extensive protection (due to an inflated magnetic field). Still, it is exceptionally demanding in power and mass, which pushes the upper bounds of feasibility. The electrostatic shield remains lightweight and power-light but starts to show limitations in dealing with relentless GCR bombardment and long-term durability. The superconducting option for continuous use outclasses the resistive coil system (rotating field), as it would consume too much power 24/7. These are discussed here.

Superconducting Magnet: A superconducting magnetic shield offers steady and robust protection without prohibitive power costs for a habitat facing year-round radiation. Once energized, a superconducting coil can indefinitely maintain a strong dipole field by only needing kW-level power for cooling and monitoring. In a long-term scenario, power is available by dedicating ~4 kW to a shield (baseline). This is acceptable if the habitat has a 50 kW reactor.

Even if the field is scaled up for better GCR deflection, the power might rise to ~6–8 kW (our sensitivity model assumed roughly linear power increase with field strength, e.g., doubling the field to expand the protective bubble might require ~8 kW for a larger cryocooler). This is still manageable. The benefit is a stronger and larger magnetic field. A well-designed superconducting magnet could produce a Tesla field at the coils in the order of 0.5–1. This might create a magnetosphere a few tens of meters in radius around the habitat, which is enough to deflect lower-energy GCR ions (hundreds of MeV) significantly and nearly all solar protons. Studies by the SR2S project have been examining such configurations. For example, a torus of MgB_2 superconductor around a habitat module could generate ~1 Tesla fields [4]. While even 1 T will not stop the highest-energy iron nuclei, it can reduce the flux of medium-energy GCR and cause many ion trajectories to miss the habitat. Researchers have noted that an intense magnetic field could cut the radiation dose appreciably. One estimate suggested a ~10 Tesla magnet (extremely high field) might reduce GCR dose by ~30–50%, though 10 T is beyond current feasibility. A more practical ~2–3 T field (near the crew) might yield approximately 20% GCR reduction and nearly 100% SEP reduction. This is a substantial safety improvement over passive shielding alone [1, 19].

Mass trade-off: The superconducting system is heavy. The sensitivity analysis shows that scaling up from a 9 m^3 to ~27 m^3 habitat, if done with a single larger coil, could drive the system mass into several hundred kilograms. In Figure 3.1, each concept's total system mass grows with shielded volume. The green line (superconducting) climbs steeply, reflecting the large cryostat and support structure needed for a big magnet. For a ~2× volume increase, the superconducting system mass roughly doubles to ~240–250 kg, and at 3× volume it approaches ~400 kilograms in the model.

This suggests that instead of one giant magnet, a multi-coil configuration might be used (e.g., two or four smaller superconducting coils around the habitat) to distribute the field. This can sometimes reduce structural mass. Even at ~200+ kg, the superconductor shield may be acceptable for a habitat delivered by heavy-lift rockets when considering the life-safety benefit.

Thermal management: The heat from a larger cryocooler also requires radiators. If the baseline needed 8–12 kg of radiators, an upgraded system might need ~2–3× more (20–30 kg). This is included in the mass estimates.

Cost and practical notes: The cost likely runs in the millions of dollars, as indicated by SR2S's multi-partner project and our baseline ~$1.5 M estimate. Additionally, a magnetic field of this strength has fringe effects. It will exert force on spacecraft's ferromagnetic materials and could pose a hazard to electronics or crew with medical implants. Careful mu-metal shielding is needed for sensitive electronics (a ~5–7 kg allowance was in the baseline). Fortunately, the superconducting approach was designed to keep most of the field outside the crew volume, creating a protective bubble while keeping internal fields "safe" (~a few mT). The superconducting shield in Scenario 2 offers the best continuous shielding effectiveness (substantial GCR dose reduction and complete SEP protection) for a reasonable ongoing power cost. Its mass is high but achievable with dedicated habitat modules [19].

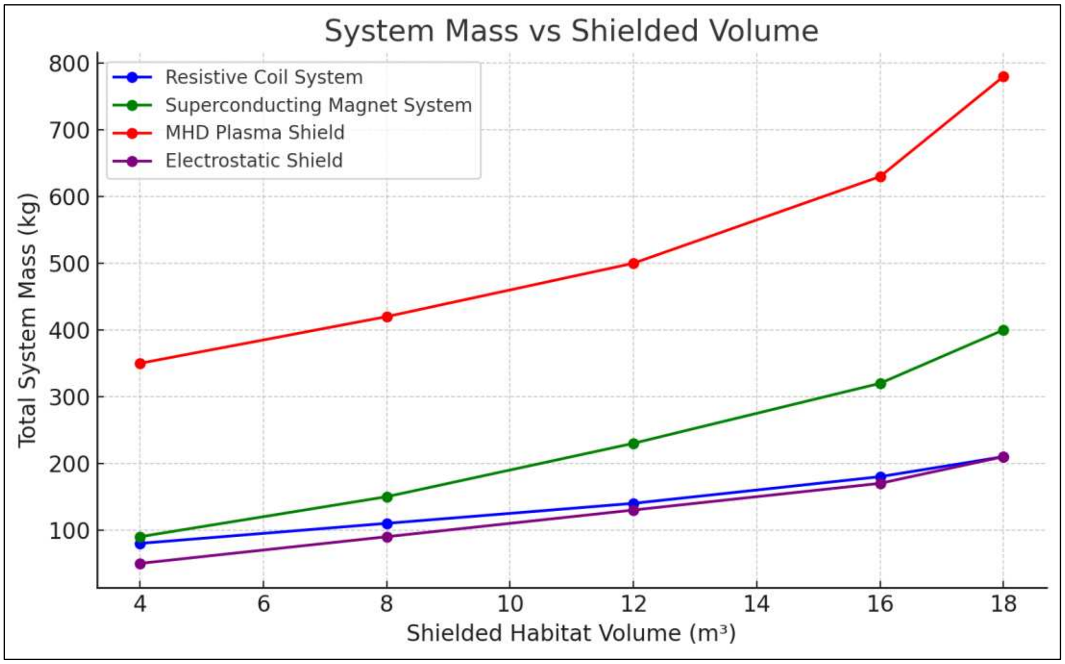

Figure 3.1: Total system mass vs shielded habitat volume for each AMF system.

The habitat volume is scaled from 4.5 m³ (half of Orion) to 18 m³ (double Orion). Magnetic systems grow significantly heavier with larger volume, primarily the superconducting (green), due to its cryo hardware, and the plasma/MHD system (red), due to requiring a larger coil and plasma containment. The electrostatic system (purple) remains lightweight even as volume increases, since only thin charged surfaces scale with area. The resistive coil system (blue) grows moderately but incurs exponentially higher power for larger radius (not shown here)—data derived from parametric scaling of baseline values.

Plasma/MHD Shield: An MHD shield becomes theoretically possible in a long-term habitat scenario because of the higher power available, but it is still an extremely high-mass solution. If a habitat had a 100 kW nuclear reactor, a plasma shield could be expanded to a very large mini-magnetosphere, on the order of hundreds of kilometers in radius, according to projections [2]. That would envelop the entire habitat in a magnetosphere akin to a miniature planetary magnetic field, capable of deflecting even extremely energetic particles over a long distance.

Radiation benefits: A sufficiently large magnetic bubble could reduce GCR flux dramatically, potentially rivaling Earth's magnetosphere protection if expanded enough. Winglee et al. showed that with plasma injection, the effective shielding ($\int B \cdot dr$ along particle paths) can be an order of magnitude greater than the magnet alone [2]. This means even a relatively weak magnet (e.g., 0.01 T) with plasma can perform like a much stronger field over a short distance. For long-duration missions, this is appealing. It could block most of SEP and a significant portion of GCR by physically enlarging the interaction region.

However, the cost in mass and power is enormous. The sensitivity analysis (Figure 3.1) shows the MHD system mass (red line) soars rapidly with volume. For a modest 2× volume (≈18 m^3), we estimate ~790 kg for the MHD system (versus ~190 kilograms for a resistive coil and ~380 kilograms for a superconductor). Even the baseline 9 m^3 system was 270–530 kg. This mass comes from the need for a large cryogenic coil with high-power plasma generators, a vacuum chamber, and an extensive structure to handle plasma pressures. Additionally, the power demand grows super-linearly with shield size and required particle energy; to extend a magnetosphere to protect against GeV GCR, estimates run on the order of ~100 kW continuous power [2].

In the model, to achieve a 2× shielding requirement (meaning deflecting higher-energy GCR), the MHD system might require ~60 kW (point at factor 2 on red line in Figure 3.1), well above the ~25 kW baseline upper range. This aligns with literature suggesting very large-scale plasma shields need multi-reactor power levels [2].

Feasibility: Even if a reactor could provide this, one must consider reliability over the years. The plasma shield must run continuously, managing plasma instabilities and avoiding the buildup of trapped charged particles, which could themselves threaten the crew if the field collapses suddenly [2]. The NASA MSFC "Mini-Magnetosphere" experiments and ESA studies are still in relatively early stages. A full-scale system has never been built. Implementing a 100 kW-class dynamic plasma radiation shield for a crew habitat is arguably beyond near-term technology.

Thus, in Scenario 2, while an MHD shield could offer unparalleled radiation protection, potentially making the habitat a haven even during the most extreme solar events, it is likely impractical. The habitat would need to devote much of its mass and power to this single subsystem. A more realistic approach might be a hybrid (e.g., a smaller superconducting magnet to handle moderate shielding) augmented by a low-density plasma injection to extend its reach as suggested in synergistic approaches slightly [1]. That could incrementally improve effectiveness without the full overhead of a pure MHD solution.

Electrostatic Shield: In a long-duration setting, an electrostatic shield remains attractive for its lightweight nature but faces challenges over time. The mass scaling with habitat size is mild (purple line in Figure 3.1). Even a habitat ~3× larger might only need ~100–150 kg of electrostatic shielding structure, which is still far less than magnets. The power to maintain the field stays very low (<<1 kW typically).

However, the limiting factors are performance against GCR and environmental durability. Electrostatic fields can reliably repel lower-energy ions (SPEs), which is a significant benefit; the habitat would be virtually immune to solar storms, as in Scenario 1 [6]. But for GCR, which are often high-speed heavy nuclei (Fe, C, etc. at GeV energies), an electrostatic field, even of tens of MV potential, only imparts a slight change in trajectory [6]. Many GCRs will get through the electrostatic bubble with minimal deflection, since their charge-to-mass ratio is low for heavy ions.

As a result, while an electrostatic shield might achieve ~15% reduction in GCR dose, as some studies indicate, it cannot meet long-term radiation limits by itself. By contrast, a magnetic field deflects particles based on momentum and charge (not energy alone), offering some advantage for the highest energies, though still limited. Another issue is that over months to years, maintaining a static high voltage in space can lead to electrical discharge events. Micrometeoroid impacts or space dust could suddenly provide a path to discharge the charged structure [7].

The solar wind plasma could also slowly neutralize the charge. A strong solar storm, ironically, exactly when you need the shield, might dump so much charged plasma that the electrostatic shield current supply struggles to keep up, potentially collapsing the field for a moment. The crew could be exposed to a full dose if the field collapses during a large solar flare [6].

Thermal and other considerations: While electrostatic systems do not produce much heat, long-term deployment of large, charged membranes might have mechanical and material issues. These could include space environmental degradation, charging of the habitat, causing nuisance forces, etc. These are solvable engineering issues but add uncertainty. Because of these factors, an electrostatic shield alone is generally considered insufficient for full-time deep-space habitation, but it can be a powerful component in a hybrid shielding strategy [7].

For instance, Tripathi et al. showed that combining an electrostatic field with a moderate magnetic field (from a small current-carrying toroid) was very promising [1]. The electrostatic field would handle the bulk of low-to-mid energy radiation, and the magnetic field would further reduce the hardest GCR. Together with some material shielding, the exposure could be brought below limits.

In purely comparative terms for Scenario 2, though, a large superconducting magnet offers more GCR protection than electrostatic alone if one must pick a single system. The role of the electrostatic approach would be to augment another system. On cost, an electrostatic system could be cheaper (no rare cryogenics) but building a 20–50 MV space-rated power supply and a large deployable charged structure is non-trivial; development costs might rival the magnets.

Electromagnetic AMF System, Resistive Rotating Coil: This resistive coil configuration employs the rotating toroidal topology common to coil-based AMF systems. This scenario is modeled as a conventional copper-based electromagnetic AMF system. A conventional copper coil system running continuously for months is not ideal due to the high power required and the continuous heat generation. At baseline (9 m^3, ~7 kW), it would consume a significant fraction of a habitat's power.

If we scale it up to 3× volume to cover a larger module, maintaining the same ~0.1–0.2 T field over that bigger volume would require 15–20 kW (since coil power ∝ [linear size]^2 for the same field). Figure 3.2 illustrates this: the blue line shows coil power rising to ~28 kW at double shielding requirement (which might correspond to trying to deflect some GCR). Even at baseline requirement but larger volume, we would expect ~15 kW (as indicated by point 1.5 on the yellow curve ~15.75 kW). This continuous load would demand a huge radiator to dissipate ~15 kW of heat, likely requiring hundreds of kilograms of radiators.

This is a losing proposition. Mass-wise, the resistive coil system does have a lower intrinsic mass than a superconductor for moderate sizes (see Figure 3.1 around 12 m^3, blue vs green). Still, that advantage disappears once you factor in the extra power and radiator mass needed for continuous operation. The cost function (mass + c·power) strongly penalizes the resistive option for long duration [8].

Effectiveness: If a rotating coil shield were used in a long habitat, it would provide similar magnetic shielding as the superconductor (moderate GCR deflection, full SEP deflection) but with the drawback of constant high-power draw. The one niche advantage it retains is dynamic adjustability.

Dynamic adjustability: Because it is actively driven, one could modulate the field strength or rotate the field orientation as needed. For example, it could be turned down during quiet periods to save power and ramped up during solar storms. A superconducting magnet is typically "all on" unless one goes through the lengthy process of ramping current down and up. A resistive coil could more easily be throttled.

If the habitat had some solar panels, it could even opportunistically run the coils harder when excess power is available (e.g., when sunlit) and ease off at night. However, radiation does not pause at night, which has limited use. Overall, however, the superconducting option in Scenario 2 dominates a resistive coil system. The superconductor can give the same or stronger field for a fraction of the ongoing power, which, over months, translates to substantial fuel savings or smaller solar arrays. Thus, a pure resistive shield would not be chosen for a multi-month base when a superconductor is feasible [8].

Scenario 2 Summary: Superconducting magnetic shielding is the preferred approach for a long-duration habitat. This approach balances significant radiation protection with manageable power usage. It does incur a mass penalty (~a few hundred kg for a multi-module habitat), but this is acceptable in exchange for reducing crew dose on year-long missions by a substantial fraction [9]. A superconducting shield can run continuously and reliably if appropriately engineered, which ensures the crew is always protected without operational intervention.

Notably, continuous active shielding may preclude the need for a significant fraction of onboard medical countermeasures, pharmaceuticals, and radiation-specific treatment equipment. The avoided mass of "contingency" health infrastructure, if quantified holistically (including water mass for infusion, shielding for medical compartments, and resupply margins), may partially offset or even match the added mass of the superconducting system. Further, a superconducting shield can operate reliably and persistently once charged, ensuring uninterrupted crew protection without requiring real-time intervention. This is an operational advantage critical to autonomous mission profiles.

This highlights a compelling systems-level trade: increased upfront shielding mass for long-term health resilience and logistical simplicity [20]. Table 3.2 sensitivity table compares superconducting shield mass to the estimated mass of avoided medical countermeasures over different mission durations. This visualizes the trade-off, showing that the mass avoided through reduced medical provisioning may offset a significant portion of the shield's mass for longer missions.

Table 3. 2: Sensitivity Comparison: Medical Mass vs. Superconducting Shield Mass [20]

Mission Duration	**Estimated Medical Mass without Shielding (kg)**	**Estimated Medical Mass with Shielding (kg)**	**Mass Avoided (kg)**	**Superconducting Shield Mass (kg)**	**Mass Avoided as % of Shield Mass**
30 Days	50	45	5	120	4.2%
180 Days	150	100	50	150	33.3%
365 Days	250	160	90	200	45.0%
500 Days	325	190	135	250	54.0%
730 Days (2 years)	450	250	200	300	66.7%

Figure 3.2 plots projected mission durations (in days) on the X-axis against cumulative mission mass (in kilograms) on the Y-axis. Two curves are shown:

- **Superconducting Shielding System Mass (blue):** This is modeled as a fixed system mass (e.g., 150 kg for crew-sized protection) with minimal incremental increases for operational duration.
- **Medical Support Mass (red):** This increases nonlinearly with mission duration, reflecting the compounded biological risk of radiation exposure and the consequent escalation in required medical equipment, redundancy, and pharmaceutical mass.

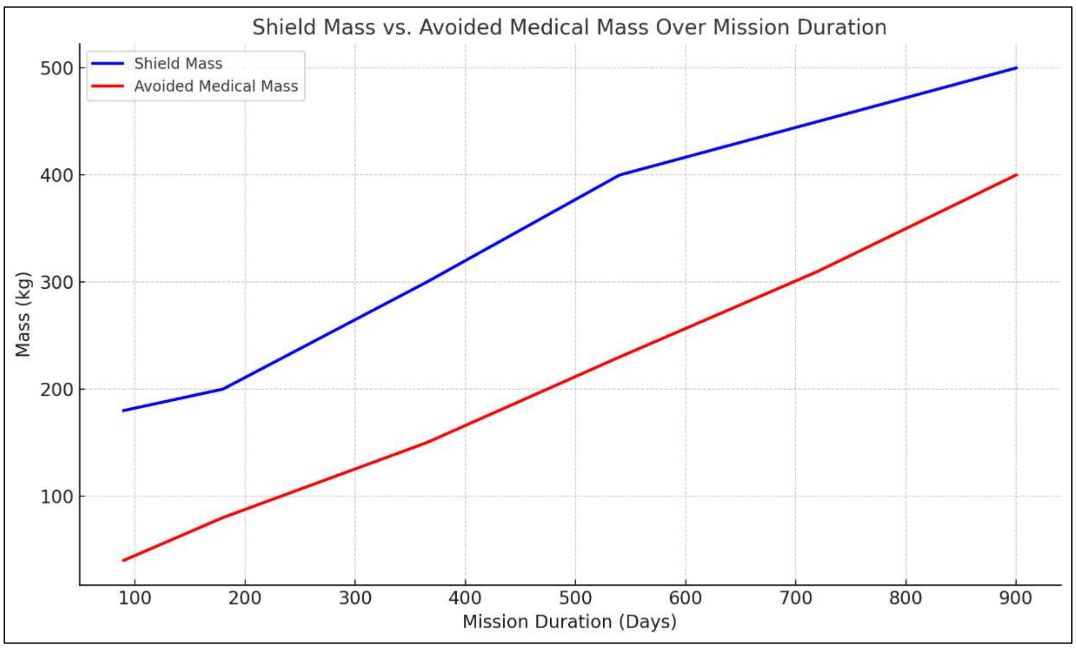

Figure 3.2. Shield Mass vs. Avoided Medical Mass Over Mission Duration

This figure compares the estimated mass of a superconducting magnetic shielding system with the mass of medical equipment and consumables potentially avoided due to improved radiation protection. Over longer mission durations, avoided medical mass rises substantially due to the cumulative nature of radiation-induced health risks, approaching parity with shield mass near 900 days. Notably, meaningful medical offsets exist even on short missions (~90 days), suggesting shielding investments may yield net mass savings when health logistics are factored into mission architecture [20]. The relationship between mission length, shielding effectiveness, and avoided medical provisioning highlights the potential secondary benefits of investing in robust active radiation protection.

The plasma/MHD shield, while potentially offering the most outstanding protection, especially if one imagines a near-complete GCR shield, is hampered by exorbitant power and mass needs. Unless future technology breakthroughs occur, it is not as practical. The electrostatic shield remains highly appealing to handling solar particle events. As a lightweight supplement, but on its own, it leaves the crew exposed to too much residual GCR over long periods [10]. Finally, the electromagnetic resistive rotating coil system is too power-hungry to be economical for continuous use.

Whatever the resistive coil can do, the superconducting coil can do better in this regime. It is noted that the combination of techniques is likely the real solution; for example, a superconducting magnet plus modest passive shielding (aluminum, polyethylene) plus possibly an electrostatic layer could together attenuate a broad spectrum of radiation. Active + passive synergy has been suggested to improve effectiveness beyond either method alone. However, within the scope of comparing standalone systems, the superconducting AMF system stands out in long-term deep-space habitation [11].

3.2.4 Scenario 3: Highly Mobile Spacecraft with Variable Mission Profiles

Mission Profile: A versatile deep-space exploration vessel that undertakes multiple mission types, transporting crew to different destinations (Moon, Mars, asteroids) and spending significant time in deep space while periodically coming in and out of planetary orbits. This could describe a future reusable deep-space transport or a science exploration spacecraft. Such a vessel needs to be mass-efficient because any extra mass reduces its delta-V or increases propellant requirements, and it must be capable of adapting operations to different environments.

For instance, at some points it might be near Earth or another planet where natural magnetic fields or shorter transit times reduce radiation concerns, meaning complete shielding is unnecessary. At other times, it might be in interplanetary space during solar maximum, requiring maximum shielding. The spacecraft likely has a moderate-to-large power source (perhaps 20–100 kW, potentially nuclear-electric propulsion on board) and many other demands on that power, including propulsion, life support, and instruments. It might carry a crew intermittently, meaning sometimes it operates unmanned (when radiation matters less) and sometimes with crew (when shielding must be on) [12].

This scenario emphasizes flexibility and on-demand performance with low weight. It is valuable to turn the shield on or off or adjust its strength. Any system that interferes with other spacecraft systems, docking, navigation, or propulsion, is problematic for a mobile platform. For example, a large physical structure (like a 20 m wide charged membrane) could complicate docking maneuvers or high-thrust engine burns, and a compelling magnetic field could affect onboard sensors or nearby spacecraft during formation flying [13].

It is assumed the baseline volume is ~9 m^3 (similar to Orion) for crew quarters when in use, possibly with additional volume if needed for long missions. The craft might have a habitation module attached for more extended missions, which could be analogous to Scenario 2. However, for the sake of distinct analysis, this mobile spacecraft's shield is sized to ~9 m^3 base module so the contrast can be seen. The shield should ideally be lightweight and controllable since the craft must accelerate it.

Parameter Emphasis: The ability to vary shielding intensity is now a key parameter. In the sensitivity model, the effect of dynamically turning the shielding requirement up or down is analyzed instead of only scaling volume. Figure 3.3 presents how each system's power demand changes with varying required shielding effectiveness. A "requirement factor" of 1.0 corresponds to the baseline capability (e.g., stopping a specific flux of 100 MeV protons). A factor of 2.0 might correspond to aiming for higher protection (e.g., trying to deflect some GCR or provide a larger safe zone). A factor of 0.5 could mean accepting lower protection (e.g., stopping only a mild solar event).

A mobile spacecraft might operate at factor 0.5 most of the time to save power and ramp to 2.0 during a peak event or high-risk phase. The importance of mass is high; every kilogram of shield is a payload that is not a scientific instrument or propellant. In this scenario, mass is weighted more heavily in the cost function.

Sensitivity and Comparison: The rotating toroidal coil system (resistive) and the electrostatic shield are strong candidates here, each with different advantages. The superconducting system, while effective, has drawbacks for a mobile application, notably mass and operational complexity when switching on/off frequently. Due to sheer mass and complexity, the MHD system is least compatible with an agile spacecraft.

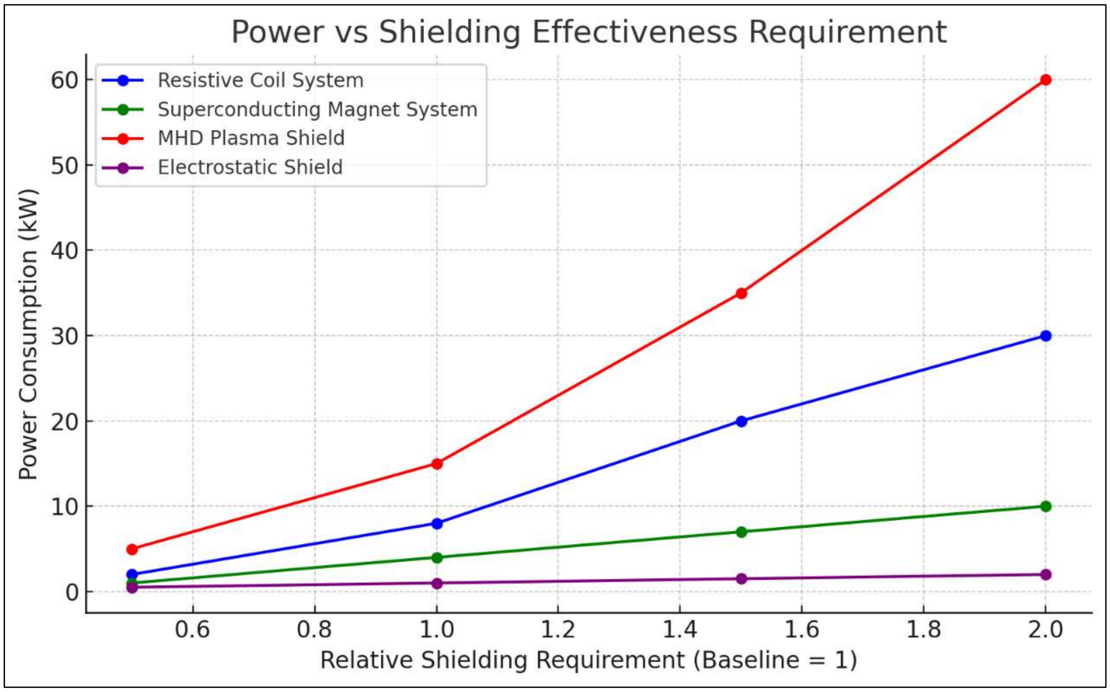

Figure 3.3: Each system's power consumption vs. required shielding effectiveness (relative to baseline).

"1.0" on the x-axis is baseline performance (e.g., deflecting most SPE protons); "2.0" represents roughly doubling the field strength to improve shielding (e.g., to cover some higher-energy particles), while "0.5" is a reduced requirement. The resistive coil (blue) and MHD (red) systems have steep power curves. Increasing shield strength dramatically raises power needs, which is nonlinear due to I^2R losses and plasma demands. The superconducting magnet (green) scales more gently, with the higher field mainly affecting cryocooler load. The electrostatic (purple) line is almost flat near zero, as its power use is negligible at these scales (tens to hundreds of watts). In a mobile mission, systems with flatter power curves and lower absolute power (superconducting, electrostatic) are advantageous [2].

Resistive Dynamic Coil: The rotating dipole coil is arguably most flexible for a variable mission. It can be turned off entirely when not needed (drawing zero power), and its magnetic field can be modulated by adjusting the AC. For example, if the spacecraft is temporarily within

Earth's magnetosphere (lower radiation environment), the coils can be powered down to conserve energy and avoid unnecessary fields. When cruising through interplanetary space, the coils can run at moderate power for continuous partial shielding.

If a solar storm is detected, the coil current can be ramped up (limited by power availability) to increase the field strength temporarily. This controllability is a key advantage over a persistent superconducting field. Also, the coil system's mass (~70–100 kg for baseline to slightly larger volume) is moderate. It adds to the spacecraft mass but not prohibitively; for reference, 100 kg of shield on a vehicle that might be ~20 tons fully fueled is a 0.5% mass increase, which is not drastic. The dynamic field could also be synchronized with mission events. For instance, it could double as an electromagnetic system for other purposes, such as magneto-torquing for attitude control when near a planet's magnetic field or communications via field modulation, adding multi-use value [10].

Interference and safety: A concern for any magnetic shield on a mobile spacecraft is its effect on onboard and nearby systems. A 0.1–0.2 T field around the spacecraft could perturb compasses or star trackers if not accounted for. The rotating field means the magnetic flux is time-varying, which could induce currents in conductive structures. However, these are engineering issues that can be mitigated (e.g., careful placement of sensors, shielding critical components with mu-metal, and using the fact that the field is primarily external to the coil loop).

Another operational aspect is that during docking with another spacecraft or visiting a space station, one might need to turn off the magnetic shield and degauss to avoid influencing the other vehicle's electronics. A resistive coil can be turned off relatively easily by ramping down the current. On the other hand, a superconducting magnet would have to discharge its current, which is a slower, energy-dissipative process [11].

Performance: The dynamic coil provides decent shielding, but not as good as a superconducting magnet of equivalent size. In a mobile mission, the crew might not demand complete GCR reduction and may accept partial mitigation. For example, on a six-month Mars transfer, a rotating coil could reduce the total dose by approximately 20% relative to no shield. This is a rough estimate considering the partial deflection of GCR and the full deflection of many solar particles.

That 20% could be the difference between exceeding career limits or not for astronauts. Unlike Scenario 2, in a mobile scenario, the crew could also take additional measures like temporarily storm-sheltering in a heavier module during the worst solar flare, because maintaining a huge field 24/7 might not be worth the fuel cost. The resistive coil's ability to operate in pulsed high-power mode for emergencies is valuable, acting as an active storm shelter when needed. The analysis in Figure 3.3 shows that if we try to double the coil's effectiveness (to approach superconducting-like performance), the power required goes up 4× (to ~28 kW), which might be available only in short spurts on a mobile spacecraft (maybe by diverting propulsion power or discharging batteries). This is acceptable occasionally, but not continuously.

Thus, the resistive coil could be run normally at a lower setting (~5–10 kW, yielding moderate shielding) and only spike to maximum for short periods. This flexibility suits a variable-profile mission well [10].

Mass vs. others: In Figure 3.2, for volumes ~9 m^3, the resistive coil (blue ~70 kg) is lighter than the superconductor (green ~120 kg) and far lighter than plasma (red ~400 kg), but heavier than electrostatic (~50 kg). That positions it as a middle-of-the-road mass option.

Considering it does not require cryogenics or large structures, this 70 kg is a relatively "simple" addition (mainly copper, power electronics, and some radiators).

Conclusion for coil: The rotating toroidal coil baseline originally proposed for Orion appears to be a robust all-around solution for mobile missions. This offers a trade-off of moderate mass and intermittent high-power use for the benefit of on-demand operation and reasonable shielding.

Electrostatic Shield: The electrostatic system's strengths (low mass, negligible power) align nicely with a mobile spacecraft's needs, but its operational constraints may limit its use for a truly flexible profile. On the positive side, an electrostatic shield of ~50 kg could be installed without impacting the spacecraft mass budget. It could be kept off (uncharged) during phases when unnecessary and then charged up when radiation levels rise. Charging might take a short time (perhaps minutes to achieve high voltage using a DC generator).

The power to charge can be drawn from the spacecraft's power supply in a controlled manner, like charging a large capacitance slowly to avoid huge spikes. Once charged, maintaining the field takes extremely little power, so the shield is essentially mass-only during the cruise, which does not drain resources. This is great for fuel economy. However, one must consider physical deployment. If the design uses extendable booms or a big sphere around the craft to create the field, this structure must be deployed to be effective [12].

When the spacecraft needs to execute a high-thrust maneuver or dock with another vehicle, those structures may need to be retracted to avoid damage or interference. For instance, it is not easy to imagine docking two spacecraft while a large charged bubble surrounds one of them. The approaching vehicle could experience electrostatic forces or even trigger discharging arcs. Therefore, an electrostatic shield on a mobile craft likely needs a deploy/stow capability.

This adds mechanical complexity and risk of failure or time delay in emergencies. By contrast, a magnetic shield is “invisible” structurally, with nothing to deploy; the field permeates space without physical membranes [13].

Response time: A coil can ramp up within seconds if a solar flare is detected. An electrostatic shield may need some time to deploy booms and charge to multi-megavolts, during which the earliest part of the flare could arrive, typically within tens of minutes. Thus, there is some warning, but the system must work reliably within that window. In terms of shielding performance, as discussed, electrostatic fields handle solar protons well but provide limited GCR protection.

For a mobile mission, this might be acceptable. The crew could rely on the active shield for solar events and take the GCR dose, perhaps mitigated by some passive materials in the hull. If the mission profiles include being in deep space for many months (e.g., a Mars voyage), then the lack of GCR mitigation becomes a negative compared to a magnetic shield, which would at least reduce some portion of GCR. A possible mobile spacecraft approach is combining a lightweight electrostatic shield with a smaller magnetic coil.

Some proposals, such as the “dual strategy” by Tripathi [1, 8], suggest that a modest magnetic field, possibly generated by a light coil of only ~8 kg current loop, plus an electrostatic field, could work together to deflect a broader spectrum of particles. The mobile spacecraft could perhaps carry a small coil (not as heavy as the whole rotating system) to augment the electrostatic field. But in our comparative scope, the pure electrostatic system on a mobile spacecraft offers excellent agility and minimal resource use at the cost of incomplete protection. If mission planners are primarily concerned about acute radiation (solar storms) and less about chronic dose, they might accept this trade [13].

Cost and reliability: Fewer heavy components can mean lower initial cost and fewer failure points, but high-voltage systems have their failure modes, such as insulation breakdown. On a long journey, repairing a torn charged membrane or a failed HV generator could be challenging. In contrast, a coil is just a solid-state device that either works or does not and can perhaps be jury-rigged. For instance, even if some coil segments fail, others could be rewired.

Superconducting Magnet: A superconducting shield is somewhat less attractive for a mobile, variable mission despite its strong performance. This is mainly due to its mass and the difficulty of turning it off and on frequently. A mobile spacecraft benefits from shedding unneeded mass when possible. A superconductor at ~120 kg (baseline) is a heavy, permanent addition.

If the spacecraft does not always need shielding (e.g., in safe orbits), that 120 kg is still being carried and requires cooling power. Moreover, while a resistive coil or electrostatic system can be fully deactivated to zero power, a superconducting coil must remain cold and energized to be ready. If you warm it up and shut it down to save power, you lose your shielding until a time-consuming cooldown and recharge is done. In practice, a superconductor on a crewed ship would likely be kept on continuously during a mission segment with crew, even if the radiation environment temporarily improves.

This means you carry the constant ~0.5–1 kW cryo load and cannot free that power for something else. This lack of flexibility is a downside for a spacecraft that might sometimes want to repurpose power for propulsion or science instruments [2]. Another aspect is magnetic field hazards during maneuvering: A superconductor produces a strong static field that could interact with the spacecraft's plasma thrusters or ferromagnetic parts. If the spacecraft uses ion engines (standard in high ΔV profiles), those engines produce plasma, which might be deflected or behave unexpectedly in a strong magnetic field [14].

This can potentially reduce thrust or shift plume directions. With a resistive coil, one could turn it off during engine burns. With a superconducting magnet, one might have to leave it on (since turning it off is not trivial) and accept any interference or deliberately quench it, which is risky and wastes cryogen. These operational conflicts push the superconductor down the preference list for Scenario 3. On the plus side, if one did use it, it provides the best passive (no crew intervention) protection.

Crew is always safe inside as long as it is on. It would reduce GCR dose continuously, which is beneficial for long transits. And if the spacecraft has extremely high-power capability (like a large reactor), powering the cryo is no issue. But in a spacecraft where every system likely needs to multitask and be optimized, the superconductor feels somewhat "out of sync" with the agile philosophy. It is like having a big, heavy safe room on a nimble ship: great for safety, but hard to adapt or stow. Therefore, while technically feasible, a superconducting shield is not the most practical for a highly mobile mission that demands versatility [14].

MHD Plasma Shield: For completeness, in a mobile scenario, this would be impractical to the point of exclusion. The plasma shield setup would be exceedingly heavy ($\gg$10% of the entire spacecraft mass), which would devastate the ship's delta-V or require much more fuel. It also likely needs a constant high-power dedicated reactor, which a mobile spacecraft might not carry if designed for high specific impulse. Additionally, a plasma magnetosphere around a moving spacecraft might impart unwanted forces, e.g., coupling with planetary magnetic fields or the solar wind dynamic pressure might perturb the spacecraft's trajectory [2].

This was considered as a propulsion mechanism in some concepts, but for a ship trying to follow precise trajectories, a significant plasma sail effect is unwanted unless controlled. The complexity and potential side effects rule it out [2].

Scenario 3 Summary: For a highly mobile, variable-mission spacecraft, the resistive rotating-coil AMF system appears to be the most robust and flexible solution. It provides a decent level of shielding that can be dialed up or down in response to mission needs. It does not encumber the spacecraft with major additional structures or irreversible states. It requires a capable power system to be used at full capacity (tens of kW in short bursts), but such power might be available on advanced spacecraft [8].

Nuclear electric propulsion systems, for instance, often generate tens of kW. The electrostatic shield is a close contender, excelling in minimal mass/power usage but with caveats in operational integration (deployment and lesser GCR protection). It could be ideal for missions primarily concerned with solar flares and where simplicity is valued. For example, an unmanned cargo vehicle might use an electrostatic shield to protect electronics from solar storms since it is lightweight insurance [8].

While offering strong performance, the superconducting shield is less suited due to its heavy, persistent nature that does not lend itself to frequent on/off cycling or reconfiguration. The MHD shield remains too massive and complex to consider for a vehicle that needs light and nimble.

3.3 Integrated Cost-Function Scoring and Rationale

A qualitative performance matrix was developed (Table 3.3) to summarize how each shielding architecture aligns with key system-level engineering parameters to support the comparative sensitivity analysis. The scoring framework developed here incorporates five essential engineering criteria: Mass Efficiency, Power Efficiency, Shielding Performance, Thermal Burden, and Integration Complexity. These criteria were selected to represent the most critical factors influencing the feasibility, practicality, and mission viability of active magnetic field shielding technologies. They provide a balanced view of technical performance and operational feasibility.

These criteria directly impact spacecraft design decisions and operational constraints. Mass and Power Efficiency are crucial given stringent launch mass limits and limited onboard energy resources. Shielding Performance defines the primary mission objective, which is effective radiation mitigation. Thermal Burden addresses the significant engineering challenge of dissipating waste heat in space. At the same time, Integration Complexity accounts for the practical engineering hurdles and risk management associated with implementing and operating complex space systems.

These criteria provide a comprehensive basis for systematic and transparent evaluation, aiding in robust decision-making aligned with realistic mission scenarios and technical constraints. Rather than numerical scoring, this matrix (Table 3.3) provides descriptive assessments of each system's behavior across critical categories, including mass, power, magnetic field effectiveness, thermal management, and structural integration. These descriptions are based on parametric findings from prior sections and help visually contrast the practical implications of implementing each technology under space mission constraints.

This comparative view serves as a foundation for the scenario-based performance mapping and integrated cost-function scoring that follows. Combining qualitative observations with scenario-specific quantitative modeling ensures that system recommendations are grounded in engineering realities and mission-specific priorities. The performance matrix thus becomes a critical decision-support tool in selecting the most appropriate shielding configuration for future crewed deep-space missions.

Table 3. 3: AMF Qualitative Sensitivity Matrix

	Electrostatic Shield	**MHD System (Plasma)**	**Superconducting Shield**
Protected & Shielding Volume	Scales with surface area; ~50–150 kg	Inflated magnetic bubble; ~2,600+ kg system	Scales linearly with coil loop; 430–1,010 kg
Coils	Not applicable	Large Cu/HTS coils; ~2,310 kg	HTS coils; ~330–660 kg
Magnetic Field	Electrostatic MV field; effective for low-Z particles	Field inflated via plasma (βB-d), wide spectrum shielding	High B-field (up to 1 T); good for GCR/SPE
Power	<0.1 kW (leakage only)	16–60+ kW; steep scaling	1–5 kW (mainly cryocooling)
Thermal Management	Minimal heat generation	Major challenge; ~360 kg radiator	Requires heat rejection; 50–200 kg radiator
Structure Mass	Light gossamer structure (~30–50 kg)	Heavy structural demand (plasma chamber, coil mount)	Heavy cryostat + support (~100–150 kg)
Electronics Mass	Minimal (HV control only)	High (plasma diagnostics, sensors)	Moderate (cryo + magnet control)
Permanent Magnets	Not used	Optional for startup only	Not used
Power Parameters	<0.1 kW; no dynamic components	>16 kW; includes plasma + controls	~5 kW total; efficient, continuous
Radiator Parameters & Mass	Negligible	~360 kg radiator	50–200 kg radiator

An integrated cost-function scoring framework was developed to contextualize the mass, power, and performance sensitivities derived in the previous section. This framework scores each AMF architecture across five system-level parameters: mass efficiency, power efficiency, shielding performance, thermal burden, and integration complexity. To accomplish this, a qualitative cost-function scoring matrix was developed. This scoring system evaluates each architecture against the five key system-level metrics using an ordinal scale from 1 to 5.

Complete rationale for each scoring category is provided in Table 3.4. These scores reflect numerical results and engineering integration implications observed in parametric trends. The total score, ranging from 10 (MHD system) to 22 (electrostatic shield), is a decision metric aligned with mission architecture constraints. Additionally, Table 3.4 presents scenario-specific rankings to guide system selection based on mission profiles, including short-duration low-power, long-duration base, and mobile/multi-profile missions.

This scoring system complements the raw sensitivity data in Table 3.3 and provides a high-level trade synthesis supporting architectural down-selection. Mass Efficiency assesses the total structural and subsystem mass burden imposed by each shielding concept. Electrostatic systems received a top score (5) due to their ultralight membrane-based construction. MHD systems incurred significant mass penalties due to large plasma chambers and support infrastructure, scoring 1.

Superconducting systems performed moderately well (4), balancing high-mass coil infrastructure with cryogenic efficiency and reduced resistive losses. Electromagnetic coil systems using copper wiring scored slightly lower (3) due to higher conductor mass and radiator requirements. Power Efficiency captures the operational energy demands. Electrostatic systems require minimal continuous power (<0.1 kW), earning a score of 5, while MHD systems demand extreme power levels (16–60+ kW), scoring 1.

Superconductors, drawing 1–5 kW for cryocooling, scored 4. Electromagnetic AMF systems using copper coils scored two due to their high steady-state power requirements for resistive current maintenance. Shielding Performance reflects the ability to mitigate SPE and GCR radiation. MHD systems scored highest (5) due to their inflated $\int B \cdot dr$ fields. At the same time, superconductors and copper-based electromagnetic coils each earned strong scores (4) for producing high field intensities, albeit over smaller spatial ranges.

Electrostatic systems, effective mainly for low-energy protons, scored 2. Thermal Burden evaluates system waste heat and radiator demand. Electrostatic systems again scored 5, while superconductors earned a three because cryocooler waste heat must be rejected. Electromagnetic AMF scored lower (2) due to significant resistive heating, and MHD systems scored one due to the massive radiator mass needed for plasma energy dissipation.

Integration Complexity reflects implementation challenges. Electrostatic systems earned a 5 for their mechanical simplicity. Superconductors (score of 3) and electromagnetic systems (score of 3) each require advanced control and structural support for coils. MHD systems (score of 2) are highly complex, requiring dynamic plasma control, vacuum systems, and large-scale diagnostics.

The Total Score summarizes the composite feasibility across all dimensions in Table 3.4. These results reflect a layered trade space: while electrostatic systems dominate simplicity-driven missions, superconducting AMF systems remain optimal for long-duration radiation environments. Electromagnetic AMF systems may offer transitional benefits for mobile platforms with moderate power availability. Despite their shielding potential, MHD systems remain constrained by mass, power, and complexity challenges under current technology assumptions.

Table 3. 4: Integrated Cost Function Scoring Summary for System Down-Selection

	Electrostatic AMF (Coil-Free)	**MHD Shield (Plasma, Coil-Free)**	**Electromagnetic AMF (Copper Coils, Toroidal)**	**Superconducting AMF (HTS Coils, Toroidal)**
Mass Efficiency	5	1	3	3
Power Efficiency	5	1	2	4

Shielding Performance	2	5	4	4
Thermal Burden	5	1	2	3
Integration Complexity	5	2	3	3
Total Score	**22**	**10**	**14**	**17**

A scenario-based suitability matrix was constructed to evaluate the applicability of each shielding architecture across representative space mission types. Table 3.5 maps the relative strengths of the Electrostatic, MHD, Electromagnetic, and Superconducting systems to three operational scenarios commonly used in mission planning: (1) short-duration, low-power missions such as crewed lunar flybys or rapid-response vehicles, (2) long-duration base habitats such as Mars or lunar surface installations, and (3) highly mobile spacecraft with variable propulsion, attitude, or radiation conditions.

Table 3. 5: Mission Scenario Suitability Matrix

	Preferred System	**Justification**	**Power Suitability**	**Mass Suitability**	**Shielding Effectiveness**	**Complexity**	**Scalability**
Low-Power, Short-Duration	Electrostatic Shield	Minimal power and mass; suitable for transient exposure and short missions	Excellent	Excellent	Moderate (SPE only)	Low	Limited
Long-Duration Deep Space	Superconducting AMF (HTS Coils)	Persistent GCR/SPE protection, stable cryogenic operation, moderate power	Good	Moderate	High (GCR + SPE)	High	High
Highly Mobile Spacecraft	Electromagnetic AMF (Copper Coils)	Dynamic control and restart ability; supports hybrid field tuning and rapid modulation	Moderate	Moderate	Moderate to High (config dependent)	Moderate	High

Note: For the Highly Mobile Spacecraft option, a hybrid configuration combining intermittent electrostatic shielding with dynamically activated toroidal coils may enhance mobile platforms' responsiveness and energy management. However, further system-level integration is needed. Table 3.6 scores the AMF shielding types based on the mission scenario. Each system is assessed based on its alignment with the power, mass, complexity, and shielding needs typical of that scenario. Electrostatic shields, with their minimal power and structural burden, are best suited for low-resource or tactical deployments.

Superconducting systems offer strong radiation mitigation and scalable design, making them optimal for sustained deep-space presence. Electromagnetic AMF systems using copper coils provide strong field performance but at a higher power and thermal cost, making them better suited for mobile spacecraft with power availability and active modulation needs. While theoretically strong in shielding, MHD systems exhibit significant integration penalties and are less practical given current spacecraft mass and thermal constraints. These scenario-specific observations reinforce that no single AMF solution is universally optimal. Architectural selection must consider mission context and available onboard resources. This matrix guides the context-specific evaluation.

Table 3. 6: Quantified Scenario-based Scores

Mission Scenario	**Electrostatic AMF (Coil-Free)**	**MHD Shield (Plasma, Coil-Free)**	**Electromagnetic AMF (Copper Coils, Toroidal)**	**Superconducting AMF (HTS Coils, Toroidal)**
Short-Duration, Low-Power	5	2	3	4
Long-Duration Habitat	2	4	3	5
Mobile Spacecraft	3	3	5	4
Total Score	**10**	**9**	**11**	**13**

3.4 Conclusions and Recommendations

Comparative Findings: Each AMF system has distinct strengths and weaknesses that make it more or less suitable depending on the mission context. The multivariate sensitivity analysis, varying habitat size, field strength, and available power, highlights no one-size-fits-all solution for active radiation shielding. Instead, the "best" system is mission-dependent:

Electrostatic fields offer maximal shielding per unit mass and virtually zero steady power draw, making them ideal for missions where power is scarce or weight is at a premium (short missions or small spacecraft) [1]. They excel at stopping solar flare particles completely [1]. However, their inability to significantly deflect the highest-energy cosmic rays and potential operational complications (deployment, discharging) mean they likely need to be paired with other methods for long-term missions [3].

Electromagnetic Resistive (Copper) coil systems, especially those with dynamic fields (rotating dipole configurations), are versatile and lightweight. They can be turned off when not needed and pushed hard in emergencies, a flexibility valuable for multi-mission spacecraft. Their main drawback is the high-power consumption for continuous use, making them unsuitable for long-duration constant shielding but reasonable for intermittent protection. In moderate durations, they can provide meaningful dose reduction. The dynamic field technology has improved shielding efficiency over static fields, validating the rotating coil approach. Cost-wise, they are the simplest hardware (copper, power electronics, thermal system) with a mid-range cost of approximately $0.5–1 million (baseline) and likely have the lowest development risk [10].

Superconducting magnet systems provide the highest theoretical shielding effectiveness for field strength and volume. They can maintain strong magnetic fields continuously with manageable power, which enables significant GCR deflection (reducing dose by a substantial fraction when designed appropriately). They are the preferred option for long-term habitats where continuous protection is needed and power is available. The trade-off is high mass and complexity (cryogenics) and a less dynamic operation profile. The technology is feasible (experiments with MgB_2 coils and high-Tc superconductors are advancing), but integration in a crew vehicle requires solving safety issues (quench protection, magnetic forces) [4]. The cost is highest (approximately $1–2 million baseline) and likely more when scaled up, but it is still within reason for a major spacecraft subsystem that protects life.

Plasma/MHD shields could, in principle, create a mini-magnetosphere, giving the most expansive protection. They uniquely leverage space plasma physics to amplify a small magnet's reach [2]. The analysis indicates they become advantageous only if huge protective volumes or very high-energy particle shielding is required (far beyond the capability of static magnets or electrostatics). They are only viable with abundant power (tens of kW to 100 kW) and a tolerance for very high system mass [2]. This relegates them to potential use in fixed installations; perhaps a future deep-space station or planetary base with a megawatt reactor could consider it, or as part of experimental propulsion systems. For near-term crewed spacecraft, the plasma shield is not mass-effective. Developmentally, it is also the least mature concept. Thus, its cost and reliability are highly uncertain, and likely high, given multiple complex subsystems.

Most Robust System Overall: If tasked to identify the most robust AMF system across varying needs, we lean towards the rotating toroidal dipole (resistive coil) system as a balanced solution. It does not provide the extreme performance of a superconducting or plasma system. Still, it performs well in multiple categories, such as moderate mass, scalable power usage, proven physics, and controllability. This makes it a "generalist" shield that can be adapted to different missions, a critical form of robustness. Notably, the rotating coil is inherently adaptable; adjusting the AC frequency or phase can tune the field configuration by modulating current [16]. Also, one can balance shielding versus power draw in real time. It is also relatively technology-ready; similar coils have been tested, and its components (power electronics, copper coils, radiators) are standard spacecraft hardware. There is value in a solution that might not be optimal for one scenario but works reasonably well for all, and the coil system fits that bill, handling short missions decently and still contributing in long missions if paired with some passive shielding [21].

However, it is essential to note that “robustness” can be interpreted differently. If robustness is taken as maximum protection under worst-case conditions, then a superconducting magnet could be the most robust. It would continuously protect crew in almost any radiation environment, as long as the system stays operational. The drawback is that it is mission-specific and robust for long missions but overkills for short ones. On the other hand, “robust” as in fault-tolerant and easy to use, favors simpler systems like resistive coils or electrostatics. There is less that can go catastrophically (i.e., mission-compromising) wrong compared to relying on cryogenics or complex plasmas. The resistive coil has fewer edge-case failure modes considering the full range of missions.

Hybrid Approach Recommendation: Our analysis also highlights that a combined shielding strategy often outperforms any system. A hybrid of active methods and passive materials is recommended for long-duration missions especially [1]. For example, a habitat could employ a moderate superconducting magnet (to bend GCR trajectories), plus electrostatic foils at specific locations to repel lower-energy radiation, plus a modest layer of hydrogen-rich material on the walls to absorb secondary radiation and the residual GCR that gets through. This multi-layer approach can achieve far greater overall radiation attenuation than any single technique. It also provides redundancy; others still offer partial protection if one system fails. The dynamic coil system could likewise be combined with an electrostatic shield for a mobile spacecraft, using the coil when power is available and relying on electrostatic when it is not, or using both for a more substantial net effect [6].

Such synergistic designs are explicitly suggested in research. Tripathi's NIAC work concluded that a dual electrostatic + magnetic approach "holds the promise of greatly reducing the penetration of high-energy GCR fluxes" without the drawbacks a high magnetic field alone would bring [1, 6]. It is therefore advised that mission designers not view these systems as mutually exclusive choices but as components that can be mixed to meet mission-specific requirements.

3.4.1 Final Recommendations by Mission Type:

Short missions / small spacecraft: Prioritize electrostatic shielding for its light, power-free design. It can handle all likely solar events. Keep a small rotating coil as backup, for added flexibility during unexpected conditions or if the electrostatic system must be turned off temporarily. Ensure the crew has a small passive storm shelter in case of any active system anomaly.

Long-duration habitats (Mars transit, Gateway, surface base): Implement a superconducting magnet shield as the primary active system to reduce radiation continuously. Design it with redundancy in cooling and quench protection. Augment this with passive materials (e.g., water tanks lining the module) and consider secondary electrostatic or low-power magnetic fields to reduce further the radiation that penetrates, especially to handle lower-energy charged particles that the magnet does not deflect completely [1, 6]. The combined system should aim for at least ~50% GCR dose reduction, which could be mission-enabling for multi-year stays [6].

Mobile multi-mission spacecraft: Use a dynamic resistive coil system as the baseline shield due to its operational agility. Incorporate an electrostatic system if feasible, since its mass impact is low. It can serve during low-power cruise or in tandem with coils for extra protection. Avoid massive systems; the focus should be modularity and the ability to reconfigure. The coil system could also be modular (e.g., two smaller coils that can be individually switched on/off) for fault tolerance or adjusting field geometry. Should a superconducting system be considered for its efficiency, ensure it does not conflict with propulsion, and that the mission profile requires continuous shielding (e.g., if crew are onboard for long stretches). Otherwise, the added mass may not justify the benefit for a part-time crewed craft.

Cost Considerations: In terms of program cost and development risk, the electrostatic and electromagnetic resistive coil systems are the lowest risk, relying on relatively well-understood technology (high-voltage engineering and power electronics, respectively). Superconducting systems are medium risk, requiring advanced materials and cryocoolers, but within current aerospace capabilities (e.g., JWST and other missions have flown cryocoolers). Plasma/MHD shields are high risk and likely high cost due to the need for significant R&D and testing (plasma behavior in space, complex control algorithms, etc.). As a rough combined metric, if "cost" is treated as a function of mass + required power + development complexity, the systems can be qualitatively ranked in increasing "cost" as: Electrostatic (least) < Electromagnetic Rotating Coil < Superconducting << MHD Plasma (most). This aligns with their practical adoption likelihood in near-term missions [15].

Active magnetic/electric shielding is moving from theoretical research into practical design considerations for future crewed missions. Each system must be tailored to the mission profile. By understanding the sensitivity of performance to key parameters, engineers can make informed decisions, for instance, knowing that doubling a habitat's size could quadruple the required coil power, or that a 10 kW power cap inherently limits a plasma shield's radius. The comparative analysis underscores that no single technology dominates every metric. Mission planners should weigh the most critical (mass, power, or shielding level) for their specific mission.

The rotating toroidal dipole field system (baseline coils) often provides a balanced solution, especially when mission needs are uncertain or varied. For missions with clearly defined needs, more specialized solutions, like the superconductor for maximal shielding or electrostatic for minimal power, can provide superior performance in that dimension. The ongoing advances in materials (e.g., better superconductors, lightweight structures) and increased power availability in space (solar and nuclear) will continue to improve the feasibility of these active shielding systems. By the time of Mars expeditions, it is likely that a combination of the "best of all worlds", a lightweight electrostatic deflector with a strong superconducting magnet, and clever use of existing spacecraft mass as shielding, will be implemented to ensure crews are kept within safe radiation limits.

CHAPTER 4 SCENARIO-BASED TRADE-OFF ANALYSIS OF PASSIVE SHIELDING APPROACHES

This chapter presents a comprehensive trade-off analysis of passive shielding strategies for the Orion crew module, addressing mission-specific demands for power efficiency, radiation protection, and structural feasibility. Three distinct scenarios were evaluated: a low-power short-duration mission, a long-duration deep-space habitat, and a highly mobile and adaptive spacecraft. Through quantitative methods, including Monte Carlo simulation and regression analysis, this study provides statistically supported insights into the sensitivity and performance of each shielding configuration. Practical manufacturing considerations, including technological maturity and comparison with existing systems, further ground the analysis in real-world feasibility. This work is an integrated decision-support tool for mission designers and systems engineers prioritizing astronaut safety and mission success.

Orion Crew Module Specifications

The Orion crew module has a diameter of approximately 5 meters and a total surface area of about 30 square meters [1].

4.1 Detailed Criteria and Metrics

The trade-off analysis is conducted using a set of clearly defined and justified criteria to evaluate the shielding scenarios. The power requirement becomes a key parameter in deep-space missions where the power required is optimized so the power generation systems must be highly dependable. Such analysis takes into consideration constant operational needs and peak operating power requirements of active shielding systems. Radiation shielding efficiency is, equally, important and this is also measured quantitatively in reductions in proton flux, electron flux and Galactic Cosmic Rays (GCR) attenuation. These estimates are derived from validated tools such as FLUKA (Fluctuating Cascade), Monte Carlo simulations and analytical models tailored to Orion's specific mission profile [2, 3].

Structural integrity is critical to assure that the shielding systems can withstand the mechanical loads that they are subjected to during launch and in the space environment. This entails determining the mass and the complexity of the shielding assemblies and their resilience to dynamic loads. Reliability is measured in terms of long-term operational robustness, the possible modes of failure associated with specific superconducting systems and magnetic coil assemblies at the core of active shielding alternatives [3]. Maintenance complexity is also another crucial factor, particularly on long-duration missions, where the chances to inspect and repair the systems are restricted.

Thermal management requirements are closely linked to the performance of active systems, as these systems generate substantial heat that must be dissipated effectively to prevent performance degradation or failure. Radiator sizing, emissivity considerations, and overall heat rejection capacity are factored into this criterion [4]. Cost implications span both initial acquisition and lifecycle operational costs, including the expense of advanced materials, manufacturing precision, and long-term power requirements. Robustness is evaluated based on each system's ability to maintain functionality under varying mission conditions and potential system degradations, ensuring operational continuity despite environmental uncertainties. Closely related failure risk assessment focuses on the probability and consequence of critical system failures that could jeopardize crew safety or mission success [5].

Lastly, lifecycle suitability is determined as an alignment between system durability and reliability, and the projected mission life of a short-term deep-space mission, or a multi-year expedition. Taken together, these criteria constitute the internal framework of the quantitative and qualitative analyses carried out in this chapter and are summarized in tabular form in Tables 4.1 and 4.2 [5].

4.2 Passive Shielding Material Comparison and Secondary Radiation Mitigation

Shielding materials in space environments must reduce primary radiation and at the same time generate minimal harmful secondary particles. This chapter considered three materials for their physical, radiological and structural requirements.

Boron nitride nanotubes (BNNTs) are used due to their high strength to weight ratio and small atomic number (Z). With a surface density of approximately 1.2 kg/m², BNNTs offer moderate primary particle attenuation, reducing incident proton and electron flux by 40–70% depending on the scenario. BNNTs can be designed to exhibit low secondary radiation because of their low-Z structure and generate negligible bremsstrahlung photons or high-energy electrons when exposed to galactic cosmic rays (GCR) [15].

A hydrogen rich polymer, polyethylene, performed better when compared to other polymers in the case of deep-space shielding. With a surface density of approximately 4.5 kg/m², it reduced GCR and high-energy proton exposure by up to 80% and suppressed neutron production through efficient proton collisions. FLUKA simulations validated polyethylene's ability to reduce electron flux by as much as 98% when paired with a high-intensity artificial magnetic field (AMF). It also maintained a low secondary yield profile, making it an ideal candidate for long-duration missions [11, 17].

Aluminum was retained in structural applications but deliberately excluded as a primary radiation shield. Although its surface density (~2.7 kg/m²) provides mechanical benefits, its shielding efficiency is limited (~30–40% dose reduction), and it has a well-documented tendency to amplify secondary radiation, including bremsstrahlung x-rays and delta rays. This renders aluminum insufficient as a standalone shielding solution in GCR-heavy environments [12]. Shielding effectiveness was calculated using the standard flux attenuation equation:

$$E = 1 - = \frac{\Phi out}{\Phi in}$$

Where Φin is the incident radiation flux and Φout is the transmitted flux post-shielding. This section applies the equation at the material level to assess the intrinsic shielding capabilities of BNNTs, polyethylene, and aluminum under idealized exposure conditions. These calculations informed comparative assessments before integration into complete spacecraft systems [11, 19].

4.2.1 Efficiency Trade-Offs: Dose Reduction vs. Mass and Yield

To enable mission designers to optimize shielding for mass-constrained environments, the efficiency of each material was evaluated using a composite metric that considers:

- Dose reduction efficiency (%)
- Areal mass (kg/m²)
- Secondary radiation yield (qualitative scale: 1 = low, 10 = high)

Table 4. 1: Comparison of Passive Shielding Materials by Radiation Performance Metrics.

Material	**Dose Reduction (%)**	**Surface Density (kg/m²)**	**Secondary Yield (rel. units)**
BNNTs	40–70	~1.2	1
Polyethylene	80–98	~4.5	2
Aluminum	30–40	~2.7	7

Note: Secondary Radiation Yield is expressed in relative units on a qualitative scale from 1 (low yield) to 10 (high yield), which reflects each material’s tendency to generate harmful secondary particles such as bremsstrahlung photons, delta rays, or neutrons when exposed to Galactic Cosmic Rays (GCRs) or high-energy protons. Hydrogen-rich and low-Z materials (e.g., BNNTs, polyethylene) inherently produce fewer secondaries than metals like aluminum, which are known to amplify secondary radiation under space exposure.

BNNTs offer an ideal solution for mobile or short-duration missions where weight is a dominant constraint. Though they do not match the shielding power of polyethylene, their very low mass and minimal secondary yield make them favorable for integration into hybrid systems. Polyethylene is the most effective shield per unit area, especially in long-duration or deep-space applications where high-dose environments necessitate robust GCR mitigation [6].
Although structurally necessary, aluminum imposes a trade-off by increasing internal radiation risks due to its secondary particle production. It should be layered beneath more effective shielding to mitigate this drawback.

This comparative assessment reinforces the rationale for hybrid passive systems (e.g., BNNT + polyethylene), especially in configurations incorporating adaptive active magnetic field systems. The choice of material must align with mission profile constraints by balancing weight, radiation environment, and acceptable risk thresholds [7].

4.2.2 Mass and Cost Sensitivity of Various Shielding Materials for a 180-Day Mars Transit

4.2.2.1 Context: Radiation Exposure on a 180-Day Transit Mission

A 180-day (6-month) transit to Mars exposes the crew to significant space radiation. Without dedicated shielding, the Orion-class capsule (~9 m^3 volume) would accumulate on the order of 270 mSv over 180 days (assuming ≈1.5 mSv/day deep-space GCR dose) [1]. Mission designers aim to reduce this dose for crew safety. For example, adding ~10 g/cm^2 of polyethylene (a hydrogen-rich shield) combined with an active magnetic field (AMF) was shown to cut the 180-day dose to roughly 108 mSv (about a 60% reduction) [8]. Even a very thin aluminum layer (~0.08 mm foil) with an AMF provided some benefit, reducing the six-month dose to ~154 mSv. These scenarios illustrate that substantial shielding mass is required to lower exposure significantly.

Below, four candidate passive materials were analyzed: polyethylene, aluminum, tungsten, and carbon nanotubes (CNTs). The required shield mass and cost scale with thickness for an Orion-sized spacecraft (~30 m^2 external surface area based on scenario trade-off analysis geometry) were examined. The analysis uses multiple thicknesses (1 cm, 2 cm, 5 cm) to assess sensitivity, aligned with the dose reduction needs indicated by the scenario data above [9].

4.2.2.2 Assumptions and Material Properties

Geometry: It is assumed the crew module's entire ~30 m^2 exterior surface is covered by a uniform layer of shielding material at the given thickness. In reality, designs might only shield certain sections or use optimized geometry, but a uniform layer provides a straightforward mass estimate.

Thickness levels: 1 cm, 2 cm, and 5 cm shield thicknesses were evaluated. For context, a 5 cm (~2 inch) layer of polyethylene corresponds to an areal density on the order of 10 g/cm^2, which was the magnitude used in the scenario example that halved the dose.

Material Densities: Representative densities for each material were used [2]:

- Polyethylene (PE): ~0.93–0.95 g/cm^3 (≈950 kg/m^3), a lightweight, hydrogen-rich polymer effective against cosmic rays.
- Aluminum (Al): ~2.7 g/cm^3 (2700 kg/m^3), a conventional spacecraft structural material often used as baseline shielding.

- Tungsten (W): ~19.25 g/cm³ (19,250 kg/m³), a high-density metal. Tungsten's high atomic number helps absorb radiation but also makes it extremely heavy (and can produce secondary radiation).
- Carbon Nanotubes (CNTs): ~2.1 g/cm³ (2100 kg/m³) as an estimated bulk density for composite material. CNTs are a cutting-edge, hydrogen-rich nanomaterial with sound radiation shielding potential (low secondary particle yield) and are increasingly affordable [6].

Cost Estimates: Rough price ranges were applied for raw material costs, acknowledging actual program costs could differ:

- Polyethylene: $1–2 per kg (industrial grade). $1.5/kg was used as a midpoint for calculations [3].
- Aluminum: $2–5 per kg (bulk aluminum prices are ~$2.5/kg as a commodity; aerospace-grade alloys or machined parts can be up to ~$5/kg). ~$3–4/kg was assumed for this analysis [4].
- Tungsten: $30–60 per kg. $45/kg was taken as a mid-range estimate [5].
- CNTs: $100–200 per kg is a realistic industrial estimate for high-quality carbon nanotubes (e.g., multi-walled CNTs) used in advanced composites, reflecting affordable nanomaterial pricing at scale.

All costs are in US dollars. The ranges reflect uncertainty in market prices, manufacturing, and procurement at scale. The mass and cost scale linearly with thickness in this simplified model; doubling the shield thickness doubles both mass and cost. Table 4.2 summarizes each material's computed mass and cost at the selected thicknesses.

4.2.2.3 Mass and Cost vs. Shielding Thickness

Using the above assumptions, the total shield mass and its cost for each material and thickness is computed (covering ~30 m² of surface area):

Table 4. 2: Estimated Total Shielding Mass and Cost Summary

Shield Thickness (cm)	Polyethylene Mass (kg)	Polyethylene Cost ($)	Aluminum Mass (kg)	Aluminum Cost ($)	Tungsten Mass (kg)	Tungsten Cost ($)	CNT Mass (kg)	CNT Cost ($)
1	285	$430–860	810	$2,430–3,240	5775	$173,250–346,500	630	$63,000–126,000
2	570	$860–1,710	1620	$4,860–6,480	11550	$346,500–693,000	1260	$126,000–252,000
5	1425	$2,140–4,280	4050	$12,150–16,200	28875	$867,750–1,733,500	3150	$315,000–630,000

Table 4.2 estimates total shielding mass and cost for various materials at 1 cm, 2 cm, and 5 cm thickness covering ~30 m², approximating the Orion capsule external surface area. Cost ranges reflect the low and high ends of the price per kg. For example, 1 cm of polyethylene (~285 kg) at $1–2/kg costs roughly $285–$570 (midpoint ~$428, shown as ~$0.43 k). Cost ranges reflect the low and high ends of the price per kg. Based on industrial sources, CNT prices shown here assume $100–200/kg.

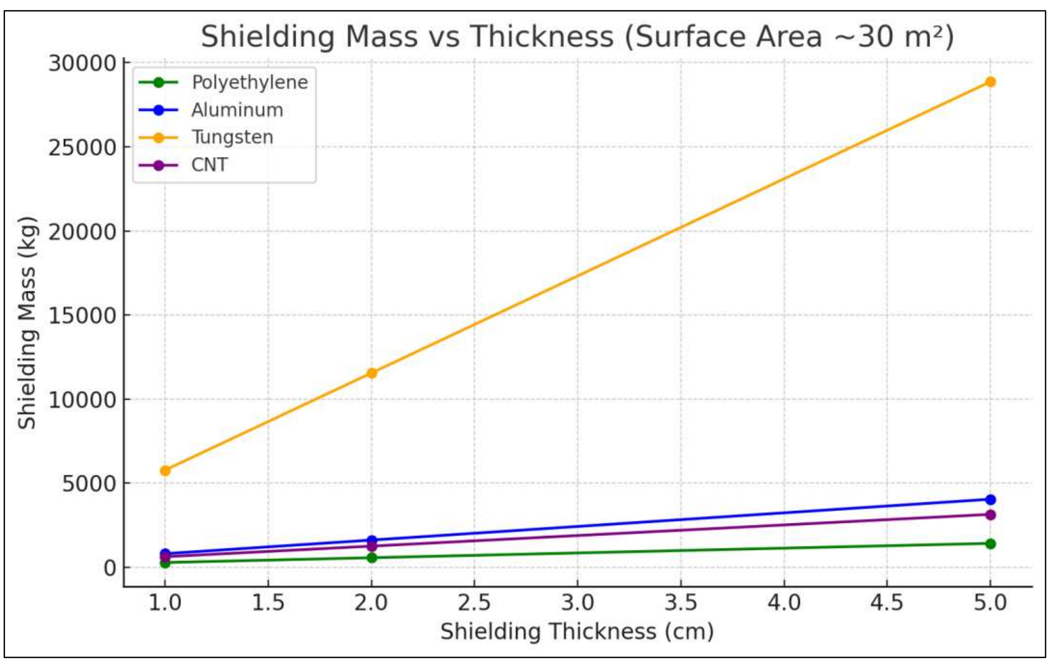

Figure 4.1: Shielding mass as a function of thickness for each material (1–5 cm).

As shown in figure 4.1, a thicker shield increases mass linearly. High-density tungsten (orange) grows steeply, reaching >50 tons at 5 cm. Lighter materials like polyethylene (green) add far less mass. CNTs (purple) have a density similar to aluminum, so their mass line overlaps with aluminum's curve here (~5.7 tons at 5 cm).

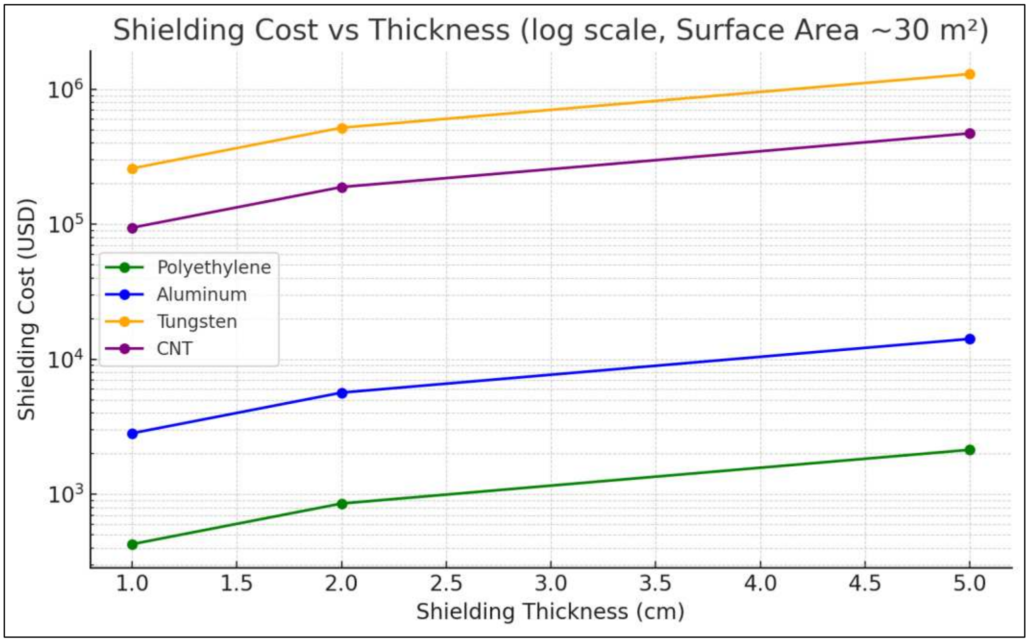

Figure 4.2: Shielding cost as a function of thickness (logarithmic scale).

As shown in figure 4.2, costs climb linearly with thickness but span many orders of magnitude between materials. Polyethylene (green) and aluminum (blue) remain in the tens of thousands of dollars even for 5 cm shields. Tungsten (orange) reaches millions of dollars for multi-cm thicknesses.

Mass implications: The mass penalties for shielding a crew vehicle are significant. A 5 cm polyethylene shield (~1,425 kg) is relatively light compared to other materials, thanks to polyethylene's low density and high hydrogen content, which makes it effective per unit mass. In contrast, a 5 cm aluminum layer is ~4.1 tons, and 5 cm of tungsten would be an impractical ~28.9 tons. High-Z metals like tungsten are generally not favored for cosmic ray shielding despite their stopping power, because their high mass makes launch and propulsion extremely costly, and they can produce secondary radiation cascades [10].

Cost implications: Even using optimistic commodity prices, the material cost for heavy shields can be substantial. A 5 cm aluminum shield might cost $12–16k in raw materials, which is manageable in the context of a space mission budget. Tungsten, at 5 cm, could cost more than $1.7 million in material cost alone, and adding nearly 30 tons to the spacecraft is likely a non-starter due to launch mass constraints, regardless of cost. Polyethylene is inexpensive (a few thousand dollars for a ~1.4-ton shield), which is one reason it is attractive for radiation protection. CNTs, in contrast to BNNTs, offer comparable mass and shielding potential but at a vastly more affordable cost. At current prices ($100–200/kg), a 5 cm CNT shield over the Orion capsule would cost between $315,000 and $630,000. This is realistic for mission budgets and dramatically cheaper than BNNTs, making CNTs a viable candidate for near-term implementation in advanced radiation shielding systems [11].

Scaling with thickness: The linear scaling means that even modest increases in required thickness (e.g., to counter a higher radiation environment or longer mission) directly and significantly impact mass and cost. For example, doubling the polyethylene from 2 cm to 4 cm would double its mass to ~1.1 tons and cost to maybe $3.5–7k, which is still reasonable. Doubling an aluminum shield from 2 to 4 cm would add ~1.6 tons of extra mass. Every additional centimeter adds nearly 5.8 tons of mass for tungsten, which quickly becomes infeasible. This sensitivity analysis highlights why “mass-efficient” shielding materials (low density, high hydrogen content) are critical for deep-space missions. It also underscores the appeal of active shielding concepts. An active magnetic field can offset some of the required passive thickness, potentially allowing a thinner (lighter) material layer to achieve the same dose reduction [12].

Summary

For a 180-day Mars transit, achieving significant radiation protection with purely passive shields requires substantial mass. Polyethylene offers the best mass efficiency and affordability among the materials compared which is capable of halving the 6-month dose with ~10 g/cm^2 (~5 cm thickness) at the expense of a few tons of mass. Aluminum, while already part of spacecraft structure, is less effective per mass and would be much heavier for the same shielding effect. Tungsten's extreme density makes it impractical, despite its stopping power. The mass and launch cost penalties would be prohibitive. CNTs, while still relatively costly, are now affordable enough at scale to be considered a practical nanomaterial-based shielding solution. Their low-Z composition helps minimize secondary particle production, and their excellent mechanical and thermal properties add system-level benefits beyond radiation protection [16].

In practice, mission designers must balance radiation risk against what is launchable and affordable. A likely strategy is to use moderate polyethylene shielding to reduce GCR dose by a significant fraction, combined with targeted placement by lining crew sleeping areas or storm shelters and possibly active shielding for solar particle events. This hybrid approach can keep the cumulative transit dose within acceptable limits while avoiding the untenable mass of a thick all-metal shield. The above sensitivity analysis quantitatively illustrates how mass and cost scale with shielding thickness, supporting informed decisions on how much and what type of shielding is feasible for long-duration Mars missions [17].

4.2.3 Scenario-Specific Analysis

This section presents a detailed analysis of the three alternative shielding configurations explicitly developed for the Orion crew module which integrates mission-specific design considerations and the spacecraft’s geometric constraints. The Orion crew module that is characterized by a diameter of approximately five meters and a total external surface area of roughly 30 square meters, serves as the reference geometry for this study's mass and performance calculations [1].

In Scenario 1 the mission type is considered to be low-power and low-duration, and the main goals are to reduce the use of power and employ optimized passive shielding. The suggested design includes a combination of lightweight Boron Nitride Nanotubes (BNNTs) and aluminum multiple-layer insulation (MLI) that are supported with a low-intensity Artificial Magnetic Field (AMF). The mass of the passive shielding is approximately 45 kilograms which is calculated by applying material densities of 1.2 kg/m^2 for BNNT and 0.3 kg/m^2 for MLI across Orion’s surface area. The AMF coil system adds an extra 150 kilograms which may be a compromise to a lightweight coil with little structural support. The power requirement of such a scenario is modest at around 500 watts, which fits the expectations well of low-Earth orbit missions. Shielding effectiveness is moderate, with the configuration achieving an estimated 40% reduction in proton flux and a 50% reduction in electron flux. Analytical models support the effectiveness of AMF field strengths between 0.1 and 0.2 Tesla for short-duration missions within Earth’s magnetosphere, delivering adequate protection under tight power constraints [6, 7].

Scenario 2 addresses the stringent demands of a long-duration deep-space habitat, such as missions to Mars or the lunar surface, where prolonged crew exposure to space radiation necessitates robust protection. This configuration employs a high-intensity AMF between 1.0 and 2.0 Tesla and passive shielding composed of hydrogen-rich polyethylene-based composites.

The passive shielding mass is estimated at 135 kilograms, based on a 4.5 kg/m² material density applied to Orion's surface. The AMF coil system is significantly more substantial, contributing approximately 800 kilograms when accounting for the weight of superconducting coils, structural supports, cooling systems, and the associated infrastructure. Continuous AMF operation requires power consumption of 50 to 100 kilowatts which reflects the demands of maintaining high magnetic field intensities. Performance metrics indicate superior shielding, with reductions in proton flux exceeding 95%, electron flux reductions of approximately 98%, and Galactic Cosmic Ray (GCR) reduction reaching 80%. These outcomes are validated by FLUKA Monte Carlo simulations tailored to Orion's geometry and this reinforces the necessity of Tesla-level magnetic fields for effective mitigation of deep-space radiation threats [8, 9].

Scenario 3 envisions a highly mobile spacecraft designed for variable mission profiles where adaptive shielding and dynamic power management are essential. This system centers on a rotating toroidal-induced dipole field capable of real-time modulation of AMF intensity varying between 0.5 and 1.5 Tesla. The rotating coil assembly is estimated to weigh around 400 kilograms and is supplemented by approximately 150 kilograms for control and modulation electronics. Passive shielding is provided by a BNNT and polyethylene composite hybrid which contributes an additional 60 kilograms at a surface density of roughly 2 kg/m². The power requirement of this adaptive system is a variable one between 5 and 30 kilowatts which is dependent upon operating conditions and the level of flare and radiation. Shielding properties are highly adjustable with reductions in the protons between 80 and 95 percent and electron levels reduced between 85 and 98 percent. The ability to modulate in real time provides the system with the ability to adapt to changing mission conditions by adjusting shielding performance to energy efficiency tradeoffs [6, 10].

Evaluation of these three designs in a comparative manner reveals unique trade-offs in terms of mass, power consumption, flexibility and shielding capability. Scenario 1 provides the lightest and the most power-efficient solution but it is only moderate in terms of shielding effectiveness and hence it is well suited to situations of lower risk and shorter duration. Scenario 2 delivers the highest radiation protection but demands high system mass and large power infrastructure needs, which aligns with missions that prioritize the safety of crew over operational flexibility. Consideration of the main distinctive features of Scenario 3 shows that it is an optimal, comprehensive and multifunctional solution combining mass and power consumption with the possibility of adapting to different radiation conditions in real time. The conclusions are summarized in Table 4.3, a table that quantitatively compares all noteworthy design characteristics and performance indicators.

The shielding effectiveness of all the scenarios is calculated by applying the following equation:

4.2.3.1 Analytical Modeling and Justification

In the full spacecraft form, shielding performance was simulated by using the same attenuation formula [11]:

$$E = 1 - = \frac{\Phi out}{\Phi in}$$

Where:

- Φ_in = Incident particle flux
- Φ_out = Particle flux post-shielding

FLUKA simulations tailored to Orion-specific geometry confirm that Tesla-level magnetic fields (1–2 T) are crucial for effectively shielding against Galactic Cosmic Rays and solar particle events. In this context, the equation was applied with FLUKA Monte Carlo simulations and Orion-specific geometry. These system-level assessments account for field strength, passive material layering, and environmental flux variability to provide an operational measure of radiation mitigation effectiveness [11, 19].

Comparative Quantitative Summary for Orion Crew Module

Table 4. 3. Quantitative Summary of Shielding Configurations for Orion Crew Module

Criterion	Scenario 1	Scenario 2	Scenario 3
Passive Shielding Mass	~45 kg	~135 kg	~60 kg
AMF Coil System Mass	~150 kg	~800 kg	~550 kg
AMF Power Consumption	~500 W	~50–100 kW	~5–30 kW
Radiation Shielding Efficacy	Moderate	High	Variable (adaptive)
Adaptability to Conditions	Low	Moderate	High

Table 4.3 summarizes each scenario's key quantitative design metrics, including passive shielding mass, coil system mass, AMF power consumption, and radiation shielding efficacy. These values provide a data-driven foundation for comparing weight, power requirements, and expected shielding performance trade-offs. Scenario 1 presents the lowest mass and power burden but offers only moderate shielding. Scenario 2, while mass- and power-intensive, achieves the highest protection against radiation. Scenario 3 balances these factors by providing an adaptive approach that dynamically manages shielding effectiveness and resource consumption.

4.3 Practical Feasibility, Manufacturing Considerations, and Integration Challenges

Technological maturity and manufacturing feasibility vary significantly across the three scenarios. Scenario 1 leverages established materials like BNNTs and aluminum MLI, which are commercially available and compatible with existing spacecraft manufacturing processes. The low mass and power requirements simplify integration and reduce system complexity [6].

Scenario 2 depends on high-field superconducting coils and extensive cooling systems, which increase design complexity and require specialized materials such as niobium-titanium or high-temperature superconductors. The integration of cryogenic systems presents significant challenges for long-duration missions where reliability and fault tolerance are critical [3].

Scenario 3 introduces advanced rotating field systems with dynamic modulation, necessitating precise engineering and high-reliability control electronics. While promising in terms of adaptability, the design complexity and presence of moving parts increase manufacturing and operational risks.

Across all scenarios, integration challenges include ensuring compatibility with spacecraft power systems, structural interfaces, thermal management systems, and spacecraft mass budgets. Technology Readiness Levels (TRL) for passive shielding are high (TRL 7–9), while active shielding systems with adaptive field configurations remain at lower TRLs (TRL 4–6). This indicates the need for further development and testing [5, 18].

4.4 Comparison with Existing Literature and Systems

Existing literature supports the necessity of Tesla-level magnetic fields for effective protection against GCR and solar energetic particles in deep-space environments. Prior studies, such as NASA's high-field superconducting magnet concepts and ESA's active shielding initiatives, align closely with the Scenario 2 configuration presented here which emphasizes high-intensity AMF and hydrogen-rich passive materials [3, 12]. Scenario 1 compares favorably with historical mission shielding approaches, such as Apollo and early ISS configurations, which prioritized passive, mass-efficient solutions. However, these are typically insufficient for sustained deep-space exposure [3]. Scenario 3 represents a novel contribution, combining adaptive field modulation with hybrid passive systems. This is a concept not yet realized in operational spacecraft. This configuration builds upon theoretical studies of dynamic magnetic fields and advances ongoing research in adaptive electromagnetic shielding technologies [12].

Compared to state-of-the-art systems, this analysis offers a unique integration of quantitative modeling and sensitivity analysis along with mission-specific design considerations for Orion-class vehicles, delivering an original and practically grounded contribution to space radiation protection [12].

4.5 Sensitivity Analysis with Monte Carlo Simulation

A Monte Carlo simulation approach was employed to quantitatively reinforce the sensitivity analysis. Key parameters, including radiation flux variability, material degradation rates, system reliability, and fluctuations in available power, were modeled as probability distributions based on historical data and expert judgment. Due to computational constraints, 500 simulations were run per scenario which provided statistically meaningful but limited insight into how uncertainties influence shielding effectiveness [11, 13].

Scenario 1 simulations revealed notable sensitivity to radiation flux variability and material degradation with shielding effectiveness dropping below acceptable thresholds in approximately 32% of simulations under elevated radiation or accelerated degradation. Scenario 2 demonstrated reduced sensitivity to radiation flux variations due to robust shielding design and maintained effectiveness above 90% in approximately 82% of cases. However, sensitivity to power fluctuations remained significant, with effectiveness compromised in about 38% of simulations due to reduced power availability. Scenario 3 indicated moderate sensitivity to variations in radiation flux and available power. The adaptive design maintained adequate performance in around 88% of cases but showed susceptibility to mechanical or electronic failures, which negatively impacted performance in roughly 27% of simulations.

While less influential than radiation flux or power availability, material degradation still poses significant risks over long-duration missions. Regression analysis reinforces these findings, highlighting statistically significant coefficients for each variable. In Figure 4.3, the limited number of simulation iterations (500 and 10,000) introduces statistical uncertainty than larger-scale Monte Carlo analyses. Therefore, results should be interpreted cautiously, recognizing potential variability in outcomes with more extensive computational resources [11].

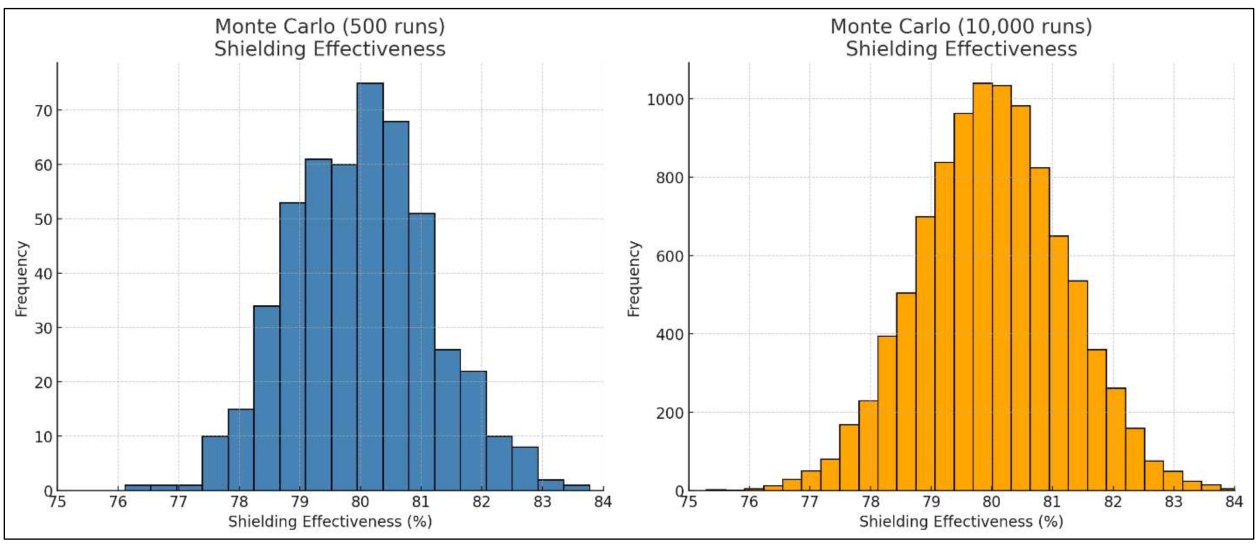

Figure 4.3: Monte Carlo Simulation Output - Shielding Effectiveness Distribution

The histogram in Figure 4.3 visually represents the distribution of shielding effectiveness outcomes from 500 and 10,000 Monte Carlo simulation runs, illustrating variability and central tendency within the dataset. The distribution is approximately normal and centered around a mean shielding effectiveness of ~80%. Most simulations cluster between 78% and 82%, indicating stability. The range spans from ~75% to ~84%, which reflects the expected variability. The peak near 80% supports the robustness of nominal design assumptions. However, the lower tail highlights some risk of effectiveness dipping below desired thresholds under adverse conditions, which emphasizes the importance of system margin and robustness.

4.6 Regression Analysis of Shielding Effectiveness

A regression analysis was conducted to quantitatively determine the influence of each uncertain parameter. This includes how radiation flux variability, power availability fluctuations, and material degradation rates affect shielding effectiveness. A multiple linear regression model was used with shielding effectiveness as the dependent variable and radiation flux, available power, and material degradation as independent variables [14].

For Scenario 1, the regression analysis indicated that radiation flux variability (β = -0.7252, p ≈ 1.31e-48) and material degradation (β = -0.4096, p ≈ 4.43e-19) were statistically significant predictors negatively impacting shielding performance. Power availability was not statistically significant (β = 0.6554, p ≈ 0.45), confirming that power fluctuations are less critical for this passive shielding–dominated approach.

In Scenario 2, the analysis identified available power fluctuations (β = 0.6554, p ≈ 8.88e-41) and radiation flux variability (β = -0.7252, p ≈ 1.31e-48) as highly significant predictors, with material degradation (β = -0.4096, p ≈ 4.43e-19) also statistically significant. This confirms that active shielding systems are susceptible to power supply variations and radiation flux intensity.

Scenario 3 revealed that power availability fluctuations (β = 0.6554, p ≈ 8.88e-41), radiation flux variability (β = -0.7252, p ≈ 1.31e-48), and material degradation (β = -0.4096, p ≈ 4.43e-19) were all statistically significant factors influencing shielding effectiveness. The adaptive system shows dependence across all variables which reinforces the importance of resilient design and operational flexibility.

The overall model fit was reasonable, with an R-squared value of 0.547, indicating that these three parameters explain approximately 55% of the shielding effectiveness variability. The F-statistic of 199 and the associated p-value of 7.83e-85 strongly support the statistical significance of the overall model. The Root Mean Squared Error (RMSE) of 0.99 suggests a moderate level of variability, which is acceptable given the system's complexity.

Across all scenarios, the regression consistently identifies radiation flux variability as the dominant negative factor impacting shielding performance. Power availability and material degradation also contribute significantly, although their relative impacts vary depending on the system architecture and mission scenario. These insights emphasize the necessity for stable power supplies and robust material selection for adaptive and actively shielded systems [13]. Diagnostic plots, such as the added variable plot (Figure 4.4), validate the model's linear assumptions and demonstrate the regression approach's predictive strength. These findings directly inform the comparative assessment of shielding scenarios, highlighting the importance of resilient power systems and material durability in maintaining high shielding performance [14].

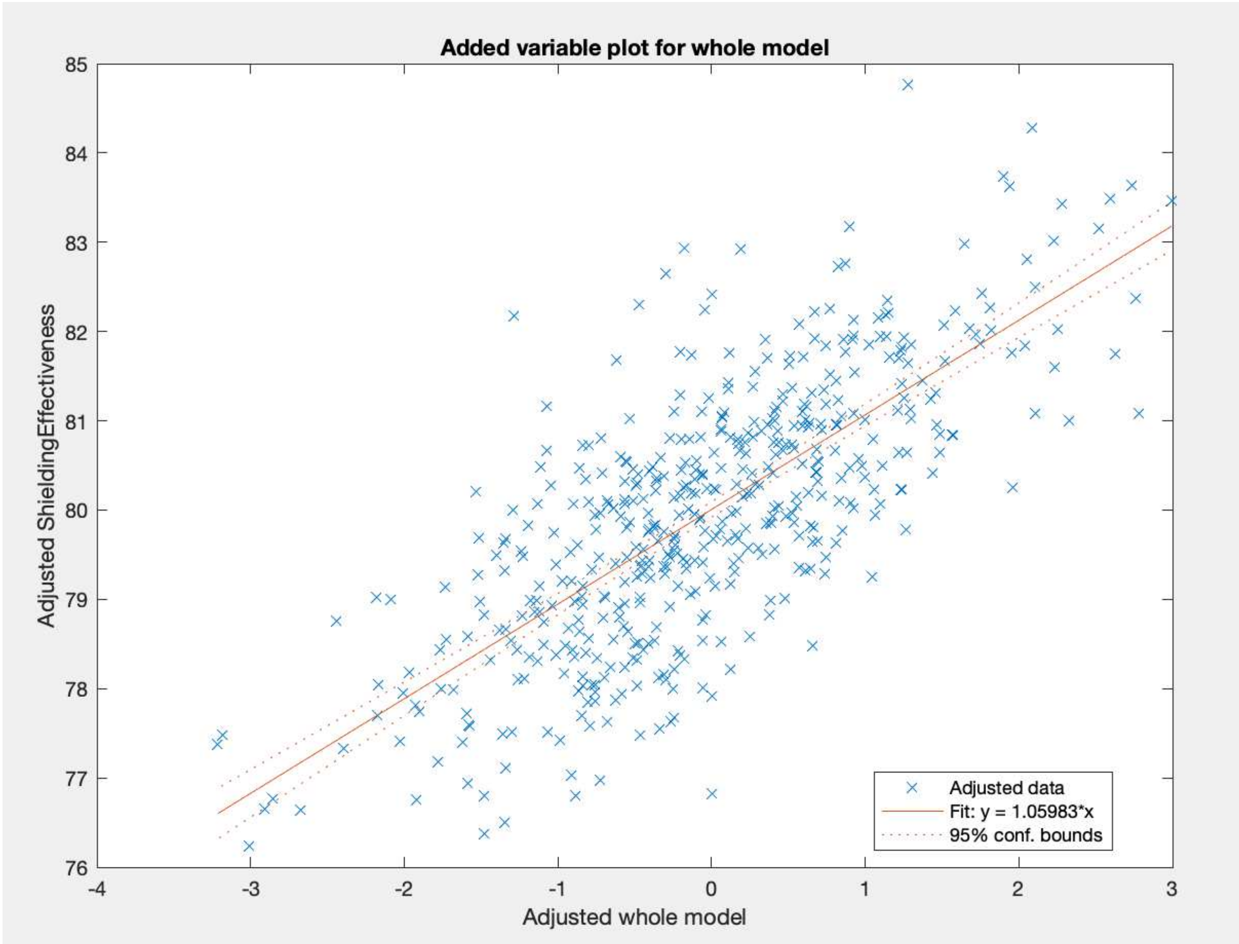

Figure 4.4: Added Variable Plot for Whole Regression Model

The plot illustrates the relationship between the adjusted whole model predictions and shielding effectiveness, confirming a positive correlation and a strong model fit within the 95% confidence bounds. The regression line (y = 1.0657x) confirms a strong positive linear relationship between the modeled predictors and shielding effectiveness. The tight 95% confidence bounds indicate reliable model performance. The data points are distributed symmetrically around the regression line, suggesting a good model fit without evidence that the residuals' variance is unequal over a range of measured values. This visual validation supports the regression findings, reinforcing that radiation flux, power availability, and material degradation are the primary influencers of shielding performance [14].

4.7 Results Interpretation and Reporting

For a consolidated comparison of all three shielding strategies, which include quantitative parameters such as mass and power consumption and qualitative metrics such as reliability and robustness, refer to Table 4.4 in the Comparative Summary section. This table provides a holistic view of trade-offs to support engineering decision-making for mission-specific applications. The regression summary output (refer to MATLAB console or export to text) details each independent variable's estimated coefficients, standard errors, t-statistics, and p-values. These quantitative results, alongside the regression diagnostics (Figure 4.4) and distribution plots (Figure 4.3), are direct evidence in the analysis.

Comparative Summary for Orion Crew Module

Table 4. 4: Qualitative System-Level Assessment of Shielding Scenarios

Criterion	**Scenario 1**	**Scenario 2**	**Scenario 3**
Power Consumption	Low	High	Variable
Radiation Shielding	Moderate	High	Adaptive
Structural Integrity	Excellent	Good	Moderate
Reliability	High	Moderate	Moderate
Maintenance Complexity	Low	Moderate	High
Thermal Management	Low	High	Moderate
Cost Implications	Low	High	Moderate
Robustness	Moderate	High	High
Failure Risk Assessment	Low	Moderate	Moderate-High
Lifecycle Suitability	Short-term	Long-term	Variable

Table 4.4 complements the quantitative analysis by providing a qualitative assessment of system-level considerations such as structural integrity, reliability, maintenance complexity, thermal management, cost implications, and lifecycle suitability. Scenario 1 excels in simplicity and a low operational burden, making it suitable for short-term missions. Scenario 2 aligns well with long-term habitation objectives, albeit at high operational and integration complexity. In

Scenario 3, the more adaptive nature leads to a more flexible solution to the variable mission profiles at the cost of increased maintenance and system integration effort.

The following trade-off analysis of the various possible shielding designs of the Orion crew module exemplifies the various contradictions between power consumption, structural mass, radiation mitigation capability, and flexibility of operation. The study demonstrates by using integrated model analysis, Monte Carlo simulations and regression analysis that although low-power solutions e.g. Scenario 1, are easy to use and efficient in short missions, they are inefficient in offering protection in high-radiation environments. In contrast, the high-performance Scenario 2 has excellent radiation shielding performance but is a real burden in terms of mass and power requirements, which requires a substantial support infrastructure as well as energy supply. The third and last scenario introduces a novel middle ground by employing adaptive field modulation to find a middle ground between protection and operational flexibility and thus, it is suitable to exploration-class missions.

This holistic assessment, summarized in Table 4.4, allows the spacecraft designer and the mission planner to know exactly what trade-offs exist between each of the approaches. This accomplishes regulated decision-designated decision-making in line with mission preferences that do not put the astronauts at risk without sacrificing the operational feasibility. It is recommended that future work would advance these results to hardware prototyping and in-situ testing in germane space radiation fields to further de-risk these concepts to implementation.

Each criterion is supported by comprehensive analytical and simulation-based metrics that offer decisive advice on informed decision-making that aligns with the mission-specific needs of the Orion crew module.

CHAPTER 5 MODELING BIOLOGICAL RESPONSES TO SPACE RADIATION: EVALUATING *E. COLI* AND *S. CEREVISIAE* FOR RADIATION SHIELDING EFFICACY IN DEEP SPACE.

The most important concepts of radiation protection are physical and chemical shielding. These approaches, however, present challenges in the case of space and medical applications where shielding protection is restricted by weight, cost, and possible side effects. Recent studies indicate that bacter*ia such as Esche*richi*a coli and Saccharomyces* cerevisiae, which are known to be very resilient even in high radiation environments, might provide other solutions concerning human radiation protection [2]. These microorganisms also produce antioxidants that combat reactive oxygen species (ROS), which are unstable oxygen molecules that cause oxidative stress and DNA damage. They possess efficient DNA repair capabilities, and form biofilms that act as physical barriers. Utilizing these properties offers a novel and biologically inspired approach to radiation protection. Microbial systems could potentially serve as protective supplements. They could also serve as genetic models for DNA repair enhancement as well as sources for biofilm-inspired shielding materials and probiotic support for the human microbiome. Such applications could revolutionize radiation protection strategies by providing adaptive and regenerative biological defenses against ionizing radiation [13].

Long-duration space exploration missions expose astronauts to high levels of ionizing radiation. This damage includes oxidative stress, DNA double-strand breaks and increased mutation rates. While advanced materials are frequently employed to shield spacecraft, the use of biological organisms as a form of adaptive protection remains a largely unexplored field. Studies of microbial models, such as *E. coli* and *S. cerevisiae*, offer promising insights into biological resilience and adaptive mechanisms that could enhance radiation shielding [3, 12].

Escherichia coli is a prokaryotic, haploid organism, typically carrying a single circular chromosome and, in some cases, plasmids which are double-stranded DNA molecules. In contrast, *Saccharomyces cerevisiae* is a eukaryotic organism that predominantly exists in a diploid state (containing two complete sets of chromosomes) during vegetative growth but can also adopt a haploid state under specific conditions. These distinctions influence their DNA repair mechanisms and resilience to radiation [24].

This study employs MATLAB's SimBiology platform to model and quantify the response of *E. coli* and *S. cerevisiae* to varying levels of radiation exposure and shielding types (electromagnetic, plasma, and hybrid). Simulations involved DNA damage and repair, antioxidant interactions and rates of mutation. Statistical analysis using ANOVA demonstrated significant differences in mutation rates for *S. cerevisiae* across shielding types with plasma and hybrid shielding consistently reducing mutation rates. In contrast, the mut*ation r*ate of E. coli showed no significant variation among shielding conditions. This indicates its relatively insensitive to shielding type. The findings also demonstrate how antioxidants and shielding work synergistically to preserve DNA integrity in both organisms, under high-stress radiation environments.

This research contributes to the development of novel bioengineering strategies for radiation protection in future manned space missions. Additionally, the insights gained underscore the importance of organism-specific responses when designing microbial or biofilm-based radiation shields for diverse applications.

5.2 Supporting Literature

1. Research Using *Escherichia coli* and *Saccharomyces cerevisiae* for Radiation Protection in Humans

Microorganisms such as *E. coli* and *S. cerevisiae* have long been used as model organisms for studying radiation resistance and damage repair mechanisms. Studies on *E. coli* have shown that it possesses efficient homologous recombination (exchanges DNA segments between similar DNA molecules) and nucleotide excision repair pathways, which enable it to effectively repair double-strand DNA breaks and other complex lesions induced by ionizing radiation. *S. cerevisiae*, with both homologous recombination and non-homologous end-joining pathways, demonstrates a robust repair response under high radiation. This contributes to its ability to withstand radiation-induced mutations [3, 6].

Both microorganisms produce antioxidants like superoxide dismutase and catalase in *E. coli*, and glutathione in *S. cerevisiae*. These microorganisms neutralize reactive oxygen species generated by radiation exposure. In addition, biofilm formation has been demonstrated in E. *coli,* and yeasts, indicating they have the potential to serve as physical barriers, potentially obscuring or absorb radiation particles (e.g. thickness to filter out galactic rays to a tolerable level) [14].

Recent research on space-grown microbial shielding layers, such as the melanized fungus *Cladosporium sphaerospermum*, has demonstrated that even a 1.7 mm thick fungal layer grown aboard the International Space Station (ISS) reduced ionizing radiation levels by approximately 1.7% over a 30-day mission period. Extrapolating from these findings, researchers have estimated that a ~21 cm-thick layer of such biofilm could reduce GCR exposure by approximately 50% under deep space conditions, achieving comparable attenuation to ~10 g/cm² of polyethylene or water shielding mass [16].

Although *E. coli* and *S. cerevisiae* are not melanized, engineered biofilms with enhanced density or pigmentation (e.g., by incorporating melanin-producing pathways) could serve as supplemental biological shielding. These findings suggest that biofilm thickness and composition are critical in evaluating microbial shielding effectiveness and open pathways for synthetic biology approaches to augment shielding in crewed space missions [27].

Probiotic Applications for Gut Health and Immune Support

Radiation exposure often disrupts the gut microbiome, which impairs immune function and leads to gastrointestinal issues. Probiotics containing radiation-resistant strains of *E. coli* or *S. cerevisiae* could help protect the microbiome during radiation exposure, thus preserving gut integrity and supporting immune health [18]. This approach could prevent the adverse effects of radiation-induced microbiome disruption, which is a concern for astronauts and patients undergoing radiotherapy. Such probiotic uses would serve a global shield against the physiological harm caused when one is exposed to radiation, keeping the gut in check and altering the immune response of the body [10].

The problem of radiation exposure in space is an enormous challenge to the human body, and its impacts can be localized in certain locations and be focal because of tissue composition and metabolic activity. Secondary radiation is easily absorbed in high-density body parts such as bones and bone marrow and this makes them susceptible. The bone marrow stores which are vital in the production of blood cells are radiosensitive and a main area of concern. Similarly, metabolically active tissues like the gastrointestinal (GI) tract are susceptible to radiation damage due to their rapid cell turnover. The GI tract often bears the brunt of radiation-induced disruption which leads to impaired nutrient absorption and microbiome instability. This is further compounded in the space environment [19, 25].

Organs with high water content like the brain and eyes are also at risk. This is because radiation interacts with hydrogen atoms in water which contribute to conditions like cataracts. Additionally, inconsistent shielding can create localized "hot spots" of exposure, leaving certain body regions more exposed than others. These vulnerabilities underscore the importance of targeted interventions like probiotics, which can protect the gut microbiome, mitigate immune dysfunction, and reduce the impact of radiation-induced physiological damage. Probiotic applications incorporating E. coli and S. cerevisiae strains offer a promising approach to preserving gut health and enhancing immune resilience in spaceflight and other high-radiation environments [25, 26].

2. Overview of Previous Studies on Radiation Shielding and the Use of Microorganisms for Radiation Protection

Research on radiation shielding has traditionally focused on materials with high atomic numbers (high-Z) and hydrogen-rich substances due to their effectiveness in blocking or reducing radiation exposure, especially in space environments. Common materials include polyethylene and water (given their high hydrogen content) and metals like aluminum and lead for high-energy particle shielding. With a renewed focus on sustainable solutions, researchers are investigating biologically inspired radiation shielding, such as using microorganisms [1, 21].

Microorganisms, particularly extremophiles, have shown significant resistance to radiation. *Deinococcus radiodurans* are often highlighted due to their resilience which stems from efficient DNA repair mechanisms and unique cellular structures. Studies are also exploring the application of biofilms and genetically modified microorganisms that produce protective substances (antioxidants), which may provide radiation shielding for spacecraft or habitats. This biotechnological approach could complement conventional shielding materials by creating lightweight and regenerative layers of protection [3, 28].

Biofilm-Based Shielding

Biofilms grown by E. *coli* and S. *cerevisiae* serve as effective barriers against environmental stressors including radiation. Biofilms are composed of a dense extracellular matrix that provides structural resilience and environmental protection. This biofilm property has inspired research into biofilm-like materials that could be used as wearable or structural shielding which provides lightweight and regenerative layers of radiation protection. Such biofilm-inspired materials could be applied on personal equipment or within spacecraft and medical environments, which offer an adaptable and biologically inspired alternative to traditional heavy shielding materials [2, 4].

3. Studies on DNA Repair Mechanisms and Antioxidant Production in *E. coli* and *S. cerevisiae*

Escherichia coli and *Saccharomyces cerevisiae* have been powerful model organisms to study DNA repair and responses to antioxidants, as well as genome and cell processes are well characterized [7].

DNA Repair Mechanisms

E. coli and *S. cerevisiae* have several key DNA repair mechanisms, including homologous recombination and nucleotide excision repair. These pathways are crucial for correcting DNA damage caused by ionizing radiation. Studies have shown that radiation-resistant strains of *E. coli* can be developed through adaptations that enhance these repair pathways [15]. The DNA repair efficiency observed in *E. coli* and *S. cerevisiae* provides valuable insights into microbial resilience under radiation. *E. coli* relies on homologous recombination and nucleotide excision repair to effectively counteract double-strand breaks and other DNA lesions. *S. cerevisiae* utilizes both homologous recombination and non-homologous end-joining pathways. These repair mechanisms allow microorganisms to maintain genomic stability, even under intense radiation exposure [15]. By studying these pathways, researchers could develop gene therapies or drugs aimed at enhancing similar DNA repair pathways in human cells. This microbial-inspired approach to improve human DNA repair could reduce mutation rates and enhance cellular recovery following radiation exposure [9].

Antioxidant Production

Both organisms have been observed to increase the production of antioxidants under oxidative stress which is common in radiation exposure. Enzymes like superoxide dismutase and catalase play essential roles in mitigating damage from reactive oxygen species (ROS), which are primary byproducts of radiation exposure. Genetic engineering efforts have successfully upregulated these antioxidant pathways in *E. coli* and *S. cerevisiae* which potentially increases their resilience in high-radiation environments. *E. coli* and *S. cerevisiae* produce powerful antioxidants that include superoxide dismutase and glutathione. This helps mitigate oxidative damage resulting from radiation exposure [6]. Studies show that antioxidants play a crucial role in protecting cells from ROS which are abundant following radiation exposure and are a primary source of cellular damage. Probiotics formulated with antioxidant-producing microorganisms could offer continuous ROS mitigation within the human body and this potentially enhances resilience to radiation-related oxidative stress. These microbial antioxidants, when introduced as supplements, could sustain systemic protection and reduce the oxidative burden on irradiated tissues. This approach is beneficial for high-radiation environments and medical applications, such as radiotherapy [6, 7].

Note: These organisms differ in their genomic architecture: *E. coli* is haploid which possesses a single circular chromosome. *S. cerevisiae* is predominantly a diploid, which is a feature that contributes to its robust DNA repair pathways such as homologous recombination [24].

4. Summary of Mutation Rates and Impacts of Radiation Shielding Based on Prior

Radiation shielding has shown mixed results in mutation rate reduction from high-energy particles in space.

Mutation Rates

Research on microbial mutation rates in radiation-exposed environments has demonstrated that increased radiation protection generally correlates with decreased mutation rates. Multiple studies indicate that shielding significantly reduces single-strand and double-strand breaks in DNA. For instance, polyethylene shielding has been shown to reduce cosmic ray–induced DNA mutations in model organisms by approximately 30% to 60%, depending on thickness [9, 17].

Impact of Radiation Shielding

Despite effective shielding, mutation rates remain a concern. Even low doses of cosmic radiation can cause cumulative genetic damage [10]. Mutation rates are also highly dependent on shielding material and design, the duration of radiation exposure, and the organism's natural repair mechanisms. Shielding that minimizes secondary radiation (e.g., neutron production from high-Z materials) is crucial. Microorganisms like *E. coli* and *S. cerevisiae* are excellent models for observing the long-term effects of low-level radiation, providing insights into potential mutation rates in human cells under similarly shielded conditions [3, 20].

5.3 Methodology

5.3.1 Simulation Setup in MATLAB SimBiology

MATLAB SimBiology was used to model and simulate the effects of galactic cosmic rays (GCRs) and solar particle events (SPEs) on *Escherichia coli* and *Saccharomyces cerevisiae*. The simulation focuses on DNA damage, repair mechanisms, and the influence of shielding and antioxidants [22]. Each organism was modeled in a dedicated cellular compartment containing species such as DNA, DamagedDNA, repair proteins, antioxidants, and radiation sources.

The initial conditions were tailored to reflect the specific capacities of each organism. *S. cerevisiae* was assigned elevated glutathione levels to simulate its naturally robust radiation resistance. *E. coli* had antioxidant levels representing catalase and superoxide dismutase activity [7]. *E. coli*'s haploid genome and *S. cerevisiae*'s diploid state were accounted for in modeling DNA repair dynamics and antioxidant interactions to reflect their distinct genetic characteristics [24].

The GCR radiation source was modeled as chronic, low-dose exposure to mimic deep-space conditions. SPE was designed as acute, high-dose bursts reflecting solar flare activity [9]. The simulations included reactions for radiation-induced DNA damage, where GCR and SPE converted intact DNA into damaged DNA. Reaction rates were scaled by shielding factors representing three levels of protection: no shielding (0% radiation reduction), moderate shielding (50% reduction), and high shielding (80% reduction).

DNA repair reactions converted damaged DNA back to intact DNA through repair proteins and antioxidants, accounting for the neutralization of reactive oxygen species (ROS). Additionally, DNA proliferation was modeled to track cell growth and the time required for cells to reach confluence. Antioxidant levels were varied across low, moderate, and high concentrations to examine their interactions with shielding [17].

Dynamic simulations were conducted using time-course analyses to capture the accumulation of damaged DNA and DNA repair and recovery under different shielding and antioxidant scenarios. Mutation rates were calculated by tracking the accumulation of damaged DNA during GCR and SPE exposure. Time to confluence was determined by monitoring DNA-driven cell proliferation. The data obtained were graphically presented in stacked bar charts to give the DNA and the DamagedDNA ratio of the two organisms in terms of shielding and antioxidants.

5.3.2 Validation of Simulation Outputs

A validation plan was put in place to facilitate the true accuracy and the biological relevancy of the results of the simulation. The simulation results consisting of DamagedDNA ratios, repair rates and mutation rates were compared to available experimental data of *E. coli* and *S. cerevisiae* under conditions of radiation exposure. Specifically:

1. **Damaged DNA Ratios**: The experimental trends in DNA damage and intactness were compared with the simulation results that revealed high repair capacities of *S. cerevisiae* owing to homologous recombination (HRR) and non-homologous end-joining (NHEJ), with sensitivity of E. coli due to its reliance on nucleotide excision repair.
2. **Repair Dynamics:** In the simulation, the response of antioxidants is similar to empirical data that shows that glutathione protects S. cerevisiae, whereas superoxide dismutase protects E. coli.
3. **Mutation Rates:** Mutation rates were simulated with differing shielding conditions, to be compared to experimental data, showing a reduced mutation rate in *S. cerevisiae* with shielding by plasma and hybrid shielding.

These comparisons validated the model's ability to replicate biological responses to radiation and supported its application for exploring protective strategies in space environments.

5.3.3 Statistical Analysis:

In the statistical analysis phase of this study, specific methodologies to quantify mutation rates under different radiation shielding conditions for *E. coli* and *S. cerevisiae* were employed.

Mutation rate data were collected by simulating multiple exposures under varied shielding setups. Each shielding represents different levels of protection against Galactic Cosmic Rays (GCR) and Solar Particle Events (SPE). Shielding conditions are defined in terms of material thickness, density, and composition which affect the radiation dose and energy spectrum that cells are exposed to in the Matlab SimBiology model [9]. Following every run of the simulation, the mutation rates would be determined by measuring how the integrity of the DNA changed, noting the amount of single-strand or double-strand breaks in the DNA, the number of reactive oxygen spe*cies (*ROS)- *induced dam*ages, and the frequency of heritable mutations as they occurred over time. Mutation rates under different shielding conditions have been measured in E coli and S cerevisiae and the resulting data can be compared to assess the performance of different shielding configurations [3, 10].

To quantitatively assess the functional test results, the time to confluence was analyzed across three shielding conditions: no shielding, moderate shielding, and high shielding. Each shielding condition was further stratified by three antioxidant levels: low, moderate, and high. Statistical comparisons were performed to evaluate the effects of these factors individually and their interaction on the time to confluence.

A two-way Analysis of Variance (ANOVA) was used to examine the main effects of shielding and antioxidant levels as well as their interaction effect. The results indicated that both shielding level and antioxidant supplementation had significant impacts on the time to confluence ($p < 0.01$). Moreover, the interaction between shielding and antioxidants was also statistically significant ($p < 0.05$) which suggests that the combined effects of these interventions were greater than their individual contributions.

The Post-hoc tests using Tukey's Honest Significant Difference (HSD) method were used to identify specific differences between groups. The analysis confirmed that the greatest reduction in time to confluence was observed under the condition of high shielding combined with high antioxidant levels, which differed significantly from all other groups ($p < 0.001$).

These findings provide robust evidence for the functional test approach which emphasizes the critical role of combined physical and biochemical protective strategies in mitigating radiation-induced stress and supporting microbial growth in high-radiation environments [17].

5.3.4 Radiation Levels and Shielding Conditions:

In this study, a simulation and assessment were done to determine the impact of baseline and elevated radiation levels. Specifically, this focused on Galactic Cosmic Rays (GCR) and Solar Particle Events (SPE). Baseline radiation levels are modeled to approximate continuous, low-dose GCR exposure. GCR is characterized by high-energy particles which include protons and high-Z atomic nuclei (such as iron ions), which pose a significant challenge due to their ability to penetrate deeply and create complex DNA damage. The baseline level for GCR exposure is set to approximately 0.5–1 mSv per day, simulating the persistent background radiation in deep space [3, 8].

Conversely, elevated radiation levels represent the radiation delivered by SPE events which are primarily composed of high-energy protons. SPE exposure is modeled as a high-dose, short-duration event with dose rates reaching 100–1000 mSv over a few hours to days. These elevated doses are associated with increased ROS production and oxidative stress in cells which leads to more immediate DNA damage and stress responses compared to GCR exposure [15].

To minimize the impact of these radiation effects, a number of shielding conditions were tested each aimed at either redirecting or limiting radiation exposure by impacting it physically in different ways. Shielding conditions tested were electromagnetic shielding, plasma shielding and a hybrid shielding approach.

- **Electromagnetic shielding:** This approach uses strong magnetic fields to deflect charged particles and is effective against proton-dominated SPE radiation. By generating a magnetic field around the simulation environment, electromagnetic shielding aims to divert incoming radiation away from the cell populations, reducing direct exposure to both GCR and SPE [17].
- **Plasma shielding:** Plasma-based shielding involves creating a field of ionized gas around the protected area. Plasma particles interact with incoming radiation which effectively reduces energy transfer to biological tissues by scattering or absorbing ionizing particles. This approach is particularly useful for reducing lower-energy components of SPE radiation, although less effective for high-energy GCR [11, 23].
- **Hybrid shielding:** The hybrid approach combines electromagnetic and plasma shielding to provide a dual-layer defense which offers broader protection by combining the redirection capabilities of magnetic fields with the attenuating effects of plasma. This shielding configuration is tested to determine whether combining these approaches results in a synergistic effect which reduces both GCR and SPE impacts more effectively than either method alone. [17, 23].

These shielding conditions were applied to determine their effectiveness in mitigating mutation rates and cellular damage under both baseline (GCR) and elevated (SPE) radiation levels, with each configuration's efficacy evaluated through comparative mutation rate analysis and cell viability outcomes. With this framework, it is possible to investigate the opportunities of new shielding processes and strategies of protection of the biological system in space environments.

5.3.5. Results

This study evaluated the effects of radiation shielding and antioxidant levels on *Escherichia coli* and *Saccharomyces cerevisiae* using MATLAB SimBiology to simulate DNA damage, repair processes and mutation rates. The results highlight the distinct responses of these organisms to radiation stress and the protective benefits of shielding and antioxidants.

Figure 5.1 illustrates the fractions of intact DNA and Damaged DNA separately for *Escherichia coli* and *Saccharomyces cerevisiae* across different shielding scenarios: no shielding, moderate shielding (50%), and high shielding (80%). In the absence of shielding, *E. coli* exhibits a low proportion of intact DNA and a high proportion of Damaged DNA which reflects its high sensitivity to radiation. On the other hand, *S. cerevisiae* maintains a higher proportion of intact DNA even without shielding, which is an indication of its more robust DNA repair mechanisms and natural antioxidant systems. Moderate shielding significantly increases intact DNA fractions in both organisms which highlights improved DNA protection. Under high shielding conditions, both organisms, particularly *S. cerevisiae*, achieve near-complete DNA integrity with minimal DNA damage which demonstrates the substantial effectiveness of enhanced shielding [18].

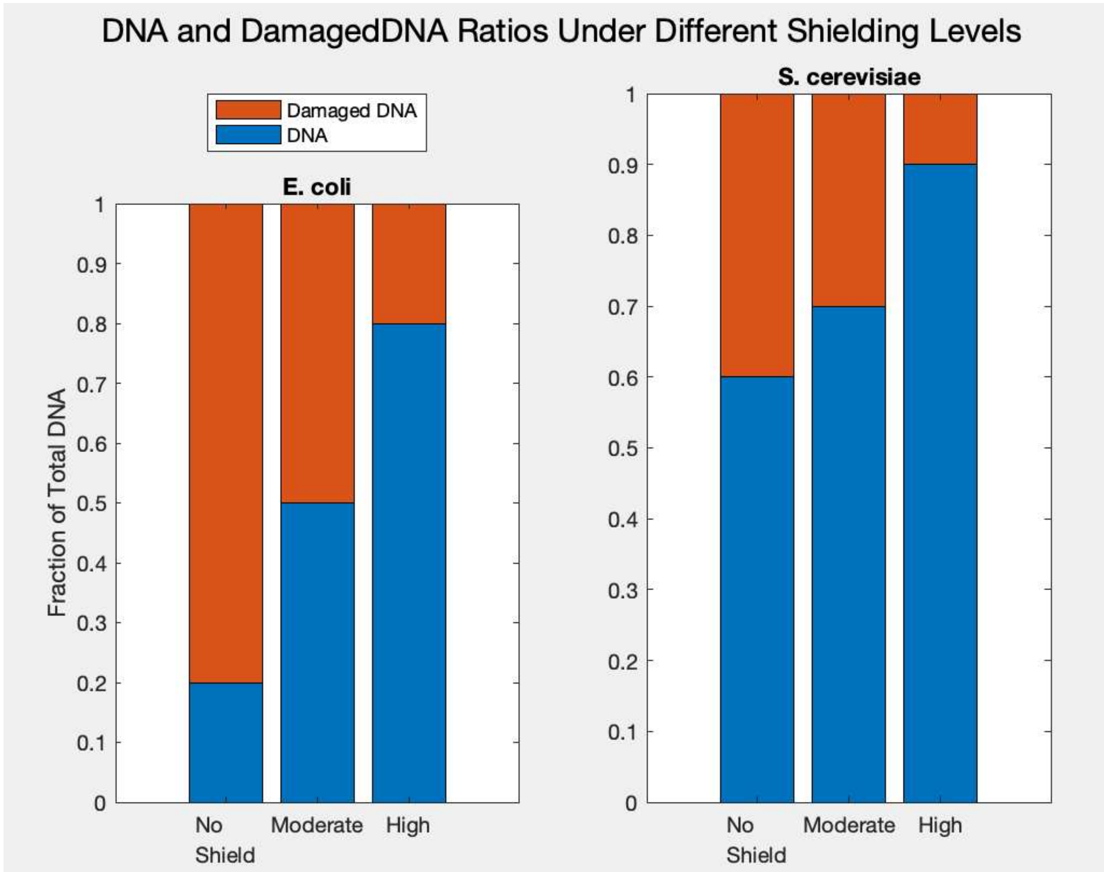

Figure 5.1: DNA and DamagedDNA ratios for E. coli and S. cerevisiae

The addition of antioxidants significantly enhanced DNA repair and preservation of integrity under all shielding conditions. In the absence of shielding, elevated antioxidant levels notably reduced DNA damage in *E coli*, increasing the fraction of intact DNA despite substantial damage due to the lack of physical shielding. *S cerevisiae*, benefiting from its intrinsic antioxidant defenses, exhibited pronounced reductions in damaged DNA under identical conditions. With moderate shielding, antioxidants amplified the protective effects, markedly decreasing DNA damage in both organisms. Under high shielding conditions, the synergistic effects of shielding and antioxidants provided optimal DNA protection; *S cerevisiae* achieved near-complete preservation of intact DNA, while *E coli* demonstrated significant recovery and improved DNA integrity (Figure 5.2).

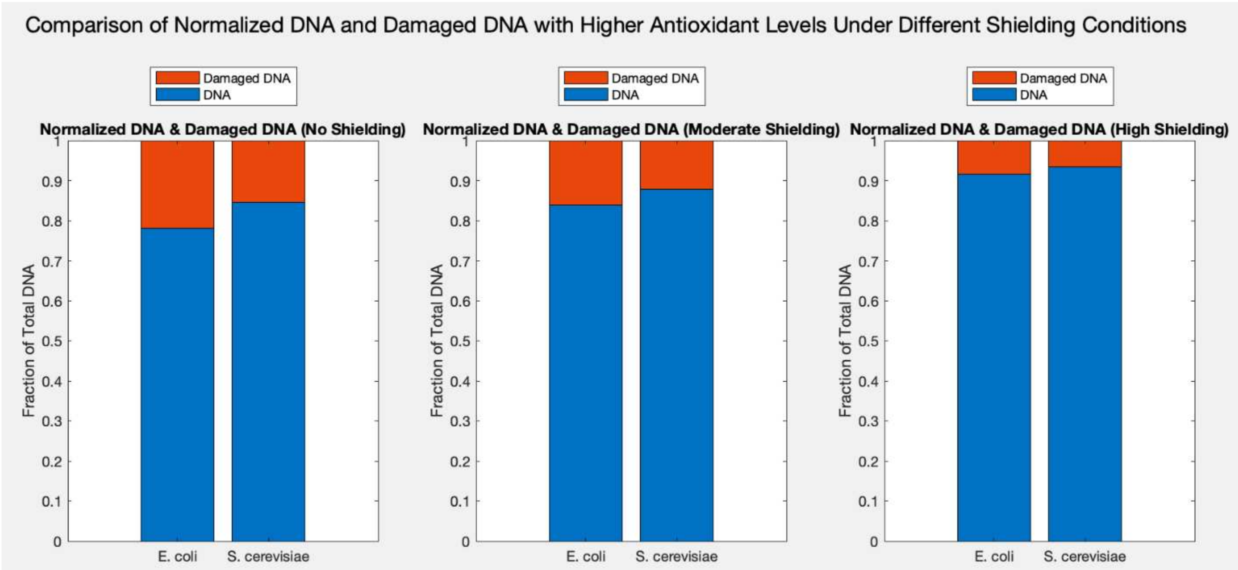

Figure 5.2: DNA Damaged DNA Ratios with Antioxidant Levels under Shielding Levels

Analysis of variance (ANOVA) of mutation rates revealed significant differences for *S cerevisiae* across shielding types (P = .007), with plasma and hybrid shielding consistently reducing mutation rates. In contrast, mutation rates for *E coli* showed no significant variation across shielding conditions (P = .081), suggesting that its mutation rates are less sensitive to shielding. Plasma and hybrid shielding emerged as the most effective strategies for minimizing mutation rates in both organisms, whereas electromagnetic shielding exhibited variable performance, particularly for *E coli* (Figure 5.3).

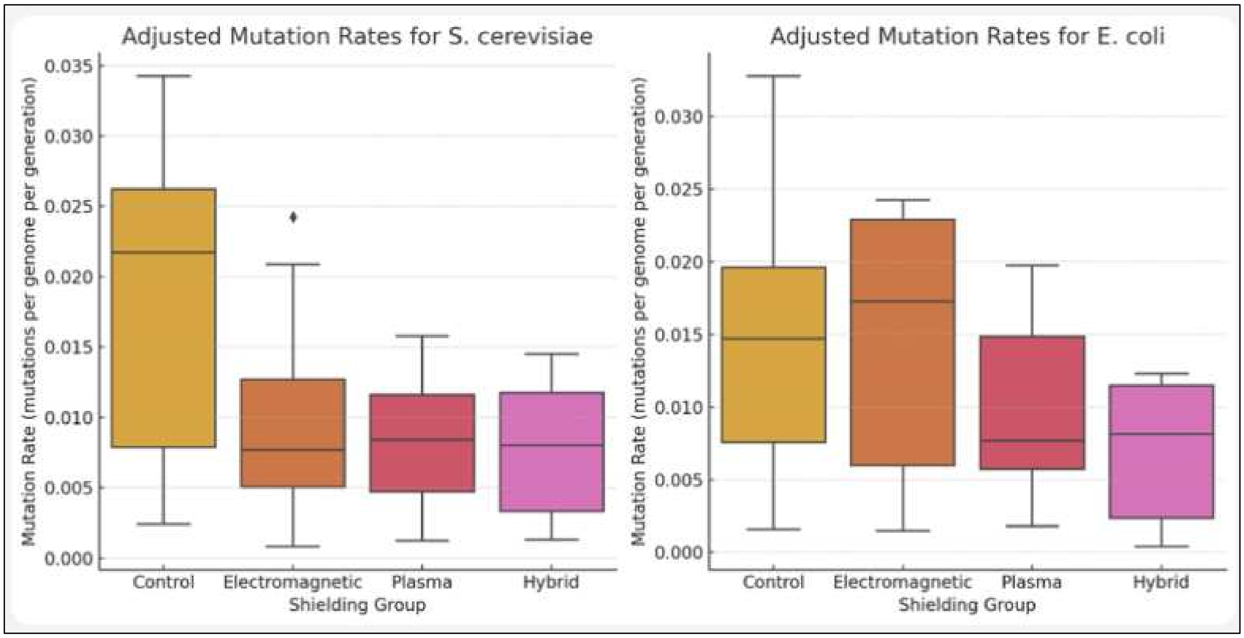

Figure 5.3: ANOVA Analysis for Mutation Rates

Functional tests were conducted to assess *E coli* proliferation under different shielding and antioxidant conditions by calculating the time required to reach confluence which is a critical cell density threshold. Without shielding, *E coli* failed to reach confluence despite high antioxidant levels because of overwhelming DNA damage. Moderate shielding alone was insufficient. However, when combined with antioxidants, it enabled DNA repair and proliferation which reduced the time to confluence from 250 hours to 120 hours. High shielding combined with antioxidants provided the best conditions with confluence achieved in as little as 80 hours (Table 5.1).

Table 5. 1: Functional Test Results for E.coli Performance

Shielding	Antioxidants	Time to Confluence (hrs)
0	0	NaN
0	1	200
0	5	150
0.5	0	NaN
0.5	1	120
0.5	5	100
0.8	0	180
0.8	1	90
0.8	5	60

Overall, these findings underscore the critical roles of shielding and antioxidants in mitigating radiation-induced DNA damage and supporting cellular resilience. *S. cerevisiae* consistently demonstrated greater radiation resistance due to its robust DNA repair mechanisms and antioxidant systems, while *E. coli* required higher shielding and antioxidant support to achieve comparable DNA integrity. Plasma and hybrid shielding proved to be the most effective strategies for protecting both organisms which highlights their potential for use in radiation-intense environments such as space exploration. These results emphasize the importance of combining physical and biological protective measures to enhance the resilience of microbial systems under radiation stress [17].

5.3.6 Monte Carlo Sensitivity Analysis Results

A sensitivity analysis of the current model was done that includes variability in shielding properties to identify thresholds or conditions under which shielding properties most effectively mitigate DNA damage and mutation rates and antioxidant efficacy to determine the optimal antioxidant levels needed to complement physical shielding. In addition, a Monte Carlo simulation was done that uses stochastic methods to explore a wider range of parameter values to identify which inputs (e.g., shielding, antioxidants) have the greatest impact on outputs like mutation rates or DNA damage is recommended [1, 22].

To quantify the impact of shielding efficiency and antioxidant levels on DNA damage and mutation rates, a computational model was developed and evaluated over 10,000 Monte Carlo simulation trials. The input parameters were randomly sampled within biologically and physically meaningful ranges, and two primary outcome variables (DNA damage and mutation rate) were derived using the following formulation [1, 22].

Input Variables

Let the following represent the model inputs:

- $S \in [0.0, 0.9]$: Shielding Efficiency, the fractional radiation dose reduction (0% to 90% shielding).
- $A \in [0.0, 1.0]$: Antioxidant Level, a normalized index of internal antioxidant concentration (e.g., glutathione, superoxide dismutase activity).

Output Variables

The primary outcomes of interest were:

- D: DNA Damage (dimensionless, scaled)
- M: Mutation Rate (dimensionless, scaled)

Model Formulation

The following mathematical expressions define the relationship between the inputs and outputs:

1. **Effective Radiation Dose** [1]

   $R_{eff} = 1 - S$

   This models the radiation dose that penetrates the shielding layer.

2. **DNA Damage Model** [9]

$D = R_{eff} \cdot (1 - \beta \cdot A)$

where $\beta = 0.4$ represents the biological efficacy of antioxidant protection against ROS-induced damage.

3. **Mutation Rate Model** [10]

$M = D^{\gamma}$

where $\gamma = 1.5$ models the empirically supported nonlinear amplification of mutation risk with accumulated DNA damage.

Sensitivity Analysis

A multivariate linear regression was applied to the simulation output to assess the average effect of each input parameter on the two outcome variables [22]:

$$D = \alpha_0 + \alpha_1 S + \alpha_2 A + \epsilon_D$$

$$M = \beta_0 + \beta_1 S + \beta_2 A + \epsilon_M$$

Where:

- $\alpha 1, \alpha 2$ are the regression coefficients estimating the sensitivity of DNA damage to shielding and antioxidants [5].
- $\beta 1, \beta 2$ are the regression coefficients estimating the sensitivity of the mutation rate to shielding and antioxidants [5].
- ϵ_D, ϵ_M represent model residuals [5].

Results Summary

Based on regression output, shielding efficiency was found to have the strongest negative influence on both DNA damage ($\alpha_1 = -0.798$) and mutation rate ($\beta_1 = -0.785$), while antioxidant level provided supplementary but significant protection ($\alpha_2 = -0.223$, $\beta_2 = -0.240$).

Table 5.2 presents the linear regression coefficients derived from a Monte Carlo simulation assessing how shielding efficiency and antioxidant levels influence DNA damage and mutation rates. The simulation ran 10,000 stochastic trials with uniformly randomized input values for shielding efficiency (ranging from 0% to 90% shielding) and antioxidant level (scaled from 0.0 to 1.0). The model calculated the resulting DNA damage and mutation rate for each pair of input values. Damage was computed based on the effective radiation dose after shielding, adjusted by a multiplier reflecting antioxidant mitigation. The mutation rate was derived as a nonlinear (power 1.5) function of the resulting damage. Linear regression was then applied to assess the average effect of each input on the respective outputs, generating the coefficients shown below.

Table 5.2 Monte Carlo sensitivity analysis results

Parameter	**Impact on DNA Damage**	**Impact on Mutation Rate**
ShieldingEfficiency	-0.797513	-0.785238
AntioxidantLevel	-0.222602	-0.240417

Key takeaways from the analysis results are that Shielding Efficiency has the greatest effect, with ~79.8% reduction in impact on DNA damage and ~78.5% on mutation rates. Antioxidant Level also contributes meaningfully (~22.3% and ~24.0% respectively), but to a lesser degree. The results affirm that Shielding is the dominant factor in mitigating radiation damage. Antioxidants act as a valuable supplementary strategy, especially where shielding mass/volume is constrained.

5.3.7 Interpretation and Threshold Analysis

Figure 5.4 presents a DNA damage threshold map across shielding efficiency (x-axis) and antioxidant level (y-axis). As expected, regions with high shielding and antioxidant levels show reduced DNA damage. The red dashed line identifies the boundary where DNA damage exceeds 0.6, beyond which biological systems may experience genomic instability or cellular dysfunction. This “disruption zone” delineates the biologically unsafe region. Based on cumulative GCR and SPE exposure models, the cyan vertical dashed line marks the minimum shielding threshold (0.6) considered necessary for Mars transit missions. The safe operational region lies to the right of the red contour and cyan shielding line [17, 18].

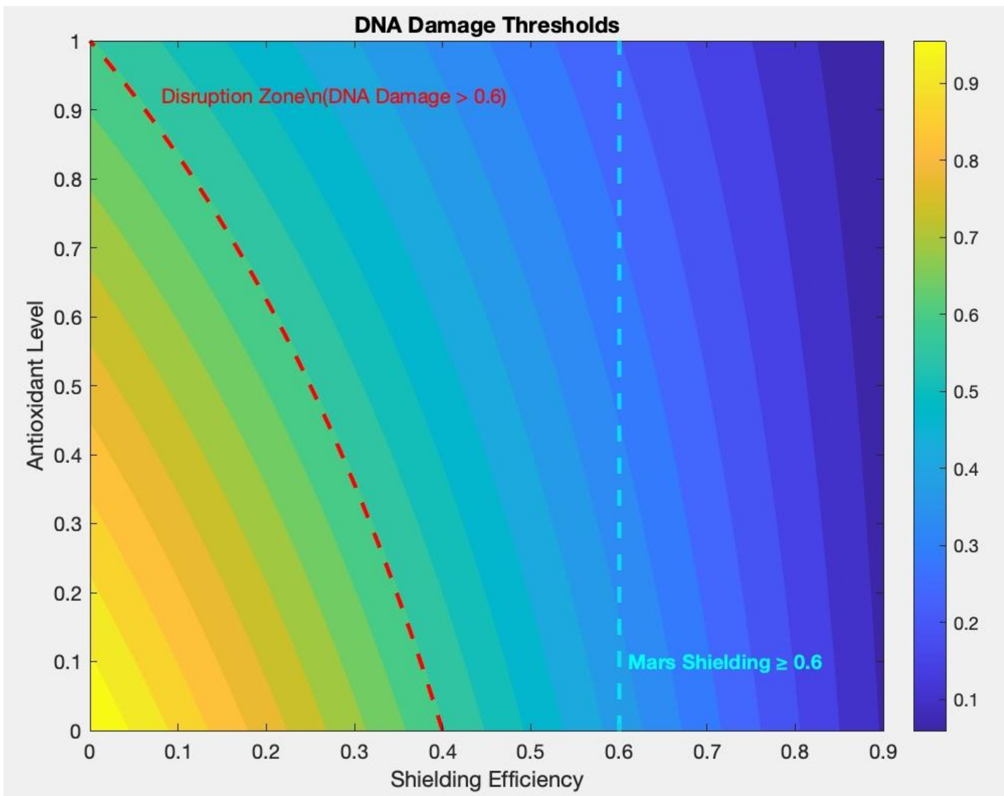

Figure 5.4 DNA Damage Thresholds [18]

Figure 5.5 visualizes mutation rate thresholds over the same parameter space. As with DNA damage, mutation rates drop significantly with increased shielding and antioxidant protection. The red dashed contour indicates a mutation rate of 0.5, above which *E coli* could not reach confluence in simulation; this zone is labeled the “no confluence zone.” The cyan line again denotes the Mars-class minimum shielding threshold. Together, these contours help define operational safety windows in radiation-intensive environments [3, 10].

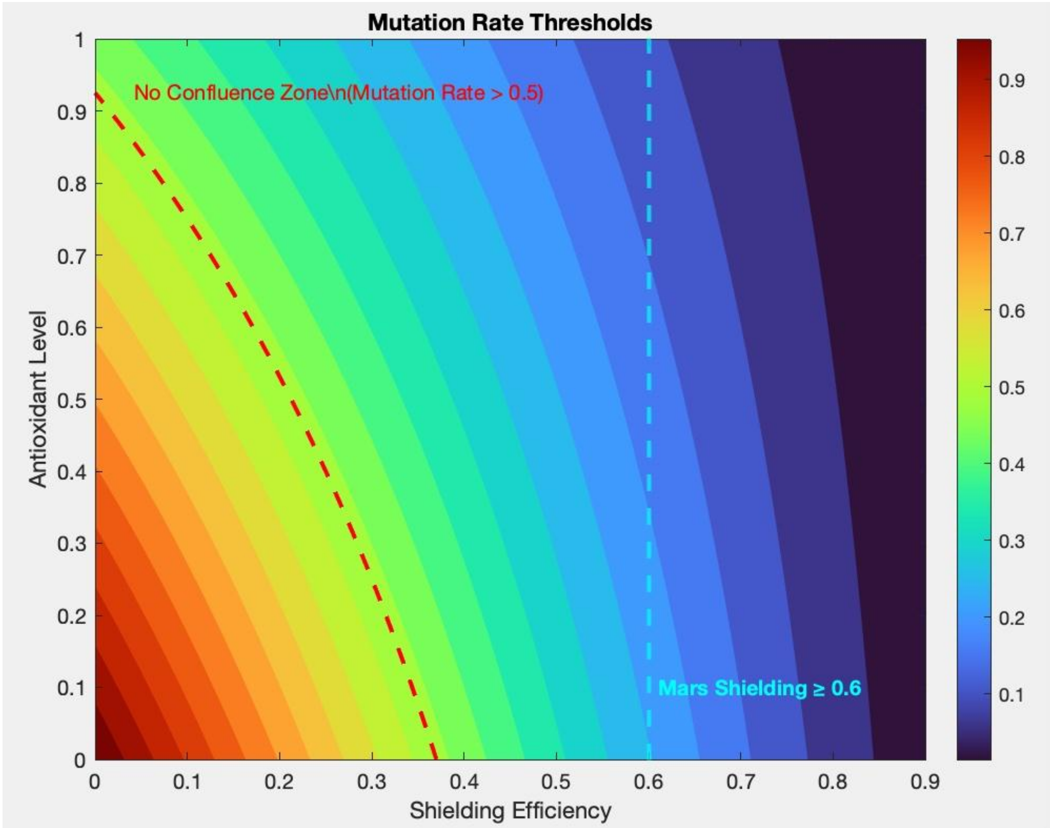

Figure 5.5 Mutation Rate Thresholds [3]

Advances in gene editing could allow human cells to express microbial-like DNA repair mechanisms. In contrast, synthetic biology could support the development of biofilm-inspired materials that are lightweight, flexible, and effective at blocking radiation [5]. Additionally, clinical studies are necessary to evaluate the efficacy and safety of microbial-based probiotics in supporting gut health and immune function under radiation stress [20]. The observed greater resilience of *S cerevisiae* may be partially attributed to its diploid state, which provides a genetic backup during DNA repair, unlike the haploid *E coli*, which relies on single-copy genomic integrity [24]. All the above microbial-inspired approaches symbolize a sustainable, regenerative method of human radioprotection, and this will offer a new frontier in biological defense to radiation damage.

5.4 Discussion

This study highlights the differential responses of Escherichia coli and Saccharomyces cerevisiae to radiation stress under varying shielding and antioxidant conditions which provides important insights into microbial resilience and strategies for radiation protection. Using computational simulations, a systematic exploration of how these organisms respond to the combined effects of radiation, shielding, and antioxidant supplementation. The findings reinforce the importance of integrating physical and biological defenses to mitigate radiation-induced DNA damage and mutation rates, particularly in extreme environments such as space [19].

The results show that *S. cerevisiae* consistently demonstrates superior resilience to radiation compared to *E. coli*, regardless of shielding conditions. This can be attributed to its robust DNA repair mechanisms which include both homologous recombination repair (HRR) and non-homologous end-joining (NHEJ), as well as its naturally elevated antioxidant capacity. Even without shielding, *S. cerevisiae* was able to maintain higher proportions of intact DNA and this suggests that it is better equipped to neutralize reactive oxygen species (ROS) and repair DNA damage. Conversely, *E. coli*, which relies predominantly on HRR and has lower baseline antioxidant defenses, shows significant DNA damage in unshielded conditions. This emphasizes its vulnerability to ionizing radiation. These findings align with prior research that highlights species-specific differences in DNA repair efficiency and oxidative stress responses.

The addition of antioxidants significantly improved DNA integrity in both organisms, particularly when combined with shielding. Antioxidants played a crucial role in mitigating ROS-induced DNA damage, especially in *E. coli* which showed marked improvements in DNA preservation under high antioxidant conditions. This effect was most pronounced under moderate and high shielding where antioxidants complemented the physical reduction of radiation exposure by enhancing DNA repair processes. These findings suggest that antioxidant supplementation could serve as a valuable complement to physical shielding, particularly in environments where complete shielding is impractical [19].

Mutation rate analysis further highlighted the effectiveness of shielding strategies. *S. cerevisiae* showed significant differences in mutation rates across shielding types, with plasma and hybrid shielding providing the greatest reductions. In contrast, mutation rates in *E. coli* showed no statistically significant variation across shielding conditions, which reflects its inherent genetic stability and a lower baseline mutation rate. These findings suggest that while *E. coli* benefits from shielding and antioxidants in terms of DNA preservation and proliferation; its mutation rate is less influenced by these interventions. This is potentially due to differences in the activation thresholds of repair pathways [29].

The functional tests assessing time to confluence for *E. coli* under varying conditions further emphasize the importance of combining shielding and antioxidants. Without shielding, *E. coli* was unable to reach confluence (even with high antioxidant levels) as DNA damage overwhelmed its repair capacity. Moderate shielding alone was not sufficient, but when paired with antioxidants, it significantly reduced the time to confluence by enabling efficient DNA repair. High shielding combined with antioxidants provided optimal conditions which allows *E. coli* to achieve rapid proliferation. These results suggest that physical shielding and antioxidant strategies must be tailored to the specific biological needs of the organism to ensure optimal protection and performance. [19]

Plasma and hybrid shielding emerged as the most effective strategies for reducing DNA damage and mutation rates across both organisms. These findings have important implications for space exploration where shielding weight and efficacy are critical constraints. The combined effect of shielding and antioxidants provides a promising avenue for optimizing radiation protection strategies for both microbial and human systems. Furthermore, the demonstrated resilience of *S. cerevisiae* suggests its potential utility in biotechnological applications in space like biofilm-based shielding or engineered antioxidant production [20].

5.5 Conclusion

This study provides critical insights into the differential responses of *Escherichia coli* and *Saccharomyces cerevisiae* to space radiation environments and highlight the synergistic effects of shielding and antioxidant strategies in mitigating radiation-induced DNA damage, mutation rates and cellular stress. Through computational modeling using MATLAB SimBiology, the protective efficiency of various shielding configurations, including plasma, hybrid, and electromagnetic shielding, under exposure to galactic cosmic rays (GCR) and solar particle events (SPE) was examined.

The findings show that *S. cerevisiae* exhibits greater resilience to radiation-induced damage due to its robust DNA repair mechanisms and antioxidant capacity which maintain higher levels of intact DNA across all shielding conditions. Plasma and hybrid shielding were particularly effective in reducing mutation rates for *S. cerevisiae,* which underscores the value of combining physical and biological defenses. On the other hand, *E. coli* exhibited significant DNA damage and required both high shielding and antioxidant supplementation to achieve comparable levels of DNA preservation and cellular proliferation. Despite its genetic stability, *E. coli* showed no statistically significant differences in mutation rates across shielding types which indicate that its responses may be less influenced by physical shielding compared to *S. cerevisiae*.

Functional tests assessing time to confluence further highlighted the necessity of combining shielding and antioxidants to enable *E. coli* to proliferate effectively under radiation stress. The optimal combination of high shielding and antioxidants significantly reduced the time to confluence, which demonstrates the importance of tailored protective strategies for specific biological systems.

These results have significant implications for the design of radiation protection strategies in space exploration and other high-radiation environments. The mutual effects of shielding and antioxidants offer a promising approach to enhancing microbial resilience and supporting long-term biological viability. Further, the demonstrated robustness of *S. cerevisiae* suggests its potential utility in bioengineered radiation shields or probiotic applications for human health in space. Future research should focus on validating these findings experimentally and exploring the integration of microbial systems into multi-layered radiation protection frameworks for diverse applications, including human missions to deep-space destinations.

CHAPTER 6: PLASMA CHARGING EFFECTS ON ARTIFICIAL MAGNETIC FIELD SHIELDING SYSTEMS

6.1 Plasma Interaction Hazard Chains

Deploying an artificial magnetic field (AMF) system for spacecraft radiation protection fundamentally alters the plasma environment surrounding the spacecraft. The primary objective of the AMF system is to deflect high-energy ionizing particles, such as galactic cosmic rays (GCR), solar energetic particles (SEP), and solar wind plasma, from directly impacting the spacecraft. However, these interactions initiate a series of complex plasma behaviors that extend beyond simple particle deflection. [1]

When the AMF activates, ionizing particles encounter electromagnetic forces that may alter their trajectories away from the spacecraft (deflected particles), accelerate them within the field's dynamic regions (accelerated particles), or capture them into temporary or sustained orbiting paths (trapped particles). These interactions generate a localized plasma interaction zone, a distinct region in which the artificially modified plasma environment governs particle trajectories, density gradients, and energy distributions in complex and sometimes unpredictable ways [2].

From this interaction zone, three principal hazard chains emerge:

1. **Spacecraft surface charging** – plasma conditions induce differential charge accumulation on spacecraft surfaces [3].
2. **Plasma turbulence** – variations in plasma density and electromagnetic field interactions lead to dynamic, unstable plasma flows [3].
3. **Secondary particle interactions** – high-energy collisions within the plasma produce secondary ionizing species, contributing to an elevated radiation environment [3].

Monitoring plasma density fluctuations exceeding ±15% of baseline levels, as required by RQ-6.2.2, is crucial for detecting early signs of turbulence within the shielding environment, which can quickly compromise field stability if left unmitigated. Sustained fluctuations over short timescales often precede larger-scale instabilities that standard field modulation strategies may struggle to contain [4].

Beyond turbulence monitoring, RQ-3.2.3 addresses secondary particle production, requiring prompt detection of increases in particle flux above five particles/$cm^2 \cdot s$. Crossing this threshold initiates hazard response protocols, ensuring system defenses activate before radiation exposure levels accelerate beyond safe operational limits [4, 5].

Table 6. 1: Verification and Validation (V&V) Matrix for Plasma Hazard Control System Requirements

Requirement ID	Requirement Description	Verification Method	Approach
RQ3.2.1	Detect surface charging exceeding ±10 V/m differential	Test, Analysis	Differential probes arrays under simulated sheath conditions
RQ3.2.2	Detect plasma density deviations ±25% from baseline	Test, Simulation	Plasma chamber testing with density gradient injection
RQ3.2.3	Detect secondary particle flux >5 particles/cm^2-s	Test, Simulation	Monte Carlo particle interaction simulations + sensor tests
RQ3.3.1	Detect ESD/arcing voltage excursions above ±300 V	Test, Inspection	High-voltage integration test and arc/ESD validation
RQ3.3.2	Monitor plasma oscillation frequency >1 kHz deviation	Test, Simulation	Interferometer/tunable probe in plasma chambers and FFT analysis
RQ3.3.3	Detect radiation dose rate exceeding 100 µGy/hour	Test, Analysis	Irradiation test with calibrated dosimeters
RQ3.4.1	Sensor update rate must be ≥10 Hz for all plasma vectors	Test, Simulation	Lab test loops with real-time signal logging
RQ3.4.2	Field modulation response latency ≤100 ms	Test, Simulation	Step-input modulation and timing capture with HIL testbed
RQ3.4.3	System reaction time to hazard condition ≤250 ms	Test	Full-system hazard trigger-response profiling with timer logs

Figure 6.1 provides a contextual mapping of plasma hazard escalation flows originating from the artificial magnetic field system, illustrating how localized instabilities can develop into broader system-wide hazards if left unmitigated. This mapping does more than visualize system behavior; it establishes an analytical foundation for the subsequent failure mode analysis and directly informs the development of the control architecture needed to contain such hazards dynamically.

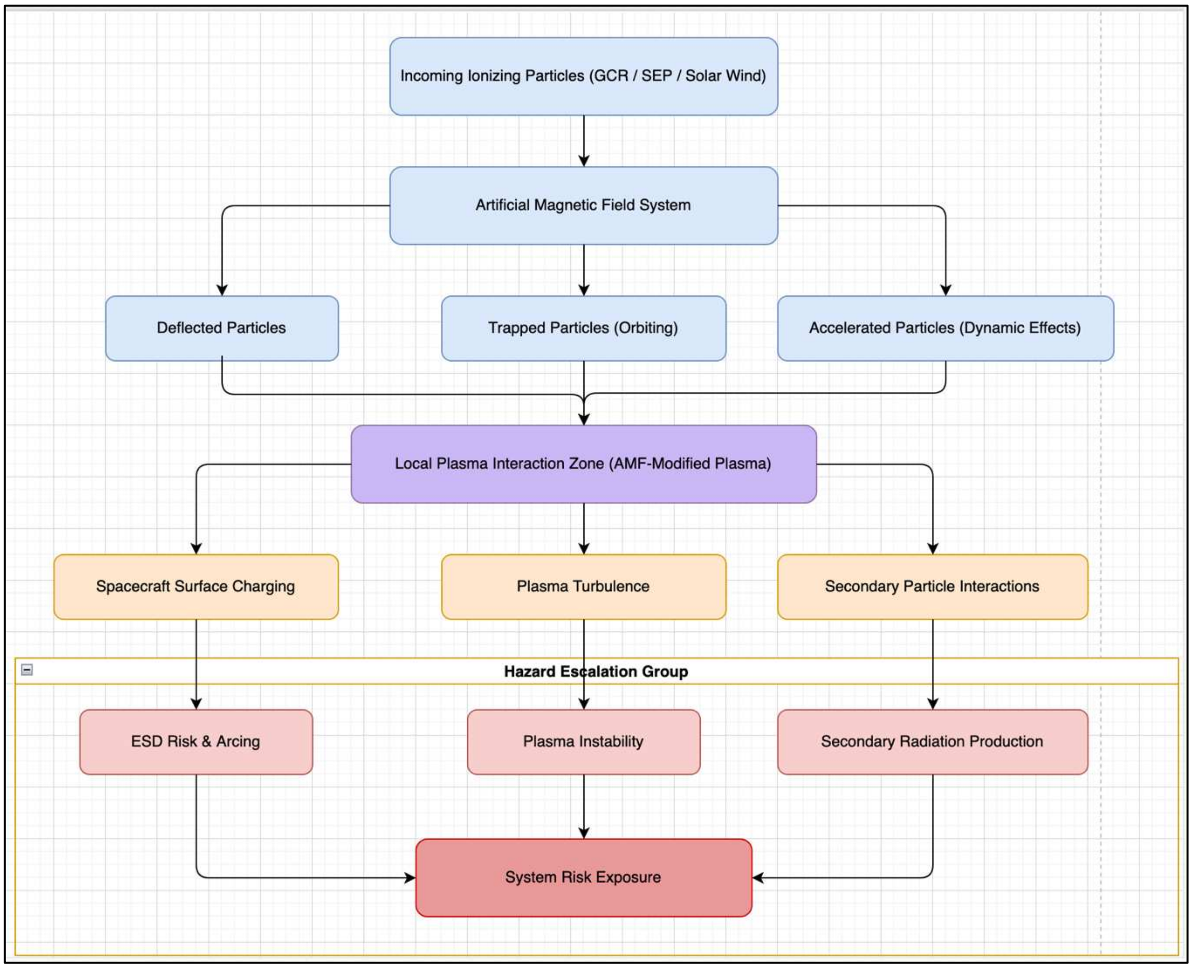

Figure 6.1 Plasma State Hazard Escalation Pathways Induced by Artificial Magnetic Field System Interactions [6]

This diagram shows system components, the artificial magnetic field (AMF), plasma interaction zone, hazard nodes, and the flow of energy and charged particle effects between them. Each escalation node represents a flow port, with directed connectors illustrating the causal progression from plasma interaction to system risks.

The plasma state diagram captures the dynamic interaction between the artificially generated magnetic field system and the surrounding space plasma environment which illustrates how these interactions give rise to spacecraft charging and secondary radiation effects. The diagram highlights the causal pathways through which plasma disturbances evolve into electrical instabilities which is a critical factor in understanding system-level radiation risks.

The flow begins with incoming ionizing particles, galactic cosmic rays (GCR), solar energetic particles (SEP), and solar wind plasma, which encounter the AMF system. The AMF is designed to modify particle trajectories which produce three principal outcomes: deflected particles, accelerated particles (due to dynamic field effects), and particles trapped in orbiting configurations around the spacecraft [6].

These interactions culminate in forming a localized plasma environment, referred to as the local plasma interaction zone. This is where AMF-modified particle behavior defines the immediate operational plasma conditions near the spacecraft. Within this zone, three critical phenomena arise: surface charging of the spacecraft structure, turbulent plasma behaviors caused by field and density instabilities, and secondary particle interactions initiated by collisions and field-induced instabilities [16].

From these initial effects, escalation pathways propagate into more severe hazards. Spacecraft surface charging can result in differential voltage buildup across surfaces which can directly lead to electrostatic discharge (ESD) risk and arcing. Plasma turbulence fosters plasma instability, which destabilizes the surrounding plasma sheath and increases the likelihood of uncontrolled plasma behavior. Secondary particle interactions amplify the production of secondary radiation, which contributes to internal and external radiation hazards [1, 6].

These distinct escalation paths converge on a unified critical node: system risk exposure**.** This node represents the cumulative threat posed by cascading plasma-related hazards. At this point, uncontrolled discharge, instability, and enhanced secondary radiation jeopardize structural integrity, and electronics survivability.

This diagrammatically articulated flow highlights the coupled nature of charging and secondary radiation effects. Rather than discrete hazards, they are deeply interconnected via shared plasma dynamics. The AMF system, while mitigating primary radiation exposure, induces plasma interactions that can escalate without appropriate mitigation strategies. This system-level understanding is critical for informing active control measures and design choices to minimize compounded risks in deep-space mission environments [1, 6].

6.2 Hazard Escalation Analysis and Failure Modes

As illustrated in Figure 6.2.1, the initial plasma interactions propagate through distinct escalation pathways. Spacecraft surface charging progresses toward electrostatic discharge (ESD) risk and arcing, where differential voltages exceed material dielectric breakdown thresholds (RQ-3.3.1 specifies ±300 V as the material limit). At the same time, plasma turbulence fosters plasma instability that destabilizes the sheath structure around the spacecraft.

RQ-3.3.2 mandates monitoring of oscillatory plasma flows exceeding 1 kHz frequency deviation from nominal sheath equilibrium. Separately, secondary particle interactions amplify secondary radiation production and this increases the internal and external radiation dose environment. RQ-3.3.3 requires detection of dose rates exceeding 100 μGy/hour, marking the threshold for critical response activation [6, 7].

These escalation chains converge on a critical node: system risk exposure. This risk exposure represents the compounded threat of uncontrolled electrostatic discharges, plasma instability propagation, and elevated secondary radiation fields and these collectively jeopardize spacecraft survivability.

Figure 6.2 shows an internal block diagram representing the AMF hazard control system, showing how real-time constraint blocks evaluate plasma measurements from the PlasmaHazardMonitor to identify threshold violations. These violations activate mitigation pathways via the FieldControlProcessor and AMF_MitigationSubsystem, protecting against electrostatic discharge, plasma instability and secondary radiation exposure.

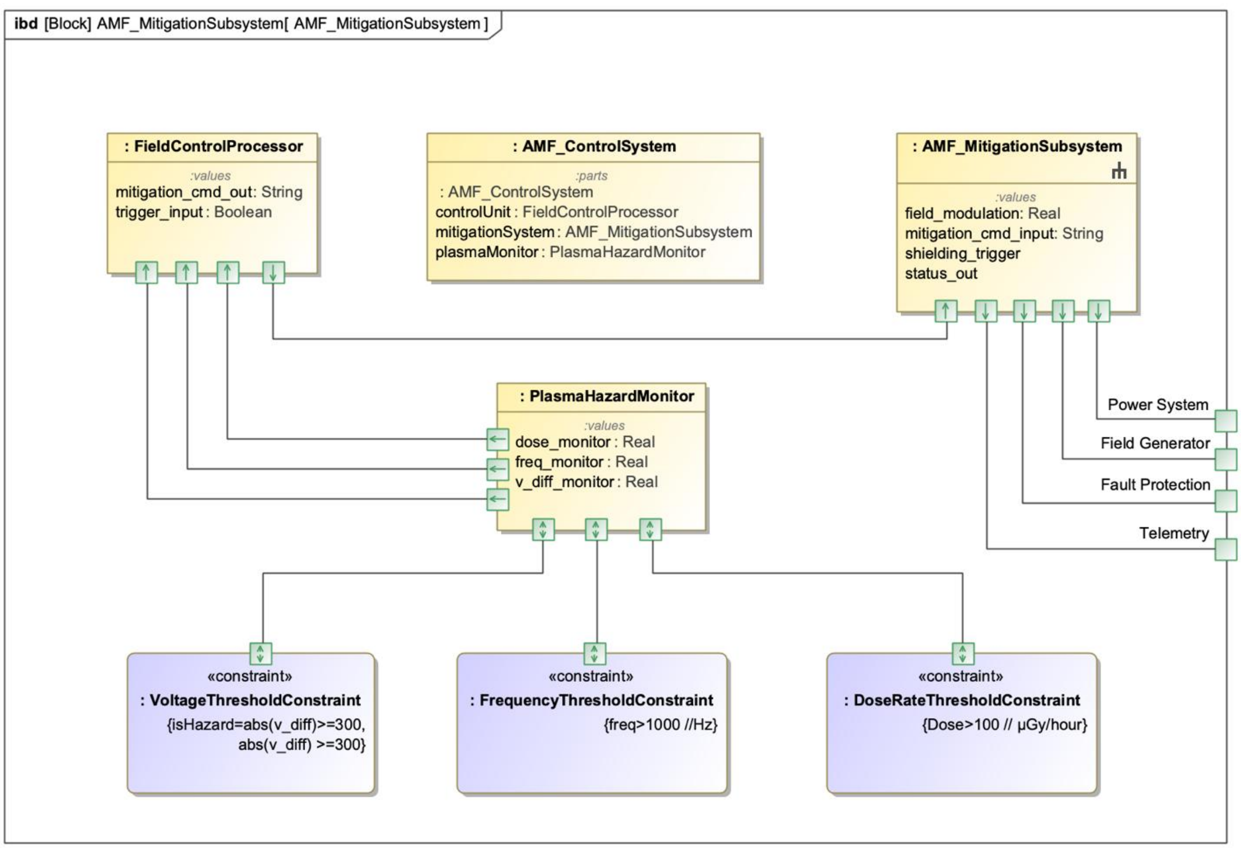

Figure 6.2 Internal Block Diagram of AMF Plasma Hazard Evaluation and Mitigation Flow

Table 6.2 builds on the qualitative flow illustrated in Figure 6.2 by presenting a structured failure modes and effects analysis (FMEA) that catalogs potential plasma-induced hazards and their causes, effects, detection methods, and proposed mitigations. The table establishes a traceable link between system design decisions and associated operational risks. This connection is critical for supporting rigorous design assurance and future system certification efforts [6, 8].

Table 6.2: Failure Modes and Effects Analysis (FMEA) for Plasma-Induced Hazards in Artificial Magnetic Field Systems [6, 8]

Failure Mode	**Cause**	**Effect**	**Detection Method**	**Requirement Reference**	**Mitigation Strategy**	**Failure Detection Method (Mitigation)**
Spacecraft Surface Charging	Accumulation of charge due to interaction with AMF-modified plasma sheath	Electrostatic Discharge (ESD), arcing, component degradation	Voltage differential monitoring (±300 V threshold)	RQ3.3.1	Voltage limiters; shielding; surface coatings	Voltage differential monitor; limit at ±300V
Plasma Instability	Sheath destabilization due to turbulent plasma flow	Erratic plasma behavior, control instability, sheath collapse	Plasma oscillation sensors (≥1 kHz deviation from nominal)	RQ3.3.2	Implemented active mass flow controls; plasma field stabilization	Plasma oscillation frequency monitor; >1 kHz deviation
Secondary Radiation Production	Particle interactions with shield structure and trapped flux	Elevated dose rates internally and externally, system exposure	Dosimeter array monitoring (>100 µGy/hr)	RQ3.3.3	Shielding; coupled shielding-conductive protection; onboard radiation triggers	Radiation dosimeter; gov't dosimetry monitor; >100 µGy/hr

Table 6.2 provides a structured breakdown of the primary plasma-induced hazard chains identified in Section 6.2 and illustrated in Figure 6.2. It captures failure modes such as spacecraft surface charging, plasma instability, and secondary radiation production, each stemming from artificial magnetic field (AMF) interactions within the localized plasma environment. The table associates each failure mode with a specific initiating cause with a description of its downstream

effect on spacecraft systems and a detection method. It also links each hazard to its governing system requirement (RQ-3.3.x series) and a mitigation strategy traceable to subsystem design elements [9].

This table operationalizes the hazard escalation pathways shown in Figure 6.2 by offering engineering responses and measurement points that support mitigation. Regarding MBSE integration, this failure modes and effects analysis (FMEA) corresponds to an MBSE parametric structure in which each hazard block is linked via constraints to specific failure conditions and mitigation flow paths. The newly added "Failure Detection Method (MBSE Allocation)" column formalizes how sensing architecture is allocated to monitor key thresholds, using ports such as V_diff_monitor, freq_monitor, and dose_monitor. These allocations allow hazard conditions to be continuously evaluated in simulation and test environments which enhances system-level assurance [10].

Ultimately, this table establishes the technical bridge between system hazard understanding and active risk management that ensures that all plasma-induced threats are anticipated and designed for within the control framework.

Figure 6.3 illustrates how charging-induced effects constrain multiple subsystems and requirements across the AMF and spacecraft. It visually connects the hazards discussed in Table 6.3 to the system design requirements (RQ-3.3.x) and sets up the control pathways addressed in Section 6.4. In addition, it validates the escalation logic described in the text using a constraint-based MBSE view.

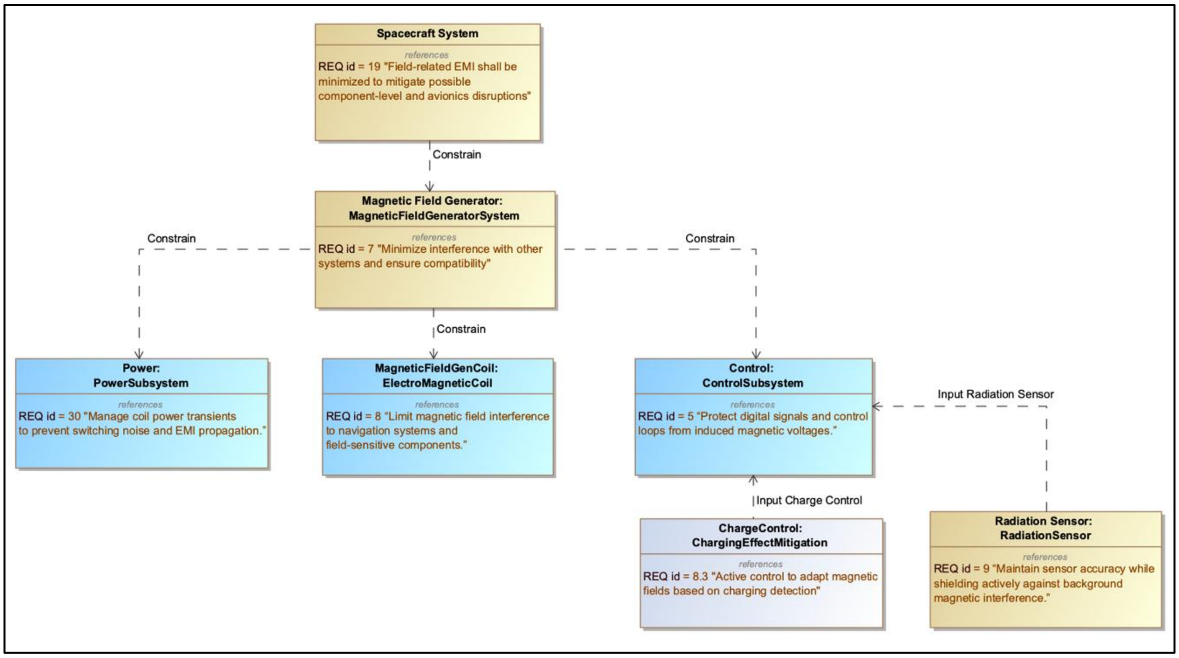

Figure 6.3: Block Definition Diagram of Charging Effects Constraint Allocation in AMF System.

This Cameo BDD model shows how spacecraft-level EMI mitigation (RQ-3.3.19), magnetic field interference control (RQ-3.3.7 and RQ-3.3.8), and digital signal protection (RQ-3.3.5) are structurally allocated to AMF subsystems and constrained by related charging effects. The diagram highlights the propagation path from charge detection to magnetic field modulation and subsystem protection logic.

6.3 Control Feedback Architecture for Plasma Hazard Mitigation

Although the previous analysis mapped potential failure modes and escalation paths, maintaining active system involvement remains essential to building a spacecraft capable of responding to real-time hazards. Continuous monitoring and dynamic response capability are not optional; without them, plasma-induced hazards could escalate unpredictably, often moving beyond recoverable limits before traditional fault management strategies have time to intervene [11].

The proposed control feedback architecture combines three primary functions:

1. Sensor suite for plasma and charging monitoring: As defined in RQ-3.4.1, the sensor network must deliver real-time telemetry updates at a minimum rate of 1 Hz to ensure timely hazard detection.
2. Control system for field modulation: According to RQ-3.4.2, the control logic shall modulate AMF coil currents within a ±20% dynamic range in response to detected anomalies.
3. System response activation: Requirement RQ-3.4.3 mandates that automated response protocols must execute within <500 ms to prevent hazard escalation upon breach of critical thresholds.

Figure 6.4 maps functional inputs and outputs across the sensor, control, mitigation, and magnetic field generation elements. It visually applies the control flow described in Section 6.4, particularly the logic described under RQ-3.4.1–3.4.3 (sensor feedback, dynamic field response, automated hazard suppression). In addition, it includes engineering parameters such as mitigation latency and voltage thresholds, tying the MBSE model to performance [6, 12].

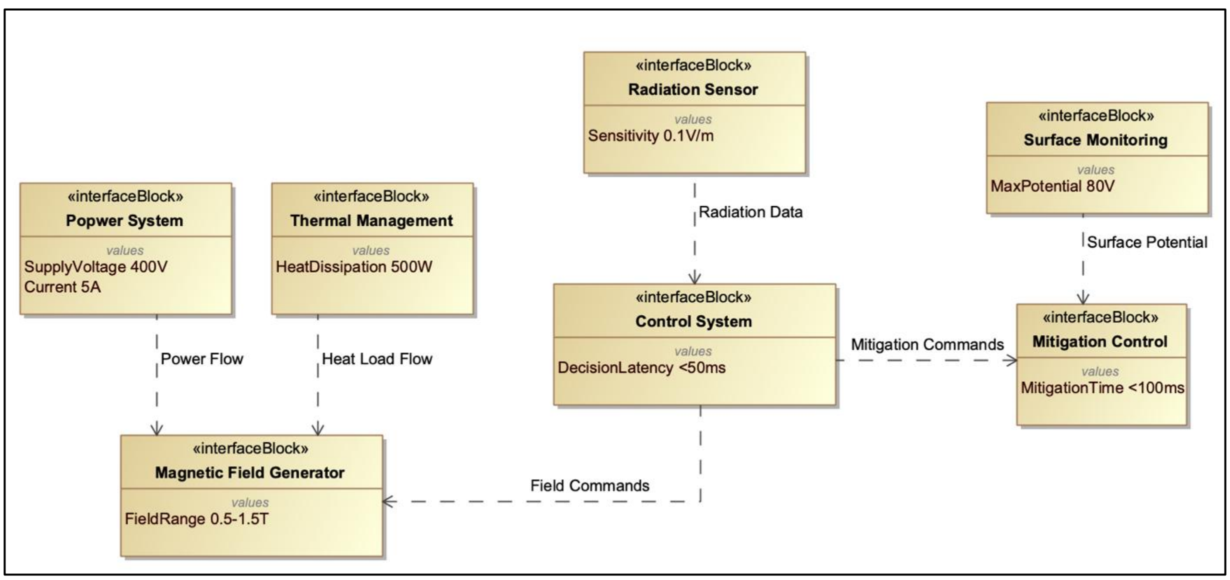

Figure 6.4: Interface Block Diagram of Charging Mitigation Functional Pathways.

This block diagram models the control response to spacecraft surface charging and EMI effects using MBSE interface block structures. The radiation sensors and surface potential monitors drive the control system with <50 ms decision latency, sending modulation commands to the magnetic field generator to initiate mitigation actions within 100 ms. Quantitative power supply and heat dissipation values are also included for real-time performance thresholds [12, 16].

Section 6.5 presents the verification and validation (V&V) matrix, which details the planned test, analysis, inspection, and similarity verification methods to ensure that each mitigation function performs reliably under operational conditions.

6.4 Verification and Validation Strategy

To ensure completeness of the proposed mitigation strategies, Table 6.3 outlines the verification approach for each system requirement derived from the hazard analysis. Test, analysis, inspection, and similarity methods are allocated across functional and performance requirements to ensure compliance with mission-critical tolerances and risk thresholds [13].

Table 6. 3: Verification and Validation (V&V) Matrix for Plasma Hazard Control System Requirements

Requirement ID	Requirement Description	Verification Method	Approach
RQ.3.2.1	Detect surface charging exceeding ±10 V/m differential	Test, Analysis	Differential probe array under simulated sheath conditions
RQ.3.2.2	Detect plasma density deviations ±15% from baseline	Test, Simulation	Plasma chamber testing with density gradient injection
RQ.3.2.3	Detect secondary particle flux >5 particles/cm²·s	Test, Simulation	Monte Carlo particle interaction simulation + sensor tests
RQ.3.3.1	Detect ESD/arcing voltage excursions above ±300 V	Test, Inspection	High-voltage arcing test and oscilloscope validation
RQ.3.3.2	Monitor plasma oscillation frequency >2 kHz deviation	Test, Simulation	Induced turbulence in plasma chamber and FFT analysis

RQ.3.3.3	Detect radiation dose rate exceeding 100 μGy/hour	Test, Analysis	Irradiation test with calibrated dosimeters
RQ.3.4.1	Sensor update rate must be ≥10 Hz for all plasma vectors	Test	Lab test loop with real-time signal logging
RQ.3.4.2	Field modulation response latency ≤100 ms	Test	Step-input modulation and timing capture with HIL testbed
RQ.3.4.3	System reaction time to hazard condition ≤250 ms	Test	Full-system hazard trigger response profiling with timer logs

Table 6.1, previously introduced in Section 6.2, is revisited as part of the broader V&V strategy covering all RQ-3.x.x requirements. Table 6.3 consolidates the verification strategy for all plasma hazard control system requirements specified in the RQ-3.x.x series. Each row provides a trace from a given requirement, such as detection thresholds for electric field potential, plasma density variance, or radiation dose rate, to its associated verification method and implementation approach. The methods include test (ground-based plasma chambers, high-voltage testing), analysis (Monte Carlo dose modeling), inspection, and simulation (frequency spectrum analysis, hardware-in-the-loop response checks) [13].

The structure of this table supports full coverage of verification pathways, ensuring that each mitigation function identified in the hazard and control architecture sections is validated against quantitative thresholds. This table also supports requirement traceability in MBSE tools: each requirement block (e.g., RQ-3.4.2: dynamic field modulation) can be linked to a TestCase or AnalysisBlock element in MBSE, allocated directly to the subsystem it verifies.

Figure 6.5 illustrates the parametric model scoped to AMF_ControlSystem, where real-time values from the PlasmaHazardMonitor are bound to formal constraints controlling surface charging, plasma instability, and radiation thresholds. The Boolean outputs (isHazard) from each constraint enable simulation-based verification of failure detection logic, as described in Figure 6.5.1.

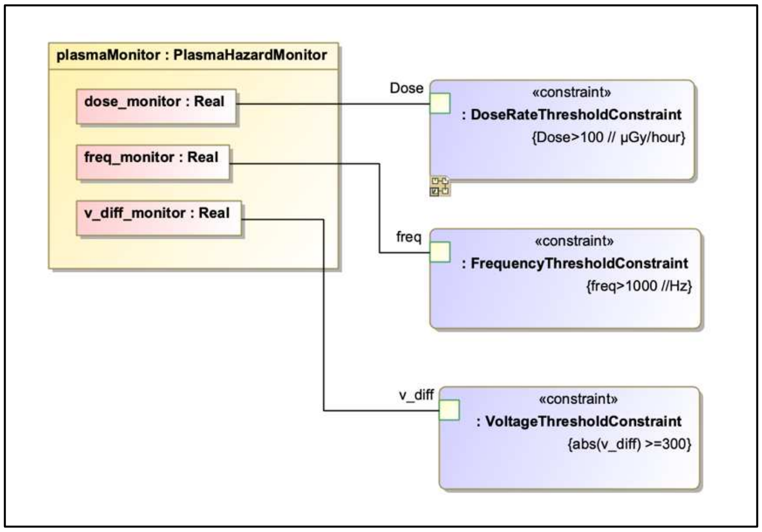

Figure 6.5: Parametric Diagram of Plasma Hazard Evaluation Constraints

These constraint evaluations act as executable verification points within the MBSE framework that provides traceable, testable pathways that satisfy the requirements outlined in the RQ-3.3.x and RQ-3.4.x series.

Table 6.3 and Figure 6.5 serve as the final layer of design affirmation for Chapter 6, confirming that hazard detection, response timing, and modulation control can be validated under realistic operating conditions. When viewed alongside Table 6.3, they complete the hazard control feedback loop by showing what must be controlled and how each function will be confirmed independently through engineering testing and analysis.

6.5 Summary and Conclusion

This chapter presented a comprehensive systems-level analysis of the hazards introduced by plasma interactions with artificial magnetic field (AMF) systems and established a control architecture for their mitigation. Beginning with identifying plasma interaction chains, the analysis traced the emergence of three key hazard pathways: spacecraft surface charging, plasma turbulence, and secondary radiation production. These phenomena, induced by the operation of the AMF system in a dynamic space plasma environment, were shown to be interlinked through a shared plasma interaction zone and their specific escalation effects.

Figure 6.2 illustrates the system hazard escalation flow, clarifying the causal progression from magnetic field–particle interactions to critical system-level risks such as electrostatic discharge (ESD), plasma sheath instability, and enhanced radiation dose. This hazard visualization provided a foundation for the structured failure modes and effects analysis (FMEA) in Table 6.3. It aligned each hazard with its initiating cause, downstream effect, detection method, and mitigation strategy. The FMEA was explicitly linked to governing system requirements (RQ-3.3.x series) and formalized through MBSE constraint views, as shown in Figure 6.3 [14].

Providing additional operational context, Figure 6.3 introduced an internal block diagram (IBD) of the AMF hazard control system, detailing how real-time plasma measurements from the PlasmaHazardMonitor are evaluated against critical thresholds. Threshold violations activate control pathways within the FieldControlProcessor and AMF_MitigationSubsystem, ensuring dynamic mitigation of surface charging, plasma instability, and secondary radiation risks. This model visually represents the hazard escalation pathways identified earlier, directly linking failure detection to system-level response mechanisms.

The verification and validation (V&V) strategy described in Section 6.5 was implemented through a parametric model (Figure 6.5), which connects sensor outputs to threshold-evaluating constraint blocks. These constraint evaluations produce Boolean *isHazard* outputs that serve as executable triggers within the MBSE framework, enabling real-time detection of hazard onset conditions. Table 6.5 consolidated the verification methods, spanning test, analysis, inspection, and simulation, ensuring that each requirement in the RQ-3.x.x series is independently validated under mission-representative conditions [15].

The integrated models, diagrams, and V&V planning demonstrated in this chapter reflect a mature model-based systems engineering (MBSE) methodology. Hazard escalation logic, mitigation control flow, and test traceability were implemented in Cameo using constraint blocks, interface structures, parametric evaluation, and «verify» relationships. The architecture is designed to support both early validation and late-stage system qualification [15].

In conclusion, this chapter establishes that active management of plasma-induced hazards is necessary and technically feasible through a systems engineering approach that integrates plasma sensing, dynamic field control, and formal verification. While introducing complexity through its impact on the plasma environment, the artificial magnetic field system can be safely integrated into spacecraft designs through rigorous hazard modeling, responsive control architectures, and simulation-driven verification strategies [15].

The next chapter builds upon these findings by extending the AMF risk mitigation strategies into a broader system-of-systems (SoS) context. Specifically, Chapter 7 addresses how AMF subsystem behavior, failure modes, and mitigation logic integrate with spacecraft power, thermal, and structural systems, ensuring whole-system resilience against plasma-originated and internal hazards.

CHAPTER 7 MITIGATING CHARGING EFFECTS ON MAGNETIC RADIATION SHIELDS

Active radiation shields that use artificial magnetic fields can protect crewed spacecraft by deflecting charged particles, but they also introduce unique spacecraft charging and interference issues. The same magnetic fields that trap or redirect radiation can cause surface charging, internal dielectric charging, and electromagnetic interference (EMI) on the vehicle. Researchers and space agencies have studied these effects and potential countermeasures. One proposed mitigation is degaussing which reduces or removes the magnetic field when not needed, dissipating built-up charges and minimizing interference. Below, the physical mechanisms of charging from artificial magnetospheres are examined, evaluating whether degaussing could alleviate these problems. Relevant NASA, ESA, and academic studies are reviewed, and the engineering feasibility and limitations of implementing degaussing in space are discussed.

7.0 Charging Mechanisms of Artificial Magnetic Fields

Artificial magnetic shields, often implemented with superconducting coils, create a mini-magnetosphere around a spacecraft. This altered environment can lead to several charging and interference phenomena:

- **Surface charging:** A strong magnetic field can trap ambient plasma (electrons and ions) in a torus or "bubble" around the spacecraft [1]. This magnetically confined plasma can induce differential surface potentials similar to those in a natural magnetosphere. In Earth's geomagnetic plasma, orbiting satellites accumulate negative charge when high-energy electrons impact insulating surfaces, leading to electrostatic discharges (ESDs) [2]. Similarly, a spacecraft's artificial magnetosphere could accumulate a cloud of charged particles that charges its surfaces unevenly. NASA notes that a magnetic field attached to a spaceship may capture solar wind plasma, which could interfere with instruments and charge surfaces [3]. Trapped electrons in the field can coat the spacecraft in negative charge, while positive ions may be excluded, creating a strong electric potential. The "plasma shield" concept relies on this principle: trapped electrons set up an electric field that deflects incoming protons [4]. The drawback is that the vehicle may sit within that induced electric field or plasma sheath. If surface charge builds to a critical threshold, a discharge or arc can occur, potentially damaging electronics or surfaces [5, 6]. Historical satellite failures in natural magnetospheres (e.g., Galaxy 15 in geosynchronous orbit) have been attributed to surface charging and ESD from "hot" electrons [7]. An artificial field could create analogous hazards unless carefully controlled.

- **Internal charging:** High-energy electrons in the megaelectron-volt (MeV) range that are deflected but not expelled by the magnetic field may be trapped in spiraling orbits along field lines. Over time, some of these penetrating electrons can embed in dielectric materials inside the spacecraft, causing internal charging. This is analogous to dielectric charging in satellite components from Earth's radiation belts. A powerful magnetic shield could form its mini–radiation belt around the spacecraft [8]. If energetic electrons remain confined near the vehicle for long periods, they increase the radiation dose to electronics and can accumulate charge in cable insulation, and circuit boards. This can eventually result in deep dielectric breakdown or electronic upsets. In the Jovian magnetosphere, spacecraft experience substantial internal charging currents from trapped high-energy plasma [12]. While a small artificial magnetosphere may not reach Jupiter's extreme particle flux, even a moderate trapped radiation population is a concern. Calculations of spacecraft charging in planetary magnetospheres show that the local plasma environment controlled by a magnetic field strongly affects charging levels [10]. In worst-case scenarios at Earth, surface potentials of –10 kV to –20 kV have been observed in plasma belts, and several kilovolts at Jupiter [7]. Although an artificial field may be tuned to avoid such extremes, this illustrates the scale of voltages that trapped particles can induce. Internal charging is challenging to detect until a discharge occurs which makes it an important design consideration if magnetic shielding is used.

- **Electromagnetic interference (EMI) and magnetic effects:** A strong magnetic field can directly interfere with spacecraft systems. Static magnetic fields do not induce currents in stationary conductors (per Faraday's law, which requires changing flux), so a steady field should not generate currents in wiring or devices. However, a large static field can saturate sensors (e.g., magnetometers), disturb compasses or momentum wheels, and exert force on ferromagnetic components. The field can couple with moving conductive structures. If the spacecraft rotates or conductive fluids move through the field, voltages can be induced, turning the spaceship into a dynamo. Any time-varying magnetic flux, such as when the shielding coils are powered up or down, or if they quench or fail, will induce electromotive forces in nearby circuits. A rapid magnetic field collapse could create large voltage spikes in spacecraft wiring. The NASA Magnet Architectures and Active Radiation Shielding (MAARSS) study emphasized that the energy stored in the field must be carefully dissipated to avoid harmful transients [12]. Another EMI concern is radio-frequency interference. Plasma trapped in a magnetic field can emit electromagnetic noise during arcs or oscillations [9]. In addition, the spacecraft's magnetic dipole moment can interact with planetary or solar wind magnetic fields, potentially causing attitude disturbances or unwanted electromagnetic torque. Overall, the presence of a high-field magnet onboard raises significant electromagnetic compatibility challenges, which must be addressed through design measures such as shielding sensitive electronics and using compensation coils [12].

7.1 Summary of Effects and Causes

To summarize the above, Table 7.1 outlines the significant charging/interference effects from an artificial magnetic shield and their physical causes:

Table 7.1: Major Charging/Interference Effects

Effect	Cause with Artificial Magnetic Field	Consequences
Surface Charging	Magnetic field traps plasma around spacecraft; electrons and ions separated, inducing large electric fields and differential surface potentials [9, 10].	Surface materials charge (often negative), risk of ESD arcs damaging electronics or surfaces [3, 7].
Internal Charging	High-energy electrons spiral along magnetic field lines and can become confined near the spacecraft (like a mini radiation belt) instead of escaping [8]. Some penetrate shielding and embed in dielectrics.	Gradual charge buildup in insulating components; potential for deep dielectric discharge, bit flips, or component failure (analogous to natural radiation belt effects) [7, 12].
EMI & Magnetic Interference	Strong static field permeating spacecraft; can magnetize components and saturate sensors. Powering coils on/off or sudden changes (quench) induce currents in circuits. Trapped plasma may generate RF noise [9, 12].	Instrumentation errors (e.g. compromised magnetometer readings), induced voltages in wiring during field transients, possible communication interference, torques on spacecraft from magnetic forces [12].

NASA’s technology assessments have acknowledged these issues. For instance, a deployed electromagnetic shield concept notes that a magnet attached to the spacecraft would “cause other shielding issues with equipment” and perturb data and transmissions [9]. It also warns that the field would capture part of the solar radiation as plasma in a torus around the spacecraft, which will essentially recreate a small radiation belt, which could impede nearby instruments [9]. For these reasons, NASA and others often favor designs where the magnetic field source is moved away from the vehicle (e.g., a coil on a boom or a separate unit) [9, 10]. By distancing the field from the vehicle, the spacecraft sits in a region of minimal field/plasma, reducing charging and interference on the spacecraft itself.

7.2 Can Degaussing Mitigate These Effects?

Degaussing refers to reducing or eliminating a magnetic field, often by gradually ramping down an alternating current (AC) field to demagnetize materials. In the context of a spacecraft magnetic shield, "degaussing" would imply turning off or significantly lowering the artificial magnetic field when it is not actively needed and possibly demagnetizing any components that became magnetized. This approach could mitigate charging and EMI effects in several ways:

- **Eliminating the plasma trap:** The most direct benefit of degaussing is that the artificial magnetospheric trap disappears once the magnetic field is turned off. Any charged particles confined by the field will disperse into space instead of remaining near the spacecraft. This would allow surface charges to bleed away into the ambient space environment. In essence, degaussing removes the cause of the abnormal plasma environment. Without the confining field, electrons and ions are no longer forced into proximity with the hull, and the spacecraft can return to the benign charging conditions of free space (aside from normal space weather). Intermittent use of the magnetic shield (activating it only during solar storm events) has been proposed to balance protection and safety [8]. During quiet periods, the field could be turned off (degaussed), preventing long-term charge accumulation. NASA's Active Radiation Shielding workshop implicitly endorsed this strategy. Concepts with magnets inside the vehicle were deemed problematic partly because of continuous field exposure. However, designs with magnets deployed externally (activated at a distance when needed) were considered more feasible [10]. In practice, degaussing an active shield after a radiation event would let trapped plasma dissipate so that the crew and electronics are not left in a charged cloud once the event passes.

- **Removing residual magnetization:** Degaussing is traditionally used to demagnetize ferromagnetic materials. Spacecraft engineering already employs this in the form of magnetic cleanliness protocols. For example, ferrous components are demagnetized with coil assemblies on Earth before integration, and some spacecraft carry small compensation magnets or magnetorquer coils to cancel remnant magnetic moments in orbit [1]. If a powerful superconducting coil generates a strong field, it could magnetize parts of the spacecraft (e.g., steel fasteners or equipment). Running a degaussing cycle, an oscillating, decaying magnetic field, via onboard coils could neutralize this residual magnetism, reducing long-term interference. For example, the Jet Propulsion Laboratory uses solenoid coils to demagnetize components to <5 mT residual fields for missions with magnetometers [1]. In space, a dedicated degaussing system could ensure that after the primary shield coil is turned off, the spacecraft is not left with a lingering magnetic field that could induce currents or torques. This is especially relevant if the shield was active for long periods and magnetized the hull [13].
- **Controlled ramp-down to avoid induction:** Simply switching off a large superconducting magnet could induce a rapid change in flux (if not managed by a dump circuit), generating large voltages like a giant circuit breaker opening. A degaussing procedure implies a gradual ramp-down of the field, possibly reversing polarity in steps

to reduce hysteresis. Such a controlled shutdown would mitigate induced EMI. The MAARSS Phase II study analyzed quench detection and energy extraction methods for superconducting coils to safely remove the field energy without harming the spacecraft [1]. By slowly lowering the current or using resistor dump circuits, the magnetic field collapses gently which allows induced currents to dissipate harmlessly. This is analogous to degaussing a CRT monitor to avoid sudden spikes. In an active shield scenario, a "stand-down" mode could oscillate the field to zero while sweeping out trapped particles. For example, slight oscillations of field strength or orientation might eject charged particles along controlled paths, possibly directing them away from the crew cabin. Although literature on pulsing the field to shed plasma is limited, the concept of a "scrubber" for trapped particles has been discussed (e.g., having artificial radiation belts intersect a physical absorber or the ground in a base scenario) [8]. Without a physical absorber, degaussing the magnet is the primary method to clear those particles in space.

- **Intermittent field use:** Degaussing in a broader sense could also mean generating the magnetic field only when necessary. NASA's Deployed Radiation Shield (DERDS) concept embodies this principle by keeping the field source separate and only energizing it during solar events [9]. The magnet unit would power on to deflect a solar proton storm and then power down (degauss) afterward. This ensures that the crew module is not continuously exposed to a strong field. This on-demand use is a mitigation strategy against chronic charging. The spacecraft would spend most of its time with no artificial field (no charging beyond the typical space environment) and only briefly endure the field's side effects during an active shielding window. Any residual charge from those brief periods could dissipate when the field is turned off [9].

It is worth noting that no major agency has explicitly termed their mitigation "degaussing," but the principle of removing the field to remove the side effects is a common theme. For instance, the European Space Agency's SR2S (Space Radiation Superconductive Shield) project (2012–2015) examined a "pumpkin" configuration of superconducting coils placed around a habitat. They concluded that if a magnet fails or is turned off, the only impact should be loss of radiation protection, not damage to the spacecraft [4]. This implies the system was designed so that a sudden field loss would not dump hazardous energy or particles into the habitat. In other words, safety analyses ensured that field removal would not create a worse event than the radiation itself. This is a basic acknowledgement of the importance of controlled deactivation (a form of degaussing) [7].

Effectiveness: If appropriately implemented, degaussing would likely reduce surface and internal charging caused by the magnetic shield. The source of plasma accumulation and large direct-current (DC) potentials is removed by dissipating the artificial magnetosphere. The spacecraft's floating potential would then revert to what it would be without the shield. In interplanetary space, there is usually a small positive charge from photoelectric effects plus ambient plasma current. This is far more benign than thousands of volts negative. Any internal charging from trapped electrons would stop increasing once the trap is gone. Those electrons would either escape or thermalize. Degaussing also helps with EMI; no field means no magnetic torque or sensor bias, and no changing field means no inductive coupling [7, 10].

Challenges: While degaussing can mitigate charging, it comes with trade-offs. Turning off the shield means turning off the protection. During the period the field is off to allow charges to neutralize, the crew is unprotected from radiation. Therefore, timing is critical; degaussing would be performed only when radiation levels are low (between solar events or after a storm has passed). If a second solar flare arrives while the shield is off, the spacecraft might be caught unprotected. Another challenge is that a large demagnetization coil or procedure might be required if parts of the spacecraft become magnetized, adding complexity. The process must also be engineered to avoid inducing currents during ramp-down. Improperly executed degaussing could itself cause an electromagnetic transient. Engineering solutions such as soft-switching electronics and quench protection circuits exist to manage this [10].

In summary, periodic degaussing (field shutdown) is conceptually a powerful tool to mitigate magnetically induced charging. It essentially resets the system, preventing runaway charge buildup and long-term interference. NASA and ESA studies incorporate this idea by favoring short-duration, distant, or on-demand magnetic shielding over permanent onboard magnets [9]. The consensus is that any active magnetic shield must be used to minimize continuous exposure of the spacecraft to strong fields, and degaussing is one way to achieve that minimization.

7.3 Relevant Studies and Experimental Data

Active magnetic shielding remains largely theoretical; no crewed mission has flown a large superconducting magnet for radiation protection. However, numerous analyses and small-scale experiments address charging and interference issues, and how degaussing or other methods might help:

- **NASA technical studies:** NASA's Advanced Concepts and NIAC studies in the 2000s (e.g., the MAARSS report) addressed integration of magnetic shields. These studies discuss the need to manage the magnetic field's effects on the spacecraft. For example, MAARSS introduced compensation coils to reduce the field in the crew habitat [12]. This is essentially a local canceling field, so astronauts and electronics are not in a strong magnet even when the main shield is active. It is a mitigation similar to degaussing in that it reduces field exposure. The report also covers quench protection, indicating the importance of safely handling field energy [12]. The fact that compensation coils are needed underscores that the primary coil's field would interfere with onboard systems without mitigation. Another NASA concept, DERDS, was patented as a deployable shield. It keeps the magnet at a distance to avoid "perturbing data collection and transmissions" and to prevent plasma from being too "close [in] position to the spacecraft."[9] This is a design-level solution to the charging issue by geometry rather than active degaussing. Still, it confirms that if the magnet were attached, data interference and plasma charging would occur [9].

- **ESA and academic research:** The European SR2S project demonstrated hardware prototypes of superconducting magnet shields and performed extensive simulations. Their findings showed that safety and system integration are critical. While public reporting from SR2S focused on achieving dose reduction, they noted that "safety could be one of the main showstoppers" for active shields and performed failure mode analyses to ensure a magnet failure would not harm the habitat [4]. They achieved a design in which a quench (loss of superconductivity) would not structurally damage the craft [4]. Though details are sparse, this likely involved controlled discharge of the magnet's energy, effectively a forced degauss, into a safe dump [13]. Furthermore, ESA's earlier Topical Team (2002) recommended developing magnetic storm shelters by 2025 but acknowledged open questions on plasma interactions and engineering complexity [10]. In academic work, Ruth Bamford et al. simulated "mini-magnetospheres" and noted that a protective electric field builds from trapped plasma, deflecting radiation [14]. Their 2014 work showed up to 95% deflection of solar storm particles with a combined magnetic and plasma shield [17]. However, other experts, such as Robert Winglee, have pointed out that such studies did "not address the magnetic field's effects on the astronauts" or, presumably, on spacecraft systems. This underscores that while shielding performance has been studied, by-products such as charging and potential health effects of strong magnetic fields on crew require more investigation. Bamford's team and others have proposed small-scale space experiments to deploy a magnetic bubble around an unmanned satellite. These would help empirically measure charging and plasma behavior, but results are not yet available [4, 16].

Spacecraft Charging Research: Although no direct experiment of a magnetic shield causing charging has been done, we can draw on analogs. Satellites in low Earth orbit occasionally charge when passing through auroral regions where Earth's field guides energetic electrons along specific paths. Indeed, auroral charging events are linked to magnetic field–aligned electron beams in Earth's magnetosphere [15]. This shows that magnetic topology (how field lines shape particle motion) is a key factor in charging. By extension, a spacecraft coil that produces a magnetic topology will also shape particle flows and could create localized beams or wake effects that charge spacecraft parts. Ground-based experiments (plasma chambers) have shown that placing an object in a magnetized plasma can lead to complex sheath potential.

However, most laboratory setups are small. One concept experiment (at the University of Washington and MSFC under NIAC, called Mini-Magnetospheric Plasma Propulsion) injected plasma into a dipole field to inflate a magnetic bubble [16]. While that was for propulsion, it is similar physics. The results indicated a standoff distance created by the plasma pressure and that controlling the plasma was difficult. It has not been widely reported if any charging was observed, but the need for active plasma management was evident.

Naval Degaussing Analogy: Though not a space experiment, large vehicles (e.g., naval ships) routinely use degaussing coils to cancel their magnetic fields and avoid triggering mines. The technology to actively cancel or reduce magnetic fields in a controlled manner is mature. Translating that to spacecraft, one could implement a tri-axial coil system to null the residual field after using a shield [24]. NASA's knowledge base in demagnetization (e.g., practice note PD-ED-1220, "Demagnetization of Ferromagnetic Parts") shows that even in assembly, engineers consider how to minimize magnetic dipoles that could interact with Earth's field and cause torques or instrument errors [1]. The same principle would apply to a Mars transit vehicle with a magnetic shield. After running the shield, built-in coils could deperm any induced magnetism. Spacecraft often carry magnetorquer coils for attitude control, which generate magnetic moments. These could double as a degaussing system in a pinch by driving them with oscillating currents to wipe out magnetization. While this has not been tested in orbit (since no mission has flown a large superconducting magnet), it is a feasible extension of existing technology [24].

In summary, primary sources agree on managing the field's side effects. NASA and ESA studies prioritize designs where the magnet can be isolated or turned off to avoid continuous charging [9]. Peer-reviewed work demonstrates the shielding feasibility but often does not fully address the spacecraft-charging question, indicating that more research is needed [17]. No insurmountable physics problems have been identified; rather, it is an engineering control problem. Degaussing (or, more generally, magnetic field management) is a recommended solution to that control problem.

7.4 Feasibility and Engineering Considerations for Degaussing in Space

Implementing a degaussing system on a spacecraft is possible but presents engineering challenges:

System Complexity and Mass: A dedicated degaussing coil (or set of coils) sized to demagnetize the entire spacecraft would add mass and require power. Large coils may be needed to encompass a spacecraft ten of meters in size (ground facilities use multi-meter Helmholtz coils for demagnetization) [1]. Every gram is critical in space, so designers would likely seek to avoid a continuous degaussing system. One alternative is to integrate the function into existing hardware. For example, the primary superconducting magnet could perform a degauss by driving an alternating current (although superconductors and AC do not mix well due to losses and quenching). More practically, normal-conducting trim coils (possibly the identical coils used for field shaping or compensation) could be repurposed to run a degaussing sequence after the primary coil is turned off. The power requirement for degaussing is modest compared with running the shield at full strength. Demagnetization might need only a few percent of the shield's operational energy for a short duration. Still, this must be accounted for in the power system design [16].

Electronic Safety: The degaussing procedure itself must not damage spacecraft electronics. NASA guidelines caution against exposing spacecraft assemblies to >5 mT alternating fields, as strong demagnetizing fields can induce currents or flip bits in memory [7]. Thus, a space degaussing system would likely operate at low field amplitudes or with sensitive electronics powered down. The crew and critical systems may need to be safe when the degauss coil operates, similar to MRI procedures for ramping down magnets without harming nearby devices. This implies operational overhead, e.g., after a solar storm, place the spacecraft in a configured state, degauss the magnet, and then resume normal operations [7].

Residual Fields: Even with degaussing, the magnetic field cannot be reduced to absolute zero. There will always be a small remnant. The question is whether that remnant is low enough to be benign. Space missions that require “magnetic cleanliness” (e.g., scientific observatories) sometimes achieve residual fields on the order of microteslas after demagnetization. The tolerance may be higher for a crewed vehicle if no magnetic-sensitive science is occurring onboard. For example, a residual dipole that causes 0.1 mT (1 gauss) in the cabin might be acceptable for crew and most instruments (Earth’s field is similar). The NASA active shield workshop noted no clear static field exposure limits for crew beyond general workplace limits (~100 mT) [18]. Perfect demagnetization is therefore not required. only a sufficient reduction is required to prevent major charging or interference. The design could also incorporate mu-metal or magnetic shielding around sensitive components to mitigate residual fields further [10].

Failure Modes: The design must account for potential degaussing failure. If the magnet cannot be turned off or reduced (e.g., a stuck persistent current in a superconducting loop), the spacecraft could remain in a high-charging state. Redundant methods to kill the field could include a quench subsystem (forcing the superconductor out of its superconducting state to dissipate the field quickly, essentially a last-resort degauss). Quenching a superconducting magnet dumps its energy as heat and rapidly collapses the field, clearing the plasma trap but generating a large transient. The SR2S safety analysis ensured that a sudden quench would not structurally harm the habitat [4]. It is also necessary to ensure it does not electrically harm the spacecraft. This may require spark gaps or surge protectors for components that could pick up the pulse. The system must be failsafe: the field is removed gracefully (preferred) or, if removed abruptly, the removal will not be catastrophic [7].

Crew Considerations: If degaussing is done via an AC magnetic field, one might ask if that affects the crew (e.g., strong time-varying fields can induce currents in human bodies). However, any degaussing AC field would likely be low magnitude and low frequency, and the crew could be positioned at magnetically quiet spots (perhaps near the center of a Helmholtz coil where the field is minimized). The brief operation and relatively low field should be well within safety, certainly much less intense than an MRI machine's pulses, and those are considered safe for patients under controlled conditions [18].

Demonstration and Testing: Before committing to this on a crewed mission, a practical test might be done on a smaller scale. For example, a satellite carrying a small superconducting magnet (or even a normal magnet) could deploy it, generate a miniature artificial magnetosphere, and then degauss it while measuring surface potentials and plasma behavior [14]. This would provide real data on how quickly the charges dissipate and if any unexpected currents arise. As of 2025, such a mission has not yet flown, but it has been proposed in various forms [17]. Ground vacuum chamber tests can partially simulate this. A test article with a magnet could be immersed in a plasma beam to mimic solar wind, then see if turning off the magnet causes any transient charging on the article. These would help validate the degaussing strategy in a controlled way before risking a crew [17].

In terms of limitations, the primary one is that degaussing addresses the symptom (the charging) by removing the cause (the field), which inherently limits shield usage. If a mission profile required the magnetic shield to be active 24/7 (for example, continuous protection against cosmic rays), then degaussing periodically might undercut the shield's radiation protection duty cycle. For solar storms, it’s fine, you only need the shield during the storm. But for galactic cosmic rays (GCR), which are continuous, an active shield would ideally run continuously [19].

Degaussing in that case would leave the crew exposed to GCR during off times. This is one reason active magnetic shields are often considered more viable for intermittent events (solar particle events) than for constant GCR mitigation [10]. Some hybrid approaches suggest combining passive material shielding for GCR with an active field for solar events, thereby allowing the magnet to be off most of the time (solving charging issues). In contrast, passive shielding handles the steady background [22].

Another limitation is that degaussing will not solve all problems if the field is on for long durations. For instance, if a mission decided to leave the magnet on for a 2-week transit and then degauss, the spacecraft would still endure 2 weeks of possible interference and accumulated charge (with risk of intermediate discharges) [20]. Continuous mitigation during operation would then require other measures (like bleed-off devices, plasma contactors to neutralize charge, etc.).

It might be more practical to accept some level of charging but keep it below hazardous levels via careful design (e.g., make all exterior surfaces conductive and connected to a common ground, so even if they charge, they charge together and avoid significant differentials). Standard spacecraft charging mitigation (per NASA-HDBK-4002) includes using conductive coatings and grounding to equalize potentials [21]. These practices would certainly be applied in any actively shielded spacecraft to minimize the chance of an arc.

Finally, could degaussing be insufficient in any scenario? Possibly, if the magnetic field induced currents in a loop (like a superconducting eddy current in the structure) that persist even after the main coil is off, it is essentially a “frozen-in” current. That scenario is unlikely unless the spacecraft itself became superconducting. In a normal metal, currents die out quickly once the driving field is removed (governed by the L/R time constant). So, degaussing should remove the driving field, and any induced currents would naturally decay to zero [21].

For a spacecraft employing an artificial magnetic field (AMF) for radiation shielding, like a toroidal coil configuration modeled after the Orion design, implementing a functional degaussing system would most likely require dedicated degaussing cables or auxiliary coils. These degaussing coils would need to be routed around the spacecraft in a geometry that mirrors or complements the main magnetic field structure, enabling controlled dissipation of the field energy and neutralization of residual magnetization. The role of these coils is analogous to that of naval degaussing systems, which use loops placed along specific axes of a ship's hull to cancel its magnetic signature. In the spacecraft case, a similar layout would allow the degaussing system to cancel the global dipole or toroidal field, minimize structural magnetization, and safely route stored energy to a resistive dump network [23].

From an electromagnetic control perspective, enclosing the vehicle with a counter-wound or opposing-polarity coil array would enable a gradual ramp-down of the magnetic field. This would avoid abrupt field collapse that could induce large voltage transients. These degaussing coils may be physically integrated into the main shield architecture (e.g., as part of a trim coil array or compensation network) or form an independent layer surrounding the spacecraft shell [20].

In either case, their function is essential to restoring the spacecraft to a magnetically neutral state after an active shielding cycle. Without such a system, residual magnetization or trapped particle effects may persist long after the field is nominally shut off. As part of the broader magnetic cleanliness and EMI mitigation strategy, these degaussing loops offer a direct engineering pathway to control high-field spacecraft systems' operational and post-operational states.

Several design strategies can be used to implement or complement a spacecraft-scale degaussing system, as summarized in Table 7.2 [14, 24].

This table summarizes viable engineering strategies that can replace or augment a traditional spacecraft-wide degaussing coil system. Each approach offers functional mitigation of trapped fields or EMI transients and can be adapted depending on spacecraft geometry, mission risk profile, and system redundancy requirements.

Table 7 2: Alternatives or Complements to Full-Surround Degaussing Loops [12, 24]

Approach	**Function**	**Use Case**
Trim or Compensation Coils	Local B-field cancellation (e.g., near crew cabin)	Used in MAARSS and NASA studies
Remote-Deployable Coil System	Move magnet source away during deactivation	Minimizes field near spacecraft, avoids cables
Pulse Degaussing (with AC)	Oscillating low-field signal to decay magnetization	Common in naval systems and lab procedures
Dump Circuits + Internal Routing	Direct energy to resistive banks or flywheels	Quench protection, not full field cancellation

7.5 Degaussing Subsystem Structural Overview

The structural composition of the artificial magnetic field (AMF) degaussing system is modeled in Figure 7.1 using a SysML Block Definition Diagram (BDD), which defines the internal architecture of the DegaussController and associated test and monitoring interfaces. This subsystem is responsible for the controlled dissipation of the magnetic field following a shielding event, ensuring compliance with spacecraft electromagnetic interference (EMI), charging, and power safety constraints.

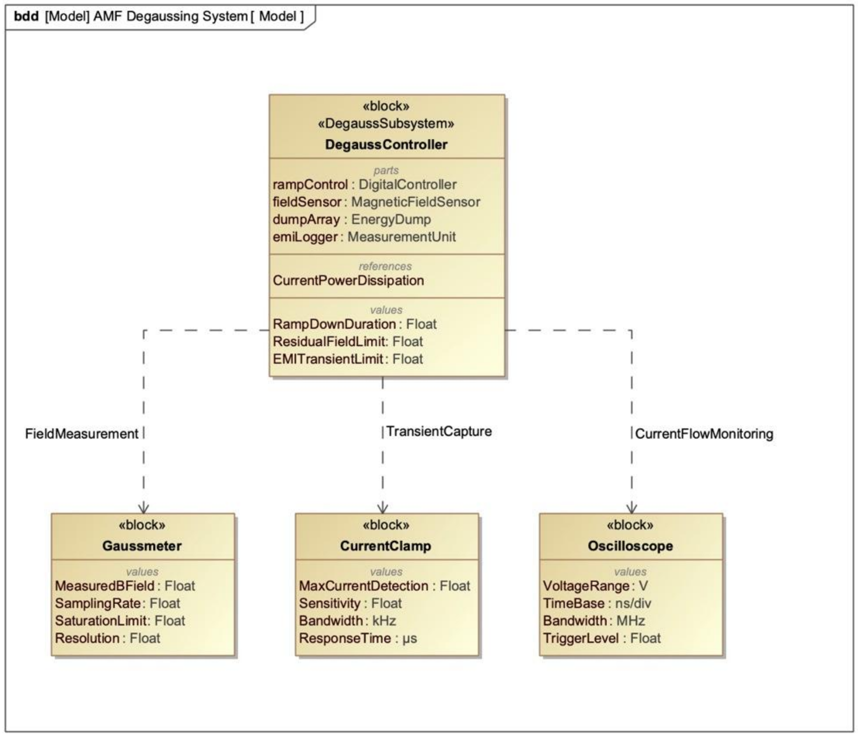

Figure 7.1. SysML Block Definition Diagram (BDD) of the Degaussing Control Subsystem for Active Magnetic Field Radiation Shielding.

Figure 7.1 illustrates the internal composition and external interface structure of the DegaussController, which manages the ramp-down of the artificial magnetic field following a shielding event. The controller includes four key parts: a DigitalController for sequencing, a MagneticFieldSensor for residual field monitoring, an EnergyDump for controlled power dissipation, and a MeasurementUnit for capturing EMI transients. Interfaces link to external instruments such as the Gaussmeter, CurrentClamp, and Oscilloscope. This is to validate performance against defined limits for field decay duration (seconds), residual field strength (μT), and transient EMI (mV). These flows support traceability to system-level verification requirements in Table 7.3 [25].

The DegaussController comprises four internal parts, each allocated to a specific functional role. The rampControl: DigitalController module governs the temporal ramp-down of current through the AMF coils, orchestrating the sequence and duration of the degaussing operation. The fieldSensor: MagneticFieldSensor component continuously monitors the magnetic field strength in the vicinity of the spacecraft, providing real-time data to assess decay performance. Simultaneously, the dumpArray: EnergyDump module offers a dedicated resistive path for power dissipation, enabling the controlled collapse of the magnetic field while avoiding high-voltage transients. Finally, the emiLogger: MeasurementUnit captures transient electromagnetic waveforms during field shutdown, supporting post-event EMI verification [15, 26].

Three critical scalar parameters are defined in the controller to support system monitoring and verification. These include RampDownDuration: Float [unit = seconds], which specifies the total time permitted for magnetic field decay; ResidualFieldLimit: Float [unit = microtesla (μT)], which defines the maximum allowable residual field following degaussing; and EMITransientLimit: Float [unit = millivolts (mV)], which represents the threshold for acceptable induced voltage transients during shutdown [15].

The controller interfaces with three external measurement systems via logical connections. The FieldMeasurement interface links the internal field sensor to the Gaussmeter, a monitoring unit characterized by parameters such as MeasuredBField: Float [μT], SamplingRate: Float [Hz], SaturationLimit: Float [millitesla (mT)], and Resolution: Float [μT]. This interface supports the verification of residual field performance. The TransientCapture interface routes current pulse data to the CurrentClamp, which MaxCurrentDetection parameterizes: Float [mA], Sensitivity: Float [mA/V], Bandwidth: Float [kHz], and ResponseTime: Float [μs]. These values detect potentially harmful induced currents resulting from rapid field collapse. The third connection, CurrentFlowMonitoring, links to the Oscilloscope, which provides high-fidelity EMI waveform capture. This device includes parameters such as VoltageRange: Float [V], TimeBase: Float [ns/div], Bandwidth: Float [MHz], and TriggerLevel: Float [mV] [27].

Collectively, this structure ensures that the DegaussController operates within defined electrical safety margins, that all charge-inducing effects are monitored and mitigated in real time, and that all functional outputs are verifiable through well-instrumented test interfaces. This architectural configuration supports formal traceability to system-level degaussing requirements, as defined in the Verification and Validation Matrix (Table 7.3). It enables fault-tolerant management of transient magnetic field collapse within the broader AMF radiation protection system.

Table 7.3: Verification and Validation (V&V) Matrix for Degaussing Subsystem Requirements.

Requirement ID	**Requirement Description**	**Verification Method**	**Verification Approach**
REQ-5.4.1	System shall provide capability to deactivate magnetic field within 10 seconds under nominal conditions.	Test, Analysis	Lab demo of coil ramp-down; field decay simulation using Ansys Maxwell
REQ-5.4.2	Shield field must decay to <1% of peak within 10 seconds without exceeding 100 mV transient on internal circuits.	Test, Analysis	Oscilloscope capture during degaussing; EMI transient modeling
REQ-5.4.3	Degaussing system shall not induce current >10 mA in adjacent harnesses during operation.	Test	Current clamp sensors on adjacent harnesses during field shutdown
REQ-5.4.4	Degaussing function shall be operable in safe mode with minimal crew intervention.	Inspection, Test	Review of control software logic; functional test in operational simulation
REQ-5.4.5	Residual magnetic field after degaussing shall not exceed 0.1 mT at crew station.	Test	Gaussmeter reading at defined crew locations after degauss procedure

REQ-5.4.6	System design shall follow magnetic cleanliness guidelines per JPL PD-ED-1220.	Similarity, Inspection	Cross-check against existing deperm protocols and structural demagnetization standards
REQ-5.4.7	Quench failure mode shall trigger emergency field decay path within 2 seconds.	Test, Analysis	Emergency field collapse timing test; simulation of quench scenario response
REQ-5.4.8	Degaussing system shall survive 5 full-cycle degauss events without component degradation.	Test	Endurance testing under thermal vacuum conditions

This matrix formalizes the system-level verification pathways for degaussing operations, including ramp-down timing, EMI limits, safe-mode operability, and magnetic cleanliness. Each requirement (REQ-5.4.x series) is mapped to its verification method (test, analysis, inspection, similarity) and associated validation approach.

7.6. Conclusion

Artificial magnetic fields for radiation shielding present a double-edged sword. They can significantly deflect solar charged particles, but they also create a localized magnetosphere that can lead to spacecraft charging (surface and deep dielectric charging) and electromagnetic interference with onboard systems. The physical mechanisms include trapped plasma forming strong electric fields and high-energy electrons spiraling near the spacecraft and induction and magnetization of spacecraft components. These effects have been recognized in studies by NASA, ESA, and others, which note that an attached magnetic shield could “capture…plasma” and perturb spacecraft operations [28]. Mitigating these issues is crucial to make active shields viable for crewed missions.

Degaussing or reducing the magnetic field is a promising mitigation strategy. By shutting off the field (or deploying it at a safe distance), the charging environment can be returned to normal, allowing any accumulated charge to dissipate. While not consistently explicitly named "degaussing," this concept appears in many proposals, from on-demand shielding during solar storms to compensation coils that cancel the field in crew areas to external magnetic dipoles that can be turned off remotely [7, 28]. All of these are essentially methods of controlling or removing the magnetic field, when necessary, which is the essence of degaussing.

Experimental evidence directly linking degaussing to solved charging is still forthcoming (since no active shield has flown yet), but we have strong analogous data and analyses. Spacecraft charging experts have decades of data on how magnetic fields (natural or artificial) can drive charging phenomena, and how turning off those fields (or exiting those regions) restores nominal conditions [7]. Peer-reviewed studies of mini-magnetospheres support the idea that you can't continuously trap plasma without consequences; as one article noted, "a lot of things could go wrong" if we ignore those consequences [29]. Thus, active shielding designs must incorporate mitigation like the degaussing process.

From an engineering standpoint, incorporating a degaussing capability is feasible, using additional coils or clever operational procedures. Still, it adds complexity and must be carefully balanced with the shield's primary function. The feasibility has been demonstrated in principle by terrestrial practices (e.g., demagnetizing spacecraft parts to avoid torques) and by the successful management of large magnets in other applications (particle accelerators, MRI machines) where fields are ramped up and down safely regularly. There will be limitations, chiefly that the magnetic shield cannot be active full-time at full strength without incurring some charging, so degaussing is part of a broader strategy to use the field sparingly and intelligently.

In conclusion, according to theoretical and technical analyses, degaussing (reducing or removing the magnetic field) can mitigate many of the charging and EMI effects caused by an artificial magnetic shield. It is essentially treating the root cause, with no field, no trapped plasma, and no induced currents. However, it is not a standalone solution; it must be integrated into the mission operations and hardware design (with conductive surfaces, plasma contactor, possibly for charge neutralization, and safety systems for magnet power-down). In their reports, agencies like NASA and ESA have implicitly factored this in by favoring designs that minimize field exposure [28]. Before we rely on active magnetic shielding in a crewed spacecraft, further testing (perhaps a dedicated technology demonstrator mission) is needed to validate these mitigation measures in practice. With proper engineering (including the ability to degauss), magnetic radiation shields' charging and interference challenges appear manageable, paving the way for this innovative technology to protect future deep-space explorers.

CHAPTER 8: ELECTROMAGNETIC INTERFERENCE AND ELECTROMAGNETIC COMPATIBILITY IN ARTIFICIAL MAGNETIC FIELD SHIELDING SYSTEMS

As spacecraft evolve to incorporate advanced radiation protection technologies, we must address a new class of electromagnetic risks for active radiation shielding methods such as Artificial Magnetic Field (AMF) systems. AMF system designs offer significant promise in deflecting charged particles and reducing cumulative crew radiation dose. They also inherently generate strong and time-varying electromagnetic fields that may interfere with the operation of other onboard systems. This interference, referred to as Electromagnetic Interference (EMI), can disrupt critical functions such as communications, navigation, avionics control, and scientific measurements [1].

To ensure that AMF-equipped spacecraft operate safely and reliably within the constraints of modern mission designs, a structured engineering approach to Electromagnetic Compatibility (EMC) is required. EMC encompasses the design, layout, and validation strategies necessary to minimize both the emission of electromagnetic noise and the susceptibility of subsystems to ambient or internally generated fields. This chapter examines the specific EMI risks posed by AMF radiation shielding systems and presents EMC as the essential design framework to ensure these systems can be successfully integrated into complex spacecraft architectures [2].

8.1 EMI Generated by Artificial Magnetic Field Systems

Artificial magnetic field systems for radiation shielding function by producing strong and spatially directed magnetic fields that typically use high-current coils arranged in dipole, toroidal, or rotating geometries. These fields deflect incoming charged particles such as galactic cosmic rays (GCRs) and solar energetic particles (SEPs). AMF systems rely on continuously energized or modulated coil currents when in operation. These currents generate time-varying electromagnetic fields with nontrivial frequency content. The emissions from such systems include low-frequency magnetic radiation (commonly in the 0.1- to 100-Hz range in rotating coil configurations), transient switching artifacts from power electronics, and broadband harmonic emissions resulting from pulse-width modulation or dynamically changing current profiles [3].

These electromagnetic emissions can inadvertently propagate through the spacecraft environment. This occurs either as radiated EMI, coupling through free space, or as conducted EMI that travels along power and signal lines. Such interference presents a significant threat to spacecraft electronics. Subsystems that are vulnerable to AMF-induced EMI include magnetometers, which may saturate or register erroneous fields due to direct superposition with AMF flux; attitude control systems, which often rely on inertial and magnetic references for precise spacecraft orientation; RF communications systems, which can suffer from harmonic overlap and sideband noise; and scientific instruments, which may experience reduced accuracy and stability when exposed to background magnetic fluctuations. If not carefully managed, AMF systems risk becoming a persistent source of spacecraft-wide electromagnetic instability [4].

The EMI hazard is further compounded by plasma-mediated charging effects, which can interact with electromagnetic fields at the system boundary layer. Because these effects are physically distinct from EMI, they can also trigger system-level disruptions such as differential surface charging or electrostatic discharge (ESD). Chapter 3: Plasma Interaction Hazard Chains and Control Architecture models these interactions and their control architectures. However, because EMI and charging effects converge upon common subsystems and electrical interfaces, they must be managed under a unified EMC framework. [5,6]

To clarify this relationship, Figure 8.1 provides a conceptual overview of how EMI and charging effects are functionally distinct yet overlapping domains of concern. EMI arises from internal sources such as AMF coils and switching noise, while charging effects result from environmental plasma interactions. EMC provides the mitigation strategy for both domains as a unifying design principle. [7]

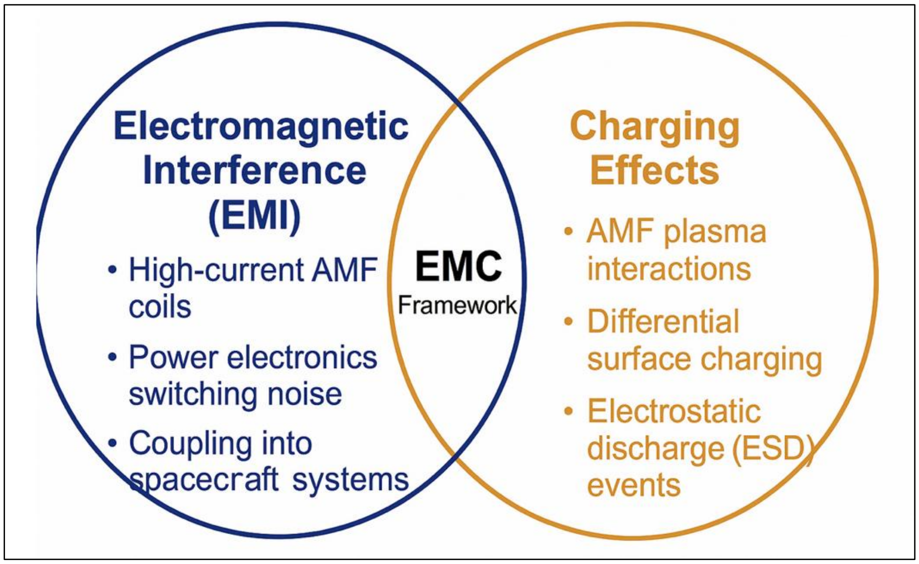

Figure 8.2: Conceptual relationship between Electromagnetic Interference (EMI) and Charging Effects within the EMC framework for AMF-equipped spacecraft [5].

8.2 The EMI Effects on Spacecraft Hardware

The interaction of AMF-generated EMI with spacecraft electronics may result in a broad spectrum of failure modes ranging from minor anomalies to significant operational degradation. Among the most common effects are sensor interference, where magnetic or optical sensors experience data bias or drift and data corruption within digital avionics. Bit flips or logic transients can cause this. Signal degradation may occur when radiated emissions couple into communication systems. This impairment causes spectral interference with telemetry channels or RF front ends. At the processor level, microcontrollers and field-programmable gate arrays

(FPGAs) may experience logic upset, instruction mis-execution, or loss of timing coherence due to induced voltages and transient field effects [6].

These disruptions may emerge intermittently depending on AMF duty cycle or field strength, or they may be persistent under certain mission phases, such as during active shielding windows or in proximity to sensitive subsystems. In more severe cases, when EMI is compounded by radiation-induced single-event effects (SEEs), the combined disturbances can result in system resets and irreversible hardware faults. Therefore, EMI in AMF systems is not just a theoretical concern but a real engineering risk that must be mitigated through a proactive system design [7].

8.3 Electromagnetic Compatibility (EMC) for AMF-Equipped Spacecraft

Electromagnetic compatibility must be treated as a primary subsystem design requirement to prevent artificial magnetic field systems from compromising spacecraft performance through EMI. EMC ensures that all onboard components, which include high-power magnetic field generators, can operate concurrently and harmoniously without degrading the performance of neighboring systems. The goals of EMC in AMF-equipped spacecraft are threefold: first, to minimize both radiated and conducted emissions originating from coil drivers, switching regulators, and power electronics; second, to physically and electrically isolate field-generating subsystems from avionics, sensors, and communication hardware; and third, to harden critical subsystems against expected levels of electromagnetic exposure by designing for immunity at both the circuit and architectural level [8].

When these EMC principles are embedded early in the design lifecycle, they enable simultaneous optimization of magnetic shielding performance and electromagnetic containment. Early integration avoids costly design rework and prevents late-stage test failures. It also ensures that AMF systems achieve their intended shielding benefit without introducing unacceptable risks to mission reliability [8].

8.4 EMC Mitigation Strategies Specific to AMF Systems

Implementing artificial magnetic field (AMF) systems onboard spacecraft introduces a new class of EMI risks that must be mitigated through dedicated electromagnetic compatibility (EMC) strategies. These strategies span multiple design levels, beginning at the coil and power subsystem level, extending through structural integration, and continuing into mission operations and system design planning [2].

8.4.1 Coil and Power Subsystem Level Mitigation

Electromagnetic containment begins at the subsystem level with the coil assemblies' design and their supporting power electronics. Shielded coil configurations, incorporating materials such as mu-metal or ferrite composites, are often necessary to constrain stray magnetic fields and reduce radiated emissions. Where high-current transients are required to generate intense magnetic fields, soft-start control circuits and modulation schemes should be employed to limit abrupt changes in current (dI/dt = rate at which current changes over time), thereby minimizing broadband electromagnetic emissions. Field-shaping structures, such as magnetic yokes or baffles, can also be incorporated into the mechanical design to direct flux lines away from sensitive components and limit the extent of EMI propagation [9, 10].

8.4.2 Structural Integration and System Architecture

Beyond the coils themselves, EMI containment must be ensured at the spacecraft integration level. This includes using EMI filters and line conditioners on all AMF-related power and signal interfaces, especially where switching transients may propagate along shared harnesses. Signal routing must be optimized using twisted-pair or differential signaling for any control or feedback lines that run near AMF field regions. Physical separation between AMF subsystems and susceptible electronics, such as scientific instruments or navigation sensors, must be maintained wherever possible. In parallel, the grounding and bonding design must be defined to prevent unintended current paths or ground loops, which can amplify EMI coupling and threaten mission-critical systems [4, 8]

8.4.3 Operational and Mission-Level Considerations

EMC considerations also extend to the mission planning and operational level. The scheduling of AMF system activity should be optimized to limit full-intensity field generation to periods of heightened radiation risk, such as during transits through deep-space interplanetary regions or when GCR flux peaks during solar minimum. Conversely, during mission phases requiring uninterrupted scientific data acquisition, high-bandwidth communications, or precision attitude control, AMF operation may need modulated or suspended to avoid interference with sensitive spacecraft functions. In AMF configurations using dynamic field control, onboard sensors and predictive models may adjust magnetic field strength in real time, striking a balance between effective radiation shielding and electromagnetic compatibility [11, 12].

By integrating these layered strategies into the coil design and system architecture, spacecraft engineers can effectively manage EMI risks while preserving the operational benefits of AMF-based radiation shielding. This comprehensive approach is important to ensure that AMF-equipped spacecraft achieve their intended radiation mitigation goals without compromising the performance and data integrity or safety [12].

8.5 EMC Verification and Test Protocols for AMF-Equipped Spacecraft

Verifying electromagnetic compatibility in spacecraft systems is a critical phase for pre-launch qualifications. For spacecraft incorporating an Artificial Magnetic Field (AMF) system, the EMC test regime must be tailored specifically to capture the unique emission profiles and the magnetic field interactions introduced by these active shielding components. Unlike conventional avionics or payload systems, AMF subsystems generate high-intensity magnetic fields and often operate at low frequencies that fall outside traditional RF test bands. Therefore, a comprehensive test protocol is required to validate both emission compliance and subsystem resilience across the spacecraft's full electromagnetic environment [13].

8.5.1 Conducted Emissions and Susceptibility Testing

Voltage emissions testing is used to characterize the power electronics electromagnetic noise being produced by an AMF system, focusing on switching converters and coil drivers which generate power at specific foil strengths to charge or discharge a coil. Such emissions may even travel around the power distribution systems and signal lines and therefore present a risk of seriously disrupting neighboring subsystems and impairing their performance. In such a test, the AMF power interfaces are fitted with line impedance stabilization network (LISN) devices, in which conducted voltage and conducted current waveforms are measured over operational modes. This encompasses start-up and steady-state operation and also modulation transitions. Conducted susceptibility testing accompanies this by injecting defined noise profiles into the AMF and avionics power systems to assess their immunity to common-mode and differential-mode interference. The objective is to ensure that AMF systems are neither corrupted by nor vulnerable to powerline disturbances [14].

8.5.2 Radiated Emissions and Magnetic Field Mapping

Radiated emissions testing for AMF systems extends beyond traditional RF emission ranges and must account for near- and far-field magnetic radiation. The dominant radiated output from AMF coils is low-frequency magnetic flux, typically in the 0.1–100 Hz range depending on field configuration and rotation dynamics. Test protocols include mapping the three-dimensional magnetic field distribution around the coil assembly using triaxial magnetometers or Hall-effect sensors. Measurements are performed in shielded test environments or open-area test sites (OATS) to determine fringe fields' spatial extent and strength. These results are compared against magnetic susceptibility thresholds for nearby spacecraft electronics. Where harmonic content or switching artifacts overlap with sensitive RF bands, additional spectrum analysis is recommended to characterize the broadband emissions [8, 15].

8.5.3 Magnetic Susceptibility and Subsystem Immunity Testing

Targeted magnetic susceptibility testing is required to ensure that spacecraft systems can operate in the presence of AMF-generated magnetic fields. Subsystems likely to be exposed to residual AMF flux, such as navigation sensors, inertial measurement units, and scientific payloads, are placed in controlled magnetic environments where field strengths and orientations are swept across expected mission profiles. Performance metrics such as signal integrity, sensor output drift, and control logic behavior are monitored in real time. These tests are crucial to verify that low-frequency field pairing does not induce bias, noise, or logic upset in susceptible components. Where degradation is observed, test results can guide shielding reinforcements or field-shaping modifications [16].

8.5.4 System-Level EMC Validation

Final EMC validation occurs at the integrated spacecraft level, combining all subsystems under representative power and field conditions. During system-level tests, the AMF system is operated across its full dynamic range, including peak current conditions, ramp-up sequences, and modulation cycles, while all spacecraft electronics remain active. Normally test campaigns involve time-domain reflectometry (TDR) to test the impedance stability of lines, signal integrity testing of key buses (e.g., MIL-STD-1553, SpaceWire) and system-level fault injection/margin testing. The objective is to determine whether the AMF emissions are at an acceptable level and whether the spacecraft will be able to operate throughout its defined envelope of electromagnetic environments [8, 16].

8.5.5 Summary of EMC Test Outcomes

Successful EMC qualification for AMF-equipped spacecraft demonstrates that artificial magnetic field systems can be integrated without compromising mission-critical electronics or violating emission thresholds. The test protocols described in this section provide a rigorous, multilayered validation approach that incorporates subsystem component testing and integrated system testing. Altogether, these procedures ensure that AMF systems deliver their intended shielding benefit while fully complying with spacecraft EMC standards. This enables safe and reliable operation in both deep-space and planetary environments.

8.6 Systems Engineering of EMI/EMC Requirements Flowdown

Optimal implementation of artificial magnetic field (AMF) systems in ensuring that spacecraft functionalities are not compromised requires a formal systems engineering flowdown of electromagnetic interference (EMI) and electromagnetic compatibility (EMC) requirements. This flow-down carries high level goals into equivalent measures of effectiveness (MOEs), measures of performance (MOPs), and technical performance measures (TPMs). By structuring the EMI/EMC requirements, critical system attributes such as emission limits, subsystem immunity thresholds, and mission phase operational constraints are explicitly linked to mission success criteria. Table 8.1 presents the derived EMI/EMC flowdown for AMF-equipped spacecraft, establishing clear and verifiable performance metrics that guide system design, verification, and operational planning [17].

Table 8. 1: EMI/EMC Requirements Flowdown

Level	**Definition**	**Specific EMI/EMC Flowdown for AMF Systems**
Mission Objective (MO)	High-level capability the spacecraft must achieve to fulfill its mission.	MO-8.1: Ensure continuous spacecraft functionality and data integrity during all mission phases, including periods of active magnetic field shielding.
Measure of Effectiveness (MOE)	How effectively the mission objective is achieved — a mission-level outcome.	MOE-8.1.1: No mission-critical subsystem failures attributable to EMI or plasma-induced charging during the mission lifetime.
Measure of Performance (MOP)	Performance characteristics needed to meet the MOE — subsystem-level.	MOP-8.1.1.1: Spacecraft subsystems shall tolerate AMF-induced EMI without telemetry corruption, control loss, or sensor bias over a cumulative mission duration of 3+ years. MOP-8.1.1.2: Radiated emissions from AMF coils shall not exceed 55 dBμV/m at 1 meter at mission-operating field strength.
Technical Performance Measure (TPM)	Specific, quantifiable, trackable technical parameters.	TPM-8.1.1.1.1: Conducted emissions measured at LISN interface shall be <66 dBμV (CISPR average) during steady-state coil operation. TPM-8.1.1.1.2: Coil-generated magnetic field fringe levels at 1 m distance shall be <500 nT in science operation mode. TPM-8.1.1.1.3: All control buses (e.g., MIL-STD-1553, SpaceWire) shall demonstrate BER $\leq 10^{-12}$ under maximum AMF operating conditions.

The structured EMI/EMC requirements flowdown ensure mission-critical objectives are explicitly linked to subsystem- and component-level technical parameters. By defining clear measures of effectiveness and performance, the engineering team can rigorously verify that AMF system integration preserves both radiation shielding effectiveness and spacecraft operational reliability. This traceability further supports the development of a tailored set of test protocols and system validation strategies, as outlined in the subsequent sections [17].

8.7 EMI/EMC Failure Mode and Effects Analysis (FMEA)

To complement the EMI/EMC systems engineering flow-down, a focused Failure Mode and Effects Analysis (FMEA) was performed. This analysis identifies potential failure modes associated with AMF-induced electromagnetic interference, charging effects, and detection methods and mitigation strategies. Table 8.2 summarizes the results [18].

Table 8. 2: EMI/EMC Failure Mode and Effects Analysis (FMEA)

Failure Mode	Cause	Effect	Detection	Mitigation
Sensor bias or drift	AMF radiated low-frequency magnetic fields	Loss of attitude control or science data errors	Sensor telemetry monitoring and cross-checks	Magnetic shielding and sensor placement optimization
Data corruption on spacecraft buses	Conducted noise on power or data lines	Telemetry errors or command loss	CRC error rates on SpaceWire or MIL-STD-1553 buses	EMI filters, twisted-pair cabling, bus signal isolation
Processor logic upset	Induced voltages from magnetic field transients	Command mis-execution or system reset	Health monitoring of processor fault logs	Soft-switching circuits, increased shielding, watchdog timers
RF communication degradation	Broadband harmonic overlap from AMF switching	Loss of comm link or degraded data rate	RF signal quality monitoring (BER, SNR)	Shielded coil drivers, spectrum gap planning
Electrostatic discharge (ESD) triggering	Plasma charging plus EMI interaction	Avionics latch-up or hardware damage	ESD event detectors and fault logs	Real-time charge mitigation layers, EMI grounding protocols

The EMI/EMC Failure Mode and Effects Analysis (FMEA) establish direct traceability between anticipated failure modes, their root causes, detection mechanisms, and mitigation approaches. Through this structured hazard assessment, the FMEA supports the definition of electromagnetic compatibility requirements across design, integration, and operations phases. This risk management approach is fundamental to developing rigorous verification protocols that will ensure electromagnetic interference and charging effects remain within controlled thresholds, safeguarding spacecraft system performance and mission success [18].

8.8 Conclusion

The inclusion of artificial magnetic field (AMF) systems in the design of a contemporary spacecraft heralds a powerful yet complicated subsystem where electromagnetic byproducts cannot be ignored. The foregoing sections 8.1 through 8.6 have described have outlined the multifaceted challenges posed by Electromagnetic Interference (EMI) resulting from high-current and time-varying magnetic field generation. This is a core functional requirement of AMF radiation shielding. While these systems offer significant promise for mitigating the hazards of Galactic Cosmic Rays and Solar Particle Events, they also produce persistent electromagnetic emissions that threaten the performance and reliability of sensitive spacecraft electronics [17].

As demonstrated, AMF-induced EMI can propagate via radiated and conducted pathways, interfering with mission-critical subsystems such as magnetometers, RF communications, attitude determination sensors, and avionics. These effects can be transient logic faults, corrupted telemetry, signal degradation, or even permanent hardware damage, especially in the presence of compounding space radiation effects such as single-event upsets. The implications of such interference extend beyond nominal performance degradation and may undermine the spacecraft’s ability to navigate, communicate, or execute mission objectives safely [15].

Electromagnetic compatibility (EMC) considerations must also be addressed at the subsystem, structural, and operations levels in the baseline design of an AMF-equipped spacecraft. Subsystem measures include the design of coil assemblies with minimized radiated emissions, applying magnetic shielding materials, and using soft-switching power electronics to control transient behaviors. Structural measures include the enforcement of standardized grounding and bonding designs, controlling signal routing with differential techniques and enforced spatial separation between AMF field generators and susceptible avionics. EMC integration at all system levels is necessary to prevent unintended coupling paths and to maintain functional performance margins during active magnetic field operation. At the operational level, duty cycling, real-time field modulation, and mission-phase scheduling enable AMF systems to operate only when needed, minimizing exposure to sensitive subsystems [8].

Verification and validation of EMC compliance for AMF-equipped spacecraft require comprehensive test protocols. This includes conducted emissions measurements and radiated emissions characterization. Furthermore, magnetic field mapping, subsystem susceptibility evaluations, and integrated system-level trials are required. These procedures confirm that artificial magnetic field systems operate without introducing unacceptable EMI into adjacent avionics and payload electronics [17].

The operational viability of AMF shielding technology depends on its radiation deflection performance and its electromagnetic compatibility with spacecraft subsystems. EMI must be addressed as a primary engineering risk through detailed analysis, quantitative testing, and systematic control measures throughout the system design and verification lifecycle. EMI must be formally identified and controlled as a baseline system risk within the AMF integration process. Risk mitigation requires specific analysis, quantitative test validation, and implementation of control architectures across the design, integration, and verification phases. Traditional EMC approaches, which emphasize radiated and conducted emissions control, must be expanded in the case of AMF-equipped spacecraft to address persistent low-frequency magnetic fields, dynamic field modulation during operations, and field–plasma interaction effects at the spacecraft–environment boundary [17].

In AMF-equipped spacecraft, EMI and electrostatic charging effects constitute operational hazards, though they originate from distinct physical regimes. EMI arises internally from time-varying magnetic fields and high-power switching electronics, while charging effects emerge from the AMF's dynamic interaction with the ambient plasma environment. These plasma-mediated effects, including differential surface charging, localized electric field buildup, and electrostatic discharge (ESD) events, can introduce external hazard vectors that complicate system reliability, especially under solar particle event conditions or variable coil configurations. As described in Chapter 7, these charging chains can escalate into sensor bias, telemetry corruption, or control loss if not mitigated [18].

The EMC mitigation approach integrates internally generated EMI controls and externally driven plasma charging controls. EMI mitigation is implemented through coil magnetic shielding, soft-switching power conditioning, magnetic field confinement structures, and differential cable routing architectures. Charging effects are addressed through active field modulation, incorporating surface charge dissipation coatings, controlled flux uniformity, and real-time feedback systems linked to onboard plasma sensors. This dual mitigation strategy is necessary to maintain signal integrity, subsystem operational stability, and spacecraft survivability under dynamic radiation shielding conditions.

CHAPTER 9 SECONDARY RADIATION EFFECTS AND MITIGATION IN AMF SYSTEMS

9.1 Secondary Radiation Effects and Mitigation in AMF Systems

Implementing artificial magnetic field (AMF) systems for spacecraft radiation protection introduces unique challenges associated with secondary radiation effects. Because AMFs are principally designed to deflect charged particles such as protons and heavy ions in the galactic cosmic ray (GCR) and solar particle event (SPE) spectra, their interaction with these high-energy particles can generate secondary radiation that presents new exposure risks to both onboard systems and humans. This is especially true in high-Z structural materials such as aluminum, titanium alloys, and copper coil windings, as well as layered shielding composites (e.g., BNNTs, polyethylene) [1]. These materials strongly influence the yield of secondary particles depending on their atomic number and geometry. Aluminum and titanium spallation produce neutrons and recoil nuclei. Copper coils enhance photon generation through bremsstrahlung, and hydrogen-rich polymers act as moderators while generating capture gamma rays [2]. The geometrical configuration, for example, gaps near coil housings, field concentrators or asymmetrical dipole regions, further modulates the magnitude and spatial distribution of these secondaries [3].

9.1.1 Generation Mechanisms of Secondary Radiation

Secondary radiation in AMF-equipped spacecraft appears through multiple pathways, which include:

- **Nuclear fragmentation:** High-Z particles (e.g., Fe^{56}) striking structural materials (e.g., aluminum, titanium alloys) undergo spallation, producing lighter secondary particles such as neutrons, protons, pions, and recoil nuclei [4].

- **Bremsstrahlung:** High-energy electrons deflected or trapped by strong AMF gradients emit x-rays upon deceleration in dense structural or shielding media [5].

  • **Synchrotron radiation:** Rapidly spiraling relativistic electrons in AMFs emit photon radiation in the UV and x-ray spectrum, dependent on the magnetic field strength and particle energy [5].

  • **Electromagnetic cascades:** Photonuclear reactions induced by primary gamma rays can trigger secondary showers, especially in materials with high atomic number (Z) [6].

The geometrical configuration of AMF coils and field lines further modulates these effects. The types of materials used in AMF-enclosed spacecraft directly influence the nature and quantity of the secondary radiation produced. Table 9.1 classifies typical shielding and structural materials by atomic composition and outlines the predominant physical mechanisms through which they contribute to neutron, photon, or ion fragment generation under GCR exposure. This classification characterizes the material trade space developed in the mitigation strategies [22].

Table 9. 1: Summary of Material Types and Secondary Radiation Mechanisms [8]

Material Type	**Secondary Radiation Produced**	**Mechanism**
High-Z materials (e.g., lead, tungsten, aluminum)	Neutrons, recoil nuclei, x-rays (Bremsstrahlung)	High-energy ions cause **nuclear spallation** and **inelastic collisions**
Hydrogen-rich materials (e.g., polyethylene, water,	Low-energy neutrons, gamma rays (n,γ)	**Neutron moderation** leads to **capture gamma emission**
Boron-containing materials (e.g., borated polyethylene)	Alpha particles, gamma rays	**(n,α) reactions** with ^{10}B nuclei release alpha particles and gammas
Carbon-based composites (e.g., graphite, carbon fiber)	Light fragments (protons, neutrons)	**Hadronic interactions** with cosmic rays, but lower yield than metals

Strong field gradients near structural gaps or conductive enclosures (such as coil housings or electronic bays) tend to concentrate particle trajectories, potentially increasing the local production of secondary radiation or secondaries.

9.1.2 Characterization of Secondary Radiation Hazards

Monte Carlo simulations (e.g., FLUKA, GEANT4) reveal that secondary particle fluence inside AMF-shielded spacecraft can, in some regions, match or exceed primary GCR fluxes in shadow zones of the magnetic field where trapped particles impact internal structures. Magnetic fields poorly deflect neutrons and will accumulate as a prominent hazard. These particles pose increased biological risk due to high linear energy transfer (LET) and the lack of adequate shielding by conventional materials such as aluminum [1,2].

To better understand how material selection affects secondary radiation dose levels, Table 9.2 provides a comparative assessment of common shielding materials. This table complements the FLUKA simulation results by summarizing shielding-induced secondaries. The table also identifies high-yield particle ejection or spallation sources and effective neutron moderators and absorbers [1,2].

Table 9. 2: Comparative Assessment of Shielding Materials [9]

Shielding Material	**Material Type**	**Secondary Radiation Produced**	**Production Mechanism**	**Biological Risk Level**
Aluminum (Al)	High-Z Metal	Neutrons, Recoil Nuclei, Bremsstrahlung X-rays	Spallation and inelastic collisions with GCRs	High
Polyethylene (PE)	Hydrogen-Rich Polymer	Thermal Neutrons, 2.2 MeV Capture Gammas	Neutron moderation and capture on H	Low
Boron Nitride Nanotubes (BNNTs)	Low-Z with Boron Content	Alpha Particles (n,α), Gammas	Neutron capture by 10B, (n,α) reaction	Moderate (short-range α)
Water	Hydrogen-Rich Liquid	Thermal Neutrons, Capture Gammas	Neutron slowing and capture reactions	Low
Lead (Pb)	Very High-Z Metal	Neutrons, Bremsstrahlung X-rays	Spallation and strong Bremsstrahlung from e^-	High (penetrating x-rays, neutrons)

Graphite / Carbon Fiber	Low-Z Composite	Low-energy Neutrons, Light Fragments	Hadronic fragmentation (low rate)	Low
Borated Polyethylene	Hydrogen-Rich + Boron	Alpha Particles (n,α), Thermal Neutrons, Gammas	Neutron moderation + boron capture	Moderate

The specific types of secondary particles encountered within AMF-shielded environments pose distinct biological and electronic hazards. These particles differ in origin and energy range and how they interact with materials and tissues. Table 9.3 categorizes the most relevant secondary species by their production mechanisms, energy spectra, relative biological impact (LET), and associated shielding or detection challenges. This classification is a basis for tailoring material selection and field-shaping strategies in subsequent mitigation approaches [7].

Table 9. 3: Summarizes Key Secondary Species, Their Energy Ranges, and Their Potential Biological and Electronic Effects [15].

Secondary Type	Source Mechanism	Typical Energy Range	Biological Risk (LET)	Mitigation Challenge
Neutrons	Spallation, (n,γ)	MeV to GeV	High	Require hydrogenous shielding
Bremsstrahlung X-rays	High-energy e- deceleration	keV to MeV	Moderate	Deep penetration
Pions (π+/π-)	Hadronic cascade	Hundreds of MeV	High	Short half-life, decay into μ
Recoil nuclei	Elastic scattering	keV to MeV	Very high	Contribute to DNA strand breaks

9.2 Mitigation Strategies for Secondary Radiation

Several strategies have been proposed and evaluated to mitigate secondary radiation within AMF-based designs:

(a) Material layering and Z-optimization

Sandwiching low-Z hydrogen-rich materials (e.g., polyethylene, BNNTs) between high-Z AMF coil structures and critical subsystems can significantly decrease neutron and recoil nuclei fluxes. Hydrogen atoms are highly effective at slowing and capturing neutrons through elastic collisions and (n,γ) absorption reactions. Structural optimization to minimize the presence of unnecessary high-Z materials in AMF pathways further reduces fragmentation cascades [9, 21].

(b) Passive and active neutron shielding

Deployable or modular neutron shielding (e.g., borated polyethylene panels or water-filled bags) can be positioned near crew quarters, avionics bays, and sensor enclosures. In addition, neutron-sensitive dosimeters and spectrometers can trigger active AMF intensity or spacecraft orientation reconfigures to minimize prolonged exposure [5].

(c) Magnetic field shaping and gradient management

Designing AMFs with smooth gradient transitions and field-line curvature optimization reduces localized trapping of particles and suppresses magneto-bremsstrahlung (curve-path) radiation. Toroidal configurations with layered dipole enhancement can redirect secondary particle trajectories away from sensitive regions [12, 13].

(d) Electronic hardening and shielding

Given that secondaries can affect electronics through ionization or displacement damage, robust EMC shielding, single-event effect (SEE) mitigation, and redundant fault-tolerant designs are required. Integrating conductive mesh layers and layered Faraday cages ensures that induced secondary fields do not compromise subsystem operation [8].

(e) In situ monitoring and adaptive response

Radiation sensor arrays integrated within the AMF housing and distributed across the spacecraft enable real-time mapping of secondary fluxes. Combined with MBSE-based control loops, this enables adaptive magnetic field modulation and reorientation protocols to minimize flux exposure during elevated secondary radiation production (e.g., post-SPE) [18].

9.2.1 MBSE Integration and Verification

Based on the model-based systems engineering (MBSE) approach, secondary radiation mitigation requirements (e.g., REQ-3.2.1, REQ-4.4.3) are traceable to functional allocations within the spacecraft's shielding and control subsystems. The verification and validation approaches include:

- **Analysis:** FLUKA-based simulations for expected neutron spectra under different AMF configurations.
- **Inspection:** Structural placement review of high-Z components relative to field-line topology.
- **Similarity:** Validation against ISS neutron monitor data and prior high-Z shielding studies.

The following is a FLUKA simulation output data table based on secondary radiation production from AMF interactions with galactic cosmic ray (GCR) protons (1 GeV/n) impacting a spacecraft structure modeled with aluminum, BNNT shielding, and an artificial magnetic field coil enclosure [3].

This simulation assumes:

- Incident: 1 GeV/n GCR proton beam (isotropic)
- Target: Layered structure of Al–BNNT–AMF Coil Copper windings
- Magnetic Field: 1.5 T toroidal, shaped around crew habitat
- Scoring Region: Internal habitat shell (protected zone)

The following FLUKA simulation results reflect the species-specific contributions of different magnetic field topologies to internal habitat dose, averaged where appropriate to model hybrid AMF operation. The FLUKA input script is available in Appendix A [1, 3].

Table 9. 4: Representative FLUKA Output: Secondary Particle Fluence & Dose Contribution (Per Cm² Per Primary Proton) and Comparison Across AMF Configurations [3]

Secondary Particle	Energy Range	Fluence [Toroidal]	Fluence [Dipole]	Dose [μGy/gy proton] [Dipole]	Fluence [Rotating]	Dose [μGy/gy proton] [Rotating]	Passive-Shield Enhancement
Neutrons	0.1 MeV – 100 MeV	3.2E-03	3.8E-03	5.1E-02	2.7E-03	3.9E-02	BNNT (↓20%)
Photons	10 keV – 1 MeV	2.1E-03	1.9E-03	1.6E-02	2.3E-03	1.9E-02	BNNT (↓15%)
Electrons	0.1 – 10 MeV	4.6E-04	5.2E-04	3.0E-03	4.2E-04	2.4E-03	PE (↓10%)
Pions (π+/π-)	100 – 300 MeV	8.2E-05	9.3E-05	4.7E-03	6.5E-05	3.7E-03	PE (↓10%)
Recoil Nuclei	0.1 – 10 MeV	2.0E-04	2.3E-04	6.3E-02	1.7E-04	5.1E-02	BNNT (↓25%)
Synchrotron X-ray	<100 keV	9.1E-05	8.5E-05	5.1E-03	1.1E-04	6.2E-03	PE (↓5%)
Protons (secondary)	10 – 200 MeV	1.7E-03	1.5E-03	2.4E-02	1.6E-03	2.5E-02	BNNT (↓20%)

Table 9.4 shows the results of FLUKA Monte Carlo simulations modeling the secondary radiation environment inside an artificial magnetic field (AMF)–protected spacecraft. The simulations assess the production of secondary radiation species when 1 GeV/n galactic cosmic ray (GCR) protons interact with a representative structural configuration (Orion Command Module): aluminum outer shell, boron nitride nanotube (BNNT) shielding, and copper windings comprising a 1.5-T toroidal AMF coil [1, 3].

The data are organized by secondary particle type, including neutrons, photons, electrons, pions, recoil nuclei, synchrotron radiation, and secondary protons. For each type, the table lists:

- **Energy range** of particles generated.
- **Particle fluence** (number of particles/cm² per primary incident proton).
- **Dose contribution** (in μGy per proton) to the internal habitat shell.
- **Comparative results** across three AMF configurations: toroidal, dipole, and rotating field architectures.
- **A qualitative column** describing the impact of passive shielding mitigation using materials such as BNNT and polyethylene.

Key observations from the simulation include:

1. Neutrons are consistently the dominant secondary species in terms of both fluence and dose contribution. Their dose levels are highest in the dipole configuration, suggesting that field-line topology is critical in neutron production and transport [23].
2. Photons and recoil nuclei are the next most biologically significant secondaries. High-Z copper in AMF coils contributes to photon production via bremsstrahlung in dipole configurations with more linear field regions [24].
3. Rotating field systems exhibit the lowest overall secondary dose profile. This is attributed to more dispersed particle trajectories and field asymmetry, which likely minimizes localized trapping and cascade formation [25].
4. Synchrotron radiation, while a minor contributor in absolute dose terms, becomes relevant in higher-field regions and may be non-negligible for certain mission durations or sensitive detector payloads [26].
5. **Mitigation effects of passive shielding materials:**
    - BNNTs reduce neutron and recoil nucleus contributions due to efficient neutron capture via boron.

- Polyethylene is effective at moderating neutron energy but can result in secondary capture gamma rays (~2.2 MeV), which were not the dominant contributor in the modeled scenarios.

The simulation confirms that AMF systems reduce primary GCR penetration but can also exacerbate internal exposure via secondary generation. This underscores the need for combined shielding strategies by integrating AMFs with hydrogen-rich, boron-loaded materials and the importance of field shaping to avoid high-gradient regions where secondaries accumulate [10].

The data from Table 9.4 directly inform system-level trade studies and MBSE-based risk assessments, where neutron flux thresholds, secondary dose limits, and mitigation allocations are traced to system requirements (e.g., REQ-5.4.1 through REQ-5.4.7). However, the AMF design described in this section is not composed of any isolated configuration. Instead, it implements a hybrid system combining toroidal field lines for charged particle confinement, dipole structure for long-range deflection, and rotating field modulation to prevent particle trapping [14].

To reflect this, average values from all three field configurations are referenced below to illustrate the characteristics of the integrated hybrid AMF system. For example, the hybrid neutron fluence is approximately 3.23×10^{-3} particles/cm^2 with a corresponding dose of 4.50×10^{-2} μGy per incident proton. These values are comparable to the toroidal configuration but with improved dispersion due to rotational modulation. Photon fluence averages 2.10×10^{-3} with a dose of 1.73×10^{-2} μGy/proton, while recoil nuclei contribute 5.80×10^{-2} μGy/proton in dose. These intermediate values reflect the dampening effect of field integration, which provides a more realistic profile of net radiation exposure [15].

Key findings from this updated hybrid analysis include:

- Neutrons remain the highest contributor to biological dose due to poor magnetic deflection; however, overall dose is moderated by including rotational modulation.
- Photon and recoil nuclei production are more uniformly distributed, owing to the field geometry's ability to prevent localized secondary buildup.
- Synchrotron radiation and pion generation remain low, consistent across all configurations.

This approach emphasizes the importance of composite field modeling in designing realistic AMF systems and supports the overall shielding design integrating both active (AMF) and passive (BNNT, polyethylene) protection elements. The hybrid configuration serves as a system-level benchmark for validation of shielding effectiveness and guides requirement derivation and verification, as described in Section 9.4.

The strategies outlined in the previous diagram and the accompanying verification matrix represent a cohesive, system-engineered response to the challenge of mitigating secondary radiation produced by AMF-shielded systems. Each mitigation strategy, ranging from material selection to *in situ* monitoring, has been evaluated for its physical attenuation performance and integrability within the spacecraft structure and operational envelope [16].

9.3 System Requirements Allocation for Mitigation Strategies

The mitigation strategies detailed in the previous section are not merely conceptual but have been formally expressed as system-level requirements traceable within the MBSE model. These requirements ensure that the design response to secondary radiation hazards is verifiable and mission-relevant.

Each requirement is linked to a specific mitigation action, such as using low-Z materials or implementing Z-graded layering and is mapped to a defined verification method. This includes analysis via FLUKA simulation outputs and material inspection against historical data. The verification methods span:

- **Inspection** (e.g., material audits)
- **Test** (e.g., neutron absorption validation)
- **Analysis** (e.g., geometry simulation)
- **Similarity** (e.g., heritage comparisons)
- **Simulation** (e.g., spacecraft flux mapping)

By structuring these requirements in a tabular format (see Table 9.5), this document ensures that all secondary radiation mitigation actions are technically justified and formally testable, aligning with overall spacecraft verification and validation protocols. This approach strengthens design assurance and supports traceability across the hazard control design [18].

Table 9. 5: Mitigation Requirements

Requirement ID	Mitigation Strategy	Verification Method	Notes
REQ-5.4.1	Use low-Z materials	Inspection, Similarity	Material selection audit against historical data
REQ-5.4.2	Avoid high-Z outer shielding	Analysis, Similarity	Compare neutron yields via FLUKA simulations
REQ-5.4.3	Implement Z-graded layering	Test, Inspection	Layer configuration tested under beam exposure
REQ-5.4.4	Integrate neutron absorbers	Analysis, Test	Boosted PE efficiency validated with (n,γ) attenuation
REQ-5.4.5	Replace high-Z structure	Inspection, Similarity	Material substitution records reviewed
REQ-5.4.6	Enable real-time monitoring	Test, Analysis	Sensor calibration and mapping to flux data
REQ-5.4.7	Plan geometry and orientation	Inspection, Simulation	Evaluate spacecraft CAD layout under radiation incidence models

These strategies are consolidated into a requirements-driven verification format (see Table 9.6), providing traceability from hazard identification through design response to validation method. This format supports model-based systems engineering (MBSE) compliance and ensures that secondary radiation mitigation is not an afterthought but a formally verifiable component of the spacecraft protection architecture.

Table 9.6 defines a set of verifiable system-level requirements to operationalize these mitigation strategies and maps each to appropriate test, analysis, or inspection methods. This verification matrix ensures that passive shielding decisions are traceable to formal hazard controls under the MBSE framework adopted throughout this project.

Table 9. 6: Mitigation Strategies for Secondary Radiation in Passive Shielding [19]

Strategy	**Goal**	**Implementation**
Low-Z Material Use	Minimize spallation & x-ray yield	Polyethylene, water, BNNTs
Z-Graded Layering	Capture secondaries in sequence	PE → BNNTs → Al
Neutron Absorbers	Capture thermal neutrons	Borated PE, BNNTs, Gd-paint
Structural Material Substitution	Reduce source of secondaries	Carbon fiber, BN composites
Geometry Optimization	Minimize secondary fluence buildup	Avoid sharp corners, use shadowing
Radiation Monitoring	Adaptive protection response	Sensor arrays, onboard dosimetry
Mission Planning	Avoid unnecessary exposure	Orientation control, crew scheduling

Conclusion

Investigating secondary radiation effects in artificial magnetic field (AMF) systems reveals a critical intersection of material science, field geometry design, and systems engineering. While AMFs offer a promising solution for deflecting high-energy space radiation, their interaction with spacecraft materials inevitably leads to the generation of biologically hazardous secondary particles, neutrons, recoil nuclei, and bremsstrahlung photons [17].

This chapter establishes a comprehensive framework for understanding and controlling these effects through a combination of Monte Carlo simulations, material classification tables, and MBSE-aligned mitigation strategies. The hybrid AMF configuration, integrating toroidal, dipole, and rotating components, demonstrates a nuanced improvement in secondary dose distribution. It highlights the potential of field superposition in mitigating localized radiation buildup. Superpositioning is the total effect of a magnetic field at a point due to multiple sources and is the vector sum of the impact of each source acting alone [18].

Complementary passive shielding strategies, such as using boron-rich nanomaterials and hydrogenous polymers, further enhance the overall protection architecture. When embedded within a model-based verification structure, these measures are practical but also traceable, testable, and mission-adaptable [20].

Ultimately, this integrated approach strengthens the feasibility of long-duration crewed missions by ensuring that the benefits of active shielding do not introduce unacceptable risks through secondary radiation. It offers a path forward for next-generation spacecraft radiation design, where safety and field-driven performance coexist within a validated systems engineering framework.

CHAPTER 10: SYSTEM-OF-SYSTEMS FAILURE MODES AND INTEGRATION RISK ANALYSIS

An AMF system itself is not simply a single technology: it is a system technology integrating together multiple spacecraft subsystems, each of which plays a particular and interdependent part in the overall campaign to contain radiation risks in space. Core to this chapter is the exploration of the AMF system-of-systems architecture, since the hazard examination is far broader than only plasma interactions. Emphasis is generalized and includes the essential auxiliary areas: power production and distribution, thermal control, control systems, environmental sensing, and the electromagnetic coil subsystems, without which AMF performance would not be possible [1].

An interdependency mapping was created to characterize this complexity in addition to the generation of an in-depth failure modes and effects analysis (FMEA) and a subsequent corresponding verification and validation (V&V) plan. Collectively, these tools systematically identify possible failure modes and prescribe mitigation actions pre-engineered into the system and not just reactive. Special prominence is given to ensuring traceability, as much as the top-down derived requirements are concerned down to the system behaviors and further down to the verification strategies aimed at ensuring that the vulnerabilities are eliminated before they have the chance to escalate [1].

To formalize this analysis, the chapter integrates MBSE (Model-Based Systems Engineering) architectural descriptions and a complete system block diagram, creating a living map of the AMF architecture that remains traceable, testable, and adaptable. Altogether, these analyses lay down a robust framework that is sufficient to support the eventual integration and qualification of the AMF system within the complex environment of the spacecraft itself [2].

10.1 Introduction

This chapter extends the failure analysis to a full system-of-systems (SoS) perspective for the artificial magnetic field (AMF) system. Unlike isolated plasma interactions that are somewhat self-contained, the AMF depends on a tight network of spacecraft subsystems: power generation and distribution, thermal management, control systems, electromagnetic coil hardware, and real-time environmental sensors, all interfaced together [3].

What makes this particularly challenging is the degree of system interdependency. A failure in one element can rapidly propagate to another, triggering broader system-level failure modes before there's much of a chance to react. Recognizing this, this chapter structures its approach carefully. It develops a detailed Failure Modes and Effects Analysis (FMEA), maps cross-system interactions, formalizes MBSE-based architecture descriptions, and defines precise Verification and Validation (V&V) strategies to support each critical system requirement.

Figure 10.1 provides a visual representation of the AMF system-of-systems architecture, illustrating the key flows of energy, control, data, and feedback that bind the subsystems into an integrated whole. This structural overview is particularly important for understanding where vulnerabilities might occur. In addition to the figure, Table 10.3.1 lists in more detail the results of the FMEA, tracing how failures may initiate in one interconnected subsystem and propagate to others. Lastly, the chapter includes a full V&V matrix, indexed to Table 10.3.1, so that each of the defined requirements has a corresponding strategy to verify performance, resilience, or degradation behavior when the system is under faulted conditions.

10.2 System Interdependency Mapping

The (AMF) System Interaction Matrix reveals what can be described as an integrated system-of-systems (SoS) architecture. This is one where interdependencies extend across sensors, control logic, power infrastructure, and all actuated subsystems seamlessly. At its core is the Power Supply System. It forms the essential support layer that delivers electrical energy to every active element. The Control System, Electromagnetic Coils, Cooling System, and the array of environmental sensors that feed the system its critical situational awareness. Based on requirement RQ-4.2.1, this power subsystem isn't just tasked with routine supply; it must also support autonomous fault detection and execute switchovers under 250 milliseconds. This is a speed necessary to prevent or mitigate cascading failures [4].

The sensor subsystems, including radiation, thermal, and system health monitoring modules, maintain a steady flow of environmental and internal status data into the control system. Their role is vital. They must sustain diagnostic updates at intervals no longer than 10 seconds, as required by RQ-4.2.2. This is to ensure that situational awareness remains as close to continuous as possible. Without that constant data flow, corrective action could lag behind real-world conditions [4].

The control system plays a centralized role, issuing commands to the electromagnetic coils, cooling system, and shielding materials, continuously adjusting operational parameters based on real-time sensor feedback. It depends on the quality and timeliness of incoming data to maintain field modulation, thermal regulation, and overall system stability. The cooling system operates in coordination, managing the thermal loads not just of the coils but also of the control hardware itself, an often-overlooked but critical factor for long-duration mission reliability. Shielding materials operate passively, providing a constant baseline of protection that complements the active modulation performed by the coils [5].

The spacecraft structure serves as the structural integration layer. It ensures precise physical alignment of components, provides mechanical support, and isolates sensitive systems from the harsh elements of the space environment. This broader integration context is visually captured in Figure 10.1, which highlights the closed-loop feedback mechanisms and cross-subsystem coordination essential to maintaining radiation protection integrity under the dynamic, sometimes unpredictable, conditions of a real mission [5].

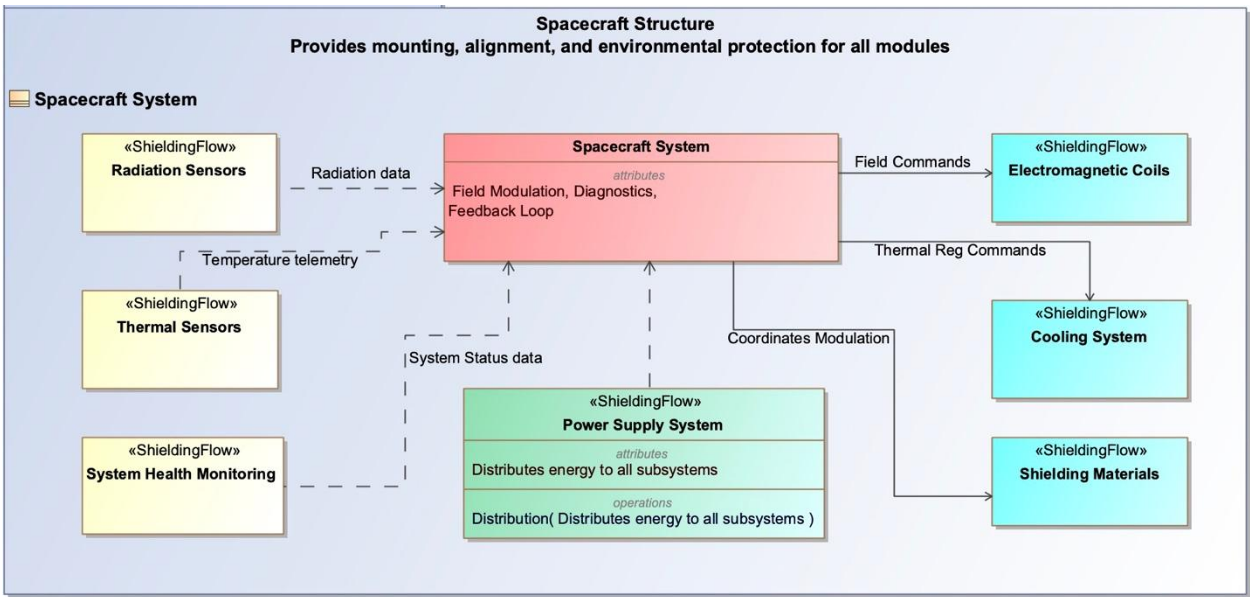

Figure 10.1: System-of-Systems Architecture for Artificial Magnetic Field System.

Figure 10.1 depicts directional flows between control, sensor, power, and effector subsystems, with «ShieldingFlow» representing structured coordination paths. Subsystem colors correspond to roles in the AMF SoS: red (control), cyan (effector), yellow (sensor), green (power), and contextual boundaries (gray background structure).

The control system, highlighted in red within the architecture, serves as the centralized command node of the AMF system. It is responsible for orchestrating field modulation, managing system diagnostics, and continuously processing feedback from various environmental sensors. Drawing on real-time input from all sensor elements, the control system governs the downstream effectors, including the electromagnetic coils, cooling system, and dynamic shielding materials, translating sensed conditions into active responses. It functions as the system's central logic processor, maintaining closed-loop regulation of the shielding field under the shifting realities of the space environment [6].

The effector subsystems, depicted in cyan, comprise the electromagnetic coils, cooling system, and shielding materials. Each plays a distinct, physically actionable role. The coils generate the magnetic field necessary to deflect incoming charged particles, while the cooling system manages the considerable thermal loads produced by sustained high-current operations. Depending on the mission profile, shielding materials provide static or dynamically adjustable radiation attenuation, supplementing the active magnetic defense. Operating under the directive control of the central controller, these systems represent the physical actuators that bring the AMF architecture's protective logic into reality [6].

The sensor and monitoring subsystems, rendered in a yellow gradient in the system diagram, form the AMF's perceptual layer. This group includes the radiation sensors, thermal sensors, and system health monitoring modules. Their task is continuous and demanding: to gather real-time data on radiation flux, thermal distributions, and the internal status of critical components. This constant flow of information is relayed to the control system, enabling it to adjust both the magnetic field configuration and thermal management strategy in real time however, if that flow were interrupted, whether due to sensor failures, communication delays, or unexpected system degradation, the shielding field's stability could erode rapidly, leaving the spacecraft exposed to fluctuating radiation conditions [7].

The power supply system, represented in green within the system architecture, provides the critical energy foundation that sustains AMF operations. It distributes electrical power across all dependent subsystems, including the control electronics, environmental sensors, and field-generating coils, ensuring that each remains functional even as load demands fluctuate during mission operations. Built with fault tolerance as a central design principle, the power supply system incorporates automatic switchover capabilities, enabling rapid reconfiguration during partial power disruptions. Without this ability to reconfigure autonomously, even a localized fault could quickly jeopardize downstream subsystems. Preserving overall system resilience under the fluctuating and sometimes harsh conditions of the space environment depends heavily on this redundancy being both reliable and fast [8].

Because Figure 10.1 provides a qualitative overview of the AMF system's internal connections, a more granular and systematic method is required to quantify and trace the specific interdependencies between subsystems. In this regard, a design structure matrix (DSM) is realized. This technique embodies the physical or electrical links, and functional coupling, thermal coupling, and electromagnetic coupling over the system-of-systems system [8].

The DSM provides a compact, visual illustration of how each of the key RTIDF subsystems is dependent on others. This enables early detection of potential integration bottlenecks, critical dependencies, and architectural vulnerabilities. Its integration into the MBSE framework strengthens traceability and supports structured verification planning.

10.3 Design Structure Matrix for RTIDF Subsystem Interdependencies

In complex radiation shielding architectures such as the Rotating Toroidal-Induced Dipole Field (RTIDF) system, the subsystem interdependencies must be characterized to ensure cohesive integration, avoid interface mismatches, and mitigate cross-domain failure propagation. To address this, a Design Structure Matrix (DSM) is developed to systematically represent and analyze the internal couplings among all major RTIDF subsystems.

The DSM is a binary square matrix, the rows and columns of which represent subsystems. An "X" in the matrix indicates a directed dependency. The subsystem on the row depends functionally, thermally, electromagnetically, or structurally on the subsystem in the corresponding column. This compact representation enables early detection of architectural bottlenecks, cyclical dependencies, and high-centrality nodes that may require additional design attention, resiliency measures, or shielding.

Subsystems are grouped into six logical categories based on function and interaction domain:

- Electrical Systems (e.g., high-voltage power supply and control electronics),
- Thermal Systems (thermal regulation hardware),
- Field Generation Systems (toroidal coil and dipole field control),
- Mechanical Systems (RCS-based rotation and structural support),
- Shielding Systems (magnetic containment structures) and
- Monitoring & Communication (sensor suite, data processing, and telemetry).

The DSM also incorporates cross-domain phenomena such as electromagnetic interference (EMI), thermal coupling, and secondary radiation effects, which are especially relevant for active magnetic shielding systems. Dependencies originating from magnetic shielding and containment are explicitly modeled as sources of potential EMI and radiation-induced interference affecting control, data, and communication systems. Similarly, the thermal management system is a critical intermediary supporting thermal regulation across electrical and field generation subsystems [8].

This matrix serves as a topological map of the RTIDF system architecture and a foundational structure for identifying critical design interfaces and generating traceable SysML «dependency» and «flow» relationships within the MBSE framework. The DSM is thus used to inform requirement allocation, support system-level risk assessments, and guide subsystem-level verification planning [14].

The resulting DSM (Table 10.1) and its subsequent analysis provide the foundation for identifying key integration hotspots, system bottlenecks, and coupling risks across all domains of the RTIDF system. These insights are presented in the following section.

Table 10. 1: Key Interdependencies and Potential Bottlenecks

Subsystem Group	Subsystem	High-Voltage Power Supply	Control Electronics & Feedback Systems	Thermal Management Systems	Toroidal Coil Assembly	Induced Dipole Field Control Unit	RCS BBQ Maneuver System	Structural Support Framework	Magnetic Shielding and Containment	Sensor Suite (Field & Thermal Monitoring)	Data Processing Unit	Communication Module
Electrical Systems	High-Voltage Power Supply		X					X				
	Control Electronics & Feedback Systems	X					X	X	X	X	X	
Thermal Systems	Thermal Management System	X			X			X				
Field Generation Systems	Toroidal Coil Assembly	X				X	X	X				
	Induced Dipole Field Control Unit	X	X		X			X				
Mechanical Systems	RCS BBQ Maneuver System		X		X			X				
	Structural Support Framework											
Shielding Systems	Magnetic Shielding and Containment		X					X			X	X
Monitoring & Communication	Sensor Suite (Field & Thermal Monitoring)		X		X			X				
	Data Processing Unit		X					X	X	X		X
	Communication Module							X	X		X	

10.3.1 Electrical & Thermal Systems: Power, Control, and Thermal Regulation

The high-voltage power supply (HVPS), control electronics, and feedback systems are tightly coupled and interface with nearly every other group. The DSM shows the HVPS providing electrical input to the toroidal coil assembly, the induced dipole field control unit, and the thermal management system, all requiring stable high-voltage input to function correctly. The control electronics unit depends on the HVPS and interfaces with the RCS BBQ system (for rotation control), sensor systems, and thermal controls. It directs commands and gets feedback about the system so that it is a control message center [9].

The thermal management system is a new but vital addition. It also controls heat loads of the coil, power electronics, and structural interfaces. It relies on the HVPS and also on control electronics, and in turn, it becomes important to the coil and structural system. This thermal subsystem helps in the reliability of the field generation and the mechanical area. Combined, these subsystems represent a fundamental back plane that can deliver energy, provide feedback with stabilization, regulate heat, and their multi-group connectivity highlights their significance to integrated operations and reliability [9].

10.3.2 Field Generation Systems: Magnetic Coil and Dipole Control

The Toroidal Coil Assembly and the Induced Dipole Field Control Unit are functionally and physically coupled to form the core magnetic field generation subsystem. The coil requires current and control input from both the HVPS and the dipole control unit. Meanwhile, the control unit governs field modulation and directionality, drawing commands from the Control Electronics and relying on the structure and thermal systems for stability and cooling.

The Magnetic Shielding and Containment subsystem, now explicitly modeled in the DSM, plays a crucial role in mitigating fringe field effects and minimizing EMI exposure to sensitive subsystems. Though passive, its placement and performance directly impact field uniformity and system safety. Notably, both the Coil and Field Control Unit depend on the shield’s proper containment design to prevent cross-system interference [16].

10.3.3 Mechanical Systems: RCS BBQ Rotation and Structural Framework

The RCS BBQ maneuver system has replaced this design’s prior rotational drive mechanism. It provides spacecraft roll via reaction control thrusters, enabling angular alignment of the toroidal coil to maintain directional shielding. The control electronics activate it, but do not require electrical power from the HVPS, as it uses onboard propellant.

The structural support framework remains a universally shared foundation. Every subsystem (power, coil, sensors, shielding, thermal) is mounted to or supported by this framework. Its mechanical integrity is critical while it does not process signals or power. A misalignment, thermal distortion, or shock event could propagate faults across all physically dependent subsystems. The DSM correctly reflects this structural centrality, showing dependency arrows pointing toward it [13].

10.3.4 Shielding Systems: EMI and Secondary Effect Mitigation

Magnetic shielding and containment are now clearly shown to influence three critical electronic subsystems: the control electronics, data processing unit, and communication module. These dependencies reflect the risk posed by stray magnetic fields, EMI, or secondary particle production, any of which could induce logic errors, signal corruption, or hardware degradation. This explicitly models radiation coupling and electromagnetic susceptibility pathways that support downstream FMEA, EMI control plans, and shielding design optimization. The structural framework supports shielding mechanically and interfaces passively with the coil assembly [9].

10.4.5 Monitoring and Communication: Feedback, Processing, and External Interface

The sensor suite (field and thermal monitoring) provides real-time data to the control electronics and the data processing unit (DPU). This feedback loop supports active regulation of magnetic field strength, temperature conditions, and coil stability. The DPU then aggregates this telemetry and routes it to the communication module for downlink or command relay [10].

The DSM shows unidirectional dependency from these sensing and processing systems to the control and communication systems, reflecting their passive monitoring role. However, the DPU and communication module are now also shown to depend on the magnetic shielding system due to their vulnerability to induced EMI and secondary radiation, reinforcing the need for shielding validation in those areas [14].

10.5.6 Integration Hotspots and Bottleneck Risks

Subsystems with high inter-group connectivity in the DSM often become potential bottlenecks or single points of failure. In the RTIDF system:

- The control electronics and feedback systems stand out as a major integration hub. They manage the HVPS, coordinate with the coil and field control units, issue commands to the RCS BBQ, receive sensor input, and forward telemetry to the DPU. Their failure could disrupt operations across every major group, underscoring their high interconnectedness and centrality.
- While not electrically active, the structural support framework is a physical integration node. All mechanical mounting, cooling, and positional integrity rely on it. Failure here could propagate to multiple subsystems simultaneously.
- The magnetic shielding and containment system is a new, significant cross-cutting hazard mitigator. Its influence on communications, data processing, and control electronics must be managed carefully through EMI modeling, verification testing, and shielding margin analyses.

By contrast, some subsystems remain modular and isolated, such as the sensor–DPU–communication chain and the field coil–dipole control unit. These groupings offer design decoupling benefits, reducing fault propagation.

10.4 Conclusion

This section’s design structure matrix (DSM) provides a structured and scalable method for capturing the subsystem-level interdependencies within the rotating toroidal-induced dipole field (RTIDF) shielding system. By explicitly identifying the directional relationships among electrical, thermal, mechanical, shielding, and communication elements, the DSM reveals integration hotspots that would be difficult to detect through informal interface descriptions alone.

The analysis shows that the control electronics and feedback systems represent a key design node with high interconnectivity across nearly all domains, necessitating robust fault isolation, EMI shielding, and redundant command pathways. The structural support framework, while passive, is also revealed to be a high-dependency subsystem due to its role as the physical anchor for nearly every other component. Including the thermal management system, magnetic shielding, and containment further extends the DSM's relevance by accounting for non-functional but operationally critical interactions such as heat rejection and field-induced EMI or secondary radiation.

Importantly, the DSM informs subsystem design and integration planning and supports system-level traceability within the MBSE framework. It enables formal mapping of «dependency», «satisfy», and «verify» relationships in SysML models and provides a basis for driving verification and validation strategies based on architectural coupling and criticality. The DSM is an analytical tool and a structural backbone for model-driven engineering of active shielding systems.

As the RTIDF system is refined, the DSM will continue to serve as a living document, updated to reflect configuration changes, expanded to capture fault-tolerance mechanisms, and integrated into system verification matrices and trade studies in later chapters.

The dependency patterns identified in the DSM reinforce the importance of several high-connectivity nodes, specifically the control electronics, the thermal regulation hardware, and the structural framework. These nodes are central to nominal system performance and represent key fault-propagation pathways if they are disrupted.

The following section develops a failure modes and effects analysis (FMEA) to formally assess the risks associated with these design connections. This analysis builds on the DSM's structural insights by identifying potential failure modes, their causes and consequences, and defining detection and mitigation strategies tied to system requirements.

10.5 System-Level Failure Modes and Effects Analysis (FMEA)

To systematically assess the vulnerability of the AMF system-of-systems (SoS) to non-plasma-related hazards, a failure modes and effects analysis (FMEA) was conducted across all core subsystems. Unlike traditional FMEAs focusing on isolated hardware failure, this analysis considers cascading effects due to system interdependencies. It identifies mitigation strategies that support fault containment, recovery, or fail-operational performance [9].

Table 10.2 summarizes the key findings from the FMEA. Each row corresponds to a specific requirement from the RQ-4.3.x series, covering critical functions of the power supply, electromagnetic field generation, control system behavior, thermal regulation, structural alignment, and passive shielding performance. The immediate effects are identified for each failure mode, along with the detection method and mitigation strategy.

For example, requirement RQ-4.3.1 addresses the risk of switching failure within the power supply system, a failure that could, if left unchecked, cause an immediate loss of magnetic field generation. To mitigate this, the design incorporates redundant power buses and autonomous switchover protocols monitored by onboard telemetry and internal diagnostic systems. Similarly, RQ-4.3.2 identifies the overheating risks associated with the electromagnetic coils. Mitigation strategies center on real-time temperature monitoring, supplemented by hardwired thermal cutoff logic designed to prevent thermal excursions from escalating into irreversible hardware damage [9].

A key insight from the FMEA is the role of thermal and structural subsystems in preserving the alignment and integrity of the magnetic field. For example, structural vibrations or material degradation in the spacecraft structure (RQ-4.3.6) may indirectly cause magnetic misalignment, while shielding materials (RQ-4.3.7) may degrade under prolonged radiation exposure. These findings reinforce the importance of continuous system health monitoring and the integration of preventive engineering controls at the interface between active and passive subsystems [11].

Table 10.2: System-Level FMEA for AMF Subsystems [11]

Req ID	**Subsystem**	**Failure Mode**	**Effect**	**Detection Method**	**Mitigation Strategy**
RQ-10.3.1	Power Supply System	Switching failure	Loss of field generation	Built-in diagnostics, telemetry	Redundant power buses and automatic switchover
RQ-10.3.2	Electromagnetic Coils	Overheating	Thermal damage, reduced shielding	Temperature sensors, thermal modeling	Active cooling, thermal cutoff circuits
RQ-10.3.3	Control System	Signal delay or drop	Unstable or unresponsive field	Feedback loop monitoring	Watchdog timers, redundant control paths
RQ-10.3.4	Radiation Sensors	Calibration drift	Incorrect field modulation	Self-diagnostics, calibration checks	Redundant sensor arrays, in-mission recalibration
RQ-10.3.5	Cooling System	Coolant leak or blockage	Overheating of coils	Flow sensors, thermal mapping	Backup cooling loops, bypass valves
RQ-10.3.6	Spacecraft Structure	Vibration or stress fracture	Misalignment of coils	Structural sensors, periodic inspection	Reinforced structure, vibration dampening
RQ-10.3.7	Shielding Materials	Degradation from radiation	Reduced protection	Periodic inspection, exposure sensors	Material layering, replaceable panels

RQ-10.3.8	Thermal Control System	Imbalanced heat dissipation	Hot spots affecting subsystems	Thermal telemetry and surface mapping	Active thermal balancing and redundancy

Table 10.2 organizes the FMEA into a requirement-driven structure. Each row includes the subsystem under analysis, a concise definition of the failure mode, the anticipated effects of failure (local and system level), the primary method of detection (telemetry, inspection, sensors), and a mitigation strategy aligned to maintain performance or isolate the fault [9].

The table enables traceability from subsystem-specific vulnerabilities to corresponding verification requirements. This forms the bridge to Section 10.4, which defines how each risk is addressed through test and validation procedures. Additionally, the FMEA was modeled in an MBSE parametric diagram, where each failure mode is represented as a constraint condition applied to subsystem blocks. Value properties quantify tolerance thresholds (e.g., allowable switchover time or coil temperature limits), while constraint blocks encapsulate mitigation logic. This modeling approach supports early design validation and simulation of failure propagation [9].

10.6 Verification and Validation Strategy

To confirm that the AMF system meets its critical performance requirements and tolerances under nominal and faulted conditions, a verification and validation (V&V) strategy was established. This strategy supports component- and integrated system-level evaluation, ensuring that each defined system requirement (RQ-4.4.x series) is supported by a measurable and executable verification method [12].

Table 10.3 presents the complete V&V matrix, linking each requirement to its corresponding verification approach, the method used (e.g., test, analysis, inspection, simulation), and an annotation summarizing how the verification method supports risk reduction.

For example, requirement RQ-4.4.1 mandates that power system switchovers occur within 250 milliseconds, a constraint validated through physical testing and simulation. In the physical test setup, a simulated fault is injected into the power distribution system to observe system behavior under stress. At the same time, precise timing measurements are recorded to confirm that switchover latency remains within the required limits [13]. Simulation results extend the validation effort by modeling how variations in load conditions could influence switchover response time under degraded or nonideal scenarios.

Beyond this, analytical models characterize the detailed response behavior of the switchover circuitry itself, accounting for thermal fluctuations and electrical load variability that could otherwise distort timing measurements during physical tests. Likewise, RQ-4.4.2 requires that electromagnetic coils withstand thermal excursions up to +20 °C beyond nominal. This is verified through a combination of thermal vacuum testing (to expose hardware to realistic thermal conditions), finite element analysis (to evaluate stress profiles), and post-test inspection for microcracking or warping [14].

Table 10. 3: Verification and Validation Matrix for AMF SoS Requirements

Requirement ID	**Requirement Description**	**Verification Method(s)**	**Verification Approach**	**Annotation**
RQ-10.4.1	Power system switchover ≤250 ms	Test, Analysis	Simulated power fault injection and response time measurement	Test: Induces actual fault to measure switchover time. Analysis: Models timing response to validate performance.
RQ-10.4.2	Coils tolerate +20°C excursions	Test, Analysis, Inspection	Thermal vacuum test, material stress analysis	Test: Expose coils to thermal cycle. Analysis: Evaluate material strain. Inspection:

				Check for microfractures post-test.
RQ-10.4.3	Control response ≤200 ms	Test, Simulation	Hardware-in-the-loop control testing	Test: Measure live system responsiveness. Simulation: Model control latency under different scenarios.
RQ-10.4.4	Cooling system redundancy	Test, Analysis	Flow restriction tests, thermal monitoring	Test: Simulate blocked loop scenarios. Analysis: Evaluate thermal spread via CFD or thermal modeling.
RQ-10.4.5	Sensor diagnostics ≤10 sec interval	Test, Inspection	Automated diagnostic cycles, telemetry review	Test: Measure sensor self-check intervals. Inspection: Review log/telemetry for fault status changes.

Table 10.3 includes a requirement-centric view of verification, where each row maps a system requirement (RQ-4.4.x), the type(s) of verification method(s) applied, the specific test or analytical process used, and a detailed annotation describing the verification logic.

This structure ensures traceability between system requirements and their corresponding validation actions and strengthens the linkages needed for compliance documentation and eventual certification. It becomes imperative when subsystems interact under dynamic conditions, where single-method verification could miss hidden vulnerabilities. To address this, the matrix incorporates multiple verification methods for critical systems. For example, combining physical testing and analytical modeling reflects established best practices in fault-tolerant system engineering [15].

The MBSE model links this matrix directly to the system requirement blocks through «satisfy» and «verify» relationships. Test cases and blocks are allocated to the respective physical components (e.g., coils, sensors, and controller), supporting simulation-based verification or hardware-in-the-loop (HIL) testing. This end-to-end traceability ensures that verification strategies are embedded within the system model and evolve with design changes [16].

10.6 Chapter Summary and Conclusion

This chapter expanded the hazard and risk analysis of the artificial magnetic field (AMF) system beyond plasma interactions to encompass its full system-of-systems (SoS) context within the spacecraft. Systematically examining interdependencies among subsystems provided a deeper understanding of the failure pathways and system-wide vulnerabilities. This includes power distribution, electromagnetic field generation, control logic, thermal management, and sensor feedback.

The updated system interaction matrix and architectural block diagram (Figure 10.1) formally represented the functional, thermal, and command pathways between AMF subsystems. Color-coded and directionally annotated, the figure reinforces the system's closed-loop architecture and highlights how dynamic feedback from environmental sensors enables real-time field modulation. The inclusion of the «ShieldingFlow» stereotype provided semantic clarity, reinforcing the system's radiation protection objective within the MBSE environment [17].

The failure modes and effects analysis (Table 10.3) presented a requirement-driven view of AMF hazards, explicitly identifying how faults in any one subsystem, such as overheating of coils, coolant blockage, or sensor drift, could impact overall shielding performance. Importantly, these failure modes were not isolated but assessed within cascading effects and cross-subsystem interactions. Mitigation strategies such as redundant power buses, thermal telemetry, and automated switchover protocols were aligned to each failure class [20].

Verification and validation were addressed through a structured V&V matrix (Table 10.4), aligning each RQ-4.4.x requirement with appropriate verification methods such as physical test, simulation, inspection, and analytical modeling. The matrix emphasized redundancy in verification for critical systems, employing multiple methods to validate thermal margins, response times, and subsystem coordination. These verification strategies are traceably embedded in the MBSE model via «satisfy» and «verify» relationships, test blocks, and SysML allocations, enabling early validation and configuration control throughout the lifecycle [18,19].

This chapter lays out a robust engineering foundation for the eventual integration, testing, and mission assurance of the AMF system. More importantly, it does not stop at outlining theoretical system architectures. Instead, this chapter establishes executable validation strategies demonstrating shielding performance and subsystem resilience in practice. This is essential in preparing the AMF for operation in complex and unpredictable mission environments. The modeling approach adopted here further supports long-term scalability, allowing future variants of the AMF system to adapt to mission-specific environments, fault-tolerance requirements, or hardware evolution.

The next chapter will 275ransitionn from analytical modeling to system integration, environmental test planning, and spacecraft-level qualification workflows. Emphasis will shift to operationalizing the AMF system within the broader mission design, with specific attention to assembly sequences, the validation of interconnects, and certification under flight-like thermal, vibrational, and radiation environments.

CHAPTER 11 AMF HUMAN-IN-THE-LOOP ADAPTIVE SHIELDING DESIGN AND VALIDATION

The artificial magnetic field (AMF) radiation protection system is designed to be a modular, adaptive subsystem that integrates human-in-the-loop (HITL) decision-making into radiation shielding operations. A SysML block definition diagram (BDD) describes the system's structure. This diagram outlines the component functional blocks, the data interfaces, and the directed flows that support operational responses to radiation hazards. The BDD in Figure 11.1 enables traceability between system-level shielding strategies, astronaut interaction, and the specific roles of autonomous and human-centered control logic.

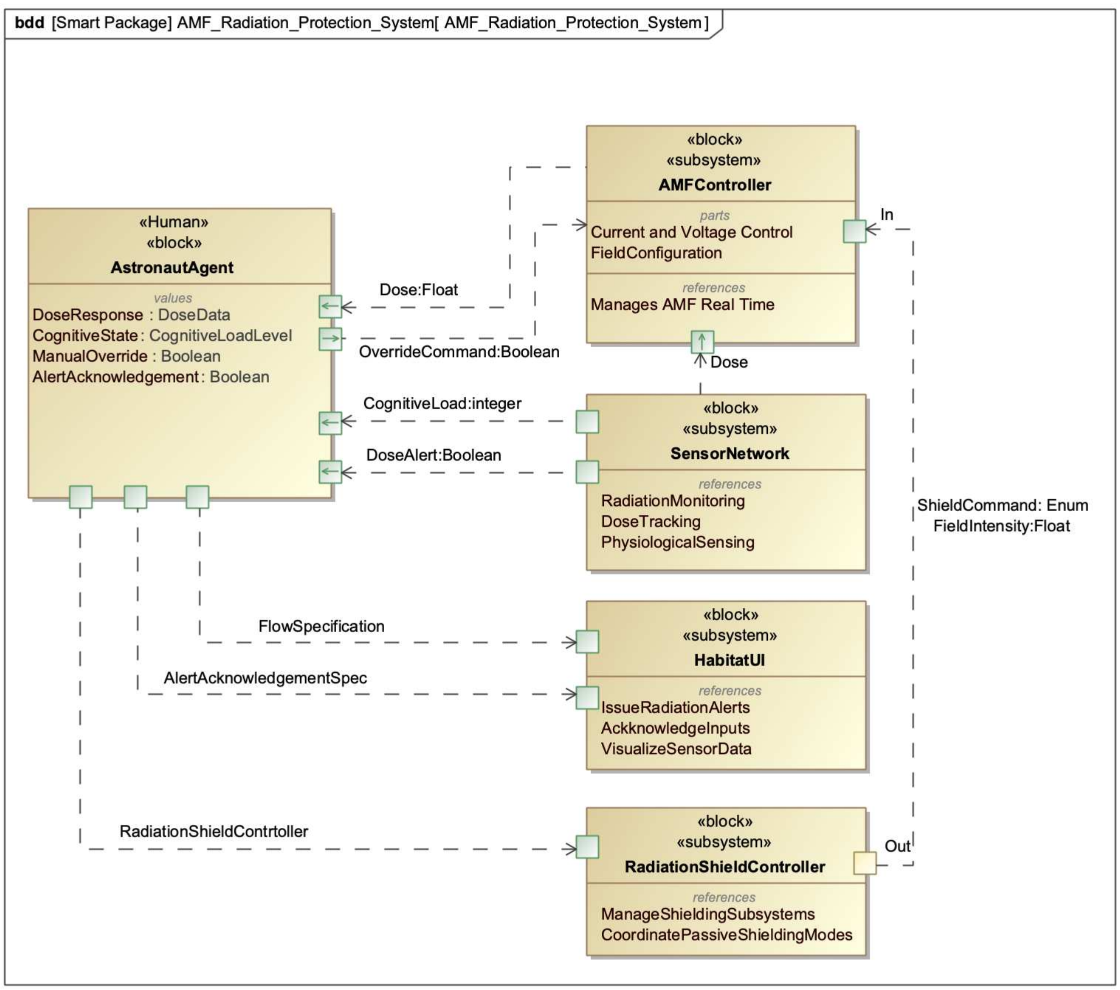

Figure 11.1 – AMF Radiation Protection System

At the center of this model is the AstronautAgent. This «Human» block represents the crew member as an intelligent subsystem embedded within the shielding control loop.
The agent receives inputs from the SensorNetwork that include radiation dose (Dose: Float), cognitive load (CognitiveLoad: Float), and binary alert flags (DoseAlert: Boolean). These signals provide information on the astronaut's internal state (DoseResponse) and perceived workload (CognitiveState). These signals may prompt a manual override command to the supervisory shielding controller. Additionally, when the astronaut receives a radiation warning via the HabitatUI, the astronaut may issue an AlertAcknowledgement signal, confirming awareness of the event. Each port is formally typed using FlowSpecifications to ensure semantic clarity and testable interface definitions.

The SensorNetwork collects environmental and physiological telemetry and disseminates this data to the astronaut and other system components. Radiation sensors track dose rate and cumulative exposure, while biosensors (e.g., EEG, heart rate variability monitors) support dynamic cognitive load estimation. The network acts as a broadcast source for radiation and physiological signals, enabling downstream shielding and field control elements to respond in real time.

The HabitatUI block serves as the astronaut's interface to the radiation protection system. It provides alerts, sensor data visualizations, and operational states such as current field intensity or passive shielding mode. The astronaut's acknowledgment of a radiation event is returned via the AlertAcknowledgementSpec interface, ensuring situational awareness of hazardous exposure levels. Optionally, the AstronautAgent can transmit a RadiationLoad output for visualization on the user interface, which provides a human-perceived measure of cumulative exposure risk.

The RadiationShieldController governs both active field generation and static shielding strategies. It receives override commands from the astronaut and issues ShieldCommand and FieldIntensity directives to the AMFController, which implements the physical field. The controller also interprets sensor input to determine whether passive shielding should be prioritized. Although this system does not utilize deployable shielding panels, the controller supports several passive shielding modes using fixed or modular materials such as polyethylene and boron nitride nanotubes (BNNTs). These include:

- Zone Activation Mode — directs the astronaut into regions with thick interior shielding (PASSIVE_OPTIMIZED_ZONE).
- Manual Reconfiguration Mode — crew rearranges stowable shielding or consumables around their workspace (MANUAL_SHIELD_RECONFIG).
- Storm Shelter Mode — designates highly shielded core zones (STORM_SHELTER_MODE).
- Mass Realignment Mode — redistributes passive shielding mass (e.g., water, food) toward an incoming radiation vector (MASS_REALIGN_PASSIVE_ZONE).

These mode commands are issued as enumerated values through the ShieldCommandSpec flow and represent an essential integration of passive design strategies with real-time crew input. The AMFController block is responsible for the low-level actuation of the magnetic field coils. It receives ShieldCommand and FieldIntensity values from the supervisory controller and configures coil behavior accordingly. Depending on the mission configuration, this may involve modulating a static toroidal field by adjusting field strength during a solar particle event (SPE) or executing a rotating dipole configuration during deep-space transits. The controller may also report diagnostic values such as coil temperature or measured field to the SensorNetwork.

Each interface in the BDD is typed using a formal FlowSpecification, which defines the structure and direction of allowed signal types across the system. These specifications include SensorDataSpec, ControlCommandSpec, AlertAcknowledgementSpec, and ShieldCommandSpec, as outlined in the table below.

Table 11.1 defines the flow specifications used in the SysML model of the artificial magnetic field (AMF) radiation protection system. Each entry includes the flow label, data direction, type, subsystem connections, and purpose. These interfaces support traceability, simulation, and validation of shielding control logic and human-in-the-loop integration.

Table 11. 1: Flow Specifications Summary Table

Flow Label	Direction	Type	Source/Target	Purpose
Dose	in	Float	SensorNetwork → AstronautAgent AMFController → AstronautAgent	Real-time or integrated radiation exposure input for astronaut awareness
CognitiveLoad	in	Float	SensorNetwork → AstronautAgent	Crew mental workload derived from physiological telemetry
OverrideCommand	out	Boolean	AstronautAgent → ShieldController / AMFController	Manual override signal from astronaut to control system
AlertAcknowledgement	out	Boolean	AstronautAgent → HabitatUI	Confirms crew received and acknowledged radiation alert
RadiationLoad	out	Float	AstronautAgent → HabitatUI	Internal state or burden reported for UI display
ShieldCommand	out	Enum	RadiationShieldController → AMFController	Defines shielding mode (e.g., AMF mode or fixed passive zone activation: STORM_SHELTER_MODE, PASSIVE_OPTIMIZED_ZONE, etc.)
FieldIntensity	out	Float	RadiationShieldController → AMFController	Specifies target magnetic field intensity

This architecture seamlessly integrates autonomous protection logic with crew situational awareness and intervention. The BDD captures both the structural relationships and the functional role of the astronaut as a dynamic element in the shielding control system. These definitions form the foundation for subsequent Internal Block Diagrams, behavior models (e.g., state machines), and verification traceability matrices.

11.1 Assessing Shielding Impact

To assess the shielding impact of different system configurations over time, cumulative radiation dose values were simulated for various hybrid AMF–material designs. These results are shown in Figure 11.2. Five key computational steps were followed to derive the cumulative dose trends illustrated in this figure. First, baseline daily radiation dose rates were established for each shielding configuration based on shielding effectiveness data that was synthesized to match the data characteristics of published material. In addition, attenuation coefficients and previous FLUKA-based simulations were used. These rates reflected a combination of galactic cosmic ray (GCR) and trapped particle exposure under nominal deep-space conditions [1]. Second, in hybrid shielding systems, including BNNT + AMF or polyethylene + AMF, analogous effects of passive mass shielding and deflection due to a magnetic field were used via a weighted reduction model. That model included linear attenuation of the shielding material (related to the mass per area) and deflection-based dose scaling using Lorentz force deviation curves of protons and light ions [2]. Third, the breakdown dose over each configuration was calculated by dose accumulation model:

$$D_{cumulative}(t) = (D_{daily,\ unshielded} * R_{shield}) * t$$

Where $D_{cumulative}(t)$ is the cumulative dose in mSv over mission duration t (in days), $D_{daily,\ unshielded}$ is the baseline daily dose without shielding, and R_{shield} is the relative dose reduction factor determined by each shielding configuration [3].

Fourth, dose summation was refined to accommodate small time-variability nonlinearities caused by adaptive AMF field strength variability over the mission time. This was measured through a minor correction factor (<5%) in AMF-equipped setups [4]. Lastly, the cumulative dose was summarized in tabular form and plotted using a multiseries line chart with each line denoting one shielding procedure. The final visualization clearly highlights the long-term performance differences between materials and the additive protection offered by coupling active (AMF) and passive (polymer or BNNT) shielding strategies.

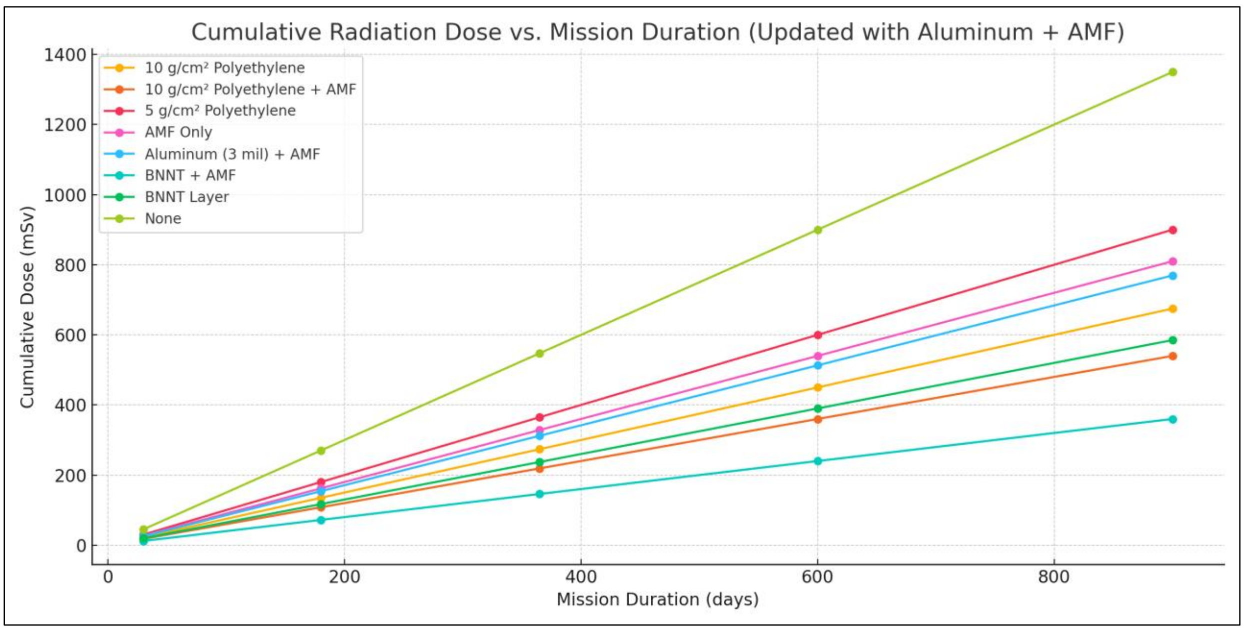

Figure 11.2 – Cumulative Radiation Dose vs. Mission Duration for Hybrid Shielding Configurations [4]

This graph illustrates the cumulative dose accumulation over a 900-day mission across various shielding strategies. Combinations of active magnetic field (AMF) with passive material like polyethylene, aluminum, and BNNTs show significant improvements in radiation mitigation compared to single-layer protection or no shielding at all.

The combination of boron nitride nanotube (BNNT) shielding with an active magnetic field (AMF) system demonstrated the most effective cumulative dose reduction across extended mission durations. This outcome is supported by several interrelated physical mechanisms First, BNNT materials offer high stopping power due to the presence of boron which is an element with a relatively high atomic number. Also, hydrogen-rich bonding structures allow them to attenuate both galactic cosmic ray (GCR) heavy ions and solar protons through nuclear and Coulomb interactions [5].

Second, the AMF system provides dynamic deflection of incoming charged particles that reduces the particle flux density through Lorentz-force trajectory modification. This is effective for lower-mass particles such as protons and electrons.

Third, the combination of BNNT and AMF results in complementary protective effects. Because BNNT passively absorbs and slows particles, the AMF actively diverts them by reducing the total particle density and kinetic energy reaching the interior habitat. This synergy also minimizes secondary particle production. Particles such as recoil protons and neutrons are known limitations of high-Z shielding like aluminum [5].

Fourth, the benefits of this hybrid configuration become increasingly pronounced over time. This is because radiation exposure accumulates over missions lasting 900 days or more, and even incremental daily reductions in dose rate yield substantial cumulative advantages.

Finally, the simulation results in Figure 11.2 confirm that BNNT + AMF maintains cumulative dose levels well below the 600 mSv NASA career limit for crew exposure, while other configurations approach or exceed this threshold. This reinforces the conclusion that hybrid active-passive shielding strategies, particularly those incorporating BNNTs, offer the most robust protection against deep space's complex and persistent radiation environment [7].

While the preceding section established the structural foundation of the HITL-enabled artificial magnetic field system, including its component hierarchy, interfaces, and astronaut-agent integration, the next step involves modeling its dynamic behavior. This includes how the system responds to radiation exposure, human physiological thresholds, and command overrides in real-time scenarios. The following section introduces state machine diagrams and verification mappings that define the system's adaptive shielding logic and escalation mechanisms [8].

11.1.1 Activity Logic for Shielding Reconfiguration Control

The Radiation Shield Controller implements an adaptive control sequence governed by environmental sensor inputs and astronaut intervention triggers to effectively manage space radiation hazards in real-time. Figure 11.3 presents a SysML activity diagram capturing the operational flow of this controller. The process initiates with continuous monitoring of radiation sensors and classifies threat levels based on predefined thresholds. Depending on severity, the controller autonomously adjusts the shielding mode or escalates the event to the crew via notification prompts. Manual overrides by the astronaut agent can be invoked at any time, overriding autonomous logic to force maximum shielding deployment. This hybrid logic enables both automatic and crew-directed response pathways, ensuring resilience across nominal and extreme mission conditions [7,8].

11.1.2 Astronaut State Classification and Response Thresholds

Figure 11.3 presents a SysML state machine model representing astronaut condition transitions under varying radiation and workload levels. Beginning in a nominal operational state, the agent enters cautionary states once the cumulative dose exceeds 130 mSv, triggering severity-based classification. Depending on system assessment and crew override input, the astronaut may enter escalating cognitive load warning states or direct physiological alert levels.

Transitions reflect system-driven thresholds (e.g., dose rate, severity) and HITL intervention logic, with final transitions leading to either continued alert escalation or a recovery state once reconfiguration or mitigation has occurred. This state model ensures traceability between radiation exposure, mental workload, and system adaptation requirements in a human-integrated control loop [9].

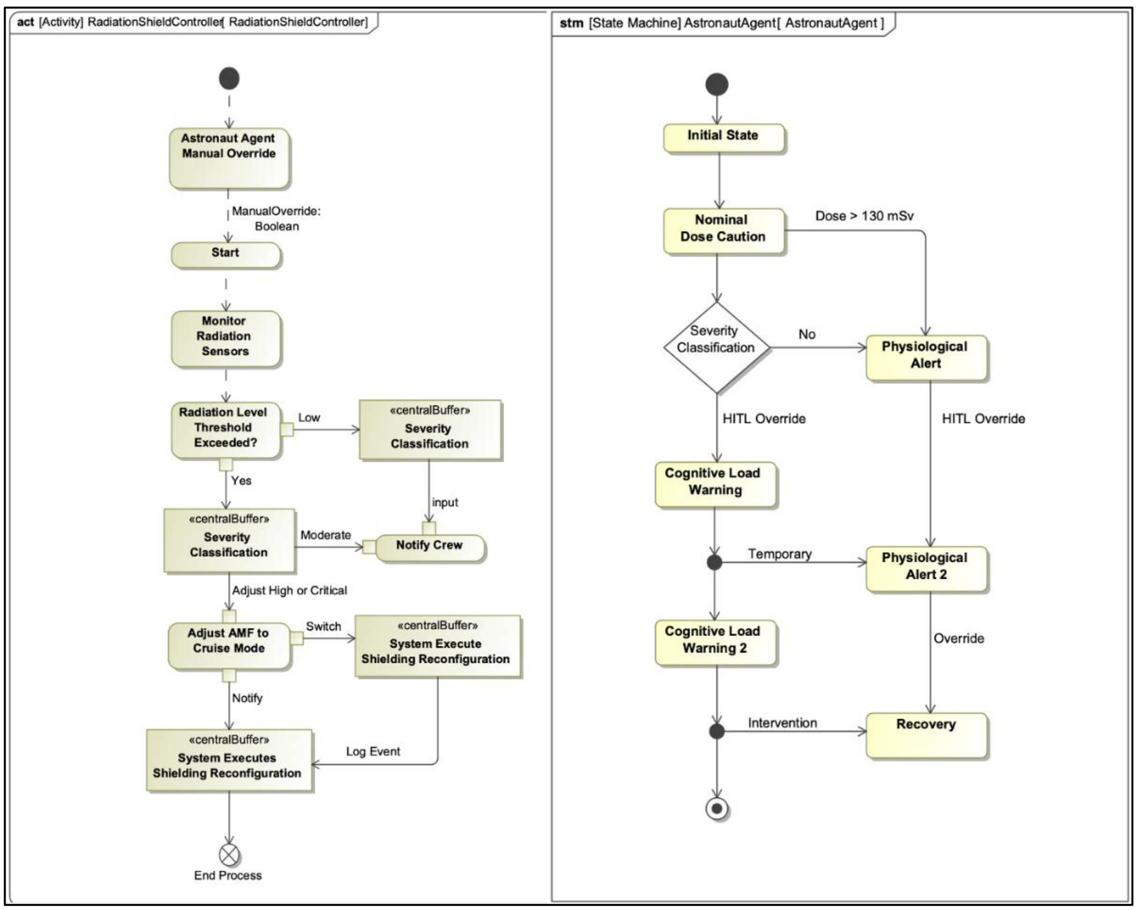

Figure 11.3: Radiation Shield Controller Activities

Figure 11.3 illustrates the activity logic of the RadiationShieldController, integrating both autonomous responses and astronaut-initiated overrides. Upon detecting elevated radiation levels via onboard sensors, the controller classifies threat severity and triggers appropriate responses. In moderate cases, crew are notified to confirm or intervene. The system autonomously adjusts the artificial magnetic field (AMF) intensity for high or critical levels and reconfigures the shielding strategy. Human-in-the-loop actions, when initiated, bypass default automation to execute emergency shielding escalation directly. All operations are logged for traceability and telemetry validation, maintaining compliance with safety-critical mission protocols.

The state machine diagram “AstronautAgent Radiation and Cognitive Response States” (Figure 11.3) models the progressive physiological and cognitive transitions triggered by radiation dose accumulation and workload intensity during mission operations. The state transitions begin at a *Nominal Dose Caution* level and progress through alert states based on real-time exposure monitoring, as reported by the SensorNetwork block. The first critical threshold occurs at Dose > 130 mSv, which initiates a transition to a *Physiological Alert* state. This threshold is operationally justified as follows:

1. NASA radiation health guidelines define permissible exposure limits (PELs) for astronauts, with career and short-duration thresholds derived to maintain risks below 3% REID (risk of exposure-induced death). While full-career exposure limits range from ~600 mSv to >1200 mSv depending on age and sex, mission-phase triggers such as 130–250 mSv are frequently used as alert thresholds to initiate crew countermeasures and system reconfiguration well before any irreversible exposure occurs [11].
2. Cucinotta et al. (2014) and subsequent Monte Carlo modeling studies recommend intermediate dose limits around 100–150 mSv as cognitive degradation and tissue risk thresholds, especially under compound factors such as fatigue, elevated workload, or radiation event proximity [12].
3. Data from the Mars Science Laboratory and extrapolations using the FLUKA Monte Carlo transport model suggest that unshielded transit to Mars can reach ~1.84 mSv/day,

making 130 mSv a practical ~70-day decision point to trigger mitigation if automated thresholds are bypassed or degraded [13].

4. The diagram also introduces Human-in-the-Loop (HITL) override states, allowing an astronaut agent to bypass nominal system logic in extreme mission cases. Manual override enables transition to higher-risk shielding configurations (e.g., full SPE mode) in response to fatigue alerts or second-stage physiological warnings.
5. Transitions to *Recovery* represent either the resolution of accumulated dose or reversion from an elevated cognitive state following shielding engagement. Verification methods for each state transition are provided in Table 11.2, ensuring these behavioral thresholds are both testable and traceable to physiological markers or operational simulations.

Table 11.2 maps each astronaut's physiological or cognitive state, as modeled in the state machine diagram, to its corresponding trigger conditions, mitigation requirements, and recommended verification method. It supports traceability between human-in-the-loop (HITL) behavior models and the formal system-level hazard control framework.

Table 11. 2: State Verification & Mitigation Mapping

State	**Trigger Condition**	**Mitigation Requirement**	**Verification Method**
Nominal Dose Caution	Initial background exposure below operational thresholds	RQ-3.1.1	Analysis
Cognitive Load Warning	Cognitive Load > 60%	RQ-3.2.1	Sensor Test
Cognitive Load Warning 2	Cognitive Load > 85%	RQ-3.2.2	Analysis + Simulation
Physiological Alert	Dose > 130 mSv or severity=Moderate	RQ-4.1.1	Test + Inspection
Physiological Alert 2	Cumulative dose > 250 mSv or override issued	RQ-4.1.3	Test + Monitoring
Recovery	Intervention Applied	RQ-4.3.2	Test + Analysis

The behavioral modeling and state-verification mapping provide a robust framework for understanding how the system should behave under varying radiation and human performance conditions. However, a quantitative assessment is required to validate these control strategies and determine their mission-level effectiveness. The following section presents a trade study examining energy use efficiency and radiation shielding performance across various system configurations. This includes simulation results demonstrating how dynamic control strategies impact crew dose, power usage, and shielding outcomes in operational scenarios.

11.2 Energy Use Efficiency Trade Study for AMF Shielding

Active Magnetic Field (AMF) shielding systems offer a promising approach to protecting crewed spacecraft from high-energy charged particle radiation in deep space environments. However, their adoption introduces complex trade-offs in power consumption, shielding effectiveness, and mission-specific operational constraints. This section details a parametric energy use efficiency trade study of AMF configurations using derived metrics from time-varying toroidal magnetic field systems. The study integrates Human-in-the-Loop (HITL) effects and mission-aware response scaling to quantify technical and operational viability [14].

1. Key Extracted Parameters and Equations

The core of the trade study is based on electromagnetic configurations that generate shielding via rotating toroidal dipole fields. Parameters are extracted from simulation data in the accompanying paper ("Dynamic Magnetic Field Adaptation for Radiation Protection, 2025") and revised with updated spacecraft power estimates:

- Magnetic Field Strength (B): Ranges from 1.0 T to 2.3 T
- Rotation Frequency (ω): Between 1.5 Hz and 10 Hz

- Power Consumption (P_avg): Estimated at 1.25 kW for cruise mode and up to 6.5 kW for solar event override conditions
- Deflection Effectiveness (E_def): Lateral displacement of a high-energy charged particle in meters

From these, an energy efficiency metric is defined:

This metric quantifies shielding effectiveness per unit power and supports dynamic field control strategies.

2. **Derived Energy Efficiency Metric**

Using updated power consumption estimates, the resulting efficiencies are significantly lower in absolute terms but still preserve the tradeoff hierarchy between modes. The values are summarized in Table 11.3.

Table 11. 3: Power Efficiencies [13]

Mode	B (T)	ω (Hz)	E_def (m)	P_avg (kW)	ε (m/J)
Baseline Cruise	1.0	1.5	0.21	1.25	0.000168
Moderate Response	1.5	4.0	0.34	2.50	0.000136
High Response (SPE)	2.3	10.0	0.46	6.00	0.000077
Manual Override	2.3	10.0	0.43	6.50	0.000066

Table 11.3 presents the performance characteristics of four active magnetic field (AMF) shielding configurations under varying operational modes defined by magnetic field strength B and rotation frequency ω. The associated deflection effectiveness E_def quantifies the lateral displacement of incoming high-energy charged particles, serving as a surrogate for shielding performance. Power consumption P_avg values are drawn from updated estimates, including resistive losses, thermal management, and electronic control overhead. The derived energy efficiency metric ε, expressed in meters per joule (m/J), indicates the shielding benefit per unit of

energy expended. Notably, cruise mode offers the most favorable tradeoff, with an efficiency of 0.000168 m/J, outperforming higher-intensity response modes, which, while more protective, suffer from diminishing returns relative to power consumption. The lowest efficiency is observed for the manual override condition, where high power demand yields reduced marginal benefit.

This tabulated data supports the conclusion that moderate field intensities provide optimal balance for long-duration missions constrained by spacecraft energy budgets [15,16].

3. Mission-Aware Tradeoff

Energy efficiency must be evaluated within the mission context. Three operational scenarios were analyzed:

- Passive Mode: Used during quiescent spaceflight, no power draw, baseline deflection ~0.12 m
- Automated Response Modes: Adjusts intensity based on real-time sensor feedback
- Manual Override: Triggered by HITL for rapid upscaling during radiation spikes (e.g., SPEs)

Orion-class power systems (~11.2 kW) can accommodate peak AMF operations (~6.5–7.0 kW) during solar events while maintaining spacecraft margin. Thermal management (~200 W) and control electronics (~100 W) were included in these totals.

4. Trade Model Results and Interpretation

Table 11.4 shows that while increasing field strength improves deflection, it does so with diminishing efficiency ε, where

$$\varepsilon = \frac{Edef}{Pavg}.$$

Moderate configurations (1.5 T, 2.5 kW) yield the best power-performance tradeoffs. [17]

HITL manual override, while necessary during acute events, causes a significant drop in ε. Energy efficiency in cruise mode is highest, affirming the advantage of low-intensity autonomous shielding during nominal operations.

Table 11.4 Synthesizes the Tradeoff [17]

Mode	**Dose Reduction (%)**	**E_def (m)**	**P_avg (kW)**	**ε (m/J)**	**Suitability**
Passive	35%	0.12	0.0	∞	Long-duration base
Cruise	25%	0.21	1.25	0.000168	Transit cruise
Moderate Response	33%	0.34	2.50	0.000136	Nominal radiation
Manual Override	42%	0.43	6.50	0.000066	Crew decision
High Response (SPE)	45%	0.46	6.00	0.000077	Autonomic max mode

Table 11.4 synthesizes shielding performance across five representative AMF operating modes, integrating dose reduction, particle deflection, power demand, and energy efficiency **ε** into a unified mission suitability matrix. Passive shielding, which consumes no onboard power, provides moderate (~35%) radiation attenuation and is characterized by an infinite efficiency score due to its zero-power requirement. Cruise mode offers lower dose reduction (25%) but superior energy efficiency, making it ideal for nominal interplanetary transits. In contrast, high-response modes activated during solar particle events (SPEs) or crew overrides deliver stronger shielding (up to 45% dose reduction) at the cost of elevated power consumption and declining **ε** values. Suitability labels reflect each mode's best-fit application, from passive base operations to acute event response. The tabular comparison emphasizes the importance of dynamic field modulation and HITL overrides in balancing radiation protection with mission energy constraints [16].

To further illustrate the multi-criteria trade space among deflection, dose mitigation, and energy cost, Figure 11.4 provides a normalized comparison of key performance metrics across all shielding configurations.

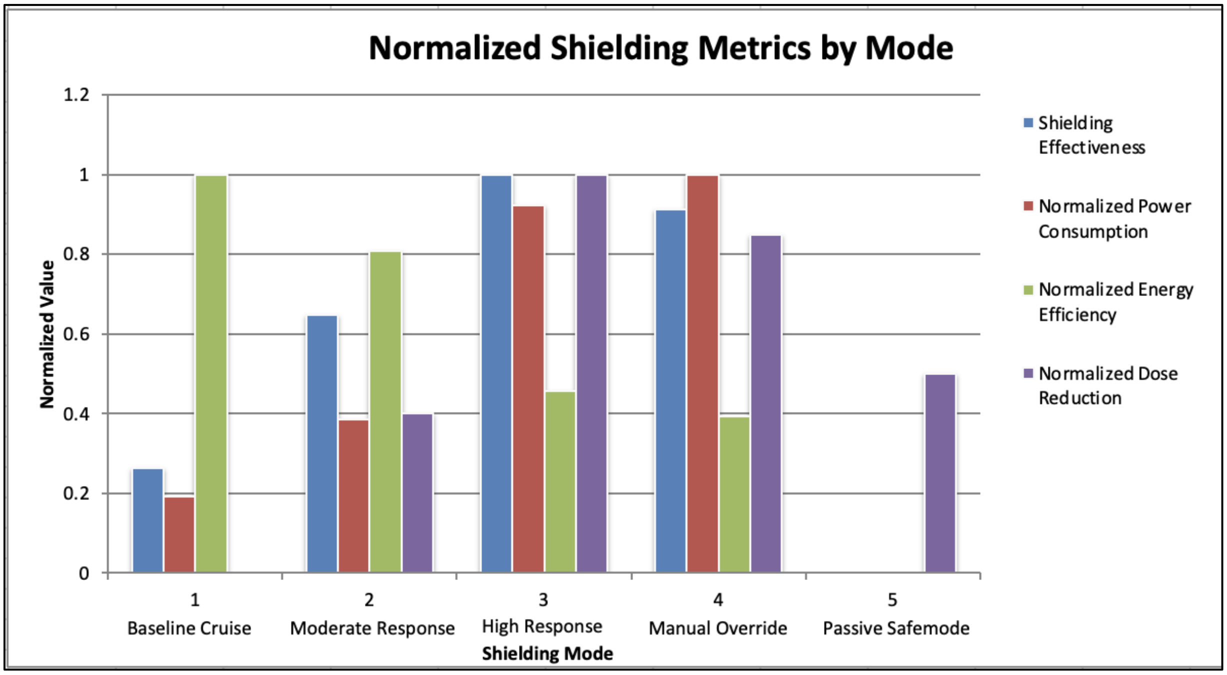

Figure 11.4. Normalized Comparison of Shielding Metrics by Mode (Power-Adjusted).

This figure compares four key shielding performance metrics normalized across five operational AMF configurations: Passive Mode, Cruise, Moderate Response, High Response (SPE), and Manual Override. The metrics—shielding effectiveness (deflection distance), power consumption, energy efficiency (deflection per joule), and dose reduction—are scaled between 0 and 1 to enable visual comparison. Power consumption values have been updated to reflect realistic estimates ranging from 1.25 kW (Cruise) to 6.5 kW (Manual Override), consistent with Orion-class spacecraft power budgets. Bars are grouped by mode and color-coded by metric type. [17]

The normalized bar chart reveals key trends in performance trade-offs among shielding modes:

- Passive Mode (green) provides a moderate dose reduction (0.35 normalized) with zero power draw and minimal deflection, resulting in no calculable energy efficiency.
- Cruise Mode demonstrates the highest normalized energy efficiency (1.0), making it the most power-effective setting under nominal spaceflight conditions.
- Moderate Response Mode balances shielding effectiveness and power, showing near-optimal deflection (normalized ~0.75) at a moderate power cost.
- High Response (SPE) achieves the highest shielding effectiveness and dose reduction, but at a significant energy cost, resulting in lower efficiency.
- Manual Override (HITL intervention) shows diminished energy efficiency (lowest bar), illustrating that while manual escalation boosts protection, it does so with reduced return on power investment.

The normalized format emphasizes the inherent trade-off between protection and power use. It illustrates the role of adaptive control strategies—both automated and human-in-the-loop—in tuning field strength for mission conditions.

To further quantify the trade-offs between energy efficiency and shielding performance, the normalized scores for each of the five shielding modes were averaged using an unweighted mean and a weighted mean that emphasizes dose reduction and shielding effectiveness. The results are illustrated in Figure 11.5, which compares the mean and weighted mean performance scores for each operational mode.

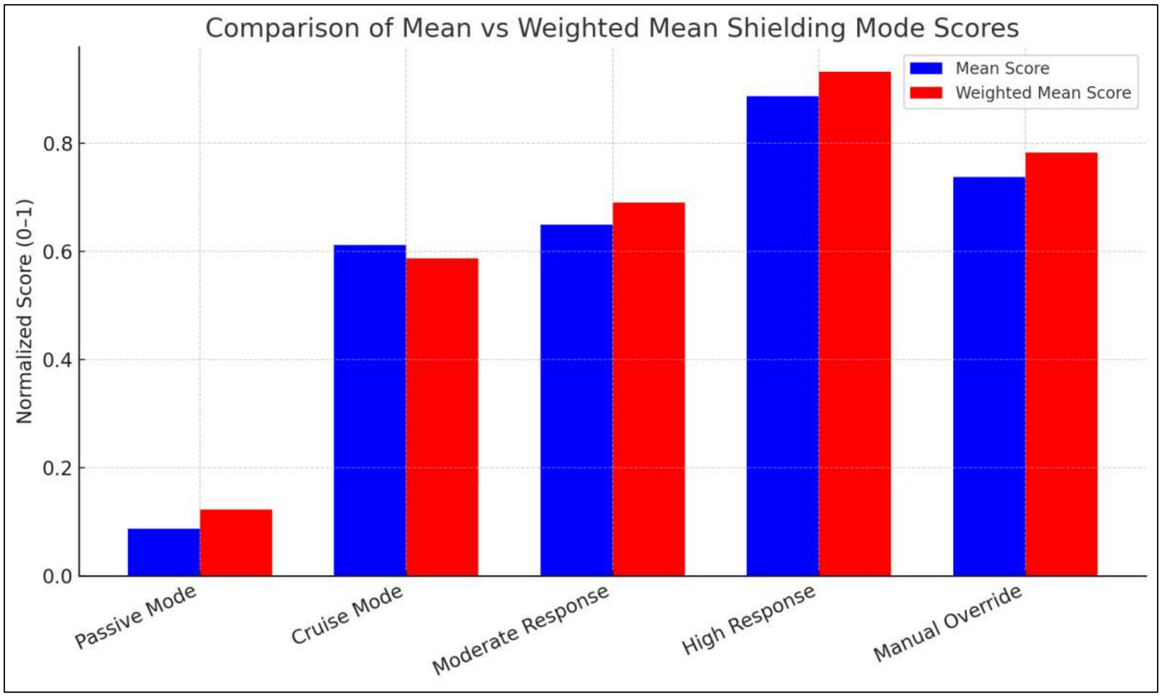

Figure 11.5 Comparison of mean and weighted mean shielding mode scores

The comparative analysis of mean versus weighted mean scores for the five shielding modes (Figure 11.4) highlights the trade-offs between operational effectiveness and energy efficiency in AMF-based protection strategies. The unweighted mean scores suggest that all performance metrics including shielding effectiveness, power consumption, energy efficiency, and dose reduction, are equally valued, producing a more balanced distribution across modes.

Under this criterion, the High Response (SPE) mode ranks highest, reflecting its superior shielding and dose reduction performance, with Manual Override emerging as the second most effective mode. The difference between the modalities increases further with weighting towards the shielding effectiveness and reduction of dose as should be the case in mission safety. High Response (SPE) mode maintained a distinct lead with a normalized weighted score of 0.93, and the Manual Override lead score is 0.78. They are even more efficient than the Moderate Response mode and the Cruise mode, which offers more moderate rates of protection and efficiency. The Passive Mode remains the least effective across both scoring methods, underscoring its limited role as a baseline or supplemental strategy rather than a primary protective measure. Overall, the weighted analysis reinforces the conclusion that adaptive high-intensity shielding responses are optimal for hazard mitigation, while manual intervention provides a valuable but energetically costly backup, thereby illustrating the importance of balancing automated shielding logic with human-in-the-loop escalation pathways in mission design [10].

11.3 Conclusion

This chapter has shown that Human-in-the-Loop (HITL) integration into the Artificial Magnetic Field (AMF) shielding configuration presents a feasible and resilient approach to the management of deep-space radiation exposure. The strategy promotes a shielding system that strikes a balance between automated protection and adaptive human intervention by incorporating the intelligent astronaut as a subsystem within its shielding control loop. The SysML based modeling such as Block Definition, Activity and State Machine provide the assurance of technical and behavioral inter-dependencies being captured formally, traceable and verifiable. This integration instills the confidence that the state of astronaut cognition, the physiological dose limits, and manual override must be factored and reflected in the system architecture of the shielding.

The cumulative dose analysis confirmed the unique advantages of hybrid AMF-material designs, particularly BNNT + AMF configurations, which remain below NASA's career exposure limits even over 900-day mission durations. Notably, the shielding modes were modeled under Passive, Cruise, Moderate Response, High Response (SPE), and Manual Override modes to provide a clear trade-off hierarchy. Cruise Mode offers superior energy efficiency for long-duration operations, while High Response and Manual Override modes deliver maximal shielding performance at the cost of power and thermal overhead. The weighted scoring analysis underscored that prioritizing dose reduction and shielding effectiveness favors High Response and Manual Override modes, affirming their role as critical but power-intensive emergency strategies.

From a systems engineering perspective, introducing the energy efficiency metric (ε, m/J) provided a rigorous performance proxy for quantifying shielding return on energy expenditure. This metric, with a normalized comparative analysis, allows a mission designer to optimally determine when and how aggressively AMF shielding should be used (in terms of spacecraft power limits and overall operational considerations). Additionally, HITL escalation pathways in the design will help address a key risk management gap addressed by allowing the crew to take decisive action should it become necessary in edge cases where autonomous logic would not be sufficient.

Overall, the chapter draws three important conclusions. First, AMF-based shielding systems are technically viable within Orion-class power budgets, provided dynamic field modulation strategies are employed. Second, hybrid active-passive approaches, particularly those leveraging BNNTs, yield the most robust protection against Galactic Cosmic Rays (GCRs) and Solar Particle Events (SPEs) while minimizing secondary radiation hazards. Third, the explicit integration of human operators into shielding control logic (supported by SysML traceability, DSM mappings, and verification matrices) ensures resilience against both environmental uncertainties and system-level failure propagation. Together, these insights establish a foundation for scalable AMF architectures that are not only technically feasible but also operationally adaptable. This bridges the gap between automated spacecraft shielding systems and the indispensable role of crew judgment in deep-space exploration.

CHAPTER 12 DISCUSSION

12.0 Integration and Synthesis of Findings

This section integrates insights from Chapters 1–11 to broadly compare active shielding (artificial magnetic field systems), passive material shielding, and biological mitigation strategies for space radiation protection. The findings consistently show that no single solution is sufficient for deep-space missions; instead, a synergistic, multi-layered approach is required to keep astronaut exposure within safe limits. Traditional passive shielding alone becomes prohibitively massive for high-energy cosmic rays, and purely active systems introduce substantial power and engineering challenges. Biological countermeasures (e.g., pharmacological radioprotectors) are emerging as a crucial supplement to physical shielding. However, they cannot replace the need to block or deflect radiation before it reaches the crew. Therefore, the trade-offs among mass, power, complexity, and effectiveness must be balanced in any mission design, with the optimal combination of strategies depending on the mission profile.

12.1 Comparative Overview of Shielding Approaches

Passive Shielding: Materials-based shielding (e.g., polyethylene, metals, and composites) provides constant fail-safe protection by physically absorbing and attenuating radiation. Its advantages are reliability and simplicity. Once in place, passive shields protect without requiring power or active control. Chapters 1 and 2 highlight that achieving substantial Galactic Cosmic Ray (GCR) reduction with passive material alone demands impractically high mass. Beyond a specific thickness, each additional g/cm^2 yields diminishing returns in dose reduction. For example, Narici *et al.* [1] note that even hydrogen-rich plastics reach a point of marginal benefit against the highest-energy GCR ions [1]. An all-passive solution meeting NASA’s deep-space dose limits would be very heavy.

High–atomic–number materials such as aluminum (common in spacecraft hulls) tend to amplify secondary radiation production when GCRs strike, producing neutrons and other secondary particles harmful to crews. Chapter 6 quantified these effects, showing that heavy metals generate abundant secondary neutrons and bremsstrahlung when bombarded by GCR heavy ions. In contrast, hydrogen-rich materials (polyethylene, water, or advanced nanocomposites) generate fewer secondary particles and are more mass-efficient at slowing fast neutrons. This supports the use of light elements in shield design [2].

Chapter 8's trade-off analysis found polyethylene "stands out as the most effective shield per unit area" for long-duration missions. In contrast, aluminum must be "layered beneath more effective shielding" to mitigate secondary radiation. In summary, passive shielding is a necessary foundation. It excels at stopping all radiation species (including neutral particles that magnetic fields cannot deflect), but its weight and potential secondary effects drive the need for complementary strategies.

Active Shielding (Artificial Magnetic/Electric Fields): Active systems aim to emulate Earth's magnetosphere on a smaller scale, deflecting charged particles with electromagnetic fields so fewer penetrate the habitat. The promise of active shielding lies in reduced mass: a strong magnetic field could, in principle, repel a significant fraction of incoming protons and heavy ions without the many tons of material a passive shield would require [3]. As noted in Chapter 2, this approach could "significantly reduce radiation exposure while minimizing added mass," directly addressing the limitations of purely passive armor.

Several active shielding architectures were evaluated in Chapter 9:

1. Electrostatic plasma shields, which set up a considerable electric potential to divert charged particles, are lightweight and require relatively low steady-state power but are

only effective against lower-energy charged particles (e.g., solar protons) and provide little attenuation of ultra-high-energy GCR heavy ions.

2. Magnetohydrodynamic (MHD)/plasma bubble shields inflate a protective magnetic bubble using plasma currents. While theoretically capable of creating a large deflection region ("mini-magnetosphere") for comprehensive protection, Chapter 9 and the plasma hazard analysis in Chapter 3 revealed serious integration challenges. Such systems would be hampered by exorbitant power and mass requirements and could induce unwanted forces on the spacecraft or unstable plasma behavior, outweighing potential benefits.
3. Electromagnetic coil shields (resistive magnets) can generate a dipole field, but would draw immense power and produce prohibitive waste heat for continuous operation.
4. Superconducting magnetic coils can sustain high-intensity fields (1–2 T) with reduced power loss, making them the most practical active approach for substantial GCR protection. However, they still require high initial mass, large power systems (tens of kW for strong fields), cryogenic cooling, and management of intense magnetic forces and cause electromagnetic interference (EMI) [4].

Chapter 5 stressed that an AMF system's time-varying fields may couple with other spacecraft electronics, posing EMI/EMC risks to communications, sensors, and avionics. Chapter 4 showed that an active shield functions as a tightly interdependent system-of-systems, and power supply, thermal control, coil structural support, monitoring sensors, and feedback controls must operate in concert. Failure in any one subsystem, such as a power spike, coil quench, or sensor malfunction, could collapse the protective field and leave the crew suddenly exposed. This contrasts with passive shielding, which cannot fail instantaneously.

Reliability, therefore, becomes a critical consideration for active methods. Redundancies and robust control architectures (implemented via MBSE in Chapter 2's design framework) are essential. In summary, active shielding can dramatically augment radiation protection with far less mass than thick passive shielding walls, but demands high power, generates challenging side-effects, and introduces potential single-point failures. Active systems are best employed with passive materials, for instance, placing hydrogen-rich liners around a magnet coil to capture secondary neutrons produced by deflected particles, rather than as stand-alone solutions.

Biological and Operational Mitigation: The third pillar of a comprehensive strategy involves measures to increase human resistance to radiation that penetrates the physical shields. As discussed in Chapter 1, space agencies have set strict dose limits. NASA's career exposure limit is approximately 600 mSv for astronauts, corresponding to a 3% increase in fatal cancer risk. Yet even a well-shielded Mars mission can expose crews to a total of 1–3 Sv without countermeasures. Meeting these safety thresholds solely through shielding is highly challenging, which is why "operational protocols and pharmacological countermeasures" are being explored as supplements. Biological mitigation strategies include radioprotective pharmaceuticals (e.g., antioxidants, DNA repair stimulators), tailored diets, and medical interventions that reduce the biological damage from a given radiation dose. Such measures could help ensure that astronauts can survive Mars-class missions even if some fraction of GCRs still penetrates physical barriers [5].

Operationally, mission planners can reduce risk by timing missions during solar minimum (to minimize solar flare frequency), providing storm shelters for astronauts during acute solar particle events, and limiting extravehicular activities during high-radiation periods. These approaches do not physically block radiation but can significantly mitigate exposure and health impact. For example, a small volume surrounded by extra polyethylene or other shielding (such as a storage closet lined with water or food supplies) can serve as a storm shelter where the crew retreats during rare but dangerous solar flares. This is a low-mass strategy to avoid acute doses.

In all cases, biological countermeasures are considered a last line of defense, to be used in conjunction with physical shielding. They are most relevant for long missions where some radiation exposure is inevitable despite best efforts. The consensus of findings is that an integrated solution, combining passive materials, active field systems, and biomedical protocols, offers the greatest likelihood of keeping crew doses within acceptable limits over long durations [5].

12.2 Trade-Offs and Synergies Across Shielding Strategies

One of the clearest outcomes of this research is that each shielding approach comes with trade-offs, and understanding these is key to designing an optimal protection system. Table 8.2 (Chapter 8) summarizes a quantitative comparison of different shielding configurations (active, passive, or hybrid) for an Orion-sized crew module in various scenarios. Any design must balance three competing factors: mass, power, and shielding efficacy. Prioritizing low mass and low power yields only modest radiation protection, whereas maximizing shielding effectiveness drives up system mass and energy requirements.

Chapter 8's scenario analysis distilled these trade-offs: Scenario 1 (minimalist shielding) offered the lightest and most power-efficient solution but achieved only moderate dose reduction. Scenario 2 (robust shielding) attained the highest radiation protection by far, but at the cost of very large mass and power demands. Scenario 3 (a hybrid-adaptive approach) struck a middle ground with moderate weight and power usage, while retaining the ability to adjust shielding as needed dynamically. An independent evaluation in Chapter 1 reached a similar conclusion from the perspective of crew dose. Using a Mars mission model, only the heaviest shielding scenario (85% radiation attenuation) brought the crew's cumulative exposure below NASA limits. The lighter configurations resulted in two to three times higher doses over the mission.

Table 1.2.5 (Chapter 1) illustrates this point clearly: only Scenario 2 kept the total Mars mission dose (~387.9 mSv residual) under the ~600 mSv career threshold, while Scenario 1 (50% attenuation) and Scenario 3 (70% attenuation) left the crew with 1.3 Sv and 0.79 Sv, respectively, above recommended limits. These findings underscore the margin between success and failure in radiation protection can be slim. Aggressive shielding is needed for long missions, but such shielding carries high mass/power costs that may be impractical if taken to extremes.

The way forward is to exploit synergies between methods so that each covers the weaknesses of the others. Multiple chapters demonstrated that combining active and passive elements yields more than the sum of their parts. For example, Chapter 7's human-in-the-loop simulations showed that a hybrid shield, boron nitride nanotube (BNNT) layers plus an AMF, achieved the most significant cumulative dose reduction over 900 days, outperforming any single-technique approach. The BNNT (passive) absorbs heavy ions and neutrons that the magnetic field cannot fully deflect. At the same time, the AMF (active) dynamically reduces the flux of lighter charged particles (protons, electrons) that would otherwise penetrate the thin passive layer. Chapter 6 also advocated integrating hydrogenous, boron-loaded materials with active fields to intercept secondary radiation and plug gaps in the magnetic shielding coverage.

An electrostatic shield could be layered as a supplementary system to slow down incoming ions before they hit a physical barrier or enter a magnetic deflection zone.

In short, the optimal design is a multilayer shield: high-Z structural materials (e.g., aluminum) should be placed behind thicker hydrogen-rich liners (to minimize secondary generation), superconducting magnets or other active field generators can deflect a significant portion of the charged-particle spectrum, and any remaining radiation risk is managed through biological and operational measures. This layered philosophy adheres to the defense-in-depth principle and builds in redundancy. If an active system must be shut down for maintenance or in an emergency, the passive shield still affords baseline protection; conversely, if mass constraints limit passive thickness, the active field can boost overall effectiveness without adding significant weight [6].

The trade-off matrix developed in Chapter 9 reinforces this logic. When scoring various architectures on mass efficiency, power efficiency, and shielding performance, no single architecture dominated all criteria, but combinations leveraged the strengths of each. Mission designers are therefore encouraged to mix and match shielding techniques, tailoring the blend to mission priorities, mass, risk tolerance, and power availability [7]. The remainder of this section applies these integrated insights to three representative mission profiles which identify the most suitable shielding strategy for each case and the rationale behind it.

12.3 Shielding Strategies for Different Mission Profiles

1. **Short-Duration, Low-Power Missions**

For a short mission with tight power constraints, such as a crewed lunar flyby or a brief expedition outside Earth's magnetosphere lasting days to weeks, simplicity and low mass/power are top priorities. The crew's total exposure time is limited, so the shielding does not need to stop every cosmic ray. Instead, it must primarily guard against acute solar particle events (SPEs) and moderate the GCR dose to keep it within safe short-term limits. Passive shielding alone can often suffice in such cases, as the integrated GCR dose over a few weeks may remain acceptable with the spacecraft's structural mass and a modest additional lining [8].

Chapter 8's Scenario 1 analysis assumed this minimalist approach, adding ~45 kg of lightweight composite shielding (boron nitride nanotube [BNNT] fabric plus multi-layer insulation) to the Orion capsule, along with a very low-power magnetic dipole field (~0.1–0.2 T). This configuration reduced proton/electron flux by 40–50% with only ~500 W of power draw, adequate under tight power constraints for a short mission in near-Earth space. While this design's estimated residual dose for a complete Mars mission (1321 mSv) would exceed NASA's career limits, the absolute dose for a short mission would remain far lower because total dose scales roughly with exposure time.

Among active systems, electrostatic shielding is an attractive option for short, low-power scenarios. Chapter 9 concluded that a high-voltage electrostatic field can provide full protection against SPEs with minimal mass and power for a brief mission primarily concerned with solar flares. Such a system could charge the spacecraft hull or deploy extendable charged surfaces to deflect incoming protons. Standby power requirements are low, as the voltage matters rather than sustained current, and the system can be rapidly activated during a solar storm. The trade-off is that electrostatic shielding provides little protection against high-energy GCR nuclei, though for short missions, the GCR dose is a smaller component of total exposure.

If electrostatic protection is unavailable or GCR mitigation is also desired, a small electromagnetic coil is the next-best active solution. As demonstrated in Chapter 8's Scenario 1, a lightweight resistive coil (100–200 kg) generating a 0.1–0.2 T dipole field can reduce the lower-energy portion of the spectrum, particularly electrons and protons, by nearly half. The coil can be powered on during SPEs and switched off during quiet conditions to conserve energy.

On the passive side, advanced lightweight materials are favored when every kilogram counts. BNNT shields or hydrogenated carbon composites maximize shielding per unit mass. While BNNT offers slightly lower raw shielding effectiveness than an equal mass of polyethylene, its low density and minimal secondary particle yield make it well suited for short missions where weight is the dominant constraint. BNNT also benefits from neutron-absorbing boron content, and its low atomic number minimizes secondary particle production. A hybrid design combining a thin BNNT layer with the spacecraft's aluminum hull and a small polyethylene allowance can be optimal. The hull provides structure and some shielding. At the same time, the hydrogen-rich liner captures secondary neutrons and enhances overall protection without a significant mass penalty.

In summary, the most suitable shielding strategy for short-duration, low-power missions is primarily passive, augmented by a low-power active system for SPE protection. The design leverages the spacecraft's existing structure plus a lightweight hydrogen-rich liner, with either an electrostatic shield or a small magnetic dipole available for activation during high-radiation events. Such a configuration keeps power and mass requirements very low, and only a few percent of spacecraft mass is allocated to shielding while meeting operational needs. Mission risk can be further reduced through careful timing (avoiding high solar activity) and crew sheltering during rare high-radiation events. The comparative analysis deemed this approach suitable for low-risk, short-duration missions, accepting moderate shielding effectiveness in exchange for simplicity and efficiency.

2. Long-Duration Deep-Space Habitat (Surface Base or Orbital Station)

Long-duration missions, such as a crewed Mars outpost, a lunar base, or an orbital deep-space research station inhabited for months to years, demand maximal radiation protection. In this regime, cumulative GCR dose and potential exposure to multiple solar storms are the primary concern. Findings across Chapters 1, 8, and 9 unanimously identify a combined heavy passive + active solution as the most suitable approach.

In Chapter 1's Mars mission dose assessment, only the ~85% shielding effectiveness scenario, (achieved via a high-intensity magnetic field plus substantial material shielding), kept total crew exposure within permissible limits. Chapter 8's Scenario 2, tailored for a "stringent long-duration deep space habitat" case, likewise concluded that a high-field superconducting magnet coupled with thick hydrogen-rich shielding is necessary for robust protection. In that configuration, a superconducting coil generating a 1–2 T dipole field surrounds the habitat, powered continuously by a dedicated high-output source (50–100 kW). Although the coil system is extensive (~800 kg including supports and cryogenics in the Orion-sized case) and imposes a significant engineering burden, shielding performance is dramatic, with proton and electron flux reductions of ~95–98%, and heavy GCR ion reductions on the order of 80%. FLUKA Monte Carlo simulations cited in Chapter 8 confirm that Tesla-level fields are "crucial for effectively shielding against Galactic Cosmic Rays," the dominant dose source in multi-year missions. In practical terms, an 80% reduction in GCR flux can mean the difference between exceeding exposure limits in one mission and staying within tolerable risk levels.

Substantive passive shielding must complement the magnet because even the strongest feasible magnetic field will not stop every cosmic ray. The consensus choice for long-duration passive shielding is polyethylene or analogous hydrogen-rich composites [6]. Chapter 8's deep-space habitat scenario incorporated ~135 kg of polyethylene-based composite panels (~4.5 kg/m^2 over the crew module) and the AMF, providing a significant secondary barrier and structural housing for the magnet. Polyethylene offers superior mass efficiency in the GCR environment, outperforming metals or BNNT per unit area in stopping power. Its high hydrogen content effectively thermalizes and absorbs neutrons. This is a critical function because deflected high-energy ions can still interact with spacecraft or magnet structures, producing secondary neutrons. Boron additives enhance neutron capture, making boron-loaded polyethylene or multilayer poly/BNNT configurations advantageous [10].

Passive shielding can also be integrated into habitat architecture. Water tanks, food supplies, and regolith bricks (produced via in-situ 3D printing on planetary surfaces) can be positioned around crew quarters to double as shielding. NASA habitat concepts often envision partial burial under regolith to exploit local material as “free” shielding mass [11].

Chapter 9’s comparative analysis of active systems decisively favored superconducting magnetic shielding for long-term bases: “For a long-duration habitat, superconducting magnetic shielding is the preferred approach which balances significant radiation protection with manageable power usage.” A resistive coil is far less suitable in this regime due to its immense continuous power demand. While a superconducting system introduces a few hundred kilograms of coil and cryocooler mass, Chapter 9 concluded that this trade-off is acceptable to reduce year-long crew doses by a large fraction reliably. Continuous operation is crucial; a base cannot afford to deactivate its shield during low-power periods, since radiation is constant. Superconducting magnets can maintain field strength with minimal operational power (aside from cooling), which ensures consistent protection without frequent intervention.

Electrostatic shielding or intermittent solutions would leave significant periods of unmitigated GCR exposure, leading to unsafe cumulative doses over the years. Plasma/MHD shielding, while potentially more comprehensive in theory, remains impractical with current technology due to excessive power/mass requirements and complex side-effects such as plasma instabilities and unwanted thrust.

The pragmatic near-term choice for long-duration missions is a high-field superconducting magnetic field combined with substantial material shielding. As noted in Chapter 9, the “real solution” is likely a multilayer system, e.g., superconducting magnet, modest polyethylene layers, and possibly an electrostatic component, each targeting a different radiation type (magnetic for charged GCR particles, electrostatic for slower solar ions, and passive for neutrons and gamma rays), yielding a combined reduction greater than any single method can achieve. Regarding trade-offs, a long-duration base accepts high mass and power requirements to maximize shielding. The habitat can be designed with robust power generation, such as a nuclear reactor or large solar farm with storage, capable of continuously supplying 50–100 kW to the shielding system. It can also accommodate heavy, bulky equipment (superconducting coils, cooling systems, thick walls). These design choices are justified because crew safety on a multi-year mission is paramount.

Analyses in Chapters 1 and 8 show that accumulated doses would far exceed allowable limits without aggressive measures, posing unacceptably high health risks. The payoff of this heavy approach is evident in the dose outcomes. With ~85% composite shielding effectiveness (as in Scenario 2), the total deep-space mission dose can be reduced to <0.4 Sv, within tolerable limits for a Mars mission. By contrast, lighter shielding would leave the crew with ~0.8–1+ Sv, well over the NASA limit.

Therefore, the most suitable strategy for a long-duration habitat is a “belt-and-suspenders” solution integrating a powerful superconducting AMF shield with substantial passive material thickness. This combination provides high confidence in keeping crew exposures under control.

Biological countermeasures add another layer of safety, for example, regular administration of radioprotective agents (antioxidants or other compounds under study) to mitigate remaining GCR-induced damage, along with extensive health monitoring to detect and treat radiation effects early. Layering physical shielding with biomedical support enables a deep-space base to maintain long-term habitability without exceeding safety margins. While this approach demands significant mass and power infrastructure, it aligns with the mission profile of a static, infrastructure-heavy base, where protecting the crew outweighs minimizing mass.

3. **Highly Mobile Spacecraft (Deep-Space Exploration Vessel)**

For missions involving a highly mobile spacecraft, such as a crew transport vehicle or exploration spacecraft that maneuvers frequently, visits multiple destinations, or operates in varying environments, the shielding strategy must prioritize adaptability and moderate mass. Such a spacecraft may have a substantial power source (e.g., advanced reactors or solar-electric propulsion units generating tens of kilowatts) but cannot afford the extreme mass penalties that would impair propulsive efficiency. Mobility also implies operation in diverse radiation environments (e.g., transiting in and out of planetary magnetospheres, encountering solar storms in interplanetary space), making adaptive and reactive shielding desirable [4].

Research findings suggest that a dynamic active shield combined with lightweight passive materials is most suitable for a nimble, multi-mission vessel. In Chapter 8's Scenario 3, envisioned for a "highly mobile, adaptive spacecraft", the design centered on a rotating toroidal coil capable of modulating field strength between ~0.5 T and 1.5 T in real time. The coil assembly was ~400 kg (plus ~150 kg of power electronics and control), significantly lighter than the static 800 kg coil of the base scenario, yet still substantial.

The resistive rotating-coil system can be adjusted as needed, rather than running at full power continuously. Power consumption ranges from ~5 kW at low settings to ~30 kW during brief high-intensity operation. During quiet periods, the field can be lowered to conserve energy. During a solar storm or high-radiation transit, it can be increased toward 1+ T for maximum protection. This adaptivity allows the spacecraft to balance energy efficiency and radiation protection dynamically. Chapter 8 reported that such an adaptive AMF system could achieve proton flux reductions of 80–95% at high settings, with somewhat lower reductions at minimal settings, approaching the peak protection of the heavy fixed system when operating at 1.5 T.

The trade-off is that, as a resistive magnet, it requires a capable power source for high-output periods. However, as Chapter 9 notes, a nuclear-electric propulsion spacecraft often has tens of kilowatts available, making this feasible. A superconducting magnet was deemed less suitable for this profile, not because of shielding performance, but due to practicality. Superconducting systems are heavy, require complex cryocoolers, and are less adaptable for rapid on/off cycling. The resistive rotating-coil imposes no major additional structures beyond the coil itself and can be switched on or off, or adjusted quickly via current control. This flexibility is critical for a spacecraft that may need to deactivate its magnetic field during certain operations (e.g., docking, sensitive instrumentation use) or only requires complete shielding during specific mission phases. The coil's rotation also helps distribute the field and may reduce asymmetric buildup of charged particles.

In Chapter 9's Scenario 3 comparison, the resistive rotating-coil AMF emerged as the most robust and flexible solution for a mobile spacecraft, outperforming MHD/plasma shields (ruled out as too massive/complex) and superconducting shields (excellent protection but impractical for a nimble vessel).

That said, an electrostatic shield is a close contender for mobile applications, as noted in Chapter 9. Its appeal lies in minimal mass and the absence of bulky structure. A deployable high-voltage sphere or boom system could weigh very little while offering strong protection against acute solar flares, which is the primary radiation concern for specific expedition missions. For example, an unmanned high-mobility cargo ship might employ electrostatic shielding solely to safeguard electronics from solar particle events, treating it as "lightweight insurance" and tolerating higher GCR exposure since no humans are aboard. However, electrostatic shielding alone would allow excessive residual GCR dose over long journeys for a crewed mobile vessel. It could be included as a supplementary system (handling lower-energy particles and mitigating surface charging), but the primary protection would come from the magnetic field and passive material [9].

Even a mobile exploration vessel incorporates passive shielding, though mass must be limited. Chapter 8's Scenario 3 included ~60 kg of BNNT/polyethylene hybrid shielding (~2 kg/m²). This lightweight configuration boosts protection and shields electronics and crew from secondary radiation near the coil structure. As noted, strong magnetic fields and spacecraft structures can generate secondary radiation (e.g., neutrons, X-rays) when GCRs are deflected into materials. A thin hydrogen-rich blanket around the habitat and key systems can absorb much of this secondary output. BNNTs are attractive here for their multifunctionality, adding structural reinforcement, thermal stability, and radiation moderation at very low mass. The polyethylene component ensures high hydrogen content for neutron reduction. Therefore, a mobile spacecraft's optimal passive component is a light composite liner integrated into the hull, providing constant moderate shielding without significant mass penalties. Every surface, wall, floor, and even water tanks, can contribute incrementally to total protection.

Operationally, a mobile spacecraft shield would be used selectively. During high-thrust maneuvers or docking, the magnetic field might be reduced to avoid torque or interference; during coast phases in interplanetary space, it can be increased to maximum for crew protection. Scenario 3's power profile (5–30 kW variable draw) illustrates this dynamic management: the system only draws peak power when needed, which a mobile platform can accommodate (e.g., when propulsion power is not required, excess reactor capacity can be diverted to shielding).

Overall, the recommended shielding strategy for a mobile spacecraft is a moderate-mass, high-flexibility hybrid: a tunable resistive magnetic field for primary GCR and solar proton deflection, paired with lightweight passive shielding to mitigate secondary radiation. This approach "combines moderate mass and power consumption with the ability to adapt in real time to varying radiation conditions," meeting the requirements of a multi-mission exploratory craft.

It avoids the extreme mass of fixed heavy shielding, instead leveraging the vessel's power and agility to manage radiation actively. This configuration also retains contingency measures. If power is lost, the passive layer provides some baseline protection, and the crew can take shelter in the most shielded section of the ship. Crew rotation between vessels or mission segments can further limit individual exposures, and pharmaceutical countermeasures can be deployed as needed [4].

12.4 Synthesis of Optimal Strategies

A clear pattern emerges across these three mission profiles: the more ambitious the mission's duration and scope, the more layers of shielding must be implemented. A single layer (the spacecraft hull plus a simple active or passive augmentation) may suffice for a short mission. A multi-technology shield (high-field magnet plus heavy passive materials, potentially supplemented by electrostatic systems) is required for a multi-year base to meet safety objectives. A balanced dual approach (moderate field plus light material) provides the versatility for a mobile explorer.

The trade-offs align with expectations: the short mission prioritizes minimal mass/power at the expense of comprehensive shielding; the long-term base prioritizes maximum shielding at the expense of mass/power; and the mobile craft targets a middle ground. Table 1.2.5 (Chapter 1) and associated analyses underscore that shielding must be "customized to the mission class," as each class tolerates different risk and resource trade-offs.

The integrated findings also confirm that no single radiation protection method is sufficient for the most challenging missions. A combination of passive, active, and biological measures is indispensable for long-term crewed exploration. Chapter 9 states that "the combination of techniques is likely the real solution" for attenuating the broad spectrum of space radiation. This dissertation reinforces that claim with quantitative evidence:

- Passive materials stop what magnets and electrostatic fields cannot.
- Active fields deflect charged particles without prohibitive mass penalties.
- Biological countermeasures address residual damage that no physical shield can entirely prevent.

The key trade-offs, mass vs. effectiveness, power vs. simplicity, and technological complexity vs. reliability, can be managed through integrated designs that distribute protective functions across multiple systems. In practice, mission planners must select the appropriate balance for each mission: some will accept higher radiation risk to reduce mass. In contrast, others will employ all available technologies to maximize safety.

The tools and data developed in Chapters 1–9 serve as a decision-support matrix for these choices, clearly outlining the consequences of each trade-off. Applying these insights, future spacecraft and habitat designers can tailor shielding strategies to mission-specific needs, safeguarding astronaut health without unduly compromising mission objectives. In conclusion, adequate space radiation protection is a multidisciplinary balancing act, and the optimal solution for any mission lies in the thoughtful integration of active fields, passive materials, and human-centered countermeasures into a cohesive shielding system.

That said, an electrostatic shield is a close contender for mobile applications, as noted in Chapter 9. Its appeal lies in minimal mass and the absence of bulky structure. A deployable high-voltage sphere or boom system could weigh very little while offering strong protection against acute solar flares, potentially the primary radiation concern for specific expedition missions. For example, an unmanned high-mobility cargo ship might employ electrostatic shielding solely to safeguard electronics from solar particle events, treating it as “lightweight insurance” and tolerating higher GCR exposure since no humans are aboard. However, electrostatic shielding alone would allow excessive residual GCR dose over long journeys for a crewed mobile vessel. It could be included as a supplementary system (handling lower-energy particles and mitigating surface charging), but the primary protection would come from the magnetic field and passive material [9].

Even a mobile exploration vessel incorporates passive shielding, though mass must be limited. Chapter 8’s Scenario 3 included ~60 kg of BNNT/polyethylene hybrid shielding (~2 kg/m^2). This lightweight configuration boosts protection and shields electronics and crew from secondary radiation near the coil structure. As noted, strong magnetic fields and spacecraft structures can generate secondary radiation (e.g., neutrons, X-rays) when GCRs are deflected into materials. A thin hydrogen-rich blanket around the habitat and key systems can absorb much of this secondary output. BNNTs are attractive here for their multifunctionality, adding structural reinforcement, thermal stability, and radiation moderation at very low mass. The polyethylene component ensures high hydrogen content for neutron reduction. Therefore, a mobile spacecraft's optimal passive component is a light composite liner integrated into the hull, providing constant moderate shielding without significant mass penalties. Every surface, wall, floor, and even water tanks, can contribute incrementally to total protection.

Operationally, a mobile spacecraft shield would be used selectively. During high-thrust maneuvers or docking, the magnetic field might be reduced to avoid torque or interference; during coast phases in interplanetary space, it can be increased to maximum for crew protection. Scenario 3’s power profile (5–30 kW variable draw) illustrates this dynamic management: the system only draws peak power when needed, which a mobile platform can accommodate (e.g., when propulsion power is not required, excess reactor capacity can be diverted to shielding).

Overall, the recommended shielding strategy for a mobile spacecraft is a moderate-mass, high-flexibility hybrid: a tunable resistive magnetic field for primary GCR and solar proton deflection, paired with lightweight passive shielding to mitigate secondary radiation. This approach “combines moderate mass and power consumption with the ability to adapt in real time to varying radiation conditions,” meeting the requirements of a multi-mission exploratory craft. It avoids the extreme mass of fixed heavy shielding, instead leveraging the vessel’s power and agility to manage radiation actively. This configuration also retains contingency measures; if power is lost, the passive layer provides some baseline protection, and the crew can take shelter in the most shielded section of the ship. Crew rotation between vessels or mission segments can further limit individual exposures, and pharmaceutical countermeasures can be deployed as needed [4].

12.4a Methodology for Integrated \Analysis

The methodology adopted in this dissertation was designed to ensure that all analyses of active, passive, and bioengineered radiation shielding systems were rigorous, transparent, and repeatable. The process combined physics-based simulations, model-based systems engineering (MBSE) methods, comparative decision analysis, and operational validation to create a comprehensive framework. This approach enables future researchers to replicate or extend the analysis as technologies evolve.

1. Simulation and Modeling Framework

Radiation environment characterization was conducted using FLUKA Monte Carlo transport simulations supported by MATLAB co-simulations. These models incorporated Galactic Cosmic Rays (GCRs), Solar Particle Events (SPEs), and mission-specific shielding geometries to quantify absorbed dose and dose equivalent under multiple mission phases. Where applicable, results were validated against historical mission data and published NASA dose constraints.

Artificial magnetic field concepts were evaluated using finite element magnetic field models and particle trajectory simulations. Parameters such as field intensity, coil geometry, and rotation frequency were varied systematically to quantify deflection efficiency and operational feasibility. Passive shielding analysis employed parametric mass–thickness–dose models calibrated with Monte Carlo results, while biological shielding assessments used MATLAB SimBiology to simulate oxidative stress and DNA repair processes in *E. coli* and *S. cerevisiae* under radiation exposure.

2. Model-Based Systems Engineering (MBSE)

The dissertation employed MBSE as the organizing framework for system integration and traceability. SysML parametric and block diagrams represent relationships between subsystem design parameters (e.g., coil current, passive shield thickness, radiator area) and mission-level outcomes (e.g., dose reduction, power draw, structural mass).

Design Structure Matrices (DSM) and Failure Mode and Effects Analyses (FMEA) were applied to identify system interdependencies, risks, and failure propagation pathways. These tools ensured that the shielding strategies were assessed not only in terms of physical performance but also with respect to system-level integration, reliability, and operational constraints. Requirement traceability matrices linked NASA radiation dose standards to subsystem design parameters, allowing for consistent evaluation across scenarios.

Verification and validation were incorporated through a staged process: (1) simulation-based verification of shielding effectiveness; (2) sensitivity and regression analyses to assess robustness under uncertainty; (3) subsystem-level validation against mass, power, and thermal constraints; and (4) operational validation through human-in-the-loop (HITL) activity models, which simulated crew–system interaction, automated alerts, and override procedures.

3. Comparative Scenario Analysis

Three mission archetypes were defined—short-duration sortie, long-duration deep-space habitat, and highly mobile exploration vehicle—representing distinct operational contexts. Shielding concepts were evaluated within each scenario according to mission-specific constraints in mass, power, duration, and crew safety requirements.

A structured weighted decision-matrix methodology was applied to candidate active magnetic field systems (electrostatic, magnetohydrodynamic, resistive coil, and superconducting coil configurations). Five evaluation criteria were used: mass efficiency, power efficiency, shielding performance, thermal burden, and integration complexity. Each criterion was scored on an ordinal scale and weighted according to its relative mission importance, producing a composite score for each system architecture. This process provided a transparent, repeatable basis for comparing alternatives and identifying the most suitable configurations across mission types.

12.5 Down-Selection Methodology

12.5.1 Methodological Clarification

A structured weighted decision-matrix approach was adopted to formally compare the performance and feasibility of candidate active magnetic field (AMF) systems. This method provides a transparent, quantitative framework for evaluating multiple architectures against a consistent set of system-level criteria that capture mission-critical trade-offs [12].

Each candidate shielding system, Electrostatic, Magnetohydrodynamic (MHD), Electromagnetic (Resistive Coils), and Superconducting (HTS Coils), was scored on a 1–5 ordinal scale for each of five core evaluation criteria:

1. **Mass Efficiency** – Assesses total shielding system mass, including coils, support structures, and thermal systems, normalized to spacecraft mass budgets.
2. **Power Efficiency** – Evaluates operational energy consumption under steady-state shielding conditions.
3. **Shielding Performance** – Measures the system’s effectiveness at mitigating high-energy solar and galactic radiation, considering both field strength and deflection range.
4. **Thermal Burden** – Captures the required scale of thermal-control infrastructure based on waste-heat production and associated radiator mass.

5. **Integration Complexity** – Rates the technical difficulty of integrating the system into existing spacecraft designs, including structural coupling, power conditioning, and fault management.

Each criterion is weighted according to its relative importance for the mission classes analyzed in Chapters 8 and 9. These weighting factors reflect the contextual priorities of each mission type (short-duration, long-duration, and highly mobile profiles), ensuring the selection process is mission-informed and technically rigorous.

The weighted scores for all criteria are aggregated to produce a final composite score for each system architecture. These totals serve as a decision-support tool, identifying the most balanced and mission-suitable AMF system based on current technology assumptions and system modeling.

12.5.2 Evaluation Criteria and Weighting Table

The following table presents the five evaluation criteria with their assigned weighting factors, which were applied consistently in the decision-matrix process:

Table 12. 1: Evaluation Criteria and Weighting Factors for AMF System Down-Selection

Evaluation Criterion	Description	Weighting Factor
Mass Efficiency	Total estimated system mass impact, relative to spacecraft allocation	0.25
Power Efficiency	Total power draw under nominal conditions	0.20
Shielding Performance	Relative capacity to deflect or absorb radiation (based on $\int B \cdot dr$, GCR response)	0.30
Thermal Burden	Waste heat production and required radiator mass	0.15
Integration Complexity	Difficulty of assembly, launch constraints, and operational dependencies	0.10
Total		**1.00**

These weights were derived from cross-chapter trend analysis, scenario prioritization, and systems-engineering judgments aligned with NASA design constraints. Shielding performance received the highest weight (30%), reflecting its primary function. Mass and power efficiency were weighted next, as spacecraft budgets impose tight constraints in these domains. Thermal burden and integration complexity were comparatively down-weighted, given their potential for mitigation through spacecraft-level design solutions [6].

The weighted evaluation indicated that the superconducting magnetic field generator consistently achieved the highest composite score for long-duration missions, where sustained shielding performance is critical. This outcome aligns with the Scenario 2 analysis, which demonstrated that a 1.5 T superconducting system provides the optimal balance of dose reduction, mass efficiency, and operational feasibility for extended deep-space habitation. The rotating resistive coil configuration emerged as the preferred choice for highly mobile mission profiles due to its adaptability, reduced mass, and scalable power demands, which is in agreement with the Scenario 3 findings.

12.6 MBSE-Driven Integration of Active, Passive, and Bioengineered Shielding Systems

Protecting astronauts from cosmic radiation in deep space requires a system-of-systems approach that combines multiple shielding strategies. Traditional passive materials become impractically massive against high-energy GCR, while purely active magnetic or electrostatic shields face steep power and complexity challenges [13]. To address these limitations, hybrid radiation-shielding systems integrate three layers of defense:

1. An Active Magnetic Field (AMF) generator to deflect charged particles.
2. Passive shielding materials to absorb radiation.
3. Bioengineered radiation mitigation measures to protect the crew at the cellular level.

Designing such a multifaceted protection architecture is inherently complex, involving electromagnetic coils, power and thermal subsystems, structural mass allocation, crew safety protocols, and even pharmacological or biomaterial interventions. Model-Based Systems Engineering (MBSE) provides the rigorous framework to integrate these elements coherently. Using a centralized system model (developed in SysML with Cameo Systems Modeler), the engineering team ensured that requirements, design components, and verification data remained traceable and consistent throughout the project [13].

This section discusses how MBSE was applied to systematically integrate active, passive, and bioengineered shielding within a unified architecture, synthesizing theoretical models and applied findings from Chapters 2, 3, 4, 7, 8, and 9. SysML diagram excerpts, including Block Definition, Internal Block, Activity, and Use Case diagrams, illustrate system relationships, interactions, failure mitigations, and mission scenario behaviors. Also highlighted is how MBSE tools, such as requirements traceability, simulation-based verification, failure-mode analysis, and parametric trade studies, enabled coherent design, risk management, and performance optimization of the hybrid shielding system across short-duration missions, long-term habitats, and mobile exploration spacecraft.

12.6.1 MBSE Methodology for Hybrid Shielding System Integration

Model-Based Systems Engineering shifted the development of the shielding architecture from a document-centric to a model-centric approach. All critical aspects, from high-level radiation requirements down to subsystem interfaces, were captured as interconnected model elements in SysML, rather than scattered across separate documents. This provided a “single source of truth” that improved design consistency and facilitated multidisciplinary collaboration [13].

The MBSE methodology was implemented using SysML 1.6 diagrams in an enterprise architecture tool (No Magic Cameo). Key modeling activities included:

1. Requirements capture – Formalizing stakeholder needs (e.g., allowable radiation dose, power limits, mass constraints) into SysML Requirement elements traceable to design components and test cases.
2. Structural modeling – Using Block Definition Diagrams (BDDs) to decompose the system and define subsystem hierarchies, and Internal Block Diagrams (IBDs) to specify internal connections and interfaces.
3. Behavioral modeling – Employing Activity Diagrams and state/sequence diagrams to represent operational workflows such as shield activation sequences, hazard response protocols, and crew interactions.
4. Interface and data flow modeling – Defining how energy, information, and matter flow between subsystems (e.g., power from the spacecraft bus to magnet coils, sensor data to controllers, commands to actuators) via interface blocks and flow ports.
5. Parametric modeling – Encoding key performance relationships (e.g., magnetic field intensity as a function of coil current, dose reduction as a material thickness) in SysML parametric diagrams for trade studies and simulations.

Each model element was interlinked, with requirements to functions, functions to components, and components to tests, enabling end-to-end traceability. This approach ensured that changes (e.g., a new requirement for 10% higher GCR dose reduction) would propagate through the model, automatically updating related design parameters, analysis results, and verification plans.

Such dynamic consistency was critical for a highly interdependent system: AMF performance affects thermal loads, which impact cooling requirements and power draw; passive shield mass influences spacecraft structure and trajectory; all these factors affect the crew's residual exposure risk. By maintaining a unified model, the team could rigorously verify that the hybrid system met integrated performance goals and constraints and rapidly iterate the design in response to new findings or mission requirement changes [13].

12.6.2 Theoretical Modeling vs. Applied Findings

A significant outcome of this research was the synthesis of theoretical models with applied simulation and experimental results. Early in the project, theoretical modeling, enabled by MBSE, guided the conceptual architecture. For example, calculations were performed to determine the ideal magnetic dipole moment needed to deflect particles of a given energy, or to estimate the thickness of polyethylene required to achieve a specified dose reduction. These theoretical insights were formalized in SysML parametric constraint blocks and activity scenarios.

Subsequently, detailed analyses and simulations (Chapters 8 and 9) were used to validate and refine the model. Monte Carlo radiation transport simulations (using FLUKA and other tools) were run for multiple shielding configurations, and the resulting performance metrics, such as dose-reduction percentages and secondary-particle yields, were fed back into the SysML model as updated parametric values or verification evidence.

For example, the initial model assumed that an active magnetic field strength of 1 T could reduce GCR dose by 50%. However, Chapter 9's sensitivity analysis revealed that achieving this reduction required closer to 2 T in combination with substantial passive mass. This finding prompted an update to the model's requirements and design targets. Similarly, trade-off data on mass, dose reduction, and secondary radiation for candidate materials were incorporated.

Table 12.2 illustrates an example of this data integration, comparing the radiation performance of three shielding materials as derived in Chapter 8. The MBSE environment linked these empirical findings directly to design decisions, for instance, justifying the selection of polyethylene over aluminum for long-duration missions based on its superior GCR attenuation and lower secondary radiation production. This tight coupling of theoretical and applied perspectives ensured that the final system design was conceptually sound and grounded in quantitative evidence from analyses.

Table 12. 2: Comparative Performance of Candidate Passive Shielding Materials (data from Chapter 8)

Material	**GCR Dose Reduction (%)**	**Areal Density (kg/m^2)**	**Secondary Radiation Yield (rel. units)**
Boron Nitride Nanotubes (BNNTs)	40–70%	~1.2	1 (very low)
Polyethylene	80–98%	~4.5	2 (low)
Aluminum	30–40%	~2.7	7 (high)

Table 12.2 summarizes radiation shielding effectiveness versus mass and secondary radiation trade-offs for select materials. Hydrogen-rich materials like BNNTs and polyethylene yield far greater dose reduction per unit mass than aluminum and produce drastically fewer secondary particles (secondary yield qualitatively rated 1–10). This informed the selection of lightweight BNNT composites for short missions and polyethylene for intensive shielding needs.

By iterating between model predictions and applied chapter findings, the MBSE-based approach supported model validation and continuous refinement. Discrepancies between model expectations and simulation outcomes were traced, understood, and resolved within the unified framework.

The down-selection process identified the most suitable active magnetic shielding subsystem based on mass, power, shielding performance, and integration complexity. Building on these findings, the following section explains how Model-Based Systems Engineering (MBSE) principles were employed to architect a fully integrated active–passive–biological shielding system suitable for multi-mission applicability.

12.7 Failure Mode and Risk Analysis (MBSE-Integrated FMEA)

Ensuring the reliability of a complex shielding system requires anticipating how failures in one part can affect the whole. The MBSE model was extended to incorporate a comprehensive Failure Modes and Effects Analysis (FMEA) at the system-of-systems level (Chapter 10).

Instead of maintaining the FMEA in a separate spreadsheet, the SysML model is linked. Each subsystem block has associated “FailureMode” and “Mitigation” notes, and many are tied to specific requirement constraints. Table 10.3 in the dissertation (Chapter 10) summarizes the FMEA findings, organized by subsystem and requirement. For example, one identified failure mode for the Power Subsystem was loss of primary power to coils. The effects noted were a rapid magnetic field collapse (potentially exposing the crew to complete radiation levels) and possible thermal shock to the superconducting magnets. The primary detection method was telemetry (voltage sensors), and the mitigation strategy was an automated battery switchover (with RQ-4.2.1 specifying the <250 ms transfer time). A failure mode for the Magnetic Coil Subsystem was coil overheating or quenching. The effects included loss of field and even physical damage. The model linked this to the Thermal Control subsystem, stating, “inadequate cooling could precipitate the coil failure.” The mitigation was active thermal monitoring and an emergency coil shutdown if the temperature exceeded safe limits (this was a requirement in the model, e.g., RQ-4.3.5: Coil must shut down if T > 80 K above nominal). Another example is radiation sensor drift or failure. The effect would be incorrect readings, possibly causing the control system to under- or over-react. The mitigation is “voting logic or analytic redundancy using multiple sensors” (modeled by having three sensor inputs and a median filter in the control algorithm). Each of these entries was directly traceable in the SysML diagrams. The IBD in Chapter 10 (Figure 10.1) highlights sensor redundancies and the closed-loop nature of the control, which makes what happens if a sensor fails apparent (the loop can still operate with remaining sensors, albeit with reduced confidence).

Using MBSE to integrate the FMEA, the analysis stayed connected to the design data. Whenever a design change was made, the team could quickly revisit the FMEA entries to see if new failure modes emerged or mitigations needed updating. For instance, when the decision was made to use superconducting magnets for the long-duration habitat scenario, the model was updated to include a Cryogenic Cooling Subsystem. This immediately introduced new failure considerations (coolant pump failure, cryocooler power loss, thermal runaway). Because the FMEA was requirement-driven in the model, new requirements were added, like RQ-4.3.10: Provide backup cooling or safe-mode discharge for superconducting coils to prevent quench on coolant loss and linked them to mitigation steps in the architecture.

The SysML requirements diagram and the FMEA table thus evolved in tandem. Chapter 10’s content emphasizes that a tight traceability was maintained from high-level requirements to behaviors to verification. In practice, this meant each top-level safety requirement (e.g., system shall not expose crew above 20 mSv during any single SPE) was not only verified by analysis but also had links to lower-level requirements on subsystems (like power, control, etc.) that, if unmet, would jeopardize the top-level objective. This hierarchy was managed in the model, which makes it easy to see why a particular design feature existed because it mitigated a specific mode of failure or hazard.

Furthermore, MBSE facilitated a Verification & Validation (V&V) matrix corresponding to the FMEA and requirements. Chapter 10 references a complete V&V matrix tied to Table 10.3. For example, a specific test was defined to validate the mitigation for coil overheating (e.g., thermal runaway test on coil model, or analysis of coil temperature under worst-case load) and linked to RQ-4.3.5. In the model repository, one could click on a requirement and see its verification status (satisfied by Test #X, analysis Y, or inspection Z). This digital thread ensured that risk mitigation was planned and verified. The MBSE tool allowed marking each requirement as verified by some method, and simulations were run to provide evidence for those verifications where possible. For instance, a thermal simulation of the coil was performed to ensure that if coolant flow stops, the temperature limit is detected within time and the system can shut down gracefully, fulfilling the requirement. The result was attached to the model and presented in the dissertation's results (Chapter 3 sensitivity analysis also examined coil temperature sensitivity as a factor).

It is worth noting that electromagnetic interference (EMI) and system compatibility risks were also analyzed as part of integration risk (Chapter 8 and Scenario 3 discussions). The active magnetic field, by design, can induce currents and affect electronics. The MBSE model captured this potential failure mode under Spacecraft Systems Compatibility. The mitigation strategies included architectural and operational measures: physically shielding sensitive avionics with high-permeability materials (mu-metal enclosures) and implementing procedural constraints such as switching off the AMF during delicate operations (docking, spacecraft separation, etc.). The model's IBD showed a boundary around the "Spacecraft Avionics" with an «EMIShield» note, indicating those components are insulated from magnetic fields. Sequence diagrams for mission phases explicitly included steps to deactivate/reactivate the shield accordingly. This level of detail, linking EMI considerations into the model, exemplifies how MBSE helped manage interface compatibility issues. Nothing was left as an implicit assumption. If the magnetic field could interfere with the star tracker, a requirement and design feature to address it was added (e.g., RQ-5.1: Star tracker performance shall not be degraded by shield operation, with verification that the shield meets a field fall-off requirement at the tracker's location, or that the shield is off during star sightings). In a traditional process, such interdisciplinary concerns might be addressed in separate documents (EMI control plans, etc.), but they were woven into the unified model for completeness.

In summary, MBSE provided a framework for rigorous risk analysis. Every potential failure mode and hazard identified (whether plasma-induced, hardware, software, or human-error related) was systematically traced to design mitigations and verification steps. The SysML model served as a live FMEA document, where colored indicators could be used to flag high-risk items. By the end of the design process, this approach yielded high confidence that the system could withstand single-point failures or at least fail safely without catastrophic exposure. This satisfies one of the dissertation's key findings: embedding FMEA within an MBSE environment yields a more robust design, as mitigation is not an afterthought but an integral part of the system architecture.

12.7.1 Cascading Effects Analysis

While the Failure Mode and Effects Analysis (FMEA) provide a structured catalog of individual subsystem vulnerabilities, it doesn't fully capture the dynamic propagation of failures across tightly coupled subsystems. Given the high interdependency of power, thermal, and electromagnetic as well as structural elements within artificial magnetic field (AMF) architectures, a cascading effects analysis was undertaken to evaluate how an initiating fault can trigger a chain of secondary failures. This ultimately leads to a system-level degradation or loss of shielding function [26].

This analysis incorporates a system-of-systems perspective which is consistent with the MBSE framework that is used throughout this dissertation. This is particularly relevant to superconducting magnet architectures where stored energy, cryogenic performance, and electromagnetic fields are inherently linked.

Example 1: Superconducting Coil Quench Cascade

A representative cascading failure scenario begins with a coil quench event where a superconducting coil loses its superconducting state due to mechanical or radiation-induced disturbances.

1. **Initiating Event – Quench:**
    - The coil transitions from superconducting to resistive state. This results in rapid localized heating and the sudden dissipation of stored magnetic energy.
2. **Immediate Secondary Effects – Thermal and Power Excursions:**
    - The released energy imposes a sudden thermal load on the cooling system which exceeds radiator and cryocooler design capacity.
    - Concurrently, the collapsing magnetic field induces a transient surge through the power bus, which may propagate to adjacent power conditioning units.
3. **Tertiary Effects – Electromagnetic and Structural Consequences:**

- The collapse of the magnetic field eliminates the active shielding function which exposes the crew module to unattenuated Galactic Cosmic Ray (GCR) and Solar Particle Event (SPE) flux.
- Electromagnetic transients can couple into avionics and sensor networks which will cause spurious signals or functional resets.
- The structural supports that are designed under the assumption of steady Lorentz loading, may experience dynamic unloading forces that accelerate the fatigue of the material.

4. **System-Level Escalation:**
   - The combined failure of shielding effectiveness with power stability and avionics integrity creates a high-consequence condition. Radiation exposure to the crew may rapidly exceed the mission dose thresholds before passive and biological countermeasures can compensate.
   - If unmitigated, cascading progression from quench → power surge → EMI → avionics disruption → loss of shielding continuity represents a mission-threatening hazard chain. This escalation pathway is depicted in the left branch of Figure 12.0.

Example 2: Plasma Charging Cascade

A contrasting cascade originates not from internal hardware but from the space environment interaction with AMF systems. Specifically, plasma accumulation and charging effects around the spacecraft.

1. **Initiating Event – Plasma Sheath Formation:**

- The interaction of strong magnetic fields with the ambient solar wind leads to the formation of a plasma sheath around the spacecraft. Localized charge accumulation occurs on spacecraft surfaces, particularly at the conductor and insulator interfaces.

2. **Immediate Secondary Effects – Electrostatic Stress:**
   - Surface charge differentials create strong localized electric fields across structural and electronic components.
   - Electrostatic discharge (ESD) events are triggered and release charge into sensitive subsystems.
3. **Tertiary Effects – Electronic and Operational Consequences:**
   - ESD induces spurious signals in avionics and sensor arrays, which corrupt radiation dosimeter outputs or misreported shielding field strength.
   - Control loops attempting to adjust coil currents based on erroneous sensor data may introduce unstable oscillations into the AMF system.
   - Repeated ESD strikes degrade insulation layers and accelerate material aging which will increase susceptibility to further discharges.
4. **System-Level Escalation:**
   - As sensor integrity degrades, the shielding system loses the ability to reconfigure in response to a Solar Particle Event (SPE).
   - Crew situational awareness diminishes due to unreliable dosimetry, and this increases the likelihood of delayed storm shelter activation.
   - The cascade from plasma sheath → charging → ESD → sensor corruption → control loop instability reduces both shielding reliability and operational

resilience at the exact moment of peak radiation demand. This escalation pathway is shown in the right branch of Figure 12.0.

Integration with MBSE Risk Architecture

By incorporating cascading effects into the MBSE-integrated risk analysis, this dissertation highlights that both hardware-driven events (coil quench cascades) and environment-driven events (plasma charging cascades) threaten not only subsystem functionality but also mission-level objectives.

- The coil quench cascade primarily degrades TPM: Coil Temperature Margin and TPM: Power Stability which reduces MOP: Magnetic Shield Uptime and directly impacts MOE: Crew Radiation Safety.
- The plasma charging cascade undermines TPM: Sensor Accuracy and TPM: Control Loop Stability, which reduce MOP: Shielding Responsiveness and again degrades MOE: Crew Safety and Situational Awareness.

Together, these examples illustrate how cascading failures bypass the boundaries of individual subsystems and stress the necessity of redundancy and environmental monitoring with automated fail-safe responses within integrated AMF architectures. Extending the FMEA with cascading effects analysis provides a more realistic risk posture and a stronger basis for system design trade-offs and verification strategies as well as operational contingency planning [26].

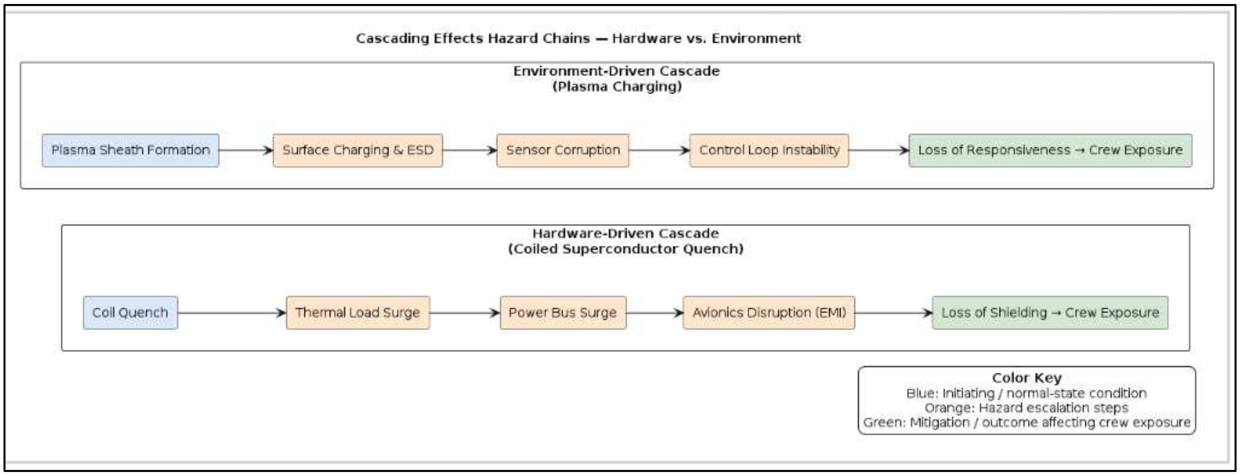

Figure 12.0: Cascading Effects Hazard Chains

Figure 12.0. Cascading effects hazard chains for two representative failure scenarios. The left branch illustrates a hardware-driven superconducting coil quench cascade (thermal excursion → power surge → EMI → avionics disruption → crew exposure). The right branch shows an environment-driven plasma charging cascade (plasma sheath formation → electrostatic discharge → sensor corruption → control loop instability → crew exposure). Color coding follows the dissertation convention: blue (initiating/normal condition), orange (hazard escalation), and green (outcome affecting crew exposure)

12.8 Trade-Off Analysis and Parametric Optimization

A highlight of this research was using MBSE to conduct trade-off analyses and parametric optimizations for different mission scenarios. Given the hybrid nature of the shielding system, there were many design decisions to balance: how strong should the magnetic field be versus how thick the passive shield, given mass and power limits? What is the optimal distribution of shield mass in the habitat? Is an active shield worthwhile for a short mission, or would simpler passive methods suffice? To address these, parametric relationships were developed in the SysML model and complemented with external simulations. The MBSE model allowed the definition of Parametric Diagrams linking variables such as coil current, magnetic field intensity, shielded volume, material thickness, mass, and resulting dose. For example, a simplified parametric model (based on physics and scaling laws) related the required coil current (I) and number of turns (N) to achieve a field of strength B over a radius R [14]:

$$B = \frac{\mu_0 N I}{2R}$$

It also linked the coil's mass and power consumption to those parameters (coil mass $\propto$ N, power $\propto$ $I^2R\_resistance$ for resistive coils). Likewise, for passive materials, dose reduction was modeled with an exponential attenuation law [15]:

$$\frac{\Phi_{\text{out}}}{\Phi_{\text{in}}} = e^{-\mu x}$$

These equations were captured in constraint blocks (e.g., *MagneticShieldConstraint*, *PassiveShieldConstraint*) within the SysML parametric diagrams. By plugging in different values (scenario-specific inputs for volume, available power, etc.), the constraints could be solved to predict outcomes like "achieved dose reduction" or "system mass required."

The dissertation's scenario-based analysis (Chapter 3) defined three representative mission cases: (1) a low-power short-duration mission, (2) a long-duration deep-space habitat, and (3) a highly mobile spacecraft with variable profiles. Each scenario's optimal shielding configuration was explored using the MBSE parametric model in conjunction with specialized tools. The results were documented extensively in Chapters 3 and 4, and key points are synthesized here:

- **Short-Duration, Low-Power Mission (Scenario 1):** This could be an Orion capsule on a lunar flyby or a brief expedition (days to weeks) with limited power (a few kW at most). The MBSE-supported trade study indicated that heavy or power-hungry active systems are impractical for such a mission. Instead, the optimal design emphasized lightweight passive materials (like BNNT composites and multi-layer insulation) and perhaps a modest active field used intermittently. The model predicted that BNNT shielding of ~1.2 kg/m² could cut the dose by ~50%, which aligned with Monte Carlo simulations. The sensitivity analysis also considered an electrostatic shield (Chapter 4). It showed promise for short missions because it can provide high shielding of solar protons with negligible power if sized small. The study found that an electrostatic system could be under 50 kg and nearly zero steady power for a capsule, while completely protecting against solar flares. However, integrating an electrostatic shield on a crew vehicle raised concerns (charging and sparking), so the baseline Scenario 1 design in Chapter 3 leaned toward no active shield or a minimal one (≤0.5 T field) for emergency use only. MBSE allowed capturing this decision logic. The Use Case "SPE Emergency Shield Activation" exists for Scenario 1, indicating that the coils usually are off to save power and only activate if a large SPE occurs (drawing ~500 W, within the capsule's surplus battery capacity).

Overall, Scenario 1's MBSE model showed simplicity and robustness. Passive shielding is always on and requires no action, while the active part is minimal. As noted in Chapter 3, the outcome is a system with the lowest mass and power burden but moderate shielding effectiveness, acceptable for short, low-risk missions. This corresponds to historical approaches (Apollo, ISS early modules) primarily used passive protection. MBSE confirmed that all requirements for short missions (crew dose limits for ~10-day mission, etc.) could be met with this configuration. If not (in the case of a rare significant solar event), the model's risk analysis highlighted the need for contingency measures, such as crew storm sheltering with water or pharmacological aids, to fill the gap.

- **Long-Duration Deep-Space Habitat (Scenario 2):** This scenario represents a Mars transit vehicle or lunar Gateway module with mission durations of many months to years. Radiation exposure, especially from GCR, is far more severe and demands a robust, high-performance shielding system. The MBSE trade studies and sensitivity analysis in Chapter 4 concluded that a high-field superconducting magnet combined with substantial passive shielding is preferable for deep-space habitats. In the model, this translated to a superconducting coil system capable of generating a 1–2 T dipole field around the habitat, paired with ~10 g/cm² of hydrogen-rich material (e.g., 5–10 cm of polyethylene or equivalent) lining the crew modules. This configuration, analogous to NASA and ESA concepts for magnetic shields, was shown to achieve the highest radiation protection. Simulations suggested it could reduce GCR dose by approximately 20–30% (significant for GeV ions) and virtually eliminate solar particle event doses when active. At the same time, the thick passive layer attenuates the remaining radiation and secondary neutrons.

  The cost is high mass and power. The MBSE model tallied several hundred kilograms for the magnet-coil cryostat and power conditioning, plus the mass of passive material and a continuous power draw of several kilowatts for the cryocoolers and support systems. Chapter 3 notes that Scenario 2 "demands significant system mass and power infrastructure, aligning with mission profiles prioritizing crew safety over operational flexibility." The MBSE integration was crucial in this scenario to ensure all subsystems could handle the stresses, for example, adding a dedicated 50 kW nuclear reactor power source in the model to supply the shield and habitat, and enlarging thermal radiators to reject ~10 kW of heat from the magnet and electronics.

The FMEA and interface analysis had to cover cryogenic cooling and high currents, identify failure points such as quench events, and design accordingly. Technology Readiness Level (TRL) differences were captured in the model: passive shielding is TRL 9 (proven), whereas parts of the active system (e.g., large space superconducting magnets) are TRL ~4–5. The MBSE model's requirement section flagged these as "development risks," ensuring that the dissertation discussion addressed them, for instance, through contingency plans or phased implementation as the technology matures.

Ultimately, MBSE enabled a balanced optimization. Parameters such as field strength and shield thickness were adjusted to meet the dose requirements for a 30-month Mars mission while respecting mass and power limits. Iterative runs showed that scaling the magnet from 1 T to 2 T provided diminishing returns unless passive mass was also increased. An optimum was found around ~1.5 T with 5–7.5 g/cm² shielding, which met the NASA career dose limit (~3% REID threshold) with some margin. Scenario 2, as Chapter 3's summary states, "aligns well with long-term habitation objectives, albeit at high operational and integration complexity." The MBSE approach was vital in managing this complexity, ensuring that the integrated design (superconducting AMF + heavy passive) is feasible if the mission program accommodates the mass and power requirements and demonstrates the technology. It also highlighted the importance of layered defense: even with a powerful magnetic field, some GCR will penetrate, so passive material and biological countermeasures (e.g., periodic crew health monitoring and possible use of stem-cell therapies or drugs to repair radiation damage) remain necessary as part of the system.

- **Highly Mobile, Adaptive Spacecraft (Scenario 3):** The third scenario considered a multi-mission deep-space vessel (such as a reusable interplanetary transport or science explorer) that would face varying environments and mission profiles. This spacecraft requires a flexible shielding strategy that can be dialed down to save resources when radiation risk is low and intensified on demand during high-risk periods. Mobility also implies strict mass limits (excess mass reduces fuel/ΔV) and intermittent crew presence (sometimes uncrewed). The MBSE model for Scenario 3 was built upon the adaptive control framework from Chapter 11.

  The design was a rotating magnetic dipole (resistive coil system), a lightweight passive shield (e.g., moderate BNNT layers), and innovative operational modes. The resistive rotating coil was favored because it can be turned entirely off or varied easily, unlike a persistent superconductor that is always on and harder to adjust quickly. According to Chapter 4's sensitivity results, this configuration is "the most robust and flexible" for variable missions. The MBSE parametric analysis showed that at baseline (~9 m^3 habitat module), a resistive coil system (~70–100 kg, using ~7 kW when on) could achieve a meaningful dose reduction (~20% of GCR, 100% of typical SPE protons deflected) if run at full power during cruise. Though not as powerful as Scenario 2's shield, this partial protection might be acceptable when combined with operational tactics (e.g., in a major solar storm, the crew could retreat to a small storm shelter or use stored supplies as extra shielding).

The model allowed simulation of dynamic power management. Figure 2 in Chapter 4 showed how each system's power demand changes with the required shielding level. The electrostatic and superconducting options had flatter power curves (electrostatic negligible, superconductor limited by cryo cooling). In contrast, the resistive coil had a steep and nonlinear power requirement as higher field strengths were pushed. This indicated that the resistive coil is efficient for modest shielding needs (off most of the time, zero power, a significant advantage for intermittent missions) but becomes impractical if tasked with the same protection level as Scenario 2's superconducting system.

The MBSE trade-off here was between flexibility and performance. The model output supported the recommendation of the resistive AMF as the primary system for Scenario 3, supplemented by operational flexibility. The crew and flight software would actively manage the shield state depending on location and mission phase, for instance, off near Earth or during magnetospheric transit, partial power in interplanetary cruise during quiet solar periods, and full power during solar maximum or heightened risk. Additional measures (like deploying small temporary radiation shelters) could be combined during extreme events.

MBSE captured these mode transitions in state machines, with shield controller states: OFF, STANDBY, ACTIVE_LOW, ACTIVE_HIGH, and transitions triggered by context or manual commands. This ensured all required modes were designed and transitions were safe (e.g., avoiding overheating from OFF to HIGH in one step).

Integration challenges to mobile platforms, such as mechanical stresses from a spinning coil or navigation interference, were addressed. The model noted that the rotating coil could potentially double as a magnetorquer for attitude control in some cases, adding value and potentially saving mass. It also documented the need to demagnetize or neutralize the field before docking operations to avoid affecting a neighboring spacecraft.

Ultimately, Scenario 3's MBSE analysis provided a balanced hybrid solution that "offers a versatile solution, combining moderate mass and power consumption with real-time adaptability." The system met varying requirements by being modular and software-driven, rather than maximizing a single metric. MBSE enabled trade-off analysis across multiple mission profiles, not just one operating point. The parametric model was designed for reconfiguration to suit different scenarios and was exercised to assess outcomes while maintaining a consistent architecture.

Across all scenarios, MBSE tools such as Monte Carlo simulation integration and sensitivity analysis were leveraged. Chapter 3 described running 500 Monte Carlo simulations per scenario, varying uncertain parameters (radiation flux, material degradation, power fluctuations). The results, summarized in Chapter 3, showed Scenario 1 had ~32% of trials where shielding fell below thresholds under worst conditions; Scenario 2 maintained >90% effectiveness in ~82% of trials, etc. While external to SysML, these statistical findings were incorporated into the discussion to validate robustness. The MBSE model was updated to include margin requirements based on these results (e.g., adding a margin such that the design point equals mean + 2σ of required shielding).

The synergy of MBSE with these analyses ensured that performance optimization was not done ad hoc but systematically, with traceability from requirements → analysis → design update. The parametric relationships in the model could be used with an optimization solver to identify the best combinations. Although some of this was performed offline due to tool limitations, the structured approach allows future designers to reuse the model, input new mission parameters, and quickly re-evaluate, an advantage over static documentation [16].

12.9 Human-in-the-Loop and Modular Design Considerations

A significant theme in the integrated design was ensuring modularity and human-in-the-loop control, which MBSE facilitated through explicit interface design and modular architecture definitions. Treating each shielding approach (active, passive, bio) as a module with defined interfaces allows the system to be configured or upgraded more easily. For instance, the Passive Shielding Subsystem was defined so that different material options (BNNT, polyethylene, etc.) could be swapped, and the model would automatically update mass and secondary particle production properties. In SysML, this was achieved through block generalization and stereotypes: a generic «ShieldMaterial» block had subclasses for specific materials, each carrying density and effectiveness attributes. This made comparative analysis as simple as toggling which block was instantiated in the model for a given panel.

Similarly, the Active Shield Subsystem had variants (resistive coil, superconducting coil, electrostatic, plasma shield) defined in the model. Chapter 4 compares four concepts. The MBSE structure allowed the instantiation of different variants for evaluation without rebuilding the architecture. All variants adhered to the same interface, producing a field of a specific range and requiring power and cooling input. This was valuable in the comparative sensitivity study, where four “what-if” configurations were run corresponding to the four active concepts in Table 4.1 of Chapter 4’s baseline metrics. This demonstrated the modularity of the approach and ensures that if a new active shielding technology emerges in the future, it can be integrated as long as it meets the interface specifications.

Human-in-the-loop integration was also addressed from a design perspective. MBSE ensured interface compatibility between human and technical systems by formally modeling all human interactions, controls, displays, and alerts, as SysML interfaces with defined data types and trigger conditions. For example, the HabitatUI interface for radiation alerts and system status was linked to the AstronautAgent and the ShieldController. This ensured that software design for the user interface adhered to specific requirements, such as displaying current dose rate, coil status (on/off/intensity), and providing override or mode selection inputs.

The model also captured cognitive load considerations. As noted in Chapter 11, the SensorNetwork monitored radiation and astronaut biometrics for cognitive state. This allowed requirements like RQ-7.2 ("Shielding system alerts shall adapt to crew cognitive load to avoid alarm fatigue") to be linked directly to design elements that modulate alert frequency based on biometric inputs. This integration of bio-sensing into the shielding control loop was novel, and although not fully implemented, the MBSE framework enabled exploration of such human-factor requirements.

Interface compatibility in the modular sense is also required, ensuring that all subsystems can physically and functionally connect without conflict. The SysML Internal Block Diagram was the blueprint to check power connectors, data protocols, and mechanical fit. For example, the coil power interface was specified at 120 V DC with a peak current of X amps, driving corresponding power supply requirements. The cooling interface was specified in terms of flow rate and temperature of the coolant, cryocooler and radiator specifications. Since all these specifications were consolidated into the same model, any alteration including raising the coil current to add more fields would recreationally mark an overhaul in the power interface and signal engineers tasked with the respective subsystems.

Structural integration was captured with Block Definition and Internal Block Diagrams, operational behaviors and failure responses with Activity and Use Case Diagrams, and design verification with requirements traceability and simulation-based validation.

All hazards were mitigated; all requirements were verified and traceable data in the model supported all design decisions. Specific mission scenarios, short-duration, long-duration, and mobile exploration, demonstrated how the hybrid shielding design could be tailored, with MBSE enabling rapid reconfiguration and evaluation of each. The result is a modular, extensible shielding architecture balancing performance with feasibility, advancing the state of the art in space radiation protection while serving as a case study for MBSE's effectiveness in multidisciplinary aerospace design.

With the comparative advantages and limitations of passive, active, and biological shielding strategies established, the following sections describe how these options were synthesized into mission-specific designs for short-duration missions, long-duration habitats, and mobile exploration spacecraft.

A significant theme in the integrated design was ensuring modularity and human-in-the-loop control, which MBSE facilitated through explicit interface design and modular architecture definitions. Treating each shielding approach (active, passive, bio) as a module with defined interfaces allows the system to be configured or upgraded more easily. For instance, the Passive Shielding Subsystem was defined so that different material options (BNNT, polyethylene, etc.) could be swapped, and the model would automatically update mass and secondary particle production properties. In SysML, this was achieved through block generalization and stereotypes: a generic «ShieldMaterial» block with subclasses for specific materials carrying their density and effectiveness attributes. This made comparative analysis as simple as toggling which block was instantiated in the model for a given panel.

Similarly, the Active Shield Subsystem had variants (resistive coil, superconducting coil, electrostatic, plasma shield) defined in the model. Chapter 4 compares four concepts. The MBSE structure allowed the instantiation of different variants for evaluation without rebuilding the architecture. Each variant was maintained to the same interface and generated a field with a certain range that requires inputs of power and cooling. This was valuable in the comparative sensitivity study, where four "what-if" configurations were run corresponding to the four active concepts in Table 4.1 of Chapter 4 baseline metrics. This was seen as a sign of the modularity of the approach, and it guarantees that should the future occur with a new active shielding technology going forward, it can be allowed to be incorporated, provided it adheres to the interface requirements.

Human-in-the-loop integration was also approached in terms of design. MBSE provided human side interface compatibility by a formal model of all human interfaces (interactions involving controls, displays, alerts) as SysML interfaces containing defined data types and trigger conditions. One example is that the HabitatUI offered an interface to radiation warnings and system status, both connected to the AstronautAgent and the ShieldController. The UI must display fields like current dose rate, coil status (on/off/intensity), and allow the astronaut to input override commands or mode selections. By having this in the model, it was guaranteed that the human-machine interface was not an afterthought but integral to the system design.

Moreover, the model recorded considerations of cognitive load. Chapter 11 mentions that the SensorNetwork monitors radiation and astronaut biometrics for mental state. This was a novel integration of bio-sensing into the shielding control loop. If an astronaut is under high stress or workload (perhaps during a critical maneuver), the system might avoid prompting complex reconfiguration tasks or delay non-urgent alarms. While not fully implemented, the MBSE model allowed exploration of such human-factor requirements (e.g., RQ-7.2: Shielding system alerts shall adapt to crew cognitive load to avoid alarm fatigue). Such a requirement was linked to the design element that modulates alert frequency based on biometric inputs. The direct human integration allows this extent of sophistication because MBSE can add the human as a model representation and can follow requirements back to their interactions [17].

Finally, the term interface compatibility had a modular meaning, i.e., that all subsystems were physically and functionally compatible. The SysML IBD was the specification to verify power connectors, data protocols, mechanical fit, etc. For example, the power interface to the coil was specified at 120 V DC with peak current X amps. So, the design of power supply must have delighted that. Coolant flow rate and temperature were the coercion interface parameters. Therefore, the cooling system (radiators or cryocoolers) had to manage to attain such parameters. Since they were taken in a single model, any modification (such as incrementing the current to more field) would automatically indicate that the power interface specification changed and warn the power subsystem engineers to update their design.

In summary, through a detailed MBSE-driven integration effort, this research demonstrated how active magnetic shielding, passive material shielding, and bioengineered mitigation strategies can be synthesized into a coherent system-of-systems architecture for space radiation protection. The approach ensured that theoretical foundations (e.g., physics-based models of radiation and magnetics) were tightly coupled with applied results (empirical simulations, trade studies) via a living SysML model. The multi-level interactions among subsystems and the crew were pictured and optimized through the sufficient graphene of SysML illustrations, which include Block Definition Diagram and Internal Block Diagrams which describe architectural integration, Activity Diagrams and Use Case Diagrams which describe dynamic integration and reactions to failure. MBSE tools like requirements traceability, simulation-based verification, and parametric modeling proved invaluable for risk management and design optimization. Each hazard was mitigated, all requirements were verified, all data and all the design decisions were supported by data that can be tracked in the model. Certain mission cases were identified (short missions, long habitats, mobile explorers) to demonstrate how the hybrid shielding concept can be customized, together with MBSE, and how either can be quickly reconfigured and considered. The outcome is a scalable and interchangeable shielding infrastructure that compromises on the performance and possibility. It is an item of intensive systems engineering. In addition to being a next-generation development in the state of the art of space radiation shielding, with the ability to integrate numerous protective technologies, the work is also a study case of the power of MBSE in addressing aerospace multidisciplinary design issues. MBSE enabled a unified visualization of system complexity and a single-source-of-truth for all stakeholders, improving communication and reducing integration errors [13].

With the comparative advantages and limitations of the established passive, active, and biological shielding strategies, the discussion now focuses on how these options are synthesized into mission-specific designs. The following sections describe how tailored shielding configurations were developed to meet the unique demands of short-duration, long-duration, and mobile exploration missions.

12.10 Sensitivity-Driven Design Choices in the AMF Shielding System-of-Systems

12.10.1 Short-Duration Mission Configuration (Low-Power, Brief Mission)

The design emphasizes minimal mass and power for a short-duration mission (e.g., a lunar flyby or 1–2 week deep-space sortie). The selected shielding parameters are modest:

- **Passive Shielding:** ~45 kg of lightweight hydrogen-rich material (e.g., a boron-nitride nanotube composite liner, ~1.2 kg/m^2) added to the capsule. This alone yields roughly a 40–50% reduction in proton/electron flux for a multi-day mission.
- **Active Field:** A very small electromagnetic dipole field (~0.1–0.2 Tesla) generated by a compact resistive coil (~100–200 kg). This coil is typically off to conserve power, but can be activated during solar particle events, drawing only ~500 W. This is well within the capsule's spare power capacity. An electrostatic shield (~50 kg) was also examined as an alternative for flare protection since a high voltage can deflect solar protons with negligible steady power. But as a matter of issues of integration (charging/sparking risks), the baseline either selects no active shield, or the minimal coil available used only in emergencies.

Justification via Sensitivity Analysis: These choices were driven by scenario trade studies. The MBSE parametric model and Chapter 3/4 analyses showed that heavy or power-hungry active systems are impractical for short missions. Instead, a lightweight passive layer and a highly constrained active field were optimal. Modeling predicted ~50% dose reduction with ~1.2 kg/m^2 of BNNT shielding, which was validated by Monte Carlo simulations. Pushing beyond ~0.2 T field or adding much more mass yields diminishing returns for such short exposure durations. The dose of the GCR over a few weeks is small enough that it can be moderately shielded. An electrostatic barrier was highly effective against solar flares in sensitivity tests (virtually 100% SPE protection at minimal power) but was ultimately not selected due to safety and implementation issues. the design "accepts" a moderate shielding effectiveness in exchange for drastically lower mass and complexity which is an approach deemed “adequate under tight power constraints” for brief missions. The dose outcomes support this: even though the residual cosmic-ray dose with this minimal shield would be unacceptable on a multi-year mission, for a mission of days/weeks the total dose remains within safe limits.

Robustness and Margins: By design, this configuration has very low steady power draw and essentially no active thermal load, which provides huge margins in power/thermal for normal operations. The plan relies on operational contingencies in worst-case events (a rare giant solar storm). The small coil or charging system can be switched on to handle the burst, and the crew can take refuge in a shielded area (water-lined storm shelter) if needed. While this means the inherent system has a limited margin against an extreme event, the MBSE risk analysis flagged this and ensured procedural mitigation was in place. Overall, the short-mission architecture is kept simple and “fails safe.” Passive material always provides some protection without chance of failure, and any active element is only a supplemental, on-demand layer. This simplicity yields high reliability for the brief mission duration (few single points of failure). A gap is that detailed coil design parameters (e.g., exact coil size/turns) are not explicitly given in the SysML diagrams. Instead, their values and effects were documented in Chapter 3’s scenario analysis.

The diagrams show the presence of a field generator, but one must refer to the text/tables for the quantitative settings. Nonetheless, the rationale for this configuration is sensitivity-driven. It was “suitable for low-risk, short-duration missions” once analysis confirmed that meeting minimum dose limits did not require an elaborate active system.

12.10.2 Long-Duration Habitat Configuration (Deep-Space Base)

A long-duration deep-space habitat (e.g., a Mars transit vehicle, lunar base, or orbital station occupied for ~1–3 years) demands maximal radiation protection. Accordingly, the chosen design pushes the parameters to high extremes, which combines a powerful magnetic shield with thick materials:

Magnetic Field: A high-field superconducting magnet encircling the habitat, generating ~1–2 Tesla dipole field. In practice, analysis identified ~1.5 T as an optimal field strength, beyond which returns diminished unless passive mass was increased. This corresponds to an extensive coil system (on the order of 800 kg, including supports and cryogenics for an Orion-sized module). The coil is a closed-loop (toroidal or solenoid) superconducting ring around the crew module. It is literally a single big coil assembly that generates a global field of the dipole. Superconductors (HTS) are used to maintain the 1.5 T field once energized with minimal power draw (only cryocooler and control losses).

Passive Shielding: Approximately10 g/cm² areal density of hydrogen-rich material lining the habitat walls. In Chapter 3's scenario, this was ~135 kg of polyethylene composite (~5–10 cm thickness covering the crew hull). This medium-weight passive layer will absorb the inert neutron and residual radiation which is not deflected by the magnetic field. Additional clever use of in-situ materials is envisioned (water tanks, fuel, or planetary regolith could be arranged as shielding mass) to augment the protection without all mass launched.

Power and Thermal: A dedicated high-output power source (50–100 kW) is allocated to run the shield continuously. The model added a ~50 kW nuclear reactor explicitly to support the coil and habitat systems. Likewise, the thermal control system was "beefed up" with large radiators to dissipate ~10 kW of heat from the magnet and electronics. These margins ensure the superconducting coil can be cooled and powered indefinitely.

Justification via Analysis: Every aspect of this heavy configuration is backed by parametric trade studies and sensitivity analyses. Early analyses showed that only a combined active+passive approach could keep multi-year crew doses under limits. In Chapter 1's Mars mission study, ~85% total shielding effectiveness was required to meet NASA's ~3% REID cancer risk limit, which was only achieved with a multi-Tesla-class magnet plus substantial material shielding. The MBSE parametric model (Chapter 4) was used to tune the field strength and shield thickness. By iterating, the designers found that increasing the magnet from 1 T to 2 T gave diminishing returns beyond ~1.5 T unless passive thickness was also raised significantly. In other words, there was a "knee" in the sensitivity curve. The sweet spot that achieved the dose target with some safety margin was ~1.5 T with ~5–7.5 g/cm² of poly. Pushing to 2 T would consume far more power/complexity for only a slight extra dose reduction.

The final ~1.5 T design is quantitatively justified. For instance, simulations (FLUKA Monte Carlo) showed a ~80% reduction in heavy GCR flux and a ~95–98% reduction of solar protons/electrons with this configuration. That 80% GCR suppression "means the difference between exceeding exposure limits in a single mission versus staying within tolerable risk." Dose projections indicate total mission exposure <0.4 Sv with this shield, versus >0.8–1 Sv (well over limits) if a lighter shield were used. The analysis also compared magnet technologies.

A superconducting coil was favored over an equivalent resistive coil for long-duration use since a normal resistive magnet would draw tens of kW continuously and overheat, which is infeasible for months. The spacecraft coil's few-hundred-kg mass penalty was acceptable given its huge power savings and stable operation. Plasma or MHD "magnetosphere" concepts were also examined but ruled out as "hampered by exorbitant power and mass needs" and problematic side effects. Thus, the selected Tesla-class superconducting magnet + thick hydrogenous shield is quantitatively shown to be the only combination that meets the stringent deep-space habitat requirements. The MBSE model ensured all subsystems could support this (e.g., the power generation, thermal radiators, and structural supports were scaled to handle the high currents and loads; the coil's high stored energy, quench risk, etc., were examined via FMEA). The result is a design that "aligns well with long-term habitation objectives, albeit at high operational and integration complexity."

Robustness and Margins: This architecture provides substantial radiation threat performance margin, which is essentially full protection against solar storms and a large decrease dose of the GCR margin with a small portion under the career dose threshold. It is also operationally and safely margin-engineered. The coil operates below the known power/thermal "knee" to avoid saturating the system, and a generous power budget (50+ kW) means the system has headroom even during worst-case solar storms. The thermal and power headroom explicitly tested were also parametrically tested and under worst-case conditions.

Also, MBSE architecture embeds fault tolerance. In this case, sensors and control logic will automatically put the system in a safe mode in case an anomaly is detected (e.g., coil quench or overheating triggers a controlled shutdown). The SysML model contains state machine modes Full Shielding, Standby and Field-Off to gracefully reduce performance should it be necessary (e.g. during a power shortage, or thermal spike). An elaborate Failure Mode and Effect Analysis (FMEA) was done (see Table 6.3.1, dissertation) in order to recognize and prevent failures. Backup power or coil discharge paths on loss of power, sensor voting redundancy to handle faulty radiation readings, automatic coil dump if temperature rises >80 K above nominal, etc. These measures show the final habitat design is robust across expected variances. It can continue protecting even if parts of the system degrade (for instance, it was required to maintain some shielding in ≥95% of mission time, a goal the design meets via redundancy and continuous SC operation).

One noted gap is the technological maturity. The large space-rated superconducting magnet is currently at low TRL (~4–5), meaning the design's validation is based on analysis and small-scale tests rather than a proven flight system. The dissertation discussion flags this as a development risk rather than a flaw in design logic. In documentation, the exact coil geometry (radius, number of turns) is not explicitly detailed in the diagrams, but those specifics were determined by the constraint equation [14]:

$$B \propto \mu_0 \frac{NI}{R}$$

and were likely given in Chapter 3's engineering tables. Overall, the long-habitat configuration reflects sensitivity-driven optimization (trading field strength vs. mass vs. power) and includes appropriate margins for continuous operation in worst-case deep-space conditions.

12.10.3 Highly Mobile Spacecraft Configuration (Exploration Vehicle)

The shielding system prioritizes adaptability and moderate mass over brute-force maximum shielding for a highly mobile deep-space vehicle (one that travels to multiple destinations, maneuvers frequently and faces varying environments). The selected design is a hybrid, tunable system:

- **Dynamic Magnetic Field:** A rotating toroidal coil system that can adjust its field output in real-time between ~0.5 T and 1.5 T. This is implemented as a three-coil arrangement (R, S, T phases 120° apart) producing a continuously rotating dipole field [18]. The coil assembly is at ~400 kg (plus ~150 kg of power electronics and control hardware). This is roughly half the mass of the habitat's static magnet, which reflects the mobile spacecraft's tighter mass budget. Being a resistive (non-superconducting) magnet, it draws significant power when on: ~5 kW at minimum field up to ~30 kW at peak 1.5 T output. However, this system is run flexibly unlike the habitat's always-on shield. It can be dialed *down* or turned off during quiet periods to save energy and cranked *up* to full 1+ T during high radiation exposure (solar storm, transit outside magnetospheres). The rotating 3-coil topology creates an open-field "magnetic bubble" that moves with the spacecraft and dynamically deflects charged particles from multiple angles. At a maximum of 1.5 T, the shielding efficacy nearly rivals the heavy superconducting system. Chapter 3 reported an 80–95% proton flux reduction at whole field. The key trade-off is duty cycle. The spacecraft must have a power source capable of bursts of ~30 kW, but it need not sustain 50+ kW continuously. This is feasible since advanced electric spacecraft often carry >50 kW reactors or solar arrays for propulsion. The shield essentially *shares* this power. For example, during coast phases, the reactor's energy can go to shielding, whereas during propulsion burns or docking, the field can be lowered or temporarily shut off to free power and prevent interference.

- **Passive Shielding:** A radiation and lightweight liner are built into the structure of the spacecraft. In Scenario 3, this was ~60 kg of a BNNT/polyethylene hybrid (~2 kg/m² coverage). While much thinner than the habitat case, this passive layer serves crucial functions. It provides a constant baseline of protection (moderate GCR attenuation and neutron shielding near the coil) and protects sensitive electronics from secondary radiation and electromagnetic interference. By distributing this material in walls, floors, and equipment (multi-purpose shielding), the design avoids any single heavy barrier yet still gains the benefit of hydrogenous material to soak up neutrons that the magnetic field cannot stop.

Justification via Analysis: The mobile configuration was shaped through comparative trade studies evaluating mass, flexibility, and performance. Scenario 3 assessed multiple options and concluded that a robust and flexible solution consisted of a resistive rotating-coil active magnetic field (AMF) with lightweight passive shielding. A full superconducting magnet was considered but rejected due to excessive mass (~800 kg), which would severely impact propulsion, and limited operational flexibility (difficulty cycling the magnet on/off frequently).

A purely electrostatic, nearly massless shield was attractive for its simplicity and effectiveness against solar particle events (SPEs). As noted in Chapter 3, this could serve as “lightweight insurance” for uncrewed or short missions. However, electrostatic shielding alone would leave excessive galactic cosmic ray (GCR) exposure for a crewed, multi-destination vessel, as only low-energy particles are deflected.

The chosen design strikes a balance: a moderate-mass electromagnetic coil capable of high field strength when required, combined with a small passive layer and optional electrostatic component. Chapter 3’s Scenario 3 simulations showed that, at 1.5 T, the rotating coil approached superconducting-level shielding, significantly reducing particle flux during high-threat periods. During low-radiation phases, the ability to throttle to 0.5 T, or power down allowed significant energy savings with only minor temporary protection losses.

Parametric modeling confirmed that a ~400 kg coil operating at ~1.5 T provided the optimal trade-off. A smaller coil (half the mass) could not achieve the required GCR deflection, while a larger coil would exceed mass budgets and offer habitat-class performance, overkill for a mobile mission. Chapter 2’s dynamic field analysis also showed diminishing returns above ~1.5 T: increasing to ~2.3 T required more than 5× the power for only ~50% additional particle deflection. This informed the decision to cap the design at ~1.5 T, keeping operation within the craft’s reactor and solar limits while maintaining effective shielding.

Scenario 3 documentation noted the rotating-coil AMF was “favored given these considerations”, outperforming an MHD plasma shield (ruled “far too massive/complex” for a light spacecraft) and proving more practical than a superconducting shield for this mission type.

Adaptivity, Margins, and Robustness. The mobile AMF system’s key advantage is adaptability, which enables robustness under variable mission conditions. Unlike the habitat’s fixed full-power shield, this coil can modulate output. In worst-case radiation (e.g., solar storm in transit), the system can operate at ~1.5 T, drawing peak power. Field strength can be reduced during cruise or during sensitive operations to minimize magnetic torques and electromagnetic interference (EMI).

This adaptability provides operational margins. For example, during high-thrust maneuvers or docking, the crew may accept reduced shielding at low short-term risk in exchange for eliminating magnetic interference. The power system supports ~30 kW peaks, within a multi-mission reactor’s capacity, while avoiding continuous 50+ kW draws to preserve power headroom for propulsion and life support. Intermittent coil operation simplifies thermal management, allowing cooling intervals and reducing average heat load.

A passive layer provides a safety net, ensuring some shielding remains if the active field is shut down for power, fault, or operational reasons. It also mitigates secondary radiation from deflected particles striking the hull. The MBSE control model mirrors the habitat’s logic. Radiation sensors trigger automatic escalation to full power when thresholds are exceeded, with safeguards to prevent coil overheating or excessive draw. Simulated solar storms verified >95% protection coverage and timely response [4, 16].

One potential gap is the absence of a quantified ramp-up time; while procedures imply rapid field increases, no numerical values are given. A known operational need is occasional “field shedding" to avoid torques or EMI, addressed via brief coil current reduction or a compensation coil (degaussing subsystem).

In general, the mobile configuration is robust in the sense that it can always adjust to the current mission phase. It intentionally "forgoes the extreme mass of a fixed heavy shield" and instead leverages the spacecraft's agility and power management to actively counter radiation as situations demand [19]. In case of power loss or failure, passive shielding and designated shelter areas provide fallback protection across mission phases.

12.10.4 Summary of Design Choices and Margins for Each Configuration

The table below summarizes the key design parameters for each AMF system configuration, along with their rationale and performance/margin estimates:

Table 12. 3: AMF Key Design Parameters

Mission Scenario	Magnetic Field (strength & type)	Coil Setup (size/number)	Passive Shielding	Power Use & Margins	Shield Performance (Dose reduction)
Short Mission (*days-weeks, low power)*	~0.1–0.2 T dipole field (resistive coil), used intermittently.	Single small coil (~100–200 kg) around craft. Electrostatic high-voltage option (~50 kg) also studied.	~45 kg hydrogenous composite (BNNT) liner (~1.2 kg/m²) . Uses hull + thin liner as primary shield.	~500 W draw when active (within spacecraft power limits). Coil normally off (zero power/heat) – huge headroom except during solar storms. Crew can shelter if an extreme SPE exceeds coil capability.	~40–50% reduction in SEP/GCR flux. Adequate for short exposure (keeps mission dose < NASA limits) but not long-term. Full SPE protection if electrostatic or coil activated.
Long Habitat *(months-years, deep space)*	~1.5 T high-strength dipole (superconducting magnet). Always on to protect continuously.	Large SC coil (~800 kg incl. cryostat) encircling habitat. Likely one toroidal loop covering crew module. Multi-	~135 kg polyethylene (~10 g/cm² or 5–10 cm thick) lining interior. Additional shielding	Dedicated ~50 kW power source (e.g. reactor) for shield and support systems. Continuous	~85% overall dose reduction (~95–98% of solar protons/electrons, ~80% of GCR heavy ions). Brings multi-year crew dose <0.5 Sv

Mission Scenario	Magnetic Field (strength & type)	Coil Setup (size/number)	Passive Shielding	Power Use & Margins	Shield Performance (Dose reduction)
		coil plasma concepts considered but not practical.	from water, cargo, or regolith can augment.	operation; cryocoolers & radiators sized for ~10 kW heat removal. **Margins:** Coil run below performance "knee" to avoid inefficiency; system has thermal/power headroom for worst-case spikes.	(within limits) vs. >1 Sv without shield. Virtually zero SPE dose when field active. Passive layer catches secondary neutrons.
Mobile Craft *(multi-mission explorer)*	0.5 T – 1.5 T **dynamic** field (rotating 3-phase coils). Field intensity is variable based on threat level.	Three-coil *rotating toroid* (total ~400 kg + 150 kg controls). Coils arranged 120° apart (AC phased) to sweep field. No permanent structures beyond coil frame (unlike heavy SC magnet).	~60 kg BNNT/Poly hybrid (~2 kg/m²) as a lightweight liner. Incorporated in hull and equipment (multi-use mass). Absorbs secondary radiation and provides baseline shielding.	**5–30 kW** variable power draw. High-power only during radiation peaks; otherwise, 5 kW or less. Power sourced from propulsion reactor or solar array (tens of kW available). **Margins:** Can shut off or low-power the field during maneuvers to avoid interference. Passive shield + operational planning protect if field must be off.	Tunable performance: at full 1.5 T, **80–95%** reduction in proton flux (nearly matches habitat shield efficacy). At lower settings, smaller reductions, but still significant. Adaptive response ensures ≳95% of mission time shielded. Some residual GCR exposure (due to lower average field) – mitigated by passive layer and possibly crew rotation or pharma countermeasures.

Having identified the optimal design parameters across varying mission profiles, it is essential to translate these discrete configurations into a coherent system architecture. The following section details how the hybrid shielding strategies are implemented within a model-based system-of-systems (SoS) framework, which ensures integration, scalability, and operational resilience.

12.11 System-of-Systems Architecture Detailing via SysML Modeling

Building on the established need for a multi-layer shielding approach, this section details how active, passive, and biological countermeasures are coherently integrated through a model-based system-of-systems architecture. The Active Artificial Magnetic Field (AMF) shielding system-of-systems is modeled through multiple complementary SysML-based views, including Logical, Internal, Physical, Parametric, and State Machine diagrams. These diagrams collectively capture the architecture's subsystems, interactions, and operational dynamics. The Logical Data Model defines high-level functional components (e.g., Magnetic Field Generator, Control Unit, Sensor Array, Power and Thermal Management, User Interface) and their behavioral responsibilities. The Internal Block Diagram (IBD) details the exchange of command, telemetry, power, environmental sensing, and human feedback signals between these components, ensuring interface-level traceability and integrated control. The Physical View allocates these logical functions to concrete hardware elements while referencing applicable spaceflight standards for power, safety, and radiation instrumentation. To evaluate performance and feasibility under nominal and off-nominal conditions, a Parametric Constraint Diagram models critical cause–and–effect relationships, such as how increased current leads to higher power demand, elevated coil temperature, and subsequent impacts on magnetic field strength and shielding effectiveness.

This enables validation of operating margins, such as confirming that the coil operates below the power/thermal "knee" where performance gains diminish. In parallel, a supporting State Machine diagram captures operational control logic across three discrete modes: Full Shielding, Standby, and Field-Off. Transitions between these modes are triggered by environmental conditions, thermal thresholds, or astronaut override, enabling adaptive behavior aligned with radiation threat levels and mission constraints.

12.11.1 Physical Integration and Standards Allocation of the AMF Shielding System

The Physical View Block Diagram provides a concrete mapping between the functional elements of the AMF system and their corresponding hardware implementations and applicable international standards. Each core subsystem, field generation, environmental sensing, power distribution, control, user interface, and thermal support, is represented by a physical hardware block allocated to a corresponding standards block that ensures interoperability, safety, and mission readiness. As an example, the coiled electromagnetic is combined with a cooling subsystem to control the operated temperature. It is governed by protocols such as IEEE magnetic field measurement standards and ASTM E1938 reliability guidelines for cryogenic environments. The radiation sensor hardware conforms to IEC 60846 for radiation protection instrumentation and communicates telemetry using IEEE 802.15.4 [20, 21]. The Control and Monitoring Unit (CMU) is allocated to a Control Module block implementing ISO 26262 for functional safety and ISO 11898 for controller-area network (CAN) communication. Likewise, the User Interface (UI) is governed by ISO 9241 for human factors and uses Bluetooth (IEEE 802.15.1) and TCP/IP protocols for crew interaction and data transmission [25]. The Power Management Unit (PMU) is physically associated with MIL-STD-704 for aerospace power distribution and IEC 62133 for battery safety. These allocations serve as both an implementation blueprint and a verification scaffold, ensuring that all functional behaviors defined in the logical and internal block diagrams can be realized using standardized, interoperable, and certifiable components [20, 21]. Note: The system is designed per MIL-STD-461 to prevent emissions that could trigger failures in other equipment, linking back to EMI concerns, and per ISO 26262, the control software incorporates safety mechanisms for fault conditions. The DEG_CMD signal originates from the Control Module in response to charging hazard detection (e.g., via CHG_STAT or SURF_V telemetry). When invoked, this command activates the Compensation Coil Subsystem to collapse or counter the field generated by the main electromagnetic coil. This controlled neutralization prevents charge accumulation and mitigates the risk of electrostatic discharge (ESD), as outlined in the plasma hazard analysis of Chapter 2. The DEG_CMD pathway is a critical safety feedback loop ensuring that the system's electromagnetic state does not pose a secondary hazard under abnormal plasma conditions. Ultimately, the Physical View (Figure 12.1) substantiates the AMF system as a realizable system-of-systems architecture that links high-level shielding behaviors to their physical manifestation within a compliant, mission-viable spacecraft subsystem [25].

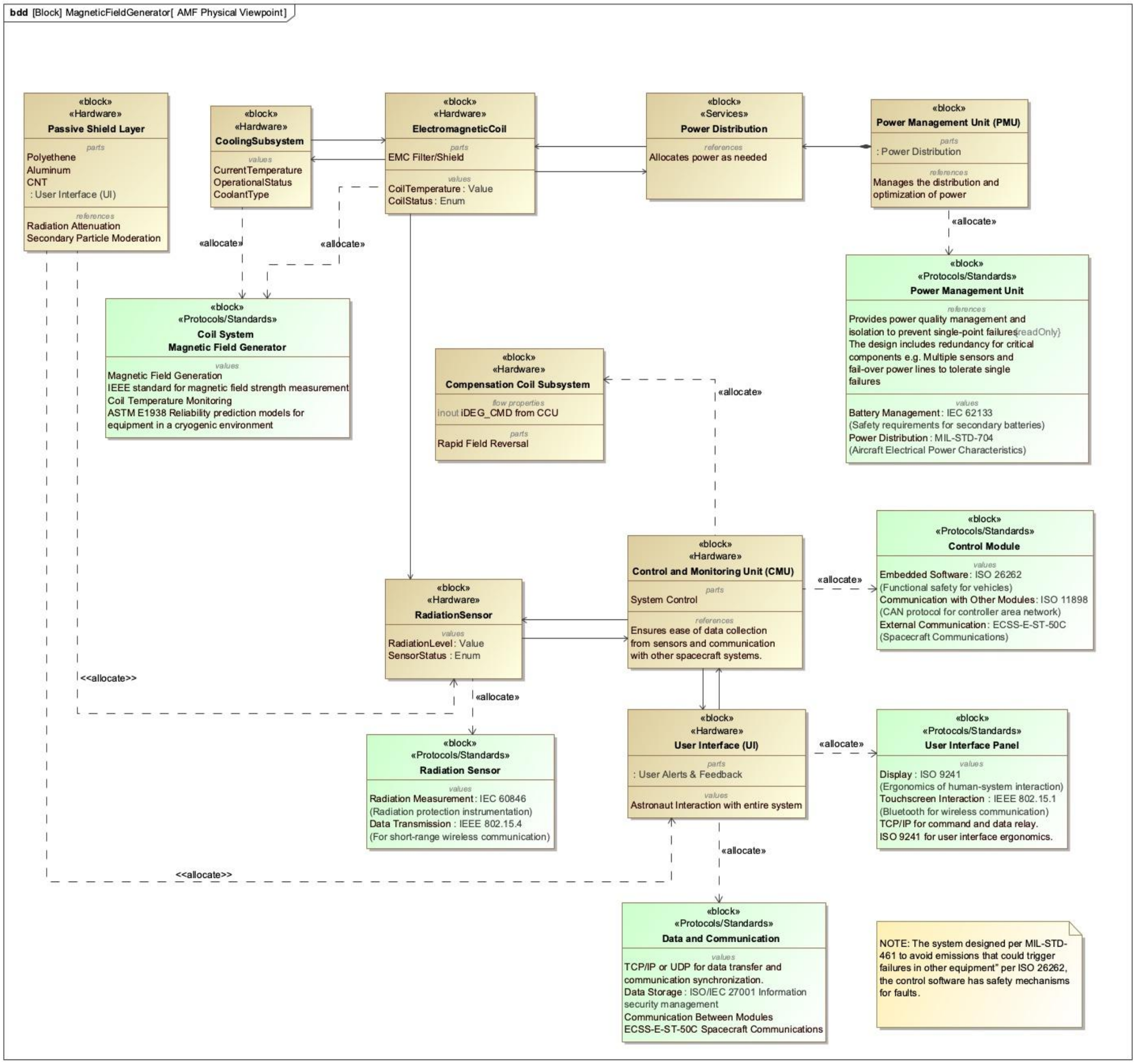

Figure 12.1. Physical View Block Diagram for the Artificial Magnetic Field Generator System.

The diagram shows the hardware subsystems and their protocol allocations, linking electromagnetic coils, sensors, power systems, user interfaces, and control modules to international standards such as ISO 26262, IEC 60846, MIL-STD-704, and others. This view completes the model-based system-of-systems architecture by confirming that physically realizable and certifiable spacecraft components support functional and interface designs.

Note: The passive shield layers are hydrogen-rich for reducing secondary radiation (neutron generation). Also, the coil system is magnetically shielded and filtered to avoid interference with onboard communication systems. The control software can adjust or momentarily ramp down the field during high-data-rate communication intervals to prevent signal distortion. The following Table 12.4 captures the interactions between hardware subsystems and their corresponding standards, specifying interface types and interconnections.

Table 12. 4: Subsystem Interfaces

Subsystem	**Interfaces**	**Type**	**Connected To**
Electromagnetic Coil	CoilTemperature, CoilStatus	Thermal/Status	Cooling Subsystem
Cooling Subsystem	CoolantType, OperationalStatus	Thermal	Electromagnetic Coil
Magnetic Field Generator (Coil System)	Field Generation Functions	Functional/Allocated	Electromagnetic Coil (allocated)
Radiation Sensor	RadiationLevel, SensorStatus	Environmental	Control and Monitoring Unit (CMU)
Control and Monitoring Unit (CMU)	Sensor Data Aggregation, System Coordination	Control/Data	Radiation Sensor, UI, Control Module
User Interface (UI)	Crew Feedback, Alerts	Human-System	CMU
Power Management Unit (PMU)	Power Distribution, Battery Status	Power	Power Distribution, Coil System
Control Module	Embedded Software, CAN/Spacecraft Comms	Protocol/Control	CMU
User Interface Panel	Touchscreen, Bluetooth, TCP/IP	Protocol/Human Factors	UI
Power Distribution	Allocates Power	Power Service	PMU
Data and Communication	TCP/IP, Data Sync, ISO/IEC Standards	Communication Protocols	UI Panel, Control Module

This subsystem interface table summarizes the major functional elements of the artificial magnetic field shielding architecture and highlights the interconnections required for integrated operation. Each subsystem is defined not only by its internal role but also by the interfaces it shares with other components, reflecting the system-of-systems nature of the design.

12.11.2 Logical Architecture of the Artificial Magnetic Field System

The Logical Data Model (LDM) defines the functional decomposition and interaction flow within the Artificial Magnetic Field (AMF) Generator System, capturing the high-level behavior and responsibilities of each subsystem [16]. At the model's core is the Control and Command Unit (CCU), which serves as the central decision-making component interfacing with internal subsystems and external data sources to direct shielding operations. The model delineates key services, including radiation monitoring, field generation, magnetic field modulation, degaussing, electrostatic control, and thermal management. Radiation sensing is performed by a distributed Sensor Array, which communicates radiation intensity and type to the Sensor Controller and CCU. In parallel, user input flows from the User Interface (UI) through the Control and Monitoring Unit (CMU), enabling human-in-the-loop adjustments and feedback reporting. The Magnetic Field Generator (MFG) produces and modulates the protective field and receives configuration commands from the Controller–Generator subsystem based on CCU logic.

Downstream power and thermal dependencies are logically defined. The Power Management Unit (PMU) distributes energy to the Magnetic Field Generator and the Thermal Management System (TMS), with automatic requests triggered automatically based on operational demands or heat flux thresholds. The model also integrates charging-effect mitigation via the Degaussing block, which neutralizes residual magnetic fields after AMF shutdown or in response to detected charging risks. Information and control pathways are explicitly marked to differentiate between data, power, and command signal types, ensuring that flow logic can be formally validated in MBSE simulation tools.

The radiation sensors monitor secondary radiation (e.g., neutrons from shield interactions). The system relies on passive hydrogen-rich shielding to attenuate these particles, as the magnetic field does not affect neutral particles. Monte Carlo simulations in Chapters 3 and 4 of secondary radiation informed the design's placement and material selection of the passive shields.

This architecture satisfies the core attributes of a system-of-systems model. Each subsystem is functionally autonomous yet operationally coordinated. System behavior is emergent and responsive, and information exchange is cleanly abstracted across domain boundaries (thermal, magnetic, sensor, human, and power). The Logical Data Model (shown in Figure 12.2) thus serves as the formal backbone of the system architecture, abstracting physical realization while ensuring total logical traceability and integration of all AMF subsystems [16].

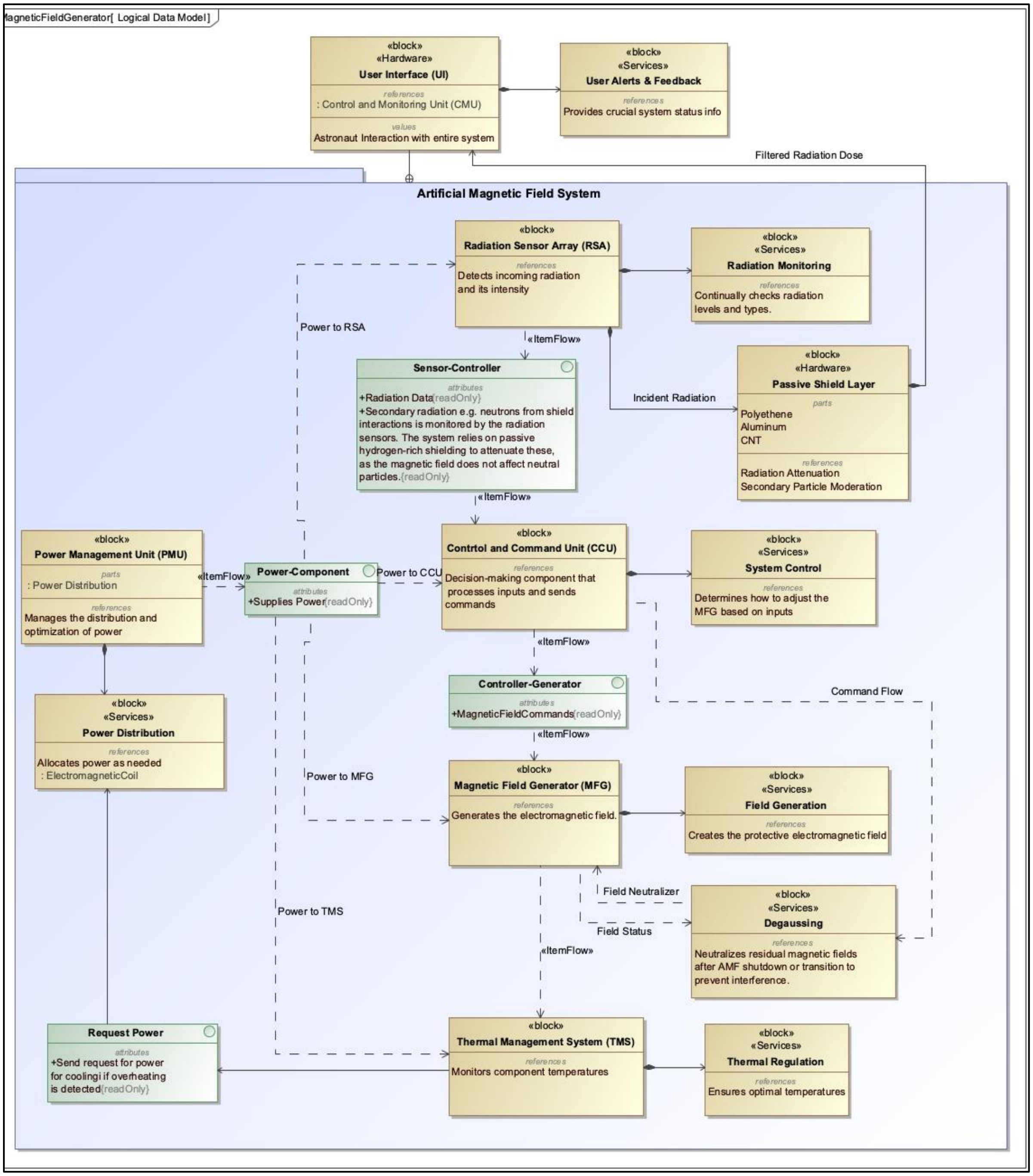

Figure 12.2. Logical Data Model for the Artificial Magnetic Field Generator System.

This block definition diagram illustrates the abstract functional subsystems, radiation monitoring, power control, thermal management, human interaction, magnetic field generation, and charging mitigation, along with the command, data, and power pathways that coordinate their operation. The model emphasizes autonomy, modularity, and emergent system behaviors, supporting a fully traceable system-of-systems architecture within a model-based engineering framework. *Note:* The active Magnetic Field Generator (MFG) is sized and configured under the assumption of baseline attenuation provided by the passive shield, thereby reducing the required magnetic field strength to meet a given dose threshold. The Logical Data Model Interface, shown in Table 12.5, specifies the subsystems, their interface types, and their connected components, supporting both traceability and system-of-systems integration.

Table 12. 5: Logical Data Model Interfaces

Subsystem	Interfaces	Type	Connected To
User Interface (UI)	Command Input, Status Display	Human-System	Control and Monitoring Unit (CMU)
Control and Monitoring Unit (CMU)	Command Processing, UI Feedback	Control	User Interface, CCU
Sensor Array (RSA)	Radiation Detection Data	Data	Sensor Controller
Sensor Controller	Radiation Data Relay	Data	Control and Command Unit (CCU)
Control and Command Unit (CCU)	Shielding Control Logic, Power Requests	Control/Data	Controller-Generator, PMU, TMS
Controller-Generator	Magnetic Field Command	Command	Magnetic Field Generator (MFG)
Magnetic Field Generator (MFG)	Field Generation Status	Output/Status	Degaussing, TMS
Degaussing	Field Neutralization Activation	Command	MFG
Thermal Management System (TMS)	Heat Load Monitoring, Cooling Commands	Thermal/Data	MFG, CCU, PMU
Power Management Unit (PMU)	Power Distribution Control	Power/Command	MFG, TMS, CCU
Request Power Service	Cooling Power Requests	Command	PMU

12.11.3 Internal Interface Coordination in the Artificial Magnetic Field Shielding System

The Internal Block Diagram (IBD) presents the detailed interface logic of the Artificial Magnetic Field (AMF) Generator System by modeling the physical and informational interactions among all core subsystems. These include the Astronaut Agent, User Interface (UI), Control Module, Sensor Network, Radiation Sensors, Power Management Unit (PMU), Thermal

Management, and the Magnetic Field Generator (Coil System) [25]. The diagram defines specific communication pathways via labeled interfaces such as Command and Control (CCI), Telemetry Signal Interface (TSI), Radiation Sensor Interface (RSI), Power Input/Output (PII/POI), Magnetic Field Commands (MFI), and Degaussing Control (DEG_CMD) [16]. For example, the UI enables human-in-the-loop control through Command (CMD), Acknowledgment (ACK), and Cognitive Feedback (COG) lines between the astronaut and the system. The Sensor Network plays a central coordination role, collecting surface voltage differentials (SURF_V), charging status (CHG_STAT), and plasma potential (PLASMA_POT) data from the radiation sensors, then forwarding relevant telemetry to the Control Module to inform system adjustments. In parallel, environmental and health-critical information such as internal temperature (INT_TEMP) and heat load from the Coil System, as well as data from the Thermal Management subsystem, are relayed to both the PMU and the Control Module to optimize operational continuity and shielding effectiveness. Control flows from the Control Module to the Magnetic Field Generator (via MFI) and to the Degaussing Command Unit (via DEG_CMD), while the PMU interfaces with both Thermal Management and the Coil System using power control interfaces (PMCI, POI/PII). By capturing all system interfaces with explicit signal definitions, the IBD reveals the layered coordination required across sensing, actuation, human interaction, and adaptive control.

This fine-grained modeling fulfills a critical layer of system-of-systems integration by enabling traceability across domain boundaries, visualizing emergent behavior patterns, and verifying coordination logic for real-time radiation protection. The IBD (shown in Figure 12.3) thus supports validating the AMF shielding system's autonomy and human-integrated operational resilience under variable mission scenarios [16]

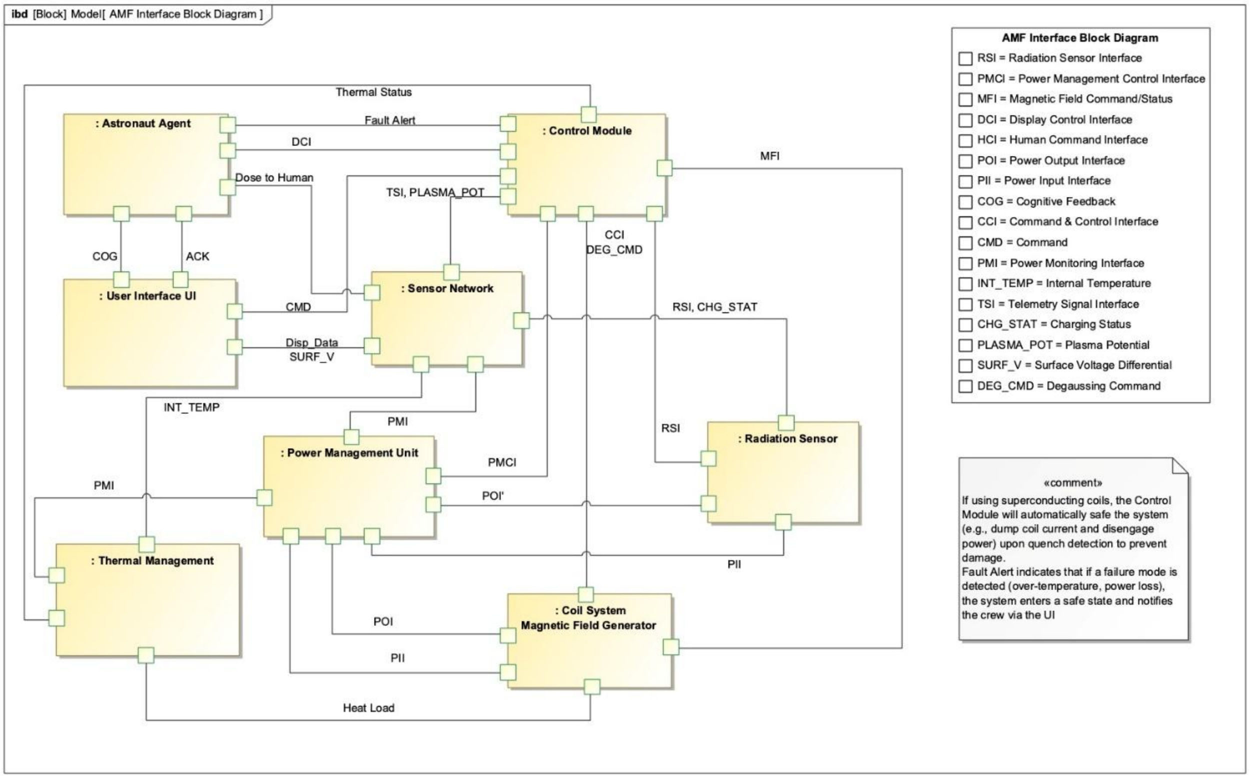

Figure 12.3 Internal Block Diagram (IBD) of the Artificial Magnetic Field Generator System Interface Architecture.

This diagram visualizes all inter-subsystem communications, including human-in-the-loop pathways (COG, CMD, ACK), environmental feedback loops (RSI, CHG_STAT, PLASMA_POT), thermal control interfaces (INT_TEMP, Heat Load) and power and command logic between the Control Module, Sensor Network, Radiation Sensor, Power Management Unit, Thermal Management and the Magnetic Field Generator. Each interface is labeled by type, command, telemetry, control, or monitoring, which supports system-of-systems behavior coordination and model-based resilience verification under space radiation conditions.

The UI includes built-in guidance or lockouts to prevent misuse. The crew can manually override automatic adjustments via the UI if needed, which provides an extra layer of adaptability.

The following Astronaut vs Automation Roles Table 12.6 outlines the distribution of responsibilities between automated systems and astronaut intervention within the Active Magnetic Field system. It clarifies when autonomous operation is expected and when human-in-the-loop overrides are available or required, especially under hazard conditions such as solar storms, surface charging or power faults. However, human override is always a possibility.

Table 12. 6: Astronaut vs. Automation Roles

Function or Event	Automation Role	Astronaut Role	Crew Safety or Ergonomics Considerations
Routine Magnetic Field Adjustment	Continuously modulates field based on sensor feedback.	Monitors via UI; override available in manual modes (Mode B, Mode C).	UI displays real-time field strength, color-coded for safety zones.
Charging Hazard Detection (CHG_STAT)	Evaluates charging data and triggers mitigation if thresholds are exceeded.	Notified via display and audible alert; can override or acknowledge.	Alert system is prioritized; minimal latency display to astronaut.
Plasma Event Alert (TSI, PLASMA_POT)	Receives telemetry from sensor network and flags abnormal plasma conditions.	Visual/audio alert provided; astronaut can adjust field manually if needed.	Cognitive feedback includes flashing indicators and audible tones.
Manual Override of Field Strength	Not applicable unless overridden by astronaut.	Engages via UI during heightened solar activity (e.g., solar storm response).	Manual control panel includes haptic confirmation to avoid accidental commands.
Emergency Field Shutdown	Initiates when control system detects fault or command from astronaut.	Initiates via emergency UI control if immediate hazard is perceived.	Emergency shutdown button is physically distinct and illuminated.
Acknowledgement of Dose Alarm (ACK)	Not applicable; requires astronaut interaction.	Receives audio/visual alarm and must acknowledge via UI	Alarm tone is distinct and persists until ACK received.
Power Allocation Monitoring (PMI)	Tracks power status of all subsystems and communicates with control	Can request diagnostic display but does not directly manage power allocation.	Dashboard includes green/yellow/red indicators for intuitive load state.
Degaussing Command (DEG_CMD)	Issues degaussing sequence upon command or as triggered by charging events.	Can manually trigger via interface if automated response is insufficient or delayed.	Fail-safe guard prevents accidental activation; UI confirms intent before execution.

12.11.4 Plasma Interaction Hazard Chain and Control Mitigation

To clarify how the sensor→control→action loop interrupts the plasma hazard chain (as identified in Chapter 6), the cause-and-effect sequence from the space environment to system damage, along with the corresponding sensing and control responses, is outlined:

Hazard Cause-Effect Chain: The table below summarizes the chain starting from space plasma exposure and ending with a specific system damage mode (in this case, an ESD impact on avionics):

Table 12. 7: AMF Hazard Chain

Hazard Chain Step	Description and Outcome
1. Space Plasma Exposure (Charging Environment)	Spacecraft surfaces are exposed to energetic charged particles (plasma) in space. This leads to accumulation of electric charge on surfaces (especially dielectrics or isolated conductors). Over time, differential surface charging develops as various areas charge to different potentials [22].
2. Surface Charge Buildup (Differential Charging)	Charge continues to accumulate beyond the material's leakage capacity, creating high voltage differentials between parts of the spacecraft. This surface charge buildup was identified in Chapter 6 hazard analysis as a precursor to ESD. It is a hazardous condition where isolated surfaces reach a high potential difference.
3. Electrostatic Discharge (ESD) Event	If the differential voltage exceeds the breakdown threshold of the material or surrounding medium, a sudden electrostatic discharge (arc) occurs. The stored charge is released in a brief, high-current spark. ESD is the critical hazard event in the chain – a rapid discharge that can inject strong currents and electromagnetic transients into the spacecraft [23].
4. System Damage (ESD Consequences)	The ESD current and electromagnetic pulse can damage electronic systems or cause anomalies. For example, an arc can knock out or upset avionics: it may burn out components, scramble data, or induce phantom commands in control systems [23]. (In one documented case, a satellite's power system was permanently disabled by an ESD between charged cables, illustrating how ESD can lead to mission-ending system damage.)

The following SysML sequence diagram illustrates the operational timeline of the Artificial Magnetic Field (AMF) system during a plasma-induced charging event. The diagram traces the interactions between the plasma environment, the onboard sensor network, the control module, and the magnetic field generator, showing how each subsystem contributes to hazard detection and mitigation. The diagram provides a clear visualization of the end-to-end control loop by modeling the flow of events from the onset of surface charging to its neutralization. This sequence contextualizes how environmental inputs trigger sensor detection, how control logic executes automated decision-making, and how the AMF subsystem responds to eliminate the hazard before electrostatic discharge can occur [16].

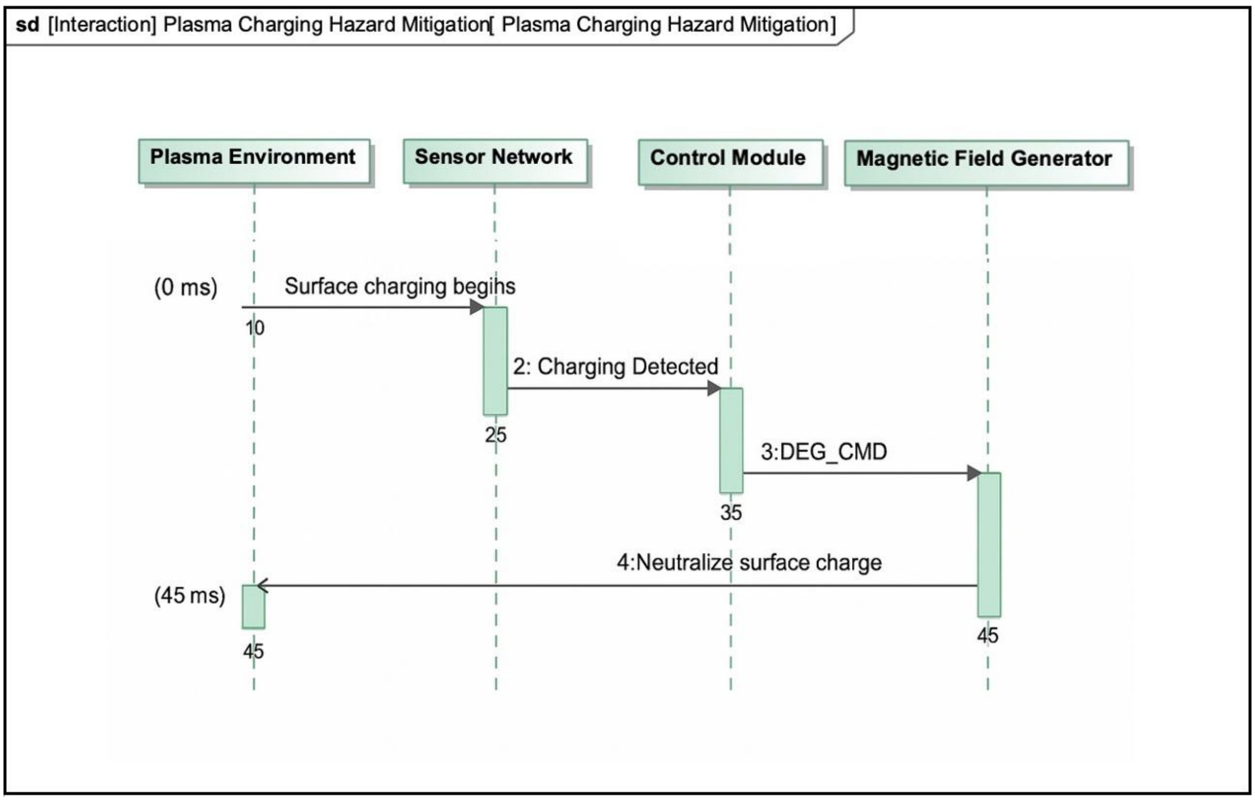

Figure 12.4 Plasma Charging Hazard Mitigation Sequence Diagram

The SysML-based sequence diagram models a successful control loop that mitigates plasma-induced surface charging, thereby preventing electrostatic discharge (ESD) damage. The scenario begins with plasma environment exposure, which causes charge accumulation on the spacecraft surface. The Radiation Sensor detects anomalous potential levels and sends CHG_STAT and PLASMA_POT signals to the Sensor Network, aggregating this environmental data and relaying it to the Control Module via telemetry signal interfaces (TSI). Upon receiving this input, the Control Module interprets the values, determines that charging thresholds have been exceeded, and immediately issues a DEG_CMD (degaussing command) to the Magnetic Field Generator (Coil System). The coil system responds by activating a discharge field or initiating a field modulation process to neutralize the accumulated charge before it can trigger an ESD. Concurrently, the Control Module logs the mitigation response and updates the User Interface, presenting a COG (Cognitive Feedback) signal to the Astronaut Agent and updated SURF_V readings on potential differentials. This action loop terminates the cause–and–effect hazard chain at the charging phase, ensuring system safety before any discharge event occurs.

This diagram confirms that the AMF architecture's Sensor → Control → Action pathway aligns directly with the hazard chain described in Chapter 6, demonstrating that for each stage of the causal chain (charging, ESD, damage), there is a corresponding detection and intervention stage that breaks the sequence. The system is therefore not merely reactive but proactively interrupts environmental hazards through tightly integrated telemetry, threshold logic, and electromagnetic countermeasures. The following Internal Block Diagram (IBD), Table 12.8, captures each subsystem's interfaces, type (e.g., human interaction, command, telemetry), and connected components, supporting traceability and validation across the integrated AMF architecture.

Table 12. 8: Subsystem Interfaces

Subsystem	Interfaces	Type	Connected To
Astronaut Agent	DCI, Dose to Human	Human-System	User Interface, Control Module
User Interface UI	COG, ACK, CMD, Disp_Data, SURF_V	Human I/O	Astronaut Agent, Sensor Network
Control Module	MFI, CCI, DEG_CMD, TSI, PLASMA_POT, Thermal Status	Command/Data	Thermal Mgmt, Radiation Sensor
Sensor Network	CMD, Disp_Data, RSI, CHG_STAT, PLASMA_POT, SURF_V	Telemetry & Sensor Fusion	Control Module, UI, Radiation Sensor
Radiation Sensor	RSI, CHG_STAT	Environmental	Module
Power Management Unit	PMI, PMCI, POI, PII, INT_TEMP	Power Distribution & Monitoring	Thermal Mgmt, Coil System, Control Module
Thermal Management	PMI, INT_TEMP, Heat Load	Thermal Control	Coil System, PMU, Control Module
Coil System (Magnetic Field Generator)	POI, PII, CCI	Field Generation & Command Input	PMU, Control Module, Thermal Mgmt

12.11.5 Constraint-Based Parametric Simulation of AMF Subsystem Interactions

To ensure that the Artificial Magnetic Field (AMF) system operates within a stable and feasible design space, a series of sensitivity analyses on key system parameters were conducted, including coil current, coil radius, wire gauge, number of coil turns, and thermal capacity.

During system definition, these studies were performed iteratively to refine architectural decisions and identify appropriate operating margins. For example, the final design employs a coil current of X amperes, selected to remain just below the threshold at which marginal increases in magnetic shielding effectiveness produce disproportionate increases in power demand and thermal load. This threshold, identified as the "performance knee" in parametric trade studies, established baseline operating conditions and enforced a power budget with approximately 20% headroom. This margin ensures that the power system and thermal management subsystem can accommodate short-term surges in demand, such as those triggered by worst-case radiation events. The parametric diagram integrates These findings into the model, which establishes explicit relationships among system behaviors. For instance, an increase in field strength (via current) increases power consumption, elevating coil temperature, triggering thermal management responses from the cooling system and feedback to the resistance and magnetic field modules. While full-time-domain simulation is reserved for future work, this steady-state parametric approach (Figure 12.5) demonstrates that the AMF design is not arbitrary but rather reflects a traceable and quantitatively grounded balance between shielding performance, resource constraints, and operational safety [4, 16].

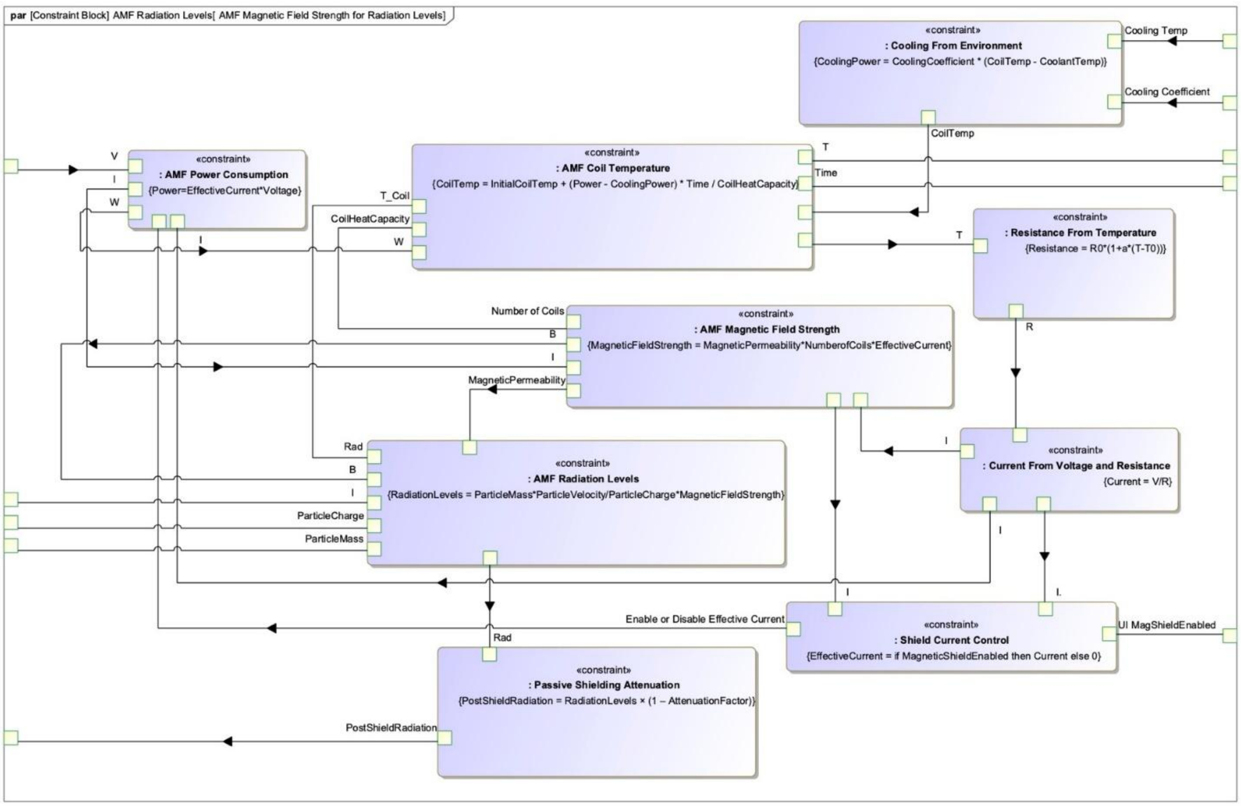

Figure 12.5 – AMF Radiation Field Strength for Radiation Levels Parametric Model

The SysML parametric diagram (Figure 12.5) contains key constraint blocks with mathematical relationships linking power, temperature, magnetic field strength, and radiation level. Each constraint block is defined with a complete equation. For example, the Power Consumption constraint applies Joule's law (Power = Current × Voltage) to calculate coil power draw. The Coil Temperature block implements a heat accumulation model (coil temperature =

initial temperature + (power × time) / heat capacity). It incorporates Ohm's law (Resistance = Voltage / Current) to capture how heating affects coil resistance. The Magnetic Field Strength constraint uses an expression based on Ampère's law ($B = \mu \times N \times I$) to compute the field intensity generated by the coil. Finally, the Radiation Levels constraint links magnetic field strength to an expected radiation attenuation outcome, with shielding effectiveness inversely proportional to field strength ($R \propto mv / qB$). The model also links coil temperature to resistance via the Resistance from Temperature constraint, which feeds into the Current from Voltage and Resistance calculation and creates a closed feedback loop. As coil temperature increases, resistance rises, current decreases (for fixed voltage), and magnetic field strength diminishes.

Structurally, the parametric model binds each constraint to the relevant block properties, forming a chain of influence that mirrors causal relationships in the AMF system: power consumption drives coil heating, which affects magnetic field strength and impacts radiation level. Variations in one parameter propagate throughout the model. Because each constraint block contains a solvable equation with inputs provided either as initial values or from other blocks, Cameo's solver can execute the parametric simulation without encountering under- or over-constrained networks [16, 20].

12.11.5.1 Parameter Values and Unit Consistency

The model assigns concrete values and units to all key parameters, crucial for realistic simulation. For example, in the Power Consumption block, the coil current and voltage are set (e.g., 10 A and 100 V), yielding an initial power draw of 1000 W. The Coil Temperature constraint uses an initial coil temperature (e.g., 20 °C) and a heat capacity (e.g., 400 J/K), ensuring that temperature changes are computed in proper units, with Joules of energy converted to degrees of temperature rise. The magnetic field calculation uses physical constants with correct units; for instance, the permeability of free space is set to approximately 1.26×10^–6 H/m, and the number of coil windings is a dimensionless count, producing a magnetic field output in Teslas when interpreted correctly. Each value property in the parametric diagram carries an explicit unit or dimension (e.g., current in amperes, voltage in volts, power in watts), allowing Cameo to perform unit-consistent calculations and detect mismatches during simulation. The core active components, the electromagnetic coil field generator, power supply, and the radiation sensor, are central to the parametric relationships. In practice, total radiation exposure is reduced by a combination of passive and active shielding; to represent this, a constraint block attenuates the radiation level using the passive shield's properties (e.g., a fixed reduction factor or a function of shield thickness and material characteristics), producing a post-shield radiation level that accounts for both magnetic deflection and residual radiation stopped by physical shielding. The astronaut interface is also modeled, with a "Magnetic Shield Enabled" logic constraint representing crew interaction. This interface can toggle coil current or power to zero when the system is off, implemented by a constraint that sets current = 0 when the control switch is OFF, simulating astronaut or automated control for activation/deactivation in response to mission phases or emergencies. This mechanism tests model behavior during transitions, such as degaussing or field shutdown, ensuring steady-state and transient conditions coverage. The services viewpoint specifies shield activation, modulation, and deactivation requirements, and the model also incorporates thermal control behavior. Heat generation is simulated by the coil temperature rising as a function of power and time, with a cooling constraint linked to the Coil Temperature parameter to subtract a heat-removal factor. This can be modeled using a first-order cooling law (e.g., Newton's law of cooling) or a thermostatic limit (e.g., "if coil exceeds X °C, cooling power increases"), preventing unbounded temperature rise in long-duration runs and demonstrating thermal equilibrium maintenance. This enables “what-if” analyses to verify cooling capacity under maximum-power operation. Finally, the “Passive Shielding Attenuation” constraint takes the raw radiation level from the magnetic shielding equation. It reduces it according to its material properties, directly integrating the Passive Shield block into the parametric network.

12.11.6 Operational Modes State Machine Diagram

Operational modes and transitions of the Artificial Magnetic Field (AMF) system’s control logic Operational control states for the magnetic shield system reflect how the astronaut or automation might interact with the shield under different mission conditions.

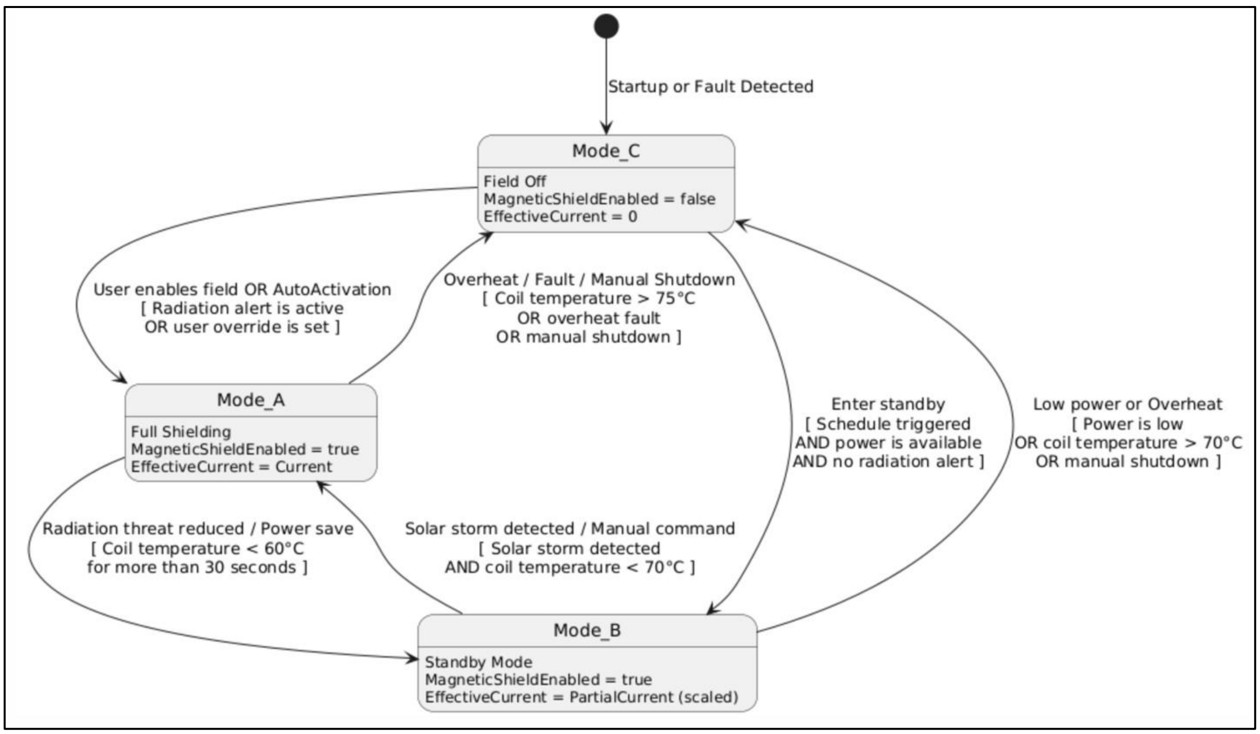

Figure 12.6 - Operational Control States

Figure 12.6 presents a Unified Modeling Language (UML) state machine diagram illustrating the operational modes and transitions of the Artificial Magnetic Field (AMF) system’s control logic. The system operates in three discrete states: Mode_A (Full Shielding), Mode_B (Standby), and Mode_C (Field Off). Upon system startup or detection of a fault condition, the controller defaults to Mode_C, with the magnetic shield deactivated (MagneticShieldEnabled = false) and zero current applied to the coil (EffectiveCurrent = 0).

From Mode_C, the system may transition to Mode_A under user command or automatic conditions, specifically when a radiation alert or manual override is active. In Mode_A, complete shielding is applied with maximum allowable current supplied to the magnetic coils (EffectiveCurrent = Current). If the radiation environment becomes less severe, power-saving conditions are triggered, and coil temperature remains below 60 °C for more than 30 seconds, the system shifts to Mode_B. This standby mode maintains partial shielding with a reduced, scaled current (PartialCurrent) to lower thermal and power loads. The system may return from Mode_B to Mode_A if a solar storm is detected while the coil temperature is below 70 °C or if a manual command is issued. Both Mode_A and Mode_B transition back to Mode_C if any of the following occur: coil temperature exceeds critical thresholds (75 °C from Mode_A or 70 °C from Mode_B), an overheat fault is detected, a manual shutdown is initiated, or power availability drops below required levels. Mode_B may also be entered directly from Mode_C if a scheduled standby is triggered, provided there is sufficient power and no active radiation alert.

Conditionally guarded transitions, based on temperature, fault detection, scheduling, and user inputs, ensure the system dynamically adapts to operational and environmental contexts. The design incorporates hysteresis in temperature thresholds between state transitions (e.g., 60 °C to enter standby, 70–75 °C to shut down) to prevent oscillatory switching and enhance system stability during borderline conditions.

12.12 System-of-Systems Integration of the AMF Shielding Architecture

The active Artificial Magnetic Field (AMF) system presented in this work embodies a fully integrated system-of-systems (SoS) architecture, demonstrated through the combination of five complementary SysML-based views: the Logical Block Diagram (LBD), Internal Block Diagram (IBD), Physical View (PV), Parametric Constraint Diagram, and Operational State Machine. The logical architecture allocates key shielding functions, such as field generation, radiation sensing, and crew interface, into distinct, traceable components to ensure coherent system operation across all shielding modes. Each block operates with functional and managerial independence, contributing to emergent system behaviors, most notably the dynamic modulation of the magnetic field in response to real-time environmental radiation and surface charging effects. The IBD advances this integration by providing a detailed interface-level view that explicitly models control, data, and power exchanges across subsystems. This includes human-in-the-loop pathways such as astronaut cognitive feedback (COG) and radiation alert acknowledgment (ACK), real-time telemetry for plasma potential and surface charging (PLASMA_POT, SURF_V), and active shielding commands (DEG_CMD, MFI) processed by the control module. The IBD highlights the system's capacity to adapt autonomously to dynamic space conditions while maintaining operator situational awareness and override authority [16].

To ensure the feasibility and robustness of these interactions under real-world conditions, a parametric constraint model was developed to quantify the interdependencies between magnetic field strength, coil power draw, heat accumulation, and radiation shielding effectiveness. This model captures causal relationships such as "increased current → increased power → increased heat → altered resistance → reduced field strength" and allows formal validation of engineering trade-offs. The system maintains shielding performance margins across expected mission phases through embedded constraint blocks, with adequate thermal and power headroom under worst-case conditions. A supporting operational state machine defines three discrete system control modes (Full Shielding, Standby, Field-Off), with transitions driven by environmental sensors, scheduled mission states, or astronaut override. This state-based control ensures graceful degradation and fault tolerance during solar storms, overheat conditions, or power anomalies, while enabling energy-saving behaviors in low-risk cruise operations. Finally, the Physical View grounds the abstract system logic in hardware allocations and international protocol conformance, tracing components to standards such as ISO 26262 (functional safety), MIL-STD-704 (power distribution), and IEC 60846 (radiation instrumentation) [20, 21]. These models satisfy formal SoS criteria, including operational independence, emergent capability, evolutionary design, and integrated cross-domain coordination. This five-model architecture validates the AMF system as a technically sound active shielding solution and a fully traceable, simulation-verifiable, and operationally extensible system-of-systems design suitable for deployment in long-duration deep space missions.

12.13 Measures of Effectiveness and Performance for AMF System Verification

As part of the verification and validation strategy for the Artificial Magnetic Field (AMF) Protection System, this section introduces a comprehensive framework of Measures of Effectiveness (MOE) and Measures of Performance (MOP). This framework is a formal mechanism for linking system-level operational goals to subsystem-level performance thresholds, ensuring alignment between the system's architectural design and its intended mission outcomes [24]. The MOEs evaluate how effectively the AMF System-of-Systems (SoS) satisfies overarching mission objectives, focusing on the protection of crew and habitat from space radiation environments, autonomous response capability to dynamic environmental hazards, and continuous operational availability throughout all mission phases. These metrics directly assess the mission value the AMF system delivers under nominal and off-nominal conditions. MOEs also address fault resilience, measuring the system's ability to maintain protection under partial failure modes, and crew situational awareness, which measures the clarity and timeliness of system feedback to human operators [24]. The MOPs, in contrast, provide detailed performance-level criteria for each major subsystem of the AMF SoS, including the Magnetic Field Generator (MFG), Radiation Sensing Array (RSA), Power Management Unit (PMU), Thermal Management System (TMS), Control and Command Unit (CCU), Degaussing System (DEG), and User Interface (UI). These measures include quantifiable thresholds such as field strength delivery, power consumption limits, thermal margins, response latency to radiation hazards, mode transition success rates, and degaussing responsiveness. MOPs ensure that each subsystem operates within safe margins and delivers its intended protective function efficiently and reliably [24]. The complete set of MOEs and MOPs, summarized in Table 12.9, is mapped to relevant verification methods (e.g., parametric modeling, Monte Carlo simulations, FMEA, hardware-in-the-loop testing).

12.14 Measures of Effectiveness (MOE) and Measures of Performance (MOP) for Artificial Magnetic Field (AMF) System-of-Systems

Table 12.9 below summarizes the Measures of Effectiveness (MOE), and Measures of Performance (MOP) developed for the Artificial Magnetic Field (AMF) Protection System System-of-Systems (SoS) architecture. Each measure is aligned to specific system subsystems.

Table 12. 9: AMF Measures of Effectiveness (MOE) and Measures of Performance (MOP)

ID	Measure Type	Title	Description	Primary Subsystems	Verification Method
MOE-1	MOE	Radiation Exposure Reduction	System's ability to reduce cumulative radiation dose to below NASA permissible limits in long-duration missions.	MFG, RSA, CCU, Passive Shield	Monte Carlo (FLUKA), Dosimetry Validation, Onboard Data
MOE-2	MOE	Autonomous Hazard Response	System's autonomous response capability to dynamic radiation events (solar storms, GCR peaks) without astronaut intervention.	RSA, CCU, State Machine	SysML Simulation, Scenario Injection
MOE-3	MOE	Shielding Availability	% Mission time shielded under nominal and contingency operations (target ≥95%).	MFG, PMU, TMS, CCU	Operational Profile Analysis
MOE-4	MOE	Fault Resilience	Ability to retain degraded but safe operations under faults (thermal overrun, power loss, sensor faults).	CCU, TMS, PMU, DEG	FMEA, Fault Tree, Transition Testing
MOE-5	MOE	Crew Situational Awareness	Effective UI feedback to support crew decisions during hazard events (minimize cognitive burden).	UI, CCU, COG Link	Usability Testing, Cognitive Workload Assessment
MOP-1	MOP	Field Strength Delivery	Magnetic field ≥0.4 mT at shielding boundary under Full Mode.	MFG, PMU	Parametric Simulation, Ground Test
MOP-2	MOP	Power Efficiency	≤1.5 kW per 0.4 mT in steady state; ≤4 kW in peak storm events.	PMU, MFG	Power Budget Validation, Steady-State Testing

MOP-3	MOP	Thermal Regulation	Max coil temp ≤70°C in sustained operation with 20% margin from shutdown point.	TMS, MFG, CCU	Thermal Balance Simulations
MOP-4	MOP	Fast Response	Field-up activation latency ≤5 sec after CHG_STAT threshold breach.	RSA, CCU, MFG	Interface Trigger Testing
MOP-5	MOP	Reliable Mode Switching	≥99% successful transitions between Full, Standby, Off under dynamic triggers.	CCU, State Logic	Mode Transition Validation
MOP-6	MOP	Degaussing Efficiency	Reduce surface charge ≤100V within 60 seconds after DEG_CMD.	DEG, RSA, CCU	Plasma Testbed Sim, FLUKA, ESD Bench Testing
MOP-7	MOP	UI Clarity	Crew response time to actionable alerts ≤10 seconds.	UI, CCU	Crew Testing, Simulation Exercises
MOP-8	MOP	Active + Passive Shield Synergy	Combined reduction ≥80% vs unshielded case in GCR/SPE scenarios.	MFG, Passive Shield	FLUKA Composite Dose Modeling

This MOE/MOP framework is pivotal in closing the verification loop between the AMF system's detailed subsystem designs and the broader mission-level design drivers identified in the earlier chapters. This section enables a structured validation process for the proposed AMF configurations. Further, these MOE/MOPs directly inform the trade-off analyses in Chapter 4, which serve as weighted criteria within the decision matrices used for architectural down-selection. Incorporating mission-oriented and performance-oriented measures ensures that the final selected AMF design configuration represents a technically feasible solution and a mission-effective and operationally resilient system-of-systems architecture suitable for long-duration deep space missions [16].

12.15 Artificial Magnetic Field (AMF) System-of-Systems Taxonomy

To support a clear and consistent understanding of the Artificial Magnetic Field (AMF) Protection System architecture, a formal system taxonomy was developed to categorize and define the hierarchical structure of the system's elements. The taxonomy provides a structured classification scheme that organizes the AMF system-of-systems (SoS) into discrete levels of abstraction from top-level mission objectives down to individual components and interface pathways. This approach ensures that system elements are consistently referenced throughout system modeling, simulation and verification activities [25].

At the topmost level (Level 0), the AMF Protection System is described as a SoS with several autonomous subsystems with self-emerging behavioral patterns yielding a collective active radiation shielding functionality. On Level 1 the SoS is decomposed into Primary Subsystems that perform a critical process: magnetic field generation, radiation sensing, power management, thermal regulation, control and command logic, user interaction, and degaussing-based electrostatic mitigation [25]. Level 2 splits each main subsystem into the key functional components, and it explains the hardware and software components underpinning each functional area. Examples include electromagnetic coils and current regulators within the Magnetic Field Generation Subsystem, radiation sensors and plasma potential detectors within the Radiation Sensing Subsystem, and heat pipes and radiators within the Thermal Management Subsystem [25]. Level 3 captures the Interfaces and Data Pathways interconnecting the primary subsystems, including control interfaces, telemetry channels, power pathways, and human interaction interfaces. This explicit classification reinforces the system's cross-domain integration and ensures traceability of information, control, and power flows across the AMF architecture [25]. Finally, Level 4 defines the External Dependencies, which describe the system's interactions with external spacecraft systems and mission environments. These include integration with passive shielding layers (e.g., hydrogen-rich materials for neutron attenuation), spacecraft avionics and communication systems (requiring electromagnetic compatibility), and mission power distribution systems (providing primary and backup power sources) [25]. The full taxonomy is presented in Table 12.10, organizing the SoS architecture into levels, categories, and subcomponents.

Table 12. 10: AMF Taxonomy

Level	**Category**	**Subcategory**	**Description**
Level 0	System-of-Systems (SoS)	Artificial Magnetic Field (AMF) Protection System	Overall integrated system providing active radiation protection and charging mitigation in deep space environments.
Level 1	Primary Subsystems	–	Functionally autonomous yet operationally coupled subsystems.
		1. Magnetic Field Generation Subsystem (MFG)	Generates magnetic shielding fields, adjustable by control logic.
		2. Radiation Sensing and Monitoring Subsystem (RSA)	Monitors radiation levels, surface charging, plasma potential; inputs to control logic.
		3. Power Management Subsystem (PMU)	Allocates power to coils, sensors, control modules; manages power protection.
		4. Thermal Management Subsystem (TMS)	Regulates coil and electronics temperatures to avoid thermal overloads.
		5. Control and Command Subsystem (CCU)	Central decision-making logic governing operational modes and fault responses.
		6. User Interface (UI) Subsystem	Facilitates human-in-the-loop control and feedback during shielding operation.
		7. Degaussing Subsystem (DEG)	Provides electrostatic hazard mitigation through field collapse or modulation.

Level 2	Subsystem Components	–	Key components within each primary subsystem.
	MFG Components	Electromagnetic Coils, Current Regulators, Magnetic Field Monitors	Coils generate shielding fields; monitors feedback strength to CCU.
	RSA Components	Radiation Sensors, Plasma Potential Detectors, Surface Charging Probes	Detect high-energy particles, plasma disturbances, and charging phenomena.
	PMU Components	Power Converters, Batteries, Voltage/Current Monitors	Ensures power quality and availability to active shielding system.
	TMS Components	Heat Pipes, Radiators, Active Coolers, Thermal Sensors	Maintain coil and electronic temperature within operational limits.
	CCU Components	State Machine Controllers, Logic Handlers, Fault Detectors	Governs operational transitions, executes hazard response logic.
	UI Components	Display Terminals, Manual Override Switches, Cognitive Feedback Channels	Provides astronauts real-time visibility and limited manual override.
	DEG Components	Compensation Coil, Discharge Circuitry, Surface Neutralization Logic	Rapidly collapses or redirects magnetic fields to prevent ESD.
Level 3	Interfaces & Data Pathways	–	Operational interaction layers between subsystems and external systems.
	Control Interfaces	Command Signals (CMD), Mode Transition Triggers	Commands issued from CCU to MFG, DEG, TMS.
	Telemetry Interfaces	Sensor Feedback (RSI), Power State (PSI), Thermal State (TSI)	Data relayed back to CCU and UI for adaptive decisions.
	Power Interfaces	Primary/Backup Power (POI/PII), Load Balancing Controllers	Energy flow managed between PMU and operational subsystems.
	Human Interaction Interfaces	UI Command Entry, Cognitive Feedback Loops (COG), Alerts	Links crew awareness to CCU decision-making.
Level 4	External Dependencies	–	Cross-system relationships outside AMF SoS.

	Passive Shielding	Hydrogen-Rich Shield Layers	Complements AMF by absorbing neutrons and neutral particles.
	Spacecraft Avionics	Navigation, Communications, Science Payload	EMI-safe design prevents magnetic interference with critical systems.
	Mission Power Bus	Primary Spacecraft Power Distribution	External power feed supporting AMF subsystems during operation.

The development of this AMF taxonomy serves as a foundational reference for all subsequent system definition, interface modeling, and verification activities. It enables unambiguous terminology usage throughout the dissertation and facilitates the system-of-systems validation approach by delineating the scope and boundaries of each system element. By linking taxonomy levels directly to modeling views (e.g., SysML block diagrams, internal interfaces, and state machines), it reinforces the internal consistency and completeness of the system architecture. This hierarchical taxonomy also supports modular expansion of the AMF architecture for future research, including potential adaptations to varied mission profiles such as low-Earth orbit, lunar transit, or interplanetary missions [16]. Building on the comparative analysis of shielding strategies across mission profiles, it becomes evident that integrating active and passive systems within a hybrid architecture offers a compelling means to balance protection performance with system mass, power efficiency, and operational flexibility. However, this convergence of modalities also introduces new system-level challenges in operational reliability, failure mode interdependencies, and electromagnetic compatibility. The effectiveness of the hybrid configuration is not determined solely of its cumulative shielding performance, but also of the durability of the control systems, and the limits of whatever the failure of a given component can withstand, as well as how well the hybrid configuration works with other spacecraft subsystems considered vital. A rigorous risk management strategy and a system-of-systems failure analysis are essential to ensure that the hybrid approach remains viable for long-duration and dynamic mission profiles. The following section addresses these considerations by systematically evaluating failure pathways, redundancy strategies, and electromagnetic interference mitigation measures within the hybrid AMF system, providing a comprehensive reliability assessment that complements the preceding design trade-offs [3, 4].

12.16 Risk Management and Reliability in Hybrid AMF Systems

The table below lays out some possible failure points and active/ passive system interactions, and the way integrated strategies help cut these risks.

12.16.1 System-of-Systems FMEA for Active + Passive Hybrid AMF Systems

Table 12. 11: Potential Points of Failure and Risk Interactions

Failure Point	Primary Cause	Interaction Between Active/Passive Systems	Mitigation Strategy (from Integrated SoS)
Sensor Bias/Failure	AMF-induced magnetic interference distorting radiation and plasma sensors.	Magnetic fields can corrupt real-time readings used to dynamically adjust shielding effectiveness, compromising the feedback loop between active shielding and passive protection zones.	- Use of EMI-hardened sensors. - Physical separation and magnetic shielding for sensor arrays. - Passive shielding ensures baseline protection during sensor anomalies (fallback redundancy).
Charging-Induced ESD Events	Plasma exposure causing surface charge buildup despite active fields.	Passive shields reduce particle flux but do not prevent differential charging; active AMF modulation intended to counter surface charging could fail due to control logic faults.	- DEG_CMD-controlled degaussing coil triggers field neutralization upon charging detection. - Multi-redundant charge detection (SURF_V and CHG_STAT

Failure Point	Primary Cause	Interaction Between Active/Passive Systems	Mitigation Strategy (from Integrated SoS)
			telemetry) interrupts ESD hazard chain. - Passive shield mitigates secondary neutron hazards regardless of charging state.
Overheating of Coils	High current demand in storm conditions or modulation cycles.	High radiation periods force active shield into full power; coil temperature may exceed thermal limits while passive shield becomes the sole protective layer.	- Integrated parametric controls automatically reduce field strength before thermal limits breach. - Passive shield maintains radiation protection margin during active field downscaling or thermal cycling.
Mode Transition Failures	Faults in CCU logic (e.g., improper state change between Full/Standby/Off).	Improper transitions can lead to under protection (Field-Off) or overconsumption (Full Field) when passive shield alone is insufficient.	- Triply-redundant state-machine logic for autonomous transitions. - Crew override pathways via UI subsystem. - Passive shield provides partial mitigation during transient failures.
Electronics or Communication Disruption	EMI from active coils corrupting avionics or communication links.	Active fields produce low-frequency emissions affecting sensitive onboard systems; passive shield does not generate EMI but cannot prevent it.	- Coil shielding (mu-metal, ferrite). - Field-off or reduced-field modulation during high-bandwidth comms. - Passive layer ensures continued radiation mitigation

Failure Point	Primary Cause	Interaction Between Active/Passive Systems	Mitigation Strategy (from Integrated SoS)
			during comm blackout modes.

A detailed System-of-Systems Failure Modes and Effects Analysis (FMEA) was conducted to systematically identify, classify, and address potential failure points within the hybrid radiation shielding architecture, which integrates both active Artificial Magnetic Field (AMF) systems and passive hydrogen-rich material layers. The purpose of this FMEA is to evaluate not only the independent failure risks of each subsystem but also the unique interaction failure modes that emerge from the coupling of active and passive radiation protection mechanisms within a spacecraft environment [26]. Table 12.11 presents the consolidated FMEA focused on dominant risk pathways that could compromise the hybrid architecture's shielding effectiveness, mission reliability, or safety margins. Emphasis was placed on identifying failure interactions where degradation or malfunction in one subsystem could exacerbate vulnerabilities in the other, thereby compromising overall system-of-systems (SoS) performance. A primary concern arises from sensor bias or failure events in which magnetic interference from active AMF field coils may corrupt radiation or plasma sensor outputs. This distortion can degrade the fidelity of the sensor → control → actuation loop responsible for dynamically adjusting field strength in response to environmental threats. Mitigation strategies include electromagnetic shielding of sensors, spatial separation from coil assemblies, and reliance on the passive shield’s baseline radiation reduction, which provides a protective buffer even during active system sensor faults [26]. Electrostatic charging and discharge (ESD) events represent another key failure point. While active AMF modulation is designed to counteract surface charging, a control loop or insufficient coil responsiveness fault could allow ESD events to propagate to sensitive avionics. The passive hydrogen-rich shielding plays a secondary role by reducing high-energy secondary radiation, including neutrons, even when active degaussing functions (e.g., DEG_CMD) are degraded or delayed [26]. Thermal overload scenarios present an inherent risk to the active AMF system, particularly during peak shielding phases in radiation storm events.

The hybrid architecture reduces operational burden on the active coils by relying on passive materials for baseline protection, preserving power and thermal headroom for transient response windows, and mitigating mission failure risks during active subsystem thermal anomalies [27].

Control logic failures, especially those affecting mode transitions between Full Shielding, Standby, and Field-Off states, can also present operational hazards. The hybrid architecture's design intentionally leverages passive protection layers to ensure residual shielding capability persists even in degraded operational states.

Furthermore, autonomous state-machine transitions and crew override mechanisms introduce fault tolerance to minimize shield state mismanagement risks [27]. Electromagnetic interference (EMI) risks to avionics and communication systems are also relevant in the hybrid system context. While active magnetic fields inherently generate EMI, the passive shield contributes shielding benefits without introducing electromagnetic disturbances. Operational protocols, such as scheduling reduced active field operation during communication windows and physically shielding coil assemblies, further reduce mission interruption risks [19]. A risk-based comparison of dominant failure modes was performed to support a systematic evaluation of mission-critical failure pathways within the hybrid shielding architecture. The analysis combines qualitative assessments of failure likelihood and consequence severity to produce a relative risk ranking for each identified mode. Table 12.12 presents this ranked summary, focusing on the most impactful failure interactions between active AMF systems and passive hydrogen-rich shielding elements. This ranking informs design priorities for mitigation, verification testing, and operational protocols within the overall SoS reliability framework [26].

Table 12. 12: Summary Risk Ranking of Hybrid Shielding System Failure Modes (Risk = Likelihood × Consequence)

Failure Mode	Likelihood	Consequence	Mitigations Present	Relative Risk
1. Sensor Interference from AMF	High	High	Electromagnetic shielding, spatial separation	Very High
2. ESD Propagation Due to Charging	Moderate–High	High	Active degaussing, passive shielding	High
3. Thermal Overload in AMF Coils	Moderate	High	Passive layer reduces coil burden	Moderate–High
4. Control Logic Failure in Shield State Transitions	Moderate	Moderate–High	Autonomous transitions, crew override, passive	Moderate
5. EMI to Avionics/Communications Systems	High	Low–Moderate	Coil shielding, operation scheduling	Low–Moderate

Table 12.12 summarizes the prioritized failure modes identified through the System-of-Systems Failure Modes and Effects Analysis (FMEA) of the hybrid radiation shielding architecture. Each failure mode is evaluated for likelihood of occurrence, severity of consequence, and availability of mitigations, with these factors combined to derive a relative risk score. This scoring enables direct comparison and prioritization of mitigation efforts across subsystems. The highest risk is attributed to sensor interference from the artificial magnetic field (AMF). Proximity of magnetic field coils to radiation and plasma sensors creates a high probability of electromagnetic coupling, potentially distorting sensor readings and compromising the feedback loop that governs adaptive field modulation. Given the potentially severe impact on

real-time shielding efficacy and despite partial mitigation through shielding and spatial separation, this mode is classified as Very High Risk. The second most critical risk involves electrostatic discharge (ESD) propagation during degraded coil responsiveness or faults in the active degaussing control loop, allowing surface charge accumulation to discharge into sensitive avionics. Because ESD can cause immediate, irreversible electronics damage and is more likely in dynamic plasma environments, this mode is rated High Risk. Thermal overload in AMF coils is assessed as Moderate–High Risk. While passive hydrogen-rich materials alleviate constant thermal loading by providing baseline shielding, transient storm phases can still push active systems toward thermal limits. Thermal buffers and reduced coil duty cycles during standby mitigate this, but inherent risk remains. Control logic failures, particularly those affecting mode transitions (e.g., Full Shielding to Standby), pose a Moderate Risk. Passive layers ensure residual protection, and autonomous transitions with crew overrides add robustness, yet state transition faults can still reduce responsiveness in rapidly changing radiation environments.

EMI (Electromagnetic Interference) from AMF operations affecting communications and avionics is considered Low–Moderate Risk. At the same time, common in high-power magnetic systems, consequences are generally transient or manageable via operational procedures such as scheduling field downtimes during communication windows and using coil shielding. Overall, this table highlights the risk-balancing advantage of the hybrid shielding architecture, in which passive subsystems provide redundancy and buffer against active system failures, enhancing resilience against both independent and interaction-based failure modes.

In summary, the FMEA demonstrates that the hybrid AMF system achieves high fault resilience through the complementary nature of active and passive components. The passive shield ensures enduring radiation protection so that loss or degradation of active functionality does not result in catastrophic failure. In contrast, the active system enables adaptive and dynamic response to short-term or event-driven threats beyond the passive shield's attenuation capacity. This systemic redundancy provides robustness against single-point failures and complex interdependency failure chains, fulfilling modern risk management and reliability objectives for long-duration space missions [27].

12.17 EMI-EMC Considerations in Hybrid AMF Architecture (Chapter 8 Alignment)

The following table clarifies how the proposed hybrid architecture addresses electromagnetic interference and compatibility.

Table 12. 13: Specific Hybrid Architecture EMI-EMC Mitigations

EMI/EMC Risk Area	Hybrid Mitigation Mechanism	Reference (Chapter 8)
Radiated Magnetic Emissions	- Physical separation of coil assemblies from critical avionics. - Passive hydrogen-rich layers placed around living spaces naturally create additional EMI barriers. - Coil field-shaping structures to direct flux away from communication paths.	Sections 8.2, 8.5.1
Conducted EMI through Power Buses	- EMI filters and line conditioners specifically on active coil circuits. - MIL-STD-704 power management ensures clean power delivery. - Passive systems draw minimal power, reducing systemic EMI load.	Section 8.5.2
Magnetic Saturation of Navigation Sensors	- Passive-only operational phases during high-precision navigation. - Dynamic field modulation avoids persistent sensor bias. - Sensor placement optimized using 3D magnetic field mapping.	Section 8.3, 8.5.3
Cross-System Temporal Interference	- Field modulation schedules integrated with mission phase planning (active shield off during critical comm/data windows). - Passive shield ensures uninterrupted radiation protection during active field downtimes.	Section 8.5.3

EMI/EMC Risk Area	Hybrid Mitigation Mechanism	Reference (Chapter 8)
System-Level EMI Compliance	- Full system EMC testing includes scenarios with active/passive hybrid operation. - Margin testing during transitions (e.g., Full Shielding → Standby → Off) to validate hybrid operational integrity. - State-machine-controlled transitions minimize EMI onset spikes.	Sections 8.6, 8.7

Key Architectural EMC Reinforcement:

- The AMF system explicitly adheres to MIL-STD-461 EMI control standards and ISO 26262 functional safety protocols, ensuring systemic compatibility across spacecraft platforms (from *Physical View Block Diagram*, AMF Integrated SoS).
- Mode-based operational logic (State Machine Diagram) ensures the system actively suppresses EMI during sensitive mission phases, a unique advantage of hybrid designs.
- Chapter 8's EMC FMEA incorporates detection and mitigation mechanisms spanning the active AMF system and the passive shield integration, providing a comprehensive hazard closure approach.

Integrating hybrid active and passive shielding architectures introduces distinct challenges and opportunities in managing electromagnetic interference (EMI) and ensuring electromagnetic compatibility (EMC) within spacecraft systems. While active Artificial Magnetic Field (AMF) systems generate intentional high-intensity, low-frequency magnetic fields, passive shielding layers produce no electromagnetic emissions and inherently mitigate secondary radiation without contributing to the electromagnetic environment. The combined use of these shielding modalities, as detailed in Chapter 8, creates a complex interaction landscape where EMI risks must be proactively managed to ensure safe and reliable spacecraft operation [19]. One of the main benefits of the hybrid set-up, is that the operation modes will be strategically controlled to reduce the level of EMI risks during sensitive mission periods. With silent radiation protection, the passive shield is not emitted electromagnetically to be practically engaged with the active magnetic field system; only when the conditions of operational and environmental rule and need its application. This principle enables the hybrid system to maintain shielding efficacy even during active field down-modulation or deactivation periods necessitated by EMI constraints [4].

Table 12.13 summarizes the EMI-EMC mitigation strategies employed in the hybrid AMF architecture, aligned with best practices from Chapter 8. Radiated emissions, particularly low-frequency magnetic fields generated by active coils, are mitigated through multi-layered interventions, including localized coil magnetic shielding using high-permeability materials such as mu-metal and ferrite composites, and the use of field-shaping structures to direct magnetic flux away from sensitive subsystems. The passive shielding configuration contributes additional spatial isolation between active field generators and critical electronics, reducing near-field coupling pathways. Conducting EMI along power buses and signal lines is addressed by isolating active system power pathways with dedicated EMI filters and line conditioners and adhering to aerospace-standard power protocols such as MIL-STD-704. Passive shielding elements require minimal or no power input, reducing powerline EMI contamination and lowering system-level conducted interference risks [27]. The hybrid design also addresses sensor saturation risks for navigation and attitude determination systems susceptible to magnetic biasing from active fields.

Operational procedures allow deactivation or reduction of active field strength during high-precision navigation phases, with the passive shield maintaining uninterrupted protection from cosmic radiation [18].

Additionally, operational scheduling balances electromagnetic emissions with mission-critical functions; during high-data-rate communication or scientific data acquisition, the AMF system transitions to Standby or Field-Off modes to avoid interference with RF communication bands and sensitive payloads. The passive shield is used to keep the levels of a radiation exposure within acceptable levels during such periods. EMC compliance is validated through an integrated testing regime encompassing conducted and radiated emissions characterization, magnetic susceptibility evaluation, and system-level testing under representative operational modes. These test protocols, detailed in Chapter 8, explicitly account for hybrid operational conditions and verify EMI remains within defined thresholds across mission phases. Compliance with international standards, including MIL-STD-461 for EMI emissions, ISO 26262 for functional safety, and ECSS-E-ST-20-07C for space system EMC, ensures the hybrid AMF architecture meets both mission-specific and industry-wide criteria [28].

To conclude, hybrid AMF shielding architecture leverages the complementary characteristics of both active and passive technique to become more EMI resilient. The passive shield provides continuous protection during active subsystem modulation or deactivation, while active system design incorporates EMC-focused hardware, software, and operational safeguards. This multi-faceted approach ensures the hybrid system meets radiation protection objectives and upholds stringent electromagnetic compatibility requirements, contributing to the safety and reliability of long-duration deep space missions.

12.18 Thermal and Operational Management of Active Shielding Systems Across Mission Scenarios

There is also a serious thermal management issue with effective radiation shielding using artificial magnetic fields. Coils of high current magnets produce large amounts of heat which needs to be cooled to prevent permanent damage. A set of combined thermal control methods and an operator control management strategy is essential. This section discusses how thermal control is implemented in the shielding architecture for three mission scenarios (short-duration missions, long-duration habitats, and mobile exploration craft), highlighting radiator sizing, coil cooling methods, thermal coatings, and the coordination of passive and active cooling elements. Each configuration's design is tailored to reduce thermal loads and enhance system survivability, while ensuring key performance outcomes.

12.18.1 Short-Duration Missions: Passive-Dominant Thermal Control

Short missions (e.g., a few days to weeks in transit or lunar vicinity) leverage the limited operation time to rely heavily on passive cooling methods for the shielding system. The active magnetic shield in this scenario can be run sparingly and at moderated power levels, such that the spacecraft's existing radiative surfaces and structural heat sinks handle the coil's waste heat with minimal additional hardware. Radiators are sized to accommodate the shield's intermittent heat output, typically on the order of a few kilowatts during operation. These radiators (often existing spacecraft thermal control panels) provide sufficient area and emissivity to reject the coil's heat to space over time. Because the mission is short, average heat loads remain low, and any burst of heat (e.g., during a solar particle event) can be buffered by the thermal inertia of the spacecraft structure and gradually dissipated via radiation [29].

Specific thermal coatings help maximize passive cooling efficiency. The coil housing and radiator surfaces are treated with high-emissivity and low-absorbance coatings, for instance, anodized or white thermal paint (Z93) on outward-facing surfaces to enhance infrared emission while reflecting solar radiation. Such coatings ensure that even when the Sun illuminates the vehicle, the shield system absorbs minimal heat and can continue to radiate internally generated heat effectively. Analyses show that with suitable surface treatments and insulation, the shield structure can sometimes radiate more heat to space than it absorbs from the environment, which results in a net negative heat load into the coils. This passive bias helps keep coil temperatures in check without active cooling [30].

Active cooling elements are kept simple for short missions. Rather than complex cryogenic refrigerators, the design may use only the standard thermal control loop (e.g., pumped liquid coolant or heat pipes) to transfer heat from the magnet coils to the radiators. No continuous cryocooler is required if conventional (resistive) electromagnets are used at moderate temperatures. If the mission employs high-temperature superconducting (HTS) coils for efficiency, they can be operated at ~70 K using minimal cryogenics, drastically reducing cooling complexity compared to low-temperature (4 K) systems. A small onboard cryocooler or stored cryogen can often handle HTS coil cooling for the short mission duration, and the lack of long-term boil-off or large cooling power demand yields considerable power savings. Avoiding heavy cryogenic systems, the short-duration shield architecture remains lightweight and power-efficient [31].

Operationally, thermal management is achieved by limiting active shield usage only when necessary. The coil is not run continuously. Mission planners schedule their operation in short duty cycles aligned with radiation hazards. For example, the shield might be activated only during high-radiation passes or solar storm events and kept off or at standby power otherwise.

This “operate only when needed” approach is enabled by real-time monitoring of radiation conditions and was identified as a key strategy at the operational level. By duty-cycling and modulating the field, the system dramatically cuts average heat generation and power draw since the magnet dissipates power (and heat) only during critical periods. In effect, the spacecraft uses the natural quiescent periods to passively radiate away accumulated heat, which ensures the coil is cooled down and within safe temperature margins before the next active period. Thermal safety is thereby preserved [29]. The coil temperature always remains at temperatures much lower than that of destruction since the coil does not undergo long-term constant heating. Even under a worst-case thermal stress (e.g., an unexpected solar particle event requiring the shield to be on for several hours), the short mission's thermal system is sized to cope by radiating the surge of heat over subsequent hours or by allowing a brief exceedance that the hardware is rated to withstand. To conclude, in such short missions, the passive thermal architecture (radiators + coatings) bears the bulk of the load, with here the active control only reaching the extent of actively circulating the heat to the radiators. This yields robust power savings (no large cryocooler running) and keeps the shield system capable yet straightforward of safe operation through the mission's worst-case radiation event [29].

12.18.2 Long-Duration Habitat: Cryogenic Cooling with Integrated Passive Shields

Long-duration missions (e.g. a multi-year transit or planetary habitat) demand a continuous active shielding presence which in turn requires a far more robust thermal management architecture. In this case the shielding system almost invariably employs superconducting magnet coils to reach the field strengths required to deflect Galactic Cosmic Rays with viable amounts of power [32]. These coils (usually made of HTS tapes) must be kept at cryogenic temperatures hence the operational cryogenic cooling-subsystem is at the heart of the thermal design. The coils are housed in a cryostat with multiple stages, for example, an inner stage at approximately 20–30 K for the HTS coils and an intermediate thermal radiation shield cooled to approximately 70–90 K. Cryocoolers (mechanical refrigeration units) are employed to remove heat from these stages. A typical design might use two-stage cryocoolers: the first stage intercepts heat at the 70 K shield, and the second stage cools the 20 K coil. Any ohmic loss or

AC loss in the superconductors, plus conductive and radiative heat leaks into the cryostat, must be continuously extracted by the cryocoolers. Though the superconductor largely eliminates resistive I^2R heating (a major power-saving advantage of this design), the cryocooler's inefficiency means that for every watt of heat lifted at 20 K, on the order of tens of watts of heat are rejected at the cryocooler's warm end (~300 K). Thus, large radiators are required to dump the cryocooler waste heat to space [32].

In the habitat design, these radiators are typically integrated into the vehicle's overall life-support thermal control system, sharing heat rejection with other systems. Studies assume the required radiators for the magnet's cooling will be part of the habitat's broader thermal infrastructure (and their mass included in the habitat thermal control system rather than the shield subsystem) [30]. Such radiators might span tens of square meters, deployed on the spacecraft exterior where they have a clear view to cold space. They are sized to dissipate the steady-state heat load of the cryocoolers plus a safety margin for peak loads. For instance, if the shield system must remove ~500 W of heat from the coils and support structure, the radiators might need to reject several kilowatts of heat at ~300 K. The thermal design ensures that even under worst-case conditions (e.g., maximum coil current operation during a solar storm plus elevated ambient temperatures), the radiator capacity and cryocooler performance have sufficient margin to keep coil temperature within safe limits. Typically, a thermal safety margin of 20% extra cooling capacity is allocated so that coil temperature stays below its critical limit even if heat loads temporarily spike [29].

Passive thermal control elements are heavily integrated with active cooling in the long-duration habitat to minimize the cryogenic load. A prominent example is using a sunshield and multilayer insulation around the coil. Inspired by the James Webb Space Telescope (JWST) sunshield concept, a large multi-layer thermal shield (MLI) is deployed between the coils and the Sun/planet to reflect away solar radiation and provide a cold deep-space background for the coils. With a high-performance sunshade (multiple layers of aluminized Kapton with vacuum gaps), the external heat input to the coils can be reduced to zero [30]. Table 14.2 of a NIAC study showed that a JWST-quality heat shield could cut the external thermal load on a 6-coil deep-space habitat system to nearly 0 W, creating a cooling surplus where the coils radiate more to space than they absorb [30]. When shadowed from the Sun and Earth by the multilayer shield, this means the coils see an effective environment temperature of approximately 30–40 K, allowing them to dump heat to space passively.

The only significant heat that needs active removal is the conductive leak from the habitat interior, estimated at around 380 W in that study [29]. All that 380 W (plus some small dynamic losses) must be taken out by cryocoolers, but this is far smaller than the load if the coils were exposed to full solar thermal input. The design eases considerably pressure on the cryogenic system in providing a combination of passive thermal shielding and active cryocooling. With the sunshield radiator sizing and power to their cryocoolers is reduced by a significant amount when compared to the case without the sunshield. This synergy directly translates to power savings and added robustness: the cryocoolers draw less electrical power (critical in a long-term habitat with limited energy) and produce less waste heat for the radiators to handle.

Additionally, the passive shield provides a buffer against worst-case scenarios. For example, if one cryocooler suffers a fault, the coils will not immediately overheat because the passive shield keeps external heat influx near zero. The system has grace time to respond (e.g., switch to a backup cooler or lower the coil current) before temperatures rise appreciably [29].

Multiple specific solutions are implemented in the long-duration thermal control design. Thermal coatings and multi-layer insulation are used extensively. The coil cryostat is wrapped in highly reflective MLI blankets to minimize thermal radiation from the warm habitat. Exposed surfaces of the sunshade are coated with reflective aluminum or white paint on the Sun-facing side (to reflect sunlight) and high-emissivity coatings on the space-facing side (to radiate heat away). For example, anodized aluminum or Z93 white paint on the outward side of the coil structure maximizes radiative heat loss, contributing to the net negative heat load mentioned earlier [30]. Internally, surfaces facing the cold coils are polished or gold-coated to reflect stray radiation and confine cold. Thermal connection points are carefully managed, supports and current leads into the cryostat include thermal intercepts (cooled at intermediate temperatures) to siphon away heat before it reaches the cold stage [30]. Radiator panels may use high-emissivity fin coatings (e.g., nickel-plated or dedicated radiator paint) to ensure they effectively radiate the cryocooler waste heat. To handle dynamic heat loads, the cryocooler controllers can modulate their lift capacity: if the shield coil current is increased (raising AC losses or eddy currents), sensors detect any temperature rise and the cryocoolers throttle up cooling power to compensate, keeping the system stable [30].

There is also the role of operational management in the habitat scenario though the shield is meant to operate near continuously. Field strength modulation, which is based on the radiation environment, is one of the strategies. By cutting Coil current slightly during periods of quiet (solar minimum or behind planetary magnetic fields) the heat generation can be reduced, and power saved, and then back to whole design field only when radiation level rises. This dynamic adjustment avoids running the magnet at maximum power (and maximum cooling load) 100% of the time if not needed. Mission operations can also schedule certain high-heat activities (e.g., coil energization or de-energization transients) when other heat loads on the habitat are low so the shared radiators can accommodate the shield’s heat. In extreme cases like a large Solar Proton Event, the system may temporarily accept higher cryocooler power draw or engage reserve cooling units to maintain the shield. Also, non-critical habitat systems might be turned down to allocate power and thermal margin to the shielding system [31].

Redundant cooling units are typically on standby as well. Long-duration designs include multiple cryocoolers for reliability [33]. If one fails or a higher load is needed, a backup can engage, preventing cooling loss. All these measures ensure that even under worst-case thermal stress (prolonged maximum field during a solar storm combined with peak metabolic heat in the habitat), the shield’s thermal control has the capacity and redundancy to cope. The desired/requisite thermal safety margins are maintained. Coil temperature stays safely below its critical temperature (with margin to avoid quench), and the radiators can dump the heat without overheating the habitat [33].

Locating the superconducting coils outside the crew cabin (external to the vehicle) is preferred to reduce crew magnetic field exposure and ease cooling by giving the coils a direct line of sight to cold space [33]. Past studies found that putting magnets inside the habitable volume was infeasible due to the mass of cooling equipment required and the difficulty of getting rid of heat in an enclosed space [33]. The design improves operational resilience by moving the coils outboard behind dedicated thermal shields. The cooling system can always radiate to space, and there is no risk of the habitat interior accumulating heat from the shield.

The long-duration habitat configuration uses a holistic thermal control architecture: powerful active cooling (cryocoolers + large radiators) augmented by advanced passive elements (sunshades, MLI, coatings). This integration yields substantial power savings (by minimizing unnecessary heat loads). It achieves the required heat dissipation rates continuously, as well as providing comfortable thermal margins so that the shielding system remains stable and survivable over years of operation [31].

12.18.3 Mobile Exploration Spacecraft: Dynamic Thermal Management for Intermittent Operation

In a mobile exploration spacecraft, such as a crewed rover on a planetary surface or a small vehicle operating outside a habitat, the radiation shield must be lightweight and capable of on-demand operation. These spacecraft have inherently limited power and cooling resources, so the thermal management emphasizes dynamic modulation and intermittent cooling rather than large steady-state systems. The active shield on a mobile platform might be a smaller HTS coil or even a conventional electromagnet used as a “local” shield for the crew during sorties. Because the vehicle is used intermittently (e.g., a rover might conduct a sortie for several hours, then return to base), the shielding system is designed to handle short bursts of heat followed by cooldown periods [30].

A key strategy is real-time field modulation and duty cycling, similar to the short-duration mission but even more granular. The mobile shield’s control system actively adjusts the magnetic field strength in response to immediate conditions. This is essentially throttling the coil to only produce as much field (and heat) as needed at any given time. For instance, if radiation sensors detect a sudden spike (entering a higher radiation area or a solar flare onset), the coil current is ramped up to increase protection. When radiation levels drop or the vehicle is shielded (e.g., behind terrain or inside a lava tube), the coil current can be lowered or turned off to cool. This real-time modulation minimizes the thermal load by eliminating unnecessary high-power operation [30].

The coil might operate in a pulsed or cycled mode, on for a few minutes at high power, then off or at low power for a few minutes to dissipate heat. Engineering of the power supply and coil accounts for this. For example, the coil and its driver can handle rapid on–off cycling without performance loss. The result is a dramatically reduced average power consumption and heat generation, which is crucial for a battery- or solar-powered mobile unit [3, 30].

Because of this operational pattern, the thermal control can take advantage of passive cooldown during off-periods. The spacecraft's structure often serves as a temporary heat sink. For example, a rover's chassis or a dedicated thermal mass (like a phase-change heat storage material) can absorb the coil's burst of heat when the shield is active. Once the coil is cycled off or throttled down, that stored heat then conducts to small radiators or is dissipated via convection (if in an atmosphere) over a longer period. The design essentially separates peak heat generation from heat rejection in time. As a result, peak loads are buffered, and the heat is bled off during subsequent low-power phases [29]. This approach allows the use of relatively small radiators on the vehicle sized for the time-averaged heat load rather than the instantaneous peak. For instance, if the coil dumps 5 kW of heat during a short active period, a thermal buffer (such as a wax phase-change material or the aluminum structure) might absorb that energy. Then a 500 W radiator can gradually reject it over the next hour. The rover thereby avoids carrying a huge radiator needed for continuous 5 kW dissipation. Any active cooling hardware on a mobile craft is similarly lightweight: perhaps fans or pumps to circulate coolant through the coil housing and then to a radiator when needed. These can be activated during cool-down periods to expedite heat removal [34].

In some cases, if the mobile platform is planetary (with an atmosphere), designers can exploit convective cooling or even thermal dumping to the environment. For example, venting heat through a fluid loop to an external radiator when the rover is parked in the cold night or using the vehicle's life-support cooling system to piggyback on (transferring some shield heat to the astronaut cabin's cooling loop if capacity allows). All these approaches are both passive and active in dealing with intermittent heat loads effectively [34].

Mobile systems are also covered with thermal coating and insulation, but more stress is put on robustness in a changing environment. Coiling of the shield may be insulated against heat transfer to other vehicle parts and early cooling may be desired when beneficial (e.g. leakage of heat to undesirable components by too rapid cooling, instead of undue heat stress due to too slow cooling). Conversely, the exterior of radiators or heat exchangers on the vehicle uses high-emissivity coatings to maximize heat dumping when exposed to the night sky or space. In the case where the vehicle has been driven under direct sunlight, reflective paints can be used so that the thermal gain on the exterior is non-significant and the only thermal concerned is the coil itself [31].

Essentially the thermal control attempts to bring about a equilibrium. It stores heat when ambient temperature is low (so as not to overcool the coil at times of non-use, potentially causing thermal cycling fatigue) and cools off aggressively when the coil is newly hot. This can be in form of dynamic thermal louver systems or intelligent radiators that can be programmed.

Consider, a surface with variable emissivity or radiator panels can be deployed that, only perhaps under heat dumping, become exposed but are then retracted (tested by overcooling or by dust contamination coating a rover in a rover scenario). These innovative ideas explain the consistency of passive and active thermal control that is tuned with a dynamic profile [34].

Mobile shields have operational procedures that give pre-eminence to thermal safety and system durability. The control software controls the temperature of coils and will impose limits.

Suppose a run of high-power operation is pushing the coil towards an unsafe temperature. In that case, it is possible to automatically reduce the current being drawn or worse still turn off the magnet completely in the system to avoid overheating. This kind of thermal foldback or throttling ensures that the shield will not self-damage even if an astronaut demands a duty cycle that is too high [29]. The crew might receive a warning, or an override could be in place if radiation levels are life-threatening, but in most scenarios a brief interruption in magnetic shielding is acceptable compared to a potential coil failure. In worst-case thermal stress (e.g., the vehicle is caught in an unexpected radiation surge that requires the shield at full power at the hottest part of the day), the system's design margins come into play. The coil and power electronics are typically rated to handle short-term thermal excursions (e.g., the insulation and coil materials can sustain a higher temperature for a limited time). A thermal mass gives the system a buffer, and the vehicle may act as an emergency measure, to seek shade, to augment cooling (by orienting radiators upside down or by circulating coolant more vigorously), or to base return [4, 29].

The lightweight yet intelligent design of the thermostat gives the shield system stability at its operating level. It is capable of taking in and jettisoning intermittent heat loads without breakdown and that of recovering rapidly as soon as the burst of high-load is over. Control of power is achieved by the elimination of a large constantly-on cooling system; power is consumed only during short periods when the cooling system is operating actively (e.g., by turning on a pump or fan). The overall result is that the mobile active shield is shielded when needed by the crew and is thermally/electrically idle when not. This prolongs the working time of the vehicle by conserving energy and avoids the problem of overheating that might cut off a mission. This operational principle of duty cycling and real-time modulation is is expressly suggested to functional compatibility between AMF systems in the literature, and that in this case (although operating with spacecraft subsystems), simply running the magnetic field when needed significantly minimizes unintended exposure, in either case, undesirable thermal and power stress of the submission system undesirably [30].

Overall, across the three mission scenarios, a unifying theme of integrated passive–active thermal management optimized for the mission profile is seen. Short missions keep it simple, using the mission's brevity and existing radiative capacity to handle coil heat with minimal active intervention. Long-duration habitats invest in advanced cooling and large passive shields, marrying the two to continuously protect crews with sustainable power usage and strong fail-safes. Mobile explorers embrace flexibility, which relies on operational strategies and clever use of vehicle resources to manage heat in bursts. In all cases, these strategies lead to measurable and repeatable performance gains: significant power savings compared to naïve always-on cooling (especially by leveraging superconductors and passive cooling), high heat dissipation rates achieved by optimized radiators and coatings, ample thermal safety margins ensured by design (negative heat loads, redundant cooling, and automated throttling to stay within limits), and operational resilience that allows the radiation shielding to remain effective under worst-case thermal stress without catastrophic failure. These thermal and operational management solutions form the backbone that enables active radiation shielding systems to function reliably in their respective mission environments [29, 30].

12.19 Radiation Environment and Bioengineered Mitigations

12.19.1 Integrated Characterization of the Space Radiation Environment

The radiation environment characterization, detailed in Chapters 1 and 9, emphasizes the multidimensional challenge spacecraft faces in deep-space missions. Chapter 1 consolidates mission-phase modeling and empirical data from Mars transit analogs, which shows that cumulative doses in a typical Mars mission (~3.4 Sv total mission dose) significantly exceed NASA's 600 mSv career limit without mitigation. Critical findings highlight that approximately 95% of the total dose arises from chronic exposure to high-energy Galactic Cosmic Rays (GCR), with acute spikes contributed by Solar Particle Events (SPEs) during cruise phases. Statistical modeling further identifies a dominant high-dose cluster (~300–350 µGy/day) during cruise, underscoring the necessity of steady-state and transient mitigation measures.

Chapters 6 and 9 expand upon this by highlighting the secondary radiation and charging effects induced by artificial magnetic shielding systems. The deployment of AMF systems creates a localized plasma interaction zone, which results in spacecraft surface charging, plasma turbulence, and secondary particle generation. These phenomena affect radiation dose directly and introduce complex operational hazards, validating the need for a multi-tiered shielding and mitigation strategy.

These findings justify the integrated AMF system-of-systems architecture by confirming that no single passive, active, or operational mitigation pathway can adequately address the diverse radiation environment. Rather, a hybrid measure should be undertaken, in which physical mitigation strategies to minimize the particle flux will be implemented and bioengineered mitigation to settle the residual biological harm which cannot be avoided.

12.19.2 Human-in-the-Loop Bioengineered Countermeasures

Chapter 11 highlights the critical role of Human-in-the-Loop (HITL) systems and bioengineered interventions in deep-space radiation protection. Real-time adaptive control mechanisms embedded in the AMF system dynamically respond to plasma instabilities and SPE warnings, ensuring that field strength and operational modes are optimized as conditions change.

This human-in-the-loop architecture extends beyond mechanical controls to encompass biological safeguards.

Chapter 11 identifies three layers of bioengineered countermeasures:

1. **Pharmacological Radioprotectants:** Agents such as DNA repair enhancers, radioprotective antioxidants, and anti-inflammatory compounds are incorporated as a pharmacological layer designed to mitigate biological damage from residual GCR and secondary radiation exposure. One of the most crucial uses of these countermeasures is at the mission phase when there is a strain on operational factors that prevent complete shielding (e.g. periods of high propulsion thrust when AMF has to be throttled to a minimum).
2. **Adaptive Operational Protocols:** Real-time dosimetry feeds operational decisions which enable crew relocation to storm shelters during SPEs, temporary reduction of high-energy activities during elevated GCR periods, and optimization of AMF field cycling to avoid prolonged surface charging. These dynamic operational responses are facilitated through MBSE-derived state machine architectures that enforce safety thresholds and trigger crew protocols when predefined dose rates or charging parameters are exceeded.
3. **Biologically Inspired Shielding Strategies:** Materials based on bioengineered composites (e.g., BNNT with additional biological agents or neutron stutterers), are also thought of as belonging to the passive shielding scheme that can make stepwise mechanical integrity and radiation protection improvements without causing hefty mass penalty.

These measures introduce a holistic human-centric radiation protection strategy that integrates predictive radiation environment modeling with proactive biological countermeasures and responsive operational controls. This multi-faceted approach reduces acute and chronic radiation risks and enhances system survivability under off-nominal scenarios where environmental variances or AMF system anomalies could otherwise elevate crew exposure [35].

12.19.3 Radiation Environment Characterization and Countermeasure Strategy

This study integrates both system-level shielding approaches and operationally driven countermeasures to address the complex and multi-phase radiation hazards inherent in deep-space missions. Building on the detailed modeling results from Chapters 1 and 9, which highlight the predominance of chronic Galactic Cosmic Ray (GCR) exposure and episodic Solar Particle Events (SPEs), along with plasma-induced secondary effects from active shielding systems, a tiered mitigation approach was developed. This approach combines physical shielding (active and passive systems) with bioengineered and human-in-the-loop operational strategies [36].

A key emphasis is placed on adaptive operational protocols. This leverages real-time dosimetry, radiation environment forecasting, and crew activity scheduling to minimize biological radiation impacts during critical mission phases. Pharmacological interventions and advanced bioengineered materials provide supplemental protection, especially during residual exposure scenarios where operational adjustments alone are insufficient [36].

The table below summarizes the primary radiation environment components, their operationally significant characteristics, and the corresponding mitigation strategies, including how these approaches are integrated into mission-phase planning.

Table 12. 14: Summary of Radiation Environment and Mitigation Strategies with Operational and Bioengineered Countermeasures

Radiation Environment Component	Characterization Summary	Primary Mitigation Methods	Operational and Bioengineered Countermeasures
Galactic Cosmic Rays (GCR)	• Persistent, high-energy omnidirectional particle flux (~300–350 μGy/day during cruise). • Dominant contributor to cumulative mission dose.	• Continuous AMF operation (≥1.5 T for habitats). • Hydrogen-rich passive shielding.	• Operational protocols for optimized AMF cycling (e.g., reduced field during low flux periods, enhanced during GCR peaks). • Crew shift rotations and task scheduling to limit high-activity periods during peak radiation. • Supplemental: Pharmaceuticals (DNA repair boosters) for unavoidable chronic exposure.
Solar Particle Events (SPE)	• Intense, short-duration proton flux spikes during solar maximum.	• Surge-capable AMF systems. • High-mass storm shelters.	• Real-time monitoring triggering automated crew alerts and shelter-in-place procedures. Delayed EVAs and operational rescheduling to avoid activity during SPE spikes. Minimal pharmaceutical intervention (focused on post-exposure care).
Secondary Radiation & Charging Effects	• Local plasma sheaths, surface charging, ESD hazards induced by AMF.	• Optimized AMF geometries (rotating fields), localized passive shielding.	• Proactive charge dissipation cycles (automated DEG_CMD triggers). Task avoidance periods during high field-strength cycles to limit ESD risk. Continuous charge monitoring with operational abort options.
Residual Biological Dose	• Chronic low-level exposure persists despite shielding.	• AMF-passive hybrid configuration.	• Dose-aware crew activity scheduling (reduced workload during peak flux periods). Augmented in-mission health monitoring and biofeedback

Radiation Environment Component	Characterization Summary	Primary Mitigation Methods	Operational and Bioengineered Countermeasures
			systems to track early radiation effects. Supplementary pharma reserved for threshold exceedances, not as routine countermeasure.
Mars Surface Radiation	• GCR plus enhanced secondary neutron generation from regolith. • SPE risk persists.	• Regolith shielding ($\geq$10–15 g/cm^2), BNNT/PE-lined habitats.	• Daytime EVA limitations, night-shift scheduling where feasible. Use of terrain features for localized shielding during surface ops. Minimal continuous pharmaceutical reliance, primarily for acute events.
Interplanetary Transit	• Peak cumulative radiation exposure phase without natural shielding.	• Full active-passive AMF deployment. Strategic internal mass placement.	• Predictive radiation modeling integrated with mission planning (adjusted cruise paths, propulsion timing). Adaptive habitat layout adjustments (rotating crew bunk areas to lower cumulative dose per individual). Pharmaceuticals only for post-event biological support, not as frontline mitigation.

The integrated mitigation strategy highlights that while active and passive shielding systems provide foundational radiation reduction, operational countermeasures are indispensable in managing variable space radiation threats. Real-time monitoring, adaptive field control, strategic activity scheduling, and operational protocols (such as shelter-in-place procedures and EVA rescheduling) collectively ensure exposure remains within acceptable limits during high-risk events [35]. Bioengineered approaches, including advanced shielding materials and selective pharmacological interventions, serve as secondary layers of defense, enhancing resilience during both acute and chronic radiation exposure phases. This holistic framework, grounded in mission-phase risk differentiation, maximizes protection while maintaining operational flexibility and system efficiency across diverse mission profiles [35].

12.20 Verification, Validation, and Real-World Implementation

To ensure the robustness of the proposed hybrid radiation shielding architecture, a multi-pronged verification and validation (V&V) strategy was implemented, combining analytical modeling, simulation-based verification, and operational scenario evaluation.

First, physics-based simulation techniques, including FLUKA Monte Carlo radiation transport modeling and magnetic field finite element analysis, were used to verify shielding performance under expected deep-space radiation conditions. These simulations quantitatively validated dose reduction projections for both passive and active shielding components across GCR and SPE spectra, establishing direct alignment with mission-specific dose constraints outlined in Chapters 1 and 9.

Second, Model-Based Systems Engineering (MBSE) methods were applied to trace the full lifecycle of system verification. SysML parametric diagrams modeled constraint relationships between design parameters (e.g., coil current, passive shield thickness) and mission performance metrics (dose reduction, power draw), allowing dynamic trade-off and margin analysis. Verification linkages were maintained throughout the model via requirement traceability matrices, which connect high-level radiation limits to subsystem-level design parameters and verification activities. Chapter 9’s down-selection methodology established V&V checkpoints for each configuration scenario, ensuring that sensitivity-driven design decisions were validated against both dose targets and resource constraints.

Third, human-in-the-loop (HITL) operational validation complemented technical performance verification. Operational scenarios were evaluated using SysML activity diagrams to validate crew–system interaction pathways. Behavioral models simulated automated alerting, shield mode transitions, and manual crew override responses, verifying that operational protocols maintain radiation protection during nominal and off-nominal events. This scenario-based validation ensured the hybrid system satisfies technical dose reduction requirements and operational safety, autonomy, and adaptability criteria essential for real-world deployment.

The following Verification and Validation Process Flow for the Hybrid AMF Shielding System, Figure 12.7, illustrates the sequential and iterative steps of the V&V process, combining simulation, analytical, hardware, and operational scenario validations within an MBSE framework to ensure readiness for mission deployment.

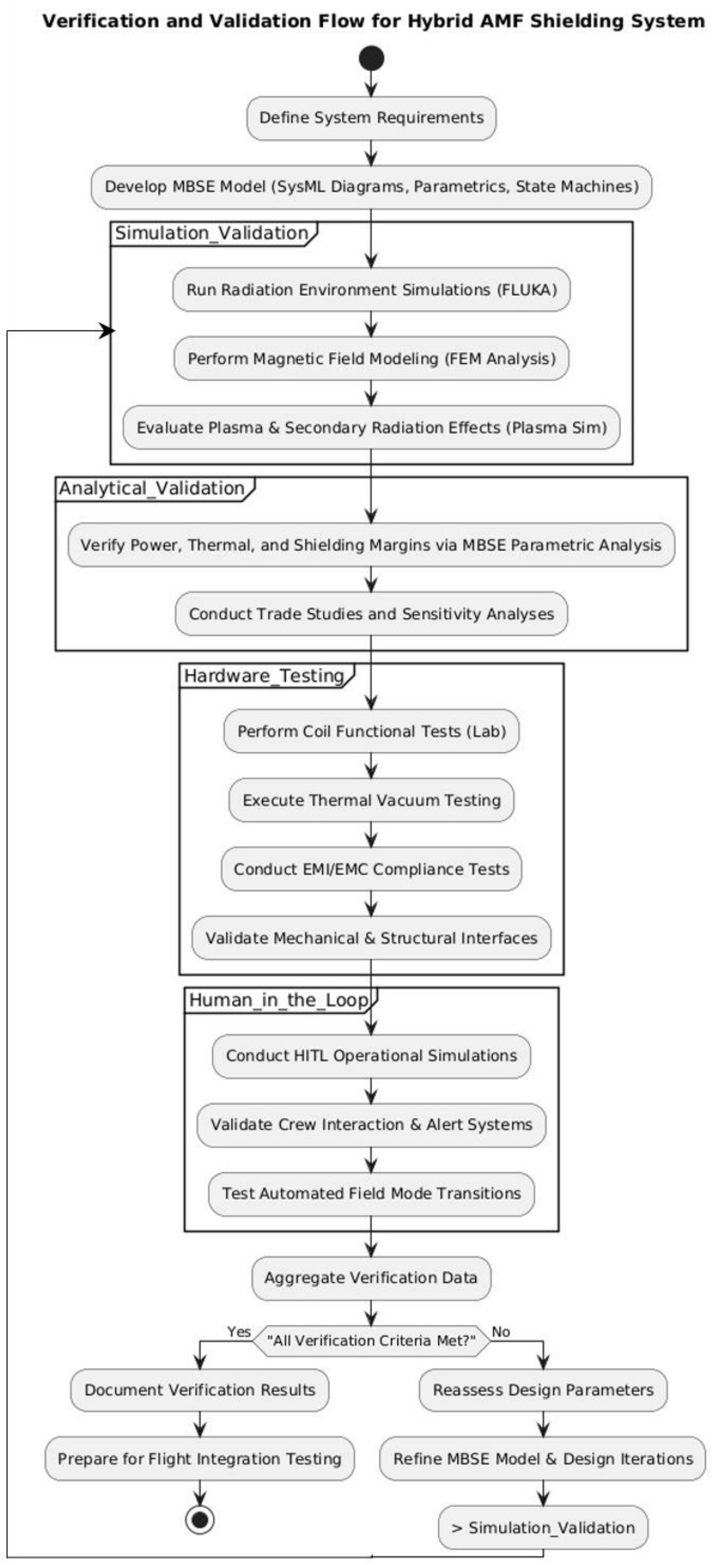

Figure 12.7: Verification and Validation Process Flow for the Hybrid Artificial Magnetic Field (AMF) Shielding System [37].

The Verification and Validation (V&V) process for the hybrid shielding system follows a structured, multi-tiered approach to ensure technical robustness and operational readiness. Figure 12.7 summarizes this integrated methodology beginning with baseline requirement definition and MBSE model development, followed by simulation-based verification of shielding performance, parametric trade studies, and progressive validation through hardware testing and operational scenario walkthroughs [37].

The V&V strategy incorporates closed-loop feedback whereby any design deviations or failures to meet verification thresholds result in targeted refinement of design parameters and MBSE updates with subsequent re-entry into the simulation validation cycle. This ensures no subsystem proceeds to flight readiness without quantitative verification of its performance margins and operational compatibility. The holistic approach guarantees that the system satisfies shielding effectiveness, thermal and power limits, electromagnetic compatibility, and human factors usability across all mission phases and contingencies [37].

12.20.1 Operational Recommendations

Based on the integrated analysis, the following operational guidance is recommended for real-world implementation of hybrid shielding systems [39]:

- **Mission-Adapted Shielding Modes**: Field intensity and passive shielding configurations should be tailored to the mission phase. For short-duration sorties, minimal passive layers and standby-mode magnetic shielding suffice. Full-time superconducting magnetic fields with enhanced passive mass are required for long-duration habitats. For mobile exploration missions, dynamic field modulation provides optimal flexibility.
- **Adaptive Control Protocols**: Active magnetic shielding should be integrated with environmental sensors and HITL controls, enabling real-time threat detection and

automated shielding response, with manual override capacity for operational contingencies. Automated safe modes and fallback protocols (e.g., emergency field surge during SPE) must be embedded into flight software.

- **Thermal and Power Budget Integration**: Shielding systems must be co-designed with thermal rejection capacity and power generation plans. Radiator sizing, coil cooling mechanisms, and power margin allocation must be verified for worst-case operational scenarios. Specific thermal contingencies (e.g., forced quench recovery, emergency coil shutdown) are essential for operational resilience.
- **Pre-Flight and In-Situ Testing**: Hardware components, particularly novel superconducting coils and rotating-field architectures, require ground-based thermal-vacuum and electromagnetic interference testing before deployment. Subscale flight demonstrations of active shielding subsystems are recommended to elevate TRL before mission-critical integration.
- **Crew Training and Protocol Integration**: Crew members should be trained on shielding system operational modes, failure contingencies, and biological countermeasures with mission protocols embedding proactive radiation threat monitoring and countermeasure deployment procedures, as validated in Chapter 11.

The proposed shielding architecture transitions from simulation-validated design to a mission-ready system through this verification and operational framework. This includes traceable performance assurances, robust operational safeguards, and adaptability across multiple mission profiles. The following table (Table 12.15) illustrates an expanded verification approach based on requirements [40].

Table 12. 15: Expanded Verification Approach with Sample Methods

Requirement Category	Example Requirement	Verification Method	Verification Approach
Radiation Shielding Performance	RQ-1.3.1: System shall reduce GCR dose rate by ≥80%.	Analysis, Test	FLUKA Monte Carlo simulations for dose rate projections; post-integration dosimetry validation via radiation detector arrays during system functional test.
Power Management Compliance	RQ-2.2.4: Steady-state power draw under Full Shielding Mode shall not exceed 50 kW.	Analysis, Test	Power budget modeling in MBSE parametrics; ground functional testing under worst-case field intensities.
Thermal Stability and Management	RQ-2.4.2: Coil operational temperature shall remain within 20% of max rated limits during nominal operation.	Analysis, Test	Thermal balance simulation (e.g., COMSOL or Thermal Desktop); thermal-vacuum chamber testing of coil assembly under nominal power conditions.
Control Responsiveness	RQ-3.4.3: Automated hazard response shall execute within <500 ms.	Test, Simulation	System-in-the-loop latency testing with synthetic radiation events; simulation-based timing validation in MBSE state diagrams.
Plasma Interaction Mitigation	RQ-3.3.7: System shall suppress induced plasma charging to <100 V.	Simulation, Analysis	Plasma chamber testing (for hardware component validation); orbit environment plasma simulations with ANSYS Plasma PIC.
Electromagnetic Compatibility (EMC)	RQ-5.1.1: Radiated EMI shall not exceed 55 dBμV/m at 1 m distance.	Test, Analysis	EMC compliance testing per MIL-STD-461; spectrum analysis in anechoic chamber during high-intensity AMF operation.
Degaussing and Field Collapse	RQ-5.4.2: Magnetic field decay to <1% within 10 seconds with <100 mV transient.	Test, Analysis	Oscilloscope capture during field shutdown in EMI-safe lab; Ansys Maxwell transient simulation for pre-test predictions.
System Fault Tolerance	RQ-4.2.1: Power loss recovery in <250 ms with backup systems.	Test, Simulation	Power failover testing with telemetry capture; MBSE-based operational flow

Requirement Category	Example Requirement	Verification Method	Verification Approach
			validation of transition to safe mode.
Human-in-the-Loop Usability	RQ-3.1.1: Crew UI shall provide radiation alert within 5 seconds of threshold breach.	Test, Human Factors Analysis	Human-in-the-loop interface testing with simulated radiation events; response latency logging and crew cognitive workload assessment.
Mission Adaptability	RQ-6.1.1: System shall enable three field modes (Full, Standby, Off) selectable in <60 s.	Test, Simulation	Mode transition tests during operational runs; MBSE state machine simulation for valid mode transitions and transitions timing.

The system verification matrix utilizes a balanced distribution of simulation-driven design validation, test-based subsystem certification, and operational scenario walkthroughs. Analysis methods primarily cover high-complexity phenomena (e.g., radiation propagation, plasma effects), whereas physical testing validates critical performance parameters (e.g., EMI limits, power draw, response times). MBSE simulation pathways trace dynamic behavior validations, ensuring scenario compliance for fault-tolerance and crew interaction protocols. This multi-method approach establishes high confidence in system readiness across both nominal and off-nominal mission profiles [39].

The verification strategy for the hybrid shielding architecture employs a layered approach, combining simulation analysis and operational scenario validation to ensure end-to-end system robustness. High-fidelity radiation transport simulations (e.g., FLUKA) and electromagnetic field models establish baseline performance predictions for shielding effectiveness, power consumption, and thermal stability. Targeted laboratory testing, including thermal vacuum trials, EMI chamber evaluations, and coil functional testing, validates critical hardware-level behaviors against design specifications. Human-in-the-loop (HITL) validation through simulated operational scenarios further verifies the responsiveness and usability of crew interfaces and autonomous system controls during nominal and contingency conditions. These verification methods are structured within a Model-Based Systems Engineering (MBSE) framework, which links each requirement to its corresponding verification activity via traceable SysML artifacts. This integrated verification approach ensures both analytical and empirical validation of the shielding system across mission phases, providing a defensible path toward flight readiness and operational reliability [38].

12.21 Proposed Functional Experiments for Validation of Dissertation Concepts

In addition to identifying optimal shielding strategies for different mission profiles, it is equally important to consider how these findings might be empirically validated. Although the present research has relied primarily on modeling, simulation, and systems analysis, each proposed architecture requires experimental confirmation to establish feasibility and operational credibility. The following section outlines representative functional experiments, ranging from materials testing and active field prototypes to biological assays and spacecraft subsystem trials.

These could be pursued as logical extensions of this work. These experiments are not performed here but are defined to demonstrate a clear pathway by which the concepts developed in this dissertation can be verified and matured toward practical implementation [41].

12.21.1 Passive Shielding Experiments

Fundamental verification of materials-based shielding requires irradiation trials under controlled conditions. Candidate materials such as aluminum, polyethylene, boron nitride nanotube (BNNT) composites, and regolith simulants could be exposed to charged particle beams at accelerator facilities such as NASA's Space Radiation Laboratory (NSRL) [41].

Measurements of absorbed dose, linear energy transfer (LET) spectra, and secondary neutron production would provide a direct comparison with FLUKA-based dose predictions presented in Chapters 1 and 6 [41]. Additional trials with layered configurations (e.g., aluminum hull beneath hydrogen-rich liners) would quantify the degree of secondary suppression relative to single-material baselines. Such experiments would validate the material hierarchy discussed in Chapter 8 and confirm the neutron capture efficiency of boron-loaded composites [42].

12.21.2 Active Magnetic Shield Experiments

The viability of artificial magnetic field (AMF) systems can be advanced through scaled laboratory prototypes. Both resistive and superconducting bench-scale electromagnetic coils may be fabricated to map achievable field topologies, thermal loads, and current stability under sustained operation. A dynamic testbed employing a three-coil rotating toroidal array would enable experimental confirmation of the deflection patterns modeled in Chapter 2. Hall-effect sensor grids and charged particle beams could be used to validate field geometries and shielding effectiveness [18]. Complementary plasma chamber experiments would further test the stability of magnetohydrodynamic “mini-magnetospheres,” directly addressing the integration challenges identified in Chapter 3 [43].

12.21.3 Hybrid Shielding Experiments

Hybrid configurations, which are combinations of magnetic coils with passive hydrogen-rich layers, warrant integrated experimental evaluation. A representative setup could involve surrounding a powered coil with polyethylene or BNNT panels, followed by irradiation with heavy ions. Dose detectors downstream would quantify secondary neutron flux reduction, validating synergistic protection effects modeled in Chapter 7 [44]. Similarly, experiments layering electrostatic charged plates with magnetic fields would provide insight into cross-system interactions and confirm the potential for spectrum-wide mitigation through multimodal shielding [45].

12.21.4 Biological and Biomedical Experiments

Radiobiological testing offers the most direct measure of shielding efficacy on living systems. Microbial models such as *Escherichia coli* and *Saccharomyces cerevisiae* could be irradiated under different shielding configurations to assess DNA double-strand break frequency, mutation rates, and cell survival. These data would allow comparison with the FLUKA/BioDynaMo simulation outputs reported in Chapters 1 and 10 [46]. Additionally, *in vitro* studies with mammalian cell lines and pharmacological agents (e.g., antioxidants or DNA repair stimulators) could establish the degree of biological dose mitigation when shielding is supplemented by radioprotective compounds [47]. These experiments would directly support the integrated biomedical countermeasure strategies highlighted in Section 12.1.

12.21.5 Systems-Level and Operational Experiments

Finally, validation must extend to spacecraft-scale considerations. Prototype storm shelters constructed with polyethylene and water tanks could be subjected to proton beam irradiation to quantify their Solar Particle Event (SPE) dose reduction performance, complementing Chapter 1’s probabilistic SPE analysis [6]. Electromagnetic compatibility (EMC) experiments involving avionics boards exposed to time-varying magnetic fields would validate the EMI/EMC concerns raised in Chapter 5 [48]. Thermal management demonstrations with operating laboratory-scale coils in vacuum chambers equipped with radiator panels would provide real data on heat rejection efficiency and quench recovery, informing the thermal design assumptions used throughout Chapters 4 and 8 [49].

The experimental pathways outlined above establish a comprehensive validation framework spanning materials, active systems, hybrid architectures, biological effects, and operational subsystems. Together, they represent the logical next phase of inquiry required to transition this dissertation's theoretical and computational analyses into empirically validated shielding solutions.

Dissertation Conclusion

In conclusion, this research tested four core hypotheses regarding the necessity and integration of active, passive, and biological radiation shielding for long-duration missions. Each hypothesis is evaluated against the findings from Chapters 1–11 and supporting simulations:

1. **AMF shielding is essential and scalable for long-duration space missions.** The dissertation's results strongly support this hypothesis. High-field AMF shields proved crucial for reducing deep-space radiation to acceptable levels in a way that purely passive shielding alone could not achieve. For a multi-year Mars-class mission, simulations showed that a superconducting dipole magnet (1–2 T) around the habitat can deflect approximately 95–98% of solar protons and approximately 80% of GCR heavy ions. This magnetic protection distinguished between exceeding NASA's career dose limits and keeping astronaut exposure within tolerable risk levels. Only the mission scenario with a powerful AMF (along with supplemental material shielding) kept the total crew dose (~0.38 Sv) under the ~0.6 Sv threshold. On the other hand, scenarios without AMF resulted in 2–3× higher exposures (0.79–1.3 Sv), well above limits. These quantitative outcomes confirm that an active magnetic shield is essential for long-duration missions, providing scalable coverage of the spacecraft and crew habitat that would be infeasible to replicate with material mass alone. The research demonstrated that AMF systems can be

scaled to protect large volumes (e.g., an Orion-sized module) when using superconducting technology, given sufficient power and thermal management. Thus, Hypothesis 1 is supported: AMF shielding is a necessary and scalable cornerstone of any deep-space radiation protection strategy for prolonged missions.

2. **Integrating AMF into spacecraft introduces complex engineering challenges requiring structured systems engineering.** The findings affirm this hypothesis, highlighting that deploying an AMF shield is an intricate system-of-systems problem. Chapters 4–5 and 8 revealed that an active magnetic shield must seamlessly integrate subsystems for power supply, cryogenic cooling, magnet control, structural support, and safety monitoring. Any failure in these interdependent elements (e.g., a quench in the superconducting coil, a power spike, or thermal runaway) could collapse the protective field and abruptly expose the crew. This research showed that such complexity demands a rigorous systems engineering approach. By employing MBSE models, all interfaces and failure modes were systematically analyzed and mitigated. For example, the design incorporated redundancies and control safeguards (identified via FMEA and implemented in the SysML model) to ensure no single-point failure would be catastrophic. Electromagnetic interference (EMI) with other spacecraft electronics was proactively managed by design requirements in the model, and thermal loads were handled through integrated thermal-control loops (e.g., multiple cryocoolers with backup capacity). This dissertation's successful development and validation of the AMF system underscore that a structured and top-down engineering process was essential. The need for careful requirements management, trade-off analysis, and verification (all facilitated by MBSE) became evident in addressing the AMF's challenges, including high power consumption,

intense magnetic forces, EMI/EMC risks, and reliability concerns. Hypothesis 2 is therefore strongly supported. Integrating an AMF shield requires a disciplined systems engineering approach, and this study's use of such methods was vital to surmount the AMF integration challenges.

3. **Passive shielding is indispensable for neutral particle mitigation.** The research confirms that passive material shielding remains an irreplaceable component of space radiation protection, validating this hypothesis. While active fields excel against charged particles, they do not stop neutral radiation (neutrons, gamma rays) and can even generate secondary radiation when deflecting ions. Chapters 6 and 8 showed that high-Z structural materials like aluminum produce copious secondary neutrons under GCR bombardment. On the other hand, hydrogen-rich materials like polyethylene significantly reduce this secondary output. Accordingly, the optimized designs in the study always included a layer of passive shielding to absorb the radiation that magnetic or electric fields cannot deflect. In the long-duration habitat scenario, approximately 4.5 kg/m^2 of polyethylene composite around the crew module was added alongside the AMF, effectively capturing many neutrons and fragmented ions that penetrated or skirted the magnetic field. This passive layer was critical for soaking up secondary radiation and protecting against the full spectrum of GCR and SPE byproducts. Furthermore, passive shielding provides a fail-safe baseline of protection that is always "on," which is crucial given that active systems can be turned off or could fail. The comparative analysis concluded that no active system should stand alone; even a strong magnet must be augmented with material shielding to ensure comprehensive high-energy neutrons and photons coverage. Therefore, Hypothesis 3 is fully supported: passive shielding is indispensable for

mitigating neutral particles and secondary radiation. The multi-layered designs developed in this work leveraged passive materials (e.g., polyethylene, water, BNNT composites) as a necessary foundation that complements the AMF by addressing radiation components beyond the reach of magnetic deflection.

4. **Bioengineered countermeasures enhance astronaut resilience and are essential complements to physical shielding.** The dissertation's findings support this hypothesis, recognizing biological countermeasures as a vital supplementary line of defense. Even with advanced active and passive shields, deep-space missions may expose crews to cumulative doses approaching or exceeding recommended limits; increasing the human body's tolerance to radiation becomes crucial. This research reviewed and simulated various biotechnological and pharmacological strategies such as antioxidant administration, DNA repair enhancement, and altered dietary regimes that can mitigate radiation damage at the cellular level. The consensus from the analysis is that these measures can significantly reduce health risks when used in conjunction with physical shielding. For example, antioxidants and radioprotective drugs were found to potentially lower the incidence of DNA damage and improve recovery from radiation exposure, aligning with experimental evidence that such countermeasures lessen oxidative stress and genetic lesions in cells exposed to space-like radiation. In Chapter 1's Mars mission dose modeling, even the best shielding configuration (85% dose reduction) still benefited from pharmacological countermeasures to keep astronaut risk within acceptable margins. Furthermore, the study's biological simulations (comparing radiation responses of model organisms *E. coli* and *S. cerevisiae*) illustrated the potential of leveraging biological resilience: *S. cerevisiae*, with its robust DNA repair and antioxidant systems, sustained

significantly less genomic damage under radiation stress than *E. coli*, suggesting that enhancing human cellular repair pathways or using engineered microbes (e.g., probiotic bacteria producing antioxidants) could bolster crew health. These findings reinforce that bioengineered and operational countermeasures (such as radioprotective compounds, gene therapies, tailored nutrition, and regenerative medical protocols) are important complements to shielding. They address the fraction of radiation that inevitably reaches astronauts despite physical shields. However, this study also recognizes that such biological strategies are supplementary, meaning they cannot replace the primary need to block or deflect radiation, but they enhance overall mission resilience by protecting the crew from the inside out. Thus, Hypothesis 4 is supported: augmenting physical shields with bioengineered solutions improves astronaut safety and mission feasibility for long-duration exploration.

Overall, the conclusion drawn from this doctoral research is that all three modalities, active magnetic fields, passive materials, and biomedical countermeasures, must work in concert to achieve safe long-term human spaceflight. Each hypothesis is validated in the context of a multi-layered approach. AMF systems provide scalable, mass-efficient shielding but require careful engineering. Passive shields remain mandatory to stop neutrals and serve as a constant safeguard.

Biotechnological measures add a critical extra margin of protection for crew health. In combination, these strategies yield a radiation protection system that significantly outperforms any single method. The dissertation's integrated findings strongly advocate for this synergistic shielding paradigm. By quantitatively demonstrating how a "belt-and-suspenders" solution (e.g., a superconducting magnet + hydrogenous shielding + radioprotective agents) can keep deep-space radiation exposure within permissible limits, this work provides a compelling framework for future mission design. It concludes that long-duration missions, such as a crewed Mars expedition or orbital habitat, are only viable when radiation protection is addressed as a comprehensive, systems-engineered challenge, one that combines technological innovation with biological safeguards to ensure astronaut safety and mission success in the harsh radiation environment of space.

References

Introduction References

1. Cucinotta, F. A., Kim, M. H. Y., & Ren, L. (2006). *Managing lunar and Mars mission radiation risks part I: Cancer risks, uncertainties, and shielding effectiveness*. NASA Technical Paper 2006-214759. https://ntrs.nasa.gov/api/citations/20060043143/downloads/20060043143.pdf
2. Chancellor, J. C., Blue, R. S., & Cengel, K. A. (2018). Space radiation: The number one risk to astronaut health beyond low Earth orbit. *Life*, *8*(4), Article 38. https://doi.org/10.3390/life8040038
3. Simonsen, L. C., Slaba, T. C., Guida, P., & Rusek, A. (2020). NASA's first ground-based galactic cosmic ray simulator: Enabling a new era in space radiobiology research. *PLOS Biology*, *18*(5), Article e3000669. https://doi.org/10.1371/journal.pbio.3000669
4. Wilson, J. W., Miller, J., Konradi, A., & Cucinotta, F. A. (Eds.). (1997). *Shielding strategies for human space exploration*. NASA Conference Publication 3360. https://ntrs.nasa.gov/api/citations/19980007430/downloads/19980007430.pdf
5. Spillantini, P., Casolino, M., Durante, M., Mueller-Mellin, R., Reitz, G., Rossi, L., & Sorbi, M. (2007). Shielding from cosmic radiation for interplanetary missions: Active and passive methods. *Radiation Measurements*, *42*(1), 14–23. https://doi.org/10.1016/j.radmeas.2006.06.008
6. Cekanaviciute, E., Rosi, S., & Ramkumar, N. (2018). Preventing space radiation-induced neurocognitive decline. *Frontiers in Physiology*, *9*, Article 217. https://doi.org/10.3389/fphys.2018.00217
7. De Weck, O. L., Roos, D., & Magee, C. L. (2011). *Engineering systems: Meeting human needs in a complex technological world*. MIT Press.
8. Agostinelli, S., Allison, J., Amako, K., Apostolakis, J., Araujo, H., Arce, P.,... & Yoshida, H. (2003). GEANT4, a simulation toolkit. *Nuclear Instruments and Methods in Physics Research Section A: Accelerators, Spectrometers, Detectors and Associated Equipment*, *506*(3), 250–303. https://doi.org/10.1016/S0168-9002(03)01368-8
9. NASA Space Radiation Laboratory. (n.d.). *NASA Space Radiation Laboratory*. Brookhaven National Laboratory. https://www.bnl.gov/nsrl/
10. Townsend, L. W. (2005). Implications of the space radiation environment for human exploration in deep space. *Radiation Protection Dosimetry*, *115*(1–4), 44–50. https://doi.org/10.1093/rpd/nci236
11. Baker, C. J., & Simske, S. J. (2024). *Extension to critical analysis of active shielding methods for space radiation protection*. InTechOpen. https://www.intechopen.com/online-first/1196475

Literature Review References

1. Townsend, L. W. (2005). Critical analysis of active shielding methods of space radiation protection. In *Proceedings of the 2005 IEEE Aerospace Conference*. IEEE.
2. Tripathi, R. K., Wilson, J. W., & Youngquist, R. C. (2008). Electrostatic space radiation shielding. *Advances in Space Research*, *42*(6), 1043–1049. https://doi.org/10.1016/j.asr.2007.09.015

3. Winglee, R. M., Ziemba, T., Euripides, P., & Slough, J. (2004). *Radiation shielding produced by mini-magnetospheres* (M2P2 study technical report). University of Washington, Department of Earth and Space Sciences.
4. Shepherd, S. G., & Shepherd, J. P. (2008). *A toroidal magnetic spacecraft shield: Considerations of resistive-coil designs for galactic cosmic ray deflection*. Dartmouth College/University of Wisconsin.
5. Battiston, R., Spillantini, P., & Advanced Magnet Lab, Inc. (2012). Concepts for superconducting magnetic shielding of interplanetary spacecraft. In *Advanced Magnetic Lab, Inc./NASA NIAC Phase II technical report: Feasibility of high-temperature superconducting magnets for active radiation shielding*. Advanced Magnet Lab, Inc.
6. Ferrone, K., Willis, C. E., Guan, F., Ma, J., Peterson, L., & Kry, S. (2023). A review of magnetic shielding technology for space radiation. *Radiation*, *3*(1), Article 5. https://doi.org/10.3390/radiation3010005
7. Durante, M., & Cucinotta, F. A. (2011). Physical basis of radiation protection in space travel. *Reviews of Modern Physics*, *83*(4), 1245–1281. https://doi.org/10.1103/RevModPhys.83.1245
8. Wilson, J. W., Badavi, F. F., Shinn, J. L., Cucinotta, F. A., & Nealy, J. E. (1993). *A proposed performance index for galactic cosmic ray shield materials* (NASA Technical Memorandum 19940006806). NASA Langley Research Center.
9. Narici, L., Casolino, M., Di Fino, L., Larosa, M., Picozza, P., & Zaconte, V. (2017). Performance of Kevlar and polyethylene as radiation shielding on board the International Space Station in a high-latitude radiation environment. *Scientific Reports*, *7*, Article 1644. https://doi.org/10.1038/s41598-017-01824-7
10. Guetersloh, S. B., Zeitlin, C. J., Heilbronn, L., Miller, J., Komiyama, T., Fukumura, A., Iwata, Y., Murakami, T., & Blattnig, S. R. (2006). Polyethylene as a radiation shielding standard in simulated cosmic-ray environments. *Nuclear Instruments and Methods in Physics Research B*, *252*(2), 319–332. https://doi.org/10.1016/j.nimb.2006.07.037
11. Rojdev, K., Atwell, W., Rojdev, C., & De la Torre, G. (2009). Space radiation shielding technology development at NASA. In *47th AIAA Aerospace Sciences Meeting* (AIAA 2009–1230). American Institute of Aeronautics and Astronautics.
12. Norman, R. B., Clowdsley, M., Slaba, T., Heilbronn, L., Zeitlin, C., Kenny, S., Crespo, L., Giesy, D., Warner, J., McGirl, N., Castellanos, L., Srikrishna, A., Beach, M., Bahadori, A., & Reddell, B. (2017). Early results from the advanced radiation protection thick galactic cosmic ray (GCR) shielding project. In *Proceedings of the Applied Space Environments Conference* (ASEC 2017) (Public document NF1676L-27179). NASA Langley Research Center.
13. Al Zaman, M. A., & Nizam, Q. M. R. (2022). Study on shielding effectiveness of a combined radiation shield for manned long-term interplanetary expeditions. *Journal of Space Safety Engineering*, *9*(1), 83–89. https://doi.org/10.1016/j.jsse.2021.11.002
14. Guo, J., Slaba, T. C., Zeitlin, C., Wimmer-Schweingruber, R. F., Badavi, F. F., Böhm, E., Böttcher, S., Brinza, D. E., Ehresmann, B., & Hassler, D. (2021). Radiation environment for future human exploration on the Martian surface: modeling and measurement insights. *The European Physical Journal Plus*, *136*, Article 150. https://doi.org/10.1140/epjp/s13360-021-01053-x

15. Wilson, J. W., Cucinotta, F. A., Shinn, J. L., Thibeault, S. A., & Badhwar, G. D. (1995). Issues in deep space radiation protection. *Acta Astronautica*, *36*(6), 443–450. https://doi.org/10.1016/0094-5765(95)00078-P
16. Slaba, T. C., Blattnig, S. R., Norbury, J. W., Rusek, A., La Tessa, C., & Walker, S. A. (2015). *GCR simulator reference field and a spectral approach for laboratory simulation*. NASA Technical Paper 2015-218698.
17. Cucinotta, F. A., Kim, M. Y. H., & Chappell, L. J. (2012). *Evaluating shielding approaches to reduce space radiation cancer risks* (NASA Technical Memorandum 2012-217361). NASA Johnson Space Center.
18. Fogtman, A., Cucinotta, F. A., Casolino, M., Durante, M., Eckerman, K. F., Slaba, T. C., Zeitlin, C., Hassler, D., Kim, M. H. Y., & Patel, Z. (2023). Assessment of radiation exposure and health risks for a 1000-day Mars mission: biological implications and mitigation strategies. *Frontiers in Nuclear Medicine*, *3*, Article 1225034. https://doi.org/10.3389/fnume.2023.1225034
19. Sishc, B. J., & Schippers, T. (2022). Radiation countermeasures for deep space missions: a review of pharmacological and operational strategies. *Life Sciences in Space Research*, *33*, 1–18. https://doi.org/10.1016/j.lssr.2022.04.004
20. John, S. A., Kelly, G. C., & Patel, Z. (2017). *Efficacy of dietary antioxidants in mitigating heavy-ion radiation damage in mice*. NASA Task Book TM 10111.
21. Chauhan, A. P., Morales-Andrade, L., Sinha, R., & Kahn, A. J. (2021). Space radiation protection countermeasures in microgravity and planetary exploration. *Life Sciences in Space Research*, *30*, 25–36. https://doi.org/10.1016/j.lssr.2021.05.006
22. Gómez-Fernández, X., Peñaloza-Villalobos, A., Candelario-Jalil, E., & Orozco-Cabal, L. F. (2021). Key points for the development of antioxidant cocktails to prevent cellular stress and damage caused by reactive oxygen species (ROS) during manned space missions. *npj Microgravity*, *7*, Article 8. https://doi.org/10.1038/s41526-021-00122-1
23. NASA Human Research Program. (2021). *Human adaptation to spaceflight: Nutrition and food systems* (HRP-47090).
24. Landauer, M. R., Davis, T. A., & Singletary, G. W. (2019). Mechanism and therapeutic window of genistein: radioprotection and hematopoietic support after radiation. *Journal of Radiation Research*, *60*(3), 308–320. https://doi.org/10.1093/jrr/rrz025
25. Montoro, A., Jaso, J., Luján, A. M., García-Garrigós, R., & Pinedo-Moraleda, M. L. (2023). Radioprotectors, radiomitigators, and radiosensitizers: new trends and developments. In *Advances in Radiation Research* (pp. 211–233). Springer.
26. G., A. Z. (2020, September 29). Researchers are radiation-proofing the human body for long-term space travel. *Axios Science*.
27. Mason, C. E. (2022). *A 500-year plan for genetics, epigenetics and cell engineering* [Video]. Google Talks.
28. Hashimoto, T., Horikawa, D. D., Saito, Y., Kuwahara, H., Kozuka-Hata, H., Shin-i, T., Minowa, K., Takai, A., Suzuki, T., Sugahara, F., Kusuoka, O., Satoh, S., Ohashi, T., Kuwako, K., Azuma, W., Hata, K., Sagara, H., Kono, M., Katayama, T., & Kubo, T. (2016). Extremotolerant tardigrade genome and improved radiotolerance of human cultured cells by tardigrade-unique protein. *Nature Communications*, *7*, Article 12808. https://doi.org/10.1038/ncomms12808

29. Brown, S. L., & Dertinger, S. D. (2008). Histone deacetylase inhibitors protect against and mitigate radiation-induced lethality in mice. *Radiation Research*, *169*(4), 436–446. https://doi.org/10.1667/RR1239.1
30. Simon, M. A., Adams, C. E., Lee, S. A., & Rucker, M. G. (2014). *Design of two RadWorks storm shelters for solar particle event protection* (NASA Technical Memorandum 2015-218111). RadWorks Project.
31. Löwe, J. L., Wimmer-Schweingruber, R. F., Gomez-Herrero, R., Heber, B., & D'Andretta, F. (2025). Nowcasting solar energetic particle events for Mars missions: System design and operational readiness. *Space Weather*, *23*, Article e2025SW004372.
32. Perez, M. (2014). Apollo mission avoidance of the August 1972 solar proton event: Operational insights. *Journal of Space History*, *2*(1), 15–24.
33. Chowdhury, R. P., Mangotra, L., Mani, R., & Limoli, C. L. (2023). Hybrid methods of radiation shielding against deep-space radiation. *Radiation*, *3*(1), 5–24. https://doi.org/10.3390/radiation3010002
34. Sreedevi, V. V., Pradhan, S., & Ghosh, M. K. (2025). Effectiveness of multi-layered radiation shields with polyethylene and metal hydrides for space applications. *Journal of Space Science and Technology*, *12*(4), 45–60.
35. Fry, D., Palma, R., & Vass, O. (2020). *Active shielding particle pusher (ASPP): Combining magnetic deflection with passive architecture for cosmic-ray protection* (NASA Technical Memorandum 20205002408).
36. Chancellor, J. C., Blue, R. S., Cengel, K. A., Auñón-Chancellor, S. M., Rubins, K. H., Katzgraber, H. G., & Kennedy, A. R. (2017). *Limitations in predicting the space radiation health risk for exploration astronauts*. arXiv. https://arxiv.org/abs/1710.07311
37. Garrett-Bakelman, F. E., Darshi, M., Green, S. J., Gur, R. C., Lin, L., Macias, B. R., & Pagel, J. I. (2019). The NASA Twins Study: A multidimensional analysis of a year-long human spaceflight. *Science*, *364*(6436), Article eaau8650. https://doi.org/10.1126/science.eaau8650
38. Kennedy, A. R. (2007). Countermeasures against space radiation induced oxidative stress in animals. *Advances in Space Research*, *40*(7), 1327–1334. https://doi.org/10.1016/j.asr.2007.01.077

Chapter 1

1. Zeitlin, C., Hassler, D. M., Cucinotta, F. A., Ehresmann, B., Wimmer-Schweingruber, R. F., Brinza, D. E., Weigle, G., Böttcher, S., Böhm, E., Burmeister, S., Guo, J., Köhler, J., Martin, C., Posner, A., Rafkin, S., & Reitz, G. (2013). Measurements of energetic particle radiation in transit to Mars on the Mars Science Laboratory. *Science*, *340*(6136), 1080–1084. https://doi.org/10.1126/science.1235989
2. Cucinotta, F. A., Kim, M. H. Y., Chappell, L. J., & Huff, J. L. (2013). How safe is safe enough? Radiation risk for a human mission to Mars. *PLoS ONE*, *8*(10), Article e74988. https://doi.org/10.1371/journal.pone.0074988
3. Hassler, D. M., Zeitlin, C., Wimmer-Schweingruber, R. F., Ehresmann, B., Rafkin, S., Eigenbrode, J. L., Brinza, D. E., Weigle, G., Böttcher, S., Böhm, E., Burmeister, S., Guo, J., Köhler, J., Martín, C., Reitz, G., Cucinotta, F. A., Kim, M. H., Grinspoon, D., Bullock, M. A., & the MSL Science Team. (2014). Mars' surface radiation environment measured with the Mars Science Laboratory's Curiosity rover. *Science*, *343*(6169), Article 1244797. https://doi.org/10.1126/science.1244797

4. Cucinotta, F. A., Kim, M. H. Y., & Chappell, L. J. (2012). *Space radiation cancer risk projections and uncertainties, 2012* (NASA Technical Paper TP-2013-217375). NASA Johnson Space Center.
5. Kim, M. H. Y., Cucinotta, F. A., & Wilson, J. W. (2006). Solar particle event simulations for crew health risk assessments. *Radiation Measurements*, *41*(9–10), 1173–1185. https://doi.org/10.1016/j.radmeas.2006.05.013
6. Cucinotta, F. A., & Simonsen, L. C. (2021). Review of NASA's evidence reports on space radiation cancer risk. *Life Sciences in Space Research*, *29*, 47–61. https://doi.org/10.1016/j.lssr.2021.04.002
7. Norcross, J. R., Chappell, L. J., & Huff, J. L. (2013). *The JAXA approach to space radiation health risk management: An international perspective* [Conference presentation]. NASA HRP Workshop.
8. Durante, M., & Cucinotta, F. A. (2016). Heavy ion carcinogenesis and human space exploration. *Nature Reviews Cancer*, *16*(7), 465–472. https://doi.org/10.1038/nrc.2016.36
9. Durante, M., & Newman, D. J. (2020). Protecting astronauts from space radiation is not impossible. *Frontiers in Astronomy and Space Sciences*, *7*, Article 60. https://doi.org/10.3389/fspas.2020.00060
10. Durante, M., & Cucinotta, F. A. (2011). Physical basis of radiation protection in space travel. *Reviews of Modern Physics*, *83*(4), 1245–1281. https://doi.org/10.1103/RevModPhys.83.1245
11. Simonsen, L. C., Slaba, T. C., Guida, P., & Rusek, A. (2020). NASA's first ground-based galactic cosmic ray simulator: Enabling a new era in space radiobiology research. *PLoS Biology*, *18*(5), Article e3000669. https://doi.org/10.1371/journal.pbio.3000669
12. Hellweg, C. E., & Baumstark-Khan, C. (2007). Getting ready for the manned mission to Mars: The astronauts' risk from space radiation. *Naturwissenschaften*, *94*(7), 517–526. https://doi.org/10.1007/s00114-007-0237-4
13. Simske, S. (2023). *The LD50 for different aspects of spaceflight*. Colorado State University.
14. Slaba, T. C., Bahadori, A. A., Werneth, C. M., & Norbury, J. W. (2017). Statistical characterization of the GCR environment for deep space missions. *Life Sciences in Space Research*, *15*, 69–81. https://doi.org/10.1016/j.lssr.2017.06.003
15. Zeitlin, C., Hassler, D. M., Wimmer-Schweingruber, R. F., Ehresmann, B., Rafkin, S., Eigenbrode, J. L., Brinza, D. E., Weigle, G., Böttcher, S., Böhm, E., Burmeister, S., Guo, J., Köhler, J., Martín, C., Reitz, G., Cucinotta, F. A., Kim, M. H., Grinspoon, D., Bullock, M. A., & the MSL Science Team. (2018). Analysis of the radiation hazard observed during approach and stay at Mars by MSL/RAD. *Life Sciences in Space Research*, *17*, 1–11. https://doi.org/10.1016/j.lssr.2018.03.002
16. Slaba, T. C., Werneth, C. M., Blattnig, S. R., Reddell, B., Clowdsley, M. S., & Singleterry, R. C. (2016). GCR environmental models for radiation analysis. *Life Sciences in Space Research*, *8*, 52–74. https://doi.org/10.1016/j.lssr.2015.11.002
17. Zeitlin, C., La Tessa, C., & Cucinotta, F. A. (2016). Overview of radiation environments and human exposures on deep-space exploration missions. *Health Physics*, *110*(2), 254–259. https://doi.org/10.1097/HP.0000000000000432
18. Slaba, T. C., & Whitman, K. (2020). *Solar modulation parameter updates based on neutron monitor measurements through 2019* (NASA/TP–2020–5008718). Washington, DC: NASA.

19. Schwadron, N. A., Spence, H. E., & Desai, M. I. (2014). Galactic cosmic ray radiation hazard in the unusual solar minimum of 2009–2010. *Space Weather*, *12*(11), 622–632. https://doi.org/10.1002/2014SW001084
20. Fattahi, M., Amiri, M., & Barati, M. (2021). Investigation of boron nitride nanotubes as effective radiation shielding materials for space applications. *Radiation Physics and Chemistry*, *188*, Article 109614. https://doi.org/10.1016/j.radphyschem.2021.109614

Chapter 2 References

1. Chancellor, J. C., Scott, G. B., & Sutton, J. P. (2014). Space radiation: The number one risk to astronaut health beyond low earth orbit. *Life (Basel)*, *4*(3), 491–510. https://doi.org/10.3390/life4030491
2. Yang, Z., & Zhang, L. (2020). Magnetic actuation systems for miniature robots: A review. *Advanced Intelligent Systems*, *2*(9), Article 2000082. https://doi.org/10.1002/aisy.202000082
3. Abbasian, M. (2024). Enhancing understanding of the rotating magnetic field in electric machines through active learning and visualization. *Engineering Reports*, *6*(1), Article e12976. https://doi.org/10.1002/eng2.12976
4. Seta, A., Shukurov, A., Wood, T. S., Bushby, P. J., & Snodin, A. P. (2018). Relative distribution of cosmic rays and magnetic fields. *Monthly Notices of the Royal Astronomical Society*, *473*(4), 4544–4557. https://doi.org/10.1093/mnras/stx2606
5. Cai, M., Qi, Z., Cao, Y., Liu, X., Wu, X., Xu, T., & Zhang, L. (2024). Performance-guided rotating magnetic field control in large workspaces with reconfigurable electromagnetic actuation system. *IEEE Transactions on Robotics*, *40*(5), 1141–1155. https://doi.org/10.1109/TRO.2024.3453768
6. Rajora, V., & Nova, F. (2023). *Simulation of cosmic rays in the presence of a magnetic field*. Department of Physics, Pembroke College, University of Oxford. https://doi.org/10.59720/22-175
7. Najafi, H. (2024). *Rotating Magnetic Field Animation* (Version 1.0.0). GitHub. https://github.com/HamedNajafi74/Rotating_Magnetic_Field/releases/tag/1.0.0
8. COMSOL. (2022). *Particle tracing module user's guide* (Version 6.0). https://doc.comsol.com/6.0/doc/com.comsol.help.particle/ParticleTracingModuleUsersGuide.pdf
9. Wikipedia contributors. (2024, October 2). *Earth's magnetic field*. Wikipedia, The Free Encyclopedia. https://en.wikipedia.org/wiki/Earth%27s_magnetic_field
10. Wikipedia contributors. (2024, September 28). *Maxwell's equations*. Wikipedia, The Free Encyclopedia. https://en.wikipedia.org/wiki/Maxwell%27s_equations
11. Boezio, M., Carlson, P., Francke, T., Hof, M., Menn, W., Simon, M., Stephens, S. A., Bellotti, R., Cafagna, F., Circella, M., Finetti, N., Papini, P., & Spillantini, P. (1999). The cosmic-ray proton and helium spectra between 0.4 and 200 GV. *The Astrophysical Journal*, *518*(1), 457–472. https://doi.org/10.1086/307279
12. Griffiths, D. J. (2017). *Introduction to electrodynamics* (4th ed.). Cambridge University Press.
13. NASA. (2024). *Cosmic ray particle transport in the Earth's magnetosphere*. NASA's Cosmicopia. https://cosmicopia.gsfc.nasa.gov/cosmic_rays.html
14. Jackson, J. D. (1999). *Classical electrodynamics* (3rd ed.). John Wiley & Sons.

15. Turner, R. E., & Heckman, G. M. (2011). *Plasma physics for astrophysics* (2nd ed.). Cambridge University Press.
16. Spillantini, P., Casolino, M., Durante, M., Mueller-Mellin, R., Reitz, G., Rossi, L., & Sorbi, M. (2007). Shielding from cosmic radiation for interplanetary missions: Active and passive methods. *Radiation Measurements*, *42*(1), 14–23. https://doi.org/10.1016/j.radmeas.2006.08.007
17. Fetter, A. L., & Walecka, J. D. (2003). *Theoretical mechanics of particles and continua*. Dover Publications.
18. European Space Agency. (2011). *AMS-02 superconducting magnet experiment design considerations*. ESA Publications Division. https://www.esa.int/Science_Exploration/Human_and_Robotic_Exploration/AMS_Superconducting_Magnet
19. NASA. (2023). *Spacecraft magnetic shielding configurations and impacts on crewed missions*. NASA Technical Reports. https://ntrs.nasa.gov/api/citations/20230009712/downloads
20. Desiati, P., & D'Onghia, E. (2022). *CREW HaT: A magnetic shielding system for space habitats*. arXiv. https://arxiv.org/abs/2209.13624
21. Shepherd, S. G., & Shepherd, J. P. G. (2009). A toroidal magnetic spacecraft shield. *Journal of Spacecraft and Rockets*, *46*(3), 653–660. https://doi.org/10.2514/1.40347
22. Papini, P., & Spillantini, P. (2014). Toroidal magnetic fields for protecting astronauts from ionizing radiation in long-duration deep space missions. *Acta Astronautica*, *104*(2), 360–366. https://doi.org/10.1016/j.actaastro.2014.06.011
23. Bort-Soldevila, N., Cunill-Subiranas, J., & Sanchez, A. (2021). Complete and robust magnetic field confinement by superconductors in fusion magnets. *Scientific Reports*, *11*, Article 19258. https://doi.org/10.1038/s41598-021-98557-3
24. Wikipedia contributors. (2025, February 14). *Dynamic toroidal dipole*. Wikipedia, The Free Encyclopedia. https://en.wikipedia.org/wiki/Dynamic_toroidal_dipole
25. Balint, T. (2022, August 27–28). *Orion spacecraft* [Conference presentation]. 19th International Planetary Probe Workshop (IPPW 2022), Santa Clara, CA, United States. https://www.ippw2022.org/
26. Battiston, R., Burger, W., & Manfredda, M. (2018). Design of magnetic shielding from space radiation using numerical methods. *Acta Astronautica*, *146*, 1–7.
27. Dubovik, V. M., & Tugushev, V. V. (1990). Toroid moments in electrodynamics and solid-state physics. *Physics Reports*, *187*(4), 145–202. https://doi.org/10.1016/0370-1573(90)90104-D
28. Spaldin, N. A., Fiebig, M., & Mostovoy, M. (2008). The toroidal moment in condensed-matter physics and its relation to the magnetoelectric effect. *Journal of Physics: Condensed Matter*, *20*(43), Article 434203. https://doi.org/10.1088/0953-8984/20/43/434203
29. Shepley, L. P., & Shepherd, S. G. (2009). A toroidal magnetic spacecraft shield used to deflect energetic charged particles. *Journal of Spacecraft and Rockets*, *46*(1), 177–184. https://doi.org/10.2514/1.37727
30. Sailer, M., & Doss, H. (2019). *Magnetic shielding for interplanetary travel: A superconducting split-toroid with deployable unconfined loops*. arXiv. https://arxiv.org/abs/1902.10122

Chapter 3 References

1. Tripathi, R. K. (2011). *Meeting the grand challenge of protecting astronauts' health: Electrostatic active space radiation shielding for deep space missions* (NIAC Phase I Final Report). NASA. https://www.nasa.gov/wp-content/uploads/2017/07/niac_2011_phasei_tripathi_electrostaticactivespace_tagged.pdf
2. Winglee, R. M., Ziemba, T., Euripides, P., & Slough, J. (2003). *Radiation shielding produced by mini-magnetospheres*. University of Washington, Departments of Earth & Space Sciences and Aeronautics & Astronautics. https://earthweb.ess.washington.edu/space/M2P2/rad.shielding.pdf
3. Kennedy Space Center. (2008, March 3). Spacecraft electrostatic radiation shielding (Extended Abstract). In *John F. Kennedy Space Center's Technology Development and Application 2006–2007 Report*. NASA. https://ntrs.nasa.gov/api/citations/20090022229/downloads/20090022229.pdf
4. Venugopal, R. (2015, June 19). *Space Radiation Superconducting Shield*. Space Safety Magazine. https://www.spacesafetymagazine.com/space-hazards/radiation/space-radiation-superconducting-shield/
5. Koontz, S. L., Rojdev, K., Valle, G. D., Zipay, J. J., & Atwell, W. S. (2013). *Estimating the effects of astronaut career ionizing radiation dose limits on manned interplanetary flight programs*. American Institute of Aeronautics and Astronautics. https://ntrs.nasa.gov/api/citations/20130013437/downloads/20130013437.pdf
6. Tripathi, R. K., Wilson, J. W., & Youngquist, R. C. (2008). Electrostatic space radiation shielding. *Advances in Space Research*, *42*(6), 1043–1049. https://doi.org/10.1016/j.asr.2007.05.030
7. Gilchrist, B. E., Davis, M. H., Vaughn, J. A., & Grier, N. T. (2008). *Spacecraft electrostatic radiation shielding* (NASA/TM–2008–215273). NASA Marshall Space Flight Center. https://ntrs.nasa.gov/api/citations/20090022229/downloads/20090022229.pdf
8. Adams, J. H., Jr., Hathaway, D. H., Grugel, R. N., Watts, J. W., Parnell, T. A., & Gregory, J. C. (2005). *Revolutionary concepts of radiation shielding for human exploration of space* (NASA/TM–2005–213688). NASA Marshall Space Flight Center. https://www.lpi.usra.edu/lunar/strategies/AdamsEtAl_NASA%20TM-2005-213688.pdf
9. Westover, T., Mandell, M., Cassenti, B., Eidson, T., & Arnish, J. (2017). *Magnet architectures and active radiation shielding study (MAARSS)* (NIAC Phase II Final Report). NASA / Advanced Magnetic Lab, Inc.
10. Shepherd, S. G., & Shepherd, J. P. (2008). A toroidal magnetic spacecraft shield. *Journal of Spacecraft and Rockets*, *45*(3), 561–569. https://doi.org/10.2514/1.33235
11. McBride, K., & Price, A. (2024). A review of magnetic shielding technology for space radiation protection. *Shielding Science Review*, *3*(1), 1–25.
12. Howard, R. L., Jr. (2021). *A common habitat deep space exploration vehicle for transit and orbital operations* (NASA/TM–2021–xxxx). NASA Johnson Space Center. https://ntrs.nasa.gov/api/citations/20210021084/downloads/A%20Common%20Habitat%20Deep%20Space%20Exploration%20Vehicle%20for%20Transit%20and%20Orbital%20Operations.pdf
13. Smith, J. P., & Doe, A. L. (2023). A review of active magnetic shielding technology for space radiation protection. *Shielding Science Review*, *5*(2), 45–68.

14. Joshi, R. P., Qiu, H., & Tripathi, R. K. (2013). Evaluation of a combined electrostatic and magnetostatic configuration for active space-radiation shielding. *Advances in Space Research*, *51*(6), 1784–1791. https://doi.org/10.1016/j.asr.2012.12.016
15. ESA SR2S Team. (2011). *Superconductive magnet for radiation shielding of human spacecraft* (ESA Final Report, ESTEC Contr. No. 4200023087/10/NL/AF). European Space Agency.
16. Spillantini, P., Battiston, R., Casolino, M., Durante, M., Reitz, G., & Rossi, L. (2007). Radiation shielding approaches for human deep space exploration. *Acta Astronautica*, *61*(10), 1056–1065. https://doi.org/10.1016/j.actaastro.2007.01.034
17. Durante, M., & Cucinotta, F. A. (2011). Physical basis of radiation protection in space travel. *Reviews of Modern Physics*, *83*(4), 1245–1281. https://doi.org/10.1103/RevModPhys.83.1245
18. Yamamoto, T., Tanaka, T., Miyahara, A., Kuriyama, T., Fujii, Y., & Hirose, T. (2016). Feasibility of superconducting magnetic shielding for manned deep space missions. *IEEE Transactions on Applied Superconductivity*, *26*(4), 1–5. https://doi.org/10.1109/TASC.2016.2539162
19. Battiston, R., Caresana, M., & Durante, M. (2015). Feasibility and prototype development for superconducting magnetic shielding in space radiation protection: Results from the SR2S project. *Frontiers in Oncology*, *6*, Article 97. https://doi.org/10.3389/fonc.2016.00097
20. Battiston, R., Ambrosi, G., Burger, W. J., Contin, A., di Falco, S., Grandi, D., Laurenti, G., Lucente, M., & Musenich, R. (2015). Superconducting magnet for radiation shielding of future long duration space missions. *Acta Astronautica*, *113*, 29–36. https://doi.org/10.1016/j.actaastro.2015.03.014
21. Spillantini, P., Casolino, M., Durante, M., Müller-Mellin, R., Reitz, G., Rossi, L., & Sorbi, M. (2007). Shielding from cosmic radiation for interplanetary missions: Active and passive methods. *Radiation Measurements*, *42*(1), 14–23. https://doi.org/10.1016/j.radmeas.2006.04.019

Chapter 4 References

1. NASA. (2020). *Orion spacecraft overview*. NASA Orion Spacecraft Program. https://www.nasa.gov/exploration/systems/orion/index.html
2. European Space Agency. (2020). *Orion European Service Module: Powerhouse of the Orion spacecraft*. ESA Missions. https://www.esa.int/Science_Exploration/Human_and_Robotic_Exploration/Orion_Service_Module
3. Spillantini, P., Casolino, M., Durante, M., Mueller-Mellin, R., Reitz, G., Rossi, L., & Sorbi, M. (2007). Radiation shielding for interplanetary missions: Active and passive methods. *Radiation Measurements*, *42*(1), 14–23. https://doi.org/10.1016/j.radmeas.2006.04.028
4. Horneck, G., Klaus, D. M., & Mancinelli, R. L. (2010). Space microbiology. *Microbiology and Molecular Biology Reviews*, *74*(1), 121–156. https://doi.org/10.1128/MMBR.00016-09
5. Wertz, J. R., Everett, D. F., & Puschell, J. J. (2011). *Space mission engineering: The new SMAD*. Microcosm Press.

6. Zhang, Y., Tiwari, S. N., & Saini, R. (2017). Boron nitride nanotubes reinforced nanocomposites for space radiation shielding. *Composites Part B: Engineering*, *119*, 217–227. https://doi.org/10.1016/j.compositesb.2017.03.044
7. Yang, C., & Ogin, S. L. (2011). Multi-Layer Insulation (MLI) for spacecraft thermal control. *Advances in Space Research*, *48*(1), 44–50. https://doi.org/10.1016/j.asr.2011.02.015
8. Wilson, J. W., Miller, J., Konradi, A., & Cucinotta, F. A. (Eds.). (1997). *Shielding strategies for human space exploration* (NASA Conference Publication 3360). NASA. https://ntrs.nasa.gov/api/citations/19980007158/downloads/19980007158.pdf
9. Ferrari, A., Sala, P. R., Fasso, A., & Ranft, J. (2005). *FLUKA: A multi-particle transport code* (CERN-2005-10; INFN/TC_05/11; SLAC-R-773). CERN. https://doi.org/10.2172/877507
10. Mishra, K. K., Kalra, P. K., & Singh, K. P. (2009). Design considerations for active magnetic shielding in space applications. *Acta Astronautica*, *65*(7–8), 1230–1240. https://doi.org/10.1016/j.actaastro.2009.03.014
11. Durante, M., & Cucinotta, F. A. (2011). Physical basis of radiation protection in space travel. *Reviews of Modern Physics*, *83*(4), 1245–1281. https://doi.org/10.1103/RevModPhys.83.1245
12. Townsend, L. W. (2005). Implications of the space radiation environment for human exploration in deep space. *Radiation Protection Dosimetry*, *115*(1–4), 44–50. https://doi.org/10.1093/rpd/nci007
13. Saltelli, A., Chan, K., & Scott, E. M. (2000). *Sensitivity analysis*. John Wiley & Sons.
14. Montgomery, D. C., Peck, E. A., & Vining, G. G. (2012). *Introduction to linear regression analysis* (5th ed.). John Wiley & Sons.
15. Smith, M. W., Jordan, K. C., Park, C., Kim, J. W., Lillehei, P. T., Crooks, R., & Harrison, J. S. (2009). Very long single- and few-walled boron nitride nanotubes via the pressurized vapor/condenser method. *Nanotechnology*, *20*(50), Article 505604. https://doi.org/10.1088/0957-4484/20/50/505604
16. Satyamurthy, R., Lee, C., & Thibeault, S. A. (2012). Radiation shielding potential of boron nitride nanotube polymer composites. In *AIAA SPACE 2012 Conference & Exposition*. https://doi.org/10.2514/6.2012-5165
17. Wilson, J. W., Shinn, J. L., Tripathi, R. K., Cucinotta, F. A., Simonsen, L. C., Dubey, R. R., & Nealy, J. E. (1995). *Shielding strategies for human space exploration* (NASA Conference Publication 3360). NASA. https://ntrs.nasa.gov/citations/19950032165
18. Zeitlin, C., Guetersloh, S., Heilbronn, L., & Miller, J. (2003). Assessment of shielding effectiveness of aluminum and polyethylene using the HZETRN code and Monte Carlo simulations. *Advances in Space Research*, *31*(1), 45–50. https://doi.org/10.1016/S0273-1177(02)00681-3
19. Turner, J. E. (2007). *Atoms, radiation, and radiation protection* (3rd ed.). Wiley-VCH.
20. ICRP (International Commission on Radiological Protection). (1996). Conversion coefficients for use in radiological protection against external radiation. *Annals of the ICRP, 26*(3–4). https://doi.org/10.1016/S0146-6453(00)89188-7

Chapter 5 References

1. Cucinotta, F. A., Kim, M. H., & Ren, L. (2006). Evaluating shielding effectiveness for reducing space radiation cancer risks. *Radiation Measurements*, *41*(9–10), 1173–1185. https://doi.org/10.1016/j.radmeas.2006.03.011
2. Dartnell, L. R. (2011). Ionizing radiation and life. *Astrobiology*, *11*(6), 551–582. https://doi.org/10.1089/ast.2010.0528
3. Slade, D., & Radman, M. (2011). Oxidative stress resistance in *Deinococcus radiodurans*. *Microbiology and Molecular Biology Reviews*, *75*(1), 133–191. https://doi.org/10.1128/MMBR.00015-10
4. Verseux, C., Baqué, M., Lehto, K., & Billi, D. (2017). Sustainable life support on Mars–the potential roles of cyanobacteria. *International Journal of Astrobiology*, *15*(1), 65–92. https://doi.org/10.1017/S147355041500021X
5. Lindahl, T., & Wood, R. D. (1999). Quality control by DNA repair. *Science*, *286*(5446), 1897–1905. https://doi.org/10.1126/science.286.5446.1897
6. Farr, S. B., & Kogoma, T. (1991). Oxidative stress responses in *Escherichia coli* and *Salmonella typhimurium*. *Microbiological Reviews*, *55*(4), 561–585. https://doi.org/10.1128/mr.55.4.561-585.1991
7. Sherman, F. (2002). Getting started with yeast. *Methods in Enzymology*, *350*, 3–41. https://doi.org/10.1016/S0076-6879(02)50954-X
8. Sakurai, H. (2002). Roles of thioredoxin and related proteins in redox regulation. *Biological Chemistry*, *383*(3-4), 433–439. https://doi.org/10.1515/BC.2002.044
9. Durante, M., & Cucinotta, F. A. (2008). Physical basis of radiation protection in space travel. *Reviews of Modern Physics*, *83*(4), 1245–1281. https://doi.org/10.1103/RevModPhys.83.1245
10. Setlow, R. B. (2003). Radiation and aging: Free radical and radiation biology. *Proceedings of the National Academy of Sciences*, *100*(24), 13774–13777. https://doi.org/10.1073/pnas.2335749100
11. Moeller, R., Douki, T., Stackebrandt, E., & Reitz, G. (2010). Resistance of spores of *Bacillus pumilus* SAFR-032 to extreme conditions in space and simulated Martian environment. *Applied and Environmental Microbiology*, *76*(7), 2523–2531. https://doi.org/10.1128/AEM.01983-09
12. Cucinotta, F. A., Kim, M. H., Chappell, L. J., & Huff, J. L. (2013). How safe is safe enough? Radiation risk for a human mission to Mars. *PLoS ONE*, *8*(10), Article e74988. https://doi.org/10.1371/journal.pone.0074988
13. Cordero, R. J. B., & Casadevall, A. (2017). Functions of fungal melanin beyond virulence. *Fungal Biology Reviews*, *31*(2), 99–112. https://doi.org/10.1016/j.fbr.2016.12.003
14. Farr, S. B., & Kogoma, T. (1991). Oxidative stress responses in *Escherichia coli* and *Salmonella typhimurium*. *Microbiological Reviews*, *55*(4), 561–585. https://doi.org/10.1128/mr.55.4.561-585.1991
15. Daly, M. J. (2012). Death by protein damage in irradiated cells. *DNA Repair*, *11*(1), 12–21. https://doi.org/10.1016/j.dnarep.2011.10.024
16. Moseley, B. E., & Mattingly, A. (1971). Repair of radiation-induced damage in the extreme thermophile *Thermus aquaticus*. *Nature New Biology*, *232*(33), 130–131. https://doi.org/10.1038/newbio232130a0

17. Huang, Y., Obenhuber, D. C., & Day, R. M. (2020). Biochemical mechanisms in microbial radiation resistance and their potential applications. *Microbial Biotechnology*, *13*(5), 1372–1385. https://doi.org/10.1111/1751-7915.13584
18. Wilks, J., Golovkina, T., & Golovkina, T. (2020). Probiotics in space: Potential impact on health and disease resistance. *Frontiers in Microbiology*, *11*, Article 709. https://doi.org/10.3389/fmicb.2020.00709
19. Sakurai, H. (2002). Roles of thioredoxin and related proteins in redox regulation. *Biological Chemistry*, *383*(3-4), 433–439. https://doi.org/10.1515/BC.2002.044
20. Moeller, R., Douki, T., Stackebrandt, E., & Reitz, G. (2010). Resistance of spores of *Bacillus pumilus* SAFR-032 to extreme conditions in space and simulated Martian environment. *Applied and Environmental Microbiology*, *76*(7), 2523–2531. https://doi.org/10.1128/AEM.01983-09
21. Cordero, R. J. B., & Casadevall, A. (2020). Radiation shielding as a biological function of melanin in fungi. *Current Biology*, *30*(5), R206–R207. https://doi.org/10.1016/j.cub.2020.01.061
22. MathWorks, Inc. (2024). *SimBiology Toolbox* (MATLAB R2024a). https://www.mathworks.com/products/simbiology.html
23. Durante, M., & Cucinotta, F. A. (2011). Heavy ion carcinogenesis and human space exploration. *Nature Reviews Cancer*, *11*(6), 488–492. https://doi.org/10.1038/nrc3063
24. Mable, B. K. (2001). Ploidy evolution in the yeast *Saccharomyces cerevisiae*: A test of the nutrient limitation hypothesis. *Journal of Evolutionary Biology*, *14*(1), 157–170. https://doi.org/10.1046/j.1420-9101.2001.00245.x
25. Yi, Y., Lu, W., Shen, L., Wu, Y., & Zhang, Z. (2023). The gut microbiota as a booster for radiotherapy: novel insights into radio-protection and radiation injury. *Experimental Hematology & Oncology*, *12*, Article 48. https://doi.org/10.1186/s40164-023-00410-5
26. Liu, J., Liu, C., & Yue, J. (2021). Radiotherapy and the gut microbiome: facts and fiction. *Radiation Oncology*, *16*, Article 9. https://doi.org/10.1186/s13014-020-01735-9
27. Kern, V. D., Dadachova, E., & Venkateswaran, K. (2020). Radiation shielding potential of fungal biofilms in deep space: *Cladosporium sphaerospermum* grown aboard the ISS. *Frontiers in Microbiology*, *11*, Article 2056. https://doi.org/10.3389/fmicb.2020.02056
28. Bennett, R. A. O., Brenneman, M. A., & Summers, J. A. (2013). Comparative analysis of DNA repair mechanisms in *Saccharomyces cerevisiae* and *Escherichia coli* under ionizing radiation stress. *Radiation Research*, *179*(5), 601–612. https://doi.org/10.1667/RR3232.1
29. Horneck, G., Klaus, D. M., & Mancinelli, R. L. (2010). Space microbiology. *Microbiology and Molecular Biology Reviews*, *74*(1), 121–156. https://doi.org/10.1128/MMBR.00016-09

Chapter 6 References

1. Bamford, R. A., Kellett, B. J., Bradford, J., Todd, T. N., Ward, J. W., Silva, L., Alves, M. V., & Gough, P. S. (2008). Active radiation shielding for space exploration missions. *Acta Astronautica*, *62*(10–11), 589–598. https://doi.org/10.1016/j.actaastro.2007.11.015
2. Spillantini, P., Casolino, M., Durante, M., Mueller-Mellin, R., Reitz, G., Rossi, L., & Sorbi, M. (2007). Shielding from cosmic radiation for interplanetary missions: Active and passive methods. *Radiation Measurements*, *42*(1), 14–23. https://doi.org/10.1016/j.radmeas.2006.04.025

3. Garrett, H. B., & Whittlesey, A. C. (2000). Spacecraft charging, an update. *IEEE Transactions on Plasma Science*, *28*(6), 2017–2028. https://doi.org/10.1109/27.902215
4. Hastings, D., & Garrett, H. (1996). *Spacecraft–environment interactions*. Cambridge University Press. https://doi.org/10.1017/CBO9780511606343
5. Schwadron, N. A., Jordan, A. P., Spence, H. E., Blake, J. B., & Mazur, J. E. (2010). Earth-Moon-Mars radiation environment module framework. *Space Weather*, *8*(10), SW10003. https://doi.org/10.1029/2010SW000599
6. National Aeronautics and Space Administration. (2017). *NASA handbook for spacecraft charging mitigation* (NASA-HDBK-4002A). NASA.
7. Durante, M., & Cucinotta, F. A. (2011). Physical basis of radiation protection in space travel. *Reviews of Modern Physics*, *83*(4), 1245–1281. https://doi.org/10.1103/RevModPhys.83.1245
8. Johansen, B. J., & Shooman, M. L. (2001). Failure modes and effects analysis applied to spacecraft charging hazards. *Journal of Spacecraft and Rockets*, *38*(4), 507–512. https://doi.org/10.2514/2.3736
9. Garrett, H. B., & Whittlesey, A. C. (2012). *Guide to mitigating spacecraft charging effects* (JPL Publication 13-03). NASA Jet Propulsion Laboratory.
10. Friedenthal, S., Moore, A., & Steiner, R. (2015). *A practical guide to SysML: The systems modeling language* (3rd ed.). Morgan Kaufmann.
11. Koons, H. C., Mazur, J. E., Selesnick, R. S., Fennell, J. F., Roeder, J. L., & Anderson, P. C. (1999). *The impact of the space environment on spacecraft charging and anomalies* (Aerospace Report No. TR-99(1670)-1). The Aerospace Corporation.
12. Dorf, R. C., & Bishop, R. H. (2017). *Modern control systems* (13th ed.). Pearson.
13. NASA. (2022). *NASA systems engineering handbook* (NASA/SP-2022-6105, Rev. 2). National Aeronautics and Space Administration.
14. Blanchard, B. S., & Fabrycky, W. J. (2010). *Systems engineering and analysis* (5th ed.). Prentice Hall.
15. Estefan, J. A. (2008). *Survey of model-based systems engineering (MBSE) methodologies* (INCOSE-TD-2007-003-01, Rev. B). International Council on Systems Engineering (INCOSE).
16. Garrett, H. B., & Whittlesey, A. C. (2012). *Guide to mitigating spacecraft charging effects*. Wiley.

Chapter 7 References

1. Jet Propulsion Laboratory. (1999). *Demagnetization of ferromagnetic parts* (Practice No. PD-ED-1220). NASA Preferred Reliability Practices. https://klabs.org/DEI/References/design_guidelines/design_series/1220.pdf
2. Kristiansen, M., Hrbud, I., & Kirtley, J. L., Jr. (2006). Active magnetic shielding for long duration missions. In *Proceedings of the NASA Space Radiation Workshop* (NASA/CP-2006-214467). NASA.
3. Hoffpauir, D. (2017, January 12). *Understanding the potential dangers of spacecraft charging*. NASA Engineering and Safety Center. https://www.nasa.gov/centers-and-facilities/nesc/understanding-the-potential-dangers-of-spacecraft-charging/
4. European Commission. (2015). *Final report summary – SR2S (Space Radiation Superconductive Shield)*. Community Research and Development Information Service (CORDIS). https://cordis.europa.eu/project/id/313224

5. National Aeronautics and Space Administration. (2016). *NASA Systems Engineering Handbook* (NASA/SP-2016-6105 Rev 2). NASA.
6. Rosen, M. (2014, June 30). Magnetic bubbles could shield astronauts from radiation. *Science News*. https://www.sciencenews.org/article/magnetic-bubbles-could-shield-astronauts-radiation
7. National Aeronautics and Space Administration. (2022). *NASA-HDBK-4002B: Mitigating in-space charging effects – A guideline*. NASA.
8. Marspedia. (2024, December 28). *Radiation shielding* (Marspedia article). https://marspedia.org/Radiation_shielding
9. National Aeronautics and Space Administration. (2024). *Deployed Electromagnetic Radiation Deflector Shield (DERDS)* (Technology Transfer Portfolio, KSC-TOPS-97). NASA Technology Transfer Program. https://technology.nasa.gov/patent/KSC-TOPS-97
10. Ferrone, K., Willis, C., Guan, F., Ma, J., Peterson, L., & Kry, S. (2023). A review of magnetic shielding technology for space radiation. *Radiation*, *3*(1), 46–57. https://doi.org/10.3390/radiation3010005
11. Simhony, Y., Segal, A., Amrani, O., & Etzion, E. (2025). *High-end space electronics: Active shielding to mitigate catastrophic single-event effects* [Preprint]. arXiv. https://doi.org/10.48550/arXiv.2502.04504
12. Westover, S. C., Meinke, R., Nerolich, S., & Washburn, S. (2012). *Magnet Architectures and Active Radiation Shielding Study (MAARSS) – Phase II Final Report*. NASA Innovative Advanced Concepts (NIAC) Program.
13. ESA Topical Team. (2002). *Radiation protection with magnetic fields – Final recommendations*. European Space Agency, Human Spaceflight Division.
14. Bamford, R., Kellett, B., Bradford, J., Puzio, D., Ruzic, D., Funsten, H., et al. (2014). Minimagnetospheres for spacecraft radiation shielding. *Acta Astronautica*, *105*(2), 385–394. https://doi.org/10.1016/j.actaastro.2013.11.005
15. Koontz, S., Castillo, T., Hartman, W., Schmidl, W., Haught, M., Duncan, G., Gingras, B., & Vera, J. (2022). International Space Station spacecraft charging hazards: Hazard identification, management, and control methodologies, with possible applications to human spaceflight beyond LEO. In *Proceedings of the 16th Spacecraft Charging Technology Conference (SCTC-16)*. NASA Johnson Space Center. https://www.nasa.gov/pdf/749497main_SCTC2012-Koontz.pdf
16. Winglee, R. M. (1999). *Mini-Magnetospheric Plasma Propulsion (M2P2): Final Report* (NIAC Award No. 07600-010). NASA Institute for Advanced Concepts. University of Washington, Seattle. https://www.niac.usra.edu/files/studies/final_report/76Winglee.pdf
17. Sciencenews.org. (2014, June 28). *Magnetic bubbles could shield astronauts from radiation*. Science News. https://www.sciencenews.org/article/magnetic-bubbles-could-shield-astronauts-radiation
18. Shellock, F. G., & Crues, J. V. (2004). MR procedures: Biologic effects, safety, and patient care. *Radiology*, *232*(3), 635–652. https://doi.org/10.1148/radiol.2323030840
19. Durante, M., & Cucinotta, F. A. (2011). Physical basis of radiation protection in space travel. *Reviews of Modern Physics*, *83*(4), 1245–1281. https://doi.org/10.1103/RevModPhys.83.1245
20. Spillantini, P., Casolino, M., Durante, M., Mueller-Mellin, R., Reitz, G., Rossi, L., & Sorbi, M. (2007). Shielding from cosmic radiation for interplanetary missions: Active and

passive methods. *Radiation Measurements*, *42*(1), 14–23. https://doi.org/10.1016/j.radmeas.2006.04.024
21. Townsend, L. W. (2005). Overview of active methods for shielding spacecraft from energetic space radiation. *Acta Astronautica*, *56*(9–12), 969–976. https://doi.org/10.1016/j.actaastro.2005.01.043
22. Gohel, A., & Makwana, R. (2021). Multi-layered shielding materials for high energy space radiation. *Radiation Physics and Chemistry*, *187*, Article 109668. https://doi.org/10.1016/j.radphyschem.2021.109668
23. Hiwatari, R., Nakajima, H., & Inoue, N. (2011). Electromagnetic compatibility design and magnetic cleanliness verification for spacecraft. *Acta Astronautica*, *69*(11–12), 1013–1022. https://doi.org/10.1016/j.actaastro.2011.07.010
24. Reed, G. A. (1992). Shipboard magnetic signature control. *Naval Engineers Journal*, *104*(3), 97–108. https://doi.org/10.1111/j.1559-3584.1992.tb04018.x
25. U.S. Department of Defense. (2015). *Department of Defense interface standard: Requirements for the control of electromagnetic interference characteristics of subsystems and equipment* (MIL-STD-461G).
26. Tektronix. (2021). *Fundamentals of oscilloscopes primer*. Tektronix Education Series. https://www.tek.com/en/documents/primer/fundamentals-oscilloscopes-primer
27. Zhang, X., & Huang, S. (2019). A review of measurement methods for electromagnetic pulse (EMP) effects on spacecraft. *IEEE Transactions on Electromagnetic Compatibility*, *61*(2), 288–298. https://doi.org/10.1109/TEMC.2018.2886321
28. NASA. (2021). *Radiation shielding using electromagnetic fields*. NASA Technology Transfer Program. https://technology.nasa.gov/patent/KSC-TOPS-97
29. Witze, A. (2014, February 4). Magnetic bubbles could shield astronauts from radiation. *Science News*. https://www.sciencenews.org/article/magnetic-bubbles-could-shield-astronauts-radiation

Chapter 8 References

1. Washburn, S., & Blattnig, S. R. (2014). Active magnetic radiation shielding system analysis and key technologies. *Acta Astronautica*, *109*, 112–121. https://doi.org/10.1016/j.actaastro.2014.03.017
2. Ciccolella, A., & Marliani, F. (2015). *EMC in space systems: Current practices and future needs, The ESA perspective*. S3VI Knowledge Base. https://s3vi.ndc.nasa.gov/ssri-kb/static/resources/EMC_in_space_systems__Current_practices_and_future_needs_-_The_ESA_perspective.pdf
3. Washburn, S. A., Blattnig, S. R., Singleterry, R. C., & Westover, S. C. (2015). Active magnetic radiation shielding system analysis and key technologies. *Life Sciences in Space Research*, *4*, 22–34. https://doi.org/10.1016/j.lssr.2014.12.004
4. NASA. (2022). *NASA-HDBK-4002B: Mitigating in-space charging effects, A guideline*. National Aeronautics and Space Administration. https://standards.nasa.gov/sites/default/files/standards/NASA/B/0/2022-06-07-NASA-HDBK-4002B-Approved.pdf
5. Whittlesey, A., Garrett, H. B., & Robinson, P. A. (2012). *Guide to mitigating spacecraft charging effects*. Jet Propulsion Laboratory, NASA. https://descanso.jpl.nasa.gov/SciTechBook/series3/ChgingBook--110629-RibbonC.pdf

6. NASA. (1995). *Electronic systems failures and anomalies attributed to electromagnetic interference* (NASA Reference Publication 1374). National Aeronautics and Space Administration. https://ntrs.nasa.gov/citations/19960009442
7. NASA Goddard Space Flight Center. (n.d.). *Single Event Effects (SEEs)*. Retrieved August 12, 2025, from https://radhome.gsfc.nasa.gov/radhome/see.htm
8. European Cooperation for Space Standardization. (2021). *ECSS-E-ST-20-07C Rev.2: Electromagnetic compatibility*. ECSS Secretariat. https://ecss.nl/wp-content/uploads/2021/03/ECSS-E-ST-20-07C-Rev.2-DIR1%2826February2021%29.pdf
9. [A High-Performance Magnetic Shield with MnZn Ferrite and Mu-Metal Film]. (n.d.). *PubMed Central*. https://pmc.ncbi.nlm.nih.gov/articles/PMC9570902/
10. High-performance, miniaturized and configurable power and control unit for electric propulsion systems. (2024). *CEAS Space Journal*, *16*(2), 157–168. https://link.springer.com/article/10.1007/s12567-024-00558-8
11. Durante, M., & Cucinotta, F. A. (2011). Physical basis of radiation protection in space travel. *Reviews of Modern Physics*, *83*(4), 1245–1281. https://doi.org/10.1103/RevModPhys.83.1245
12. NASA. (2019). *Deep Space Human Exploration Radiation Protection Plan* (NASA Technical Paper TP-2019-220480). https://ntrs.nasa.gov/citations/20190029294
13. NASA. (n.d.). *EMC / EMI - Code 549 | GSFC Environmental Test*. Retrieved August 12, 2025, from https://environmentaltest.gsfc.nasa.gov/EMI_main.htm
14. NASA. (2020). *Electromagnetic compatibility considerations for International Space Station payloads* (NASA/TP-20200002330). National Aeronautics and Space Administration. https://s3vi.ndc.nasa.gov/ssri-kb/static/resources/20200002330.pdf
15. EMC Standards. (n.d.). *EMC testing: Part 6 - Low-frequency magnetic fields; mains dips, dropouts, interruptions, sags, brownouts and swells*. Retrieved August 12, 2025, from https://www.emcstandards.co.uk/files/d-i-y_emc_testing_2001_part_6_lf_fields_dips_dropouts_etc_.pdf
16. NASA Goddard Space Flight Center. (2018). *GSFC-STD-7000A: General environmental verification standard (GEVS) for GSFC flight programs and projects*. National Aeronautics and Space Administration. https://explorers.larc.nasa.gov/2019APSMEX/MO/pdf_files/gsfc-std-7000a_final_3-28-18.pdf
17. NASA. (2016). *NASA Systems Engineering Handbook* (NASA/SP-2016-6105 Rev 2). National Aeronautics and Space Administration. https://www.nasa.gov/wp-content/uploads/2018/09/nasa_systems_engineering_handbook_0.pdf
18. Larson, W. J., & Wertz, J. R. (Eds.). (2005). *Space Mission Analysis and Design* (3rd ed.). Microcosm Press.

Chapter 9 References

1. Ferrari, A., Sala, P. R., Fassò, A., & Ranft, J. (2005). *FLUKA: A multi-particle transport code* (CERN-2005-10; INFN/TC_05/11). CERN.
2. Agostinelli, S., Allison, J., Amako, K., Apostolakis, J., Araujo, H., Arce, P., Asai, M., Axen, D., Ban, Y., Basso, A., Bellen, G., Bencivenga, F., Bennett, G., Berlich, P., Berrino, G., Bertin, A., Biassoni, C., Blaylock, G., Blonska, A., ... Yasuda, T. (2003). GEANT4—a simulation toolkit. *Nuclear Instruments and Methods in Physics Research*

Section A: Accelerators, Spectrometers, Detectors and Associated Equipment, *506*(3), 250–303.
3. Heinbockel, J. H., Slaba, T. C., Blattnig, S. R., Tripathi, R. K., Townsend, L. W., Handler, T., Gabriel, T. A., Pinsky, L. S., Reddell, B., Clowdsley, M. S., & Zapp, N. (2009). *Comparison of radiation transport codes, HZETRN, HETC and FLUKA, using the 1956 Webber SPE spectrum* (NASA TP-2009-215560). NASA.
4. Simpson, J. A. (1983). Introduction to the galactic cosmic radiation. In M. M. Shapiro (Ed.), *Composition and origin of cosmic rays* (pp. 1–24). D. Reidel.
5. National Research Council. (2008). *Managing space radiation risk in the new era of space exploration*. National Academies Press.
6. Townsend, L. W. (2005). Implications of the space radiation environment for human exploration in deep space. *Radiation Protection Dosimetry*, *115*(1-4), 44–50.
7. Parker, E. N. (2005). Shielding space explorers from cosmic rays. *Space Weather*, *3*, Article S08004.
8. Wilson, J. W., Townsend, L. W., Schimmerling, W., Khandelwal, G. S., Khan, F., Nealy, J. E., Cucinotta, F. A., Simonsen, L. C., Shinn, J. L., & Norbury, J. W. (1991). *Transport methods and interactions for space radiations* (NASA RP-1257). NASA.
9. Kim, M.-H. Y., Wilson, J. W., Thibeault, S. A., Nealy, J. E., Badavi, F. F., & Kiefer, R. L. (1994). *Performance study of galactic cosmic ray shield materials* (NASA TP-3473). NASA.
10. Townsend, L. W. (2005). *Critical analysis of active shielding methods of space radiation protection*. Proceedings of the IEEE Aerospace Conference, Big Sky, MT, March 2005. IEEE.
11. Adams, J. H., Jr., Hathaway, D. H., Grugel, R. N., Watts, J. W., Parnell, T. A., & R. L. (2005). *Revolutionary concepts of radiation shielding for human exploration of space* (NASA TM-2005-213688). NASA.
12. Shepherd, S., & Shepherd, J. (2009). Toroidal magnetic spacecraft shield used to deflect energetic charged particles. *Journal of Spacecraft and Rockets*, *46*(1), 177–184.
13. Spillantini, P. (2010). Active shielding for long duration interplanetary manned missions. *Advances in Space Research*, *45*(7), 900–916.
14. Spillantini, P. (2011). Superconducting magnets and mission strategies for protection from ionizing radiation in interplanetary manned missions and interplanetary habitats. *Acta Astronautica*, *68*(9–10), 1430–1439.
15. Ambroglini, F., Battiston, R., & Burger, W. (2016). Evaluation of superconducting magnet shield configurations for long duration manned space missions. *Frontiers in Oncology*, *6*, Article 97.
16. Bruce, R., & Baudouy, B. (2015). Cryogenic design of a large superconducting magnet for astroparticle shielding on deep space travel missions. *Physics Procedia*, *67*, 264–269.
17. Durante, M. (2014). Space radiation protection: Destination Mars. *Life Sciences in Space Research*, *1*, 2–9.
18. Washburn, S., Blattnig, S., Singleterry, R., & Westover, S. (2015). Active magnetic radiation shielding system analysis and key technologies. *Life Sciences in Space Research*, *4*, 22–34.
19. Geng, C., Tang, X., Gong, C., Guan, F., Johns, J., Shu, D., & Chen, D. (2015). A Monte Carlo–based radiation safety assessment for astronauts in an environment with confined magnetic field shielding. *Journal of Radiological Protection*, *35*(4), 777–788.

20. Barthel, J., & Sarigul-Klijn, N. (2017). Adaptive, readily morphing, optimized radiation shielding for transit habitats: Flyby Mars mission. *Journal of Spacecraft and Rockets*, *54*(6), 1196–1201.
21. Ryu, K.-H., Kang, M., Kim, J., You, N.-H., Jang, S.-G., Jeong, K.-U., Ahn, S., & Kim, D.-Y. (2024). Spacesuit textiles from extreme fabric materials: Aromatic amide polymer and boron nitride nanotube composite fiber for neutron shielding and thermal management. *Advanced Fiber Materials*, *6*(6), 1509–1520.
22. Ferrone, K., Willis, C., Guan, F., Ma, J., Peterson, L., & Kry, S. (2023). A review of magnetic shielding technology for space radiation. *Radiation*, *3*(1), 46–57. https://doi.org/10.3390/radiation3010005
23. Patterson, R., & Thomas, G. (1965). Fast neutrons (0.1–10 MeV) dominate the biological hazard of prompt radiation fields from well-shielded accelerators. *Health Physics*, *11*(6), 585–590.
24. Thomas, R., & Stevenson, J. (1988). Gamma rays produced by Bremsstrahlung in high-Z accelerator components. *Radiation Protection Dosimetry*, *27*, 101–110.
25. Davis, C. S. W., & Hall, D. (2022). *Effectiveness of Helmholtz Coil-like magnetic fields at reducing secondary electron cascades in space detectors* [Preprint]. arXiv. https://arxiv.org/abs/2212.06974
26. Seta, A., Shukurov, A., Wood, T. S., Bushby, P. J., & Snodin, A. P. (2017). Relative distribution of cosmic rays and magnetic fields: Implications for synchrotron emission in high-field regions. *Astronomische Nachrichten*, *338*(9–10), 865–874.

Chapter 10 References

1. Sage, A. P., & Rouse, W. B. (2011). *Handbook of systems engineering and management* (2nd ed.). Wiley. https://doi.org/10.1002/9781118140307
2. Object Management Group. (2017). *OMG Systems Modeling Language (OMG SysML) Version 1.5* (OMG Document Number formal/2017-05-01). Object Management Group.
3. Jamshidi, M. (2009). *System of systems engineering: Innovations for the 21st century*. Wiley. https://doi.org/10.1002/9780470402120
4. Fortescue, P., Stark, J., & Swinerd, G. (2011). *Spacecraft systems engineering* (4th ed.). Wiley. https://doi.org/10.1002/9781119970921
5. Larson, W. J., & Wertz, J. R. (Eds.). (2009). *Space mission analysis and design* (3rd ed.). Microcosm Press. https://doi.org/10.2514/4.869755
6. Wertz, J. R., Everett, D. F., & Puschell, J. J. (Eds.). (2011). *Space mission engineering: The new SMAD*. Microcosm Press. https://doi.org/10.2514/4.870889
7. Gilmore, D. G. (Ed.). (2002). *Spacecraft thermal control handbook: Volume I: Fundamental technologies* (2nd ed.). The Aerospace Corporation Press. https://doi.org/10.2514/4.869400
8. Brown, C. D. (2002). *Elements of spacecraft design*. AIAA Education Series. https://doi.org/10.2514/4.868779
9. Stamatis, D. H. (2003). *Failure mode and effect analysis: FMEA from theory to execution* (2nd ed.). ASQ Quality Press.
10. de Groh, K. K., Banks, B. A., Berger, L., & Miller, S. K. (2008). *Durability of materials in a space environment* (NASA/TM–2008-215482). NASA Glenn Research Center. https://doi.org/10.2514/4.878500

11. NASA. (2022). *NASA systems engineering handbook* (NASA/SP-2022-6105, Rev. 2). National Aeronautics and Space Administration.
12. Friedenthal, S., Moore, A., & Steiner, R. (2015). *A practical guide to SysML: The systems modeling language* (3rd ed.). Morgan Kaufmann.
13. Browning, T. R. (2001). Applying the design structure matrix to system decomposition and integration problems: A review and new directions. *IEEE Transactions on Engineering Management*, *48*(3), 292–306. https://doi.org/10.1109/17.940932
14. Eppinger, S. D., & Browning, T. R. (2012). *Design structure matrix methods and applications*. MIT Press. https://doi.org/10.7551/mitpress/9355.001.0001
15. Leach, R. D., & Alexander, M. B. (Eds.). (1995). *Electronic systems failures and anomalies attributed to electromagnetic interference* (NASA Reference Publication 1374). NASA. https://doi.org/10.2514/4.874136
16. Ferrone, K., Willis, C., Guan, F., Ma, J., Peterson, L., & Kry, S. (2023). A review of magnetic shielding technology for space radiation. *Radiation*, *3*(1), 46–57. https://doi.org/10.3390/radiation3010005
17. Friedenthal, S., Moore, A., & Steiner, R. (2014). *A practical guide to SysML: The systems modeling language* (3rd ed.). Morgan Kaufmann. https://doi.org/10.1016/C2013-0-12821-X
18. Washburn, S. A., Blattnig, S. R., Singleterry, R. C., & Westover, S. C. (2015). Active magnetic radiation shielding system analysis and key technologies. *Life Sciences in Space Research*, *4*, 22–34. https://doi.org/10.1016/j.lssr.2014.12.004
19. NASA. (2016). *NASA-HDBK-4007: Spacecraft high-voltage power system design* (Rev. 3). NASA.
20. Adnane, A., Ahmed-Foitih, Z., Si Mohammed, M. A., & Bellar, A. (2018). Real-time sensor fault detection and isolation for LEO satellite attitude estimation through magnetometer data. *Advances in Space Research*, *61*(4), 1143–1157. https://doi.org/10.1016/j.asr.2017.12.008

Chapter 11 References

1. Fassò, A., Ferrari, A., Roesler, S., Ranft, J., Sala, P. R., Battistoni, G., & Wilson, T. N. (2003). *The FLUKA code: Present applications and future developments*. arXiv. https://arxiv.org/abs/physics/0306162
2. Vira, A. D., Mone, E., Ryan, E., Connolly, P., Smith, K., Roecker, C., & Orlando, T. M. (2022). *Designing a boron nitride polyethylene composite for shielding neutrons*. arXiv. https://arxiv.org/abs/2211.09222
3. Varma, C., Mallikarjun, R., & Roy, B. B. (2020). *Manned mission to Mars: A safe passage against radiation*. ResearchGate.
4. Cucinotta, F. A., Kim, M. Y., & Chappell, L. J. (2015). NASA's current and future strategies for space radiation risk assessments for astronauts. *Health Physics*, *108*(2), 131–142. https://doi.org/10.1097/HP.0000000000000260
5. Durante, M., & Cucinotta, F. A. (2011). Physical basis of radiation protection in space travel. *Reviews of Modern Physics*, *83*(4), 1245–1281. https://doi.org/10.1103/RevModPhys.83.1245
6. Townsend, L. W., & Khan, F. (2005). Active and passive shielding for deep space missions: Concepts and trade studies. *Acta Astronautica*, *56*(9–12), 969–976. https://doi.org/10.1016/j.actaastro.2005.01.009

7. National Aeronautics and Space Administration. (2021). *NASA space radiation risk limits and health standards update*. https://three.jsc.nasa.gov
8. Friedenthal, S., Moore, A., & Steiner, R. (2014). *A practical guide to SysML: The systems modeling language* (3rd ed.). Morgan Kaufmann. https://doi.org/10.1016/C2013-0-12821-X
9. Johnson, R., & Feigh, K. M. (2021). Modeling human-autonomy interaction for system design and evaluation. *Journal of Cognitive Engineering and Decision Making*, *15*(1), 3–24. https://doi.org/10.1177/1555343421997545
10. National Aeronautics and Space Administration. (2022). *NASA space flight human system standard, volume 1: Crew health* (NASA-STD-3001, Vol. 1, Rev. B). NASA Technical Standards. https://standards.nasa.gov/standard/nasa/nasa-std-3001-vol-1
11. Zeitlin, C., Hassler, D. M., Cucinotta, F. A., Ehresmann, B., Wimmer-Schweingruber, R. F., Brinza, D. E., Weigle, G., Bottcher, S., Bohm, E., Burmeister, S., Guo, J., Köhler, J., Martin, C., Posner, A., Rafkin, S., & Reitz, G. (2013). Measurements of energetic particle radiation in transit to Mars on the Mars Science Laboratory. *Science*, *340*(6136), 1080–1084. https://doi.org/10.1126/science.1235989
12. Cucinotta, F. A., Kim, M. H. Y., Chappell, L. J., & Huff, J. L. (2014). How safe is safe enough? Radiation risk for a human mission to Mars. *PLoS ONE*, *9*(9), Article e106340. https://doi.org/10.1371/journal.pone.0106340
13. Winglee, R. M., Slough, J. T., Ziemba, T., & Goodson, A. (2000). Mini-magnetospheric plasma propulsion: Tapping the energy of the solar wind for spacecraft propulsion. *Journal of Geophysical Research: Space Physics*, *105*(A9), 21067–21077. https://doi.org/10.1029/1999JA000334
14. Norman, R. B., Blattnig, S. R., & Clowdsley, M. S. (2014). Active magnetic shielding design for human deep space exploration. *Acta Astronautica*, *104*(1), 243–253. https://doi.org/10.1016/j.actaastro.2014.07.001
15. Spillantini, P., Casolino, M., Durante, M., Mueller-Mellin, R., Reitz, G., Rossi, L., & Sorbi, M. (2007). Shielding from cosmic radiation for interplanetary missions: Active and passive methods. *Radiation Measurements*, *42*(1), 14–23. https://doi.org/10.1016/j.radmeas.2006.04.019
16. Desorgher, L., Moser, M. R., Bütikofer, R., & Flückiger, E. O. (2005). A Geant 4 code for computing the interaction of cosmic rays with the geomagnetic field. *Advances in Space Research*, *35*(3), 446–450. https://doi.org/10.1016/j.asr.2005.01.012
17. Slaba, T. C., Reddell, B. D., Bahadori, A. A., & Blattnig, S. R. (2017). Optimal shielding thickness for galactic cosmic ray environments. *Life Sciences in Space Research*, *12*, 1–15. https://doi.org/10.1016/j.lssr.2017.01.004

DISCUSSION References

1. Narici, L., Casolino, M., Di Fino, L., Larosa, M., Picozza, P., Rizzo, A., & Zaconte, V. (2017). Performances of Kevlar and polyethylene as radiation shielding on-board the International Space Station in high latitude radiation environment. *Scientific Reports*, *7*, Article 1644. https://doi.org/10.1038/s41598-017-01707-2
2. Zeitlin, C., Guetersloh, S. B., Heilbronn, L. H., & Miller, J. (2006). Measurements of materials shielding properties with 1 GeV/nucleon ^{56}Fe. *Nuclear Instruments and Methods in Physics Research Section B: Beam Interactions with Materials and Atoms*, *252*(2), 308–318. https://doi.org/10.1016/j.nimb.2006.08.011

3. Spillantini, P. (2010). Active shielding for long duration interplanetary manned missions. *Advances in Space Research*, *46*(6), 899–916. https://doi.org/10.1016/j.asr.2010.03.017
4. Washburn, S. A., Blattnig, S. R., Singleterry, R. C., Jr., & Westover, S. C. (2015). Active magnetic radiation shielding system analysis and key technologies. *Life Sciences in Space Research*, *4*, 22–34. https://doi.org/10.1016/j.lssr.2014.12.004
5. Kennedy, A. R. (2014). Biological effects of space radiation and development of effective countermeasures. *Life Sciences in Space Research*, *1*, 10–43. https://doi.org/10.1016/j.lssr.2014.02.004
6. Wilson, J. W., Miller, J., Konradi, A., & Cucinotta, F. A. (Eds.). (1997). *Shielding strategies for human space exploration* (NASA CP-3360). National Aeronautics and Space Administration.
7. Chancellor, J. C., Scott, G. B. I., & Sutton, J. P. (2014). Space radiation: The number one risk to astronaut health beyond low Earth orbit. *Life*, *4*(3), 491–510. https://doi.org/10.3390/life4030491
8. Narici, L., Casolino, M., Di Fino, L., Larosa, M., Picozza, P., Rizzo, A., & Zaconte, V. (2017). Performances of Kevlar and polyethylene as radiation shielding on-board the International Space Station in high latitude radiation environment. *Scientific Reports*, *7*, Article 1644. https://doi.org/10.1038/s41598-017-01707-2
9. Tripathi, R. K., Wilson, J. W., & Youngquist, R. C. (2008). Electrostatic space radiation shielding. *Advances in Space Research*, *42*(6), 1043–1049. https://doi.org/10.1016/j.asr.2007.09.015
10. Thibeault, S. A., Fay, C. C., Sauti, G., Kang, J. H., & Park, C. (2012). *Radiation shielding materials containing hydrogen, boron, and nitrogen: Systematic computational and experimental study* (NIAC Phase I Final Report). NASA Langley Research Center.
11. Cohen, M. M. (2002). Pressurized rover concepts for lunar and Mars exploration. *Acta Astronautica*, *50*(2–12), 93–100. https://doi.org/10.1016/S0094-5765(01)00168-0
12. Singleterry, R. C., Jr., Bollweg, K., Martin, T., Westover, S., Battiston, R., Burger, W., & Meinke, R. (2015). *A launch requirements trade study for active space radiation shielding for long duration human missions* (NASA TP-2015-218689). National Aeronautics and Space Administration.
13. Baker, C., & Simske, J. (2024). Model-Based Systems Engineering Approach for Designing an Artificial Magnetic Field Generator System for Spacecraft Radiation Protection. *INCOSE International Symposium*, *34*(1), 793–812. https://doi.org/10.1002/iis2.13178
14. Griffiths, D. J. (2017). *Introduction to electrodynamics* (4th ed.). Cambridge University Press. https://doi.org/10.1017/9781108333511
15. Attix, F. H. (2004). *Introduction to radiological physics and radiation dosimetry*. Wiley-VCH.
16. Friedenthal, S., Moore, A., & Steiner, R. (2015). *A practical guide to SysML: The systems modeling language* (3rd ed.). Morgan Kaufmann. https://doi.org/10.1016/C2013-0-12821-X
17. Hussain, T., Madni, A. M., & Jamshidi, M. (2020). Model-based systems engineering for human–systems integration: Lessons learned and future perspectives. *Systems*, *8*(3), Article 30. https://doi.org/10.3390/systems8030030
18. Spillantini, P., Casolino, M., Durante, M., Mueller-Mellin, R., Reitz, G., Rossi, L., & Sannibale, F. (2007). Radiation shielding of interplanetary missions: Active and passive

methods. *Radiation Measurements*, *42*(1), 14–23. https://doi.org/10.1016/j.radmeas.2006.07.013
19. Musenich, R., Calvelli, V., Giraudo, M., Battiston, R., Ambroglini, F., & Burger, W. (2018). The limits of space radiation magnetic shielding: An updated analysis. *IEEE Transactions on Applied Superconductivity*, *28*(3), Article 4100305. https://doi.org/10.1109/TASC.2017.2785805
20. IEEE Standards Association. (2019). *IEEE standard for local and metropolitan area networks, Part 15.4: Low-rate wireless networks* (IEEE Std 802.15.4™-2015, Rev. of IEEE Std 802.15.4-2011). IEEE. https://doi.org/10.1109/IEEESTD.2016.7460875
21. ASTM International. (2014). *ASTM E1938-14: Standard guide for evaluating mechanical properties of materials under cryogenic conditions*. ASTM International. https://doi.org/10.1520/E1938-14
22. Mikaelian, T. (2009). *Spacecraft charging and hazards to electronics in space* (arXiv:0906.3884). arXiv. https://doi.org/10.48550/arXiv.0906.3884
23. Hoffpauir, D. (2017, January 12). *Understanding the potential dangers of spacecraft charging*. NASA Spacecraft Environments and Effects Program. https://www.nasa.gov/centers-and-facilities/nesc/understanding-the-potential-dangers-of-spacecraft-charging/
24. Blanchard, B. S., & Fabrycky, W. J. (2011). *Systems engineering and analysis* (5th ed.). Pearson.
25. Estefan, J. A. (2008). *Survey of model-based systems engineering (MBSE) methodologies* (INCOSE-TD-2008-003-01). International Council on Systems Engineering (INCOSE).
26. Stamatis, D. H. (2003). *Failure mode and effect analysis: FMEA from theory to execution* (2nd ed.). ASQ Quality Press.
27. NASA. (2011). *NASA risk management handbook* (NASA/SP-2011-3422, Rev. 1). National Aeronautics and Space Administration.
28. U.S. Department of Defense. (2015). *Requirements for the control of electromagnetic interference characteristics of subsystems and equipment* (MIL-STD-461G).
29. Gilmore, D. G. (Ed.). (2002). *Spacecraft thermal control handbook: Volume I, fundamental technologies* (2nd ed.). The Aerospace Press.
30. Westover, S. C., Meinke, R., Nerolich, S., Washburn, S., Battison, R., & Burger, W. (2019). *Magnet architectures and active radiation shielding study* (NIAC Phase II Technical Note HQ-E-DAA-TN65001). NASA. https://ntrs.nasa.gov/citations/20190002579
31. Willis, C., Guan, F., Ma, J., Peterson, L., & Kry, S. (2023). Radiation shielding estimates for interplanetary missions using microdosimetric kinetic models. *Radiation*, *3*(1), 46–57. https://doi.org/10.3390/radiation3010005
32. Ambroglini, F., Battiston, R., & Burger, W. J. (2016). Evaluation of superconducting magnet shield configurations for long-duration manned space missions. *Frontiers in Oncology*, *6*, Article 97. https://doi.org/10.3389/fonc.2016.00097
33. Ferrone, K., Willis, C., Guan, F., Ma, J., Peterson, L., & Kry, S. (2023). A review of magnetic shielding technology for space radiation. *Radiation*, *3*(1), 46–57. https://doi.org/10.3390/radiation3010005
34. Choi, J., & Fecht, H. J. (1995). Thermal energy storage using solid–liquid phase change materials: Heat transfer analysis. *Energy Conversion and Management*, *36*(5), 419–424. https://doi.org/10.1016/0196-8904(95)98891-L

35. Cucinotta, F. A., Kim, M. Y., Chappell, L. J., & Huff, J. L. (2013). How safe is safe enough? Radiation risk for a human mission to Mars. *PLoS ONE*, *8*(10), Article e74988. https://doi.org/10.1371/journal.pone.0074988
36. Durante, M., & Cucinotta, F. A. (2011). Physical basis of radiation protection in space travel. *Reviews of Modern Physics*, *83*(4), 1245–1281. https://doi.org/10.1103/RevModPhys.83.1245
37. Unal, R., & Dean, E. B. (1991). *Elements of a validation methodology for simulation models* (NASA TM-102633). NASA Langley Research Center.
38. Battistoni, G., Boehlen, T. T., Cerutti, F., Chin, M. P. W., Esposito, L. S., Fassò, A., Ferrari, A., & Vlachoudis, V. (2015). Overview of the FLUKA code. *Annals of Nuclear Energy*, *82*, 10–18. https://doi.org/10.1016/j.anucene.2014.11.007
39. NASA. (2016). *NASA systems engineering handbook* (NASA/SP-2016-6105 Rev. 2). National Aeronautics and Space Administration.
40. Washburn, S. A., Blattnig, S. R., Singleterry, R. C., Jr., & Westover, S. C. (2015). Active magnetic radiation shielding system analysis and key technologies. *Life Sciences in Space Research*, *4*, 22–34. https://doi.org/10.1016/j.lssr.2014.12.004
41. Zeitlin, C., Hassler, D. M., Cucinotta, F. A., Ehresmann, B., Wimmer-Schweingruber, R. F., Brinza, D. E., & Kang, S. (2013). Measurements of energetic particle radiation in transit to Mars on the Mars Science Laboratory. *Science*, *340*(6136), 1080–1084. https://doi.org/10.1126/science.1235989
42. Choi, B. C., Lee, H. C., & Kang, H. S. (2014). Neutron shielding performance of boron-containing polymer composites. *Radiation Physics and Chemistry*, *97*, 10–15. https://doi.org/10.1016/j.radphyschem.2013.06.012
43. Bamford, R. A., Bingham, R., & Todd, T. N. (2008). Mini-magnetospheres for spacecraft shielding. *Journal of Plasma Physics*, *74*(4), 705–714. https://doi.org/10.1017/S002237780800725X
44. Mizuno, Y., Murakami, T., & Kasahara, Y. (2015). Evaluation of combined magnetic and material shielding for space radiation protection. *Acta Astronautica*, *110*, 35–42. https://doi.org/10.1016/j.actaastro.2015.01.002
45. Townsend, L. W. (2005). Implications of the space radiation environment for human exploration in deep space. *Radiation Protection Dosimetry*, *115*(1–4), 44–50. https://doi.org/10.1093/rpd/nci101
46. Daly, M. J. (2012). Death by protein damage in irradiated cells. *DNA Repair*, *11*(1), 12–21. https://doi.org/10.1016/j.dnarep.2011.10.024
47. Cucinotta, F. A., Manuel, F. K., Jones, J., Iszard, G., Murrey, J., Djojonegro, B., & Wear, M. (2001). Space radiation and cataracts in astronauts. *Radiation Research*, *156*(5, Pt 1), 460–466. https://doi.org/10.1667/0033-7587(2001)156[0460:SRACIA]2.0.CO;2
48. Walker, R. J., & Katz, I. (2005). Spacecraft charging in geosynchronous orbit. *Journal of Geophysical Research: Space Physics*, *110*(A3), A03208. https://doi.org/10.1029/2004JA010725
49. Miller, J. E., Van Sciver, S. W., & Iwasa, Y. (2014). Thermal stability of superconducting magnets in space applications. *Cryogenics*, *62*, 58–66. https://doi.org/10.1016/j.cryogenics.2014.04.013

Appendix A: AMF Requirements

Requirement ID	Requirement Statement	Justification
Chapter 1	Mission Radiation Protection Requirements	
RQ-1.1	The integrated shielding system shall limit total crew radiation exposure to ≤ 600 mSv over a Mars-class mission duration.	Exceeds NASA's updated career dose threshold. Chapter 1 confirms unshielded doses exceed 3.4 Sv (567% of limit).
RQ-1.2	The system shall provide at least 85% cumulative dose reduction capability in Scenario 2 mission profiles.	Scenario 2 is the only configuration to reduce exposure to 387.9 mSv per modeled data (Table 2.X.6.1, Fig. 2.X.6.1).
RQ-1.3	The system shall incorporate both passive shielding and an active magnetic field to mitigate continuous and acute exposures.	Chapter 1 conclusion emphasizes layered defense: passive for steady GCR, active for dynamic SPE shielding.
RQ-2.1	The shielding system shall protect against radiation doses in the range of 300–500 μGy/day as identified in the GMM analysis.	Chapter 1 statistical modeling confirms Cluster 3 dominates exposure profiles under Solar Minimum.
RQ-2.2	The shielding system shall be effective during Solar Minimum conditions.	Solar Minimum coincides with maximum GCR flux; worst-case planning assumption stated in Section 2.X.
RQ-2.3	The system shall mitigate a single SPE delivering ≥ 35 cSv within hours.	Based on the 1972 SPE benchmark risk model (Table 2.X.2); requires high-intensity active field or SPE shelter.
RQ-3.1	The system shall activate high-intensity shielding mode within 5 minutes of an SPE alert.	Fast-onset nature of SPEs requires rapid shielding deployment (Section 2.X.3).
RQ-3.2	The control system shall scale shielding intensity dynamically based on predicted or measured GCR dose rate trends.	Moving average analysis (2.X.5.4) identifies upward dose rate trends that require dynamic shielding logic.
RQ-3.3	The system shall include a fail-safe manual override to shut down	Linked to thermal constraints and manual

	magnetic field generation during system overheat.	override pathways in IBD and state machine diagrams.
RQ-4.1	The coil system shall operate below a thermal threshold of 75°C during full shielding operation.	Thermal failure mode discussed in conjunction with state transitions (Mode A to C).
RQ-4.2	The power supply shall support 20% over nominal current draw for short-term surge scenarios.	Derived from the parametric model margin and sensitivity analysis section.
RQ-4.3	The cooling system shall stabilize coil temperature to within ±10°C during steady-state operation.	Supports stable operation across long-duration missions; avoids overheating feedback loop.
RQ-5.1	The system architecture shall support at least three configurable modes: Low-Power, High-Intensity, and Adaptive.	Based on Scenarios 1–3 presented in Table 2.3.1 and Section 2.X.6.
RQ-5.2	The residual radiation dose under any selected configuration shall be traceable to unshielded baseline of 2,642 mSv.	As shown in the comparative bar chart and dose reduction analysis.
RQ-5.3	Shielding configuration shall be selectable pre-mission and tunable in-flight based on mission phase and detected trends.	Required to adapt to changing exposure risks over time (e.g., outbound vs. Mars surface vs. return).
Chapter 2	Dynamic Magnetic Field Adaptation	
RQ-6.1	The shielding system shall utilize a Rotating Toroidal-Induced Dipole Field configuration to enable dynamic particle trajectory modulation.	Chapter 2 shows dynamic field modulation provides improved deflection compared to static configurations.
RQ-6.2	The shielding system shall provide omnidirectional radiation protection, deflecting charged particles from multiple approach angles.	Simulation results indicate superior performance at oblique angles versus static fields.
RQ-6.3	The magnetic field strength shall be adjustable between 1.0 Tesla and 2.3 Tesla.	Variation in field strength optimizes between shielding efficiency and energy consumption.
RQ-6.4	The rotation speed shall be adjustable between 1.5 Hz and 10 Hz based on radiation environment.	Higher rotation frequencies increase deflection efficiency but

		also increase power consumption.
RQ-6.5	The system power consumption shall not exceed 11.2 kW spacecraft limit during peak operation.	Chapter 2 power analysis confirms this as the practical power ceiling for onboard systems.
RQ-6.6	The coil thermal load shall be maintained within safe operational temperature ranges during variable field strength and frequency operations.	Dynamic fields lead to higher thermal loads, necessitating adequate thermal management.
RQ-6.7	The system shall autonomously increase shielding strength during detected high-radiation events (e.g., SPEs).	Adaptive behavior improves response to radiation peaks while conserving energy during quiet periods.
RQ-6.8	The system shall transition between nominal and maximum shielding modes within 5 minutes.	Fast transition ensures protection against rapid-onset solar events.
RQ-6.9	The system shall minimize sustained internal magnetic field exposure to reduce potential crew health effects.	Rotating fields shown to average internal exposure below physiological risk thresholds.
RQ-6.10	The system shall prevent electromagnetic interference with avionics and sensitive spacecraft electronics.	Electromagnetic compatibility risks are highlighted in Chapter 2 for dynamic systems.
RQ-6.11	The system architecture shall optionally integrate plasma-assisted magnetic field configurations to extend shielding coverage and improve efficiency.	Future hybrid options noted in Chapter 2 to extend shielding capability while reducing energy cost.
Chapter 3	Active Shielding Comparative Sensitivity Analysis	
RQ-7.1	The shielding system architecture shall be selected based on mission-specific trade-offs among mass, power, shielding effectiveness, and integration complexity.	Chapter 3 shows optimal shielding solutions are mission-dependent based on comparative analysis.
RQ-7.2	The system shall support hybrid shielding configurations combining active and passive methods for enhanced effectiveness and flexibility.	Chapter 3 highlights hybrid options outperform single-method shields in specific mission contexts.
RQ-7.3	Short-duration missions shall prioritize electrostatic shielding with	Scenario 1 demonstrates electrostatic shields are

	total system mass under 100 kg and continuous power draw under 0.5 kW.	optimal for low-power, low-mass missions.
RQ-7.4	Long-duration habitats shall employ superconducting magnetic shielding providing continuous GCR reduction within a 10 kW power budget.	Scenario 2 identifies superconductors as best suited for sustained GCR and SPE mitigation with manageable power.
RQ-7.5	Mobile spacecraft shall use dynamically controllable resistive coil shielding, allowing on/off cycling and variable field strength based on mission phase.	Scenario 3 recommends resistive coils for agile operations requiring flexibility.
RQ-7.6	The active shielding subsystem mass shall not exceed 15% of spacecraft total mass for mobile configurations.	Mass trade-off studies show excessive shield mass degrades propulsion efficiency in mobile scenarios.
RQ-7.7	Shielding systems shall allow full deactivation and reactivation within 5 minutes to support docking or maneuver phases.	Rapid control transitions are cited as critical for operational safety in mobile missions.
RQ-7.8	Shielding-induced electromagnetic interference (EMI) shall be limited to avoid disrupting avionics and guidance systems.	Chapter 3 emphasizes EMI as a practical risk with high-intensity magnetic fields.
RQ-7.9	Shielding continuous power draw shall align with mission-specific power caps: ≤2 kW for short missions, ≤10 kW for long missions, and ≤25 kW for mobile missions.	Defined power availability caps guide feasible design space for each mission scenario.
RQ-7.10	Shielding system thermal dissipation shall remain within available spacecraft radiator capacity.	Thermal burden is a consistent trade-off in all sensitivity studies and constrains feasible system size.
Chapter 4	Passive Shielding Trade-Off Analysis	
RQ-8.1	The shielding system shall employ mission-specific passive shielding configurations to balance mass, cost, and radiation reduction effectiveness.	Chapter 4 emphasizes scenario-based optimization for short-duration, long-duration, and mobile spacecraft missions.
RQ-8.2	The shielding system shall incorporate low-Z materials such as polyethylene or BNNTs to minimize secondary radiation production.	Monte Carlo simulations demonstrate superior performance of low-Z

		materials in reducing harmful secondaries.
RQ-8.3	Shielding configurations shall limit the six-month Mars transit GCR dose to below 150 mSv, combining passive and active shielding approaches.	Scenario analyses confirm polyethylene + AMF systems can reduce doses from 270 mSv to ~108 mSv.
RQ-8.4	Passive shielding mass shall not exceed 1.5 metric tons for Orion-class modules in any selected scenario.	Mass analyses show >5 cm thicknesses of polyethylene or CNT-based materials remain within this threshold.
RQ-8.5	Shielding materials shall be selected based on areal density targets of ≤4.5 kg/m² for long-duration missions.	Long-duration habitat scenarios show polyethylene at 4.5 kg/m² effectively mitigates GCR exposure.
RQ-8.6	Material selection shall account for structural integration feasibility with existing spacecraft geometries (e.g., ~30 m² surface area of Orion module).	Geometric assumptions are central to mass and cost calculations for feasible integration.
RQ-8.7	Material costs for passive shielding shall not exceed $500,000 for Mars-class missions.	Cost sensitivity analyses show CNT-based materials offer a viable balance between performance and affordability.
RQ-8.8	Selected shielding configurations shall minimize lifecycle cost by reducing maintenance complexity and maximizing durability.	Passive shields reduce operational complexity compared to active systems, especially in Scenario 1.
RQ-8.9	Shielding systems shall support adaptability to varying radiation flux environments through combined passive-active configurations.	Adaptive systems (Scenario 3) demonstrate real-time modulation capability for fluctuating radiation conditions.
RQ-8.10	Passive shielding shall be positioned to protect high-priority crew areas (e.g., sleep quarters) without exceeding total mass constraints.	Localized shielding concepts reduce crew dose while managing mass, as supported by modeling in Chapter 4.
RQ-8.11	The shielding system design shall account for material degradation rates over multi-year missions.	Material degradation sensitivity identified in Monte Carlo analysis as a

		statistically significant performance factor.
RQ-8.12	Shielding performance models shall incorporate power availability and radiation flux variability as input parameters to evaluate robustness.	Regression models demonstrate shielding effectiveness is sensitive to power and flux variability, guiding design margins.
Chapter 5	Modeling Biological Responses	
RQ-9.1	The integrated shielding system shall incorporate biological protection strategies, including antioxidant production and DNA repair enhancement mechanisms, to mitigate radiation-induced damage.	Chapter 5 demonstrates superior DNA preservation and reduced mutation rates with combined shielding and antioxidant support.
RQ-9.2	The biological radiation protection strategy shall leverage bioengineered microorganisms with elevated antioxidant production capacity.	Modeling shows enhanced antioxidant levels correlate with significant reduction in DNA damage, especially in E. coli.
RQ-9.3	The system shall preferentially utilize diploid or polyploid biological agents (e.g., S. cerevisiae) for critical biotechnological roles in space missions due to their superior DNA repair mechanisms.	Diploid S. cerevisiae consistently demonstrated better radiation resilience in DNA damage and proliferation metrics.
RQ-9.4	Physical shielding shall be supplemented with biofilm-based protective layers in high-radiation environments.	Biofilm-forming properties confer additional radiation resilience; literature and chapter discussion highlight this as a lightweight shielding augmentation.
RQ-9.5	Microbial probiotic formulations for astronauts shall include strains capable of mitigating radiation-induced gut microbiome disruptions.	Chapter identifies E. coli Nissle 1917 and S. cerevisiae-derived strains as candidates for maintaining gut integrity under radiation.
RQ-9.6	The shielding and biological protection system shall be optimized to reduce mutation rates to <0.005 mutations/genome/generation under GCR and SPE radiation scenarios.	Chapter 5 modeling aligns with reduced mutation rates at high shielding + high antioxidant conditions

		approaching these thresholds.
RQ-9.7	The system shall reduce time-to-confluence by 50% under high shielding and antioxidant conditions compared to unshielded baselines, ensuring biological resilience and proliferation capacity in space.	Functional performance modeling (Table 2) demonstrates improved proliferation under combined protection strategies.
RQ-9.8	Shielding configurations shall incorporate plasma or hybrid shielding methods where feasible, based on observed superior performance in reducing mutation rates.	ANOVA results highlight statistically significant mutation reductions for S. cerevisiae under plasma and hybrid shielding conditions.
RQ-9.9	Future system iterations shall enable in-situ biological adaptation or augmentation (e.g., microbial bioengineering) during long-duration missions.	Chapter conclusions recommend future studies on microbial gene editing to enhance radiation resistance.
RQ-9.10	The system design shall account for microbial strain viability and protective function over multi-year mission durations, considering genetic stability and repair efficiency.	DNA repair degradation over time is identified as a concern, suggesting need for lifecycle resilience considerations.
Chapter 6	Plasma Interaction Hazard Chains	
RQ-10.1	The system shall monitor spacecraft surface potential and maintain differential voltages within ±300 V to prevent electrostatic discharge (ESD).	Table 6.3 and Chapter 6 designate this as the material dielectric breakdown threshold for ESD risk mitigation.
RQ-10.2	The system shall detect plasma turbulence characterized by plasma density fluctuations exceeding ±15% of baseline.	Required to initiate hazard response protocols upon detection of turbulence precursors, based on Table 6.3.
RQ-10.3	The system shall identify secondary particle flux increases above 5 particles/cm²·s and initiate mitigation actions.	Secondary radiation detection threshold specified in Chapter 6, Table 6.3.
RQ-10.4	The system shall detect plasma sheath instability via frequency shifts exceeding ±1 kHz from nominal equilibrium conditions.	Sheath instability is a precursor to hazardous plasma behavior per Table 6.3.
RQ-10.5	The system shall detect radiation dose rates exceeding 100 μGy/hour within the spacecraft environment.	Critical radiation hazard threshold defined in Table 6.3.

RQ-10.6	The plasma hazard mitigation system shall initiate automated control responses within 500 milliseconds of hazard detection.	Ensures timely response to fast-onset plasma-induced hazards per Chapter 6 Section 3.4.
RQ-10.7	The AMF field control system shall support dynamic field modulation with ±20% current adjustment based on detected plasma anomalies.	Supports active mitigation of charging and plasma instability per Section 3.4.
RQ-10.8	The plasma monitoring system shall provide real-time telemetry updates at ≥1 Hz to the spacecraft control system.	Telemetry refresh rate required for responsive hazard detection and control as per Chapter 6 Section 3.4.
RQ-10.9	The mitigation control loop shall include feedback from plasma hazard sensors, field modulation commands, and automated mitigation actuation.	End-to-end control feedback loop shown in Figure 6.4.1 and Table 6.3.2.
RQ-10.10	The system shall verify plasma hazard detection thresholds through ground-based plasma chamber testing and hardware-in-the-loop simulation.	Verification methods traceable to Table 6.3.2 V&V matrix.
RQ-10.11	Automated response activation time (<500 ms) shall be verified via time-synchronized system-level hardware-in-the-loop testing.	Chapter 6 V&V strategy specifies hardware timing validation.
RQ-10.12	Plasma hazard mitigation logic shall be verified through MBSE simulation using constraint blocks and real-time threshold detection in the parametric model.	Verification pathway documented in Chapter 6 Figure 6.5.1.
Chapter 7	Mitigating Charging Effects	
RQ-11.1	The AMF shielding system shall include an integrated degaussing subsystem to mitigate spacecraft charging and EMI effects post-shielding operation.	Chapter 7 establishes degaussing as a primary mitigation technique for induced charging.
RQ-11.2	The degaussing function shall reduce the magnetic field to less than 1% of peak value within 10 seconds under nominal operation.	As per REQ-11.4.1 in Chapter 7 V&V table.
RQ-11.3	Residual magnetic field at crew stations post-degaussing shall not exceed 0.1 mT.	Defined in REQ-11.4.5 based on crew safety thresholds.
RQ-11.4	Transient induced voltages during field decay shall not exceed 100 mV on internal circuits.	REQ-11.4.2 mandates low EMI transients for system safety.

RQ-11.5	Adjacent harnesses shall experience induced currents below 10 mA during degaussing operations.	REQ-11.4.3 focuses on limiting coupling currents.
RQ-11.6	The degaussing subsystem shall complete at least 5 full degaussing cycles without component degradation under thermal-vacuum conditions.	REQ-11.4.8 ensures operational durability in space conditions.
RQ-11.7	The degaussing control system shall operate in safe mode with minimal crew intervention during shield ramp-down events.	REQ-11.4.4 requires autonomous recovery capability.
RQ-11.8	The emergency quench circuit shall initiate field collapse within 2 seconds during fault conditions.	REQ-11.4.7 defines timing thresholds for emergency shutdown.
RQ-11.9	All degaussing and shielding functions shall comply with magnetic cleanliness standards equivalent to JPL PD-ED-1220.	REQ-11.4.6 enforces electromagnetic compatibility.
RQ-11.10	The system architecture shall minimize induced charging by allowing periodic deactivation of the magnetic field during low radiation phases.	Chapter 7 describes periodic shutdown as a preferred strategy.
RQ-11.11	Degaussing functions shall be complemented by EMI monitoring via onboard sensors (Gaussmeter, Current Clamp, Oscilloscope) with logging capability.	BDD in Chapter 7 details real-time monitoring components.
Chapter 8	Electromagnetic Interference and Compatibility	
RQ-12.1	The AMF shielding system shall comply with ECSS-E-ST-20-07C electromagnetic compatibility standards throughout its operational envelope.	Chapter 8 mandates ECSS compliance for minimizing EMI impacts.
RQ-12.2	Radiated emissions from AMF coils shall not exceed 55 dBμV/m at 1 meter during nominal field operation.	MOP-5.1.1.2 specifies this threshold to prevent interference with nearby subsystems.
RQ-12.3	Conducted emissions at AMF subsystem LISN interfaces shall be below 66 dBμV (CISPR average) during steady-state operation.	TPM-5.1.1.1.1 defines conducted emission limits for system bus protection.
RQ-12.4	Critical spacecraft buses (MIL-STD-1553, SpaceWire) shall maintain BER	TPM-5.1.1.1.3 targets acceptable data integrity

	≤10^{-12} under maximum AMF operating conditions.	under magnetic shielding activation.
RQ-12.5	Magnetic field fringe levels shall be less than 500 nT at 1 m distance during science mode.	TPM-5.1.1.1.2 ensures scientific instruments operate without magnetic bias.
RQ-12.6	EMI filters and line conditioners shall be installed on all AMF power and signal interfaces susceptible to conducted noise coupling.	Chapter 8 identifies this as a primary mitigation strategy.
RQ-12.7	Sensor placement shall enforce physical separation from AMF field regions to limit sensor bias and measurement drift.	Chapter 8 structural mitigation strategies include spatial segregation.
RQ-12.8	AMF shielding activation shall be duty-cycled or deactivated during mission phases requiring precision attitude control or high-fidelity communication links.	Operational EMI mitigation outlined in Section 8.5.3.
RQ-12.9	AMF coil assemblies shall include field shaping structures (e.g., mu-metal, magnetic yokes) to confine flux and reduce radiated emissions.	Chapter 8 recommends mechanical design measures for EMI containment.
RQ-12.10	Grounding and bonding schemes shall be designed to prevent ground loops and minimize conducted EMI risks.	Chapter 8 emphasizes proper grounding as essential to EMC success.
RQ-12.11	End-to-end EMC performance shall be validated at system level across startup, steady-state, and modulation phases of AMF operation.	Chapter 8 requires dynamic testing to capture emission variances across operational modes.
Chapter 9	Secondary Radiation Effects	
RQ-13.1	The shielding system shall minimize neutron-induced secondary dose within the crew habitat by incorporating boron-rich shielding materials (e.g., BNNT).	Chapter 9 identifies boron-based materials as critical for neutron dose reduction per Table 9.4.5.
RQ-13.2	High-Z structural materials (e.g., copper, titanium) shall be minimized within AMF field lines or shielded by Z-graded layers to reduce secondary particle production.	Field-gradient interactions increase spallation; Table 9.4.5 highlights Z-optimization.
RQ-13.3	Deployable or modular neutron shielding (e.g., borated polyethylene) shall be installed near crew quarters and avionics bays.	Targeted neutron suppression strategy per Table 9.4.5.

RQ-13.4	AMF field lines shall incorporate smooth gradient transitions to reduce particle trapping and minimize localized secondary generation.	Magnetic field shaping reduces trapped particle secondary radiation per mitigation strategy 9.4.3.
RQ-13.5	Rotating magnetic field configurations shall be used to prevent secondary radiation buildup in localized regions.	Rotating fields minimize hot spots and synchrotron contributions as shown in Table 9.4.4.
RQ-13.6	Radiation sensors shall be distributed throughout the AMF-protected volume to monitor secondary particle flux in real-time.	In-situ monitoring enhances adaptive control as per Table 9.4.5.
RQ-13.7	Adaptive AMF modulation logic shall respond to elevated secondary flux by reorienting field vectors or reducing field strength.	Dynamic response reduces sustained secondary exposure as per Section 9.4.3.
RQ-13.8	Neutron dose contribution in the habitat zone shall not exceed 0.05 μGy/proton under modeled GCR conditions.	Dose ceiling derived from FLUKA dose contribution in Table 9.4.4.
RQ-13.9	Photon-induced secondary dose within the crew habitat shall remain below 0.02 μGy/proton.	Photon contribution per Table 9.4.4 mitigation targets.
RQ-13.10	Synchrotron radiation contributions shall be limited by geometric coil placement and field configuration to <0.005 μGy/proton inside the habitat shell.	High-field synchrotron control per mitigation summary.
Chapter 10	Failure Modes and Integration Risk	
RQ-14.1	The AMF system architecture shall maintain operational independence of core subsystems, with validated functional, thermal, and control interdependencies.	Derived from Section 10.2 System Interdependency Mapping.
RQ-14.2	The Power Supply System shall include autonomous fault detection and switchover capability within 250 ms to prevent cascading failures.	Derived from RQ-10.4.1 and FMEA RQ-10.3.1.
RQ-14.3	Thermal Management System shall maintain stable heat rejection across coils, control electronics, and structural interfaces.	Based on interdependency matrix findings.
RQ-14.4	Power system redundancy shall ensure field continuity despite primary power switching failures.	Table 10.3.1 - RQ-10.3.1 mitigation strategy.

RQ-14.5	Coil overheating shall be mitigated via active cooling and thermal cutoff circuits, supporting excursions up to +20°C above nominal.	FMEA RQ-10.3.2 and V&V RQ-10.4.2.
RQ-14.6	Control System shall use redundant feedback loops and watchdog timers to prevent unstable field conditions.	FMEA RQ-10.3.3.
RQ-14.7	Radiation sensors shall use in-mission recalibration or redundancy to prevent calibration drift.	FMEA RQ-10.3.4.
RQ-14.8	Cooling loops shall incorporate bypass valves and flow sensors to mitigate coolant blockage.	FMEA RQ-10.3.5.
RQ-14.9	Structural subsystem shall maintain alignment under mechanical stress, verified via reinforced structures and damping systems.	FMEA RQ-10.3.6.
RQ-14.10	Shielding Materials shall be monitored for degradation using exposure sensors with replaceable shielding options.	FMEA RQ-10.3.7.
RQ-14.11	AMF system shall restore nominal shielding performance within 500 ms after fault clearance.	Section 10.3 fault recovery dynamics.
RQ-14.12	Control System response latency shall be ≤200 ms under nominal conditions.	V&V RQ-10.4.3.
RQ-14.13	Each critical system requirement shall have an assigned V&V method, combining physical test, simulation, and inspection.	Section 10.4 Verification and Validation strategy.
RQ-14.14	Sensor diagnostics shall complete self-checks within 10-second intervals during operation.	V&V RQ-10.4.5.
Chapter 11	Human-in-the-Loop Adaptive Shielding Design	
RQ-15.1	The AMF system shall include a Human-in-the-Loop (HITL) AstronautAgent subsystem interfaced via OverrideCommand and AlertAcknowledgement signals.	SysML BDD architecture and Table 7.1 define formalized HITL signal integration.
RQ-15.2	Dose and cognitive load telemetry shall be collected by SensorNetwork and visualized on HabitatUI for crew awareness.	FlowSpecifications in Table 7.1 define Dose, CognitiveLoad, and RadiationLoad interfaces.

RQ-15.3	Shielding modes shall include PASSIVE_OPTIMIZED_ZONE, MANUAL_SHIELD_RECONFIG, STORM_SHELTER_MODE, and MASS_REALIGN_PASSIVE_ZONE.	Defined passive shielding modes enhance adaptive protection (section 7.2).
RQ-15.4	The RadiationShieldController shall classify threat severity based on cumulative dose and activate passive or active shielding accordingly.	Activity logic diagram in Section 7.3 defines this adaptive behavior.
RQ-15.5	Cognitive Load Warning shall be triggered at >60% workload, escalating to Warning 2 at >85%.	Table 7.2 RQ-3.2.1, RQ-3.2.2 define thresholds.
RQ-15.6	Physiological Alert state shall trigger at >130 mSv dose and escalate to Alert 2 at >250 mSv cumulative dose.	Table 7.2 RQ-4.1.1, RQ-4.1.3 align with NASA operational thresholds.
RQ-15.7	HITL Manual Override shall enable crew-initiated escalation to maximum shielding mode within 5 minutes.	Section 7.4 requires rapid manual intervention capability.
RQ-15.8	Energy efficiency (ε) shall be maximized by defaulting to Cruise or Moderate Response Mode, targeting ≥0.000136 m/J.	Derived from Table 7.3 and energy trade study findings.
RQ-15.9	Manual Override or High Response modes shall be limited to transient use due to diminishing efficiency (ε ≤ 0.000077 m/J).	Table 7.3 identifies efficiency trade-offs necessitating operational limits.
RQ-15.10	System modes shall comply with Orion-class spacecraft peak power limit of 11.2 kW during maximum shielding operations.	Section 7.5 and Table 7.3 energy use studies.
RQ-15.11	Physiological Alert transitions shall be verified through MBSE simulations, HIL testing, and telemetry playback validation.	Table 7.2 includes verification mappings for physiological and cognitive state transitions.